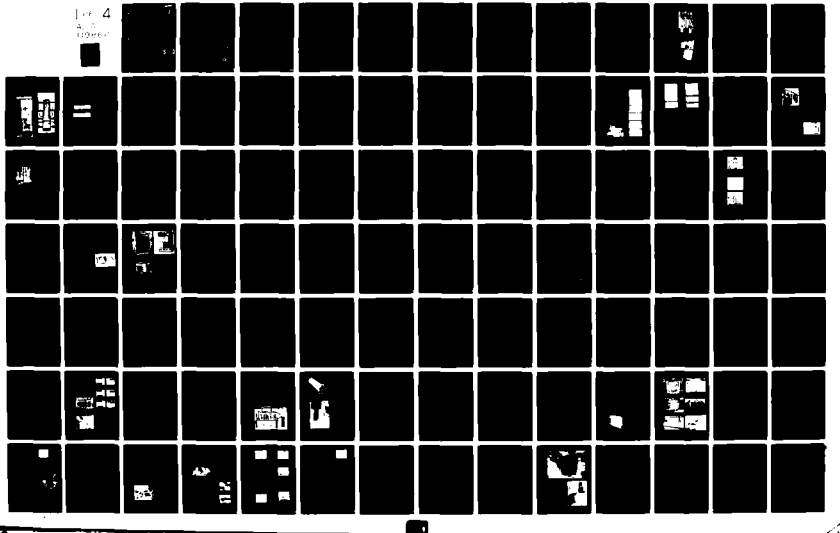
AD-A119 662 PALISADES INST FOR RESEARCH SERVICES INC NEW YORK F/G 9/5
IEEE CONFERENCE RECORD OF 1978 THIRTEENTH PULSE POWER MODULATOR--ETC(U)
1978
UNCLASSIFIED 78-CH-1371-4-ED NL



AD A119662

78 CH 1371-4 ED

IEEE

CONFERENCE RECORD OF

1978 THIRTEENTH PULSE POWER MODULATOR SYMPOSIUM

June 20-22, 1978

Sponsored by the
IEEE Electron Devices Society
In cooperation with the
Advisory Group on Electron Devices
and
The State University of New York at Buffalo
Under the management of
Palisades Institute for Research Services, Inc.

DTIC
ELECTE
SEP 28 1982
S D
D

DTIC FILE COPY

DISTRIBUTION STATEMENT A
Approved for public release;
Distribution Unlimited

82 09 27 074

78 CH 1371-4 ED

IEEE

CONFERENCE RECORD OF

1978 THIRTEENTH PULSE POWER MODULATOR SYMPOSIUM

Papers presented at the
Statler Hilton - Buffalo, New York
June 20-22, 1978

Sponsored by the
IEEE Electron Devices Society
in cooperation with the
Advisory Group on Electron Devices
and
The State University of New York at Buffalo
Under the management of
Palisades Institute for Research Services, Inc.

DTIC
COPY
INSPECTED
2

Accession For
NTIS GRA&I
DTIC TAB
Unannounced
Justification
By Per Ltr. (ACQ 22-166?
Distribution/ and Aug 82 on File
Availability Codes
Dist | Avail and/or Special
A

Library of Congress Catalog Card No.: 78-66972

Available from
IEEE Service Center
445 Hoes Lane
Piscataway, N. J. 08854

Printed in USA

Copyright © 1978 by The Institute of Electrical and Electronics Engineers, Inc.
345 East 47th Street, New York, N. Y. 10017

FOREWORD

The 1978 Thirteenth Pulse Power Modulator Symposium is the latest in a series beginning with the Hydrogen Thyratron Symposium in 1950. These conferences have provided early views of the evolution of devices and technologies in the modulator field. As a part of the Symposium, information on recent trends and current modulator applications is presented.

1978 PROGRAM COMMITTEE

S. Schneider; Symposium Chairman
Electronics Technology and Devices Laboratory (ERADCOM)

J. E. Creedon; Co-Chairman
Electronics Technology and Devices Laboratory (ERADCOM)

L. H. Klein; Secretary and Treasurer
Palisades Institute for Research Services, Inc.

A. S. Gilmour, Jr.; Chairman, Local Arrangements
State University of New York at Buffalo

H. Menown; Overseas Representative
English Electric Valve Company, U.K.

N. S. Nicholls; Overseas Representative
Royal Signals & Radar Establishment, U.K.

E. H. Beckner
Sandia Laboratories

R. A. Gardenghi
Westinghouse Electric Corporation

B. R. Gray
Air Force Rome Air Development Center

A. H. Guenther
Air Force Weapons Laboratory

R. J. Harvey
Hughes Research Laboratories

M. Kristiansen
Texas Tech University

P. N. Mace
Los Alamos Scientific Laboratory

M. F. Rose
Naval Surface Weapons Center

I. Smith
Physics International

C. M. Stickley
Energy Research & Development Administration

R. Verga
Air Force Aero-Propulsion Laboratory

T. A. Weil
Raytheon Company

Symposium included papers on:

TABLE OF CONTENTS

PAGE

SESSION I – MODULATOR TECHNIQUES

A Miniature High-Voltage High-Current Nanosecond Pulse Generator,
J. Bajda; Cober Electronics, Inc. 1

Driving Pockels Cell Gates in Multiarm Lasers,
B. M. Carder; Lawrence Livermore Laboratory 5

Operating Hydrogen Thyratrons in Parallel,
G. J. Scoles, R. L. Snelling; English Electric Valve Company, Ltd., U. K. 9

SESSION II – POWER CONDITIONING, REGULATION, AND CHARGING

A Stable Load-Invariant High-Frequency SCR Series Resonant Inverter For Radar Transmitter Applications,
R. C. Cole; International Telephone and Telegraph, Inc. 14

High-Voltage dc Power Conditioner,
D. L. Pruitt; RCA Corporation. 15

Modulator Charging System Upgrade For A 5-MeV Electron Accelerator,
D. Rogers, W. Dexter, A. Myers, L. Reginato, A. Zimmerman; Lawrence Livermore Laboratory. 19

Pulsed TWT Power Supply – A Technique For Minimizing RF Phase Instability And High-Voltage Energy,
F. Tarantino, P. Porzio; Selenia, Italy 22

Off-Resonance Transformer Charging For 250-kV Water Blumlein,
E. Cook, L. Reginato; Lawrence Livermore Laboratory 27

Precision Regulated 20-kW Modulator PFN Charging System,
C. A. Carson; Westinghouse Electric Corporation 34

SESSION III – PULSE NETWORKS

A Modular PFN With Pulse Width Agility,
H. J. Blinchikoff, R. A. Gardenghi; Westinghouse Electric Corporation. 38

PFN Loss Calculations,
S. I. Rambo, R. A. Gardenghi; Westinghouse Electric Corporation. 43

Pulse Forming Networks With Time-Varying Or Nonlinear Resistive Loads,
R. M. Roark, M. E. Parten, L. B. Masten, T. B. Burkes; Texas Tech University. 46

Peak Switch Current Enhancement Filter,
J. P. O'Loughlin; Air Force Weapons Laboratory
W. M. Moeny; Tetra Corporation 52

A New Resonance Transformer,
J. Harrison; Maxwell Laboratories, Inc. 55

SESSION IV – COMPONENTS FOR PULSE CIRCUITS

Solid-State Clipper Diodes For High-Power Modulators,
S. Levy, J. E. Creedon; Electronics Technology and Devices Laboratory (ERADCOM) 60

Low-Inductance Low-Impedance Megawatt Average Power Load,
W. Wright, Jr.; Electronics Technology and Devices Laboratory (ERADCOM) 66

Loads For High-Power Testing,
B. R. Gray; Rome Air Development Center 70

Lightweight Power-Conditioning Magnetics,
J. Welsh, R. Hauptauer, D. Lockwood; SUNY at Buffalo 71

Electro-Optic Transducers And Optical Fibers In High-Voltage Microwave Modulators,
P. Cervone, G. Scerch; Selenia, Italy 75

SESSION V – CLOSING SWITCHES

The Crossed-Field Closing Switch – A Status Report,
R. J. Harvey, R. W. Holly; Hughes Research Laboratories
J. Creedon, H. Gauch; Electronics Technology and Devices Laboratory (ERADCOM) 79

Pulse Modulator Behavior Of The Liquid Plasma Valve,
W. Wright, Jr.; Electronics Technology and Devices Laboratory (ERADCOM)
J. Bayless; Hughes Research Laboratories. 83

over

TABLE OF CONTENTS

PAGE

Development Of A 100-kV Multimegawatt Repetition-Rate Gas Switch,
A. Ramrus; Maxwell Laboratories, Inc. 88

Multichannel Surface Spark Gaps,
W. J. Sarjeant, R. S. Taylor, A. J. Alcock, K. E. Leopold; National Research Council of Canada 94

High-Repetition-Rate Burst-Mode Spark Gap,
A. Faltens, L. Reginato, R. Hester, E. Cook, A. Chesterman, T. Yokata, W. Dexter; Lawrence Livermore Laboratory 98

SESSION VI – THYRATRON SWITCHES

Flange Mounting Glass Envelope Hydrogen Thyratrons,
L. J. Kettle, C. V. Neale, B. P. Newton; English Electric Valve Company, Ltd., U.K. 102

Double-Ended Hydrogen Thyratrons For Crowbar Protection Of High-Power TWT Systems,
H. Menown, R. J. Wheldon; English Electric Valve Company, Ltd., U.K.
N. S. Nicholls; Royal Signals & Radar Establishment, U.K. 105

Double-Gap Metal Envelope Thyratrons,
R. J. Wheldon; English Electric Valve Company, Ltd., U.K. 113

Development Of A Hydrogen Thyratron Having A Long Pulse Capability,
D. Dolbear, D. Fleischer, S. Merz, R. Plante, D. Turnquist; EG&G, Inc.
N. Reinhardt; Consultant 117

Thyratrons For Short-Pulse Laser Circuits,
H. Menown, C. V. Neale; English Electric Valve Company, Ltd., U.K. 125

Multigigawatt Hydrogen Thyratrons With Nanosecond Rise Times,
S. Friedman, S. Goldberg, J. Hamilton, S. Merz, R. Plante, D. Turnquist; EG&G, Inc. 129

Development Of A 40-kV Megawatt Average Power Thyratron (MAPS-40),
J. Hamilton, S. Merz, R. Plante, D. Turnquist; EG&G, Inc.
N. Reinhardt; Consultant
J. Creedon, J. McGowan; Electronics Technology and Devices Laboratory (ERADCOM) 135

Double-Ended Thyratrons In High-Power Burst-Mode Pulse Modulator Applications,
R. B. Molyneux-Berry; Marconi Research Laboratories, U.K. 144

SESSION VII – SOLID-STATE AND GENERAL SWITCHING

Complete Characterization Studies Verify RBDT-RSR Reliability,
J. B. Brewster, G. M. Sherbondy; Westinghouse Electric Corporation 149

Hybrid SCR Switch,
D. L. Pruitt; RCA Corporation 157

Optical Drive Requirements For Laser-Activated Semiconductor Switches,
P. G. McMullin, L. R. Lowry; Westinghouse Electric Corporation 159

Improvements On Transmission Line Pulsers,
R. Dollinger, C. Scheffler; SUNY at Buffalo 163

Time-Resolved Resistance During Spark-Gap Breakdown,
W. K. Cary, Jr., J. Mazzie; Naval Surface Weapons Center 167

High-Power Switching Capabilities,
T. R. Burkes, M. Kristiansen, W. Portnoy, M. Hagler; Texas Tech University 173

SESSION VIII – SWITCHES WITH AN INTERRUPT CAPABILITY

A 100-kV 80-A Long-Pulse Switch Tube,
S. G. McNees; EIMAC Division of Varian 180

Long-Pulse High-Efficiency Switch Tube Development,
A. F. Morreall; Rome Air Development Center 183

The Use Of Vacuum Interrupters At Very High Currents,
R. W. Warren, E. M. Honig; Los Alamos Scientific Laboratory 189

The Use Of Vacuum Interrupters And Bypass Switches To Carry Currents For Long Times,
E. M. Honig, R. W. Warren; Los Alamos Scientific Laboratory 194

TABLE OF CONTENTS

PAGE

High-Repetition-Rate High-Power Pulse Tests Of Vacuum Arc Switches,
R. N. Miller, R. Dollinger, A. S. Gilmour, Jr.; SUNY at Buffalo 200

A Multimegawatt Vacuum Arc Switched Inverter For Airborne Applications,
R. N. Miller, D. C. Hopkins, C. J. King, A. Pedano, R. Dollinger, A. S. Gilmour, Jr.; SUNY at Buffalo 204

Magnetic Flux Concentration With The Anode In A Vacuum Arc Switch,
Y. Swen, A. S. Gilmour, Jr.; SUNY at Buffalo 208

Energy Considerations In The Pulsed Operation Of A Vacuum Arc Current Limiter,
C. D. Bowman, A. S. Gilmour, Jr., R. Dollinger, D. P. Malone; SUNY at Buffalo 213

Relaxation Pulsing With A Vacuum Arc Device,
A. S. Gilmour, Jr., R. Dollinger, C. N. Manikopoulos, P. Schwartz, M. Rosenfeld; SUNY at Buffalo 217

Magnetically Modulated Vacuum Arc For dc Switching,
R. Dethlefsen, J. Mylius; Gould, Inc. 222

Advances In The Development Of A Gas Discharge Switch Having A Repetitive Current Interrupting Capability,
R. F. Caristi, R. P. Simon, D. V. Turnquist; EG&G, Inc. 227

SESSION IX – RF SYSTEMS

A Modulator For The SEASAT-A Radar Altimeter,
K. Y. Ishikawa, C. T. McCown, G. E. Stronks; Hughes Aircraft Company 235

An All-Solid-State Modulator For The ARSR-3 Transmitter,
E. H. Hooper, S. R. Bird; Westinghouse Electric Corporation 242

Haystack Hill Long Range Imaging Radar (LRIR) Transmitter,
W. North; GTE Sylvania 247

High-Repetition-Rate LC Oscillator,
S. L. Moran; Naval Surface Weapons Center. 254

SESSION X – HIGH POWER/HIGH ENERGY

A 1200-MW Van-Mounted Line-Type Modulator,
P. A. Corbiere, R. E. Kolibas, J. J. Moriarty; Raytheon Company 260

Compact Megawatt Average Power Pulse Generator,
J. E. Creedon, J. McGowan, A. J. Buffa, S. Schneider; Electronics Technology and Devices Laboratory (ERADCOM) 264

Power System For A High-Power Burst-Mode Pulsed Load,
T. H. Robinson; Marconi Research Laboratories, U.K. 267

Pulse Power Requirements For Laser Isotope Separation,
P. N. Mace, W. L. Willis; Los Alamos Scientific Laboratory 274

Analysis Of An Inductive Energy High-Perveance Electron Beam Generator,
M. Weiner; Electronics Technology and Devices Laboratory (ERADCOM) 277

Inductive Storage Pulse-Train Generator,
R. D. Ford, I. M. Vitkovitsky; Naval Research Laboratory 284

High-Density Z-Pinch Pulse Power Supply,
W. C. Nunnally, C. A. Ekdahl, J. E. Hammel, L. A. Jones, K. W. Hanks; Los Alamos Scientific Laboratory 289

MG Energy Storage And Pulse Power Supply,
Karl I. Selin; The JET Project, Abingdon, Oxfordshire, U.K. 293

POST-DEADLINE PAPERS

High-Voltage Pulser Development,
Harold Watson; AiResearch Manufacturing Co. 297

Operation Of A 300-kV 100-Hz 300-kW Average Power Pulser,
M. T. Buttram and G. J. Rohwein; Sandia Laboratories 303

A MINIATURE, HIGH VOLTAGE, HIGH CURRENT NANOSECOND PULSE GENERATOR

Joseph Bajda
Cober Electronics, Inc.
Stamford, CT

Summary

This paper describes the development of a high voltage, high current, nanosecond pulse generator of small volume, low weight, and high efficiency. The pulse generator operates either single pulse or 15Hz at a pulse width of 125ns, pulse voltage of 30KV, and pulse current of 1200 amps. The 30KV, 1200 amp pulse is formed by discharging a Blumlein circuit with a triggered spark gap. A ringing choke dc-to-dc converter charges the Blumlein circuit capacitors to 30KV by transforming the 28 volt input.

Presented are factors leading to the design approach, problems encountered, and breadboard test results.

Introduction

Table I summarizes the design goals as specified in Contract Number DAAB07-77-C-2641, U.S. Army Electronics Command, Fort Monmouth, New Jersey.

TABLE I

Input Voltage	28V
Output Voltage	30KV
Peak Current	1200A
Prr	15Hz and single pulse
Pulse Width (50%)	125ns
Rise Time (10% to 90%)	20ns max.
Fall Time (90% to 10%)	40ns max.
Pulse Energy	90% min. (resistive load)
Life	10^6 pulses min.
Weight	2.0 kg max.
Volume	360 cm^3 max.
Form Factor	Cylindrical
Maximum Outer Diameter	6.3 cm

Presented in Figures 1 and 2 are schematic diagrams for the power supply and modulator for the pulse generator.

The insulation requirements of the power supply and modulator high voltage components have a significant effect on size and weight. A conventional pulse forming network (PFN) requires the network capacitors to be charged to 60KV in order to form a 30KV pulse. The 30KV voltage required to charge the Blumlein network capacitors results in a significant reduction in volume in the following areas:

1) converter high voltage transformer
2) network capacitors
3) triggered spark gap.[1]

To achieve maximum efficiency and minimum volume, the ringing-choke converter provides a uniform charging current of 5ma during approximately the full interpulse period (67 msec for a Prr = 15Hz).[4] Each charging interval of 67 msec consists of alternate primary and secondary half cycles at a switching rate of approximately 20KHz. During the primary half cycle, energy is drawn from the 28 volt input and stored in the primary inductance of the ringing-choke transformer. During the secondary half cycle, the energy stored in the primary inductance is coupled by the secondary winding to the Blumlein network capacitors.

Power Supply

The 30KV output is formed by connecting the outputs of the three secondary windings of transformer T_1 in series. Each secondary consists of 2500 turns of wire wound around a separate molypermalloy powder toroid core. The secondary start and secondary finish are terminated in corona rings separated by 0.5 inch. Each core has an outer diameter of 1.33 inches, an inner diameter of 0.76 inches, and a height of 0.46 inches. Adjacent cores are separated by 0.5 inch. The primary winding passes through the center window of all three cores and is insulated to withstand the 30KV potential difference between primary and secondary. The drive winding of transformer T_1 passes through the center of all three cores and over the primary winding. It is insulated for 15KV. Figure 3 shows a photograph of a transformer configuration utilizing two cores with the secondary windings in series.

The function of the control circuitry is 1) assure the start of the conversion action, 2) control the duration of the primary half cycle (power transistor 2N6340 conducting), 3) limit the input current, and 4) establish the correct charging voltage at the output.

Modulator

The 30KV, 1200A pulse is formed by discharging the Blumlein circuit with a triggered spark gap. Each network of the Blumlein circuit has a 12.5 ohm impedance. The high voltage trigger pulse is formed by discharging a capacitor with an SCR. A triggered transformer, having a 1:250 turns ratio, applies the high voltage pulse to the trigger electrode of the spark gap.

The 1250 pF, 30KV capacitors in the Blumlein circuit have a significant effect on the size of the pulse generator. The size of each capacitor, wound with mica dielectric, is approximately 2.25 in. x 1.75 in. x .25 in. Figure 4 shows a photograph of the Blumlein network.

Test Results

The power supply and modulator were

CH1371-4/78/0000-0001$00.75 ©1978 IEEE

integrated and operated satisfactorily at 10KV. A single secondary transformer, charges the Blumlein network capacitors to 10KV. A pulse current of 400 amps was measured through a 25 ohm load.

The modulator was operated at 30KV with an external supply. A pulse current of 1200 amps at a pulse width of 140ns was measured through a 25 ohm load at a Prr of 15Hz. The pulse rise and fall time were approximately 40ns.

Problems associated with the converter transformer have hindered operation of the power supply at 30KV. Inadequate insulation on the core, inadequate insulation on the secondary wire, and the fragile nature of secondary start and secondary finish connections to the corona rings are among the problems encountered.

Conclusions

Based on breadboard tests a practical approach has evolved to generate high voltage, high current nanosecond pulses from a battery source. The volume for a 125ns, 30KV, 1200 amp pulse generator approaches the specified requirement of 360 cm^3. Items having a significant effect on the overall size are the converter high voltage transformer and the high voltage capacitors of the Blumlein circuit.

Acknowledgment

This paper was based on work supported by United States Army Electronics Command, Fort Monmouth, New Jersey, under contract DAAB07-77-C-2641.

References

1. G. N. Glasoe and J. V. Lebacqz, eds., Pulse Generators, New York: McGraw-Hill Book Company, Inc., 1948, pp. 465-468

2. RCA Power Circuits, January 1969, pp. 163-164, 168-176

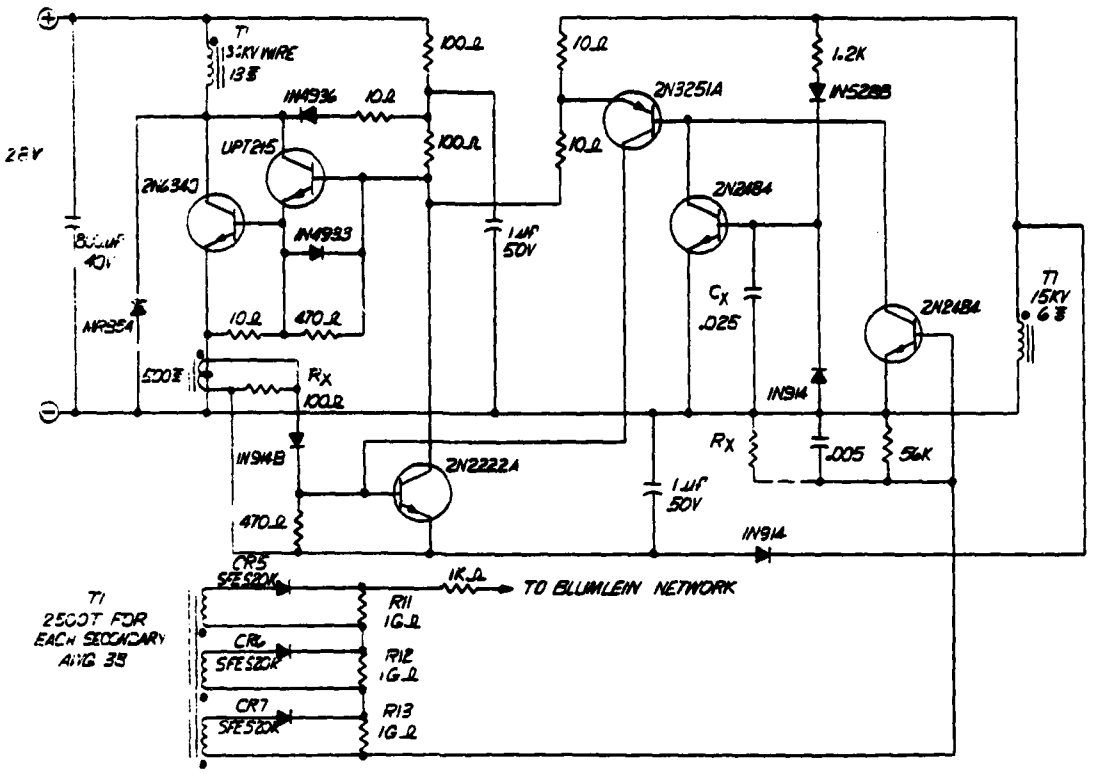


FIGURE 1 - POWER SUPPLY

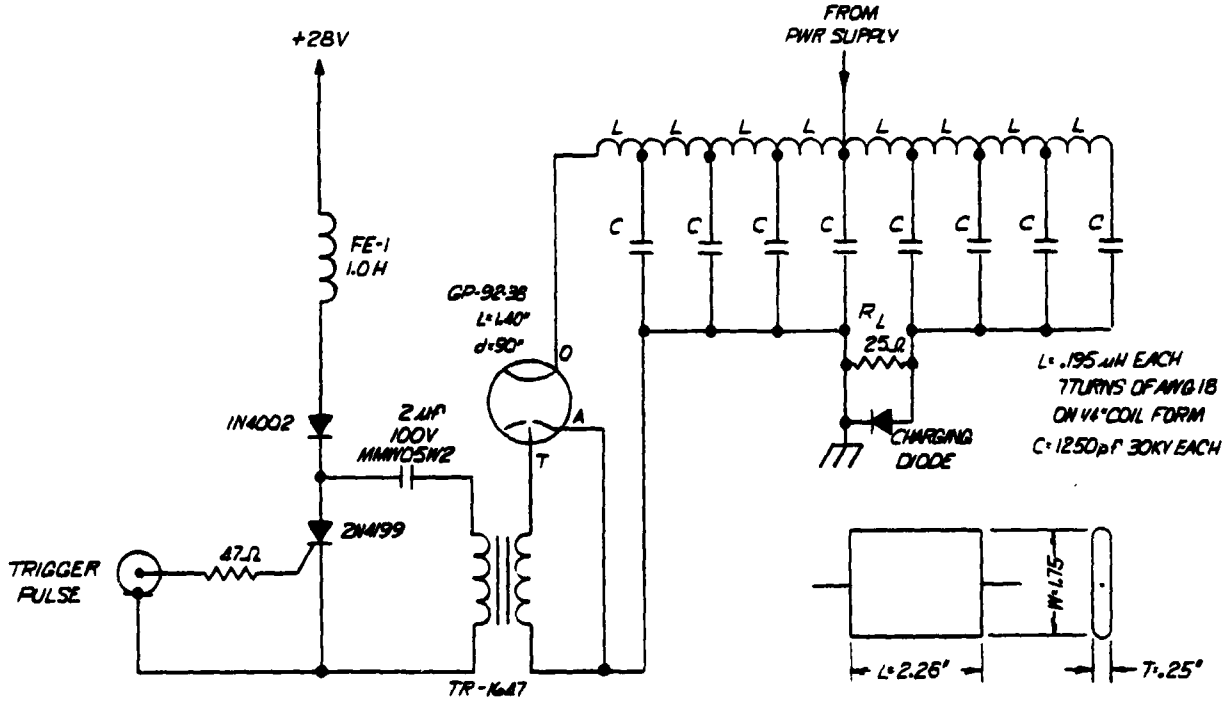


FIGURE 2 - MODULATOR

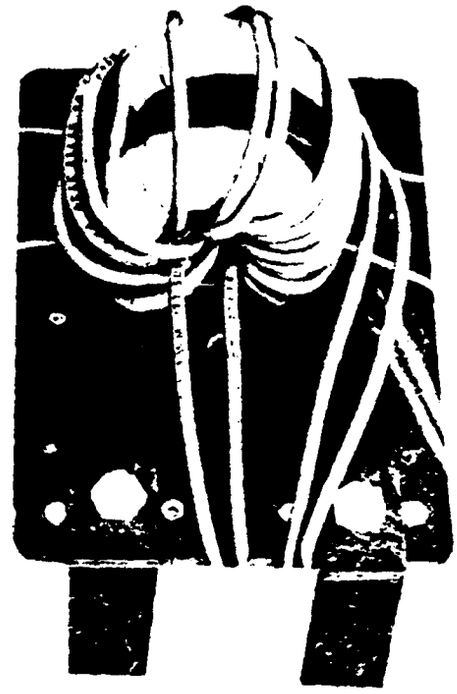


FIGURE 3
T1 POWER SUPPLY TRANSFORMER



FIGURE 4
BLUMLEIN NETWORK

Driving Pockels Cells in Multi-Arm Lasers*

Bruce M. Carder
Lawrence Livermore Laboratory
P. O. Box 5508
Livermore, California 94550

Introduction

This paper describes the method used to drive Pockels cells on the 20-arm Shiva laser for inertial confinement fusion research at the Lawrence Livermore Laboratory. Shiva became operational last fall, and has just completed a series of 20-arm target shots. It uses two Pockels cell gates in each laser arm for suppression of amplified spontaneous emission (ASE) that can damage or destroy the target before the main pulse arrives. Two additional Pockels cells are used in the preamplification stages, so that a total of 42 cells must be driven by the pulser system.

Pockels Cell Load Requirements

Each Pockels cell is a capacitive load that is driven with a 50-ohm coaxial cable. The capacitance is about 20 or 50 pF, depending upon Pockels cell size (25 mm or 50 mm diameter). The cable is terminated with a second 50-ohm "get lost" cable at the cell, Figure 1. The voltage waveshape across the Pockels cell is given by $1-e^{-t/\tau}$ for a step input applied to the cable, where the time constant $\tau = ZC/2$, Figure 2.

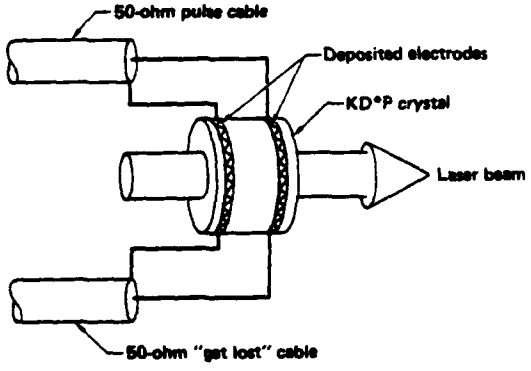


Fig. 1 Pockels Cell Layout

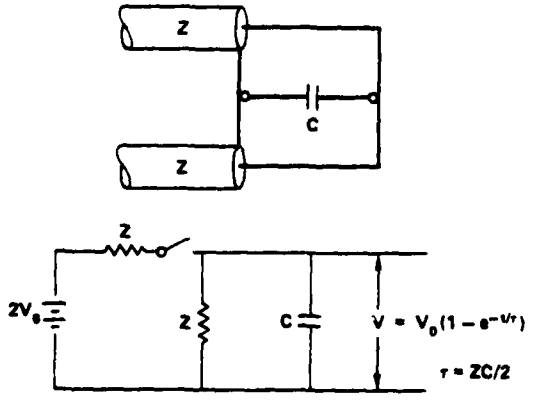
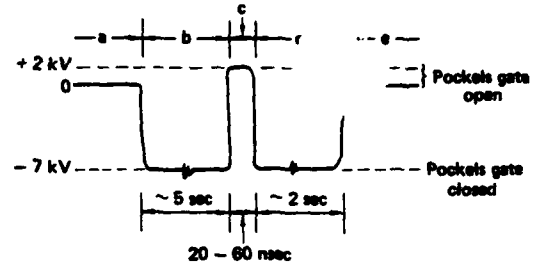


Fig. 2 Pockels Cell Schematic and Equivalent Circuit

For a 25 mm (20 pF) cell, $\tau = 20 \times 50/2 = 500$ ps, and for a 50 mm (50 pF) cell, $\tau = 50 \times 50/2 = 1250$ ps. It is desirable therefore that the pulser provide a risetime ~1 ns, so that the intrinsic capability of the Pockels cells is not degraded.

It is also desirable that the Pockels cell gates be normally open to facilitate alignment of the 20 arms with a steady-state laser. A few seconds before the laser is pumped, however, the gates must be biased closed by applying a 7 kV dc voltage to the cables. Just before the switched-out laser pulse arrives, the gate must be opened with a 9 kV fast-rise, 20 to 60 ns wide electrical pulse. The 7 versus 9 kV voltage difference accounts for dc versus pulse response of the Pockels cells. It is important that the electrical pulse falls - and that the gates close again after passage of the main laser pulse in order to prevent reflected light from amplifying backwards down the chain. A few seconds later, after inac[illegible]tion of the laser, the 7 kV bias must be turned o[illegible], restore the gates once again to their open, or t[illegible]mitting mode. The complete required voltage hist[illegible]s given in Figure 3.



a. Normally zero voltage, with pockels cell open
b. Minus 7 kV dc at ~ minus 5 seconds
c. Plus 9 kV pulse at ~ minus 10 nsec with < 2 nsec risetime and 20 – 60 nsec pulsewidth (2 kV overshoot compensates for pulse response)
d. Minus 7 kV dc until ~ plus 2 seconds
e. Zero voltage, pockels gate open

Fig. 3 Voltage history of the Pockels cell gate pulse:

Pulser Design Criteria

The initial design was for a pulse generator to provide these voltages into 50 parallel 50-ohm cables, so that any number up to 50 Pockels cells could be driven. The dc bias voltage was applied to the center conductor of each coaxial cable, and the pulse voltage superimposed thereon. The general arrangement of this pulser is shown in Figure 4. 50 pulse cables, each cut to the appropriate length, were arranged in a circle with all of the braids common, and connected to the high side of a spark gap switch. The center conductor of each pulse cable was hard-wired across the gap to the center conductor of its matching output cable. The ground shields of the output cables were tied together and connected to the ground side of the spark gap. Thus when the braids of all the pulse cables are

*Research performed under the auspices of the U. S. Department of Energy under Contract No. W-7405-ENG-48.

CH1371-4/78/0000-0005$00.75 ©1978 IEEE

charged negatively, and the gap is fired, an inverted (positive) pulse of half the charge voltage is sent down each output cable. The time duration of this pulse is simply the two-way transit time of the pulse cable.

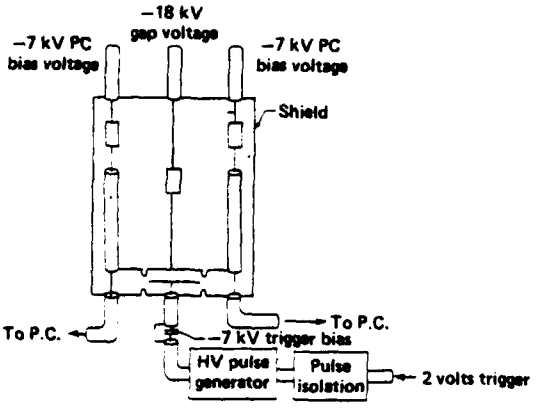


Fig. 4 Arrangement of the Pockels cell pulser using a mid-plane triggered spark gap switch.

This arrangement is convenient because it allows dc bias voltage control to be fed to each Pockels cell via the free end of each pulse cable, using resistive isolation.

Switch Design Criteria

The requirement upon the spark gap switch is a rather stringent one. It must drive a one-ohm load via a one-ohm 20 kV source, and provide about 1 ns risetime in order to preserve the fast-pulse capability of the Pockels cells. The equivalent circuit of this pulser is shown in Figure 5. A time constant of 1 ns for a one-ohm load will require the inductance to be $L = 2Z\tau = 2 \times 1 \times 1 = 2$ nH. The current for a 10 kV pulse into one ohm is 10 kA. The initial current rate of rise is $(di/dt)_{max} = V_0/Z\tau = 10/1 \times 1 = 10$ kA/ns.

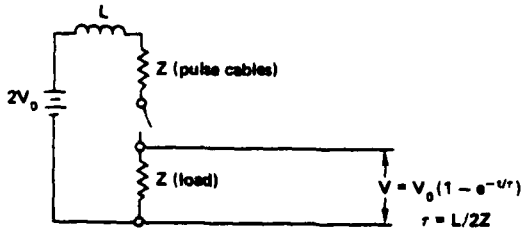


Fig. 5 Equivalent Pulser Circuit

The only known switch that would provide this performance and that could also be dc-charged and allow a reasonable pulse repetition rate, is a high pressure gas spark gap. A gas gap has a resistive phase, of time duration given approximately by J. C. Martin's formula[1]

$$\tau_R = \left(88\,\frac{\rho}{\rho}_{\text{stp air}}\right)^{1/2} \Big/ \left(E^4_{\text{MV/m}} Z\right)^{1/3} \quad \text{ns.}$$

if one uses pressurized SF_6 gas, then $\rho/\rho_{\text{stp air}} = 5\,P_{atm}$, and $E/P \sim 7$ MV/m • atm; therefore, for a 2 ohm circuit impedance,

$$\tau_R = \frac{88(5P)^{1/2}}{\left[\left(\frac{E}{P}\right)^4 P^4 Z\right]^{1/3}} = \frac{88 \cdot 5^{1/2}}{(7^4 \cdot 2)^{1/3} P^{5/6}} = \frac{12}{P^{5/6}}$$

The highest practical pressure for SF_6 is about 12 atmospheres, so the shortest resistive time for the gap is $12/12^{5/6} = 1.5$ ns unless a multiple-channel gap is employed. For example, a 3-channel, 12 atm SF_6 gap will provide $1.5/2^{1/3} = 1.0$ ns resistive time because the impedance each gap drives increases by three. A 1.5 to 2 ns resistive time was considered adequate for this requirement, however, and the pulser was developed using a small 3-electrode pressurized SF_6 spark gap switch.

The spark gap length $\ell = V/E$, and for 12 atm, SF_6 at 7 MV/m • atm, $E = 12 \times 7 = 84$ MV/m. Therefore, for 20 kV holdoff, $\ell = 20 \times 10^3/84 \times 10^6 = 2.4 \times 10^{-4}$ m or about 10 mils. The inductance of a single channel gap can be designed to be less than 40 nH/cm, so for this gap $L < 40 \times 2.4 \times 10^{-2} = 1$ nH. Since this provides an L/2Z time constant of $1/2 \times 1 = 0.5$ ns, it is apparent that the limitation on the gap risetime will be established by the resistive time phase of the gas, provided that care is taken to keep the gap inductance very low.

The Shiva Pulser System

The actual system that was constructed for Shiva comprised one six-way and two twenty-way pulsers. The dual twenty-way design was chosen because it was expected that the two sizes of Pockels cells (25 mm and 50 mm) would operate most efficiently at different voltages. So in the Shiva system, one twenty-way pulser drives all the 25 mm cells in the 20 laser arms, and the second 20-way pulser drives all the 50 mm cells.

The six-way pulser drives the two 25 mm Pockels cells on the preamplifier table. By adding this pulser to the system, we avoid the need to add a hundred feet or so of delay cable between each Pockels cell and its 20-way pulser. This cable would otherwise be required because the laser beam takes about 150 ns to travel between the preamplifier table cells and the cells on the laser arms.

The Shiva system is set up so the 6-way pulser is triggered from a master pulse generator that is fed a low-level signal from the oscillator switch-out table. The six-way then drives the two preamp table Pockels cells and it also provides delayed triggers to each of the two 20-way pulsers. The mid-plane voltage to the 20-way gap trigger electrodes is conveniently fed through the trigger cables in the same way that bias voltage is provided to the Pockels cells. The two additional 6-way outlets are used for monitoring purposes.

A pulse terminator is provided at the ends of each of the "get-lost" cables to prevent the signal from reflecting back to the Pockels cell. These terminators are 50-ohm resistive dividers, each with a series capacitor added so that the Pockels cells can be given dc bias. In addition, the resistive divider provides a 100:1 voltage reduction, with a BNC output connector that allows the pulse to any cell to be monitored.

A picture of the six-way pulser is shown in Figure 6. The Pulsar Pulspak 10A trigger generator is at the bottom, a monitoring terminator is laying on the Pulspak; the knob at the bottom of the 6-way pulser controls the trigger-pin setting via a worm gear. SF_6 pressure cables are connected at the bottom of the spark gap. Only one output cable is shown connected. The six pulse forming cables are wound up above the gap. They are each 20 feet long to provide a 60 ns pulse. The ends of these cables are connected to a plate at the top of the pulser, with the insulation and center conductors fed through. A 20 megohm resistor connects these conductors to the cables bringing in the bias and the 20-way trigger pin voltages.



Fig. 6 Shiva Six-way Pockels Cell Pulser

Figure 7 shows one of the 20-way pulsers, with all cables attached. Bias voltage is fed from the top - as with the six-way (except here it is one voltage common to all cells). The charge cable for the spark gap is seen just above the gap. Normally, these pulsers are encased in metal jackets to prevent high frequency noise from radiating into the laser bay.

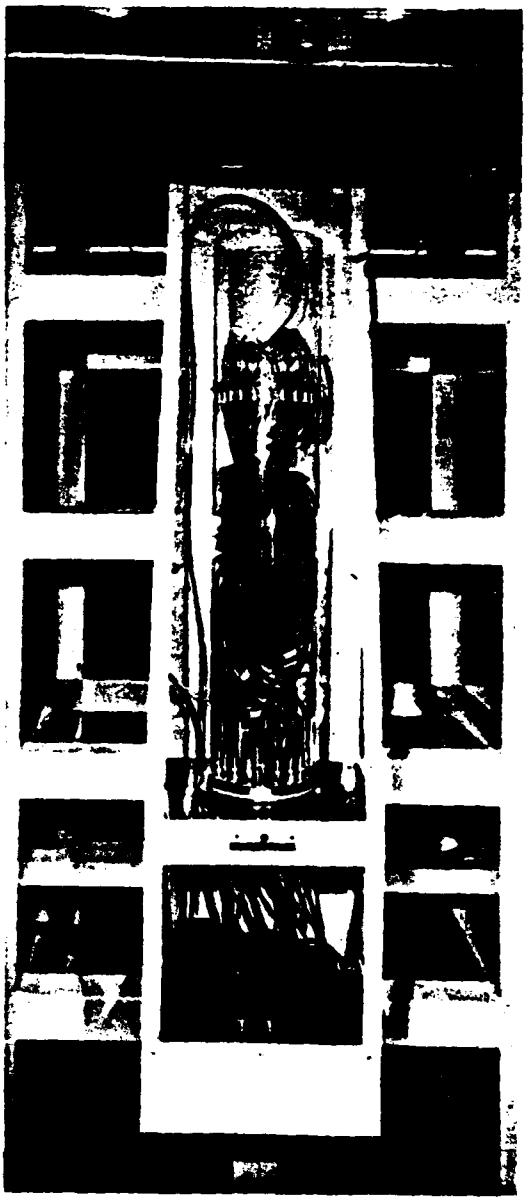


Fig. 7 Shiva Twenty-way Pockels Cell Pulser

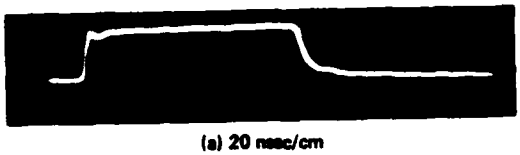
Pulser Performance

The three pulsers have been operating on the Shiva laser since October 1977. In the initial setup, some maintenance problems were encountered because the spark-gaps were pulsed up to 10 pps for hours at a time. Very close spacings are used, and sharp-edged Elkonite trigger electrodes are required. In about 10^5 pulses, the trigger pin edges become worn and the gap cannot be set for low jitter operation.

In the present mode of operation, the gaps are fired just a few dozen times a day, so they operate for weeks with no attention. Normally, an occasional few minutes of minor tweaking will establish low jitter performance.

The scope traces, Figure 8 show the waveshape from one of the 20-way pulsers. Each trace is 10 shots overlaid, with the scope trigger taken from the monitor output of the 10 kV Pulsepak trigger generator. Thus the jitter shown is through two spark gaps. The Pulsepak fires the six-way, and the six-way fires the 20-way that is being monitored.

Figure 8a shows the complete 60 ns waveshape of the 9 kV pulse. Figure 8b shows the leading edge of the pulse at 2 ns/cm sweep speed. This trace confirms the calculations of ~2 ns risetime. Note that the system jitter through both gaps can be held to less than 1 ns. (Also, the Pulsepak jitter is about 0.5 ns.)



(a) 20 nsec/cm



(b) 2 nsec/cm

Fig. 8 Twenty-way pulser waveforms. Ten traces are overlaid in each picture.

The gap producing these pulses was operated at 68 psig SF_6 with about 18 mils gap spacing. The gap voltage was 18 kV and the sharp-edge trigger pin voltage was 7 kV (both voltages were negative). It is an easy matter to set the trigger pin, since the worm-gear arrangement provides precision control - one full turn of the knob is about 1.25 mils adjustment of the pin.

Conclusions

In the Shiva system, all of the Pockels cells operate at the same voltage (7 kV bias and 9 kV pulse). Because of this, a 40-way pulser may be more desirable than two 20-ways because one spark gap is easier to maintain than two. Another possibility that we are presently exploring is to use a hydrogen thyratron in place of the 6-way gap. With specialized trigger and pulse compression techniques, it may be possible to achieve about 5 ns rise when only 6 cables are switched. This would be adequate for the Shiva or similar laser systems.

This type of pulse generator has many interesting applications. It could be designed to hold off 100 kV or so. The spark gaps are very low inductance - the present gaps are less than 2 nH. The voltage is variable over a wide range - the Shiva gaps will operate from less than 2 to over 40 kV.

Because we have noticed multi-channeling in the gaps, we are confident that they could be designed to drive up to 100 cables, and still provide a few ns risetime.

As we have noted, the pulser makes an ideal trigger generator for synchronized parallel or series firing of many gaps. One big advantage is that the trigger pin bias voltage can be fed to each individual gap via the trigger pulser itself, eliminating the need for a myriad of separate voltage dividing strings. A second advantage is that the fast-rise, flat-topped trigger pulse produces voltage doubling in even a fairly capacitive trigger electrode.

Reference

1. J.C. Martin, "Duration of the Resistive Phase and Inductance of Spark Channel", SSWA/JCM/1065/25, Atomic Weapons Research Establishment, Aldermaston, England.

OPERATING HYDROGEN THYRATRONS IN PARALLEL

G. Scoles & R. L. Snelling
English Electric Valve Company Limited
Chelmsford, Essex.

Summary

User requirements have recently become more demanding for hydrogen thyratrons. Laser driving, Torus and Plasma experiments have required new dimensions in terms of Pulse current and rates of rise of current.

The paper discusses the effect on pulse parameters of paralleling tubes and the way jitter, and delay time are affected.

Several ways of paralleling thyratrons and achieving current sharing are considered. These include "Swamp Sharing" by use of both resistors and inductors and "Forced Sharing" where coupled inductors are so connected as to force the thyratrons to accept equal currents.

Practical winding details are given including a novel "core threading" system.

For very high rates of rise the proposal is made that it is better to employ separate energy stores for each thyratron rather than to attempt true parallel working.

In practice this enables higher impedance PFN and cable systems to be designed.

Introduction

The thyratron is a switch with finite possibilities as to rate of rise of current, jitter and pulse current capability. Discussion of the physical reasons for these limitations is outside the scope of this paper and at this time the sort of figures which can be reasonably achieved from a single tube are 100KA/μs rate of rise, 20 KA pulse current and 1-3 ns jitter. It is normal in thyratron data to specify that the current and rate of rise must be limited by the external circuit and not by the tube itself.

To achieve currents and rates of rise in excess of that obtainable from a single tube it is possible to operate thyratrons in parallel. As the current through each tube must be limited to a maximum, sufficient tubes must be used to switch the complete current and steps taken to ensure that the current is equally shared.

Many of these steps are well known but it is felt that they will bear repeating and it is also worth mentioning that in all parallel systems so far, only the tetrode thyratron with its precise firing and high rates of rise has been successfully used. It is also true to say that tube geometry and care of manufacture to ensure repeatability of performance is all important.

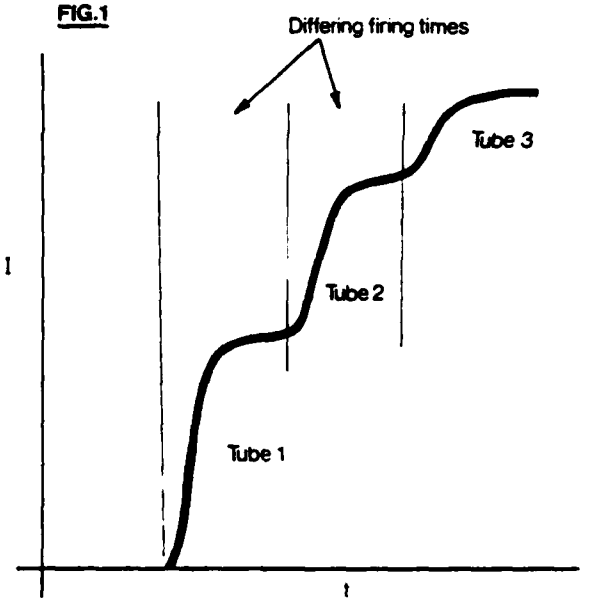
Effects of Parallel Tube Parameters on Pulse Shape

In broad terms, the rate of rise of current is controlled by the speed at which the plasma can be made to grow within the tube.

Tube jitter is affected by the way the grid is driven and the magnetic field from the heater (if supplied with ac). The maximum current is determined by the size and geometry of the tube.

Jitter, delay time and delay time drift affect the front edge of the pulse, as successive current additions are added in time or variable time sequence. See fig. 1.

FIG.1



The flat top of the pulse is relatively independent of the impedances of the tubes and current sharing during the pulse is usually within ± 10% for the individual tubes for a 20 μs pulse.

Fig. 1, shows currents through tubes in parallel when fed from separate Pfns. If a common Pfn is used then the first tube to fire may take most the current for the complete pulse.

CH1371-4/78/0000-0009$00.75 © 1978 IEEE

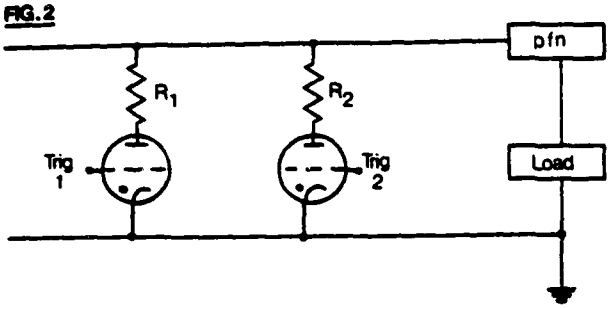
The back edge of the pulse is primarily determined by the fact that energy has been taken from the pfn or other energy bank. Secondary effects such as inverse voltage etc. can be modified by the recovery characteristics of the thyratrons.

To date current sharing has been achieved in two different ways.

Swamp Sharing

This method "irons out" differences by swamping them with a resistance or inductance in series with each tube.

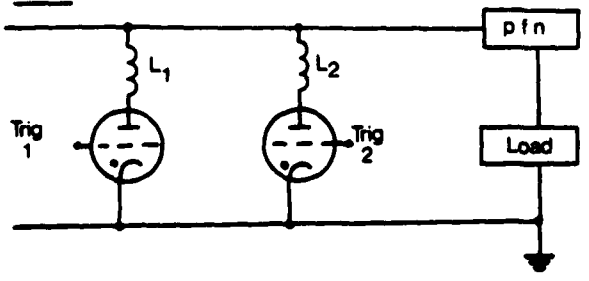
FIG.2



a) The simplest method is to include a resistance in series with each tube. This is not necessarily the best technical solution. (Fig. 2.) 100 volts is usually sufficient as a "swamp" value, therefore, each resistor will be $R = \frac{100}{I}$, where I = the current of each individual tube.

This doubles the losses during the pulse in a practical hydrogen thyratron case although it still compares very favourably with the series losses encountered in vacuum tube switches.

FIG.3



b) Better control is obtained if series inductors are used instead of resistors, (fig. 3). The inductors initially tend to force the current to rise at a similar rate in each thyratron However, if the inductor value is high enough to ensure reasonable sharing, the rate of rise of current is often adversley affected.

The rate of rise of current is given by:-

$$\frac{di}{dt} = \frac{nV}{L}$$

Where V = anode voltage
L = value of each individual anode inductor
n = number of inductors

(for a capacitively ended Pfn).

Operating thyratrons in this manner carries with it an added advantage, inasmuch as they can collectively withstand a higher inverse voltage applied immediately after the pulse since the peak currents are inversely proportional to the number of thyratrons in parallel and the rate of fall of current is controlled by each individual inductor.

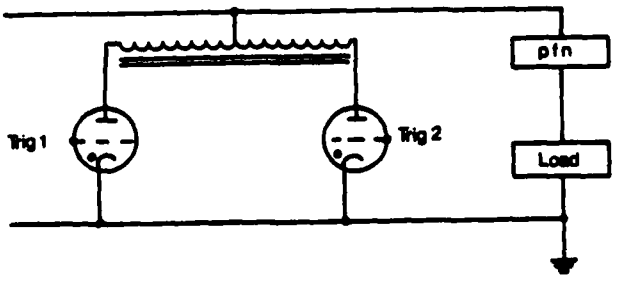
Forced Sharing

"Forced" sharing is a possibility, where out of balance current is itself used to bring about balance.

The Auto Transformer Method of Sharing

In this method a pair of thyratrons is joined to each end of a centre tapped inductor. The power being supplied via the centre tap. Ref 1.

FIG.4



The two halves of the winding must be tightly coupled by means of an iron or ferrite core, and any out of balance current increases the voltage of the side taking less current, thus restoring balance. This system can be extended to 4 thyratrons at the expense of some complications by using three centre tapped inductor which equalise pairs of already equalised thyratrons.

A Practical Case

At currents and rates of rise encountered in radar modulators, the inductors and transformers become single turns on ferrite or iron ring cores.

Assume the use of an iron core of cross section 10 cm^2 which does not saturate until the flux density exceeds one Tesla (10 K Gauss).

If the "winding" is a single turn and has 10 KV applied across it, the time to reach saturation is given by,

$$VT = N.Bsat.A$$
$$\text{i.e. } T = \frac{N.Bsat.A}{V}$$

where V = applied voltage
T = time (secs)
N = number of turns
B sat = saturation flux density (Teslas)
A = cross sectional area ($Metres^2$).

$$\text{Which is } \frac{1 \times 1 \times 10^{-3}}{10^4} = 10^{-7} \text{ secs}$$

$$= \underline{0.1 \ \mu s}$$

This means that any sharing action must be well under way within 0.1 μs.

The inductance of a single wire threaded through such a core is given by:-

$$L = \frac{\mu o \times \mu r \times N^2 A}{\ell}$$

Where L = Inductance (Henrys).
μo = Permeability of free space (Henrys/Metre).
μr = Relative Permeability of core.
N = Number of turns.
A = Cross sectional area of core ($Metres^2$).
ℓ = Mean circumference of the core, (Metres).

Assuming
$\mu r = 10^4$
$\ell = 30$ cm

This gives
$$L = \frac{4\pi \times 10^{-7} \times 10^4 \times 1 \times 10^{-3}}{3 \times 10^{-1}}$$

$$= 4 \times 10^{-5} \text{ Henrys}$$

$$= \underline{40 \ \mu H}$$

From this result and using the formula

$$VT = L \ I \ mag$$
$$\text{i.e. } I \ mag = \frac{VT}{L}$$

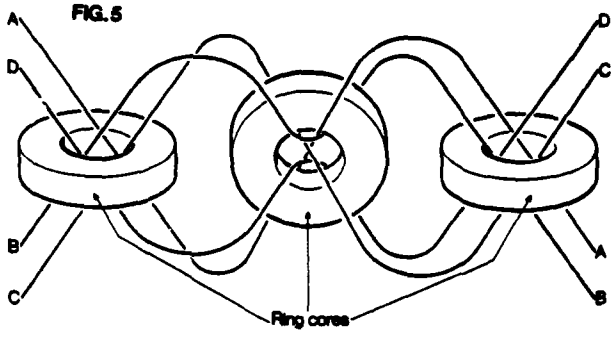
Where I mag is core magnetising current

$$I \ mag = \frac{10^4 \times 10^{-7}}{4 \times 10^{-5}} = \underline{25 \ A}$$

This is negligible in comparison with typical pulse currents of say, 1000 amperes, and thus single threadings of a core per conductor results in adequately rated components for achieving current-sharing.

One such example of what can be achieved by core threading is shown in Fig 5, an arrangement which can be used to equalise the current between four thyratrons.

FIG.5



Use of Separate Pfns

Components which are capable of storing high energies at high voltage are of necessity large.

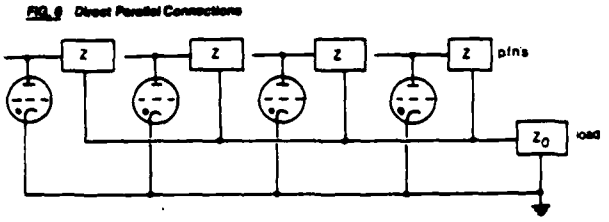
This physical size carries with it the disadvantages of high residual inductance, bulky dielectrics and long connecting distances.

Considering a co-axial energy store such as a cable, it becomes very difficult to manufacture a single cable which has high voltage capability at the low impedances necessary for very high currents.

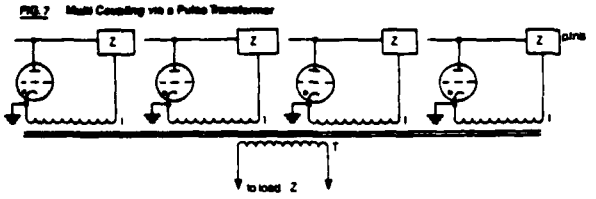
It is usual in this situation to adopt the solution where sufficient co-axial cables of standard impedance are used in parallel to provide the correct impedance.

It is obvious that this principle of paralleling can be extended to include a switching thyratron in each co-axial cable, and that the whole can be combined to produce a very fast, low impedance assembly.

Fig 6 and Fig 7 show the electrically equivalent circuits and the impedances obtained.



$Z_0 = \frac{Z}{N}$ where N is number of pl'n's



$Z_0 = \frac{Z}{N T^2}$ where I T is ratio of pulse transformer and N is number of pl'n's

PROPOSED PARALLEL LAYOUT

A single CX1175 Ceramic Thyratron in the single shot, low repetition rate, or burst mode is capable of the following parameters.

Anode Voltage	70 KV
Anode Current	20 KA
Rate of Rise	100 KA/µs

Figs 8 and 9 show a proposed layout for ten CX1175s, with a theoretical capability of:

Anode Voltage	70 KV
Anode Current	200 KA
Rate of Rise	1 MA/µs

There are obviously some engineering problems yet to be solved!

A point of principle concern is that the tubes must be made to fire simultaneously. As the rising edge of the output pulse becomes faster, jitter and drift in turn become more important, as also do tube design and repeatability of manufacture from tube to tube.

FIG. 8

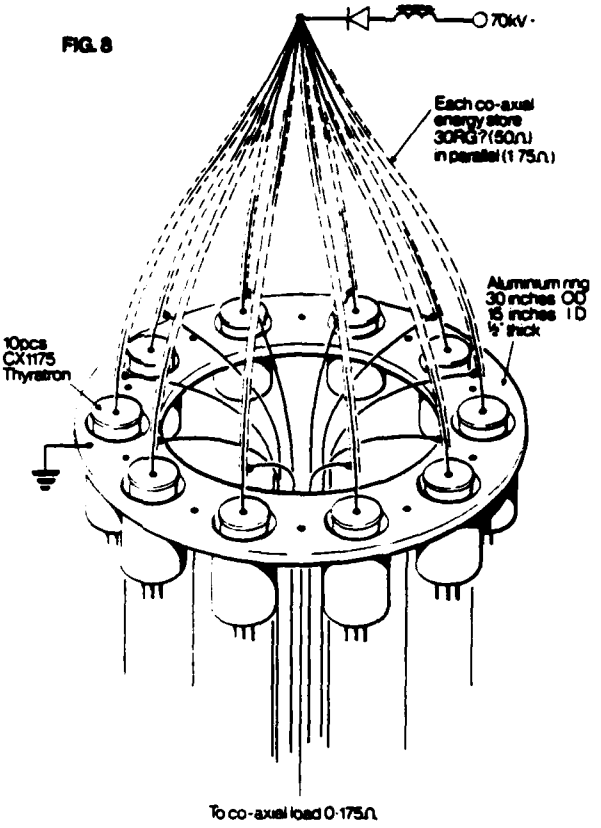
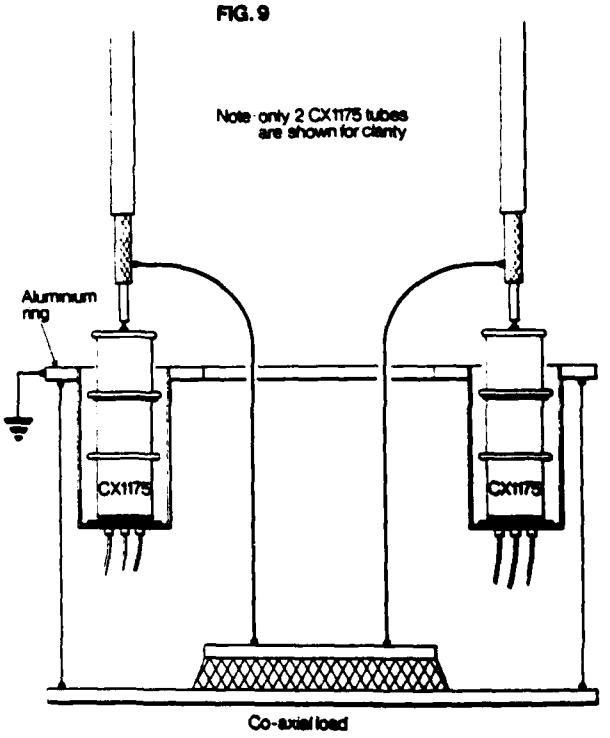


FIG. 9



The electrical layout and design must also be carefully considered and in particular the trigger circuit itself where the rising edge of the trigger pulse must be as fast as possible, of more than adequate voltage and be supplied from a very low impedance source.

Another parameter which must be considered is the tad (anode delay time). This will differ slightly from tube to tube and a variable delay must be incorporated in the trigger to each tube. This should be of the order of tens of nanoseconds.

Servo systems are in being which monitor each pulse and adjust the trigger accordingly. These systems have reduced long term drift to one or two nanoseconds.

Of particular interest to engineers working with high energy, high rate of rise applications are 2 papers written by CERN in Geneva, given in previous modulator symposium sessions. (Refs 2 and 3).

References

(1) MIT series Pulse Generators. Sec 8.11 p 343 K. J. Germeshausen.

(2) A High Voltage Thyratron Switch for the Fast Inflector H.O' Hanlon and J.P Zanasco CERN Geneva 10th Modulator Symposium.

(3) High Voltage Pulse Generators for Kicker Magnet Excitation. D C Fiander, D Grier, K D Metzmacher, P Pearce CERN Geneva, 11th Modulator Symposium.

Acknowledgements

The authors wish to thank the Directors of the English Electric Valve Co. Ltd. for permission to publish this paper.

A STABLE LOAD-INVARIANT HIGH-FREQUENCY SCR SERIES RESONANT INVERTER FOR RADAR TRANSMITTER APPLICATIONS

Robert C. Cole
International Telephone and Telegraph, Gilfillan, Inc.

A high-frequency series resonant SCR inverter has been developed for radar transmitter power conversion and regulation applications that overcomes most of the limitations of present-day high-frequency SCR inverters. Significant characteristics of the inverter circuit include stable operation and controlled resonant capacitor voltages over a wide range of input line voltages and load resistances (including short-circuit loads), fast response, and high efficiency. Low internal stored energy permits automatic reset of faults withoug destructive failure or reliance on fusing. The inverter is ideally suited for charging of capacitor loads typical of radar transmitter and other pulse-discharge applications.

An experimental inverter, operating from 208-V 3-phase ac, provides 30-kW output into a load resistor connected to the inverter through a bridge rectifier and energy storage capacitor. The inverter switching frequency is 10 kHz. Reliable operation with complete freedom from commutation failures has been demonstrated using non-preselected SCRs. Predicted control of inverter resonant capacitor voltages has been shown for all loads, including a short circuit. Two such units can be paralleled to develop a 40-Kv 60-kW regulated high-voltage power supply for a radar transmitter.

CH1371-4/78/0000-0014$00.75 ©1978 IEEE

HIGH VOLTAGE DC POWER CONDITIONER

D. L. Pruitt
RCA Government Systems Division
Missile and Surface Radar
Moorestown, New Jersey 08057

Abstract

Modern radar systems, particularly mobile systems, require high quality, compact, lightweight DC power sources.

High frequency (e.g., 10 kHz) power conditioners have been used to obtain the desired qualities.

By adapting a variation of the series inverter circuit, liberally infused with artificial line type pulse modulator technology, an effective, simple, and high performance technique has been devised. Low frequency (50 to 400 Hz) transformers are eliminated by direct full wave rectification of the AC power source. (With appropriate input filter design, power source frequencies from 50 to 400 Hz can be accommodated in one design.) A pair of suitable high frequency thyristors alternately charge and discharge a pair of capacitors through the primary of a pulse power transformer. Since the effective frequency is high (thousands of hertz), the transformer and load filter capacitor are small compared to the equivalent normal power frequency components. Operating Q is low (approaches 1), minimizing the reactive power. Regulation of the output voltage is achieved by varying the pulse recurrence frequency: from as low as zero to some maximum (e.g., 20 kHz). No load to full load regulation $< 1/2\%$ has been demonstrated. The circuit is not harmed by overload, and has a current fold-back feature. Normal operation resumes automatically when an overload is removed.

Introduction

Modern radar transmitter systems, particularly mobile systems, require high quality, compact, DC power sources. High reliability, usually associated with solid state design, is also required. In the not too distant past, designers of large radar transmitter power systems commonly achieved voltage variability (and slow regulation) by use of motor driven variacs or inductrols operating at the AC power line frequency. More recently, phase controlled thyristor techniques have been used to obtain variability and regulation, still operating at the AC power line frequency. Still more recently, designers have started using high frequency inverter techniques to obtain superior performance (faster response, high efficiency) with smaller and lighter weight equipment. The general principle is to eliminate magnetic components operating at the power line frequency (50 to 400 Hz) by direct rectification of the power line voltage, followed by a DC filter and a high frequency inverter. Output transformers, operating at the inverter frequency, are smaller and lighter than equivalent power-line-frequency transformers. Switching devices used in these inverters may be either power transistors or thyristors, and the inverter frequency may vary from 1 kHz up to 40 or 50 kHz, depending on the power requirements and the switching device characteristics.

This paper describes a version of the series inverter circuit which promises to be useful as a high performance power conditioner. DC output voltage is variable from zero to a design maximum, with no load to full load regulation of less than $1/2\%$ at normal output voltage.

Circuit Description

Figure 1 is a simplified schematic of the variable frequency series inverter power conditioner with regulated DC output voltage. Three phase input power (single phase is acceptable for low power systems) is fed through protective circuit breaker CB1 to a full wave bridge rectifier (D1 to D6). The input DC filter consists of components L1/C1/C2. C1 is an electrolytic capacitor which provides most of the energy storage, while C2 is a paper or plastic dielectric capacitor which supplies most of the pulsed inverter current. Resistor R2 limits ripple (inverter frequency) current in electrolytic capacitor C1, while resistor R1 limits fault currents in the unlikely event that both SCR1 and SCR2 "latch" on simultaneously.

C4 and C5 are the inverter pulse capacitors. C4 is charged as C5 is discharged, and vice versa. Operation is initiated by triggering SCR1, whereupon C4 is discharged, and C5 is charged, via inductor L2 and load circuit A2. L2 (in combination with C4 + C5) determines the pulse width. Load circuit A2 presents a series resistance into the charge/discharge loop, resulting in a single (half cycle) heavily damped ring. At the end of the SCR1 forward current pulse, conduction is interrupted (SCR1 does not conduct backwards), and SCR1 recovers forward voltage blocking ability. A few microseconds later, SCR2 is triggered, charging C4 and discharging C5 through the effective load resistance of A2, completing one full cycle of operation.

R3/C3 is a "snubber" circuit, which prevents excessive dV/dt on the SCRs. R4 and R5 are bleeder resistors. R6, D9, and D10, in conjunction with A3, compose the fault sensing circuit which detects excessive voltage swings at the C4/C5 junction.

The load circuit (A2) consists of a high frequency power pulse transformer followed by a full wave bridge rectifier and a capacitor input filter (C6). A compensated voltage divider feeds a sample of the output voltage to the control amplifier (A1). In A1, the output voltage sample is compared to a manually adjusted reference signal in a differential amplifier circuit to develop an error signal which in turn controls the SCR trigger frequency.

When the load circuit (A2) presents a low impedance (or short circuit) to the inverter, the normal heavily damped LRC discharge becomes an undamped LC discharge, with damaging resonant voltage buildup possible. To prevent excessive voltages, the excessive charges are returned to the storage capacitor (C2) via the L4/D7/D8 feedback circuit. Current transformer circuit A3 detects these excessive voltages, sending a fault signal to the control circuit, which then delays the next SCR trigger until after the feedback cycle is complete. Inductor L4 has a large inductance compared to L2 or L3, resulting in a feedback pulse width several times the normal discharge pulse width. This is necessary to prevent the feedback circuit from interfering with SCR recovery. In normal operation, the feedback current pulses are small, and the normal operation near maximum frequency is not inhibited (a threshold circuit is

CH1371-4/78/0000-0015$00.75 ©1978 IEEE

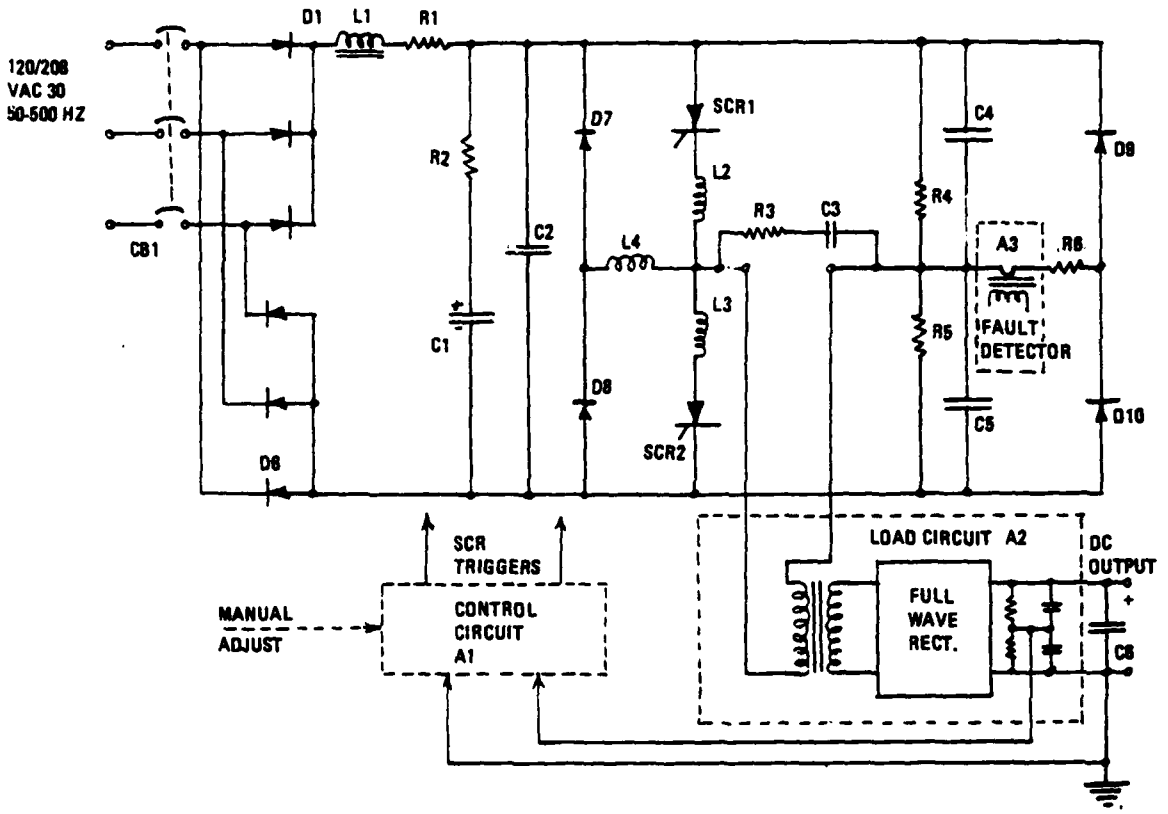


Figure 1. High Voltage DC Power Conditioner

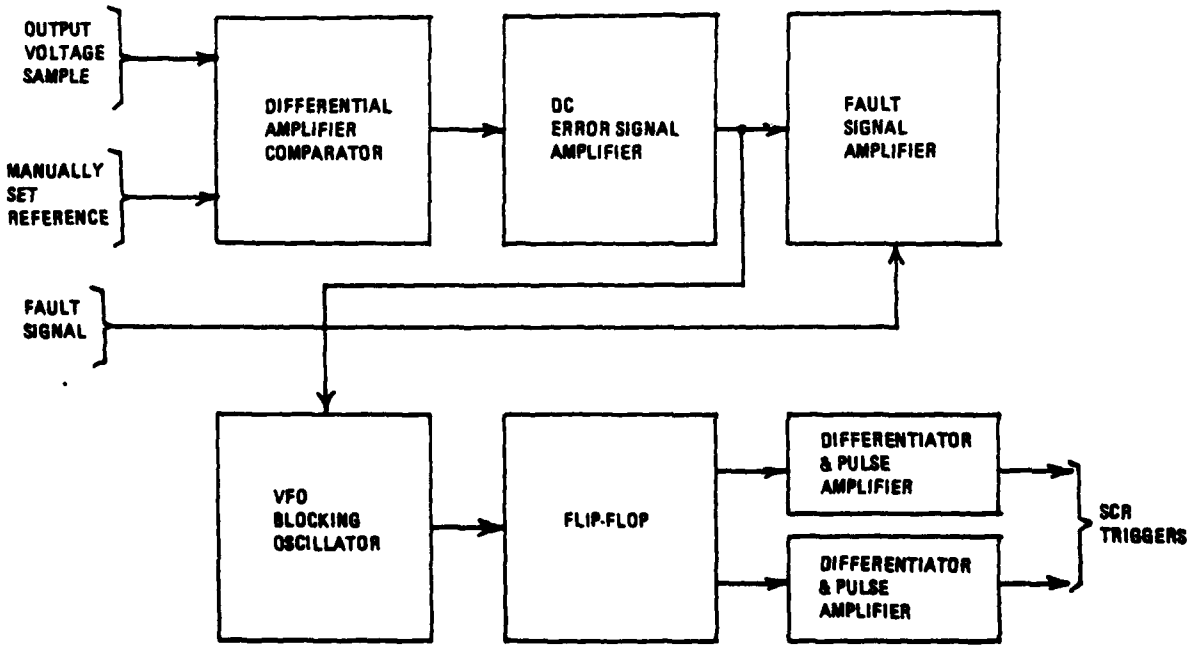


Figure 2. Control Circuit Block Diagram

provided). With a sustained short circuit, the fault circuit limits the operating frequency to about 1/8 of maximum. Thus, the circuit is short circuit proof, with a current foldback feature. When the short circuit is removed, normal operation resumes automatically. If desired in some particular application, the fault signal could also be utilized to send a trip signal to the line circuit breaker.

Control Circuit

Figure 2 is a block diagram of the control circuit. The output voltage sample (typically +5 V DC) is compared to a manually adjusted reference voltage in a differential amplifier. The DC error signal is amplified, and then applied to a voltage controlled, variable frequency, blocking oscillator. The pulse repetition rate from the blocking oscillator varies from zero to a design maximum (typically 20 kHz) as the amplified DC error signal varies from zero to maximum (e.g., 25 V). The flip-flop and output pulse amplifiers feed alternate triggers to each of the main switching SCRs.

When a low-impedance or shorted load is detected, the fault signal amplifier shorts out the amplified error signal for up to 400 μs. The circuit speed is sufficient to inhibit the very next pulse following a fault. The VFO frequency is limited to a low value (typically 2 to 3 kHz) until the fault clears.

Performance Achieved

Figure 3 is a photograph of an inverter designed as described above. The switching SCRs are a pair of RCA S7412 M devices, rated 35 A rms at 600 volts maximum. The maximum operating frequency is 10 kHz (20,000 output pulses/second). Output voltage is 30 kV DC (maximum) at 50 mA DC. No load to full load regulation is less than 1/2%. Regulation is maintained over a ±10% range on the AC input voltage. Measured efficiency was 85%.

Output ripple is a function of the size of the load capacitor (C6 of Figure 1), and the maximum energy in one pulse: 0.2% peak to peak for the circuit of Figure 3 with a 0.1 microfarad total load capacitance. For an application requiring lower ripple, additional filtering could be supplied. This equipment is capable of 2 kW output under normal conditions, with 1500 W of regulated power available, with low AC line voltage (-10%).

Figure 4 shows waveforms of the inverter operation under normal full load conditions. Figure 5 shows the same waveforms with the load short circuited. Note that the horizontal time scale is different in Figures 4 and 5; in each case, about 1-1/2 cycles of operation are shown.

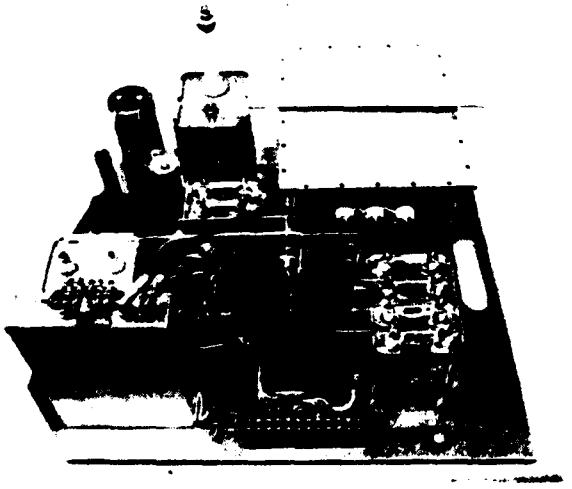


Figure 3. 1500-Watt Regulated High Voltage DC Power Supply

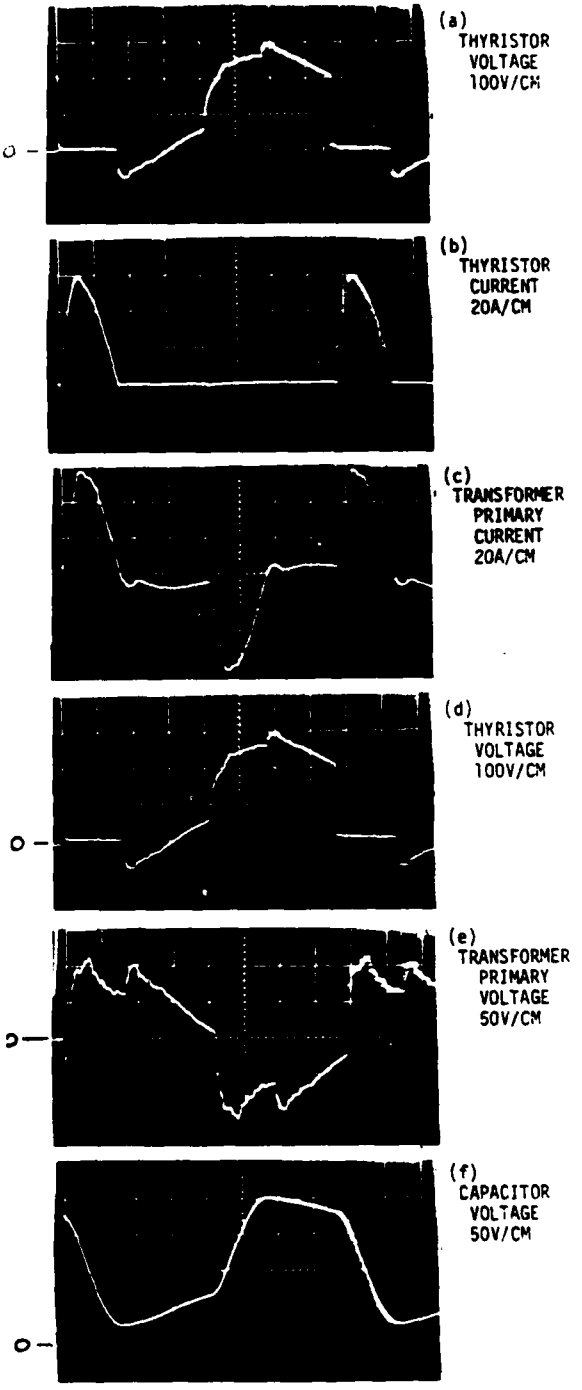


Figure 4. Inverter Waveforms, Normal Load

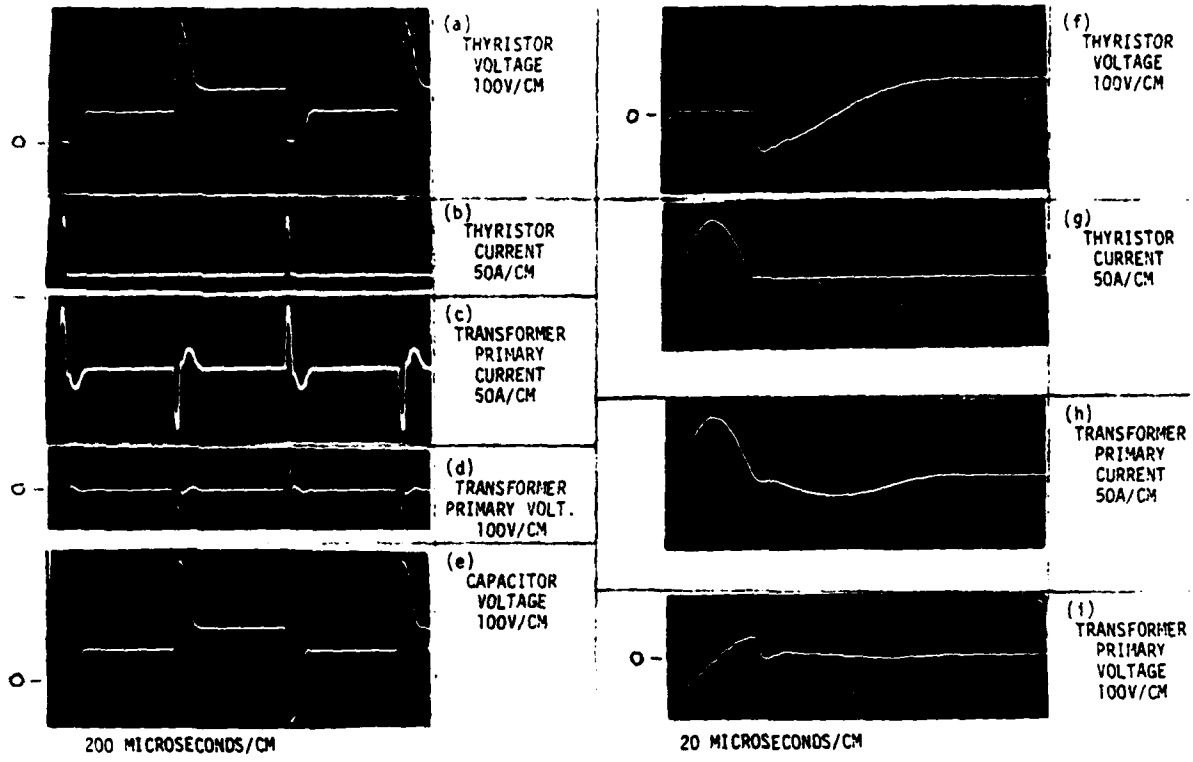


Figure 5. Inverter Waveforms, Short Circuit Load

Growth Potential

The circuit concept of Figure 1 is capable of operating at power levels far in excess of 2 kW, with appropriate choice of thyristors, components, and operating parameters. Three phase line voltages of 460 V, or even 4160 V or higher, can be accommodated by use of higher voltage thyristors, or series strings of thyristors. The inverter frequency could fall as low as 2 kHz at higher power levels, since very large thyristors are generally slower devices.

A second possibility is to operate 2, 4, 8, etc. such basic inverters with outputs in series, or parallel, or series/parallel. A common control circuit could provide properly phased SCR triggers to achieve 2, 4, 8, etc. times the basic ripple frequency. Power delivered is, of course, the same multiple of the power of a single unit. Special load sharing arrangements are unnecessary: the nature of the series inverter circuit operation leads to automatic load sharing.

A third possibility is synthesis of low frequency AC waveforms by providing an SCR output circuit as shown in the simplified schematic of Figure 6.

SCR1 is gated alternately with SCR2 to provide the positive and negative half cycles of the output AC waveform.

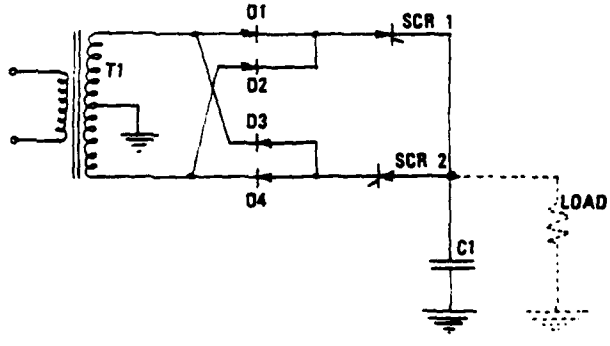


Figure 6. Simplified Schematic, AC Output Circuit

Amplitude and waveshape is controlled by frequency modulation of the inverter. An output sample, from an R/C compensated divider, is compared to the desired waveshape to generate the required error signal. Additional output filtering may be added if desired. Complex waveshapes could be synthesized in this manner. The output AC frequency must, of course, be much less than the maximum inverter operating frequency.

MODULATOR CHARGING SYSTEM UPGRADE FOR A 5-MeV ELECTRON ACCELERATOR*

D. Rogers, W. Dexter, A. Myers, L. Reginato, A. Zimmerman

Lawrence Livermore Laboratory
Livermore, California 94550

SUMMARY

The Lawrence Livermore Laboratory is currently constructing a new linear induction accelerator with a higher beam current than the Astron[1] accelerator. The new accelerator, called the Experimental Test Accelerator (ETA) will be a 5-MeV, 10-kA accelerator with a pulse width of 50-ns. Like the Astron, the principle of magnetic induction is used to obtain a linear accelerator. The modular accelerating cavities form essentially a 1:1 transformer and the change in flux in the ferrite core induces an axial electric field for the acceleration of electrons.

Since the total energy storage for the ETA is much greater than the requirement for Astron, the power system, the capacitor bank and the modulator charging system all had to be modified to provide an overall regulation of .1%. This strict regulation of the charging voltage is necessary for pulse-to-pulse repeatability.

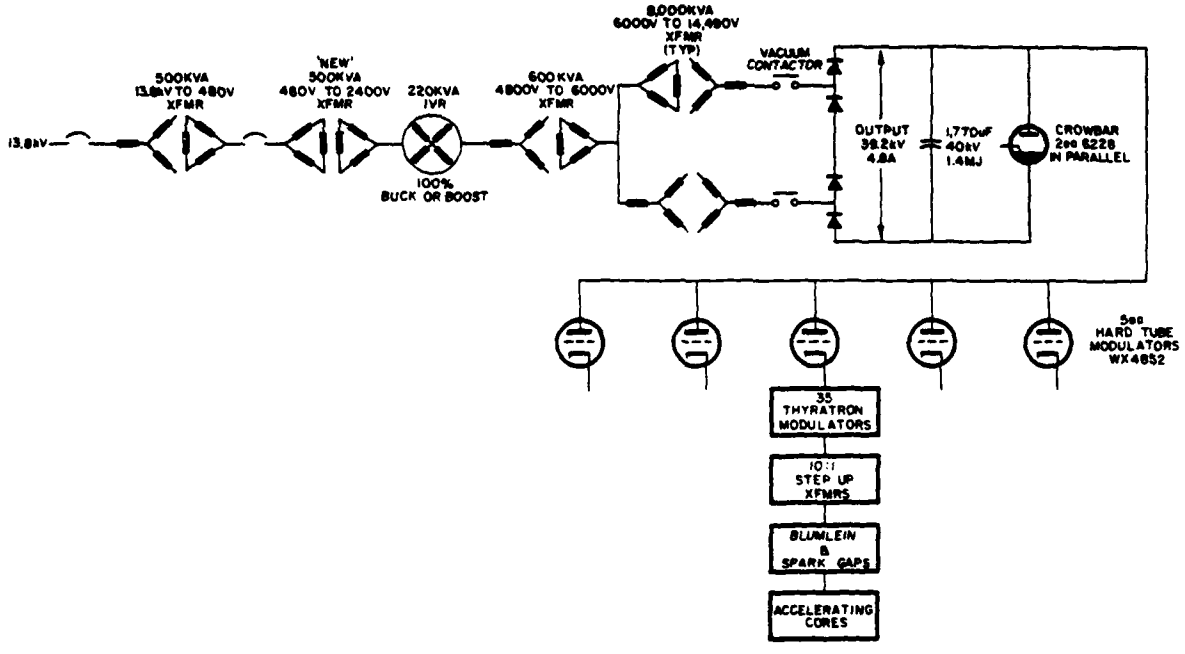


FIG. 1 ONE LINE DIAGRAM OF MODIFIED CHARGING SYSTEM

Hard Tube Modulator

The pulse forming network for the accelerating cavity consists of a Blumlein which is charged to 250-kV by an off resonance step-up transformer from a 3.3-uf, 25-kV capacitor. A total of one hundred and seventy-five capacitors are required to provide the energy storage for the burst mode capability and desired energy out. Fig. 1 is a system schematic.

With this large capacitance, 578-uf, the command resonance charge mode of charging would have resulted in an excessive amount of current and power dissipation in the WX4852 output tube. The constant current mode of charging was chosen using a voltage ramp with a duration of 250-ms. The resultant current for a 250-ms charge time is:

$$I = C\frac{\Delta V}{\Delta T} = 578 \times 10^{-6} \times \frac{25 \times 10^{3}}{25 \times 10^{-2}} = 57.8 \text{ Amps} \quad (1)$$

[1] Christofilos, N.C. et al. "High Current Linear Induction Accelerator for Electrons." RSI Vol. 35, No. 7 886-890, July 1964.

*This work is jointly supported by the U.S. Department of Energy under Contract No. W-7405-Eng-48 and the Department of the Navy under Contract N00014-73-F0012.

U.S. GOVERNMENT WORK NOT PROTECTED BY U.S. COPYRIGHT.

The hard tube modulators are shown in Fig. 2, and Fig. 3 is the schematic. Each modulator charges 35 of the 3.3-μf capacitors to 22-kV. Usual pulse rates will vary from one to five pps, however, much higher rates are required for some experiments. In such cases the accelerator is operated in the burst mode with the average rate held to the cw rate of 5 pps or less.

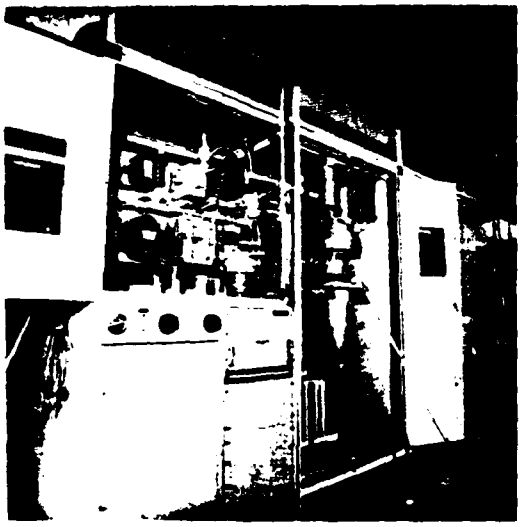


FIG. 2 FRONT VIEW OF HARD TUBE MODULATOR

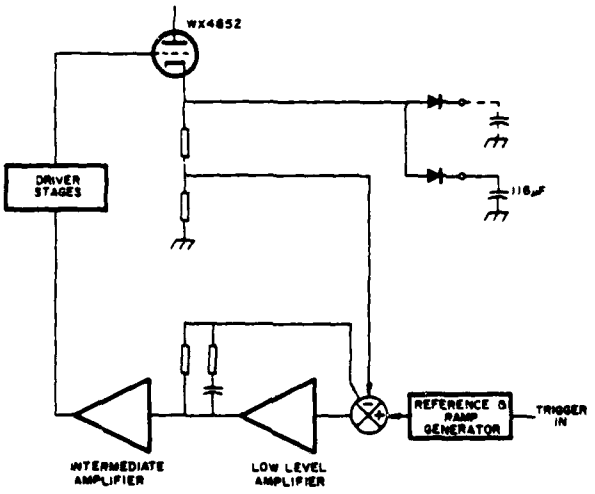


FIG. 3 CONSTANT CURRENT MODULATOR SCHEMATIC

Although five modulators are available for normal operation, it was decided to have the full system capability with any three of the modulators operational. This would result in a maximum current requirement of 23 amps from any one modulator. A maximum tube drop of 5-kV would be required for good voltage regulation; meaning the capacitor bank could be run at 30-kV, resulting in a peak power dissipation of 690-kW across the output tube. One advantage of the lower current required is that it is no longer necessary to drive the grid of the WX4852 positive to obtain the desired output current.

The basic modulator design is the same as for the Astron accelerator, the mode of the operation, output resonant charge circuit, and the low level reference system have been modified for constant current operation. Each modulator charges 116-μf worth of capacitors, thus providing one of five pulses in a burst operation. The resonant charging circuit has been removed and dual output diodes provide charging and isolation between two sequential pulses of the burst. The use of the dual output diode allows the removal of one or two modulators from the system without affecting overall accelerator operation. The 250-ms charge time was chosen so that the peak power dissipated would not exceed ratings in the anode of the 4852. Peak power, of course, occurs at the start of the cycle.

Reference and Driver Stages

The actual constant current in the output is obtained by calling for a voltage ramp from the ramp generator which is shown in Fig. 4. The time duration of

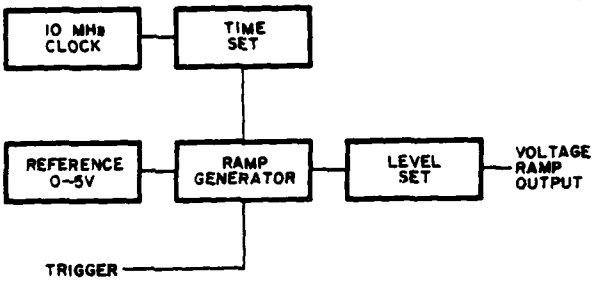
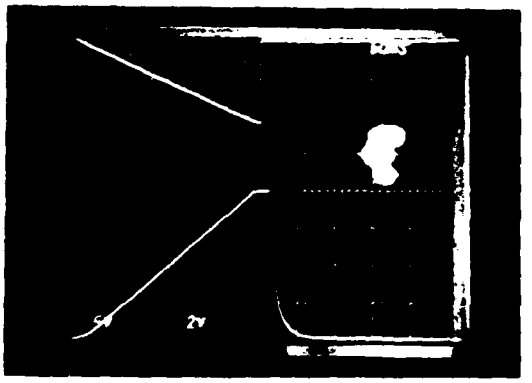


FIG. 4 BLOCK DIAGRAM OF RAMP GENERATOR

the ramp is controlled by counting down from a 10-mHz clock and is adjustable from 100-ms to 500-ms by setting the time on digital thumbwheel switches. The output of the modulator is compared to this ramp in the low level amplifier, and the error signal is amplified by the intermediate amplifier and driver stages. It is then fed to the grid of the final tube in a closed loop system. Note that since the modulators are not operated in the 1-kHz charging mode, the full closed loop gain is available for the regulated output. In our system, with a six Db/octive roll-off, the loop gain at 250-ms charge time is about ten to twenty times better than the resonant charge system of the Astron. The loop gain could be further increased at the low frequency end at a very nominal cost, should it become necessary. The ramp voltage and the output voltage are shown in Fig. 5.



TOP REFERENCE VOLTAGE 2 V/cm
BOTTOM MODULATOR OUTPUT 5 kV/cm
VERTICAL 50 ms/cm

FIG. 5

Power System and Capacitor Bank

With an output requirement of 22-kV, and allowing a tube drop of 5-kV, the power supply would have to be operated at a minimum of 27-kV. To supply the full voltage at 57.8-A would have meant a costly modification to the power system. A compromise was reached where the ratio of peak-to-average power requirements were satisfied by enlarging both the primary capacitor bank energy storage, and the power input. The original bank was 770-μf and 670-kJ. By rearranging the configuration of the bank, we were able to connect it so the total capacitance is now 1770-μf at 40-kV for an energy storage of 1.4-MJ (Fig. 6).

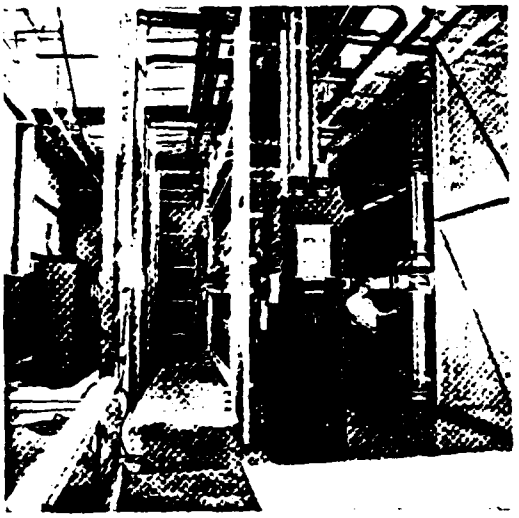


FIG. 6 1.4 MEGAJOULE CAPACITOR BANK

When running in the burst mode, the current from the power supply will be 57.8-A, with an input current of 8-A. The capacitor bank voltage will be:

$$\Delta V = \left(\frac{I_{out} - I_{in}}{C}\right) \Delta T \qquad \Delta T = .25 \text{ sec} \tag{2}$$

$$\Delta V = \left(\frac{57.8 - 8}{1770 \times 10^{-6}}\right) .25 = 7.03 \text{ kV} \tag{3}$$

The capacitor bank must be charged to a total of:

$$V_{bank} = V_{out} + V_{tube} + V_{sag} = 22 \text{ kV} + 5 \text{ kV} + 7 \text{ kV} = 34 \text{ kV} \tag{4}$$

Since the capacitor bank is rated at 40-kV and has been run at this level this should present no problem. The modulators have all been tested into a dummy load that very closely approximates the system. The charging current for a single modulator was measured at 11.2 amps, vs. 11.5 amps calculated, with an output voltage from the modulator of 22-kV and 34-kV on the bank.

Power Supply Primary Equipment

The original Astron power supply primary equipment consisted of a 20 megawatt motor-alternator for high power operation and a second circuit that could be switched to replace the motor alternator for low power operation. The low power circuit was an after thought to save wear on the high maintenance motor alternator and was assembled from components that were on hand. Because of this, some components were rated greater than others and the output was limited to about 125-kW. When the Astron accelerator was dismantled, the motor-alternator was also removed thereby limiting the output of the 15 megawatt transformer-rectifier to 125-kW.

It was decided to use this power supply for the new 5-MeV Electron Accelerator and ways were investigated to increase the output above 125-kW. Four options were considered to increase the output of the power supply by replacing the limiting components. Of course, all components could be replaced and a full 15 megawatts could be obtained, but this was not needed for the accelerator nor would the budget allow it. It was decided to replace the limiting 150-KVA, 480 to 2400 volt, transformer with a 500-KVA unit to give an output of 188-kW. A 500-KVA transformer was chosen so it would not be the limiting item if subsequent options were to be installed. 188-kW appeared to be a satisfactory starting point for the accelerator and if increased power is needed the other limiting components could be replaced, giving 474-kW. Fig. 1 shows a one-line diagram of the modified power supply.

CONCLUSION

In accelerators where a high degree of regulation is required in the electronics for beam quality, a series modulator is invariably used to provide that degree of regulation. In the Astron accelerator, the power and regulation during a beam burst was provided by the modulators and parallel systems were not necessary. When the beam power during a burst becomes very large, the modulator cost and complexity become excessive. In the ETA it was decided to reduce the modulator power requirements by charging between bursts and sequentially firing parallel capacitors to obtain the high rep rate. For example, the average ETA power during a burst is:

$$P_w = (5 \times 10^6)(10^4) \times \frac{50\ 10^{-9}}{.5\ 10^{-3}} = 5 \text{ megawatts} \tag{5}$$

Because of power losses in compensating networks, charging transformer, switch chassis and modulators, the overall input power requirements are more like 25-50 MW. This would have meant a large and very costly modulator development and primary power supply changes. For higher rep-rate requirements the accelerator power during the burst is even greater, which makes the primary power supply and modulator requirements excessive, and one has to resort to an intermediate energy storage to provide the burst energy.

REFERENCES

1. Smith, Mark E., "Recent Changes in the Astron Fast Pulsing System," 4th Symposium on Engineering Problems of Fusion Research.

Reference to a company or product name does not imply approval or recommendation of the product by the University of California or the U.S. Department of Energy to the exclusion of others that may be suitable

NOTICE

"This report was prepared as an account of work sponsored by the United States Government. Neither the United States nor the United States Department of Energy, nor any of their employees, nor any of their contractors, subcontractors, or their employees, makes any warranty, express or implied, or assumes any legal liability or responsibility for the accuracy, completeness or usefulness of any information, apparatus, product or process disclosed, or represents that its use would not infringe privately-owned rights."

PULSED TWT POWER SUPPLY: A TECHNIQUE FOR MINIMIZING R.F. PHASE INSTABILITY AND HIGH VOLTAGE ENERGY

Francesco Tarantino-Paolo Porzio

Selenia S.p.A. Rome-Italy

Summary

The ripple voltages on the electrodes of the power microwave tube limit the performances of M.T.I. radar system. When the radar employes staggered P.R.F., pulse-to-pulse ripple arises due to load duty change.

For TWT power amplifier, the variations of the cathode-body voltage cause phase and amplitude modulation of the transmitted waveform. The M.T.I. degradation results mainly from phase modulation $\Delta\Phi(t)=K_\Phi \times \Delta V_k(t)$ where K_Φ is the TWT cathode phase sensitivity and $\Delta V_k(t)$ is the cathode voltage variation.

It is possible to reduce $\Delta V_k(t)$ by increasing the value of the H.V. capacitors, but with this solution the stored energy increases too.

Series regulator is another alternative, but this means more sophisticated circuitry with decreasing of reliability and more design efforts.

This paper describes a H.V.P.S. configuration which allows to solve the problem with limited H.V. stored energy.

H.V.P.S. Description

Fig. 1 shows a basic block diagram of the H.V.P.S. designed for a grid pulsed, depressed collector TWT. There are three series connected stages to achieve the cathode-body voltage (V_k). Beam, collector and body currents are I_b, I_c and I_w respectively. Pulse width and interpulse period are t_p and T.

The first stage provides collector-cathode voltage (V_1). This power supply is obtained by a series of voltage "doublers" with an output capacitor C_1 (fig. 2). The use of voltage doublers offers the following advantages:

a) the transformer requires a simpler design, it is less expensive and allows better performances from the electrical point of view;

b) no chocke filters are required;

c) the high voltage discharge effects are limited by the intrinsically large output resistance $\left(\frac{\Delta V_{dc}}{\Delta I_{dc}}\right)$ [1].

In our case, during the time t_p, low (μs) if compared with power supply recovery time, the I_b current pulse is supplied by the capacitor C_1 (here only C_1 is taken into account). The output voltage variation is:

$$\Delta V_1(t) = \frac{I_b}{C_1} t \quad , \qquad \| o \le t \le t_p \| .$$

After the time t_p, C_1 is charged with time constant $R_{01}C_1$ where R_{01} is the output resistance of the doublers series.

The second stage (fig. 3) is a "flyback" converter whose duty cycle (δ) is controlled by the H.V. regulator. Energy is inductively stored during the transistor-ON time, then passed to the load during the transistor - OFF time. If the inductor current is continuous, the steady state output voltage is given by [2]: $V_o = nE_c \frac{\delta}{1-\delta}$. V_o, as we can see, is indipendent of the load current.

If the value of L is decreased below a minimum depending on the output current, the choke current becomes interrupted and all of the inductive energy $\frac{1}{2} LI'^2_{max}$ is discharged into the load (disregarding losses). For t_{ON} constant, the average power is constant.

We choose the constant power operation for the following main advantages:

a) the chocke size is smaller because the value of L is lower for a given output current;

b) the transistor switching-ON losses are lower because the magnetizing current is reduced to zero before the ON time occurs;

c) higher voltage gain is allowed and the stability margin of the control loop is improved because the converter is a first order system when it is used with interrupted-inductor current, instead of a second order system with continuous-inductor current operation [3], [4], [5].

In our case, considering for simplicity C_2 only, it results:

$$\Delta V_2(t) = \frac{I_w}{C_2} t \quad , \qquad \| o \le t \le t_p \| .$$

After the time t_p, C_2 is charged by a constant average current $\bar{I}_w = I_w \delta p$, where δp is the load duty (t_p/T). Since the time constant of the first stage and the response time of the H.V. control loop are very large compared with the interpulse period T, r.f. phase instability occurs if $(V_1(t) + V_2(t))$ is not compensated. For constant T, the phase instability occurs during the pulse time only; but if staggered P.R.F. is employed, pulse-to-pulse instability occurs too (fig. 4).

Load ripple compensation

The third stage allows compensation of the

CH1371-4/78/0000-0022$00.75 © 1978 IEEE

V_1 and V_2 variations due to the load pulses. The circuit operation is as follows (fig. 5): when transistor Q_2 si turned-ON by the current transformer, a current I_3 charges C_3. Hence

$$\Delta V_3(t) = -\frac{I_3}{C_3}\,t \quad , \qquad \|\, o \le t \le t_p \,\|$$

and, if

$$\frac{I_3}{C_3} = \frac{I_b}{C_1} + \frac{I_w}{C_2} \qquad (1),$$

it results

$$\Delta V_k(t) = \left(\frac{I_b}{C_1} + \frac{I_w}{C_2} - \frac{I_3}{C_3} \right) t = o, \quad \|\, o \le t \le t_p \,\|.$$

After the time t_p, C_3 discharges through the resistor R. The mean value of $V_3(t)$ is $\bar{V}_3(t) = R\bar{I}_3$ where $\bar{I}_3 = I_3\,\delta p$; if δp changes, $\bar{V}_3(t)$ also changes.

Since $\Delta\bar{V}_k(t) = \Delta\bar{V}_1(t) + \Delta\bar{V}_2(t) + \Delta\bar{V}_3(t)$, with suitable C_3 and R values it is possible to greatly reduce the $\bar{V}_k$ variations and, therefore, the pulse-to-pulse r.f. instability.
The fig. 6 shows the variation of $\bar{V}_1$, $\bar{V}_2$ and $\bar{V}_3$ due to a load duty change. The flyback converter is open loop operating and is assumed to be equivalent to a constant current source. (See Appendix).

The expressions for $\Delta\bar{V}_1(t)$, $\Delta\bar{V}_2(t)$ and $\Delta\bar{V}_3(t)$ are, for $t \ge 0$,

$$\Delta\bar{V}_1(t) = R_{01} I_b \Delta\delta_p \left(1 - e^{-1/\tau_1}\right) \qquad \text{where } \tau_1 = R_{01} C_1 \ ,$$

$$\Delta\bar{V}_2(t) = \frac{I_w\,\Delta\delta_p}{C_2}\,t \ ,$$

$$\Delta\bar{V}_3(t) = -R\,I_3\,\Delta\delta_p \left(1 - e^{-1/\tau_2}\right) \qquad \text{where } \tau_2 = R\,C_3 \ .$$

If $\Delta\bar{V}_1(t)$ and $\Delta\bar{V}_3(t)$ are series developed, results:

$$\Delta\bar{V}_k(t) = \Delta\bar{V}_1(t) + \Delta\bar{V}_2(t) + \Delta\bar{V}_3(t) =$$

$$= \Delta\delta_p \left(\frac{I_b}{C_1} + \frac{I_w}{C_2} - \frac{I_3}{C_3} \right) t \ +$$

$$- \Delta\delta_p \left(R_{01} I_b - \frac{R\,I_3}{\tau_2^2/\tau_1^2} \right) \frac{t^2}{2!\,\tau_1^2} \ +$$

$$+ \Delta\delta_p \left| \left(R_{01} I_b - \frac{R\,I_3}{\tau_2^3/\tau_1^3} \right) \frac{t^3}{3!\,\tau_1^3} - \left(R_{01} I_b - \frac{R\,I_3}{\tau_2^4/\tau_1^4} \right) \frac{t^4}{4!\,\tau_1^4} + \ldots \right| \qquad (2).$$

The first term is zero if Eq. (1) is satisfied. The second term is also zero if:

$$\tau_2 = \frac{\tau_1}{K} \qquad (3)$$

where

$$K = \frac{\frac{I_b}{C_1}}{\frac{I_3}{C_3}} = \frac{\frac{I_b}{C_1}}{\frac{I_b}{C_1} + \frac{I_w}{C_2}} < 1 \qquad (4).$$

If now the equations (1) and (3) are substituted in Eq. (2),

$$\Delta\bar{V}_k(t) = R_{01} I_b \Delta\delta_p \left| (1-K) \frac{(t/\tau_1)^3}{3!} - (1-K^2) \frac{(t/\tau_1)^4}{4!} + \ldots \right| \ .$$

Separating the terms with K and normalizing, we obtain:

$$\frac{\Delta\bar{V}_k(t)}{R_{01} I_b \Delta\delta_p} = \left| \frac{(t/\tau_1)^3}{3!} - \ldots \right| - \frac{1}{K^2} \left| \frac{(K\,t/\tau_1)^3}{3!} - \ldots \right| =$$

$$= \left| 1 - t/\tau_1 + \frac{1}{2}(t/\tau_1)^2 - e^{-t/\tau_1} \right| - \frac{1}{K^2} \left| 1 - K\,t/\tau_1 + \frac{1}{2}(K\,t/\tau_1)^2 - e^{-K\,t/\tau_1} \right| \qquad (5)$$

(see fig. 7).

Without the compensation circuit, the normalized $\bar{V}_k$ variation is:

$$\frac{\Delta\bar{V}_k(t)}{R_{01} I_b \Delta\delta_p} = \left(1 - e^{-t/\tau_1}\right) + \frac{1-K}{K}\,t \ .$$

The ratio $\dfrac{\Delta\bar{V}_k(t) \text{ without compensation}}{\Delta\bar{V}_k(t) \text{ with compensation}}$ is shown in fig. 8 where we see that low and high values of K give good ripple rejection. But from the point of view of stored energy, a minimum is found to be for $K > 0.5$. In fact, total stored energy $\mathcal{E}$ results:

$$\mathcal{E} = \frac{1}{2} V_1^2 \left| C_1 + C_2 \left(\frac{V_2}{V_1} \right)^2 \right| =$$

$$= \frac{1}{2} V_1^2 \left| \frac{I_b}{K\,\Delta V/\Delta t} + I_w \left(\frac{V_2}{V_1} \right)^2 \frac{1}{(K-1)\,\Delta V/\Delta t} \right| =$$

$$= \frac{1}{2} \frac{V_1^2\,I_b}{\Delta V/\Delta t} \left| \frac{1}{K} + \frac{1}{1-K} \frac{I_w}{I_b} \left(\frac{V_2}{V_1} \right)^2 \right| \qquad (6)$$

where $\Delta V/\Delta t \ (= I_b/C_1 + I_w/C_2)$ is the designed slope during the pulse time. The function $F(K) = \left\{ \frac{1}{K} + \frac{1}{1-K} I_w/I_b \, (V_2/V_1)^2 \right\}$ has a minimum for high values of K (fig. 8).

Conclusion

A H.V.P.S. has been described which is able to reject load ripple due to the P.R.F. stagger without sophisticated series regulator and with limited H.V. stored energy. The proposed

solution has been realized for a 2 KW transmitter. Load ripple less than $1V_{pp}$ (V_K=-11KV) has been obtained with 40% P.R.F. variation (pulse-to-pulse or pulses group stagger). The H.V. stored energy has been limited to less than 5 joules with a K value of 0.8.

The compensation circuit is a simple low voltage circuit that is open loop operating without affecting the gain and phase of cathode loop control.

Appendix

We can support the assumption of constant current source for the flyback converter in fig. 6 with the following considerations.

The mean value of the flyback output current is (see fig. 3):

$$\frac{1}{2} L I_{Lmax}^2 f \frac{1}{\bar{V}_2(t)} = \frac{1}{2} L I_{Lmax}^2 f \frac{1}{\bar{V}_{20}\left[1-\Delta\bar{V}_2(t)/\bar{V}_{20}\right]}$$

where $\bar{V}_{20}$ is the mean value of $V_2(t)$ before the load change occurs and f is the converter operating frequency. If we assume

$$\Delta\bar{V}_2(t) = \frac{I_w \Delta\delta_p}{C_2} t \quad ,$$

we have:

$$\frac{\Delta\bar{V}_2(t)}{\bar{V}_{20}} = \frac{I_w \Delta\delta_p}{\bar{V}_{20} C_2} t \quad .$$

For $\bar{V}_{20} \sim 0.3 V_K$ and $I_w \sim 0.2\ I_b$ (typical values), it is:

$$\frac{\Delta\bar{V}_2(t)/\bar{V}_{20}}{t} \sim 0.7 \frac{I_b[A]}{V_k[KV]} \frac{\Delta\delta_p}{C_2[\mu F]} \quad \left(\frac{V/V}{ms}\right)$$

For example, if I_b=1.6A, V_K=-11KV and $\Delta\delta p$=0.01, it is:

$$\frac{\Delta\bar{V}_2(t)/\bar{V}_{20}}{t} \sim - \frac{10^{-3}}{C_2[\mu F]} \quad \left(\frac{V/V}{ms}\right) \quad ,$$

i.e. 1% error after one ms if C_2=0.1 uF. Constant current source assumption is a good one for our case.

References

[1] J.S. Brugler
"Theoretical Performance of voltage multiplier circuit" IEEE J. Solid State Circuits, pp. 132-135 - June 1971.

[2] C. Van Velthooven
"Properties of D.C. to D.C. converters for switched mode power supplies"
Philips application information N. 472.

[3] F.C. LEE - Y. YU
"Modeling of switching regulator power stages with & without zero inductor-current dwell time"
P.E.S.C. 76 Record, pp. 62-72 .

[4] A. Capel, J.C. Ferrante - R. Prajoux
"Stability analysis of a P.W.M. controlled DC/DC regulator with DC and AC feedback loop"
P.E.S.C. 74 Record - pp. 246-254 .

[5] A. Capel - J.C. Ferrante - R. Prajoux
"Dynamic Behaviour and Z-Transform stability analysis of DC/DC regulator with a non linear P.W.M. control loop"
P.E.S.C. 73pp. 149-157.

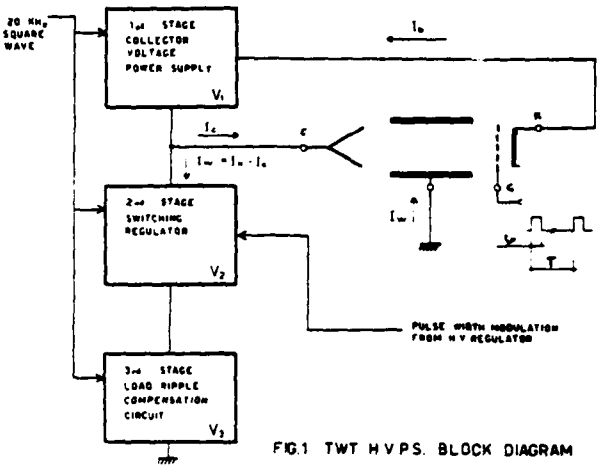


FIG.1 TWT H.V.P.S. BLOCK DIAGRAM

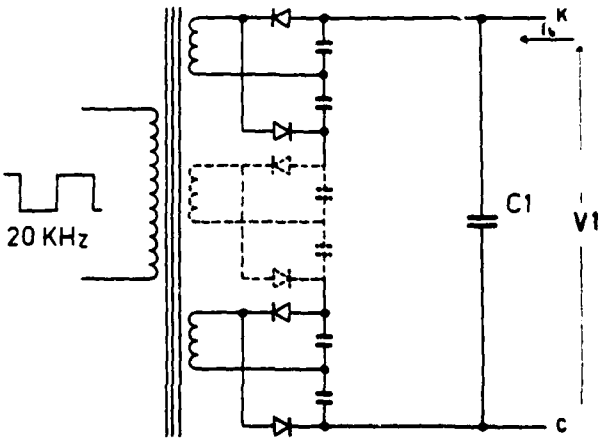


FIG. 2 COLLECTOR VOLTAGE POWER SUPPLY SIMPLIFIED CIRCUIT

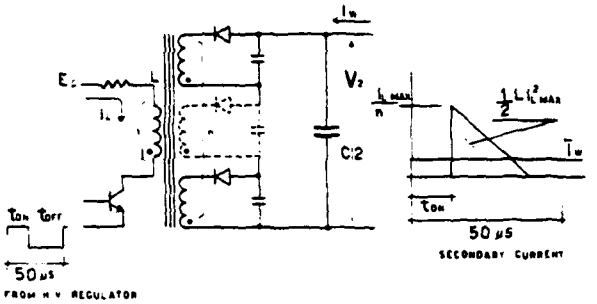


FIG 3 PULSE WIDTH MODULATED "FLYBACK" CONVERTER SIMPLIFIED CIRCUIT

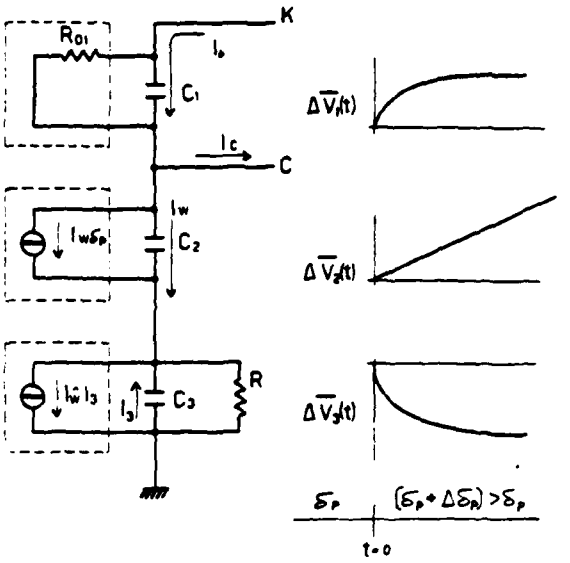


FIG 6 LOAD DUTY CHANGE

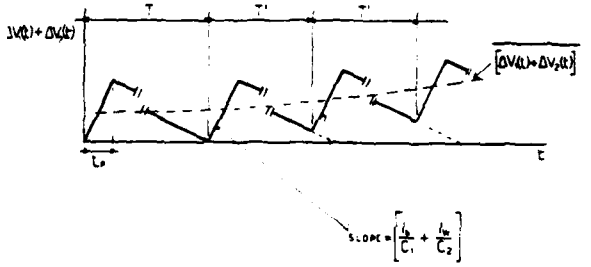


FIG 4 - STAGGERED PR.F. - PULSE TO PULSE RIPPLE VOLTAGE.

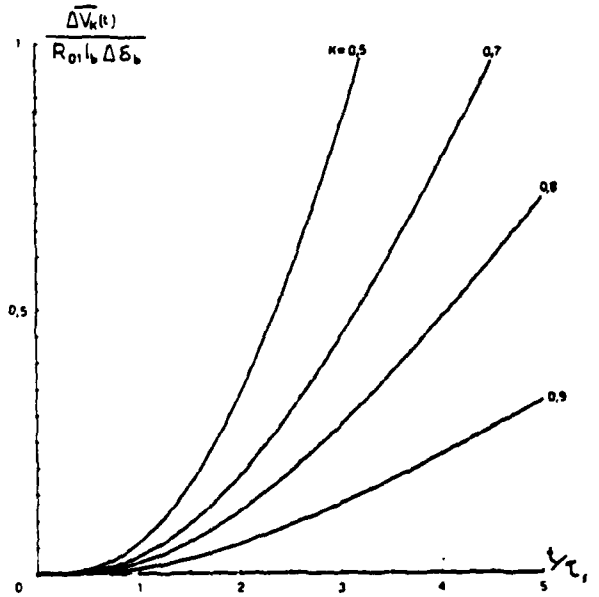


FIG.7 LOAD DUTY CHANGE. $\Delta \overline{V}_R(t)$ FOR $\frac{I_2}{C_3} = \frac{I_b}{C_1} + \frac{I_w}{C_2}$ AND $RC_3 = \frac{R_{01} C_1}{K}$

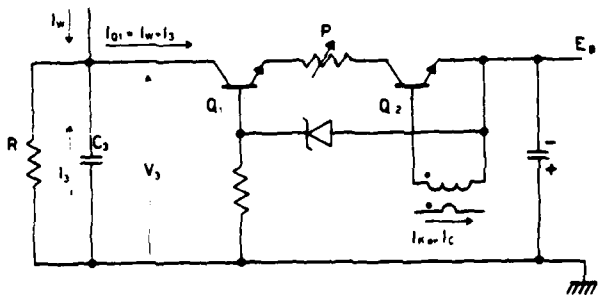


FIG 5 LOAD RIPPLE COMPENSATION - SIMPLIFIED CIRCUIT

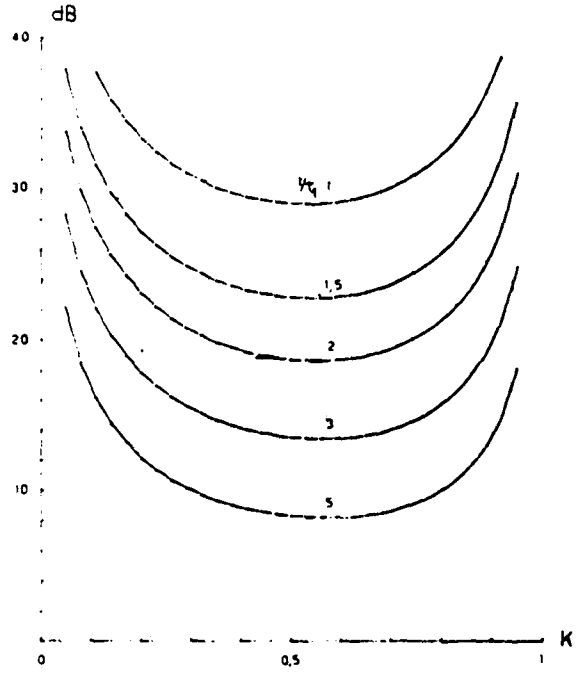


FIG 8 DUTY CHANGE - LOAD RIPPLE REJECTION

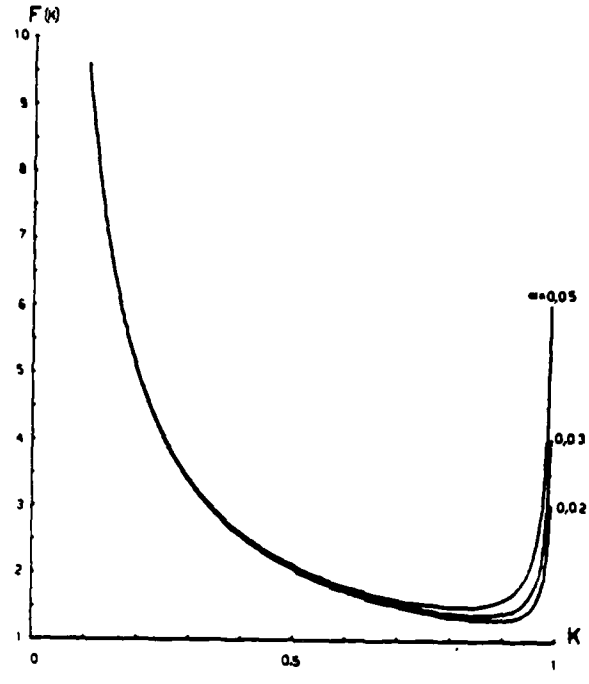


FIG. 9 $F(K) = \frac{1}{K} + \frac{\alpha}{1-K}$ WHERE $\alpha = \frac{I_W}{I_b}\left(\frac{V_2}{V_1}\right)^2$

OFF-RESONANCE TRANSFORMER CHARGING FOR 250-kV WATER BLUMLEIN*

E. Cook, L. Reginato

University of California
Lawrence Livermore Laboratory
Livermore, California 94550

SUMMARY

An off-resonance transformer for charging a 250-kV Blumlein system provides a viable alternative to other charging schemes by permitting the use of conventional thyratrons. Such a transformer must have reliability, a reasonable voltage step-up, and a non-reversing primary current. This paper presents the analysis, design, and performance data for such a transformer. The strong interrelationship between transformer design and Blumlein requirements necessitates that Blumlein description and design criterion be briefly presented prior to transformer design such that transformer load requirements be defined.

INTRODUCTION

The ETA, Experimental Test Accelerator, being built at Lawrence Livermore Laboratory is a 5-MeV, 10-kA machine. Being a linear induction machine, the accelerating potential is generated by separate modules, each capable of producing a 250-kV accelerating pulse of 50-ns duration to a 10-kA electron beam. Each module is a complete system which consists of a variety of pulse conditioning components as shown in Fig. 1. Since there are numerous modules, high reliability and long life are required of components comprising the module.

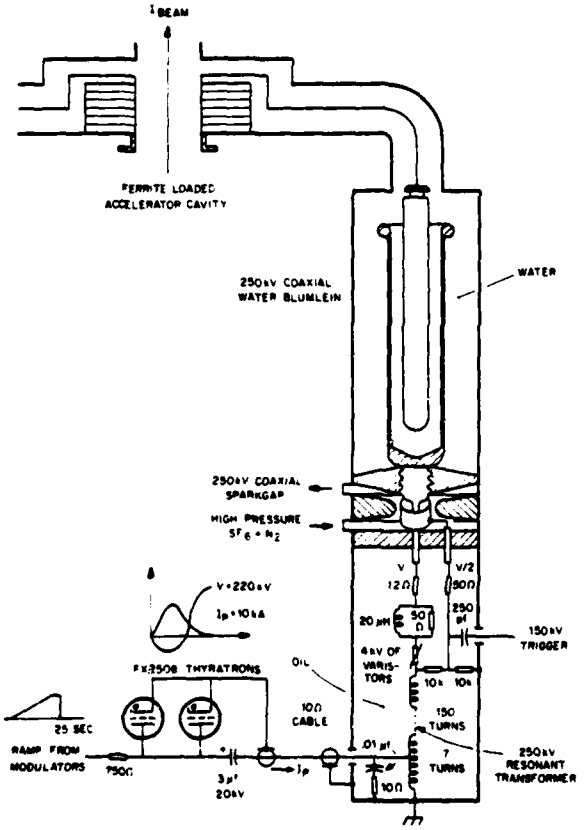


FIG. 1 ACCELERATING MODULE

The Blumlein and its charging system are considered to be an independent module subsystem. The design of either component is dependent upon the characteristics of the other, so both designs are presented. As needed, other details which influence design are described.

Blumlein Design

The Blumlein is a 10-Ω water line. The low impedance geometry is necessary as the Blumlein delivers approximately 50% of stored energy to waveshaping and compensating networks. At the cost of heavy Blumlein loading, these networks ensure that the electron beam has the desired accelerating potential. The choice of water as the dielectric permits the construction of high energy density Blumleins. This is due to water's high permittivity (~80) as opposed to permittivities of 2-3 for most oils. Water has the advantage of being able to recover from a breakdown without having formed conducting by-products (carbon, acids, etc.). However, water does require a circulation system and conditioning to remove dissolved gasses and conducting ions.

Blumlein dimensions are determined by line impedances and the degree of safety desired. The breakdown strength of water is a function of the time water has to hold off voltage. Based on a minimum charge time of 10-μs, water breakdown occurs at approximately 200-kV/cm.[1] By limiting the maximum voltage gradients to 100-kV/cm, a reasonable safety factor is provided. Using this design criterion, the Blumlein dimensions are shown in Fig. 2.

Details of mechanical construction are important if electrical parameters are to be attained. To this end, the metal electrodes are, of course, radiused to minimize or eliminate gradient magnification. In addition a 1-1/2" diameter corona ring is placed at the open circuit end of the middle conductor. Since surface preparation is so crucial, all surfaces which are in the vicinity of the higher voltage gradients are electropolished to remove whiskers and protrusions. All Blumlein components are constructed of stainless steel, which unlike aluminum, does not oxidize in very pure water and is less likely to suffer from surface damage in the event of a breakdown.

For short duration charging cycles (μs), the water Blumlein appears to the charging system as a parallel resistor, capacitor combination. Calculations based on Blumlein geometry and the dimensions of Fig. 2 show the

*This work is jointly supported by the U.S. Department of Energy under Contract No. W-7405-Eng-48 and the Department of the Navy under Contract N00014-78-F0012.

CH1371-4/78/0000-0027$00.75 ©1978 IEEE

capacitance to be 10-nF. Using the maximum realizable value for water resistivity, 18-MΩ-cm, the shunt resistance is approximately 10-kΩ. These values represent the complete load seen by the charging system. The capacitance is the dominating element as the energy dissipated into the resistor is small provided the charging time is not excessive.

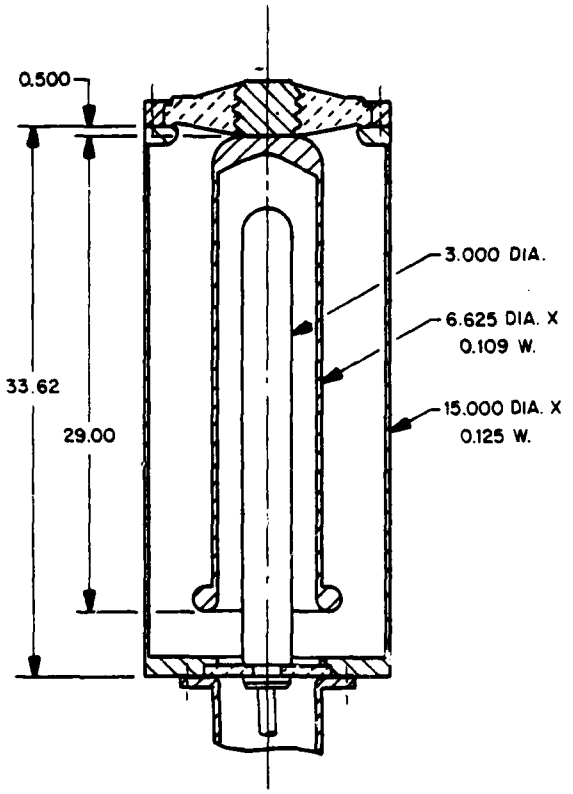


FIG. 2 BLUMLEIN DIMENSIONS

Transformer Analysis

The design of a charging transformer is influenced by many parameters; the drive, the load, step-up ratio, charge time, etc. The Blumlein load is known. The primary drive circuit is determined by the switch and its capabilities and limitations. The primary switch for this transformer is the English Electric thyratron FX 2508 (a modified CX 1159). This thyratron is used because 400 are available from the dismantled Astron accelerator.

The use of this thyratron imposes voltage and current constraints upon transformer design. The FX 2508 was designed to be pulse charged to 32-kV which cannot be done with ETA due to dc power supply limitations. In consideration of the slow (250-ms) charging rate, the tubes are derated to 20-25-kV. The FX 2508 is also specified at 2-kA peak current, however, lab tests show that at low repetition rates (5 pps) they can handle 6-kA peak current for millions of shots. A limitation of any single anode thyratron is its inability to conduct current bilaterally without internal damage. To properly handle negative current, auxiliary circuits such as diodes or perhaps double-ended thyratrons would be required. Circuit protection for the number of thyratrons to be used is not an economically feasible solution.

Based upon thyratron capabilities and limitations, the transformer is required to have a minimum voltage step-up of 10:1 and a non-reversing primary current not to exceed 10-kA. The 10-kA maximum is predicated upon using two parallel thyratrons operating at 5-kA each.

Since the load is essentially capacitive, a resonant charging transformer is logical. To determine which of several possible resonant charging modes would

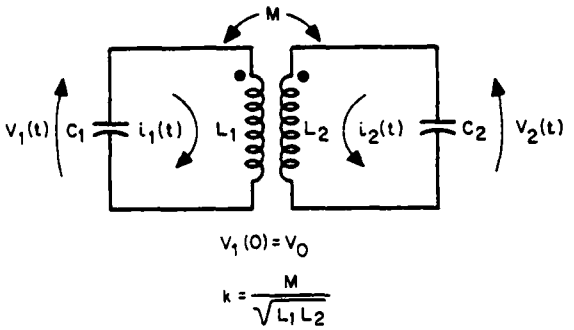


FIG. 3 RESONANT TRANSFORMER CIRCUIT

be best suited, a careful analysis of the transformer circuit is appropriate. Using the circuit of Fig. 3, the Laplace loop equations may be written for the primary and secondary currents. These are:

$$\frac{V_o}{s} = I_1(s)\left[\frac{1}{C_1 s} + L_1 s\right] + I_2(s)Ms \qquad (1)$$

and

$$0 = I_2(s)\left[\frac{1}{C_2 s} + L_2 s\right] + I_1(s)Ms \qquad (2)$$

where V_o is the initial voltage on the primary capacitor C_1, M is the mutual inductance between the primary and secondary windings and the subscripts 1 and 2 denote the primary and secondary terms respectively. Using the relationship $M=k\sqrt{L_1L_2}$ (k is the coefficient of coupling) and rearranging the current equations yields:

$$I_1(s) = \frac{V_o}{L_1} \frac{w_2^2 + s^2}{s^4(1-k^2)+s^2(w_1^2+w_2^2)+w_1^2w_2^2} \qquad (3)$$

and

$$I_2(s) = \frac{-V_o k}{\sqrt{L_1L_2}} \frac{s^2}{s^4(1-k^2)+s^2(w_1^2+w_2^2)+w_1^2w_2^2} \qquad (4)$$

where $w_1^2 = 1/L_1C_1$ and $w_2^2 = 1/L_2C_2$.

The case where the primary and secondary resonant frequencies are equal is worth considering since the equations are considerably simplified and are more easily solved. The time domain solutions for primary and secondary voltages and currents are:

$$i_1(t) = \frac{V_o}{2wL_1}\left[\frac{1}{\sqrt{1-k}}\sin\frac{wt}{\sqrt{1-k}} + \frac{1}{\sqrt{1+k}}\sin\frac{wt}{\sqrt{1+k}}\right] \qquad (5)$$

$$i_2(t) = \frac{-V_o}{2w\sqrt{L_1L_2}}\left[\frac{1}{\sqrt{1-k}}\sin\frac{wt}{\sqrt{1-k}} - \frac{1}{\sqrt{1+k}}\sin\frac{wt}{\sqrt{1+k}}\right] \qquad (6)$$

$$v_1(t) = \frac{V_o}{2}\left[\cos\frac{wt}{\sqrt{1-k}} + \cos\frac{wt}{\sqrt{1+k}}\right] \quad (7)$$

$$v_2(t) = \frac{V_o}{2}\sqrt{\frac{L_2}{L_1}}\left[\cos\frac{wt}{\sqrt{1-k}} - \cos\frac{wt}{\sqrt{1+k}}\right] \quad (8)$$

The most commonly used transformer of this type has a coefficient of coupling k = .6.[2,3] The current and voltage relationships for the primary and secondary windings are repeated here for comparison purposes (Fig. 4). The largest value of secondary voltage occurs when the maximum of the low and high frequency terms peak simultaneously. At this instant in time the primary and secondary currents are zero, and the primary voltage is zero. Theoretically, this is a condition for 100% energy transfer; in practice, because of transformer and switch losses, a 90-95% efficiency has been achieved. Unfortunately, the primary current of the transformer does reverse and the transformer cannot be used because of the decision to use existing thyratrons.

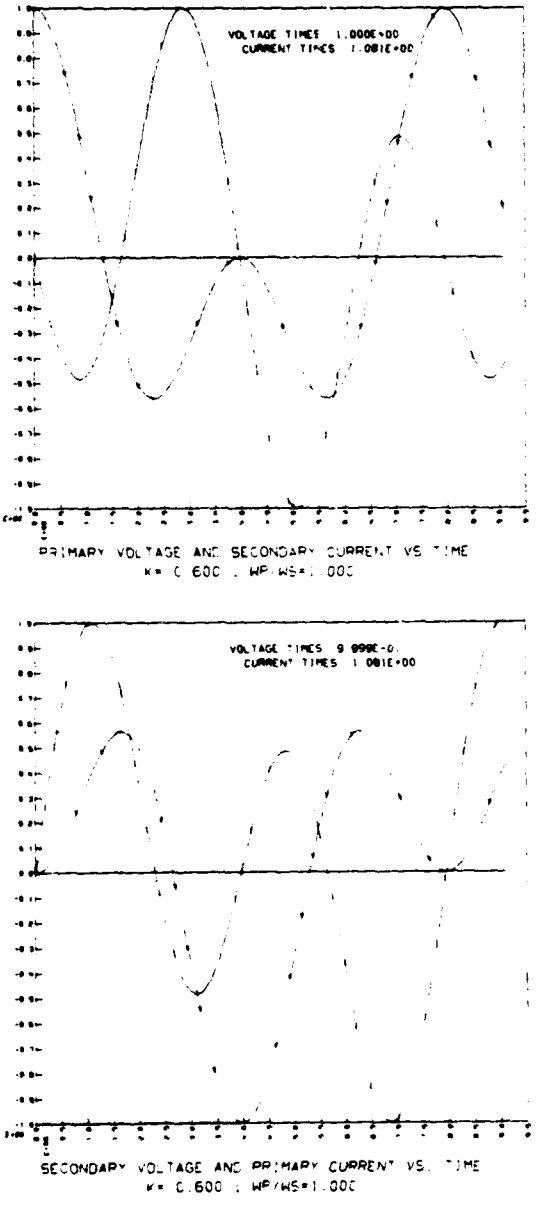


FIG. 4 PRIMARY AND SECONDARY VOLTAGES AND CURRENT FOR A TRANSFORMER HAVING k = .6 and $w_1 = w_2$

Although a thorough analysis of the primary current and secondary voltage as a function of coupling coefficient is arduous, an examination of the time domain solution indicates that for any value of coupling, the primary current does not reverse before the first secondary voltage peak. However, it is not until k > .8 that the first voltage peak begins to exceed the second voltage peak. For k = .8 (Fig. 5) the current in the primary at the voltage peak is a considerable percentage of its maximum value and even though this is an acceptable mode of operation in that it satisfies the design criterion, it is not desirable because of the low efficiency and because the unused energy in the transformer primary continues to drive the secondary thereby inhibiting sparkgap recovery. To dampen this energy, in a high rep-rate system, it becomes necessary to include lossy devices which further reduce the energy transfer efficiency. One good feature of this mode of operation is that the voltage peak occurs on the first cycle and therefore the charge time is shorter.

Having found no desirable mode of transformer operation for equal primary and secondary resonant frequencies, equations (3) and (4) must be solved for the general case where $w_1 \neq w_2$. The solutions are:

$$i_1(t) = \frac{V_o}{L_1\sqrt{\quad}}\left[\frac{w_2^2 - s_1^2}{s_1}\sin s_1 t - \frac{w_2^2 - s_2^2}{s_2}\sin s_2 t\right] \quad (9)$$

$$i_2(t) = \frac{-V_o k}{\sqrt{L_1 L_2}\sqrt{\quad}}\left[s_2 \sin s_2 t - s_1 \sin s_1 t\right] \quad (10)$$

where

$$s_1^2,\ s_2^2 = \frac{\left(w_1^2 + w_2^2\right) \mp \sqrt{w_1^4 + w_2^4 - 2\left(1-2k^2\right)w_1^2 w_2^2}}{2\left(1-k^2\right)} \quad (11)$$

and

$$\sqrt{\quad} = \sqrt{w_1^4 + w_2^4 - 2\left(1-2k^2\right)w_1^2 w_2^2} \quad (12)$$

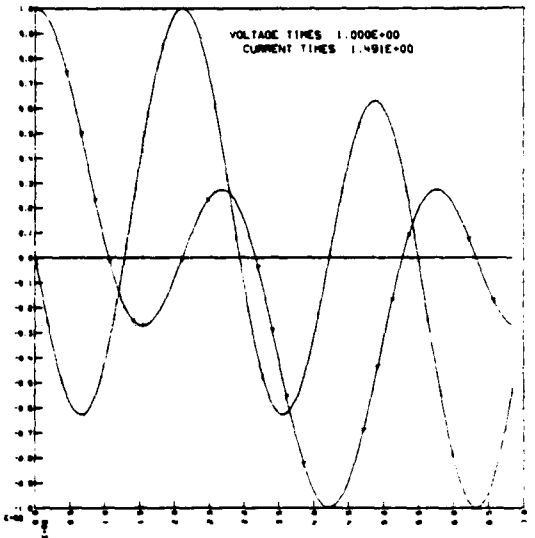
The corresponding voltages are:

$$v_1(t) = \frac{V_o w_1^2}{\sqrt{\quad}}\sqrt{\frac{L_2}{L_1}}\left[\frac{w_2^2 - s_1^2}{s_1^2}\cos s_1 t - \frac{w_2^2 - s_2^2}{s_2^2}\cos s_2 t\right] \quad (13)$$

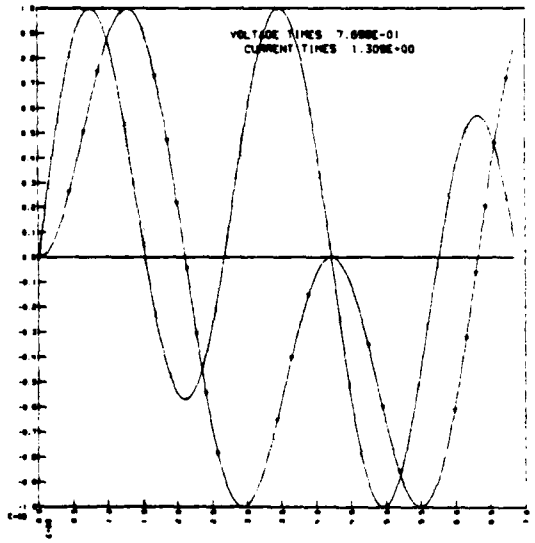
$$v_2(t) = \frac{V_o k w_2^2}{\sqrt{\quad}}\sqrt{\frac{L_2}{L_1}}\left[\cos s_2 t - \cos s_1 t\right] \quad (14)$$

Examination of equations (9 through 14) reveals that by factoring out w_1, the equations may be interpreted as functions of k and the ratio of the two frequencies. On this basis solutions for these equations are generated by computer. To add versatility to the output results, the transformer simulated has the input voltage, primary and secondary inductors, and secondary resonant frequency equal to one. Only the coefficient of coupling and ratio of primary to secondary frequencies are varied. This results in a family of voltage and current waveforms where for each value of k, a set

of curves - each curve representing a different resonant frequency ratio - is generated.



PRIMARY VOLTAGE AND SECONDARY CURRENT VS.TIME
K= 0.800 ; WP/WS=1.000

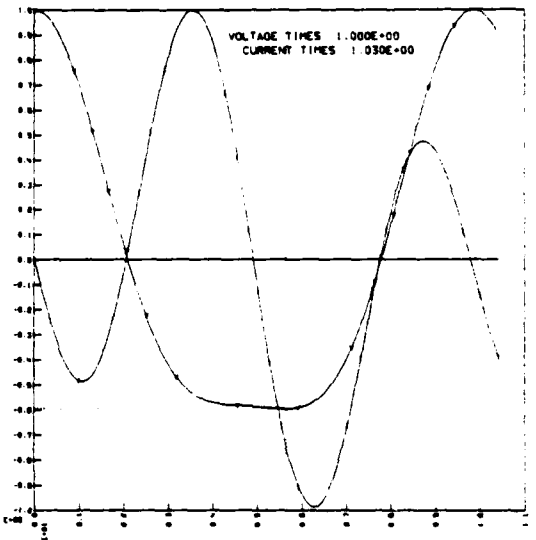


SECONDARY VOLTAGE AND PRIMARY CURRENT VS. TIME
K= 0.800 ; WP/WS=1.000

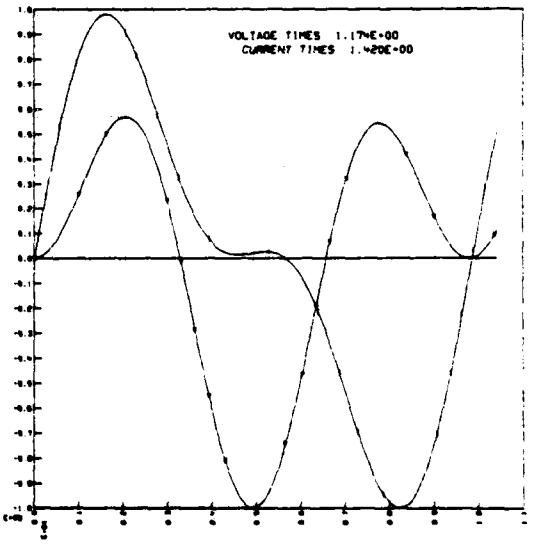
FIG. 5 PRIMARY AND SECONDARY VOLTAGES AND CURRENT FOR A TRANSFORMER HAVING k = .8 and $w_1 = w_2$

An examination of all computer generated curves reveals that a particular set of transformer parameters does indeed satisfy all the requirements. The voltage and current waveforms shown in Fig. 6 correspond to a value of coupling equal to .525 and a frequency ratio equal to .69. It should be understood that these numbers do not represent a unique solution- slight variations about either of these parameters have only slight effects on the waveforms. In fact, all values of w_p/w_s less than .69 satisfy the thyratron current requirements of non-reversal for k = .525. Furthermore, any transformer, regardless of k, has at some point a w_p/w_s at which current reversal does not occur before the secondary voltage peaks. At this point other factors become important; primary energy storage, voltage step-up, and energy distribution at the time of maximum secondary voltage. The goal now is to maintain the highest efficiency while having a minimum of energy stored in the transformer when the sparkgap is triggered.

Fig. 6 shows that the current in the primary is non-reversing and near zero at the secondary voltage peak. The primary voltage has actually reversed by 60% at this time but this energy remains in the capacitor because the thyratron opens at the zero current point. Although this case is not optimum from an energy transfer standpoint, the remaining energy has no adverse effect upon the sparkgap recovery time and does satisfy the step-up and primary current requirements.



PRIMARY VOLTAGE AND SECONDARY CURRENT VS.TIME
K= 0.525 ; WP/WS=0.690



SECONDARY VOLTAGE AND PRIMARY CURRENT VS. TIME
K= 0.525 ; WP/WS=0.690

FIG. 6 PRIMARY AND SECONDARY VOLTAGES AND CURRENTS FOR A TRANSFORMER HAVING k = .525 and w_1/w_2 = .69

Transformer Design

At this point, transformer design in terms of inductances, capacitances, current limits and voltage gains is ready to begin. The known values are Eqs. 9-14, the secondary capacitance (10-nF), k (.525), and w_1w_2 (.69). Also known are the maximum primary current (10-kA), minimum voltage gain (10:1), and the range for charging time (~10-μs). There is enough information that the other transformer values - primary inductance and capacitance and secondary inductance may be determined.

As there are several transformers which can be designed to operate under the specified limits, tradeoffs in terms of reliability and efficiency are made. For the former of these reasons, a realizable voltage step-up of 13:1 is reasonable. The higher transformer gain reduces the thyratron dc operating voltage from 25 to about 20-kV at the cost of lengthening the charging time. To offset anticipated 5-10% losses in the secondary damping circuitry and the 10% losses in the primary drive due to tube drop and cable inductance, a design voltage gain of 15:1 is required. Substituting the values of k and w_1/w_2 into the secondary voltage equation (Eq. 14) yields:

$$\frac{v_2(t)}{V_o} = .59 \sqrt{\frac{L_2}{L_1}} [\cos .92\, w_1 t - \cos 1.85\, w_1 t] \quad (15)$$

$v_2(t)$ attains its peak value at time $t \sim \pi/(.92w_1)$. Substituting this value of time into the above equation and using the design value of 15:1 for the voltage gain yields:

$$L_2 = 162 L_1 \quad (16)$$

Similarly the primary current equation becomes:

$$i_1(t) = \frac{V_o}{L_1 w_1 (1.88)} [1.37 \sin .92 w_1 t + .72 \sin 1.85 w_1 t] \quad (17)$$

The current peaks at $t \sim 2.07/1.85w_1$, and for a design peak current value of 10-kA and an anticipated primary drive voltage of 20-kV, the current equation reduces to:

$$L_1 w_1 = \sqrt{\frac{L_1}{C_1}} = 1.93 \quad (18)$$

or

$$C_1 = .270 L_1 \quad (19)$$

Knowing the resonant frequency ratio

$$\frac{w_1}{w_2} = .69 = \frac{\sqrt{L_2 C_2}}{\sqrt{L_1 C_1}} \quad (20)$$

and values of C_2, L_2, and C_1 in terms of L_1, the value of the primary inductance is easily found to be L_1 = 12.6-μH. Other transformer values are then found to be L_2 = 2.04-mH and C_1 = 3.4-μF. These values allow the determination of the secondary charging time which is 22-μs after switch closure. However, examination of Fig. 6 shows that the peak-to-peak voltage swing occurs in slightly more than half the time required to attain maximum secondary voltage. This time is slightly less than 13-μs which reasonably approaches the design value.

Transformer Construction and Testing

The transformer is a spiral wound auto-transformer as this type of construction lends itself to fast and simple manufacture. Transformer dimensions and number of turns are determined by the coefficient of coupling, the inductance values, and the container. The number of turns for the primary and secondary and the relative spacing of those windings were initially determined from standard formulae for inductance and coupling coefficient. These values were modified to account for the shielding affect of the container walls and several low voltage transformer models were constructed to insure proper performance. The low value of coupling requires a thick transformer winding and thus permits the use of relatively thick foils and insulations. The foil is capacitor grade 2-inch wide, 7 mil aluminum and the insulation consists of 6-inch wide, 7 mil mylar between two 6-inch wide, .5 mil kraft paper (for oil wicking). The thick foil minimizes corona problems and the insulation width and thickness provide a long creepage path and an insulation voltage breakdown strength far in excess of anticipated potentials-all necessary requirements for long life and reliability. As shown in the transformer cross section, Fig.7, the transformer has non-shorting curved conducting surfaces as the output (250-kV) and drive (20-kV) terminals to shape the electric fields and eliminate gradient magnification.

The final transformer winding consists of a 7-1/2 turn primary wound onto the outside of a 150 turn secondary separated by an approximate 3/16" spacer; foil and insulation dimensioned as previously described. The drive point is the junction of the primary and secondary windings. The transformer is 4 inches I.D. and 9-1/2 inches O.D.

The averaged measured values for the primary and secondary inductances and coupling for the 34 transformers constructed are approximately L_p = 11.5-μH, L_s = 2.0-mH, and k = .525. Low level operational tests using a SCR switch are shown in Fig. 8. These waveforms compare favorably with the computer generated waveforms of Fig. 6. Secondary voltage and primary current oscillograms for output voltage of 130-kV are shown in Fig. 9. The first prototype has over 100,000 shots without failure at voltages in excess of 200-kV.

The other circuitry in the transformer container (which is oil filled) provides the sparkgap midplane potential, damping, and decoupling. Referring to the schematic in Fig. 1 and to Fig. 7, these components are identifiable. The varistor in series with the high voltage output provide damping after sparkgap breakdown by becoming a large impedance at low current levels. The 20-μH, 50-Ω parallel combination decouple the sparkgap and transformer at high frequencies. The series 12-Ω resistor supplies additional damping and aids sparkgap recovery. The 20-kΩ resistor string provides the sparkgap trigger electrode with its required V/2 potential. The 250-pF capacitor is a coaxial parallel plate structure which couples the sparkgap trigger voltage to the sparkgap trigger electrode.

CONCLUSION

Using a thyratron as a primary switch imposes current restrictions with which a conventional charging transformer cannot comply. A .525 coupled transformer operating in an off-resonance mode satisfied the current requirements, but at the expense of a non-optimum energy transfer. A .6 coupled transformer can be used to overcome the energy transfer problem, but only if a bilateral switch such as a spark gap or, preferably, an inexpensive double-ended thyratron is used.

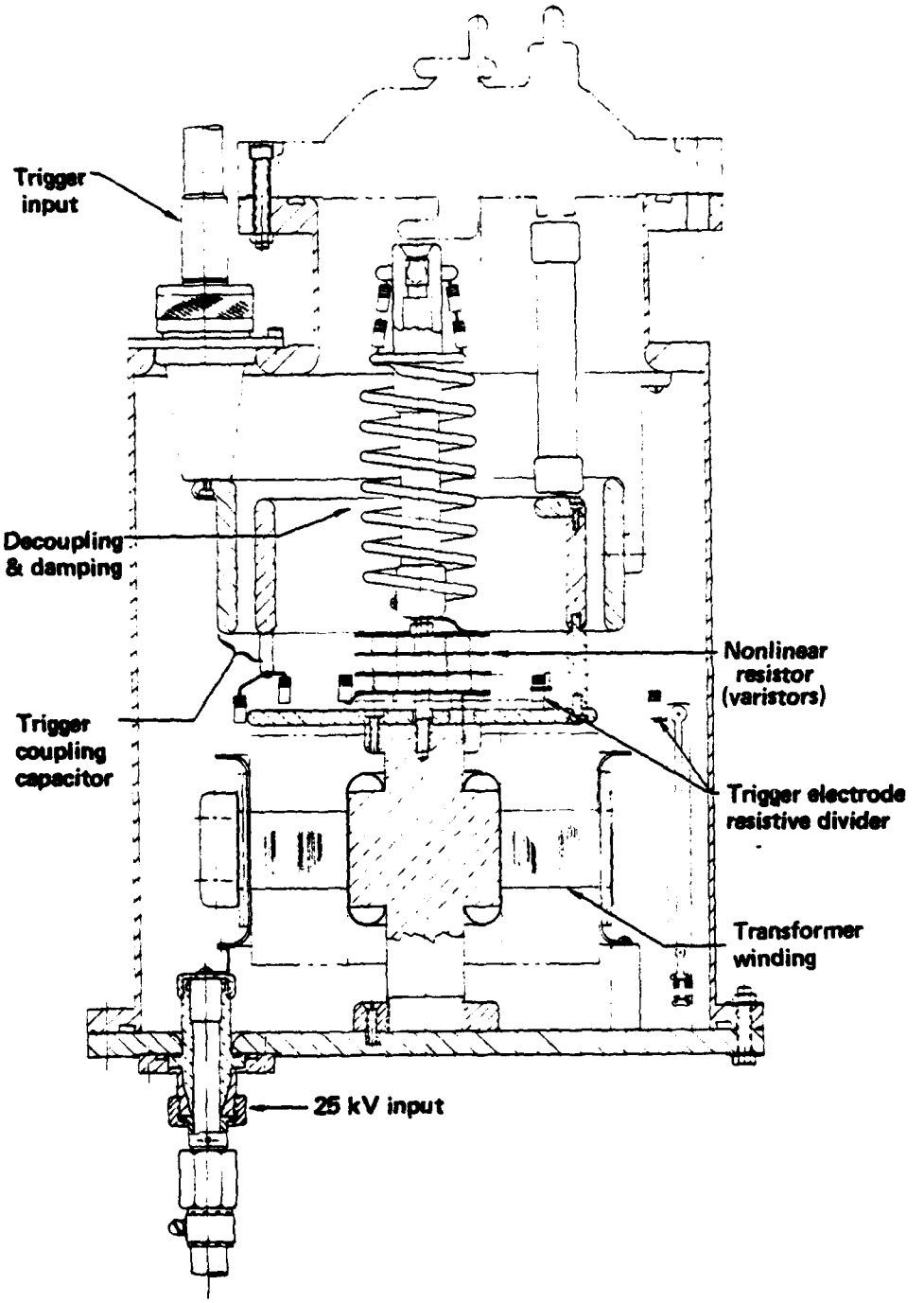


FIG. 7 TRANSFORMER CROSS-SECTION

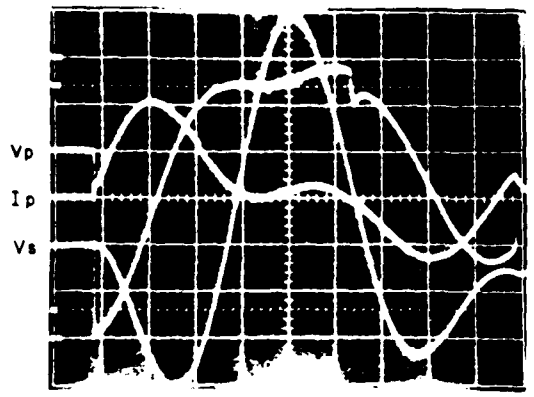
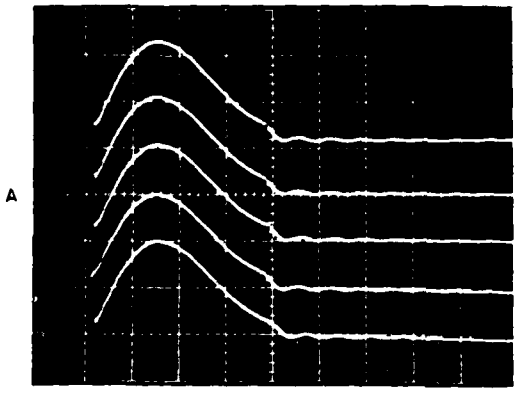


FIG. 8 LOW LEVEL MEASUREMENTS OF PRIMARY CURRENT, PRIMARY VOLTAGE AND SECONDARY VOLTAGE FOR TRANSFORMER HAVING k = .525 and w_p/w_s = .69
V_p @ 5 V/DIV, I_p @ 5 A/DIV,
V_s @ 50 V/DIV, t @ 5us/DIV.



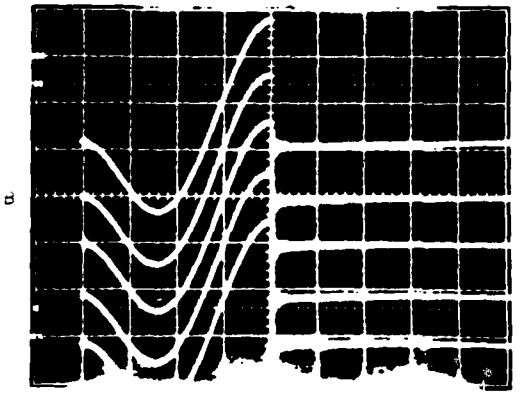


FIG. 9 SECONDARY VOLTAGE AND PRIMARY CURRENT FOR TRANSFORMER (k = .525 and w_p/w_s = .69) OPERATING AT 130-kV
9(a) I_p @ 2.6 kA/DIV, t @ 5us/DIV.
9(b) V_s @ 50 kV/DIV, t @ 5us/DIV.

REFERENCES

1. A. Richard Miller, "High Energy Density, Low Impedance Capacitors Using Pressurized Water as a Dielectric, Maxwell Laboratories.

2. E. A. Abramyan, IEEE Transactions on Nuclear Science, Vol. NS18, No. 3, June 1971, p. 447.

3. T. H. Martin,"FRIZZ - A High Voltage Impulse Tester, SC-RR-71 0341 (1971).

NOTICE

"This report was prepared as an account of work sponsored by the United States Government Neither the United States nor the United States Department of Energy, nor any of their employees, nor any of their contractors, subcontractors, or their employees, makes any warranty, express or implied, or assumes any legal liability or responsibility for the accuracy, completeness or usefulness of any information, apparatus, product or process disclosed, or represents that its use would not infringe privately-owned rights."

Reference to a company or product name does not imply approval or recommendation of the product by the University of California or the U.S. Department of Energy to the exclusion of others that may be suitable.

PRECISION REGULATED, 20 KW, MODULATOR PFN CHARGING SYSTEM

Charles A. Corson

Westinghouse Electric Corporation
Systems Development Division
Baltimore, Maryland 21203

Summary

This paper describes a new, high efficiency, regulated modulator charging system that accurately charges the pulse forming networks (PFN's) in a 14 megawatt modulator to over 3 kV without the use of a conventional high voltage power supply, or dissipative regulator. It is impervious to load open and short circuits and regulates PFN voltage precisely. The circuit stores a measured amount of energy in a transformer as $1/2\ LI^2$ and then transfers it to a PFN capacitor as $1/2\ CV^2$. This technique uses considerably less parts than previous methods and therefore produces impressive size, weight and cost reductions as well as design simplification. It also charges and regulates PFN's more efficiently than previous methods because of using less parts in the main power path and not using a dissipative regulator.

Previous Technology

Figure 1 shows the conventional method previously used for charging and regulating PFN's. It consists of three basic groups:

1. A high voltage power supply
2. A command charge group
3. A PFN voltage regulator

The high voltage power supply uses a three phase step-up transformer and six high voltage rectifiers followed by a filter choke and filter capacitor. Usually this is preceded by a line regulator (motor driven variac or 3 phase SCR controller).

The command charge group includes a charging choke, charging diode, and an SCR with its trigger circuit, to control the time at which the PFN is charged. Often the charging voltage is high enough that several SCR's are needed in series.

The PFN regulator consists of a shunt regulator connected across the PFN to remove the excess charge above the desired level that is caused by power supply ripple.

New Charging Circuit Description

A new method has been developed for charging and regulating PFN's which has been implemented in a 20 kW charging system in the ARSR-3 radar transmitter for the Federal Aviation Administration. The new method has resulted in a 4:1 reduction in size and a 5:1 reduction in weight as well as impressive reductions in cost. Forty-eight transmitters are currently in production, several of which have been shipped after an extensive test program which included environmental tests.

Figure 2 is a block diagram/schematic of the regulated charging system. Three phase power is rectified through a choke into a 300 volt electrolytic capacitor bank. When the charger control unit receives its trigger command to charge the PFN, it simultaneously energizes two transformers which drive the two transistor switches into saturation. This applies the 300 VDC power supply to the charging transformer primary. Actually, each transistor switch is made up of 36 power transistors connected in parallel. A transistor switch assembly is pictured in Figure 3. The base and emitter of each transistor is separately fused.

The voltage applied to the inductance of the transformer primary causes current to ramp up in the primary, as can be seen in the waveforms in Figure 4. The charging diode connected to the transformer secondary is polarized so that it will be reverse biased when the primary is energized. The stored energy in the primary at any given time is represented by:

$$J_p = 1/2\ L_p\ I_p^2$$, where

J_p = joules stored in the primary inductance

L_p = primary open circuit inductance

I_p = current in the primary winding

By measuring the primary current and comparing it against a stable reference, the time at which the primary stored energy reaches the desired level can be determined and used to stop the charging of the primary inductive stored energy. By removing transistor drive and turning off the two transistor switches at this time, a precise amount of energy can be measured into the primary each pulse.

When primary current flow is interrupted, the transformer voltage tries to reverse. As this voltage crosses zero, the secondary charging diode connects the transformer to the modulator PFN which has no charge. The transformer dumps its stored energy into the PFN over a period of time calculated by:

$$T_{CHG} = \frac{\pi}{2}\sqrt{L_s \times C_{PFN}}$$, where

L_s = transformer secondary inductance

C_{PFN} = the PFN capacitance

The voltage rise on the PFN is a quarter sine-wave as seen in Figure 4. The final voltage on the PFN, neglecting losses is:

$$V_{PFN} = \sqrt{\frac{2 \times J_p}{C_{PFN}}}$$

By controlling the peak primary current, the final PFN voltage can be controlled precisely. Because the pulse-to-pulse operation repeats itself, losses are constant and do not affect the pulse-to-pulse precision of the PFN voltage.

In the system that was built, the pulse-to-pulse PFN voltage accuracy was better than 0.05% for varying line voltage inputs, harmonic ripple on the 300 volt power supply and variable interpulse periods required by the radar system.

CH1371-4/78/0000-0034$00.75 © 1978 IEEE

The charging transformer is specially designed because it is used as an energy storage element. Figure 6 shows the transformer. The current sensing transformer and the high voltage charging diode are built into the assembly on the right side. Figure 5 shows the transmitter that is in production and Figure 7 shows the charging system compartment with its door open. The upper part of the compartment contains the 300 VDC power supply on the left and the transistor switches on the right along with their control unit. The bottom part of the compartment contains the charging transformer and charging diode.

System Parameters

The 20 kilowatt system that was built and tested has the following parameters:

PFN capacitance	11.3 microfarads
PFN voltage	3.1 kV (3.3 kV max)
Repetition Rate and Stagger	365 PPS 300 to 400 PPS
Pulse-to-Pulse Voltage Accuracy	± 0.02% Typical
Average (HV) Current	13 Amps DC
Primary Peak Current	500 Amps Typical (600 A max)
Transformer Turns Ratio	13.5:1
Transformer Primary Inductance	425 Microhenries
Input Power	3Ø, 60 Hz, 120/208 VAC ± 10%

The system that was built uses five 2.26 microfarad PFN's connected in parallel. These PFN's are charged in parallel and are switched with five solid state switches into a single primary of a pulse transformer that delivers a 135 kV, 105 Amp, 3 microsecond pulse to a klystron load. The modulator can be run with one of the PFN's removed leaving four PFN's connected in parallel.

Design Features

In order to protect the transistor switches from transient voltages, two diodes were included across the switches and the transformer primary that return inductive energy to the 300 volt power supply. These diodes conduct every pulse when the transistor switches are turned off. They divert the current flowing in the transformer primary back to the power supply until secondary current starts flowing. This slight delay occurs because of transformer leakage reactance which prevents instantaneous transfer of interrupted primary current into secondary current. These diodes also divert the stored energy back to the 300 volt power supply if the secondary becomes open circuited. A current sensor on the diodes indicates when the returned current is excessive, and shuts the system down.

This type of charging system is also impervious to load short circuit. Because of the polarization of the charging transformer and the secondary charging diode, the primary side of the system never sees load short circuits. When the primary side of the system is disconnected with the transistor switches, secondary current will flow through any secondary short circuit and this current is limited by the energy stored in the transformer and can never exceed the level to which the primary was limited. A secondary current sensor then reads out an overload and shuts down the system. Previous conventional systems would short circuit the high voltage power supply when the modulator shorted. This would pull very heavy currents through the charging diode and high voltage power supply until a large contactor could be opened or the main breaker tripped. This was sometimes destructive to parts in the charging system.

Another desirable feature is the fuses associated with the individual transistors in the transistor switch assemblies. Figure 8 is a schematic of a transistor switch assembly. If a transistor fails, it short circuits and blows the emitter and base fuse associated with it. Then the emitter and base terminal of the transistor assume the collector voltage. This voltage is then fed through the associated base and emitter resistors to a summing diode whose output indicates a pair of blown fuses. This signal is used to light a maintenance light which indicates that maintenance should be performed at the operator's convenience. The charging system continues to run as if nothing had happened. If more transistors should fail before the maintenance is performed, more current is fed through the summing diodes, and when more than five are failed, a sensor detects the high level and shuts down the system. This system has been run at full power with up to 25% of the transistors removed.

Because the charging diode is reverse biased during the first portion of the charging cycle, modulator switch recovery is not a problem. This system inherently provides switch recovery time and allows the charging cycle to use the entire interpulse period.

A crowbar was included in the system that is currently in production. It is connected across a tap at 10% of the transformer secondary winding. This allows the use of a low voltage SCR to divert the energy stored in the transformer. PFN voltage is monitored and if it climbs above a preset level the crowbar is triggered and the system is shutdown. This could happen if the operator turned the high voltage adjust up too high or if he tried to operate with too many PFN's removed.

Conclusions

This method of charging PFN's will be used extensively in the future because of its versatility and economy. Its main advantages are achieved because this one circuit performs the three separate functions listed earlier. It also reduced the number of high voltage components and connections in the hardware to a minimum. In summary, this new circuit offers the following advantages:

- SIMPLICITY - thus easier maintenance and troubleshooting.
- HIGH EFFICIENCY - because a dissipative regulator is not needed, and there are fewer parts in the main power path.
- RELIABILITY - because of the low power loss, low parts count and very few high voltage parts.

- SMALL SIZE AND WEIGHT - high voltage paper/oil capacitors and 60 Hz step-up transformers have been eliminated, resulting in typically a 4:1 size and weight reduction, thus providing easier maintenance.
- LOW COST - because of low parts count, minimal assembly labor and less circuits to be tested.
- HIGH ACCURACY REGULATION - comparable to existing techniques without the need for high voltage because current at a low voltage potential is controlled. This circuit is unaffected by staggered pulse repetition frequencies.

The combination of the two transistor switches and clamping diodes with an inductive load provides a fool-proof power controller that is easy to design and safely operates without stress, even during load shorts, opens, or arcs. Other production systems are currently planned that use this new charging system.

References

1. E. H. Hooper and S. R. Bird, "An All Solid State Modulator for the ARSR-3 Transmitter", Thirteenth Modulator Symposium, June, 1978, Buffalo, N.Y.
2. C. A. Corson, "A Modular Modulator for an Air Defense Radar", Twelfth Modulator Symposium, February, 1976, New York, New York.
3. This charging system was produced as part of the ARSR-3 Transmitter under FAA Contract DOT-FA75WA-3641.

NOTE: Patent application filed in 1976.

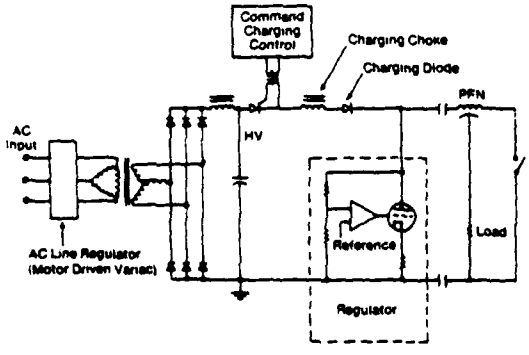


Figure 1. Conventional Charging System

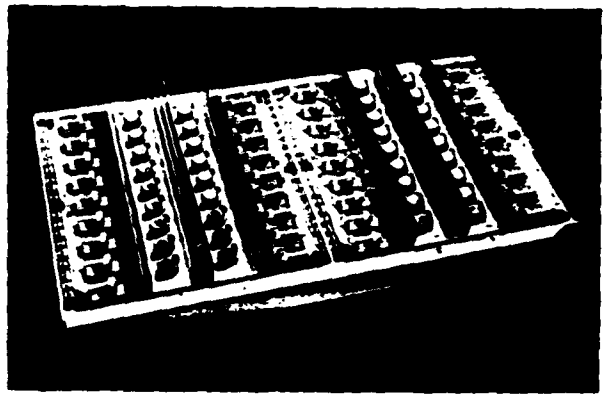


Figure 3. Transistor Tray

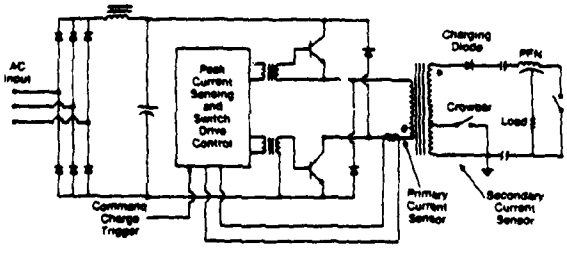


Figure 2. New Charging System

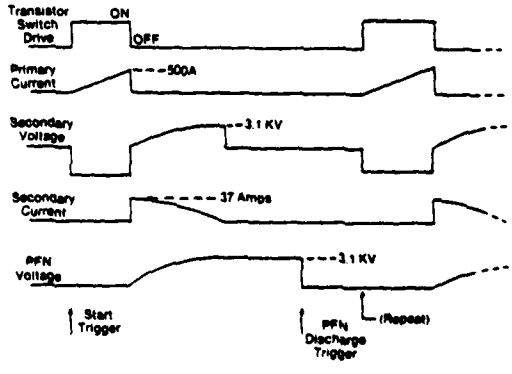


Figure 4. Operating Waveforms

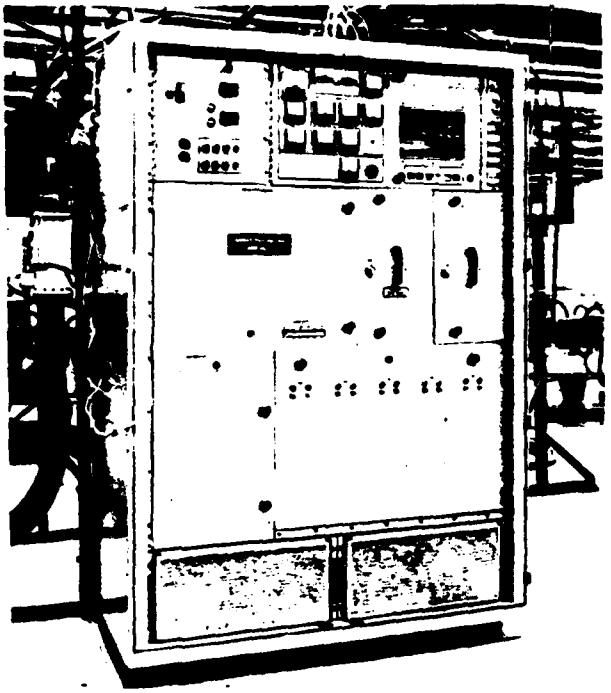


Figure 5. Production Transmitter

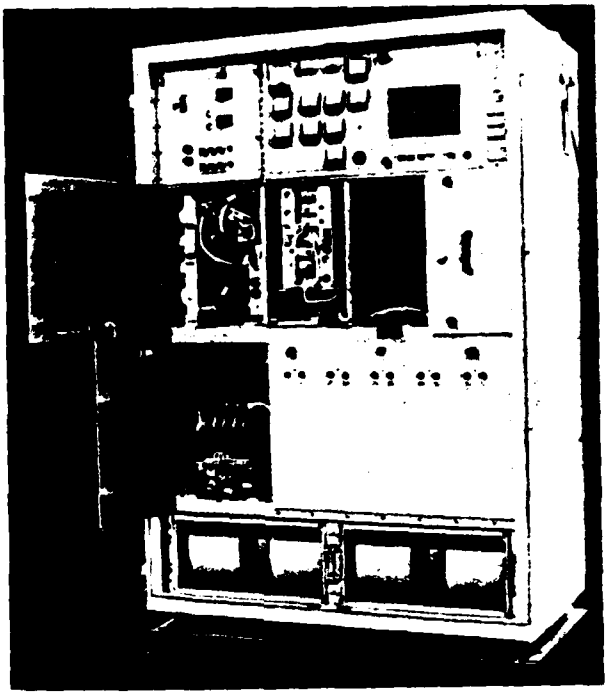


Figure 7. Charging System Compartment



Figure 6. Charging Transformer

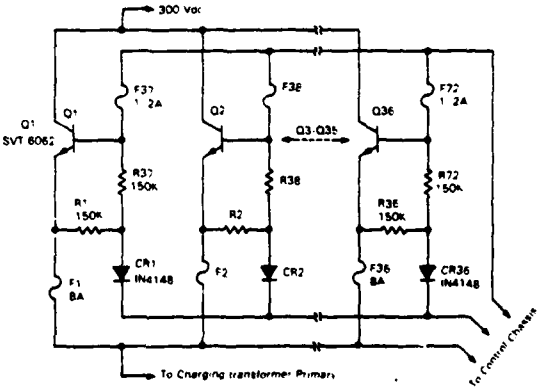


Figure 8. Transistor Switch Tray Schematic

A MODULAR PFN WITH PULSEWIDTH AGILITY

H.J. Blinchikoff
R.A. Gardenghi

Westinghouse Electric Corporation
Systems Development Division
Baltimore, Maryland 21203

SUMMARY

This paper describes the design, analysis, and realization of a lightweight, low-impedance pulse-forming network (PFN) in which identical inductor-capacitor modules can be added or removed to change pulsewidth while maintaining high pulse quality without introducing excessive pulse-top perturbations. The PFN evolved contains an input module that is optimized for a pulse-plateau ripple of ± 0.5 percent. The ripple remains within this limit as modules are added or removed from the PFN to change the pulsewidth in 2 usec steps. The optimized parameters are presented in normalized form allowing the optimum response to be achieved for arbitrary pulsewidths and network impedances.

This low-ripple response is achieved without incorporating mutual inductance into the design, therefore, easing the module tuning and assembly. Mutual inductance has been considered indispensible in PFN's, but it is a roadblock for modular construction. Its elimination as a design parameter is the key to realizing the modular PFN.

A breadboard was built and tested under high power. Included are measured responses that verify that the modular concept and optimum response can be realized in practice.

This paper is based on studies performed for the U.S. Air Force under contract number F30602-76-C-0207, RADC, Rome New York.

INTRODUCTION

This paper describes the design, analysis, and realization of a lightweight, low impedance pulse-forming network (PFN) in which indentical inductor-capacitor modules can be added or removed to change pulsewidth while maintaining high pulse quality without introducing excessive pulse-top perturbations.

The need for this type of PFN arises from the growing sophistication of modern radars, particularly transportable radars with modern ECCM capabilities. Advanced signal processing techniques require improved transmitter pulse fidelity, which depends heavily on the modulator pulse quality. Furthermore, a radar requirement exists for pulsewidth agility in which line-type modulators may be made pulsewidth variable through the use of modularized PFN's. Conventional PFN's are heavy and bulky, and the pulse-top ripple associated with these devices is considered excessive for these applications.

GOALS

In the context of this paper, the pulse-forming network (PFN) is the aggregate of pulse-forming modules (PFM's). The pulse duration of each PFM is to be 2 microseconds. Therefore, the pulse duration of the PFN can be 2, 4, 6, 8, or 10 microseconds, since the maximum number of modules considered here is five. The parameter goals for the PFM and the achieved results are given in Table 1.

TABLE 1

PULSE-FORMING MODULE GOALS AND ACHIEVEMENTS

Parameter	Goal	Achievement
Peak Power (MW)	5	5
Average Power (kW)	4	4
Charging Voltage (kV)	10	10
Pulse Duration (usec)	2	2
Pulse Repetition Frequency (pps)	400 max	400
Impedance (ohms)	5	5
Pulse-Top Variation	1% max	1% max
Weight Energy Density (joules/lb)	2 min	5.1
Max Dimension for Stack of 5 Modules (inches)	60	17.8

THEORETICAL CONSIDERATIONS

The PFN serves the dual purpose of storing the exact amount of energy required for a single pulse and discharging this energy into a load resistor R_o in the form of a rectangular pulse. An equivalent model for this pulse discharge is shown in Fig. 1, where the PFN is selected so that i(t) approximates a rectangular pulse to within an acceptable tolerance when the input voltage v(t) is the step function.

The ideal PFN is an open-circuited lossless transmission line of characteristic impedance $Z_o = R_o$ and transmission time $\tau/2$, where τ is the rectangular pulsewidth [1]. However, practical considerations rule out this line as a PFN, and in practice this distributed line is simulated by a network composed of a finite number of lumped elements.

The lumped parameter network cannot exactly simulate a distributed transmission line, so an approximation procedure must be employed to determine the network element values. Of the many possible choices for the network, the voltage-fed networks are the most commonly used because only with this type can the usual discharge switches be used. The

CH1371-4/78/0000-0038$00.75 © 1978 IEEE

energy, stored in the electrostatic field of the PFN, is transferred to the load resistor R_o when the discharge device is switched to a conducting state.

We investigated two voltage-fed network classes; the Guillemin Type E network in Figure 2(a), and the Rayleigh network in Figure 2(b). In each network all capacitors are the same. Other networks equivalent to the Guillemin voltage-fed network are given in [1], but these networks do not offer any appreciable advantages over the Type E.

The network in Figure 2(b) is the lumped-parameter approximation to the transmission line, truncated after N sections. We call it the Rayleigh network because application of Rayleigh's principle to the transmission line yields this line-simulating network. The Rayleigh network is well suited for modular separation because each section is identical. The Guillemin Type E network, because the inductors are not restricted to be the same value, produces a better approximation to the rectangular pulse than does the Rayleigh network, for the same number of elements. However, the close interrelationship among element values does not make this network adaptable for modular separation. Furthermore, careful control of the coupling between coils is required to achieve the correct response.

Type E networks with satisfactory pulse-plateau ripple are usually obtained by adjustment of the various inductors [1]; however, this is not practical if sections are added and removed as required. Analog computer simulation of Type E networks showed that excessive pulse-plateau distortion occurred whenever sections where added or removed to change the pulsewidth because the carefully chosen aggregate of section self-inductances and mutual inductance between sections was upset. For this reason, the Type E PFN was excluded as a network that meets the requirements in Table 1.

RAYLEIGH NETWORKS

The analysis of Type E networks suggested that the requirement of a variable pulsewidth could best be accomplished, and most economically, by having identical sections without mutual inductance between sections. The pulsewidth then becomes a function of the number of plug-in modules. This configuration is the Rayleigh network in Figure 2(b), where

$$L = \frac{R_o \tau}{2N}, \qquad C = \frac{\tau}{2NR_o} \qquad (1)$$

Initially we computed the current response of a six-section (N=6) Rayleigh PFN (τ = 10 usec, R_o = 5 Ω) on a digital computer because accurate values of the small pulse-top variations were not obtainable from the analog computer results [2]. The first overshoot of this network's response, was 14 percent, a figure that is unacceptable for most practical situations. However, by increasing the value of the first inductor, we considerably reduced the first overshoot and succeeding ripple. Then the three end-sections were removed. The pulsewidth halved as desired and, most important, the change in the initial overshoot and rise time due to the removal of sections was insignificant. This experiment showed that a modularized PFN without mutual inductance was feasible and proved the basis for the design of the optimum network.

Three sections (N=3) were selected as the fundamental module because it yielded a flat-top pulse whereas the two-section module yielded a rounded pulse. Nominal values from (1) are L = 1.67 μH, C = 0.067 pF. Although the pulse-top variation was considerably reduced by increasing the value of the first inductor (L_1), this one degree of freedom was not enough to reduce this ripple to the 1 percent goal. Therefore we also varied the first capacitor (C_1) to improve the response.

Computer responses in Figure 3 show the interesting trends in the pulse-top response. For a fixed value of C_1, the initial overshoot decreases as L_1 increases, but the succeeding undershoot is relatively insensitive to this change. However, as C_1 is increased, this undershoot improves. Since the pulse rise time is proportional to L_1, it is also desirable that the value of L_1 be minimized. Consequently, the optimum parameters selected were L_1 = 3.4 μH and C_1 = 0.073 μF, and the corresponding pulse response is shown in Figure 4. The ± 0.5 percent variation has been achieved and the 2 μsec pulsewidth occurs very near the predicted 70 percent value. The significant aspect about this portion of the study is that the ± 0.5 percent variation goal has been satisfied without incorporating mutual inductance between coils. Until now, mutual inductance has been indispensible in PFN's, but it is a roadblock for modular construction. Its elimination as a design parameter is the key to realizing the modular PFN and additionally the manufacture of the PFN is considerably eased. Figure 5 shows the optimum input module parameters and the Rayleigh module parameters.

The cascade of the Rayleigh N=3 modules with values L and C does not upset the initial portion of the optimized pulse. This feature is demonstrated in Figure 4 which shows the response as one and then two N=3 modules are added to the input module. The pulse-top variation remains within ± 0.5 percent and the desired pulsewidth again occurs near the 70 percent value. In this manner, an arbitrary pulsewidth can be achieved by the cascade of these identical basic building blocks. The commonality of these modules further reduces manufacturing cost and alignment time.

The optimum normalized parameters are presented in Table 2. With these values the response in Figure 4 for an arbitrary pulsewidth and impedance can be obtained. Use of this information allows a predictable response which includes the presence of the resistor R_o. This in itself is a major improvement over previous approaches, because the design procedures in [1] are based on an ideal voltage source (R_o = 0). Since there is no resistance

in the circuit, the theoretical response is periodic. When the resistor R_0 is included, the response degrades to a transient pulse that departs from the theoretical response. The above information eliminates this shortcoming of previously published design procedures.

TABLE 2

NORMALIZED PARAMETERS FOR OPTIMUM PULSE RESPONSE

Quantity	Normalized Value	To Denormalize Multiply by
L	1	$\frac{T}{6} \times R$
C	1	$\frac{T}{6} \times \frac{1}{R}$
L_1	2.04	$\frac{T}{6} \times R$
C_1	1.095	$\frac{T}{6} \times \frac{1}{R}$
Risetime (10% -90%)	1.428	$\frac{T}{6}$

78-0099-TA-17

HIGH POWER MODEL

Packaging of the high-power pulse forming module and the mating of these modules to form the final PFN require strict mechanical, electrical, and cost considerations to achieve the goals in Table 1. The PFN must be rugged and be able to dissipate the generated heat, yet it is desired to have a minimum weight energy density of 2 joules/pound. Insulation to prevent arcing and minimum lead length to avoid parasitic inductance are important electrical considerations, while cost is important for large quantity manufacture.

High-power modules were assembled using dry impregnated mica capacitors and air-core inductors. The tolerance of each component was within ±5 percent. The length of the five module assembly was 17.75 inches, easily satisfying the design goal of 5 feet for the greatest demension. Electrical connections between modules were made with No. 8 copper wire. The complete assembly is sufficiently rugged to withstand normal usage in a radar system.

We now describe the tests on the high-power model of the PFN as the pulsewidth is changed in 2 usec steps. All modules were the same except the input module, which had a larger input inductance and capacitance in accordance with the optimum design in Figure 5.

The high-power test circuit was a conventional line type modulator composed of a variable voltage power supply, charging circuit, switch tube, and load resistor. The power supply had a voltage range from 0 to 7.5 kV and a maximum power capability of 1 kW. The charging circuit was a 0.5 H inductor and a solid-state diode stack while the HY-5 thyratron acted as the discharge switch. Four 1.25 ohm air cooled woven wire resistors connected in series provided a matched 10 kW load for the PFN test.

High-power testing was performed at 10 kW peak PFN storage voltage. Figure 6 shows the pulse responses for 1, 2, 3, 4, and 5 modules while Table 3 gives the test results. The full peak and average power were met for 1, 2, and 3 modules. Laboratory power supply limitations required a reduced PRF for the 8 usec and 10 usec pulsewidths; however, the duty cycle was maintained constant.

The measured plateau ripple of the PFN high-power model was ± 1.5 percent, because the component tolerance was ± 5 percent. The design goal of ± 0.5 percent ripple will be satisfied as this component tolerance is tightened.

TABLE 3

HIGH-POWER PFN TEST RESULTS

Parameter	Number of Pulse Forming Modules				
	1	2	3	4	5
Pulsewidth (μ sec)	2	4	6	8	10
Peak Current (Amp)	1000	1000	1000	1000	1000
Average Current (Amp)	0.8	1.6	2.4	2.4	2.5
Peak Power (mW)	5	5	5	5	5
Charging Voltage (kV)	10	10	10	10	10
Rep.Frequency (pps)	400	400	400	300	250
Average Power (kW)	4	8	12	12	12.5

78-0099-TA-30

CONCLUSION

A modular pulse-forming network that does not include mutual inductance as a design parameter has been developed. Moreover, identical basic pulse-forming modules can be cascaded with the optimized input module to yield the desired pulsewidth without increasing the pulse-plateau ripple and pulse risetime. This synthesis procedure also provides the capability for electronically varying the pulsewidth by allowing the appropriate modules to be switched into or out of the circuit. Although the variable pulsewidth has been emphasized, the peak power can be increased by adding modules in parallel.

ACKNOWLEDGEMENT

This paper was based on a study sponsored by the U.S. Air Force under contract number F30602-76-C-0207, Rome Air Development Center, Griffiss Air Force Base, Rome N.Y.

REFERENCES

1. Glasoe, G.N. and J.V. Lebacqz, Pulse Generators, Dover Publications, Inc., New York, N.Y., 1965. (This book was originally published as Volume 5 in the MIT Radiation Laboratory Series).

2. Blinchikoff, J.J., Lightweight Line Pulser, Final Technical Report, RADC-TR-78-73, Rome Air Development Center, Griffiss Air Force Base, New York.

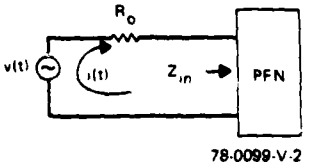


Figure 1. Equivalent Model for Pulse Discharge Current

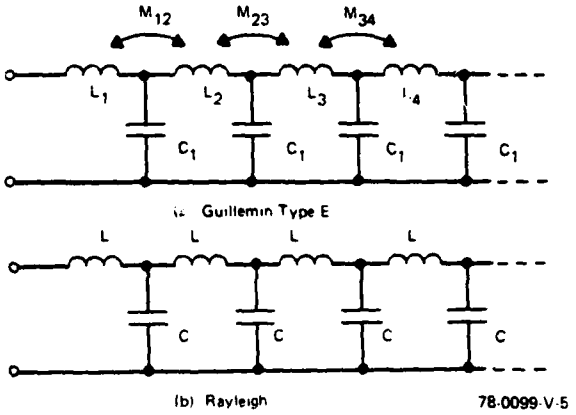


Figure 2. Pulse-Forming Networks That Were Examined

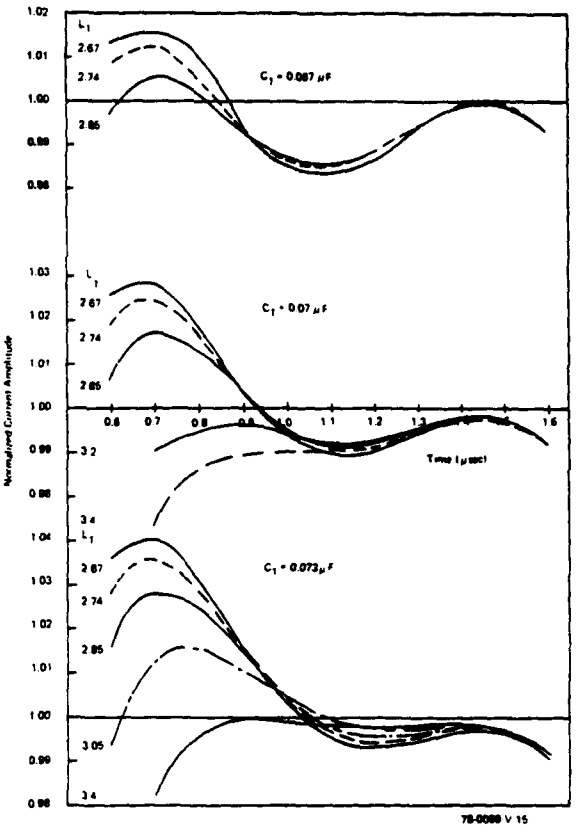


Figure 3. Pulse Responses About the Pulse Top as L_1 and C_1 Vary (N = 3 PFM)

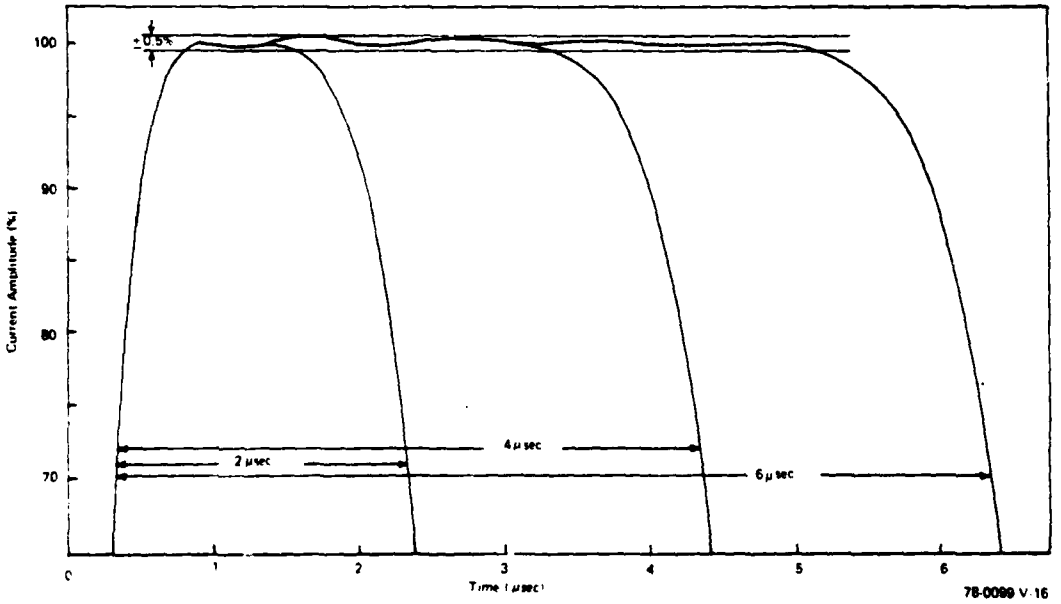
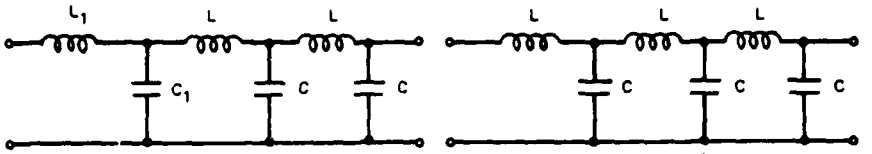


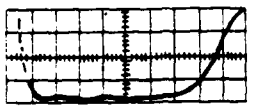
Figure 4. Pulse Responses for One, Two, and Three Modules for Optimum L_1 (3.4 μH) and C_1 (0.073 μF)



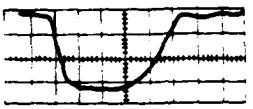
L_1 = 3.4μH C_1 = 0.073μF
L = 1.67μH C = 0.067μF

78-0099-V-18

Figure 5. Optimum Pulse-Forming Modules



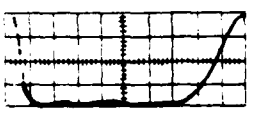
(a) 1 Module – 2 μsec/cm



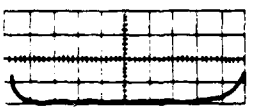
(b) 2 Modules – 1 μsec/cm



(c) 3 Modules – 1 μsec/cm



(d) 4 Modules – 1 μsec/cm



(e) 5 Modules – 1 μsec/cm

78-0099-PA-29

Figure 6. High-Power Pulse Responses of Final PFN's

PFN LOSS CALCULATIONS

S. Ivan Rambo
R.A. Gardenghi

WESTINGHOUSE DEFENSE AND ELECTRONIC SYSTEMS CENTER
Systems Development Division
Baltimore, Maryland 21203

SUMMARY

Approximation methods for the calculation of PFN losses have been used for many years. With the current availability of computer facilities to most electronic engineers today, more precise calculations can be made.

Many PFN's designed for thyratron switching have had characteristic impedances high enough that losses could be ignored safely. The recent trend to all-solid-state pulsers requiring very low Z_0 (less than 1 ohm) and high pulse current capability makes it essential that distribution of losses be determined more accurately. This paper describes a proven useful approach, using simple time-shared computer programs.

Methods are described for loss calculations by first determining the pulse current shape in each coil and capacitor in the time domain. Then these pulses are transformed into the frequency domain to determine their spectra. By knowing the Q of the coils and the dissipation factor of the capacitors and how they vary with frequency, it is easy to sum the losses for each spectral line for each component. Results agree well with experiments.

INTRODUCTION

The technique to be described for calculating PFN losses was suggested in Volume V of the MIT series. But lack of modern computer facilities prevented its extensive use until recently. The method actually used in the early years as described in Volume V utilizes a number of approximations no longer necessary, since the advent of time-shared computer facilities. For PFN's designed in the past and employing thyratron switches, characteristic impedances were usually high enough (typically 15-25 ohms) so that losses were usually low. The recent trend to high-power solid-state pulsers requiring very low Z_0 sometimes less than an ohm) and high pulse current capability makes it essential that distribution of losses be determined more accurately during the design.

The determination of losses in the inductors and capacitors of a PFN requires that the shapes of the current flow through each element be known. Then by transforming these pulse shapes to the frequency domain, power dissipation can be computed by summing the losses at each discrete spectral line. Unfortunately, the effective resistance of inductors and capacitors is a function of frequency and must be determined for accurate calculations. A fundamental limitation to accurate loss calculation is the difficulty of simulating this frequency in the time domain when computing the pulse shapes. Obviously, some pulse shape modification must occur because of this dependence. Fortunately, this effect, even for low impedance PFN's is small, and can be ignored in the cases we have examined.

CALCULATIONS

The calculation technique used can best be illustrated by a specific example. A series of computer programs were written in "basic" using the "interactive" approach where the computer requests the pulsewidth, load characteristics, number of sections desired, and pulse transformer parameters. The load can be a klystron, CFA, laser, or other nonlinear device. Data stored in the program is for a type "E", equal-capacitance, mutual-inductance, voltage-fed network of 3, 4, 5, 6 or 8 sections. Figure 1 reflects such a typical network. Figure 2 is an example of an eight-section computation using a low impedance PFN feeding a high-turns-ratio, step-up transformer for pulsing a klystron. Figure 3 shows the resultant plot of the coil currents. It can be seen that I, the current through the first coil, has a duration equal to the full pulsewidth. Current durations progressively decrease down to I_8. It is obvious from this plot that coil losses will be the greatest in L_1 and the least in L_8.

Figures 4a and 4b show similar plots for the capacitor currents. Two plots are shown with four currents on each for the sake of clarity.

Once these current shapes have been determined, at least two methods of determining the spectral distribution have been used. The simplest method is to assume the coil current pulses are trapezoidal, and the capacitor currents are pairs of half sine waves. Closed form solutions for Fourier analysis are available for these shapes. For greater accuracy, the pulses can be sampled and the data applied to FFT programs available on most time-shared facilities. Figure 5 reveals the spectrum for the first section current pulse of figure 3.

Before losses can be calculated from the above spectra, the Q or dissipation factors of the coils and capacitors must be determined as a function of frequency all the way from the first few spectral lines at the PRF to the frequency beyond which the spectral amplitude is negligible. Although measurement of coil Q over such a range is not a trivial problem because of difficulties in obtaining low loss capacitors to resonate the coils at very low frequencies, a fair approximation is usually possible. Calculation methods such as those of Butterworth are also quite good though tedious. If the coils are to be assembled in metal enclosures such as for oil- or gas-insulated PFN's, the Q must be measured "in situ." Calculations are much more difficult than for coils in "free space."

Capacitor dissipation data for PFN types as a function of frequency is not always known, and must be determined for accurate calculations. The relationship, RC = dissipation factor/2*PI*F*C), where dissipation factor is measured at 1,000 Hz, can be used with fair accuracy.

CH1371-4/78/0000-0046$00.75 ©1978 IEEE

Once the dependence on frequency of the effective resistance of the coils and capacitors has been determined, then a simple computer subroutine can be inserted in the Fourier transform program to determine loss distribution and total dissipation within the PFN. The equation:

$$P_L = \sum_{n=1}^{k} I_{L_m}^2(n) \cdot R_{L_m}(n)$$

will compute losses in coil L_m by summing the loss at each spectral line where R_{L_m} (n) is adjusted for each line to agree with measured or calculated values. Similarly, summations can be made for each capacitor. The upper *summation limit K can* be raised progressively until the contribution of added terms to the element loss can be ignored.

Applying this method of calculation to the actual network of figure 1 resulted in a total coil dissipation of 18 watts. A similar calculation using the method of Volume V of the MIT series as given on page 214 produces a total coil loss of 21 watts. The difference is less than 20 percent and may not seem significant in all but the most exacting cases. The main advantage of the calculation method described is that fewer assumptions are required, and it is easier to execute with the aid of a computer.

We have used two techniques for experimental verification of the loss calculations. Both were based on temperature rise measurements. One uses the true calorimetric method where the change in temperature of a known volume of liquid such as insulating oil is measured versus time. The other replaces the network with a resistor and power source which is adjusted to duplicate the time-temperature function of the actual network. Reasonable correlation between calculations and measurements have been obtained. These measurements verified the overall network loss. Verification of the losses in the individual network elements was considered to be too difficult to implement.

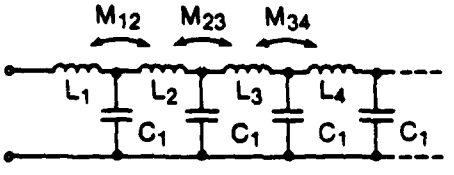
CONCLUSIONS

A method for more accurate calculations of the losses in PFN's has been described which is easier to use than older methods since fewer assumptions need to be made. Reasonable correlation between calculations and measurements have been obtained.

BIBLIOGRAPHY

Glasoe and Lebacqz - Pulse Generators - MIT Volume V

S. Butterworth - Wireless Engineer - April, 1926



78-0540-BD-6

Figure 1. Network

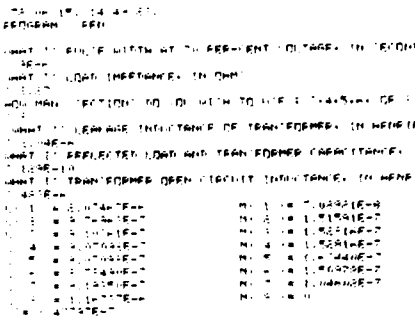
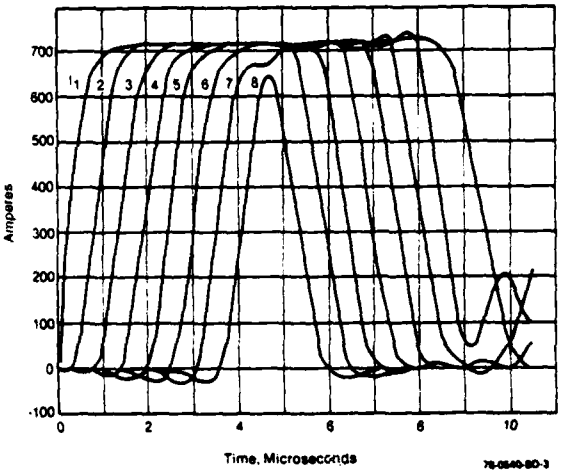
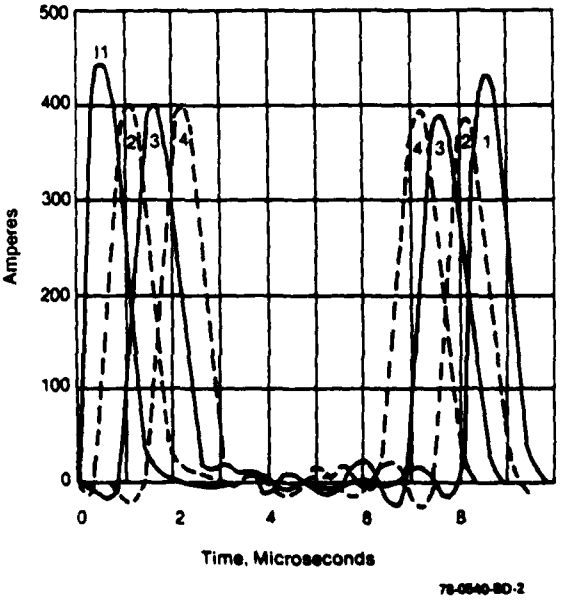


Figure 2. Eight Section PFN Computation



78-0540-BD-3

Figure 3. Coil Currents



78-0540-BD-2

Figure 4a. Capacitor Currents

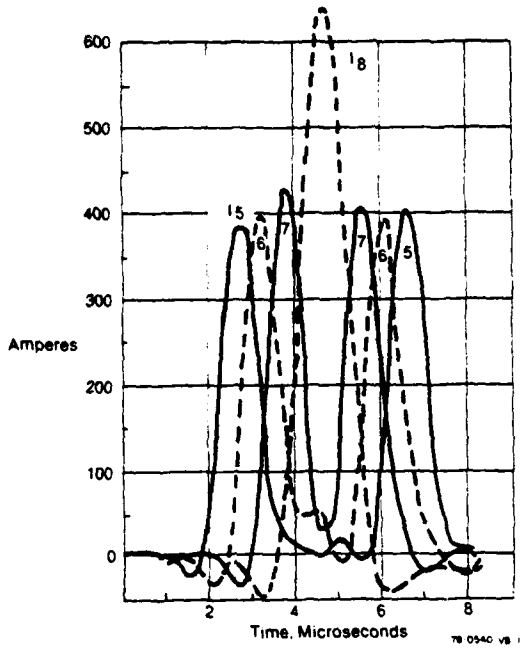


Figure 4b. Capacitor Currents

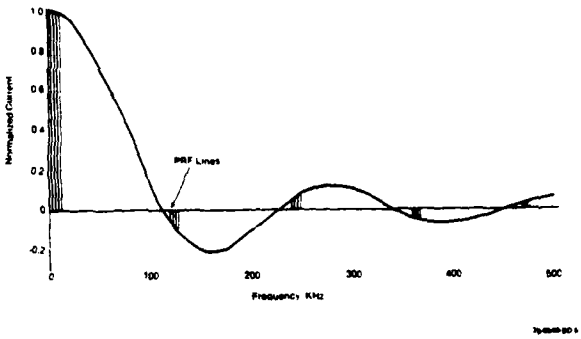


Figure 5. Envelope of PRF Lines for L_1 Current Pulse Train

PULSE FORMING NETWORKS WITH TIME-VARYING OR NONLINEAR RESISTIVE LOADS

R. M. Roark, M. E. Parten, L. B. Masten and T. R. Burkes

Texas Tech University
Lubbock, Texas 79409

Summary

High power pulse forming networks (PFN) have been in use for some time. The networks are usually designed using techniques that assume a desired pulse shape and a constant resistive load. High power gaseous discharge devices have created a need for high power pulse generation operating into time-varying resistive loads or nonlinear resistive loads. Although some work has been done in designing a PFN with a time-varying load, little has been done for the nonlinear loads in general.

In this paper a study of the effects of a time-varying or nonlinear load on a pulse forming network is presented using simulation techniques. The resultant output pulse is compared to the desired pulse using different error functions, such as mean-square error and absolute error. The sensitivity of the error function with respect to the parameters of the PFN is determined. A criteria is developed for the adjustment of the parameters of a pulse forming network to improve the pulse delivered to a time-varying or nonlinear resistive load. The form of the desired pulse, the error function and the type of resistive load can be varied to obtain a specific adjustment criteria. In one case, applying the technique to a given PFN resulted in a 46.4 percent improvement in mean-square error.

Introduction

The classical technique used in designing pulse forming networks with constant resistive loads is based primarily on the Fourier series expansion of the desired output pulse (see Fig. 1) [1]. Since i(t) is an odd function, the series contains only sine terms. Like terms in the series, the sinusoidal current produced by the circuit of Fig. 2 consists of an amplitude and frequency portion. This current is given by

$$i_k = V_c\sqrt{\frac{C_k}{L_k}}\ \sin\frac{t}{\sqrt{C_kL_k}} \qquad (1)$$

By comparing the general term of the Fourier series to that in Equation 1, the values of L_k and C_k can be written in terms of the series coefficient, b_k. The result is found to be

$$L_k = \frac{\tau V_c}{k\pi b_k I_p} \text{ and } C_k = \frac{\tau b_k I_p}{k\pi V_c} \qquad (2)$$

A network that approximates the original waveform can be realized by adding n such LC circuits in parallel. The result is the voltage-fed (type C) network in Fig. 3. In turn, this network can be converted into a large number of equivalent forms by manipulating the complex impedance function of the network [2]. Ball and Burkes have shown that the classical technique can be extended to include time-varying resistive loads [3]. However, the Fourier series method does not easily lend itself to nonlinear resistive loads.

Many achievements in designing high power pulse forming networks have been recorded[4,5]. However, consistent with the continuing development of pulse-power technology, more exotic applications have arisen. Whenever producing various pulse shapes for complex but resistive loads is necessary, the design procedure is usually not well-defined. This paper outlines a method which permits computer-aided optimization of a given set of PFN parameters based on a specific error criteria in order to better approximate the desired output pulse. In the process, sensitivities with respect to network elements can be calculated to develop a specific adjustment criteria. The optimization technique has been applied to networks designed using the classical procedure, producing significant improvements in the form of resultant output pulses. Also, some information of network element sensitivity is presented.

Preliminary Discussion

The Fourier design technique is invariant to different types of finite, real pulses. However, as Guilleman argued, the theoretical pulse should have finite rise and fall times if the series is to converge uniformly throughout [4]. Using finite rise and fall times will insure that overshoot and undershoot can be minimized as desired, usually by increasing the number of sections. A trapezoidal shaped pulse and a pulse with parabolic rise and fall are two commonly used forms.

When evaluating the performance of a PFN, it is convenient to define an error criteria which gives a measure of how well the network approximates the theoretical pulse. Defining the theoretical pulse as p(t) and the resultant output (voltage) response as v(t), the error function of the approximation, ε, is given by

$$\varepsilon(t) = p(t) - v(t) \qquad (3)$$

For a full measure, error should be amassed over the entire Fourier series period, 2τ (Fig. 1). Hence the mean-square error, E_m, is given by

$$E_m = \overline{\varepsilon^2(t)} = \frac{1}{2\tau}\int_0^{2\tau}\varepsilon^2(t)dt \qquad (4)$$

Another commonly used measure is absolute error, given by

$$E_a = \frac{1}{2\tau}\int_0^{2\tau}|\varepsilon(t)|dt \qquad (5)$$

The full advantage of an error criteria can be realized by appropriately weighing the error function according to the designers' prerogative. A weight function, q(t), can be chosen to emphasize (or deemphasize) those areas of the pulse which are of most concern. The weight function can be included in Equation 4, yielding a weighted mean-square error. The result may be written as

CH1371-4/78/0000-0043$00.75 © 1978 IEEE

$$E_m = \frac{1}{2\tau} \int_0^{2\tau} [\varepsilon^2(t) \cdot q(t)]dt \qquad (6)$$

If optimization is to proceed based on a previously defined error criteria, then enhanced improvement of various aspects of the pulse can be realized--for instance, decreased rise and/or fall time, maximum flatness, maximum energy delivered during the on period, maximum flatness in the off period, etc.

The optimization procedure is concerned with minimizing a preselected error criteria, E, with respect to the output v, subject to the network equations. The minimization of E is a function of its argument, the network parameters. The network behavior can be described in terms of its state, given as an m-dimensional set of first-order differential equations. This process can be written in the following manner:

minimum of
$$E(L,C,\ldots)$$

subject to
$$x_1' = f_1(x_1,x_2,x_3,\ldots,t) \qquad (7a)$$
$$x_2' = f_2(x_1,x_2,x_3,\ldots,t)$$
$$\vdots$$
$$x_m' = f_m(x_1,x_2,x_3,\ldots,t)$$
$$v = g(x_1,x_2,x_3,\ldots,t)$$

Letting $[x'$ represent a column vector of state variable derivatives and $\underline{x}$ a row vector of identical dimension, a more compact form is given by

minimum of
$$E(L,C,\ldots)$$

subject to
$$[x' = [f(\underline{x},t) \qquad (7b)$$
$$v = g(\underline{x},t)$$

In short, the procedure uses a standard gradient approach and is not restricted to any particular PFN; it is applicable to all of the (finite) current- and voltage- fed forms. For the purposes of this paper however, the network of Fig. 3 has been chosen to illustrate the optimization procedure. Included in the simulation program are capabilities of providing intermediate errors, sensitivities, parameter values and output plots upon request.

Optimization as a Design Criteria

A problem with any infinite series representation is the error introduced when approximating the function by a finite number of terms. How well a truncated Fourier series represents a waveform depends not only on the number of terms but on the original function itself (i.e. its convergence). Consider designing a PFN to operate with the time-varying load, r(t) in Fig. 4. Assuming that v(t) is a rectangular pulse, the product $i(t) \cdot r(t)$ is to remain relatively constant during the pulse period. The current i(t) for the given resistance is shown in Fig. 5a. The same current is shown expanded into a periodic function in Fig. 5b. As the current waveform deviates from a roughly sinusoidal shape, the n-term Fourier series can be expected to have a lower order of convergence. Therefore, it is not surprising that a finite number of Fourier sine terms fails to provide the best fit (in the mean-square sense) of the current function, especially for the general resistive load. Conventionally, more terms of the series are included in effort to reduce error. In lieu of adding sections to the PFN, another set of element values may exist which produces a more desirable pulse. Improved results may be obtained from the original set by an appropriate optimization procedure.

Consider designing a six section PFN to develop a one microsecond, one kilovolt pulse across a resistive load given by the equation

$$r(t) = 1 + t, \quad 0 \le t \le \tau \qquad (8)$$

For the duration of the pulse, the time-varying current must be of the form

$$i(t) = \frac{1}{1+t}, \quad 0 \le t \le \tau \qquad (9)$$

Expanding i(t) into an odd series (Fig. 5b) and calculating the Fourier coefficients yields twelve element values which best approximates the current pulse by the classical procedure. These values are listed in Table 1 for reference. The output pulse is shown in Fig. 6.

The above design has offered a starting point for the optimization procedure. This particular optimization was based on mean-square error and concerned with the pulse period, one microsecond. The final element values appear in Table 1 along with the percent change. The resultant pulse is shown in Fig. 7. The error has decreased 35.2 percent over the one microsecond duration. Particularly noticeable is the fall time, decreasing from .47 μs to .16 μs. Element values have varied from 0.3 percent to 13.4 percent in magnitude. For completeness, sensitivity of the error with respect to each element (at the final point) has been included in Table 1.

As a second example, an additional microsecond (2 μs) is included in the error criteria. The result is shown in Fig. 8 where a 46.4 percent improvement was noted. Again, the fall time has improved considerably. Probably the most noticeable aspect of the new pulse is the relative flatness in the off period. More energy delivered to the load can be expected. Inherent to the latter design is immunity from the large undershoot occurring in the off period. This fact becomes more important when incorporating special switching requirements in an actual network design. Similar results were obtained using absolute error.

In examining the effect conventional improvement methods would have on the original PFN design, six additional sections were added. The optimized network was better than the twelve section Fourier extension in some ways. The six section PFN had 54.5 percent faster fall time and 33.7 percent less error. However, the twelve section PFN exhibited more flatness on top of the pulse. These results have further enlightened the practical signifi-

cance of a systematic optimization procedure.

To investigate the effect of altering the load characteristics, different resistive loads were applied to a chosen PFN. Proceeding to optimize an existing network from the derived parameters due to restricted changes in the load is usually more desirable than completely redesigning the PFN. From a practical standpoint, capacitive values may be unchangeable while inductances (including mutual inductance) can be altered in meeting the new design. This concept may be particularly useful for the class of high power gaseous discharge devices. Load properties may change slightly in a time-varying or nonlinear sense due to continued use. Moreover, the PFN may be needed to operate another gaseous device. To study this phenomena, the resistive load for the derived network was changed from $r(t) = 1+t$ to a constant $R = 1$. The associated pulse is shown in Fig. 9 and is not unlike Fig. 8 in many respects. Likewise, the response in Fig. 10 is from the same PFN with a decreasing resistance $r(t) = 1 - t/4$. After optimization, the error improvement recorded was 37.4 percent and 23.1 percent respectively.

As an example of the amount of computer time required for the optimization program, the results of Table I were obtained in 8.1 CPU minutes. This time includes three output plots and intermediate result information. However, the optimization time is greatly dependent on the particular design need. Depending on the number of network parameters and the degree of improvement required, the time may be much more or much less than the example given.

Conclusion

A considerable improvement in the calculated response of PFN's for time-varying resistive loads has been made. It has been shown that the optimization procedure results in a better overall response (mean square error) than prior design procedures, even for the same number of LC sections. It should be noted that the best designs obtained with this optimization procedure results in component sections (type C network) whose natural frequencies are not harmonically related. This result leads to many interesting questions concerning established design procedures. These questions form the basis for future work on general PFN design.

The optimization procedure described has a weighted feature for error calculations. This feature allows the circuit designer to optimize a PFN's response in several ways. For instance, the fall time of the output pulse could be considerably improved at the expense of other portions of the overall response. By extending the period of optimization beyond the pulse width, a better PFN-load match can be obtained. Thus, a better transfer of energy is obtained during the pulse period itself. Likewise, rise time, maximum flatness, etc. could be optimized at the expense of other portions of the pulse. Although this paper describes the optimization only for time-varying loads, it is felt that the procedure is applicable to nonlinear loads as well. This work along with experimental verification is planned for the future.

References

[1] E. A. Guilleman, Synthesis of Passive Networks, New York: Wiley, 1957.

[2] E. A. Guilleman, Communication Networks, Vol. II, New York: Wiley, 1935.

[3] D. G. Ball and T. R. Burkes, "Pulse Generation for Time-varying Loads," Dept. of Electrical Engineering, Texas Tech University, August 1975.

[4] G. N. Glasoe and J. V. Lebacqz, eds., Pulse Generators, New York: McGraw-Hill, 1948.

[5] E. G. Cook and T. R. Burkes, "Pulse Forming Network Investigation," Dept. of Electrical Engineering, Texas Tech University, August 1975.

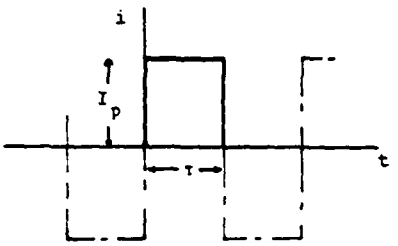


Fig. 1 An odd expansion of the desired pulse into an alternating current waveform.

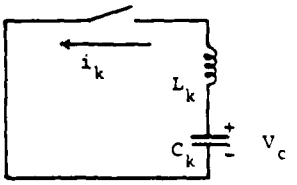


Fig. 2 An LC network to produce a sinusoidal current waveform.

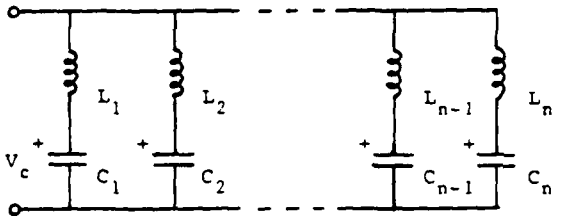


Fig. 3 The voltage-fed network derived from a Fourier series expansion of the output pulse.

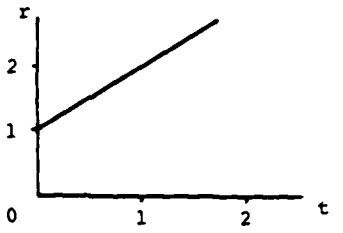


Fig. 4 The time characteristic for the resistance $r(t) = 1 + t$.

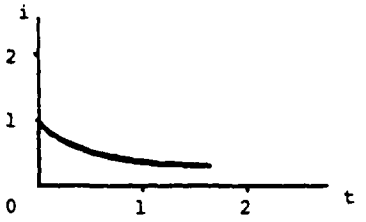


Fig. 5a The desired current response $i(t) = 1/(1 + t)$.

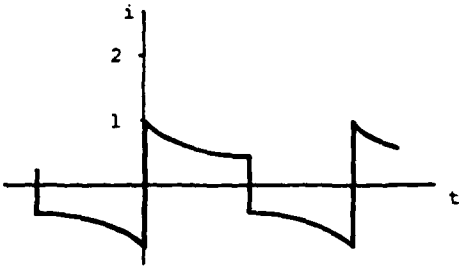


Fig. 5b The expanded current to be approximated by a six term Fourier series.

Table 1. Element values, before and after optimization, and final sensitivities for a six section PFN with $r(t) = 1 + t$.

Element	Initial	Final	Change	Sensitivity
L_1	0.3669 μH	0.404 μH	10.11 %	-0.1645
L_2	1.0754	1.0299	-4.23	-0.0109
L_3	0.3386	0.3677	8.60	-0.0634
L_4	1.00227	0.99042	-3.16	0.1510
L_5	0.3387	0.3839	13.35	0.0196
L_6	1.0069	0.9728	-3.39	-0.0372
C_1	0.27613 μF	0.2728 μF	-1.21	1.60
C_2	0.02355	0.02285	-2.96	-0.020
C_3	0.03324	0.03314	-0.30	-0.0181
C_4	0.00619	0.00599	-3.23	0.1072
C_5	0.012	0.01234	2.83	0.0078
C_6	0.00279	0.00276	-1.08	0.1168

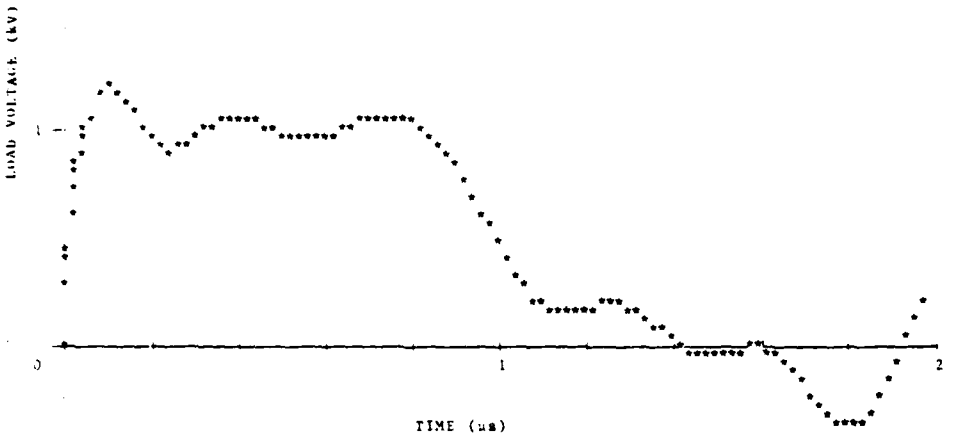


Fig. 6 Pulse of a PFN designed for $r(t) = 1 + t$ using the classical approach.

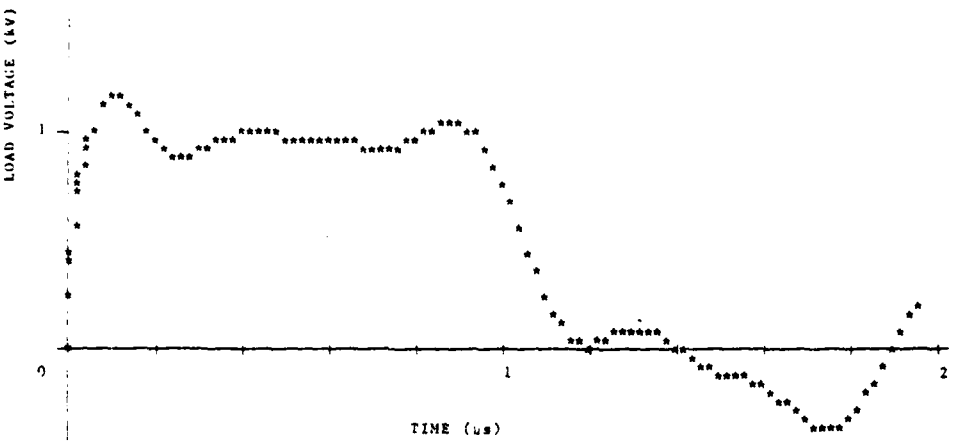


Fig. 7 Pulse of a PFN optimized over one microsecond.

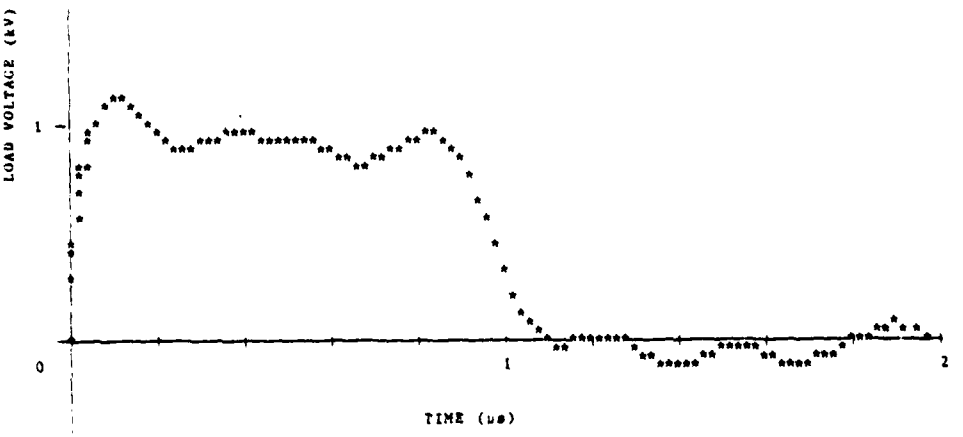


Fig. 8 Pulse of a PFN optimized over two microseconds.

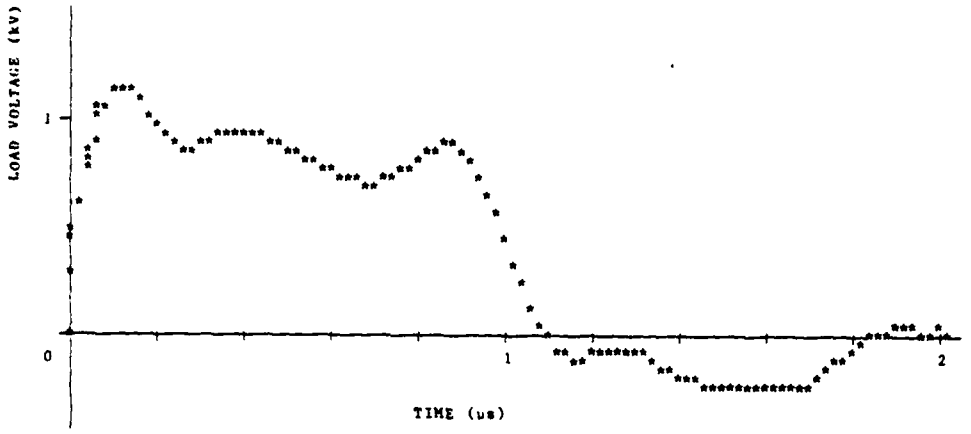


Fig. 9 Response of a PFN designed for $r(t) = 1 + t$ used with the load $R = 1$.

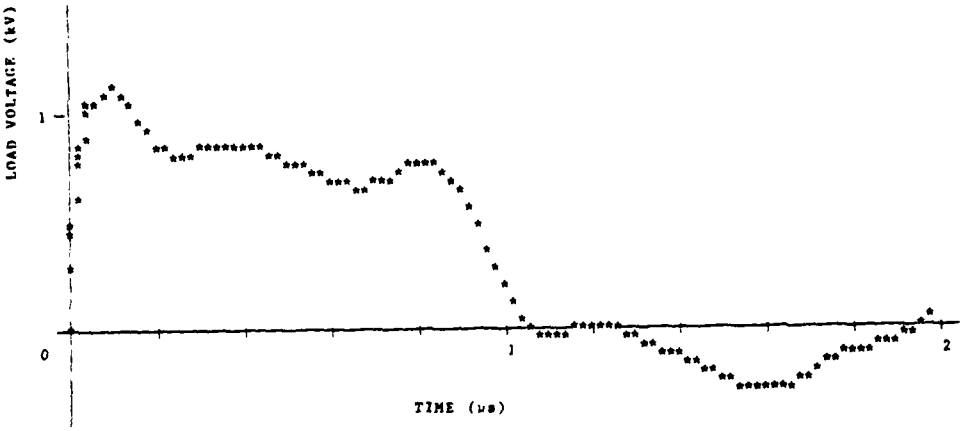


Fig. 10 Response of a PFN designed for $r(t) = 1 + t$ used with the load $r(t) = 1 - t/4$.

PEAK SWITCH CURRENT ENHANCEMENT FILTER

by

James P. O'Loughlin
Air Force Weapons Laboratory
Kirtland AFB, NM 87117

and

William M. Moeny
Tetra Corp
Albuquerque, NM

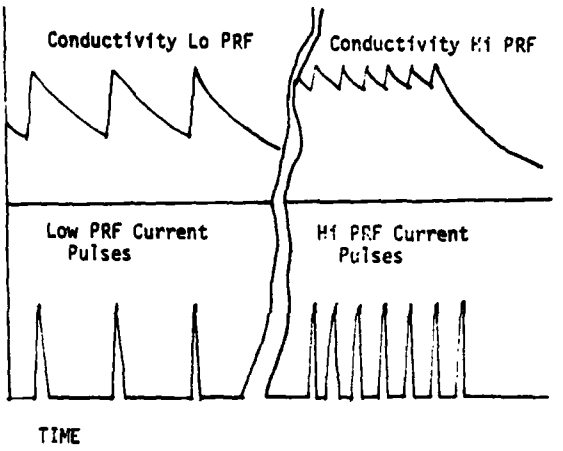
Summary

One method of providing ionization in a controlled gaseous discharge is to apply very short over voltage pulses. The voltage is typically several times the breakdown voltage of the gas but the time duration is less than the arc formation time so a complete breakdown does not occur but the gas is ionized. The level of ionization achieved depends on the total charge or equivalently the peak current delivered during the over voltage pulse. Typical parameters used on one experiment were 50 to 100 nanosecond pulses at 35 KV and repetition rates up to 500,000 PPS. A hard tube modulator was designed and built to deliver up to 200 peak amperes. Later in the experiment higher currents were desired and it was found that by using a peak current enhancement filter it was possible to deliver peak current of 350 amperes to the load while the hard tube modulator was only switching 200 peak amperes. The design and characteristics of such a filter is described in the paper.

Background

In applications such as gaseous electric lasers it is necessary to have a means of providing and controlling the electron number density. This is so because the electron number density determines the gas condictivity and there by the amount of electrical power which may be loaded into a given volume of gas. One method is to shoot high energy electrons into the gas which collide with and ionize gas molecules. (1) A second method is to irradiate the gas with ultraviolet radiation which photo-ionizes the gas. (2) A third method is to apply a high voltage pulse stress to the gas which initiates a Townsend avalanche breakdown, but before the breakdown goes to completion, that is before the formitive lag time expires, the over voltage pulse ends and thus an arc does not occur. (3) During the over voltage pulse the electron number density rises to a high value and then decays after the pulses at a rate depending on the characteristics of the gas. Thus to maintain conductivity of the gas reasonably uniform with time and above a given minimum value the pulse repitition rate of the over voltage ionization pulses must be above a certain minimum rate, Ref Fig 1.

Fig. 1



For a particular experiment on 200° K supersonic N^2 - CO^2 a hard tube modulator was designed and built to deliver 50 to 100 nanosecond 200 peak ampere pulses at 35 KV and at repitition rates up to 500,000 pps in short bursts.

The schematic diagram of the modulator is shown in Fig. 2. The modulator consists of a Velonix Model 590 pulser, the output of which is stepped up to 3000 volts with a pulse transformer and drives ~ (4) parallel 3E29's in a cathode follower configuration which in turn drives the grid of a 4C X 35,000. The screen of the 4C X 35,000 is held at 2500 volts which allows a peak plate current of about 200 amps with about 350 volts positive grid drive. The output of the 4C X 35,000 is capacitively coupled to the gas load. The 2000 V. D.C. sustainer power supply is pulse isolated from the load and 4C X 35,000 with an inductor. It is the purpose of the pulser to establish and maintain the ionization in the gas whereas the major part of the actual power loaded into the gas is provided by the 2 KVDC supply. The effectiveness of the pulse in establishing the electron number density depends almost entirely upon its peak current since the maximum duration of the pulse is limited to less than the arc formation time. The pulse shape, that is the rise and fall times are not critical.

CH1371-4/78/0000-0052$00.75 © 1978 IEEE

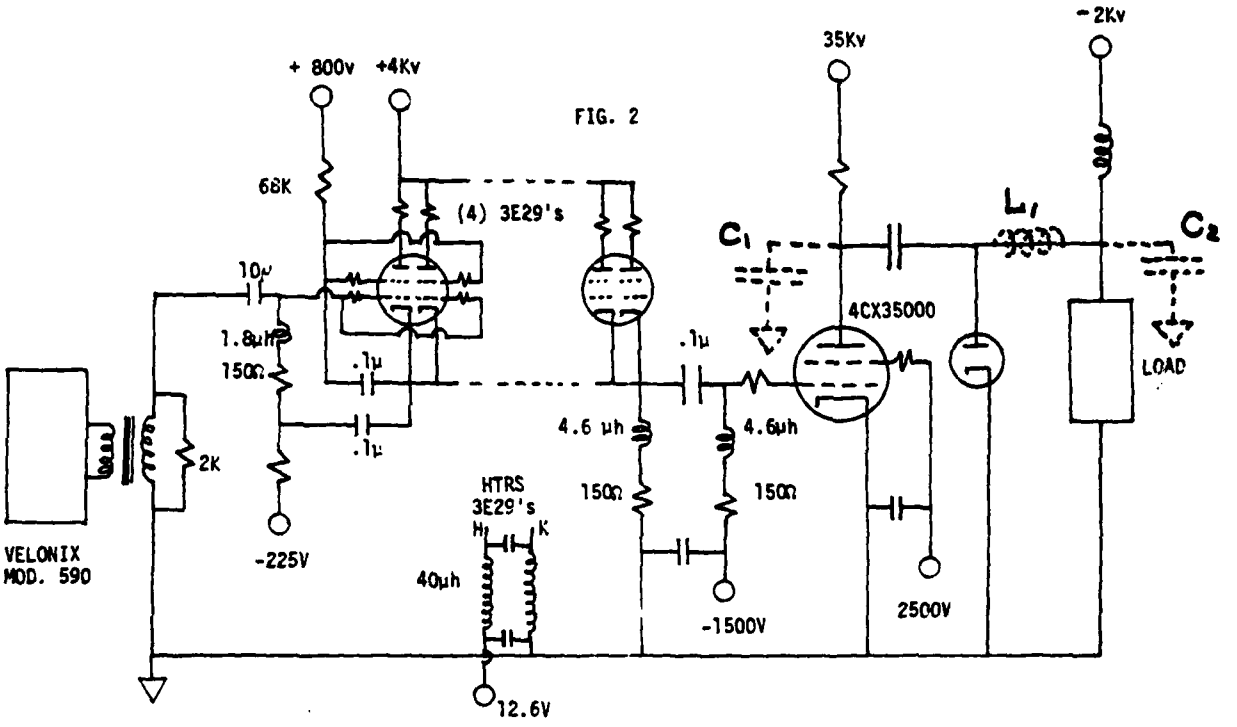


FIG. 2

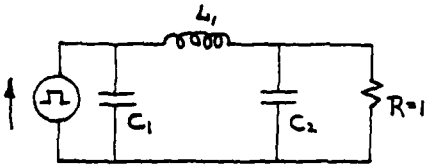


FIG. 3

EQUIVALENT CIRCUIT

$Zo = B * R = B \ (R=1)$

$B = SQRT\ (L_1 * (C_1 + C_2)/(C_1 * C_2))$

$C_2 = A * C_1$

$To = SQRT\ (L_1) * 2 * \pi/B$

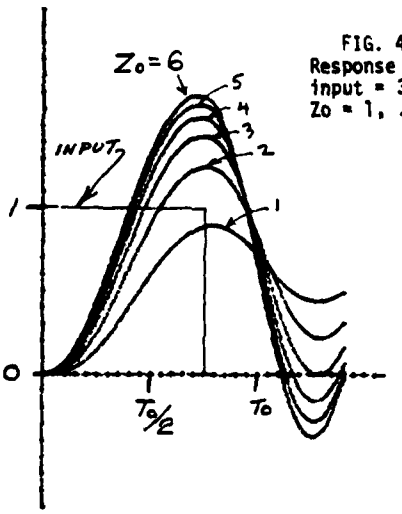


FIG. 4
Response with
input = 3 To /4;
Zo = 1, . . . 6

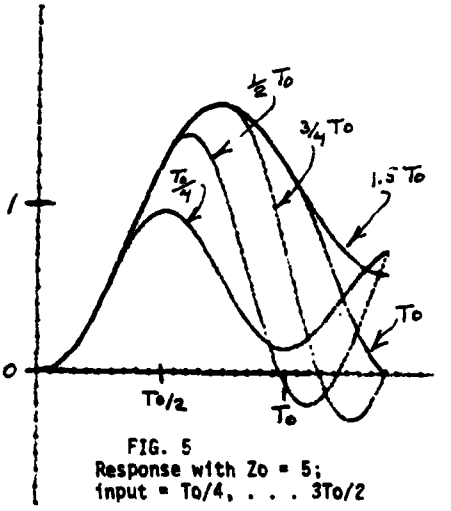


FIG. 5
Response with Zo = 5;
input = To/4, . . . 3To/2

Peak Current Enhancement Filter

It being not uncommonly the case as the experiment proceeded more peak current was desired from the modulator than it was originally designed for. The instrumentation of the installation included current monitors on both the 4C X 35,000 plate and the gas load. It had been observed that the peak current in the load was reading about 10% higher than the peak current in the tube. At first this was attributed to measurement error but accurate calibration of the current sensors and measurements made with the sensors interchanged confirmed beyond doubt that the peak load current was 10% greater than the tube current. This enhancement effect was traced to and explained theoretically by the presence of a pi section filter made up of circuit stray capacitance and inductance between and including the 4C 35,000 and the load. The circuit in Fig. 3 was used to explore the enhancement effect to determine what relationship between the parameters leads to a maximization of the enhancement. This model consists of a unit step current source, a pi section filter of C_1, L_1, and C_2 defining a characteristic impedance, and a load R such that:

(1) $Zo = B*R = B \quad (R=1)$
(2) $B = SQRT\ (L_1*(C_1 + C_2/(C_1*C_2))$
(3) $C = L_1 * B ** 2$
(4) $C_1 = (1 + A) * C/A$
(5) $C_2 = A*C_1$
(6) $To = 2*\pi * SQRT\ (L*C)$

where:

R = normalized one ohm load resistor
Zo = B = normalized characteristic impedance of the pi filter
C = effective series capacitance of C_1 and C_2
A = ratio of C_2/C_1
To = normalized time base
G = enhancement ratio, normalized peak load current

The way this circuit is set up the ratio (B) between the characteristic impedance and load resistance and the ratio (A) between the input and output capacitance can be varied over a range of values and the output peak current (normalized) is the enhancement ratio G.

This circuit was analized by computer over ranges of .1 to 10 for both A and B. It was found that over these ranges the enhancement was not effected more than a few percent by A but did depend on B. The enhancement improved as B increased and is about 1.70 for a B of 6, as shown in Fig. 4. The maximum theoretical peak current enhancement appears to be 2 as one would expect by considering the filter as a transmission line with characteristic impedance Zo terminated in R and driven by a unit source. I_{LN} delivered to the load is:

(7) $I_{LN} \approx Zo*1/(Zo + R) + (Zo - R)/(Zo + R) ** 2)$

Which has a maximum value of 2 as the ratio of Zo/R becomes large.

The response shown in Fig. 4 is for a unit amplitude input pulse width of To*3/4.

In Fig. 5 the effect of changing the driving pulse width is shown for the case of Zo = 5 and for driving pulse widths of .25 to 1.5 times To. The optimum drive pulse width is between .75 and 1.0 times To.

Although the maximum enhancement is 2 for large ratios of characteristic to load impedance it is not usually practical to use ratios greater than three or four due to the fact unreasonable over voltage stresses develop on the switch tube.

If the load resistor is non linear in a manner such that the resistance decreases with amplitude (as a gaseous load) the enhancement effect is in tne area of 10% better than for a linear load.

Conclusions

Based on experimental and theoretical data it is concluded that a current enhancement filter can be realized in a narrow pulse hard tube modulator utilizing in part the stray circuit capacitance and inductance to achieve a peak load current which may be up to twice the peak current switched by the hard tube. This filter is useful in the pulse width and rise time regime where conventional transformers are not feasible to increase the peak current capability of the modulator. Also the performance of the filter on non-linear loads such as a gaseous discharge if in the order of 10% more effective than a linear resistance load.

References:

(1) Douglas-Hamilton, D.H., et al, CO_2 Electric Discharge Laser Kinetics Handbook, AFWL-TR-74-216, AFWL, KAFB, NM p. 57, Apr 75.

(2) Denes, L.J., et al., UV Initiated CO_2 Laser Research, AFWL-TR-76-13, AFWL, KAFB, NM, Jan 77.

(3) Hill, A.F., "Continuous Uniform Excitation of Medium-Pressure CO_2 Laser Plasmers by Means of Controlled Avalanche Ionization", Appl. Phys. Let, Vol. 22, No. 12, pp 670-673, 1973.

A NEW RESONANCE TRANSFORMER

John Harrison

Maxwell Laboratories, Inc.
9244 Balboa Avenue
San Diego, California 92123

Abstract

Resonance systems have been used to provide transformer like voltage step up from a low voltage to a high voltage. However, all early systems have the disadvantage that the voltage gain is limited to the Q of the total circuit (including the load). This imposes a severe gain limit and leads to high line voltage regulation under changing load conditions when the gain is moderate. The circuit described here is a new circuit which overcomes most of these early problems. It provides a gain which is relatively insensitive to the load circuit and is mainly limited to the product of the Q of two resonant loops (i.e., the regulation of the circuit is similar to that of an iron core transformer). Furthermore, several stages can be step or series connected to provide an unlimited potential gain. The circuit is thus a competitor of the iron core transformer, and will be particularly attractive in very high voltage or high frequency circuits where adequate insulation or hysteresis loss becomes a problem.

Introduction

The circuit described in this report is a resonant circuit with characteristics similar to those of a two winding, inductively coupled transformer when it is excited from a steady state a.c. voltage, or current, source. The circuit would have a gain that is independent of the load impedance if loss free components could be used. Thus, the "ideal" lossless version of the circuit performs like an "ideal" two winding transformer. This feature is a major advance over earlier resonance systems that have been used to replace transformers. These earlier systems have a gain that varies with the load resistance. The circuit also has other features that make it superior to earlier circuits. These include:

1. A lower ratio of reactive power in the circuit to the delivered power. The reduction is substantial at high gains.

2. A much higher gain limit for a single stage of the circuit.

3. The elimination of this single stage gain limit through the use of several series connected, or ladder connected, stages. The earlier circuits could not be series or ladder connected to increase their gain limit.

As a result of these improvements, the new resonance transformer can be used as an economic replacement for a conventional transformer in many applications. Furthermore, it can operate at frequencies above the range covered by iron core transformers.

The resonant circuit described here has four basic variations. Furthermore, there is a sub-set of more complex circuits for each of these variations which are expected to be of interest to the community. However, these more complex variants will not be covered in this report.

Resonance Transformer Circuit

Figure 1(a) shows the circuit of the voltage transformer version of the resonance transformer. If we let

$$\omega = \sqrt{\frac{1}{LC}}$$

and

$$Z_o = \sqrt{\frac{L}{C}}$$

the equations for the circuit are

$$\frac{jZ_o}{G(G+1)}\, i_1 + \frac{jZ_o}{G+1}\, i_2 = \sin \omega t \qquad (1)$$

$$\frac{jZ_o}{G+1}\, i_1 + \left[\frac{jGZ_o}{G+1} + Z_L\right] i_2 = 0 \qquad (2)$$

The solution is simple. We subtract G times equation (1) from equation (2) to get

$$Z_L\, i_2 = -G \sin \omega t$$

But $Z_L\, i_2$ is the voltage across the load. Thus, the load voltage has an amplitude of G times the input voltage and is phase shifted by 180°, and the voltage gain, G, is independent of the load.

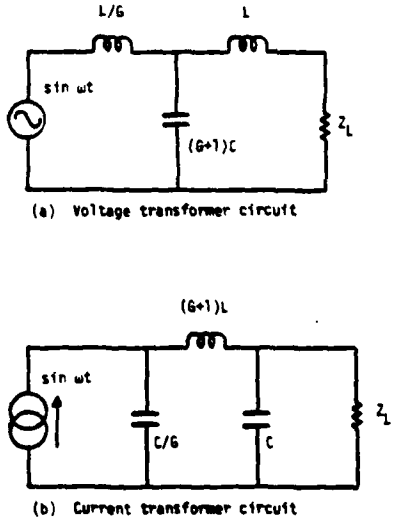


Figure 1. Resonance transformer circuits for voltage and current transformation.

CH1371-4/78/0000-0055$00.75 ©1978 IEEE

The Figure 1(a) circuit has the inverse circuit shown in Figure 1(b). This circuit is a current transformer and provides a gain of G in current that is independent of the load impedance. Both these circuits have reverse circuits in which the inductances are replaced by capacitances of equal impedance and the capacitances are replaced by inductances of equal impedance. The performance of the reverse circuits is similar to the circuits from which they were derived.

The circuits can be optimized for minimum reactive component size by providing phase correction in the load circuit. The optimum load for the Figure 1 circuit should reduce to a capacitor with a capacitance

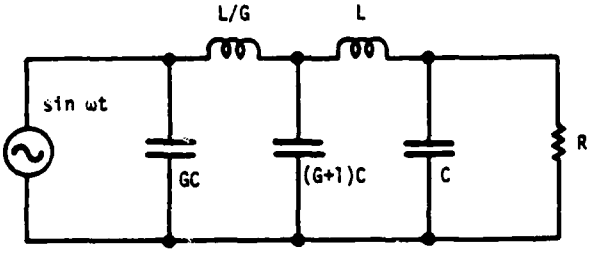
$$C = \frac{1}{\omega^2 L}$$

in parallel with a resistor with a resistance value

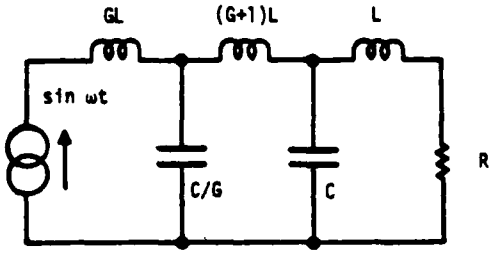
$$R = Z_0 \sqrt{G} \ .$$

The inverse circuit is optimized with an equivalently sized series inductor and resistor.

Finally, the initial and inverse circuits can be power factor corrected so that the input and output power factors are equal by adding a reactor at the input. The resulting circuits are shown in Figures 2(a) and (b).



(a) Voltage transformer circuit



(b) Current transformer circuit

Figure 2. Transformer circuits with added reactances to minimize the reactive energy and provide a unity power factor load on the source when feeding a resistive load.

The sum of the reactive power in the inductors is equal to the sum of the reactive power in the capacitors in the phase corrected optimized circuit. The ratio of the reactive power in the inductors, or capacitors, in this circuit to the active power in the resistive load is

$$\frac{VAR}{VA} = 2\left(\sqrt{G} + \frac{1}{\sqrt{G}}\right)$$

under optimum loading conditions.

This ratio of reactive to active power sets the size of the components, and thus the cost of the circuit for a given rated load.

Some Additional Features of the Circuit

The circuit has some interesting features which can be used to enhance its usefulness or to extend its range of applications. These features are:

1. Equivalent Auto-Transformer

The output of the circuit is phase shifted 180° from the input. The input and output can consequently be connected in series to provide a gain of

$$G' = G + 1 \ .$$

The resulting circuit is shown in Figure 3.

This change reduces the ratio of VAR to VA to

$$\frac{VAR}{VA} = 2\sqrt{G'-1}$$

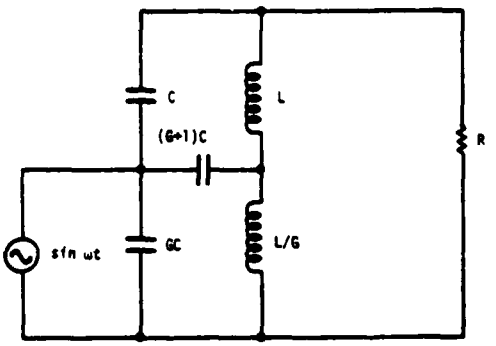


Figure 3. "Auto transformer" version of the Figure 1(a) circuit.

2. Series or Ladder Connection

Several Figure 2 circuits can be series connected to provide a gain of

$$G_T = G_s^n$$

where

G_T is the total gain

G_s is the gain per stage

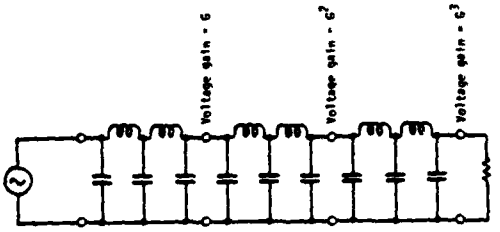
n is the number of series stages.

Similarly, the Figure 3, "auto transformer," circuit can be ladder connected to provide a gain of

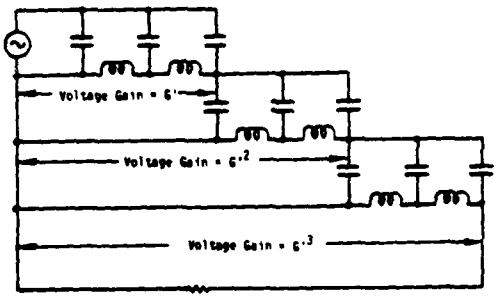
$$G_T' = G_s'^n$$

where the symbols are equivalent to the earlier case. Figure 4(a) and (b) show the resulting circuits.

This series or ladder connection reduces the ratio of VAR to VA when the gain is high. Figure 5 is a plot of VAR/VA against gain for one, two and three ladder connected circuits and demonstrates this effect.



(a) Three series corrected resonance transformer circuits



(b) Three ladder connected "auto" resonance transformers

Figure 4. Cascaded arrangement of resonance transformers used to reduce component size in high gain applications.

3. Power Factor Correction

The circuit can be used to provide the combined service of power factor correction and voltage (current) transformation by selecting the correct circuit form and reducing the VAR in the output reactor. A typical circuit of this type is shown in Figure 6. Here the inverse circuit is used and the inductance of the output inductor is reduced to compensate for a lagging power factor load. It should be noted that this circuit will also compensate for the voltage drop in an inductive connection in series with the load.

This inverse circuit and its associated reverse circuit are most useful in power factor correction applications when the voltage gain is less than unity because then the impedance of the output reactor is greater than that of the load. The Figure 2(a) circuit, and its associated reverse circuit, are most useful when the gain is greater than unity because in this case the admittance of the output reactor is greater than that of the load.

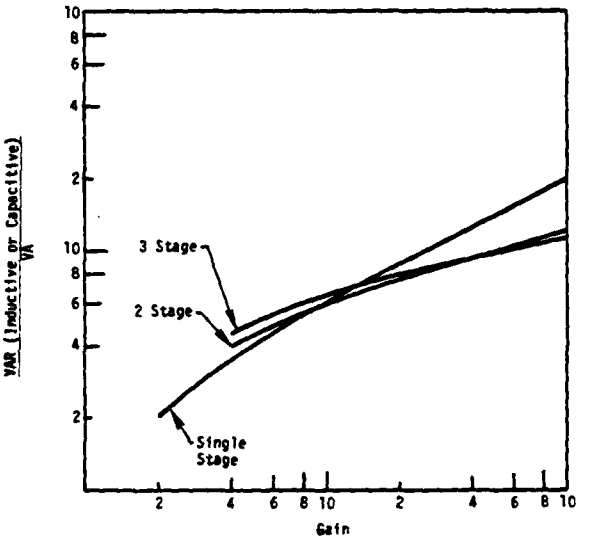


Figure 5. Ratio of inductive, or capacitive, reactive power to power output in lossless "auto" transformer circuit.

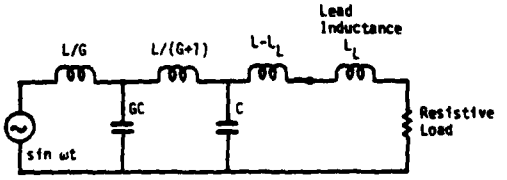


Figure 6. Circuit for combined service of power factor correction and voltage or current transformation.

4. Inverter Commutation

The circuit is a resonant circuit which can be designed to provide a leading power factor at its input terminals by reducing the size of the input reactor. Therefore, it meets the design requirements for a filter circuit to series commutate an inverter circuit, and can provide the combined service of voltage step up and series commutation of an inverter. The current transformer version, the Figure 2(b) circuit, may prove to be the best for inverter applications where a step up in voltage is required because then the impedance of the input reactance is

higher than the input impedance under optimum loading conditions. If the input inductor of this circuit is omitted, the input power factor is leading whenever the series inductance in the output circuit is less than (1 + G)L, a condition which should be easy to design into a system. The optimum value of this inductor is L, and with this value of output inductance the power factor is leading and the circuit is current limiting. This series commutating resonant circuit will, in most applications, be lighter than the circuit it replaces.[1]

5. Combined Use with a Two Winding Transformer

The circuit can be used in combination with a standard two winding transformer to reduce the mutual reactance required in the transformer and reduce the circuit regulation. Figure 7 shows a typical circuit of this type. Here the mutual inductance of a transformer replaces the shunt inductance of the central shunt inductor of the reverse circuit of Figure 1(a).

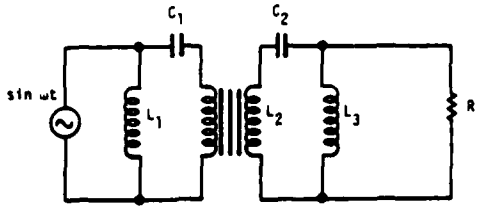


Figure 7. Variant of resonance system using a two winding transformer to provide part of the gain.

Component Loss Considerations

We will now consider how the circuit performs when real components, with losses, are used. This subject has only been studied with a series resistance in each reactive element using the circuit shown in Figure 8. This circuit shows the reactive impedances as X_n and the real impedances expressed in terms of the dissipation factor of the reactive elements. The reactive element type can be either that shown in Figure 1(a) or the equivalent reverse circuit reactors can be used. The circuit is terminated with the appropriate minimum energy output reactance. The results of the following analysis apply equally to the inverse circuits.

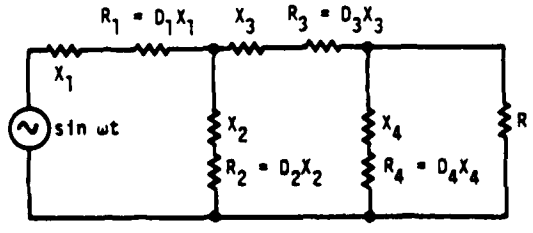


Figure 8. Circuit used in loss/gain analysis.

[1] MLR-601, "High Power MHD System Technical Memorandum, Technical Discussion of Resonance Type Voltage Step Up Systems", 1 December 1976.

The first order - neglecting D^n terms of higher order than unity and GD^n terms of higher order of D than 2 - equation for the actual gain is

$$G_A = \frac{GR\ \{1+j(D_2+D_4)\}}{\{G(D_1+D_2)+D_2+D_3-jG(D_1+D_2)(D_3-D_4)\}Z_o}$$

$$+ \{1+G(D_1+D_2)(D_3+D_4)-j(D_1-D_2-D_3-D_4)\}R$$

Here the loss term is stated in terms of the dissipation factor $D = (1/Q) = (R/\omega L) = \omega CR$ and the omitted D^n terms are in the form $D_\ell D_m$ or $D_\ell D_m D_n$.

The no load/full load regulation can be calculated using this equation and setting $R = \infty$ for the no load condition and $Z_o = R/\sqrt{G}$ for the full load condition. Figure 9 shows the resulting regulation for a single and two stage figure 2(a) circuit when the dissipation factor of the inductors is 0.02 and the capacitors 0.0025.

Lower regulation is obtained if the dissipation factor is lower, and when

$$\frac{Z_o}{R} < \sqrt{G} \quad .$$

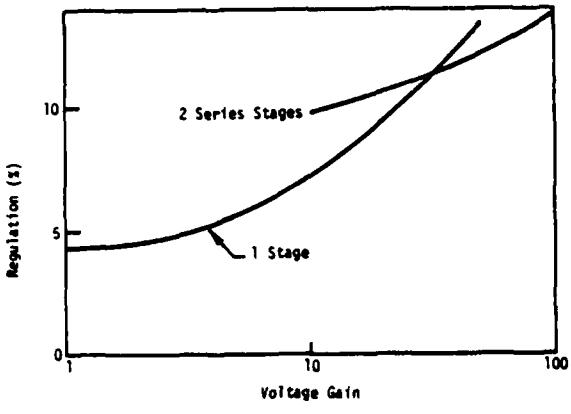


Figure 9. Regulation of single stage and 2 series stages of the Figure 2(a) circuit plotted against gain when inductors with a dissipation factor of 0.02 and capacitors with a dissipation factor of 0.0025 are used.

Comparison with Earlier Resonance Circuit

The resonance circuit shown in Figure 10 has been used for many years to obtain resonant gain under steady state a.c. conditions. The open circuit gain of this circuit is G if lossless components are used when

$$\omega = \frac{1}{\sqrt{LC}}$$

The performance of this circuit can be investigated using the variables

$$Z_o = \sqrt{\frac{L}{C}}$$

and

G_A = the actual gain .

This circuit has several fundamental limitations. The first limitation is that the open circuit gain limit is the Q of the resonant circuit where

$$Q = \frac{1}{D_1 + D_2} \quad .$$

The gain limit when the circuit is loaded is

$$G_A = \frac{R_3}{Z_o}$$

This gain is only approached when

$$G = \infty$$

and

$$Q >> \frac{R_3}{Z_o}$$

This ratio of the reactive energy in the output reactor and the active energy is

$$\frac{VAR\ (X_2)}{VA} = \frac{R_3}{Z_o} > G_A$$

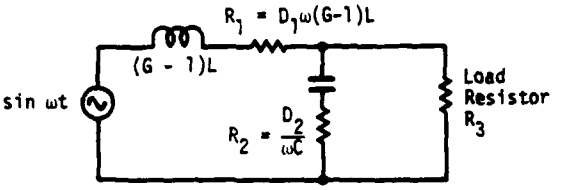


Figure 10. Conventional resonance system used for obtaining a resonant voltage gain.

The overall effect of these various features is to make a low regulation (∿10%), reasonable gain (G > 5) circuit heavy and expensive. For instance, a conventional resonance system with a gain of 5, built with inductors with Q = 50 and capacitors with Q = 400 must be twice as heavy as the new resonance system if the no load/full load regulation must be less than 10%. The new circuit would have a 6% regulation with equal components. As the gain increases the advantage in using the new system increases rapidly.

Conclusion

This paper has described a new resonance transformer that has characteristics similar to those of a two winding inductively coupled transformer. The resonance circuit can be designed to provide either current or voltage transformation, and can combine its transformer duty with power factor correction.

The circuit is a viable competitor to a conventional transformer, and is likely to prove to be superior to a conventional system in many applications.

SOLID STATE CLIPPER DIODES FOR HIGH POWER MODULATORS

By

Stephen Levy and John E. Creedon
Electronics Technology and Devices Laboratory
USA Electronics R&D Command
Fort Monmouth, New Jersey 07703

Summary

End-of-line solid state clipper diodes are essential to high power pulse modulators. These diodes are chosen to reduce the potentially damaging inverse network and switch voltages which occur when the load is less than the network impedance; especially when non-constant loads are encountered. The choice of the clipper diode stacks for a megawatt (MW) average power pulser resulted from a study of commercially available units. Destructive tests of available units gave a figure of merit of 300:1 for the maximum single shot 10 microsecond (μs) current pulse to diode rated average current. A 150 ampere (A) average current diode was chosen for the 20,000 A worst case expected in the MW pulser giving a current safety factor of better than 2:1. For the 40 kilovolt (kV) pulser operation at a 1.5:1 voltage safety factor required 60 of the 1.0 kV diodes in series. A snubber capacitor and resistor across each diode provided equal voltage division and transient turn-on protection. Transient response of the snubber protected diode stacks was modeled at low powers and later confirmed in actual MW pulser operation.

Introduction

High power line-type modulators require end-of-line clippers to protect circuit components from overvoltages due to short circuits in the load. The major components susceptible to damage are the Pulse Forming Network (PFN) capacitors, and the thyratron switch. A substantial amount of damage occurs at the anode when the thyratron is subjected to inverse voltage. One study[1] reported that the power dissipated on the tube anode varies as the square of the peak inverse voltage and that the anode "hole drilling" occurs in the approximately first 50 nanoseconds (ns) of inverse.

The large MW tubes with their lower gas pressure and commensurately longer fall of anode potential, are particularly susceptible to inverse dissipation. Voltage reversal can severely damage high energy density pulse capacitors. Life expectancy of a capacitor will decrease by a factor of 2 with only a 30 percent voltage reversal. It has been shown that in a thyratron line-type modulator the inverse voltage will be as much as 1.5 times the initial PFN voltage in the worst case of a shorted load.[2] On the other hand it is customary to design the modulator with a load impedance slightly smaller than the network impedance to produce a small negative voltage on the thyratron. The approach is to apply just enough inverse to allow the thyratron sufficient time to recover and at the same time, prevent large inverse voltages from occurring.

The most effective protection technique is the end of line (matched) clipper. A schematic of the matched end of line clipper is shown in Figure 1. The circuit consists of a diode stack and a resistive load where the resistive load is chosen equal in magnitude to the network impedance. The choice of the diode stack depends on the following factors:

a. worst case forward current
b. worst case inverse voltage
c. power dissipation
d. diode recovery

Forward Current

It was decided that parallel operation of diodes was inadvisable as the ballast resistors needed to insure proper current sharing would be impractical at the tens of kA level. The alternative was to try to find a single diode capable of handling the worst case current. For a matched clipper diode the maximum current would occur if both the modulator load R_L and the clipper load R_c were shorted. The currrent would be

$$I_p = \frac{epy}{[Zo]} \qquad (1)$$

where epy is forward anode voltage, and [Zo] magnitude of PFN impedance.

For an epy of 40 kV and a [Zo] of 1 ohm, the peak clipper current would be 40 kA. Ignoring higher order current reflections the diode chosen must be capable of sustaining 40 kA for 10 μs pulse. Our diode selection began with destructively testing diodes of different average current ratings to find if this rating would relate to its peak current handling capacity.

The test consisted of pulsing individual off-the-shelf diodes at a given current level with a 10μs pulse repeated every 5 seconds for 10 shots. After checking the diode the current was increased to its next level usually in 1 kA steps. The results are shown in Figure 2. From the best-fit-line a diode with an average current rating of greater than 75 A would be required to survive a 40 kA pulse.

Worst Case Inverse Voltage

The next most important factor is the maximum reverse voltage (epx) the stack will sustain under the worst conditions. This is when the modulator load becomes shorted and the clipper load opens. This voltage, epx, has been shown to be as much as 1.5 times epy. For a charging voltage of 40 kV the "diode" would be capable of sustaining a reverse voltage greater than 60 kV. Of course there is no one solid state diode capable of meeting this need therefore a series stack of diodes is required.

Ideally, enough diodes can be connected in series where 60 diodes with 1 kV hold off could sustain a 60 kV voltage indefinitely. In practice the reverse leakage i_R and the junction capacitance Cs of individual diodes differ significantly. Both I_R and Cs are temperature and voltage dependent. Stacked diodes require both resistive and capacitance compensation to overcome individual variations. An equivalent circuit for the series stack is shown in Figure 3.

U.S. GOVERNMENT WORK NOT PROTECTED BY U.S. COPYRIGHT.

In this figure R_F is the equivalent forward resistance of the diode, R_R is the resistance equivalent to the leakage resistance, Cs is the diode junction capacitance and C_G is the diode capacitance to ground. In our design the worst case diode leakage (T = 200°C) was 15 milliamperes (mA) at 1 kV. A resistor equivalent to 1/2 this value was selected to parallel each diode. The worst case voltage division would then divide as V_1 = 870, V_2 = 1130. Without resistive compensation the voltage would divide as V_1 = 462V and V_2 = 1538 V.

The diodes are rated at 1000 volts (V) reverse with a maximum instantaneous peak reverse voltage of 1300 V. With resistive compensation the diode would survive, however, it would fail without it.

The diode junction capacitance and stray capacitance affect the voltage division whenever the voltage rises or falls. The junction capacitance can change significantly from diode to diode. A recent article[3] stated for one type of high power rectifier the reverse recovered charge Qrr stored in the junction while it passes from forward to reverse bias, can vary by more than 300 percent. For diodes with different values of Qrr the shunting capacitors provide a current path for the stored charge to dissipate. Additionally, the external shunt capacitance must be chosen large enough to swamp out all values of junction capacitance. In the case of our clipper stack the shunt capacitor was chosen to be 100 times the typical device junction capacitance when measured at 10 V.

Power Dissipation - Worst Case

The power dissipation of the individual stack diodes is important to the determination of the cooling required. The "worst case" philosophy was used in designing the stack mounting.

In the MW modulator the "worst case" conditions which would effect the diode dissipation are:

Shorted load, system shut-down time is 16 milliseconds (ms)

epx = 40 kV PIV

Ip = 20,000 A

t_o = 10 µs pulse width

prr = 125 pps

The forward power loss per diode is[4]:

$$P_{fwd} = Eo\ I_{av} + I^2\ rms R \qquad (2)$$

where

P_{fwd} is forward power loss per diode

E_o and R are emperical constants representative of the diode selected

I_{av} is average current in the forward direction, and

I^4rms is the root-mean-square forward current through the diode

The diode chosen for the MW modulator was the 1N4594 which had an E_o of 0.825 and R of 0.0008. For the case of the shorted load the average current, I_{avg} is:

$$I_{avg} = Ip \frac{to}{T} \qquad (3)$$

where

to, pulse width is 10 µs,

Ip is the peak current, 20 kA, and

T is the pulse period, 8 ms

I_{avg} = 25 A and the square of rms current, I^2rms, is:

$$I^2rms = Ip^2 \frac{to}{T} \qquad (4)$$

$$I^4rms = 5 \times 10^5\ A^2$$

Then the forward power loss per diode is:

$$P_{fwd} = 0.825 \times 25 + 5 \times 10^5 \times 0.0008$$

or

P_{fwd} = 420 W in the case of a shorted load where the modulator will be operating for 16 ms (2 pulses).

According to the manufacturer this forward power dissipation is equivalent to an average sinusoidal forward current of 380 A which is comparable to maximum power dissipation of 560 W. For sinusoidal operation the peak power to average power dissipation is 3.14;[5] therefore the maximum (sinusoidal) peak power capacity of the modulator clipper diode is

$$560 \times 3.14 = 1758\ W$$

This is a sinusoidal equivalent to the individual diode power dissipated when conducting 20 kA for a 10 µs pulse operating at 125 hertz (Hz) rate for 2 pulses.

To verify if the chosen diode can handle this peak power, this value of 1758 W must be compared to the peak power diode heat dissipation.

The peak power in the diode produces a transient heating effect which if beyond the capacity of the diode to absorb or conduct this heat away, will destroy the unit. Again, the manufacturer provides curves of effective transfer thermal impedance for various operating times. At an ambient of 16°C and for 16 ms duration the junction to case thermal impedance is 0.09 maximum. Then the peak power that can be dissipated in the diode is limited by the maximum junction temperature of 200°C by the relationship[6]

$$P_{peak} = \frac{200 - Transient}{r_{(t)}} \qquad (5)$$

$$Peak = \frac{200 - 16}{0.09} = 2044W$$

Therefore, the diode selected for clipper operation meets the manufacturer's power handling requirements.

Power Dissipation - Normal Operation

The diodes ordinarily can dissipate 40 W each. The chosen diodes are designed to dissipate 40 W mounted in the stack in air. The normal operating

clipper current for each MW module is 8 kA. Each series stack of 60 diodes will have an average current of 5 A and an I^2rms of 2×10^4 A^2. Then the normal forward power per diode equals 20 W and the sinusoidal equivalent peak forward power would be close to 400 W. For air cooling of the diode stacks where the ambient temperature is 16°C, the diode manufacturer suggested 150 linear feet per minute through the stacks. The air flow requirement was factored into the modulator design.

Diode Recovery

The recovery of a forward-biased to a reverse-biased diode is a 2-fold process.[7] When a diode is suddenly reversed from the forward direction, the current will not immediately drop to its steady-state reverse-voltage value, I_s. It can only reach this value after the excess minority carriers are swept out of the junction, or recombine.[8] During this time the diode will conduct easily with a value determined by the external circuit impedance. Once the excess carriers are swept back across the junction, the diode voltage can begin to reverse and the diode current can drop. This period of time is called the storage time t_s.

The second part of the recovery process is called the transition time t_t, and this interval extends from the end of the storage time t_s, until the junction capacitance has been charged to the reversed-bias voltage.

Figure 5 shows the voltage and current waveforms illustrating these points. It has been shown that the storage time increases with larger forward currents; also larger reverse currents reduce storage time. A relationship expressing this is:

$$t_s = \tau \ln \left(1 + \frac{I_F}{I_R}\right) \qquad (6)$$

where τ is called the effective lifetime.

The transition time, t_t, is a function of the junction capacitance C_t and will be reduced by increasing reverse bias. According to 5(a) the estimate of t_t is $3R_LC_T$. When the capacitance is small the diode recovery can be low ns range.

A negative mis-match will cause a rapid voltage reversal on the end-of-line clipper diode stack. If the stack load were to be shorted or underdesigned then the combination of rapid voltage reversal and high reverse currents can destroy the diode stacks.[9]

Megawatt EOL Clipper Design

The clipper design chosen was based on a Westinghouse diode stack consisting of 20 each IN4594 diodes with a 30 K ohm, 10 W resistor and a 0.1 microfarad (μF), 1 kV dc capacitor across each diode.

In the first design, the clipper diode assembly, Figure 6, consisted of 3 stacks in series. Each assembly had a mating one ohm clipper resistor in series. The one ohm clipper resistor had four Carborundum type number 890 SPIROLT resistors in a series parallel combination. Originally each diode-resistor assembly was designed to parallel each of the two module PFNs. Figure 6 shows the two assemblies for a MW module housed in a fiber glass-bakelite box. The end is removed to show the interior. With the end in place, the 3 fans forced approximately 750 cubic feet per minute of 15°C air into the box plenum. The air escaped through 4 centimeter (cm) diameter holes adjacent to individual diodes. The air velocity escaping all holes was greater than 200 linear feet per minute which surpassed the manufacturer's recommended limits. This design provided a non-repetitive inverse voltage safety factor of 2, an operating voltage; safety factor of 1.5 and a current safety factor of 4. It was thought that if one diode-resistor unit opened the other PFN unit could withstand the combined fault.

A second design used two diode stacks (cut into 4 sections of 10 diodes each) in series. The clipper load resistor consisted of eight Carborundum washer resistors (0.25 ohms each), type No. 916WSR25L, stacked in a series-parallel combination to give 0.5 ohms. A view of this EOL clipper assembly is shown in Figure 7. This unit has a non-repetitive voltage safety factor of 1.3 and a current safety factor of 2.

Performance of Clipper Circuits

Normal operation of the MW modulator at an epy of 10 kV is shown in Figure 8. The anode voltage fall and load current rise occur simultaneously. The clipper current trace was subject to pick-up during the main current pulse. Ignoring the false positive-going current signal, the clipper current is seen as a series of oscillations with a period equal to the PFN pulse width of 10 μs and a maximum peak of 500 A. The anode waveform suggests that the inverse voltage never exceeds 500 V. A theoretical verification of the clipper oscillations is found in Reference 1. The question of what happens when the clipper load shorts is shown in Figure 9. There is no noticeable change in anode voltage waveform. Actually the tube current waveform looks improved. The first three clipper current peaks increased with the second peak increasing more than the first. Comparing the second peak to the second clipper current peak in Figure 8 shows a 2.5 times increase when the clipper load is shorted. The waveforms of Figure 10 were taken with both the modulator load and the clipper load shorted. In Figure 10 the anode voltage waveform shows an inverse voltage of 1.5 kV occuring 20 μs after the tube current pulse. The peak clipper current is 8 kA for a epy of 10 kV. The peak tube current is 5 kA. The tube for this worst case does show some inverse conduction at the peak of the first clipper current oscillation. After this point the tube current always stays in the forward direction and the clipper diodes continue to pass high currents in an attempt to dissipate the energy stored in the PFN. Figure 11 shows the diode clipper stack voltage and current for both the main load and clipper load shorted. This figure shows a definite phase difference in the voltage and current waveforms. From the 20 kV trace, the diode voltage is 4 kV when the current is zero and the slope of current is 2.4×10^9. When the current is zero then the voltage must be inductive. The estimated inductance is:

$$V = L \frac{\Delta_i}{\Delta_t} \qquad (7)$$

$$L = \frac{4 \times 10^3}{2.4 \times 10^9} \sim 1.7 \text{ microhenries}(\mu H)$$

The individual diode package is the DO.8 which has a flexible stranded lead which is 0.660 cm in diameter and 6.86 cm long. A solid copper wire with the same number of circular mils has a diameter of 0.583 cm. The self-inductance of 60 diode leads can be calculated from [10]

$$L = 0.002\ell \left[\ell n \frac{4\ell}{d} - 3/4\right] \qquad (8)$$

where

ℓ = length of diode lead in cm,

d = lead diameter in cm, and

L = self-inductance of a diode in μh

$$L = 0.002 \times 6.86 \left[\ell n \frac{4 \times 6.86}{0.583} - 3/4\right]$$

L = 0.042 μh per diode; then 60 diodes would have a self-inductance of 2.55 μH. This is fairly good agreement with the observed inductance.

Lastly compare a gas tube clipper, two 7890s in parallel, to the diode stack in Figure 12. The hydrogen filled triodes have inherently low inductance and could be thought to represent an ideal diode stack. The forward voltage drop of the gas tubes is only 1 kV peak while the diode stack has a 4000 V forward drop. For an epy of 10 kV with a shorted modulator load the gas clippers pass 10 kA peak which is what would be expected from a 0.5 ohm network and a clipper load of 0.5 ohm. The diode stack on the hand passes only 6 kA under the same conditions. The efficiency of the solid state diode stack can be improved.

References

1. Final Report, EG&G Inc., DA 36-039, SC-15372, "Research Study on Hydrogen Thyratrons,", pp. 101-104, June 1963.

2. Bulletin No. 401, Maxwell Laboratories, Inc., Feb 15, 1960.

3. Electronic Design, No. 5, pp. 50-53, Mar 1976.

4. Westinghouse, High Voltage Silicon Rectifier Designer's Handbook, pp. 7-36, 1963.

5. Motorola, Silicon Rectifier Handbook, pp. 3-6. 1971.

6. D. N. Vorotnikova, and G. I. Grebennikov, "Thermal Resistance of High-Power Semiconductor Devices in the Pulsed Mode of Operation," Akademiia nauk Azerbaidzhanskoi SSR, doklady vol. 27, No. 3, pp. 23-25, 1971.

7. J. Millman, and H. Taub, Pulse, Digital and Switching Waveforms, McGraw-Hill, pp. 749-759, 1965.

8. R. A. Smith, Semiconductors, Cambridge Press, pp. 444-6, 1961.

9. Westinghouse, High Voltage Silicon Rectifier, Designer's Handbook, pp. 7-47, 1963.

10. F. W. Grover, Inductance Calculations, Van Norstrand & Co., pp. 35, 1946.

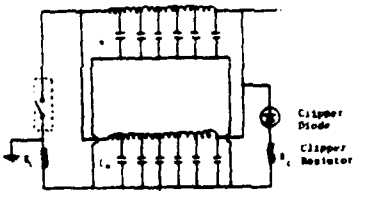


Figure 1. Modulator Circuit Showing EAK Clipper Circuit

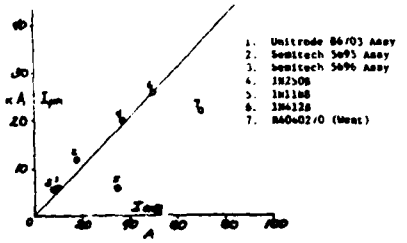


Figure 2. Peak 10 μs Pulse Current Resulting in Diode Failure Versus the Rated Diode Average Current for a Selection of Power Diodes. Diodes Pulsed Once Every 5 Seconds for 10 Shots Before Raising Current Level.

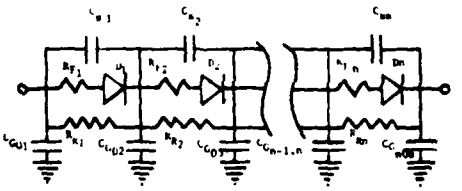


Figure 3. Equivalent Circuit for Diode Series String (diode lead inductance not shown)

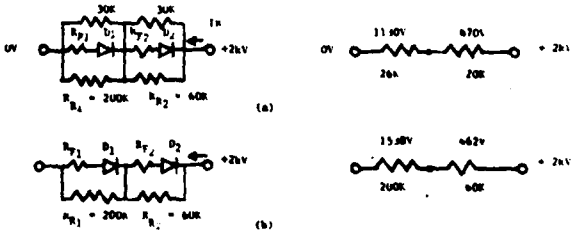


Figure 4. The Effect of Resistive Compensation on Voltage Distribution in a Two Diode Series String. (In (a) resistors were used while in (b) they were not.)

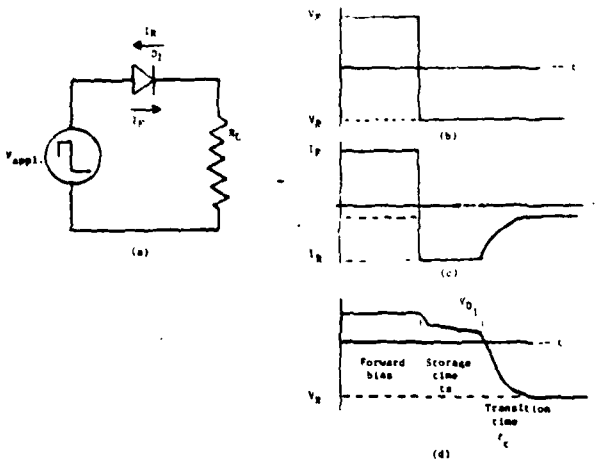


Figure 5. Stages of Diode Recovery: The waveforms shown in (b) is applied to circuit (a) with the resulting current (c) and diode voltage (d) waveforms.

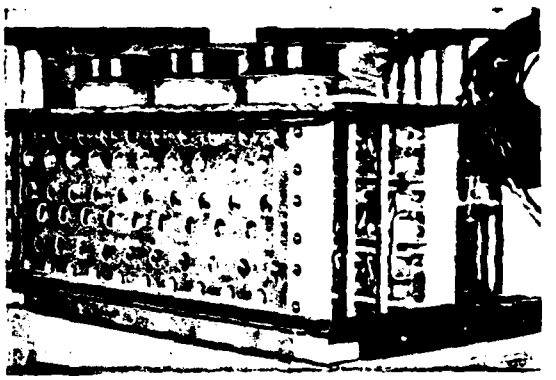


Figure 6. Original Megawatt Module EOL Clipper Diode Stacks and Housing

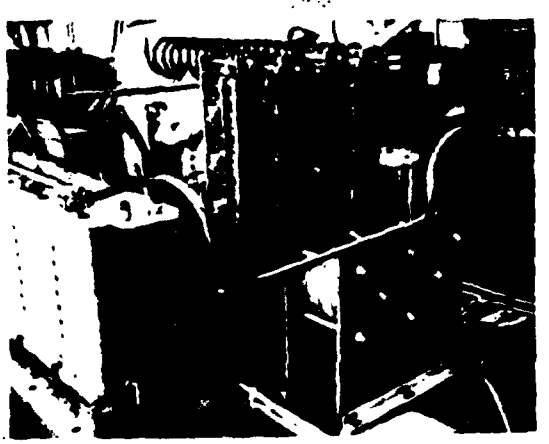


Figure 7. Other Megawatt Module with the 4 EOL Clipper Stacks, Clipper Load Connected to the Rear of the PFNs

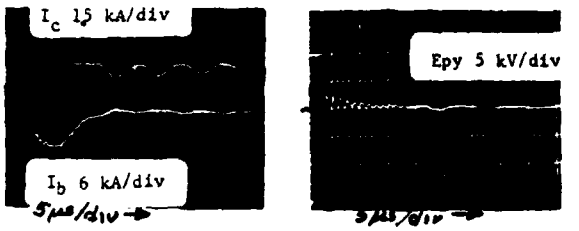


Figure 8. Normal Operation of the Modulator (R_c = 0.5Ω, R_L = 0.5Ω)

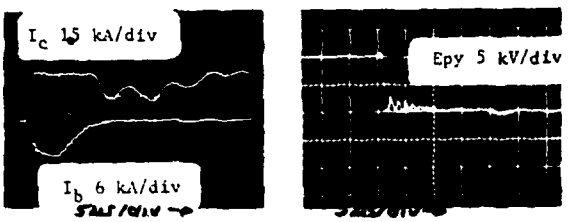


Figure 9. Modulator Operation with EOL Clipper Load Shorted (R_L = 0.5Ω)

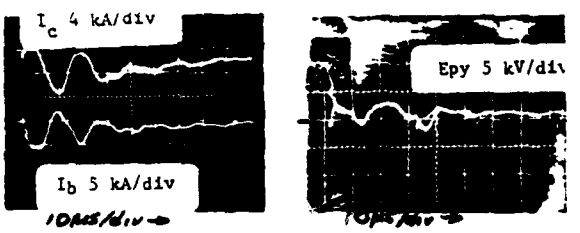
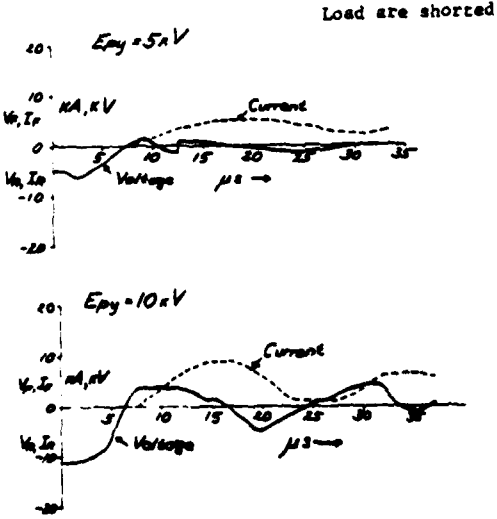


Figure 10. Modulator Operation with EOL Clipper Load and PFN Load Shorted

Figure 11. Solid State Diode Clipper Assembly Voltage and Current Waveforms at Various Epy: PFN Load and Clipper Load are shorted



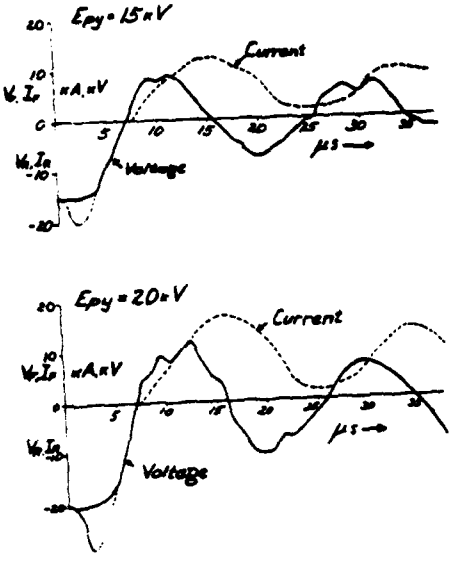
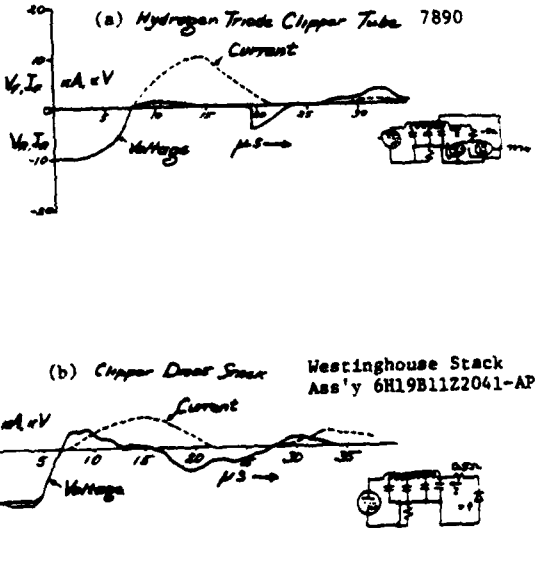


Figure 12. Comparison of Gas Tube Clipper and a Solid State Diode Stack at an Epy = 10 kV with the PFN Load Shorted.



LOW INDUCTANCE, LOW IMPEDANCE MEGAWATT AVERAGE POWER LOAD

William Wright Jr.
Electronics Technology and Devices Laboratory
USA Electronics R&D Command
Fort Monmouth, New Jersey 07703

Summary

A compact, low inductance, one-half ohm, one megawatt average power resistive load has been developed to facilitate testing of the MAPS-40 Thyratron. The flowing liquid electrolyte system uses the large thermal mass of a storage tank of electrolyte to store the energy which is dissipated through a heat exchanger after the high power run. The electrolyte starting temperature, flow rate, and allowable temperature rise determine the maximum average power into the load; the external and internal spacings and flow uniformity determine the maximum peak power; and flow rate and storage volume determine maximum running time. The load assembly consists of two parallel glass pipes 10.2 centimeters (cm) in diameter and 15.25 cm long. The active volume in each pipe is 6.35 cm long and is contained between electrodes 8.9 cm in diameter. The two sections of the load are electrically in parallel and flowing in series, putting both flow connections at ground potential. The major problem was getting the internal flow pattern uniform to eliminate local boiling and arcing across the bubbles while keeping the pressure drop low and flow high. The calculated inductance of the load assembly is 11 nanohenry (nH), and the structure lends itself to coaxial connections which reduce the overall inductance still further. Material compatibility with the electrolyte will be discussed.

Introduction

Liquid electrolyte resistors have been used in experimental modulator setups for many years.[1,2] They offer a wide range in resistance value (at least 5 orders of magnitude), flexibility in physical design, high energy absorption in a compact structure, high voltage stress, and are amenable to low inductance design. They are often easy to design and build, sometimes even trivial, and the resistive medium is forgiving, as opposed to solid resistive substances which are often damaged by overheating or overstressing. Most of the liquid resistor applications have been either single-shot or very low average power where natural cooling is sufficient to dissipate the energy. A liquid resistor for high average power, however, presents some problems.

The load described here was developed to facilitate testing of adiabatic mode modulator components (capacitors, PFN's, thyratrons). The requirements on the load were 20 kilovolt (kV), 10 microsecond (μs) pulse length, 1.0 megawatt (MW) average power, and resistance matched to PFN impedance (0.5 ohm) to within a few percent over the run time of 1 minute. The variation of electrolyte resistivity with temperature (approximately 0.8 percent per degree Celsius (°C) at 30°C), and the requirement of nearly constant resistance would have required and extremely large volume of electrolyte in a noncirculating resistor (over 4000 liters (l)), and a heat exchanger to dissipate the energy during the run would have been impractical, therefore the approach used was to build a circulating load, store the energy in the heated electrolyte and dissipate the heat during the time between runs. This approach uses the difference between the short-term average power (during a run) and long-term average power (over a period of hours) to make the heat exchanging task manageable. The system never reaches thermal stability during a series of runs but is always either heating up or cooling down.

Design Considerations

The electrical energy is deposited in the electrolyte between the electrodes in the resistor. The flow, power input, and temperature rise are related by:

$$P = 70.1\ F\Delta T,$$

where P = input power, watts
F = flow, l/min
ΔT = temperature rise, °C

When the average power is high and the peak power is moderate, the exit temperature may safely approach 100°C. However, when the peak power is also high, 800 MW in this case, high voltage stress and local boiling lead to breakdown across the steam bubbles which could cause the energy to be dissipated in a small volume, rather than uniformly, with explosive forces being generated. For a given input power and flow rate, the exit temperature depends on the entrance temperature, which is the temperature of the electrolyte in the storage tank after the cool-down cycle. For effective heat exchanging, one would like the final electrolyte temperature after cooling to be high, but for an adequate safety factor in avoiding local boiling, this temperature should be low. The required volume of electrolyte must be enough to supply cool electrolyte to the resistor for the duration of the run, allowing for a warm zone in the storage tank where the returning hot electrolyte mixes with the cool electrolyte. This warm zone can be minimized by paying attention to the flow pattern of the electrolyte return.

One of the major advantages of working in this thermal transient mode is that the rate of final energy disposal, heated city water down the drain in this case, depends only on the long-term average power, and the heat exchanger can be minimized consistent with the number of runs desired per day.

In the design of a low impedance load, one important factor is the minimum value of electrolyte resistivity. While others have used sodium chloride, nickel chloride, ammonium chloride, potassium dichromate, sodium thiosulfate, and probably a host of others, I have found that copper sulfate and sulfuric acid in water to be suitable. A concentration of 60 grams (g) hydrous copper sulfate ($CuSO_4 \cdot 5H_2O$, blue) per liter of water gives a resistivity of 70 ohm-cm at room temperautre and is about a factor of 5 away from saturation, which ensures easy dissolving, and no problems with the solute coming out of solution. The resistivity is then adjusted to the desired value by adding small amounts of concentrated sulfuric acid: about 1 percent reduces the resistivity to 12 ohm-cm.

U.S. GOVERNMENT WORK NOT PROTECTED BY U.S. COPYRIGHT.

Detailed Design

The load assembly, shown in Figure 1, consists of two resistors, electrically in parallel but flowing in series. This puts both hose connections at ground potential and prevents current flow through the electrolyte filled hoses. Each resistor is a 10.2 cm diameter, 15.25 cm long pyrex glass pipe containing two identical electrode assemblies, and both pipes are contained between two copper plates, 43.2 x 21.6 x 0.635 cm. Each electrode assembly, one of which is shown in Figure 2, is a 8.9 cm diameter by 0.95 cm thick disc on the end of a 5.1 cm diameter copper pipe. There are eight slots, each 0.95 x 2.86 cm, in the pipe behind the electrode and nine 1.25 cm diameter holes in the disc, one in the center, and one adjacent to each slot. The electrolyte flows out through the slots and divides, part through the eight holes and part through the annular gap between the disc and the glass wall. Another part of the flow is directly out through the hole in the center of the disc. The purpose of these holes and slots is to uniformly replace the heated electrolyte with cool electrolyte. In one of the previous designs, with only a large center hole, there was sparking in the electrolyte between the electrodes and near the glass wall at 800 MW peak and 1 MW average power, but not at 800 MW peak and low average power. Presumably the energy was being uniformly deposited in the electrolyte but the heated electrolyte near the walls was not being swept out by the flow, was boiling locally, and the high voltage stress was causing arcing across the steam bubbles. The calculated exit temperature, based on average temperature rise, was only 70°C. No such arcing has been seen with the slotted electrode assembly.

The glass pipes are staybolt clamped between the copper plates by a circle of eight tapped lucite rods around each pipe and sealed with neoprene gaskets which allow for a slight difference in length between the pipes. All assembly between copper pipe, copper plate, and brass disc is with lead-tin soft solder, and a reinforcing ring is used around the lower pipe to which the heavy hoses are attached. Soft solder joints have been suitable for over two years of exposure to this electrolyte mixture, but silver-solder joints eroded in a few weeks. There has been no appreciable erosion of the brass electrodes by the electrolyte.

The circulation system shown in Figure 3, uses a 750 l, 91 cm diameter, 122 cm deep polyethylene tank nearly filled with electrolyte, a 3 horsepower (hp) magnetic drive pump (March Pump, #TE-8C-MD), 5.1 cm reinforced PVC hose, and nylon or PVC plumbing fittings. The cool electrolyte is drawn from the bottom, perpendicular to the side of the tank, and the hot electrolyte is returned to the top, tangent to the circumference of the tank at two places to impart a circular flow. The flow rate is 435 l/min, which corresponds to a temperature rise of 33°C at 1.0 MW average power, and provides 80 seconds of cool electrolyte. This has not been verified because other modulator components have limited run times.

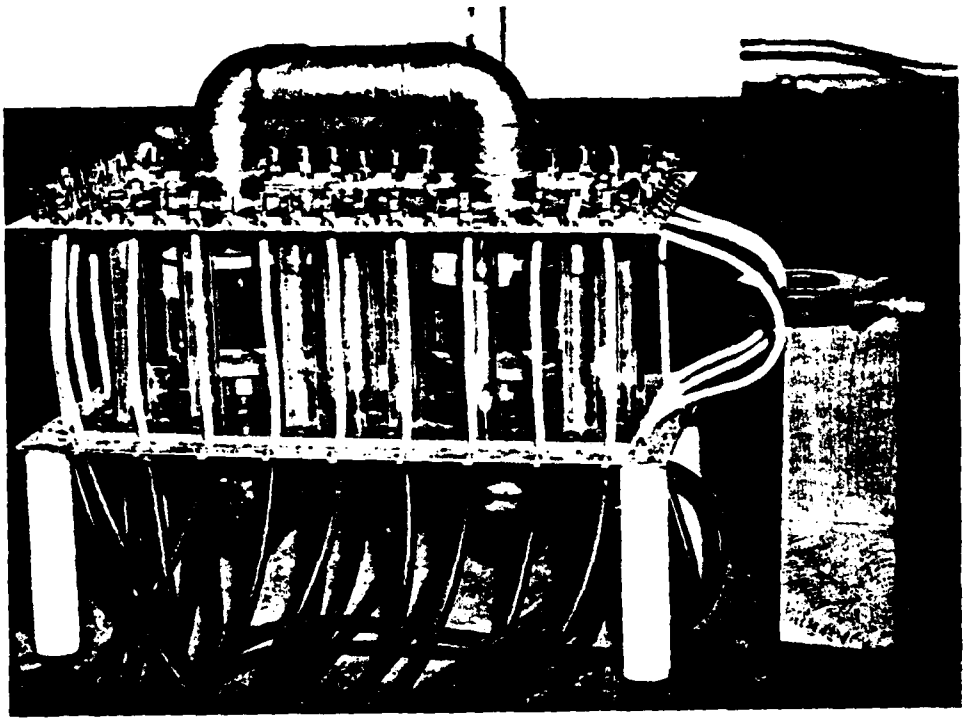


Figure 1. Load Assembly



Figure 2. Electrode Assembly



Figure 3. Circulation System

In the present application there was no requirement for closely spaced runs, the long-term average power was low, and a very simple heat exchanger could be used. Fifteen meters of 1.25 cm copper tubing was formed into a 6-coil helix, 76 cm in diameter, 61 cm high and suspended in the tank with 7.6 cm between the tank walls and the coils. The circular flow aids the transfer of heat from the electrolyte to the tap water in the coils, giving a U factor of 410 BTU/hr/sq ft/°F (837 joules/hr/cm^2/°C), and average heat removal rate of 30 kW for water flow of 18.9ℓ/min and electrolyte temperature of 50°C.

Inductance

In general, to minimize inductance one would like to maximize the length of the magnetic flux linkages created by current through a component and minimize the volume in which these linkages exist. This is normally accomplished by making a component as compact as possible, consistent with voltage breakdown, using wide or large diameter conductors, and using coaxial geometry where possible for inductance cancellation. This load can be viewed as a distorted coaxial structure where the outer conductor is an array of 50 conductors (only 25 are being used in Figure 1) evenly spaced around an 43.2 by 21.6 cm rectangle, and the inner conductor is the two paralleled electrolyte-filled glass pipes. Because of the complicated structure, a rigorous calculation of inductance is difficult, but an estimate can be obtained by using the dependence of inductance on the volume of flux-filled space, and hence on area, and the dependence on the length of the flux linkages, or magnetic reluctance, around the space between the conductors, and transforming the actual structure into an easily calculated coaxial cylinder structure with the same area (volume) and the same mean flux linkage circumference. This gives a coax with 35.4 cm outer diameter and 32.5 cm inner diameter. Using the equation for coax with a thin outer and solid inner conductor[3]

$$L = 0.002\ell \left(2n\, r_o/r_i + \tfrac{1}{4}\right) \mu H$$

gives a value of 10.2 nH. If skin effects pushed the current flow to the outer surface of the inner conductor, the inductance would be 2.6 nH for the same size coax, using the equation for two thin cylinders

$$L = 0.002\ell \left(2n\, r_o/r_i\right) \mu H$$

where ℓ = length of coax structure

r_o = radius of outer cylinder

r_i = radius of inner cylinder, all dimensions in cm.

An experimental determination of inductance can be seen in Figure 4 which shows voltage and current waveforms across the load in a 2 ohm modulator with a 170 nanosecond (ns) pulse width and 87 kA/μs di/dt. The calibration factors have been adjusted to make the amplitudes equal at the peaks where di/dt = 0. Looking at the portion of the curves from maximum positive to maximum negative di/dt, the overlay between voltage and current waveforms shows virtually no inductance. To determine the resolution of the method, voltage waveforms have been calculated for the actual current waveform and an assumed 10 nH and 20 nH inductance in series with the resistor. These waveforms are noticeably displaced from the observed voltage waveform, indicating that the resolution of the technique is better than 10 nH, and the actual inductance is less than 10 nH which agrees with the calculated estimates.

U.S. GOVERNMENT WORK NOT PROTECTED BY U.S. COPYRIGHT.

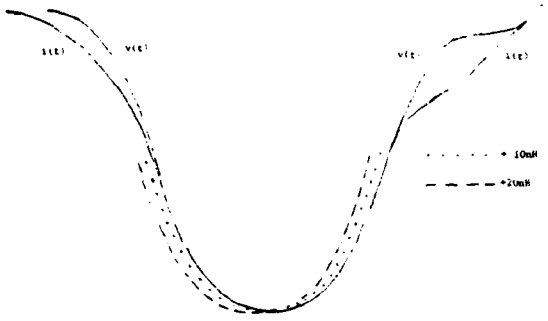


Figure 4. Current and Voltage Waveforms Across Load with Assumed Values of Inductance

Transient Resistance Variation

At the time of the first pulse, with the electrolyte flow already established, all the electrolyte in the resistor is cool. After a short time, which depends on the flow velocity and the physical size of the resistor, the entering electrolyte is cool and the exiting electrolyte is hot; this results in a reduction in resistance. Assuming a linear temperature rise through the active zone of the resistor, and a linear decrease in resistivity with temperature, the stabilized resistance is

$$R = \frac{L}{A} \frac{\rho_o^2 - \rho_o \alpha\Delta t + 3/16\ (\alpha^2\Delta t^2)}{2\rho_o - \alpha\Delta t}$$

where ρ_o = cold resistivity, ohm-cm

α = change in resistivity, ohm-cm/°C

Δt = temperature rise through load assembly, °C

L = length of active area in one load pipe, cm

A = area of one load pipe, cm^2.

The resistance of the cold load is $1\rho_o/2A$. For ρ_o = 12 ohm-cm, α = .096 ohm-cm/°C (0.8%/°C), Δt = 33°C, L = 6.35 cm and A = 81 cm^2, R_{hot} = .406 ohm, R_{cold} = .470 ohm; the decrease is 13.6%. Half of the change occurs during the first 71 millisecond (ms) of the run, the time required for the heated electrolyte to cross the active zone in the first glass pipe. There is no change for the next 131 ms while the first heated electrolyte is in the electrode assembly and cross-over pipe. The rest of the variation occurs in the next 71 ms crossing the second glass pipe. After the heated electrolyte reaches the exit pipe equilibrium is established and the resistance is constant for the duration of the run. If the load value were critical, the cold resistance could be adjusted to 13.6 percent higher than the desired stabilized resistance. The structure could be modified to reduce, but not eliminate, the time during which the resistance changes.

Conclusions

A low-impedance, low-inductance resistive load has been developed which is capable of handling a gigawatt peak power and a MW of average power for run times in the order of 60 seconds. The energy is stored in a liquid electrolyte and dissipated via a heat exchanger between runs. The resistance can be a least as low as one-half ohm and the inductance is less than 10 nH.

References

1. W. Nosch, Electrotechnik, 9 (6) 214, 1955.

2. Bishop, et al, "Plasma Physics," Journal of Nuclear Energy, Part C, Vol. 7, pp. 423, 1965.

3. F. Grover, Inductance Calculations, D. Van Nostrand, pp. 41, 1946.

LOADS FOR HIGH-POWER TESTING

Bobby R. Gray
Rome Air Development Center

The designer or test engineer of high-power systems is often faced with the problem of substituting a load for some portion of the system for the purpose of evaluating some other component in the system, trouble shooting, checkout of the system, calibration, or for system optimization. To be a truly equivalent load it must match the normal load in its reactive and resistive power relationship, its voltage/current ratios as a function of time, power-absorbing ability, polarity, and many other factors.

A test load may be required anywhere between the prime power source and the final output. It could mean a load bank on a large ac or dc power line or transformer/rectifier, a pulse-type load in the power conditioner stages of the system, or the energy output of the total system.

An example of some substitute loads discussed would be an rf load on the output of an rf amplifier, beam energy absorbers in accelerators, pulsed power load at the video level, and equivalent diode loads for modulators, etc.

("Paper available from author upon request")

CH1371-4/78/0000-0070$00.75 © 1978 IEEE

LIGHTWEIGHT POWER CONDITIONING MAGNETICS

by
James P. Welsh, President
Robert L. Haumesser, Chief Engineer
David L. Lockwood, Chief Scientist

Thermal Technology Laboratory, Inc., Buffalo, N.Y.

Summary

Recent requirements for lightweight high power magnetics which have led to increased research and development in this and related areas are explained. Transformers with specific weights in the range of 0.1 to 0.25 lbs/KVA have been developed through the utilization of improved materials, improved magnetic circuit modeling, and the application of advanced heat transfer techniques. These thermal aspects are particularly important to the size and weight reduction of magnetics. If each conductor in a magnetic device can be adequately cooled throughout most of its length, then the current density can be increased and the conductor crossectional area significantly reduced. This, in turn, results in a smaller core window and consequently, a smaller core.

The selection of suitable magnetic and insulating materials is discussed. The highlights of thermal analysis and experimentation to evolve controlled cooling of conductors is outlined. Electrical design, magnetic models, and the resultant computer aided design programs enable a designer to rapidly study the effects of changes in materials, geometry, and many other physical parameters.

Lightweight Transformer/Rectifier Units at power levels of 10 KW, 200 KW, and multimegawatt levels have been designed and fabricated. Their performance is very consistent with the computer predictions and validates the programs.

Discussion

The increasing requirements for aircraft performance, size, and electronic systems capabilities has placed electrical power demands on future power conditioning equipment which can no longer be effectively handled by existing hardware and the related technology. Pertinent to this paper is the requirement for small lightweight high power magnetics having specific weights in the range of ¼ to 1/10 lb. per KVA at 400 HZ and higher and at power levels of a few kilowatts to megawatts. The USAF Aero Propulsion Lab., at Wright-Patterson AF Base, has sponsored the R&D reported herein with the primary goal of reducing the specific weight of magnetics without sacrificing electrical performance and reliability. Emphasis in this program has been on power, inverter, and pulse transformers.

It was initially established in this program that the power, size, and weight limiting condition in transformers is the rate at which heat can be removed from the windings and to a lesser extent, the magnetic cores. Thus, one of the basic approaches in our research was to emphasize internal heat transfer in transformers and to develop thermal techniques that could provide the lowest practical thermal resistances. This permitted conductor current densities which were almost an order of magnitude greater than those in conventional transformers.

The main thrust of the program, has been to utilize modern computing techniques, advanced magnetics analyses and modeling, and thermal technology backed by extensive experimentation to develop lightweight transformer design procedures. Various experimental transformers were designed, constructed and tested to demonstrate the validity of this approach. Test results indicate very close correlation between the size, weight, and electrical performance of the experimental units and the computer derived models.

Early in the program, in order to assess the validity of the thermal approach, a series of experiments were performed to ascertain the conductor current densities which could be attained with the more effective cooling techniques. For example, it was established that vaporization cooling of typical high power transformer conductors safely permitted current densities of an order of magnitude or more than with conventional transformers. Both dielectric liquid cooling techniques were also evaluated in detail. It was concluded that the thermal aspects were particularly important to the size and weight reduction of magnetics. If each conductor in a magnetic device can be adequately cooled throughout most of its length, then the current density can be increased and the conductor corssectional area significantly reduced. This, in turn, results in a smaller core window and consequently a smaller core.

Two approaches to transformer design have been developed. The first approach, which has been called the steady state analysis routine, is basically a magnetic circuit approach. This method uses flux and flux leakage concepts to relate the primary and secondary in a transformer. The second approach, which has been called the real time

CH1371-4/78/0000-0071$00.75 ©1978 IEEE

analysis routine, is a coupled electric circuit approach in which the primary and secondary are related through their inductances.

In formulating the governing equations for transformer design, it was found that the mathematics of steady state design are not especially complex, but that the design process is complicated by the profusion of design input variables. Depending upon the application, between fifty and two hundred parameters, all interrelated by physical laws and performance criteria, are required to fully describe a design. Since many of the relationsips are not only non-linear, but are discontinuous, the manipulation of these parameters to achieve optimum results becomes formidable. However, a programmable calculator can be used for parametric analyses and design, provided a complete design optimization is not desired. Complex optimization programs for large machines have also been developed.

Since vaporization cooling techniques were determined very early to be most applicable to the high heat fluxes anticipated, much of the thermal investigation and experimentation was directed to the application of this cooling method. While a considerable amount of literature exists on the boiling process, much of it is empirical in nature and therefore limited in scope, and little if any is directly applicable to the problem of boiling in narrow vertical ducts as are found in the transformer. The analyses and experiments were directed at obtaining values of the maximum attainable heat flux without exceeding the nucleate boiling regime, and of the minimum channel width required to insure against the formation of vapor pockets with the attendant extreme temperature rises and potential burnout.

Vaporization cooling application additionally lead to other considerations. Compatability tests indicated that testing of the materials involved is desirable for a given application with a specific coolant. The high electric fields and small spacings typical of reduced size transformers lead to detailed investigations of dielectric breakdown, partially in view of the two phase nature of the dielectric coolant. Dielectric breakdown and insulation relationships and models were refined and experimentally validated for use in this program. Also, the open construction required to provide coolant passages resulted in consideration of the mechanical forces imposed on the windings, especially under overload conditions.

The gain in specific weight and size reduction is not always without a penalty, often (but not always) reduced efficiency. The efficienty of well designed conventional high power transformers is usually high in the neighborhood of 98 to 99.5 percent. The low specific weight transformers tend to exhibit 2 to 4 percent lower efficiency. This is a small penalty and often can be accomodated when an external cooling system is provided. Another penalty is the slightly degraded voltage regulation due to the increased conductor resistances in the windings of low specific weight transformers. Usually, these are small compared to the external system resistances and are offset by the relatively small increase in resistance due to much lower winding temperature rises in the low specific weight transformers. Furthur, the low specific weight transformers have shorter total conductor lengths in a given winding compared to conventional transformers, which also tends to offset the slightly degraded voltage regulation. The computer programs developed permit the tradeoff of transformer gains and penalties such as weight, size, efficienty, voltage regulation, leakage inductance, and many other parameters with respect to any given set of transformer requirements.

The transformers developed under this program are mostly continuous duty transformers. The time required for the windings to reach thermal equlibrium in a thermally adequate design is very short, much shorter than any contemplated duty cycle. Thus, from the viewpoint of the internal thermal aspects, the transformers are capable of continuous duty. However, for intermittent duty applications, the external cooling system can be reduced in size, weight, and capability to accomodate the specific duty cycle desired. Thus, a lightweight transformer system capable of any required duty cycle can be designed and developed.

There is another class of lightweight transformer which also can be designed under this program - namely the " adiabatic transformer". These are transformers which are intended for very short duty application and incorporate relatively high internal thermal resistances. The duty cycle is limited by the total quantity of heat the transformer materials can absorb without attaining excessive temperatures. The transformer must "cool down" prior to reenergization.

Safety and reliability aspects are important also. The small lightweight high power transformers developed can withstand considerable overload in spite of their small size. For example, a two hundred KVA transformer recently developed has a volume of about 300 Cu. in. When this transformer

is connected to the normal power sources which are capable of several megawatts if an internal fault occurs, it initially looks like a "bomb." However, because vaporization cooling is used, the coolant is capable of safely dissipating very large powers. Further, the operating temperatures of the transformers are typically somewhat lower than with conventional transformers. The overall reliability should equal or exceed that presently attained because the electrical, thermal, and mechanical stresses on the materials are controlled design parameters.

Figures 1 and 2 show a 50 KVA-400 HZ-three phase 208V. to 10 KV Freon cooled transformer which weighs about 15 pounds without the coolant, case, or external cooling system. It has been operated up to 100 KVA without failure and has been severely overloaded on several occasions. Fig. 3 presents a 10 KW Freon cooled transformer rectifier unit for a 10 KW inverter operating at 10 KHZ. The output is 10 KV DC at 1.0 amp. Fig. 4 presents another version of the same unit, except that this is a complete forced air cooled system. Fig. 5 is of a 700 to 1,000 HZ multimegawatt high voltage transformer rectifier unit. The forced oil cooled transformer has a specific weight of 0.08 lbs. per KVA and the complete system including the conventionally sized pump, heat exchanger, fan and structure has a specific weight of ¼ lb. per KVA. Figs. 6 and 7 show a 200 KW transformer rectifier unit with a specific weight of 0.13 lbs. per KVA. This operates in conjunction with an inverter at 10 Khz and delivers 25 KV at 8.0 amps continuous duty.

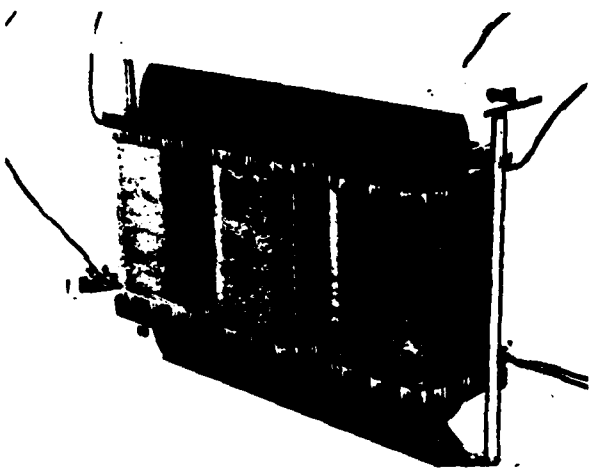


Figure 1

One problem common to these transformers is that of providing adequate input and output terminals and bushings. The large currents and/or voltages involved mandate large conductors or bushings with long leakage paths which are generally incompatable with the small sizes of the transformers. For example, with the 200 KW units, the input currents at 10 KHZ are greater than 400 amps and a low inductance is also required. With the 50 KVA transformer the primary lead size on the inside of the transformer case was No. 13 AWG, while the external lead to the primary was a No. 4. Consequently, 5/16 in. dia. stud terminals were mandated, for a 15 lb. transformer. The terminals and bushings can constitute a significant portion of the volume and weight of a low specific weight transformer.

This program, which is now in its sixth year, is continuing. The goals of reliable lightweight high power transformers with specific weights of ¼ lb. per KVA at 400 HZ or higher have been achieved. This will aid in attaining future power conditioning systems of higher power and/or reduced weight compared to the present state of the art hardware.

Acknowledgement:

The assistance of SUNYAB Dept. of Electrical Engineering personnel, under the direction of Prof. A.S. Gilmour, Jr., in the consultation, fabrication, and testing associated with this program is gratefully acknowledged.

References

Final Technical Report on Development of Lightweight High Power Transformers for Airborne High Power Supplies, Vol 1 and 2 Report No AFAPL-TR-75-15

Interim Technical Report on Development of Lightweight Transformer for Airborne High Power Supplies - Report No AFAPL-TR-76-102

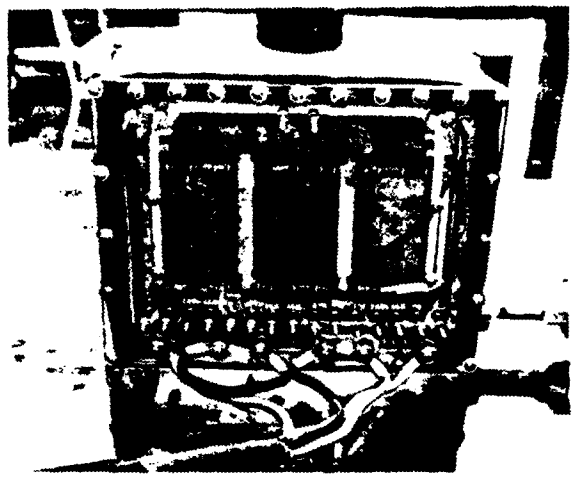


Figure 2

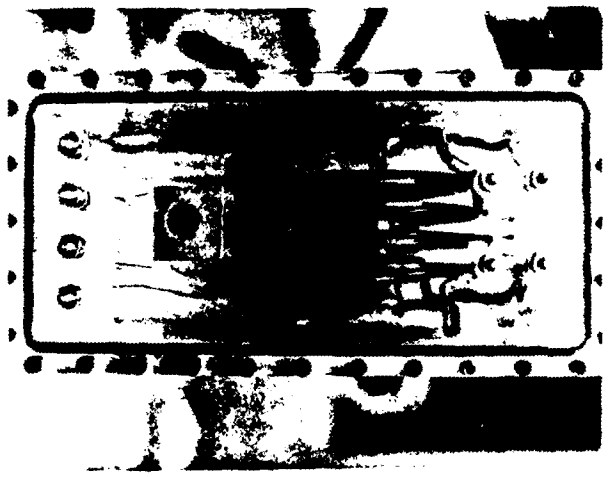


Figure 3

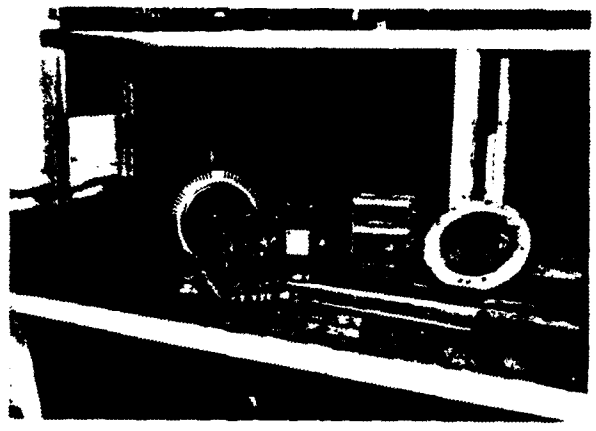


Figure 4

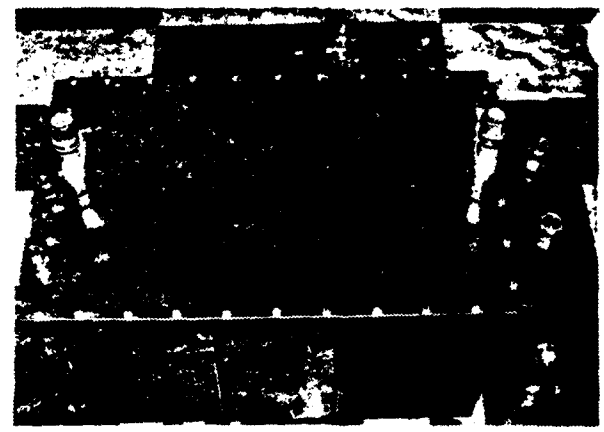


Figure 5

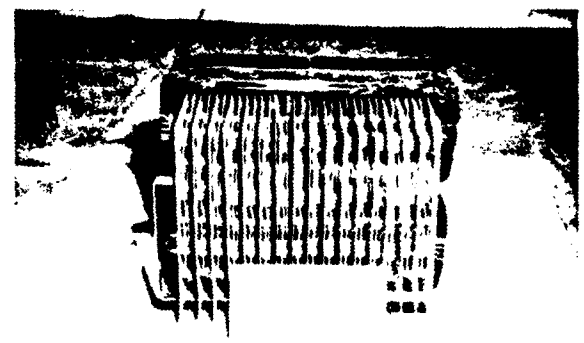


Figure 6

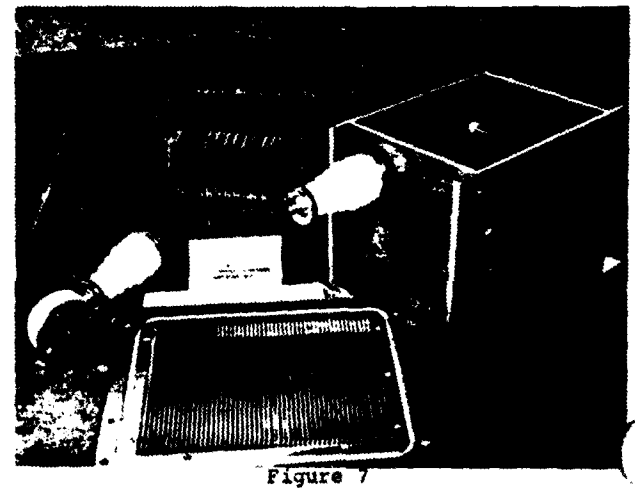


Figure 7

ELECTRO-OPTIC TRANSDUCERS AND OPTICAL FIBERS IN HIGH VOLTAGE MICROWAVE MODULATORS.

by

Piero Cervone and Giovanni Scerch
Selenia S.p.A. - Rome - Italy

Summary

This paper describes a new solution for the transfer of information through different voltage levels in a high voltage modulator for gridded microwave tubes.

The new solution is realized with the use of electro-optical transducers coupled by optic fibres.

A description of the transmission channel, the control unit and the failure indications is presented.

Introduction

As known, microwave tube modulators can be divided into two main classes:

1) Modulators for cathode pulsed tubes

2) Modulators for electron gun gridded tubes

In modern radar transmitters, for radar system with pulse compression and frequency agility, the second type is coming into general use. It is connected mainly with the superior performance that can be obtained from the points of view of flexibility, stability, transmitted pulses complexity (as any type of phase modulation, time modulation etc.). In order to use this kind of tube, it is necessary to have in the modulator many subassemblies referred to different high voltage levels (from a few kilovolt up to several tens of kilovolts). Therefore, in these modulators the problem is to know in real time the performance conditions of the equipment and consequently to operate in such a way to avoid microwave tube or component failure.
Moreover, it is necessary to give the operator information as detailed as possible in order to individuate and remove in very short time any kind of failure, thus reducing the MTTR.

The present paper proposes a solution in order to solve, having the maximum flexibility, the minimum size and high reliability three main problems of these modulators:

a) information transmission between circuits at different voltage levels and ground.

b) real time processing of all the modulator parameters.

c) carefull indication of modulator state and failures in order to reduce MTTR.

Description

Schematic block diagram.

In fig. 1 is shown the schematic block diagram of a gridded tube modulator [1] . The cathode and collector voltages are realized by two series power supplies.
On the output of the first power supply there is the crowbar which is usually necessary in order to limit at safe value the energy discharged into the tube in case of arcing. A cathode voltage regulator is added to achieve the required voltage stability.

In the diagram we can identify four different voltage levels.

Information transmission.

The information transmission system must respond to some basic requirements:

- reduced size in order to have many channels
- maximum mechanical flexibility in order to avoid constrainning the mechanical positions and dimensions due to the high voltage circuits.
- bandwidth up to few MHz to have fast response times.
- sufficient electrical insulation and absence of corona effect.

The solution choosen in our system employs electro-optic transducers coupled by optical fibres. The latter are composed of many elementary fibres of diameter 0.07 mm max bundled together to make up an external diameter of 3 mm and covered by siliconix sheath . Each elementary fibre is composed of an internal core and external coat. Denoting respectively n_0 n_2 n_1 the reflection indexes of air, core and coat and assuming $n_0 < n_2 < n_1$ its performance can be so resumed (fig.2) [2] . When a light ray coming from the air enters the fibre , it propagates in accordance with Snell's law:

$$n_0 \sin\theta_0 = n_1 \sin\theta_1 \tag{1}$$

until it reaches a boundary between the media. Here, if:

$$\sin\varphi > n_2/n_1 \tag{2}$$

then the total reflection occurs. Therefore, within the fiber the light propagates only if there is total reflection i.e the incidence angle θ_0 is lower than a critical value θ_c .

If a substitution for inequality (2) is made in (1) the following expression is obtained:

$$n_0 \sin\theta_0 < \text{N.A.} = \sqrt{n_1^2 - n_2^2} \tag{3}$$

Equation (3) defines the "numeric aperture" N.A. of the fibre and consequently the maximum possible angle of the incident ray in order to have the light transmission through the fiber. The same relationships are effective at the output end of the fibre.

For the fibres actually used the refractive indexes are respectively $n_1 = 1.63$ for the core and $n_2 = 1.52$ for the coat.

The numerical aperture is N.A. = 0.589 which corresponds to a maximum permissible incidence angle of 36°. Therefore the total aperture angle is 72°.

CH1371-4/78/0000-0075$00.75 ©1978 IEEE

The transmissione capability of these fibres have a uniform value in the range between 400 and 2500 nm. The fibres, being arranged into parallel layers, determine some non-conductive zones towards the inside of the whole Fibre, giving rise to packaging losses p_1 (within 10%, with the chosen fibre).

As far as concern transmission attenuations and to total reflection on single walls, they are evaluated to approx 10% for 1 meter.

Special care has been given to obtain maximum transmission coefficients Γ_1, Γ_2 between fibres and transducers considering the transmitting coefficient as a ratio between the average energy flux per time unit and exposed areas within the two materials on their respectively exposed surfaces. As a matter of fact, light coming from the photoemitter hits the frontal flat and optically polished surface of the fiber nucleus; part will be reflected and part will propagate inside the fiber itself.

It has been found that this transmitting coefficient is practically constant for the incidence angles between 0° and 20° and almost equal to 0,9.

This result has permitted no critical coupling between transducers and fibers. The realized system shows optics efficiency of approximately 60%.

The transmitting system is composed of a switch circuit and an electro-optic transducer which is a PN gallium arsenide infrared emitting diode with maximum spectral output at 900 nm.

The receiving system employs an opto-electrical transducer (photo transistor or photo diode) and following amplifier. We used two different types of receiver (fast and slow) according to the signal bandwidth.

Fig. 3 shows the response time of the fast channel.

The transmission system is designed in order to have light transmission when the signal is logically active. In this way the system is self-protected in case of failure itself. In fig. 4 we can see the completed transmission system.

Parameter Modulator Processor.

The signals to transmit between the different voltage levels of the modulator are mainly of two types:

1) pulses, triggers

2) logic levels able to define the modulator behaviour

All these signals are processed by a Modulator Control Unit in order to guarantee safe automatic and faultless functioning of the microwave tube and modulator and in order to give to the operator as correct as possible indications for locating and repairing faults.

Therefore the modulator is divided into many subassemblies for each of which exists a failure indication.

In the Control Unit the signals are divided in three main classes:

1) mechanical (e.g. interlocks, breakers, etc.)

2) thermal (e.g. thermometers, flow rate of refrigeration fluids)

3) electrical

For the last class, it is convenient to have further subdivisions:

a) signals for persistant failures (e.g. bias voltage absence, etc.). For these the trouble shooting can be made on-line.

b) signals for instantaneous failures (e.g. body tube overcurrent). In these cases it is necessary to memorize the error signal and therefore the trouble shooting is made via a failure table. Return from a failure condition to the ready condition is caused by a manual reset signal for the electronic memory.

In the case of contemporary failure signals the Control Unit indicates only the primary failure with the inhibition of the indicators of all secondary failures caused by the primary one.

Another characteristic of the control unit is the capability to control the power-up sequence of all parts of the transmitter including the blowers, liquid pump, filaments bias voltages, etc. until the whole transmitter is ready for operation.

The described Control Unit is realized by HLL circuits and its size is three standard printed circuit boards (20 x 16 cm).

Failure indications.

Failure signals run from the Control Unit to the indication circuits. Fig. 5 shows the schematic diagram of the system. Interface circuits adapt the HLL levels to TTL levels which then arrive at the inputs of eight-way multiplexers which are cyclically explored by two binary counters controlled by 1 KHz clock.

For each failure the coded output so obtained is decoded and goes to two 7 segments LED numerical indicators, thereby generating a two digit failure code.

At present, 47 codes have been employed. When there is an output from multiplexer a gate inhibits the cycle counting for a few seconds. Hence the operator will see at intervals a number and through a failure table will be able to locate the failure. This system permits a great reduction of the circuitry and of the number of wires needed to provide failure indications at a remote control point.

Conclusion

The system has been used since some years for many kind of transmitter (with average power from some watts up to some kilowatts). It allows a great size reduction and it is able to control in real time many modulator parameters. With the most sophisticated transmitter, we have obtained a MTTR of 20 minutes.

REFERENCES

1 G. Scerch
High power solid state modulator for coherent agile microwave amplifier
Eleventh Modulator Symposium - Sept. 1973

2 W.B. Allan
Fibre optics: Theory and Practice
Plennum Press - London 1973

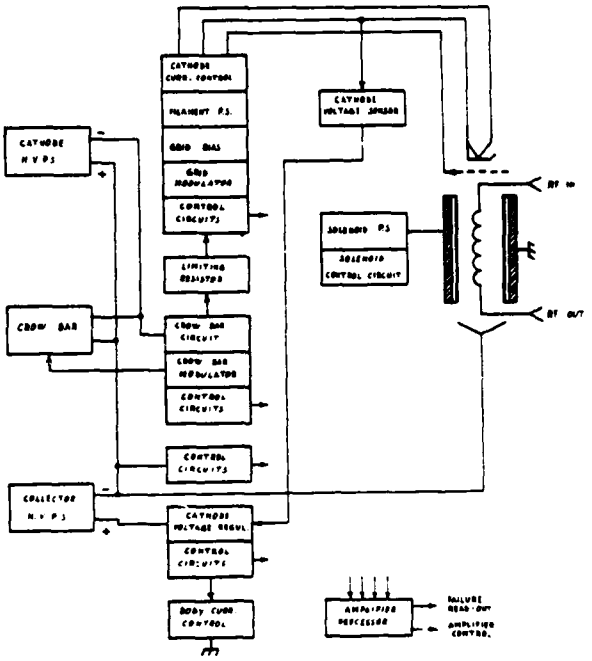


Figure 1 Amplifier schematic diagram

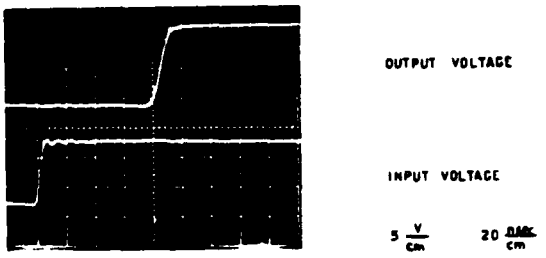
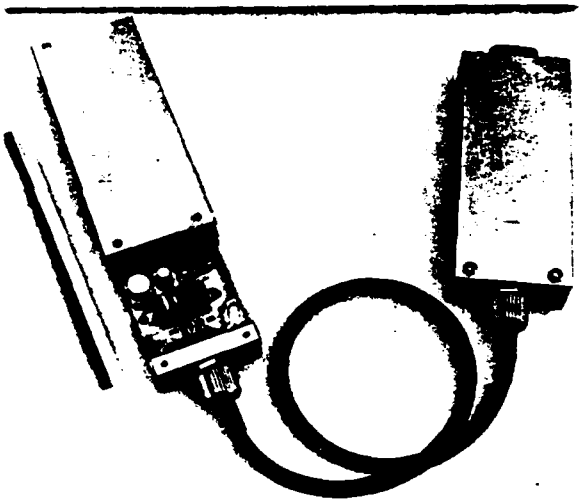
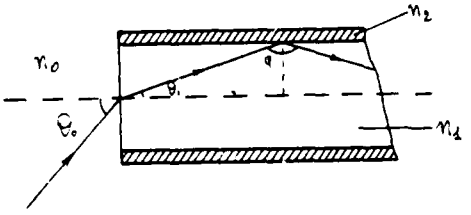


Fig 3 Response time of the fast channel

Figure 4 Signal trasmission channel





$$N_0 \sin\theta_0 = N_1 \sin\theta_2 = N_1 \cos\varphi$$

$$\sin\varphi > \frac{N_2}{N_1}$$

$$N_0 \sin\theta_0 < NA = \sqrt{N_1^2 - N_2^2}$$

Figure 2 Propagation of a light ray into an optical fibre

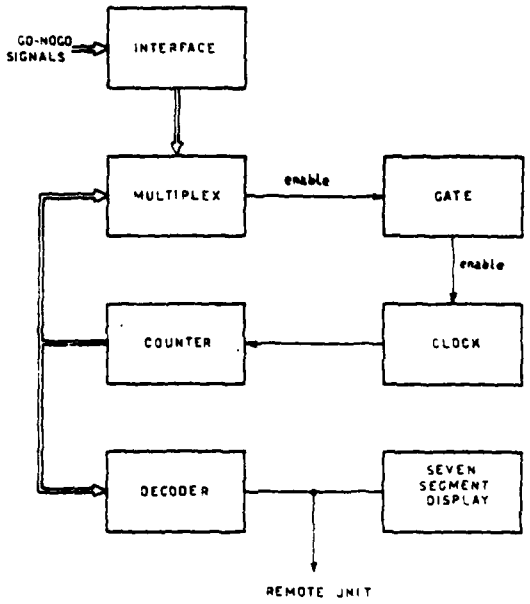


Figure 5 Failure indicator schematic diagram

THE CROSSED-FIELD CLOSING SWITCH – A STATUS REPORT*

R.J. Harvey and R.W. Holly
Hughes Research Laboratories
3011 Malibu Canyon Road
Malibu, California 90265

and

J. Creedon and H. Gauch
U.S. Army Electronics Technology and Devices Laboratory (ERADCOM)
Fort Monmouth, New Jersey 07703

Abstract

The crossed-field closing switch (CFCS) has been evaluated using a modulator consisting of 25 cables each 15.24 m long. A low-inductance 2-Ω copper sulfate load was used to terminate the modulator in its characteristic impedance. Before evaluating the CFCS in the cable modulator, studies were made of firing characteristics and mode of operation using a conventional pulse forming network of 0.5 Ω impedance matched to a copper sulfate load. The pulse width was a nominal 12 μs. Preliminary results were then obtained with the cable modulator at an anode voltage of 23 kV at a peak current of 6 kA and pulse repetition rates up to 500 Hz. The pulse width, measured at the half power points on the load, was 160 ns. Experimental results are shown for the cable modulator test, and the dependence of operating mode on circuit parameters is discussed.

Previous Results

The CFCS operates reliably at average power up to 0.8 MW at pulse repetition frequencies up to 108 Hz.[1-4] Repetitive switching at peak current levels of 20 and 40 kA at an anode voltage of 40 kV was demonstrated using a line-type modulator. The initial experimental set-up is shown in Figure 1, which also includes an oscilloscope trace showing the peak current waveform generated at an anode voltage of 40 kV. (The vertical sensitivity is 20 kA/div and the horizontal sweep is 2 μs/div.) The trace consists of approximately 16 pulses from a train of 2400 pulses in a 30 s run.

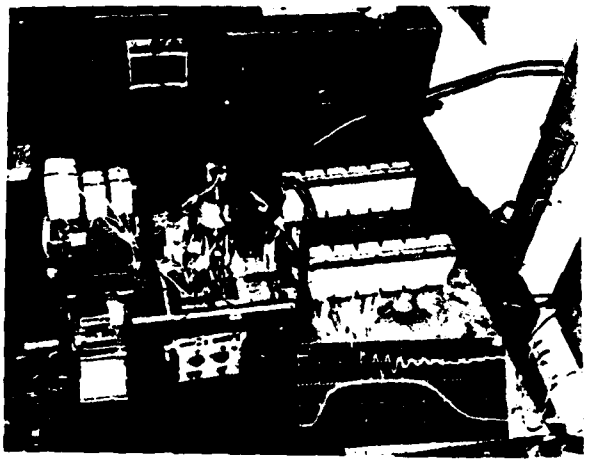


Figure 1. Initial Experimental Setup (1976)

Subsequently, the CFCS was tested in another line-type modulator of similar total impedance (1 Ω) and pulse width (12 μs) in which the current rise time (10 to 90%) was reduced from 2 to 1 μs. Peak currents of up to 47 kA were switched at average currents up to 40 A using burst lengths of a few seconds at the higher average power loadings. In general, however, the reliability was considerably reduced over that experienced in the initial phase of the evaluation. Anode voltage hold-off capability and pulse-to-pulse jitter were noticeably influenced by the operating mode, which was found to be related to peak B field value, anode voltage, and gas pressure. Unfortunately, the evaluation was somewhat clouded by an eccentricity in the grid cathode spacing (which was accidentally introduced during the refurbishing of the CFCS after the initial evaluation phase) and by the presence of several high-frequency resonances in the test circuit. To establish the circuit independent characteristics of the CFCS, a cable modulator system was constructed. This allowed examining the trigger characteristics more carefully.

Short Pulse Characteristics

Test Circuit

The circuit chosen for short pulse length operation included: a variable impedance pulse forming network (PFN) composed of 50 ft (15.24 m) lengths of RG 214/U cable, a set of low-inductance collector plates for connection to the CFCS, a matching set of load cables 15 ft (4.57 m) long, and a low-inductance $CuSO_4$ load.[5] Figure 2 shows these basic components as they were arranged in the laboratory at the Evans area of Ft. Monmouth. The PFN was draped from the ceiling to the CFCS at one end and to a groundable common terminal at the other. To date, only 25 of the possible 50 cables have been connected. This yields a 2-Ω system.

A detailed drawing of the circuit is shown in Figure 3. The inductances shown are estimated from the known geometries, and the 77-pF capacitor is the calculated internal capacitance of the CFCS. The CFCS cathode was chosen for the system grounding point. The locations A and B were the collector plate voltage sensing points, and a current transformer (CT) was normally located as shown to sample a fraction of the load current.

The calculated cable signal reflection times are 154 and 46 ns for the PFN and load cables, respectively. The PFN was charged both resistively and resonantly (as shown).

Calibration

A Tektronix 7834 400 MHz storage oscilloscope was used to record the data. The CT was a Pearson 410 with

*This work supported by the U.S. Army under Contract DAAB07-77-C-2703.

CH1371-4/78/0000-0079$00.75 © 1978 IEEE

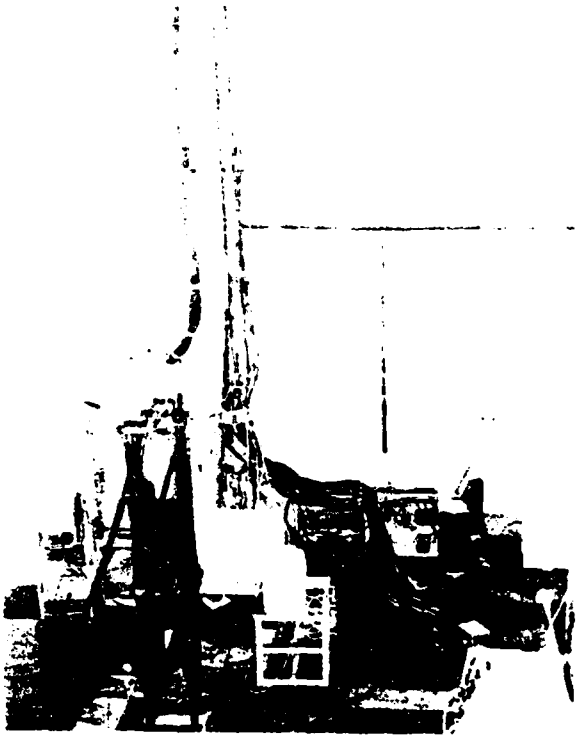


Figure 2. Experimental Arrangement

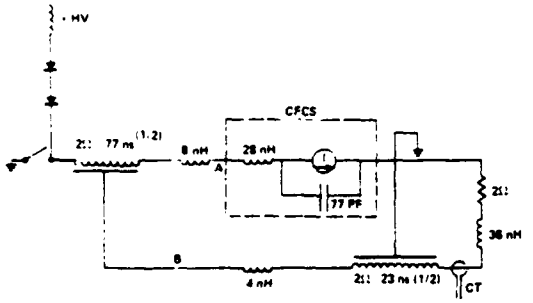


Figure 3. Test Circuit

a rated rise time of 10 ns and a 0.1 V/A output. Current transformers with higher ratios were found either to not have their rated rise time capability or to introduce too much stray inductance into the circuit being monitored to be of any use. The Pearson 410 was of marginal use. The voltage probes were Tektronix 6015s (20 kVDC, 1000:1) with 5 ns rise times.

The system response was checked at low voltage by mechanically shorting out the CFCS at point A. Figure 4(a) shows the current measured at the anode (lower trace) and the voltage measured at point B (upper traces) at 50 ns/div. The voltage noise may be pick-up noise or the natural ringing frequency of the CFCS internal capacitance.

The trapezoidal current pulse appears to have a linear 50 ns rise and a similar fall. The pulse width is about 175 ns. The fact that the top is not flat is related to the CT primary leakage inductance. Figure 4(b) shows the dramatic change in the signal (upper trace) when the CT is moved to its normal location on two of the load cable connections. The sharp features of the pulse are now washed out in the noise.

The location of the lead cables had a strong effect on the signal waveforms. Some noise coupling to the horizontal amplifier was observed at high-voltage operation. Taken collectively, this noise problem presently restricts any interpretation of the subtle features of the high-voltage data to a qualitative nature.

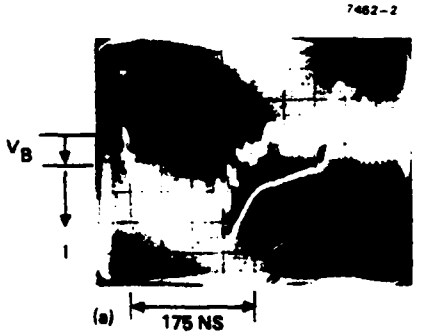
Magnetic Field and Grid Pulsers

The magnetic control field was generated by a resonantly charged thyratron pulser delivering a 60 A sinusoidal pulse with a 410 μs half period to the 100 turn field coil. The limiting frequency of this particular pulser was about 500 Hz.

The grid pulser waveforms are shown in Figure 5. The upper trace is the current (which was set to reach a peak of 80 A). The grid voltage reaches a peak of 4 kV and then drops to about 300 V on the onset of conduction. The grid was delayed in time with respect to the magnetic field pulse. This delay was variable. The pulser voltage was not changed during these experiments, although a 0.01-μF peaking capacitor was sometimes added from the grid terminal to ground.

Trigger Timing

The details of the trigger characteristics of the triode CFCS are beyond the scope of this paper. However, recent experience with low-impedance circuits has shown that the present CFCS design may be operated reliably and with low jitter. Certain precautions



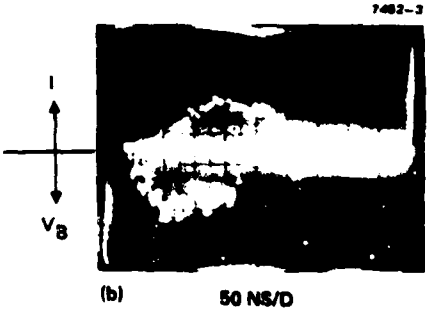


Figure 4. Low Voltage Calibration

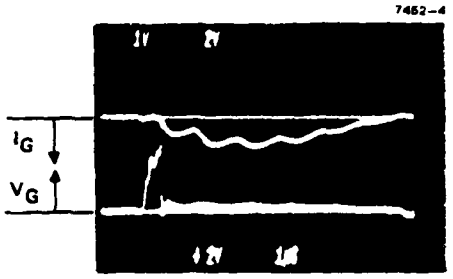


Figure 5. Grid Pulse Waveforms

must be taken to maintain a well defined operating point in parameter space to achieve this result. If one variable is altered, another must typically be changed to compensate. The critical variables in this parameter space are anode voltage, magnetic field strength, gas pressure, and grid timing.

Without pressure control, and using the magnetic field pulse trigger signal as a reference, we were able to achieve a stability of about ±10 ns in the anode fall point (some 200 μs later), during runs of about 700 pulses. This jitter level includes variations in the grid pulser and delay circuitry. A further reduction could be achieved by referencing the grid voltage signal.

Single Pulse Experiments

Figure 6 shows the load current waveform at a charging voltage of 10 kV. The peak current is 2.5 kA with a pulse shape equivalent to the calibration pulse *shape of Figure 4(a)*, but without the asymmetrical distortion produced by the CT inductance. The pulse width is 165 ns, which is consistent with the 154 ns theoretical PFN pulse width and the sensor rise times (~ 10 ns). The mismatch at the end of the pulse is probably due to the load inductance.

The anode voltage fall (measured at point A) appears to be a function of gas pressure. The initial fall is often seen at low pressure to have a gradual drop in the beginning, followed by a more rapid exponential fall. This is shown in Figure 7 at 37 mTorr of He. When the pressure is increased, the initial fall component disappears and the drop is precipitous. This is shown in Figure 8 at 50 mTorr. (Here the noise in the horizontal amplifier is most evident, negating any attempt to assign an anode fall time at this sweep speed.)

The anode fall time may be inferred by examining the foot of the current pulse rise. Any delay in fall

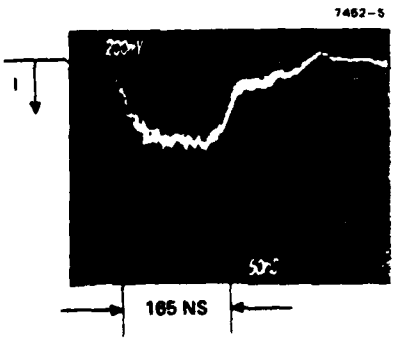


Figure 6. Load Current Waveform

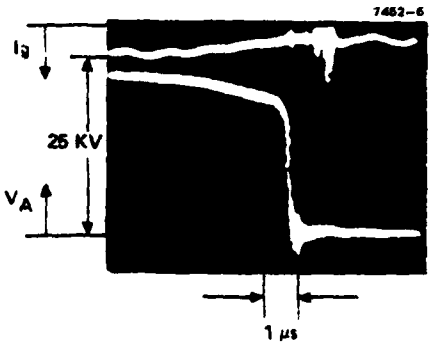


Figure 7. Anode Fall at Low Pressure

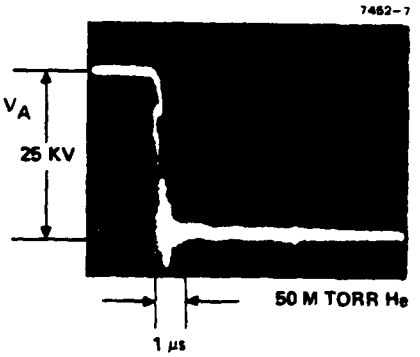


Figure 8. Anode Fall at Intermediate Pressure

would show as a precurrent. Figure 9 shows both the anode fall and the load current at 50 ns/div and at a pressure of 75 mTorr. No significant prepulse is visible. The base of the anode fall exhibits a decaying time constant of about 15 ns (exponential). This is mostly accounted for by assuming that 5 ns is due to the probe response and that the L/2R circuit time constant is 7 ns. The remainder is well within the systematic error.

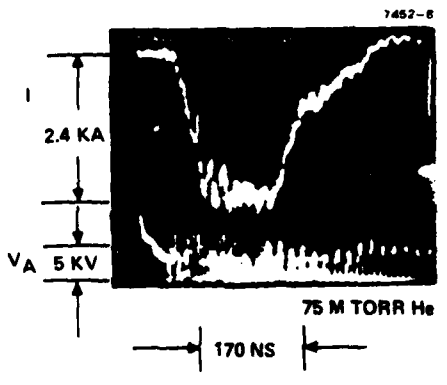


Figure 9. Anode Fall at High Pressure

Repetitive Operation

During repetitive operation, the anode voltage was set to 22 kV, resulting in peak currents of about 5.5 kA. The repetition rate was then increased to 526 Hz. Figure 10 shows the anode voltage at 10.5 kV/div using a resistive divider. The sweep speed is 1 ms/div. The upper trace is the magnetic field waveform. (The frequency limit was set by the magnetic field pulser thyratron latching in the on state.) The peak average current was then 0.5 A with 5.4 kW delivered to the load.

Summary

We previously reported operation of a CFCS at over 800 kW of average power at voltages to 40 kV and currents to 40 kA.[6] Recently, we investigated the characteristics of the same CFCS under short pulse duty. The device is presently inductively limited to rise times of 50 ns. The intrinsic rise time of the device (i.e., avalanche time) is $\lesssim$ 10 ns at pressures approaching its Paschen limit ($\sim$ 75 mTorr). As the pressure is reduced, the intrinsic rise time increases until a 1-μs prepulse is observed at 36 mTorr. Jitter times vary along with the intrinsic rise times and are of the same order of magnitude.

The CFCS has been run at over 500 Hz in the short pulse mode. Conduction appears to be in a crossed-field glow discharge. Therefore, previous simulations[1,5] suggest that the ultimate repetition rate will be limited only by the auxiliary power supplies and thermal cooling.

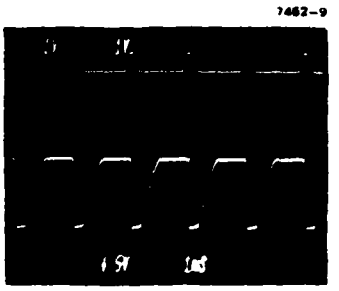


Figure 10. Operation at 526 Hz

References

1. M.A. Lutz, R.J. Harvey, and H. Alting-Mees, IEEE Trans. Plasma Sci., Vol PS-4, No. 2, June 1976, p. 118.

2. M.A. Lutz, U.S. Pat. No. 4,034,260 (7/5/77) and M.A. Lutz and R.J. Harvey, U.S. Pat. No. 4,034,261 (7/5/77).

3. M.A. Lutz, IEEE Trans. Plasma Sci., Vol. PS-5, No. 4, p. 273, Dec. 1977.

4. R.J. Harvey, R.W. Holly, and J.E. Creedon, IEEE Pub. No. 76CH1147-8 Reg 5, Proc. Int. Pulsed Power Conference, Texas Tech. Univ., Nov 9-11, 1976, p. 1B-3.

5. R.J. Harvey and M.A. Lutz, IEEE Trans. Plasma Sci., Vol PS-4, No. 4, p. 210, Dec. 1976.

6. See: W. Wright, "Low Inductance, Low Impedance Megawatt Average Power Load," these Proceedings.

PULSE MODULATOR BEHAVIOR OF THE LIQUID METAL PLASMA VALVE (LMPV)*

by

W. Wright, Jr.
U.S. Army Electronics Technology and Devices Laboratory
(ERADCOM)
Fort Monmouth, New Jersey

and

J.R. Bayless
Hughes Research Laboratory
3011 Malibu Canyon Road
Malibu, California 90265

Abstract

The LMPV is a mercury-cathode, triggered, closing switch which employs a small area mercury pool and a cooled (-30°C) condensing surface to maintain the conditions for vacuum arc operation. These conditions result in high-voltage capability, fast recovery and high current operation with negligible cathode wear. Therefore, the LMPV was considered to have potential as a high average power closing switch for modulator applications. An LMPV closing switch (LMPVCS) was built at Hughes Research Laboratories and evaluated at ERADCOM at voltages up to 150 kV, currents up to 8 kA peak and 7.5 A average, pulse lengths up to 50 us, and repetition rates up to 250 Hz. The device failed as a result of excessive anode dissipation caused by a long anode fall time on the order of 5 us. Subsequent experimentation has indicated that the fall time is reduced at increased mercury vapor pressures, however, experiments are required to define the relation between the fall time and voltage hold-off capability.

Introduction and Summary

The increasing size and complexity of pulsed power systems is leading to the requirement for closing switches capable of higher average powers, peak currents and voltages while maintaining high reliability and compactness. There are, however, few candidate closing switches which hold the promise for reliable, long-life operation at average load powers in excess of 1 MW.

The objective of the liquid metal plasma valve closing switch (LMPVCS) program** discussed herein has been to develop a new type of closing switch capable of meeting future requirements. This expected capability has been based on over ten years of development of the LMPV*** as a high-voltage dc converter valve and as a commutated dc interrupter. In these programs operation has been achieved at voltages over 200 kV, peak currents up to 40 kA and average currents over 600 A; this provided confidence that high average powers could also be achieved in relatively short pulse operation.

The objective was pursued by constructing and testing the LMPVCS shown in Figure 1. The test objectives, which are outlined in Table 1, were to use the LMPVCS to connect a PFN to a matched resistive load at an average load dissipation of 1 MW under a number of combinations of voltage, current and repetition rate. This power level was chosen to be consistent with existing test capabilities at ERADCOM while providing information concerning the scalability of the LMPVCS.

Table 1. LMPVCS Operating Goals

Parameter	Values		
Peak Charging Voltage (kV)	50	100	200
Pulse Width (μs)	20	50	50
Peak Current (kA)	8	8	4
Repetition Rate (Hz)	250	50	50
Average Current (A)	40	20	10
Average Power Delivered to Load (MW)	1	1	1
Run Time (min)	1	1	1
Minimum Off Time (min)	10	10	10

The major portion of the test program was undertaken at ERADCOM, Ft. Monmouth, New Jersey with the following conclusions:

1. A maximum average load power of 0.3 MW, which was limited by arc over in the PFN and current limitation of the high-voltage power supply, was achieved at a PFN charging voltage of 149 kV in 50 us pulsed operation. No misfires, electrical breakdown or current conduction in the reverse direction was observed under these conditions; and

2. The anode fall time was typically 5 μsec. This led to severe power dissipation in the anode and to its eventual failure. Higher average powers would not be possible unless the fall time can be reduced.

Following failure of the LMPVCS, single pulse experiments were performed with a similar LMPV at HRL in an effort to reduce the anode fall time. A fall time of 200 nsec was achieved by increasing the condenser and cathode temperatures and thereby the pressure of mercury vapor. Although the voltage hold-off capability is thereby reduced, it is possible that a relation exists between fall time and voltage hold-off which would offer the capability for high-average-power, high-voltage operation. More experimentation is required to evaluate this possibility.

The LMPVCS

A block diagram of the LMPVCS system is shown in Figure 2. The LMPV, which is the central element of this system, is shown in Figure 3 as it's being prepared for bakeout.

CH1371-4/78/0000-0083$00.75 © 1978 IEEE

The LMPV consists of a liquid metal cathode, an anode, and a condenser. The cathode is fabricated from molybdenum and contains a narrow annular groove into which mercury is fed. When any combination of the three igniter electrodes, which are located at the periphery of the mercury surface, is pulsed, arc spots form on the inner and outer periphery of the cathode groove such that the arc power is distributed and cooling is maximized. The molbdenum is wetted by the mercury and the arc spots are anchored at the mercury-molybdenum interface, thereby eliminating droplet ejection and providing gravity independence. The cathode is water-cooled at a temperature of 20-30°C for which mercury vaporization from the small mercury surface area is minimal, and the anode temperature is maintained at ∿ 50°C in order that mercury does not condense on it. The condenser is cooled to -30°C so that mercury vapor released from the cathode will condense on it. Thus, a low pressure is maintained and the valve operates in the vacuum arc mode. This results in a low voltage drop during conduction (∿30 V) combined with high recovery rates and excellent insulation integrity. The use of this liquid metal cathode in which the arc spots are anchored and mercury evaporation is controlled eliminates the main problems associated with the conventional use of mercury as a discharge cathode.

Anode temperature control is provided by a liquid loop which recirculates Dowtherm at nominally 50°C through the anode at approximately 5 gal/min. High voltage isolation of the bulk of this subsystem, which is near ground potential, from the anode is provided by dielectric hoses and the excellent dielectric properties of the Dowtherm coolant. Instrumentation is provided to calorimetrically measure the thermal input to the anode.

The condenser temperature control system employs a 1-1/2 hp refrigeration unit and a recirculating R-11 liquid loop operating at 4 gal/min to maintain the condenser at approximately -35°C during off periods. The heat capacity of the condenser and cooling system is relied upon to absorb the short-term load during operation such that the temperature of the inner wall of the condenser rises to no more than -10°C; this corresponds to a mercury vapor pressure of 10^{-4} Torr. Instrumentation is provided to permit calorimetric measurements of power input to the condenser.

Two redundant 8 ℓ/sec Varian vac ion pumps are provided to exhaust outgassing products released during LMPVCS operation.

The cathode temperature control system serves to regulate the temperatures of the cathode, surfaces which surround the cathode, and the igniters.

The ignition subsystem supplies voltage pulses to the three semiconductor type igniters as well as to a mechanically actuated igniter which is used in the event that the semiconductor igniters do not operate properly (this never occurred).

The mercury supply system contains an externally pressurized bellows-type reservoir which releases mercury to the cathode by manual command. Because the amount of mercury evolved during one operating period is small in relation to the volume contained by the cathode, feeding is only required between runs.

A control system serves to indicate subsystem status and to disable the LMPVCS if any of the cooling systems malfunction.

Experimental Evaluation

The LMPVCS was initially operated at HRL primarily to condition the cathode by wetting it with mercury but also to verify its high voltage and EMI integrity. Conditioning was achieved by operating with low dc and ac voltages at average currents up to 350 A for an accured time of about 30 min.

Testing at ERADCOM was performed using the circuit shown schematically in Figure 4. The high voltage power supply, charging resistor R_C, and the PFN characteristics were changed during the test program in order to match the range of operating parameters. The load resistor, which employs a recirculating copper sulphate and acid solution, was matched to the PFN impedance to within ∿ 10% except when the effects of mismatching were investigated. The capactive voltage divider was used to measure the rapidly varying voltage at turn-on and the resistive divider to measure the more slowly varying waveforms. Current waveforms were measured by means of the current transformer.

The operating levels are summarized in chronological order in Table 2 where V is the PFN charging voltage, I is the peak current conducted to the matched load, τ is the current pulse width, f is the repetition rate, I_{AV} is the average current delivered to the load, and T is the running time. The average current, which is calculated as $I_{AV} = If\tau$, is within 10% of the value measured using the power supply current meter.

The Sets 1-3 represent operation at up to 100 kV with the PFN and load resistance configured for impedances of 25, 12.5 and 6.25 Ω, respectively. The repetition rate was adjusted such as not to exceed the nominal maximum power supply current of ∿ 5.0 A. In these tests, no misfires (failure to fire when triggered), prefires (breakdown in the absence of a trigger pulse) or current reversals (reverse current when the voltage swings negative) were observed. During testing at a PFN impedance of 6.25 Ω, a load resistance

Table 2. LMPVCS Operating Levels

DATA SET NO.	V, kV	I, kA	τ, μSEC	f, Hz	I_{AV}, A	T, SEC
1	100	2.0	50	50	5.0	60
2	100	4.0	50	25	5.0	60
3	100	7.2	50	13	4.7	60
4	202	0	dc	-	0	120
5	127	2.4	50	36	4.3	60
6	138	2.7	50	32	4.3	60
7	149	2.9	50	30	4.4	15
8	53	3.8	20	50	3.8	60
9	15	1.0	20	250	5.0	60
10	53	3.8	20	100	7.6	35

of 5.2 Ω (20% mismatch) resulted in current reversals in only 20-30% of the conduction pulses. Figures 5 and 6 illustrate characteristic waveforms for the 50 μsec, 6.25 Ω PFN configuration. The current rise time (refer to middle trace in Figure 5) of ∿5 μsec is determined primarily by circuit parameters. The jitter was ∿4 μsec, however, it is expected that this is associated with the relatively slow rise time of the igniter current pulse. The anode fall time, the time for the voltage across the LMPV to drop from 90% to 10% of its original value, was typically 5 μs as shown in the lower trace of Figure 5 (it ranged from 3 to 10 μsec). This time, which is determined by the physical processes within the LMPV, is much longer than had been anticipated on the basis of experiments under different conditions performed at HRL. As a result of the long fall time, the anode dissipation was large; it was 6.6 kW for Data Set No. 3. As seen from Figure 6, the voltage rate-of-rise after donduction is approximately 2.2 kV/msec for the operating voltage of 50 kV.

The voltage withstand tests outlined in Table 2 were performed with a current limiting resistance of 200 MΩ in series with the high voltage power supply. A voltage of 202 kV was reached within 80 min. and held for 2 min. with no activity.

Data Sets 5-7 represent the progression of operating conditions directed toward achieving high power operation at 200 kV. Performance of these tests was limited to 4.5A average by the high voltage power supply, to 149 kV by arc-over of the PFN, and to short run times by R_C. The LMPVCS operated at the higher voltages similarly to its operation at 100 kV; with few exceptions there were no prefires, misfires or current reversals. The maximum average load power reached in these tests was 0.33 MW; the peak power was 0.3 GW.

Data Sets 8-10 were obtained using a PFN-Power Supply assembly capable of supplying 70 kV, 10 kA peak and 50 A average in 10 or 20 μsec pulses. The objective of these tests was to reach the operating levels described in the first column of Table 1. For repetition rates close to 50 Hz, the test results were similar to those obtained previously. At 50 kV and a peak conduction current of 4 kA, the anode fall time was ∿4 μsec; times as low as 1.5 μsec were occasionally observed. Calorimetric measurements of the power input to the condenser at 50 kV, 3.8 kA peak and 7.5 A average indicated that less than 4% of the total LMPV power dissipation was in the condenser; this is much less than the 30% measured for operation with 60 Hz ac. The dissipation in the cathode, also measured calorimetrically, was less than 1%. Thus, for an LMPV operating under short pulse conditions, more than 95% of the total dissipation is in the anode.

As the repetition rate was increased, misfiring begain to occur; a misfire rate of approximately 5% was observed at 250 Hz with low average power.

When the average load power level was increased to 0.2 MW at 100 Hz (Data Set No. 10) electrical breakdown of the interelectrode space occured after ∿ 30 sec. The misfire rate was also sporadically high, however, no prefires or reverse current was observed. On the third attempt to operate at this level the anode failed catastrophically and anode coolant was released into the interelectrode space. This terminated the testing.

The anode was subsequently removed from the LMPV for inspection. A spot approximately 1 cm in diameter, which was located on the anode face almost directly above the igniter in use at the time of failure, appeared to have been heated to its melting point. A narrow crack approximately 5 cm long passing through this spot was the source of coolant leakage. The high power concentration was probably due to the prescence of an electron beam during the anode fall time which is emitted from arc spots localized near the igniter; presumably the arc spots do not spread significantly during the fall time.

Although brief attempts at ERADCOM to reduce the fall time met with little success, single pulse tests were subsequently undertaken with an identical LMPV at HRL with the objective of reducing the fall time. These tests were performed using a series L-C circuit which provided a current pulse waveform similar to that existing in the damaging ERADCOM tests. For the same LMPV parameters as used in the ERADCOM tests the fall time was, as before, ∿5 μsec.

However, as the condenser temperature was varied from -40°C to room temperature, the anode fall time decreased for temperatures above about 0°C. With both the condenser and cathode at room temperature, fall times of typically 0.2 μsec were measured at voltages up to 38 kV, peak conduction currents up to 12 kA, current rates-of-rise up to 7 kA/μsec. The Paschen breakdown voltage under these conditions was ∿45 kV. This result indicates a significant relationship between mercury vapor density and the anode fall time. Further experimentation is necessary to determine the details of the relationships between temperature, fall time, and withstand voltage.

Footnotes

*This work was performed under Naval Surface Weapons Center, Dahlgren Laboratory Contract No. N60921-76-C-0139 with support from the Air Force Aero Propulsion Laboratory, Defense Advance Research Agency, and US Missile Research and Development Command.

**Bayless, J.R., and Heckl, J.P., "The Liquid Metal Plasma Valve Closing Switch," Proceeding of IEEE International Pulsed Power Conference, Lubbock, Texas, Nov. 9-11, 1976.

***Eckhardt, W.O., U.S. Patent No. 3,659,132 (1972); G. Eckhardt and W.O. Echardt, "Liquid-Metal Plasma Valve Configuration," U.S. Patent pending.



Figure 1. The LMPVCS

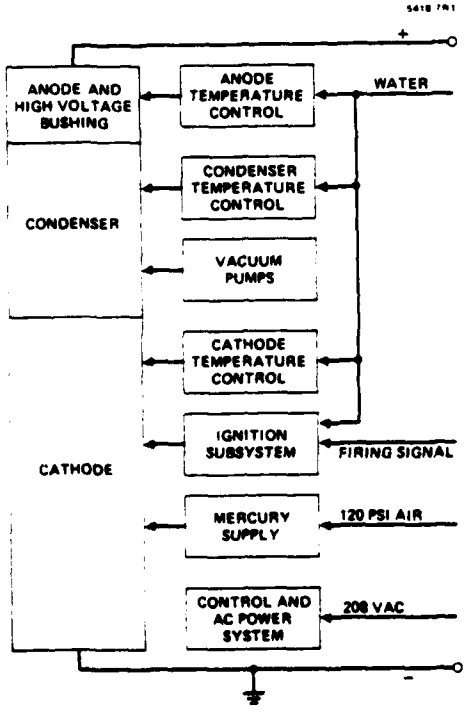


Figure 2. Block diagram of LMPVCS system.



Figure 3. The LMPV being prepared for bakeout.

7582-2R1

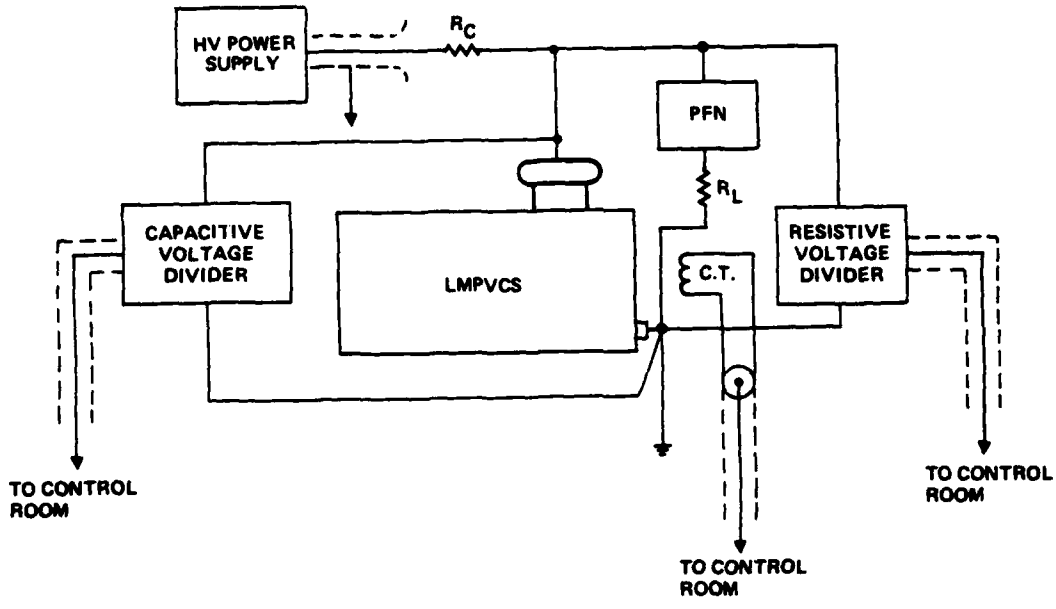


Figure 4. Schematic of test arrangement.

7582-3R1

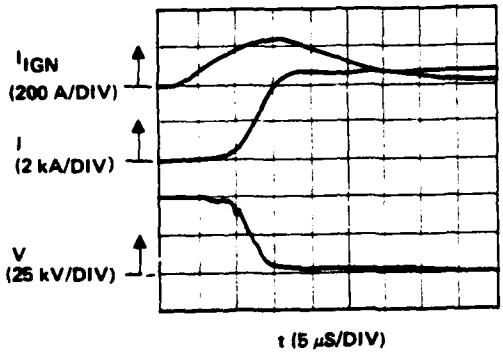


Figure 5. LMPVCS conduction waveforms. The top trace is the igniter current, the middle trace is the conduction current, and the lower trace is the anode voltage.

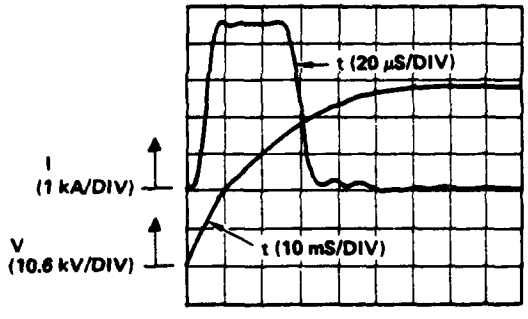


Figure 6. LMPVCS waveforms. The top trace is the conduction current and the lower trace is the anode voltage.

DEVELOPMENT OF A 100 kV MULTIMEGAWATT REP RATE GAS SWITCH*

Allen Ramrus

Maxwell Laboratories, Inc.
9244 Balboa Avenue
San Diego, California 92123

Abstract

A 100 kV gas switch has been developed and tested which is capable of controlling 5 MW average power when operated up to 250 pps repetition rate. Recovery of the switch voltage hold-off capability after each discharge was accomplished by providing both a 1 millisecond grace period during which no voltage is reapplied, and by continuously purging the switch with 40 psig pressurized air at flow rates up to 60 SCFM. The switch was tested using a simulation technique in which the switch was subjected to the same repetitive peak voltage and current as it would in controlling several megawatts of average power. Limits of switch performance as a function of air flow rate and peak voltage have been established.

Introduction

Development of high average power switching was initiated at Maxwell under contract with Wright Patterson Air Force Base early in 1974. The objective of that effort was to acquire capability to switch pfn type pulsers which operate in the voltage range of 100 kV, with impedance of tens of ohms, and power in the multimegawatt regime. To avoid the capital outlay required for such a high-power test facility, Maxwell devised a simulation technique capable of providing the *same* peak current, voltage, and charge transfer as would occur at full-rated power, but with a simulator which required only ≈10% of full power.[1,2] The simulator circuitry underwent significant development during this program and the initial prototype switch was developed capable of controlling about 5.6 MW.

The prototype switch was composed of hollow cylindrical electrodes through which high velocity compressed air flowed to purge the decay products after each discharge. A 150 SCFM flow-rate was shown to be a requirement to attain the highest power levels with this spark gap. Another parameter shown to be important was the grace period, the time following the completion of a pulse, during which no voltage is reapplied to the switch. A grace period of 1 msec was shown to be adequate to ensure acceptable switch performance.

A second program was then sponsored by Naval Surface Weapons Center with the objective of furthering this development, while utilizing the circuitry previously developed. Key accomplishments during the latter program were (1) establishment of operating parameters with extremely low malfunction rate; 100 kV, 5.6 MW switch tests occurred in which no malfunctions whatsoever occurred after 10 sec bursts at 250 Hz and (2) maintenance of high-power capability at reduced flow-rate.

These objectives were accomplished with a new switch design, called Configuration II and shown in Figure 1, which features gas flow which is highly directed at the region where sparking occurs. In contrast, the previous hollow electrode approach utilized gas flow which purged relatively large electrode areas. This Configuration II design succeeded in reducing flow to about 60 SCFM while still maintaining negligible malfunction rate over the 10-second test durations. A brief review of the electrical details in this simulation technique is contained in the next section. The convention used in specifying the peak power rating, e.g. the 5.6 MW rating indicated above, assumes the switch is intended to discharge a generator whose internal impedance is negligible compared to the load impedance; in that case, the switch charge voltage equals the load voltage. Often the load voltage is only one-half that initially across the switch because the load and internal impedances are matched. Then, for given pulse duration and current, the power rating would be 2.8 MW. Since an important application of the switches discussed in this report are pfn's with matched loads, the lower rating will be employed. For example, the 100 kV switch discussed in this paper passed 0.24 coulombs at the rate of 250 pps. Mounted in a generator of low impedance it would deliver power of 100 kV x 0.24 C x 250 pps = 5.5 MW. If in a generator of impedance matching the load, the delivered power would be 50 kV x 0.24 C x 250 = 2.6 MW.

Experimental Setup

The simulator is composed of separate high-voltage and high-current sources, as shown in Figure 2. The high-voltage source provides the >100 kV switch charge voltage, *from a high impedance source*. This recharge waveform from the voltage waveform generator (vwg) is isolated from the high current source with a switch identical in all respects to the test switch. The high-current source, which consumes most of the circuit power, is composed of a high-power circuit capable of charging a relatively large capacitor to about 8 kV.

A more detailed schematic is in Figure 4 in which (1) the current circuit, (2) the vwg circuit and (3) the trigger generator are shown.

(1) Three transformers each capable of providing 1.5 MVA reduce the power company's 12 kV to 4160V which is then rectified in a diode bridge circuit as shown in Figure 5. When the ignitron command fires, C_s is

*This development was supported by the Naval Surface Weapons Center, Dahlgren, Virginia under Contract N60921-76-C-0274.

CH1371-4/78/0000-0088$00.75 ©1978 IEEE

resonantly charged through the 1.3 mH inductor to about 8 kV.

The charge on this capacitor is important in calculating simulated load power. In a conventional circuit, the power dissipated in a resistive load is given by the equation

$$p = prf \times \int_0^T IV\, dt \quad .$$

where prf is pulse repetition frequency, T is pulsed duration, I and V are load current and voltage respectively.

For square pulses, V_o is constant and

$$p = prf\ V_o \int_0^T I\, dt$$

$$= prf\ V_o \times Q_o \text{ where } Q_o$$

is the charge transferred.

To calculate the simulated power delivered to the load in this test circuit, we use the same basic equation: $p = prf \times V_o \times Q_s$, where V_o is the peak voltage and Q_s is charge stored in C_s.

The capacitor C_s discharges through the load R_L when both switches close. The inductors and load resistor, R_L, are selected to provide about 20% voltage reversal on C_s to insure commutation of the ignitron. These circuit parameters also allow control of peak current, up to about 6 kA.

(2) Voltage Waveform Generator

In many applications for which this switch is intended, recharging the electrodes will occur relatively soon after completion of a pulse regardless of how long afterwards the switch is again required to close. In anticipation of this, the recharging voltage waveform is applied about 1 msec after a discharge. The risetime of this recharge waveform is about 1 msec. For example, for 250 prf the switches are required to hold off this full voltage for about 2 msec since the interpulse period is 4 msec. This 1 msec grace period and the 1 msec risetime were held constant throughout this program.

The voltage waveform generator is powered by a 0 - 20 kV, 10 kW power supply which charges a capacitor, typically 30 μF for maximum power tests. A thyratron discharges the capacitor into the primary of a 1:7.5 step-up transformer. The output of this transformer is passed through a pfn to provide an approximately square waveshape to the switch common-point. The diode D_3 maintains the voltage at the common-point until the switches close.

(3) Trigger Generator

During normal circuit operations the switches withstand the VWG waveform until they are triggered. The trigger circuit delivers a trigger pulse up to 200 kV with a risetime of 10's of nsec.

A 400 pF coupling capacitor is installed between the trigger circuit and the high-power circuit; this enables the trigger voltage to add to the voltage waveform generator, ensuring switch closure on the rising portion of the trigger waveform.

It is essential for the operation of this circuit that low switch jitter be maintained to ensure both switches close reliably. Installation of circuit inductance between the switches, between the test gap and the load, and between the isolation gap and the source capacitor, was found desirable to partially isolate these components. The total inductance available depends on the desired operating parameters of the circuit. For example, to attain a desired peak current of 5 kA circuit inductance of ≈20 μH is required. This inductance is placed as shown (Figure 4) to optimize circuit performance. If the inductance in a branch is too low, circuit malfunctions occur because when the switch connected to this branch fires slightly earlier than the other, the common-point voltage is abruptly reduced, thereby inhibiting closure of the second switch.

The trigger circuit is connected to the common-point via a pair of spark-plugs which provide ultraviolet illumination to the negative electrode. As the trigger voltage is applied, the spark-plugs fire prior to the breakdown of the main spark gap. The illumination is important to maintain minimum jitter. The time sequence of the main events is sketched in Figure 6.

Diagnostics

Switch Common-Point Waveform

The switch waveform is obtained with a resistive voltge divider composed of a series-string of carbon resistors connected between the common-point and ground. The monitor output is connected to a magnetic-tape recorder capable of recording at high speed to attain 300 kHz bandwidth. Playback of this recorder occurs at conventional speeds for recording on thermosensitive tape.

A Pearson current probe provides the diagnostic waveform of the recharge current flowing through L_s. Examples of this waveform, that from the voltage waveform generator, and a timing mark from the trigger generator are displayed on the tape-playback shown in Figure 7.

Periodically, conventional oscillography is employed to calibrate the current and voltage waveform, for assurance the circuit conformed to specifications. Figures 8 and 9 show discharge current and voltage respectively.

Pneumatics

A compressor system stores the compressed air required to purge the switches. The reserving volume is 60 ft^3, pressurized to about 100 psig. During a ten-second burst, this pressure normally drops to ≈65 psig. The regulators in the intake and manifolds appear to maintain pressure at approximately the preset value which is less than 50 psig

for tests to date. Figure 10 shows the flow diagram.

Flow velocity is measured with Pitot tubes located at the gas outputs of the switches. Flow readings from these tubes agree closely with flow-rate measured by reservoir pressure change. Most data to date was taken with 1550 ft/minute flowing in a 2-7/8" diameter output tube, from which is derived the 63 SCFM flow rate.

Circuit Performance

Three variants of switch malfunctions manifested themselves early in the program:

(1) Spurious triggering: switch transients were capable of triggering the ignitron in the power source.

(2) Switch prefires: with inadequate gas flow, switch prefires (restrikes) occurred, as shown in three instances of Figure 11 (in which circles point to prefiring on the voltage waveform).

(3) Switch no-fires: Figure 12 shows an example of switch no-fire. In that case, the isolation and test switches failed to break down. Therefore, the recharge current waveform is absent and the voltage waveform generator is attempting to reapply voltage. Since the switch is already charged, the voltage increases still further until self-break occurs.

Usually, switch malfunctions resulted in no significant damage to circuit components. Periodically, however, a switch would enter a so-called lock-on mode characterized by a continuous arc across the electrodes fed by the high current source. Current of $\geq$10 kA would flow for a substantial fraction of a second until a circuit interrupter actuated. The charge transfer through the switch would therefore be many tens of coulombs which tended to pit the electrodes and scorch the insulator. A typical waveform resulting from a lock-on is shown in Figure 13. These triggering problems were overcome by a careful shielding of low level timing circuits within screen rooms and by placing small, low inductance filter networks at various points within the circuit to damp transients propagating from the switches back to the components associated with the ignitron firing. Ultimately, trouble free performance was attained, resulting in ten-second bursts at 100 kV, 1/4 cb. 250 prf and 5 kA with no malfunctions.

Simulation Quality

The subject of simulation quality, that is the accuracy with which one can predict actual high-power performance levels based upon the simulation results, is not treated in detail in this paper. For spark-gaps of interest to this program the factor most relevant to high-voltage recovery is heat dissipation within the gas. Following are some general comments regarding heat dissipation within the gap due to the arc plasma.

Consider a means of comparing the heat dissipation per pulse for a switch in a simulator with that of a switch in an actual high-power circuit. In both cases, the energy dissipated in the gas during the resistive phase[4] of gap breakdown, assuming the voltage range of 100 kV, is less than about 10J. (These estimates are provided in Appendix I of ref. 3). This is small compared to the dissipated energy due to joule heating within the gap which occurs over many μsec. T. James and J. L. Browning[5] indicate an arc-drop of $\approx$150V is expected. Current of 5 kA, flowing for $\approx$50 μsec therefore provides $\approx$40 J/pulse. This suggests, if current and pulse width in the simulator are the same as those of an actual high-power circuit, approximately the same dissipations should be expected since most of this energy is dissipated during the late time of the waveform, and the current and arc-drops are approximately the same in the two cases.

Acknowledgement

The bulk of the engineering effort applied to this program was provided by the late Dennis Markins in collaboration with Richard Fitch. Our thanks also extend to P. Krickhuhn and W. Richardson for their skill in initially trouble-shooting the apparatus and for their assistance in performing the experiments.

References

1. High Power Spark Gap Switch Development, Final Report. MLR-484, May 1975.

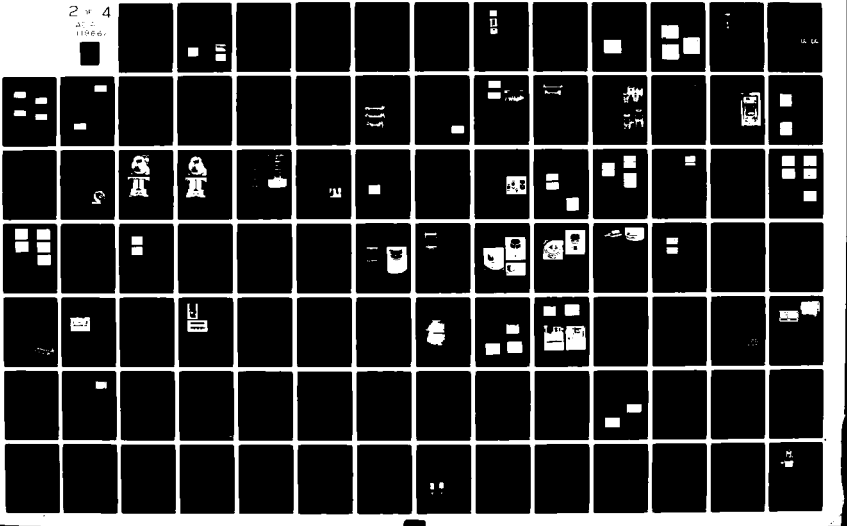
2. High Repetition Rate - High Average Power Spark Gap Switch Studies, W. Clark and V. Fargo, 1976 Pulsed Power Systems Workshop, Naval Surface Weapons Center, White Oak Laboratory, Silver Springs, Md.

3. High Power Spark Gap Optimization, Final Report, MLR-670-2, June 16, 1977. Naval Surface Weapons Center, Dahlgren Laboratory, Dahlgren, Virginia.

4. Duration of the Resistive Phase, J. C. Martin, AWRE, Aldermaston, England.

5. Arc Voltage of Pulsed High Current Gaps, T. James and J. L. Browning, UKAEA Research Group, Culham Laboratory, Abingdon, Berks.

AD-A119 662 PALISADES INST FOR RESEARCH SERVICES INC NEW YORK F/G 9/5
IEEE CONFERENCE RECORD OF 1978 THIRTEENTH PULSE POWER MODULATOR--ETC(U)
1978
UNCLASSIFIED 78-CH-1371-4-ED NL



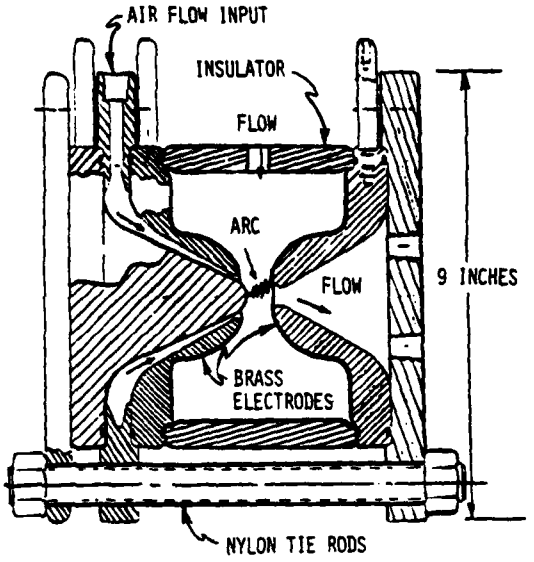


Figure 1. Configuration II rep rate spark gap switch assembly, SK68146.

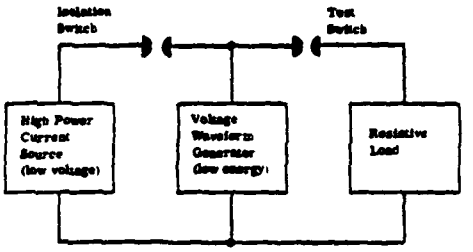


Figure 2. Simplified switch test circuit.

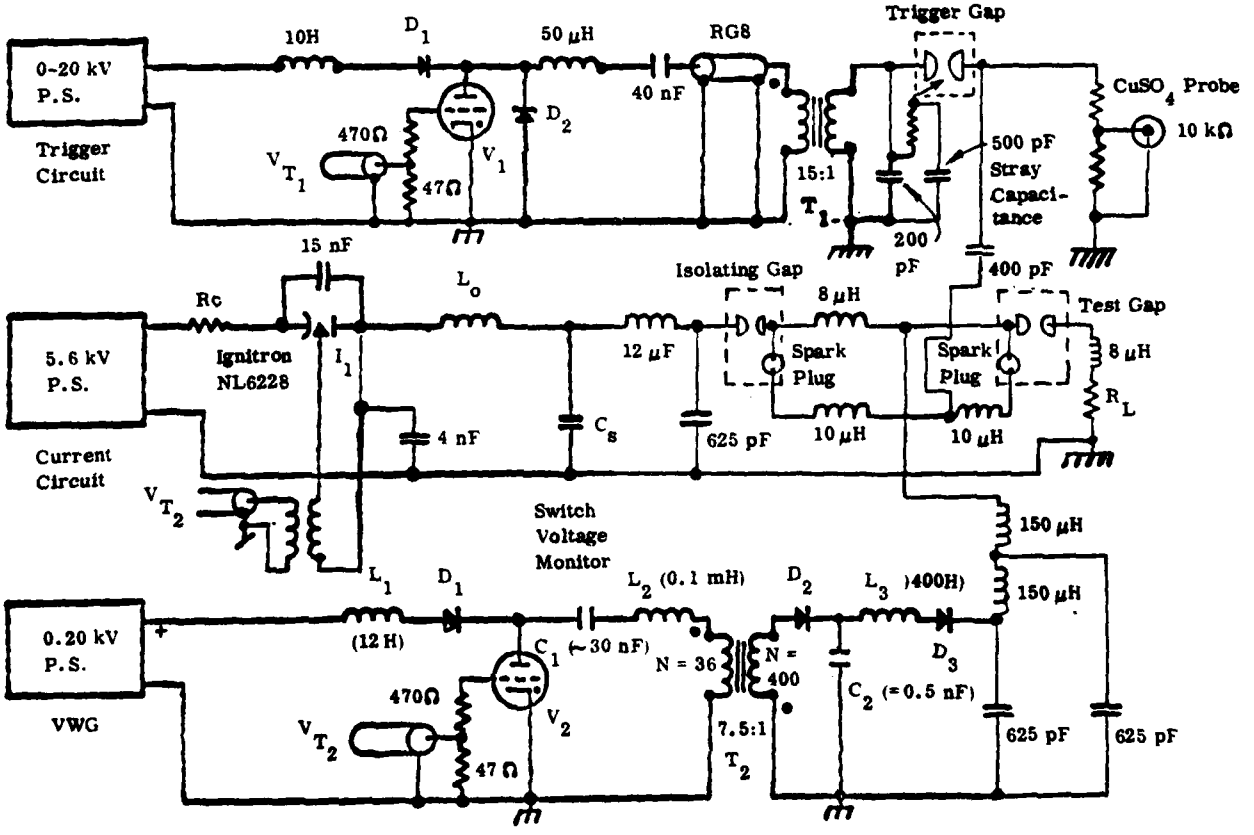


Figure 4. Updated circuit diagram for the Maxwell Laboratories, Inc. high power switch test facility.

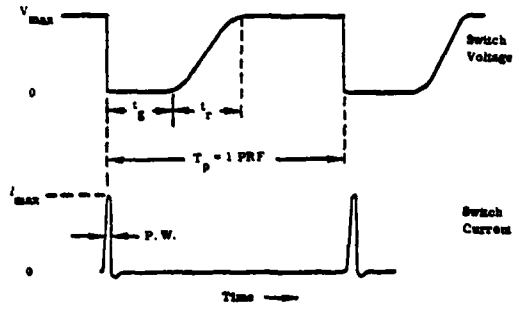


Figure 3. Idealized switch voltage and current waveforms. (P.W.-pulse width, t_g - grace period, t_r - rise time, T_p - interpulse period).

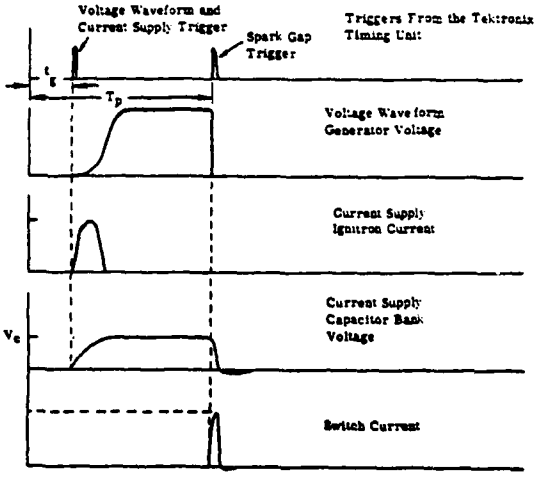


Figure 6. Time sequence of voltages and currents in the switch test facility.

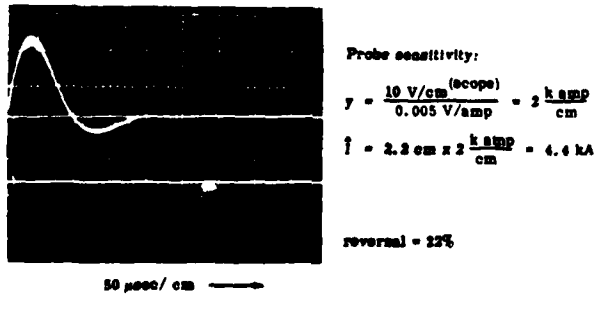


Figure 8. Load current into R_L = 0.88Ω, C_C = 8 kV, V_O = 60 kV. Sensor is a Pearson probe mod. 301A which has 0.01 V/amp sensitivity unterminated and 0.005 V/amp when terminated in 50Ω as in the present case. prf = 250 pps.

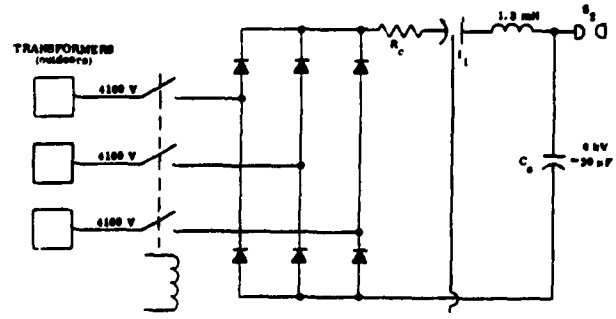


Figure 5. Main power source. 4160 volts, 3-phase with 1 MW capability is rectified to provide pulsating dc, rms = 5.6 kV dc which resonantly charges C_s to 8 kV.

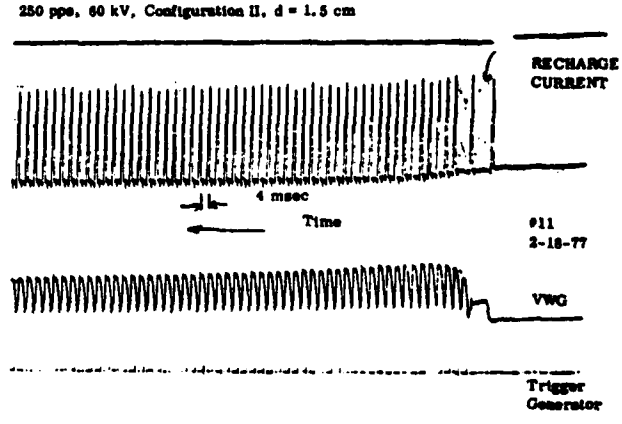


Figure 7. Magnetic tape record of recharge current and common-point voltage waveform for Configuration II switch with d = 1.5 cm.

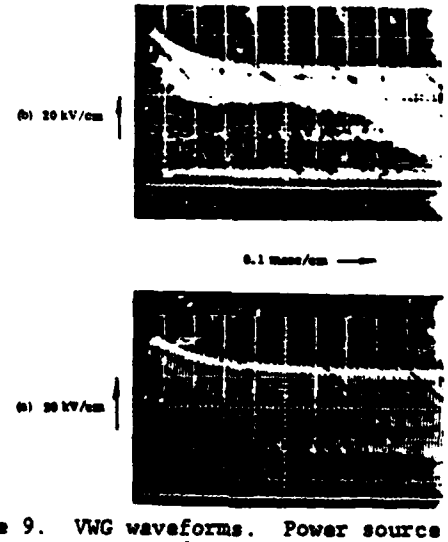


Figure 9. VWG waveforms. Power source not connected.
(a) 100 pps
(b) 150 pps
20 kV/cm, 0.1 msec/cm

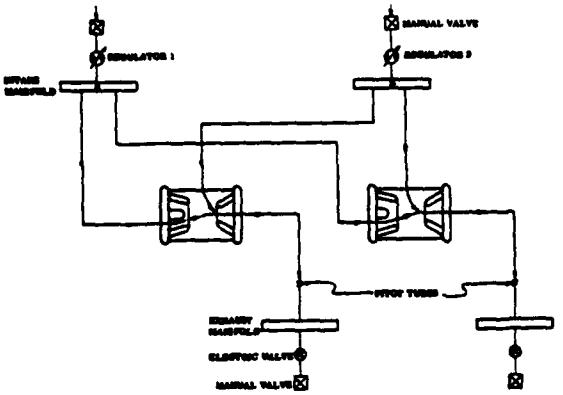


Figure 10. Air-flow diagram for Configuration II switch test.

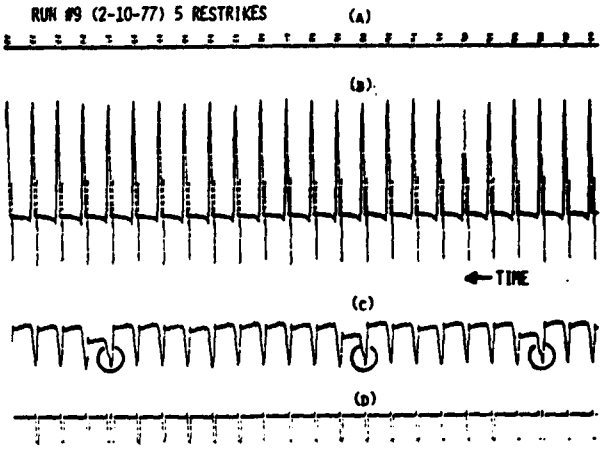


Figure 11. Run #9 (250 pps) of Configuration I switch, showing prefires (circles). Magnetic tape record of (a) ignitron trigger, (b) recharging current waveform, (c) voltage waveform generator output (common point), (d) trigger to trigger generator.

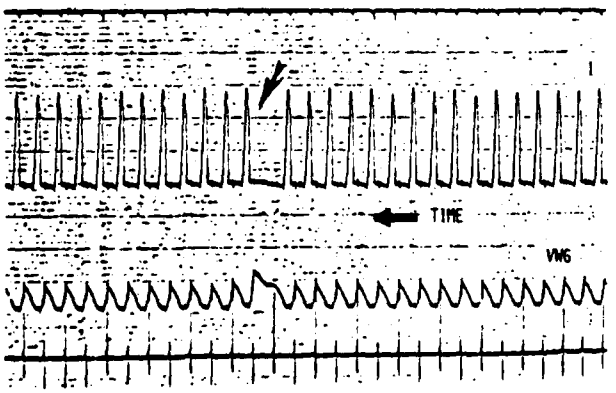


Figure 12. Recorded waveform several seconds after previous figure. The arror points to a no-fire of both switches. Recharge waveform increased voltage until self break occurred.

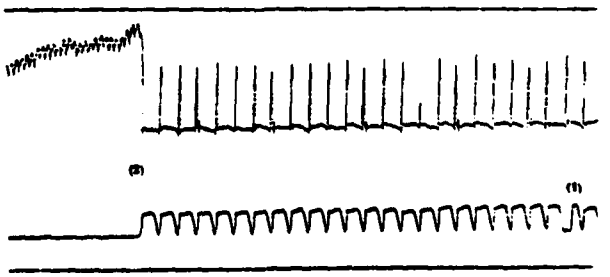


Figure 13. Magnetic tape record of recharge current and VWG waveform for early Conf. II test. Point (1) shows switch prefire, point (2) shows switch lock-on.

MULTICHANNEL SURFACE SPARK GAPS

by

W.J. Sarjeant, R.S. Taylor, A.J. Alcock and K.E. Leopold
National Research Council of Canada
Division of Physics
Ottawa, K1A 0R6, Canada

Summary

A study has been undertaken on high pressure surface discharge switches potentially capable of moderate repetition rate operation. The parametric experiments reported were carried out utilizing the gaps as transfer switches, under pulse charging conditions, between several types of low impedance transmission lines and a high pressure rare gas halide laser discharge, acting as the load. The effects of spark gap internal geometry, gas composition and controlled changes in the laser load, upon gap multichanneling, closure simultaneity and peak hold-off capability are discussed. These surface gaps, of length 66 cm, reliably close 19 channels per side (29 per meter) with a hold-off voltage greater than 120 kV and a closure simultaneity of ∿2 ns for the first 500 shots, increasing to ∿5 ns and remaining there for 10,000 shots, the test limit to date. Preliminary results at higher charging voltages have yielded intense multichanneling with hold-off voltages in excess of 210 kV.

Introduction

A low-inductance surface discharge spark gap (SSG) has been developed as a transfer switch in multiatmosphere gas discharge lasers.[1] In these lasers, the production of volume glow discharges is required for efficient laser operation and high output beam quality.[2,3] In order to achieve this with highly overvoltaged, constant E/N excitation, a low inductance transfer switch is required between the pulse charged PFN or transmission line and the laser electrodes.[4] A parametric study of this switch, sketched in Fig. 1, was thus undertaken in a test geometry shown in Fig. 2. The scale drawing of the SSG illustrates its simplicity of construction. The switch element is fabricated of 0.125 inch thick type G-30 modified polyamide rigid copper clad laminate having 2 oz. copper cladding. The copper is etched away to somewhat less than the desired 2.0 cm gap spacing with final finishing being done on an end mill, executing in addition about a 0.005 inch undercut into the laminate. This last step has been found to ensure long-term, stable multichanneling. The complete SSG unit is assembled using Viton O-rings and high strength insulating bolts.

The switch was then inserted into the laser test assembly in Fig. 2 and pressurized with high purity nitrogen. In order to characterize it, voltages, on both electrodes were measured with modified versions of a fast probe system described previously.[5] The dc resistance of each probe was approximately 3 kΩ.

The laser, similar to a diode magnetron load, was filled with the mixture required for maximum output energy, i.e., F_2:Kr:He in the ratio of 1:18:1500. For a nominal peak voltage on the transmission line of 150 kV, less than 10 kV appeared across the laser during the charging time. This voltage decreased sharply with reduced charging voltage. The peak hold-off capability of the SSG was then defined as the peak voltage appearing across the device. The effects of $\dot{B}$ contributions on the voltage monitors were checked and found to be ∿5%. Taking this and other sources of error into consideration, the empirical relations derived have an accuracy of ∿10%. The number of channels closing and their temporal evolution were recorded using high speed streak photography. Open shutter photographs of gap closure showed about 1.5 times as many bright channels as observed in the streak photographs.

Multichanneling was investigated utilizing both a ceramic capacitor PFN[1] and water transmission line,[4] with comparable results. As the latter provided potentially higher voltage capability the parametric study of SSG performance described below was executed with this system.

Results

Pulse charging of the transmission line in ∿100 ns was obtained by discharging two 0.1 μF, 100 kV storage capacitors through a single channel spark gap. Figure 3 shows (a) an open shutter photograph of the SSG breakdown, a streak photograph of (b) multichanneling and (c) gap closure. Since the imaging system also recorded the laser fluorescence (not shown) only 80% of the length of the SSG was recorded by the streak camera, so that the number of channels plotted in the following data are corrected for this. Varying the dc charging voltage from 40 to 92 kV produced strong multichanneling with suitable adjustment of the N_2 pressure in the SSG. Closure simultaneity remained within 5 ns for most test conditions, increasing to 10 ns at higher N_2 pressures. Figure 4 illustrates the dependence of the number of channels closing along the 0.66 m active length of the SSG, on the hold-off voltage of the gap. For laser gas fill pressures of 3 and 6 atm the best fit to the data in Fig. 4 gives:

$$N = 0.35\ V_h - 17 \qquad (1)$$

where N is the number of channels closing per meter (±1) and V_h is the hold-off voltage in kV.

The increased hold-off for fixed N_2 pressure is presumed to come from the faster charging time observed at higher dc voltages. The relationship between hold-off voltage and risetime is given by

$$V_h = 1.2\tau_r^{-2} \qquad (2)$$

where τ_r is the 10 to 90% rise time of the charging wave in microseconds. For a fixed

CH1371-4/78/0000-0094$00.75 ©1978 IEEE

dc voltage of 84 kV, Fig. 5 gives the dependence of V_h/N upon the pressure of N_2 in the SSG. Up to 3 atm there is a linear increase:

$$V_h/N = 2.8\ P_{N_2} - 0.8 \qquad (3)$$

where PN_2 is the SSG pressure of N_2 in atm. Above 3 atm, the peak voltage on the transmission line is nearly constant and V_h/N remains at 19. Over this range of N_2 pressures τ_r is 90 ns and the rise-time of the voltage on the laser remains at 12 ± 3 ns. This latter rise-time remained constant, to within 3 ns over a wide range of charging voltages, N_2 pressure and laser gas pressure suggesting that the duration of the resistive phase is relatively constant.[6]

In both the above cases a straight line provides a reasonable fit to the data. Initial measurements at higher charging voltages have produced denser multichanneling with hold-off voltages in excess of 210 kV. Further experiments are planned to determine the applicability of the present data, and the results of previous breakdown studies,[7,8] to the scaling of switch operation from 0.2 to up to the ∿1 MV level. At this time closure simultaneity in the switch of ∿5 ns has been observed in on-line laser operating at 10 ppm and peak charging voltages of 140-150 kV for at least 10,000 shots to date. Tests at 1 pps have recently demonstrated the unsuitability of the present substrate material for long-life operations. Initial tests with prototypes utilizing boron nitride substrates in a SSG have yielded promising results and may have direct applicability to modest repetition rate systems operating in the range of 10-20 Hz.

References

1. W.J. Sarjeant, A.J. Alcock and K.E. Leopold, "A scalable multiatmosphere high-power XeF laser", Appl. Phys. Lett., 30, No. 12, 15 June, 1977, pp. 635-637.
2. C.A. Brau, A.E. Greene and S.D. Rockwood, "Theoretical model for discharge excited rare gas halide lasers", Second Winter Colloquim on Laser Induced Chemistry, 13-16 February, 1977 and C. Brau, "Excimer Lasers", presented at the Third International Congress and International Trade Fair, 20-24 June, 1977, Munich, Germany.
3. W.J. Sarjeant, A.J. Alcock and K.E. Leopold, "Constant E/N pumping of high power rare gas halide lasers", post-deadline paper presented at the 1977 IEEE/OSA Conference on Laser Engineering and Applications, Washington, 1-3 June, 1977.
4. R.S. Taylor, W.J. Sarjeant, A.J. Alcock and K.E. Leopold, "Glow-discharge Characteristics of a 0.8 Joule High Pressure Rare Gas Halide Laser", accepted for publication in Optics. Comm.
5. W.J. Sarjeant and A.J. Alcock, "High-voltage probe system with subnanosecond rise time", Rev. Sci. Instrum., 47, No. 10, October 1976, pp. 64-68.
6. J.C. Martin, "Duration of the resistive phase and inductance of spark channels", AWRE Switching Notes, No. 9, Dec. 1965.
7. J.C. Martin, "Pressure dependency of the pulse breakdown of gases", AWRE Dielectric Strength Notes, No. 15, 26 September, 1967, and J.C. Martin, "Pulsed surface tracking in air and various gases", AWRE SSWA/JCM/745/735, May 1974.
8. J.C. Martin, "Multichannel gaps" AWRE Switching Notes, No. 10, 5 March 1970.

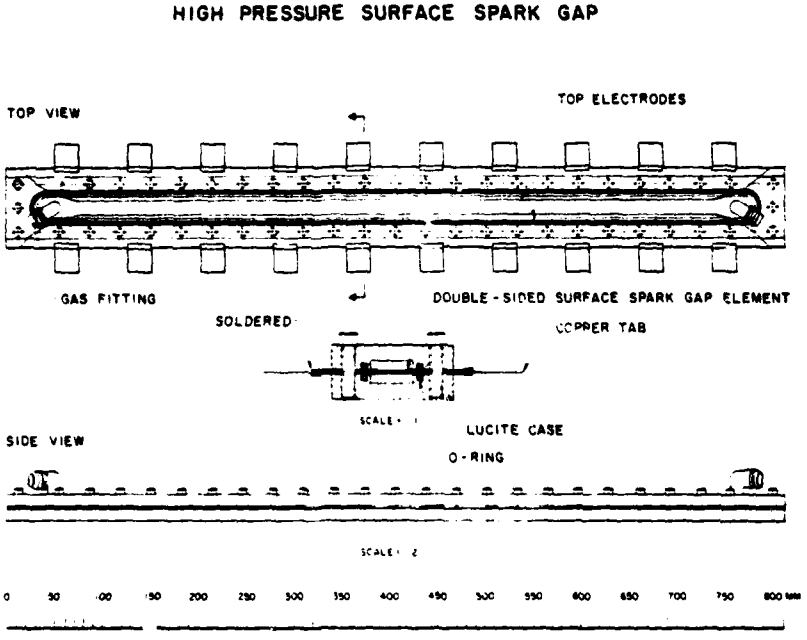


Fig. 1 Scale drawing of the pressurized multi-channel surface spark gap.

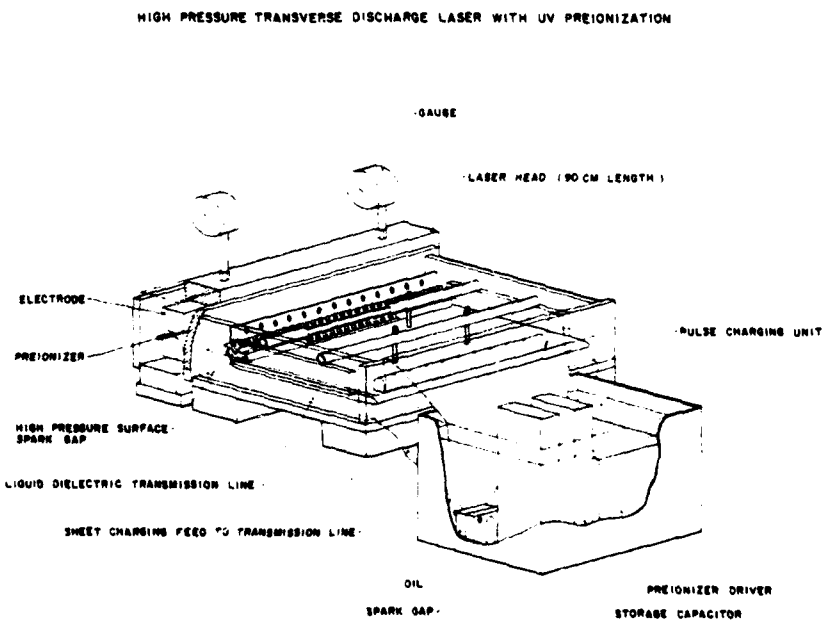


Fig. 2 Schematic representation of the complete laser system utilized as the surface spark gap test bed.

Multichanneling in 2.4 atm Surface Spark Gap

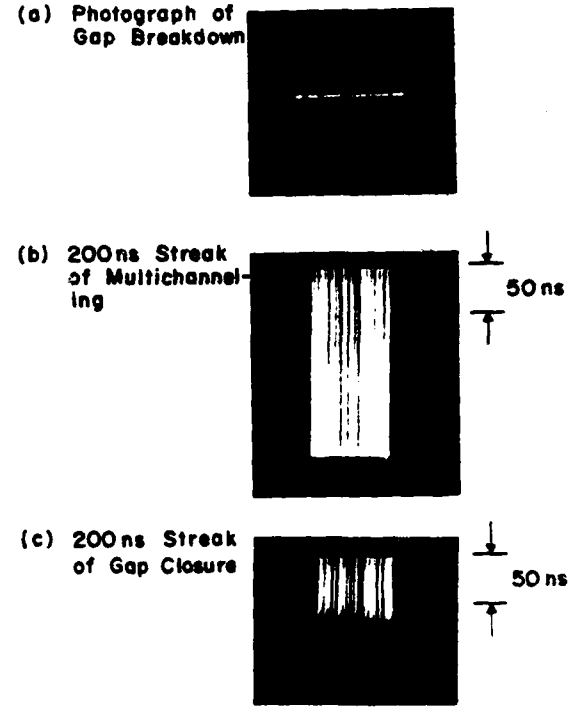


Fig. 3 (a) Open-shutter photograph of the SSG breakdown for a DC charging voltage of 84 kV and a 6 atm gas mexture in the laser.

(b) 200 ns Streak photograph of SSG multi-channeling starting 20 ns after gap closure.

(c) 200 ns streak photograph of the SSG gap closure.

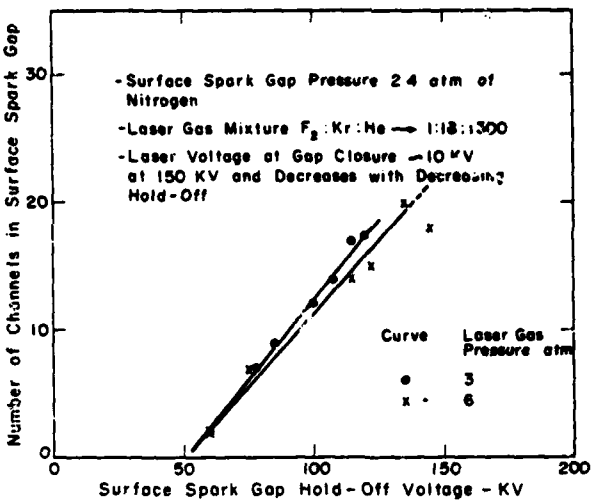


Fig. 4 Dependence of the number of channels upon the SSG hold-off voltage for fixed SSG and laser pressures.

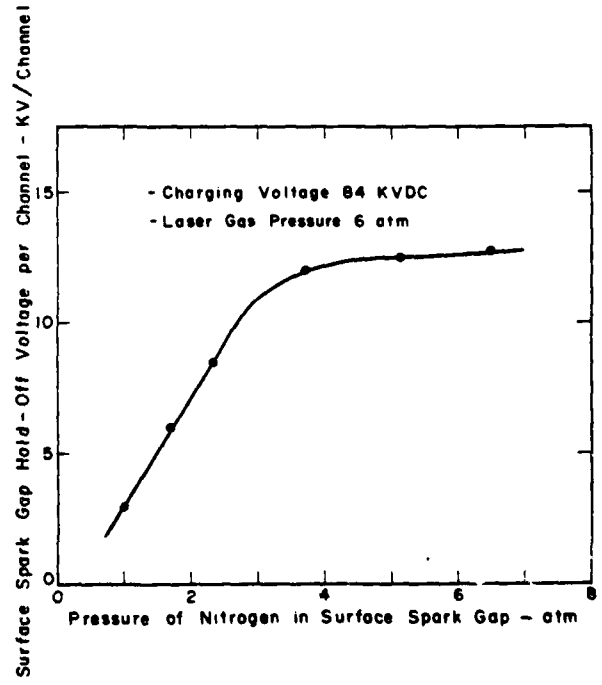


Fig. 5 Dependence of the SSG hold-off per channel as a function of the N_2 pressure for a fixed DC charging voltage of 84 kV.

HIGH REPETITION RATE BURST-MODE SPARK GAP*

A. Faltens, L. Reginato, R. Hester, A. Chesterman,
E. Cook, T. Yokota, W. Dexter

University of California
Lawrence Livermore Laboratory
Livermore, California 94550

SUMMARY

Results will be presented on the design and testing of a pressurized gas blown spark gap switch capable of high repetition rates in a burst mode of operation. The switch parameters which have been achieved are as follows: 220-kV, 42-kA, a five pulse burst at 1-kHz, 12-ns risetime, 2-ns jitter at a pulse width of 50-ns.

Spark Gap Design

The construction of the coaxial spark gap[1] is illustrated in Fig. 1. The spark gap bolts on to the lower end of a 5.2-Ω coaxial water Blumlein and is designed to switch the mid conductor to ground. The Blumlein's mid conductor feeds through a polycarbonate resin insulator which interfaces between the water

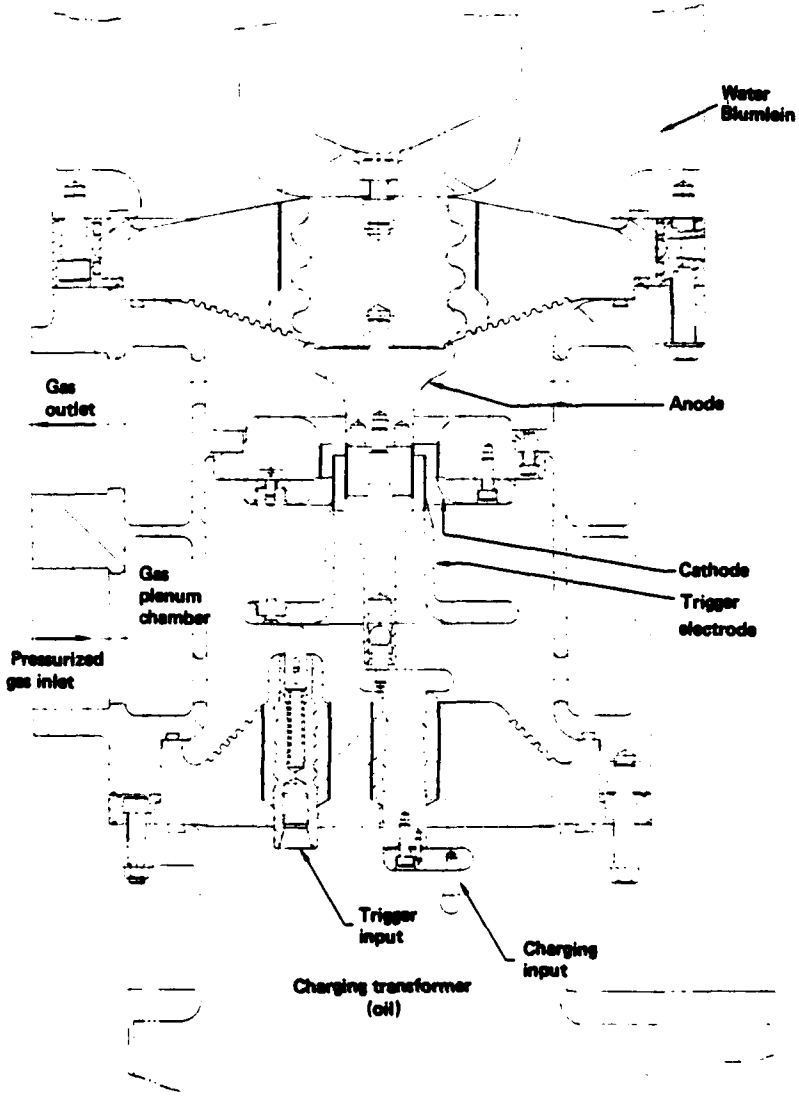


FIG. 1 SPARK GAP CROSS SECTION

*This work is jointly supported by the U.S. Department of Energy under Contract No. W-7405-Eng-48 and the Department of the Navy under Contract N00014-78-F0012.

U.S. GOVERNMENT WORK NOT PROTECTED BY U.S. COPYRIGHT.

and high pressure gas and becomes the switch's anode. This electrode continues through a second lexan insulator separating the high pressure from the oil filled charging transformer. The center electrode or anode of the switch is 3.81-cm in diameter and is made of stainless steel with a .76 mm thick, 3.18-cm long tantalum insert where the actual arc is to occur. The trigger electrode is a concentric cylinder 30 mils thick and 3.18-cm long, also made of tantalum. The ground electrode or cathode is stainless steel with a .76 mm thick cylindrical tantalum insert 1.91-cm long and 6.76-cm in diameter. The tantalum cylindrical liners are made to give the spark gap long life and to be easily replaceable after wearing out. Concentricity of tantalum inserts is maintained with 5 mils maximum deviation. The coaxial cylindrical geometry was adopted for two main reasons: long life and high rep-rate. The trigger electrode is expected to wear uniformly in the axial direction with no change in the spark gap electrical characteristics. The 30 mil tantalum cylinder can then wear for 2-cm axially before replacement should be necessary.

Secondly, since we chose to achieve the 1-kHz rate by blowing gas through the spark gap, the coaxial geometry assures high gas velocity and low pressure drop. The chamber on the outside of the spark gap reduces the pressure drop and provides uniform gas flow through trigger to ground and trigger to anode.

The interface insulators were made of polycarbonate resin because of their strength and resistance to high voltage tracking. Some cold flow problems were encountered when we tried to use cast epoxy for those insulators.

Charging System

In order to obtain high rep-rates, careful attention must be given to the charging system. Fig. 2 shows the charging pulse to the Blumlein and spark gap being triggered at the peak of this wave form. A resonant transformer coupling coefficient of .525 was chosen because this gives current non-reversal in the

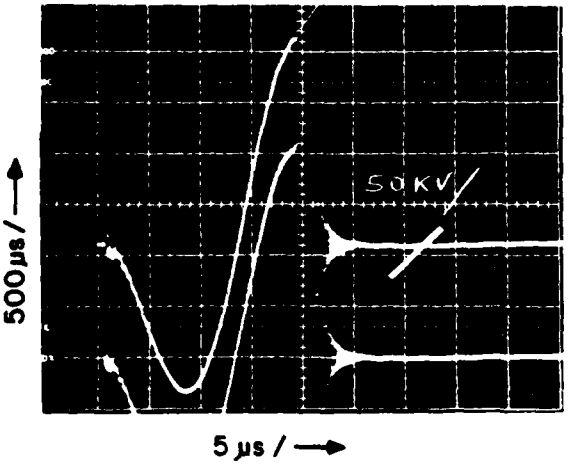


FIG. 2 BLUMLEIN CHARGING VOLTAGE

primary or thyratron switch. The current in the primary switch at peak output voltage is nearly zero and most of the energy is switched out of the Blumlein by the spark gap. These are nearly optimum conditions for arc snap-out in the switch. If, for example, a coupling coefficient of .8 is used, steps must be taken to dissipate the energy still remaining in the transformer which acts to maintain the spark gap arc with only amperes flowing. To insure quick arc snap-out and recovery times short with respect to 1-ms, we installed some linear resistance and some non-linear resistance (varistors). Although these resistors are not necessary in an ideal energy transfer system, in the practical case, they provide damping (<50-µs) of the residual energy.

Gas System

The test setup for the gas flow system consisted of a Roots type blower in a pressure tank closely connected to the plenum chamber of the spark gap. We did not have means for varying the flow rates in the switch but only pressure and gas mixtures. No extensive studies were made of gas mixtures but several were tried and for our rep-rate and voltage requirements it appears that 6-8% (gage) of SF_6 with Nitrogen has given us satisfactory results. The gas flow rate for this mixture was about 4-cm/ms; this is expected to be about 5-cm/ms in the final accelerator system. The pressure drop in the spark gas was about 3 psi at 80 psig gas pressure. It is expected that once in operation the gas mixture will be changed periodically and some of the contaminants may be removed between changes by mechanical and chemical filtration.

Test Results

The test results indicate qualitatively what is expected of the spark gap. Fig. 3 shows the relationship between rep-rate, voltage and pressure. The air flow remained relatively constant as pressure was varied. The graph shows that the closer the switch is run to the self-breakdown mode, the lower is the rep-

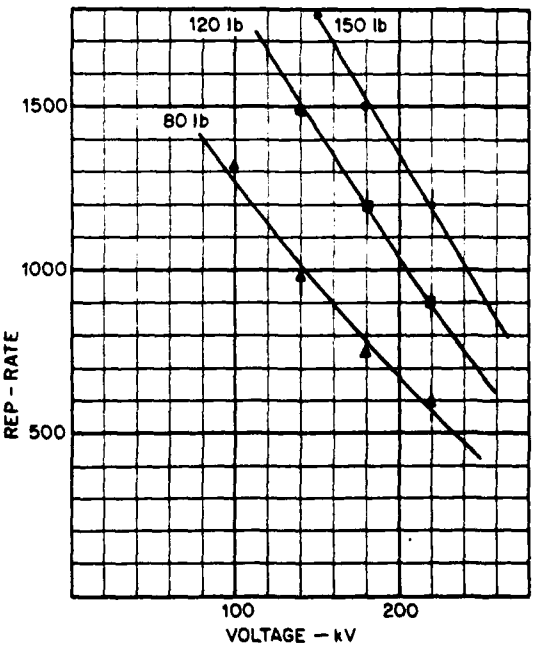


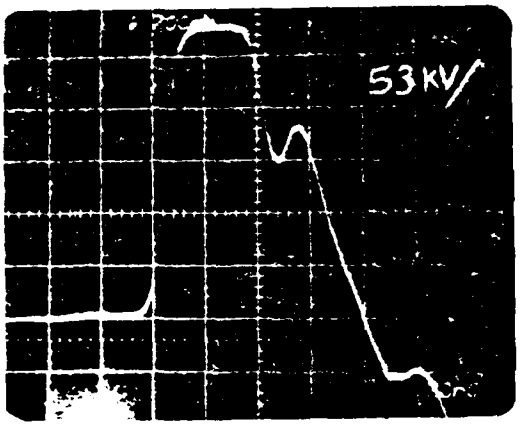
FIG. 3 REP-RATE VS. VOLTAGE AND PRESSURE

rate. As the voltage is lowered, the rep-rate increases and one is limited only by the trigger amplitude on how low in voltage or high in rep-rate it is pos-

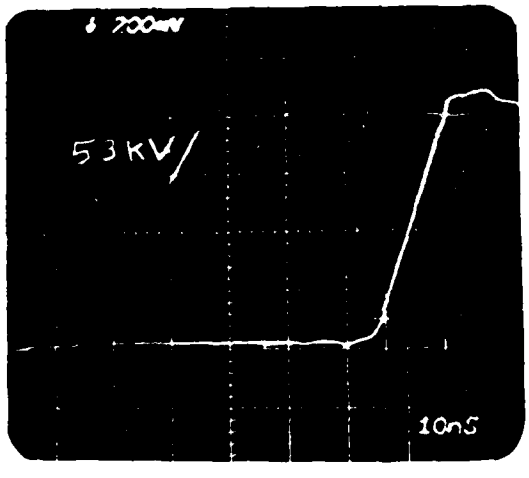
sible to go. Fig. 4a shows the output pulse into a cooper sulfate load connected to the Blumlein by a 1-m water transmission line. The 10-90% rise time is 12-ns and some improvements on this rise time were observed when a trigger pulse with faster rise time was used (Fig. 4b). The decrease in rise time is an indication that multiple arcs are occurring, thus decreasing the arc inductance.

Jitter

The trigger electrode is biased at the natural mid equipotential that it is designed to follow and is pulsed negatively or toward ground, producing a high field at the edge leading to electron emission and breakdown. The trigger pulse for the test was generated by a ferrite loaded transformer with geometry much like an induction accelerator unit. This transformer has a step-up of nine and produces 125-kV, 100-ns pulse with 30-ns rise time. A 50-Ω resistor in series with the trigger electrode terminates the trigger cable once spark gap breakdown has occurred. Before breakdown, the load impedance is high and the pulse voltage doubles.



(a) PULSE INTO $CuSO_4$ LOAD



(b) 10-90 RISETIME

FIG. 4

The final trigger for the spark gap will be generated from a Blumlein with faster rise time. The jitter measurements were made with the trigger transformer and yielded the results shown in Fig. 5. These results

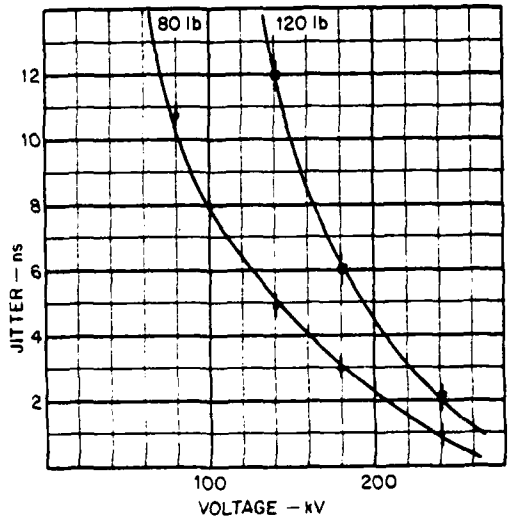


FIG. 5 SPARKGAP JITTER AS A FUNCTION OF PRESSURE AND VOLTAGE

were not unexpected. As the self-breakdown of the spark gap is approached, the jitter becomes less, and conversely as the voltage is reduced, the jitter increases until the gap no longer triggers. Fig. 6 shows the jitter of ten shots superimposed.

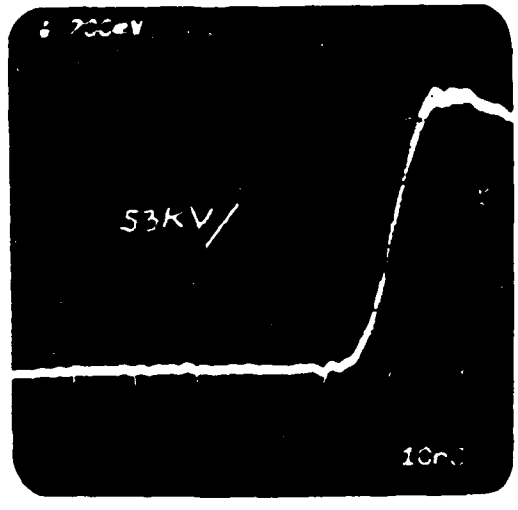


FIG. 6 TEN SHOTS SUPERIMPOSED

Spark Gap Wear

The spark gap was tested at full voltage for 10^5 shots at less than maximum rep-rate. The electrodes were then removed and inspected. The anode and cathode tantalum liners showed practically no wear. The majority of the arcing had occurred at the edge of the trig-

ger electrode but a few stray arcs occurred lower down toward the insulator where the electrode is reduced in diameter. The trigger electrode showed uniform wear at the edge except for one spot (Fig. 7). This wear spot occurred because sometime during the test the spot



FIG. 7 TRIGGER ELECTRODE AFTER 10^5 SHOTS

welding had come loose and the tantalum electrode became tilted to one side. Even with this shift the spark gap operated normally. If one assumes uniform wear to this electrode for 2-cm, the projected life appears to be greater than 10^7 shots. For the 10^5 shot test the insulators upstream of the air flow showed a small amount of debris deposited on them. These insulators could be shielded, as in the LBL ERA[2] gap, if necessary.

CONCLUSION

We have carried the spark gap development to the point where we feel satisfied that all the requirements of rep-rate, voltage, currents, rise time, jitter and expected lifetime for the ETA have been met.

With further development of the existing technology of gas-blown spark gap, it is likely that rep-rates of a few kilohertz at full voltage will be achieved. It appears that because the blower power requirements are proportional to the cube of the velocity, a few kHz may be the practical limit with this technique. After completion of the ETA, we hope to do further development to find the limits of the existing spark gap.

[1] A disclosure of invention has been made by A. Faltens.

[2] Avery, R., et al., "The ERA 4-MeV Injector, IEEE Transactions in Nuclear Science, Vol. NS18-No. 3.

Reference to a company or product names does not imply approval or recommendation of the product by the University of California or the U.S. Department of Energy to the exclusion of others that may be suitable

NOTICE

"This report was prepared as an account of work sponsored by the United States Government. Neither the United States nor the United States Department of Energy, nor any of their employees, nor any of their contractors, subcontractors, or their employees, makes any warranty, express or implied, or assumes any legal liability or responsibility for the accuracy, completeness or usefulness of any information, apparatus, product or process disclosed, or represents that its use would not infringe privately-owned rights."

FLANGE MOUNTING GLASS ENVELOPE HYDROGEN THYRATRONS

L.J. Kettle, C.V. Neale,
and B.P. Newton

ENGLISH ELECTRIC VALVE CO. LTD.
CHELMSFORD, ESSEX

Summary

The stacked grid and anode assembly of conventional ceramic thyratrons does not provide a reservoir of neutral gas near the anode which is as large as that in a glass envelope tube. In consequence, when a trip or kick-out occurs in many pulse modulator applications, the follow through current may cause a ceramic thyratron to quench and conduct in a metallic spark mode, thus causing irreparable damage to itself.

The paper describes recently developed hydrogen thyratrons which combine the advantages of the open structured glass envelope tubes, capable of high amp. second ratings for their size, with the conventional low inductance flange mountings normally associated with ceramic envelope tubes.

When used in simple low inductance housings, these tubes are capable of handling rates of rise of current in excess of 50 kA/µs.

Wave-form pictures are given showing performance of current carrying capability versus time. In this manner it becomes obvious that the amp. second rating of the glass tube is several times that of a ceramic.

Introduction

There are many applications for hydrogen thyratrons which demand a long and/or a fast rising pulse capability coupled with a relatively low duty cycle. Traditionally, the former requirement has been satisfied by using a plug-in glass envelope hydrogen thyratron. These tubes have a compact electrode structure, mounted within a large glass envelope allowing good gas circulation to replenish the anode-grid region during conduction. The grid apertures are large enough to prevent arc extinction, and they are capable of maintaining long current pulses, unlike the over baffled positive grid designs of the past.

High Rates of Rise of Current

Glass tubes are fairly inductive due to the long leads to the cathode structure, and have, as a consequence, a limited switching speed. Coaxial housings for glass thyratrons tend to minimise these inductance effects (Ref. 1).

The new flange mounted glass envelope hydrogen thratrons, CX1558 and CX1559, incorporate the annular apertured grid structure from the glass tetrode mounted directly on to a metal flange. (Fig. 1). This enables the tube to be bolted into a coaxial housing for minimum inductance. The heater and reservoir connections are made via flying leads thereby eliminating the need for plug-in sockets, which are becoming more difficult to obtain. With strip line or cable systems, rates of rise of current in excess of 50 kA/µs are obtainable.

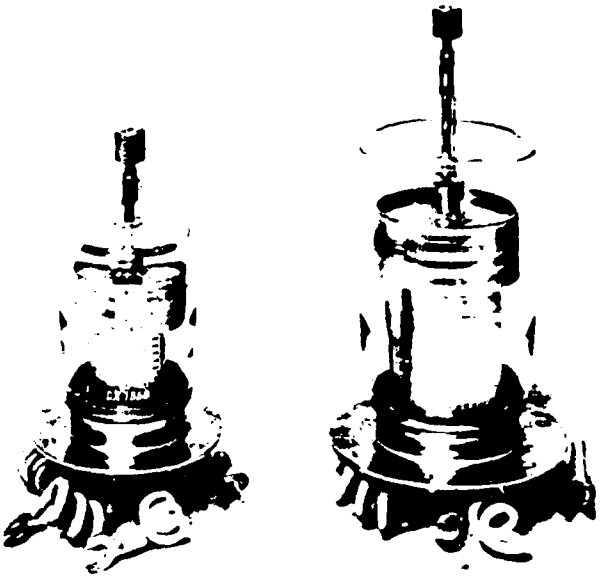


FIG.1

Long Pulse Discharges

The above features make the tube attractive for use in circuits where high amp. second ratings are required due to modulator trip-outs or for crowbar protection of sensitive circuit elements.

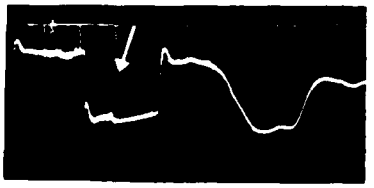
Where average power is low, such tubes are an economic alternative to ceramic envelope types, and a more rugged alternative to plug-in glass envelope tubes of the same size.

Experiments conducted in co-operation with Mr N S Nicholls of R.S.R.E.(M.O.D.)circa 1960 using glass thyratrons of the 5949 type produced rather surprising results, in that some types exhibited classical quenching whilst others did not. A 200 µs pfn was used

CH1371-4/78/0000-0102$00.75 © 1978 IEEE

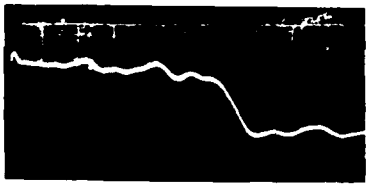
for the experiments and it was found that the negative grid tetrode CX1140 thyratron did not quench at 500 A, whereas 5949 tubes with positive grid characteristics, in which the grid apertures were baffled and segmented, usually showed quenching within about 20 μs at this current level.

FIG.2 CURRENT WAVEFORM FX229 (5949) SHOWING QUENCHING AFTER 20 MICROSECS. (Scale: 10 microsecs and 240 Amps per division)



Recently these results were corroborated using a low rep-rate system (2 p/min). with a 60 μs, 2 Ω. pfn and load. At 30 kV, the tube under test has to attempt to switch a pulse of 7,500 A, 60 μs, Fig. 2 shows a classical case of quenching at 500 A, 20 μs with an obsolete FX229 (5949). Fig. 3 shows an FX297, triggered inverse diode, switching 1,000 A for 60 μs without quenching.

FIG.3 FX297 PASSING 1000 AMPS FOR 60 MICROSECS WITHOUT QUENCHING. (Scale: 10 microsecs and 500 Amps per division)



About 20 years ago, the CX1140 was used successfully in an experimental modulator at 6 p/min switching 30,000 A, 20 μs pulses. Tube weakness in this case was confined to the glass pinch seal, where inadequately welded flexible leads were blown apart by the force from the current pulse. Tubes with satisfactorily welded leads stood up to this although problems with the pfn capacitors were never really overcome. Crowbar ratings for the CX1140 and CX1159 were established from these experiments.

With the advent of ceramic thyratrons, which were developed for both rugged and high power applications, glass hydrogen thyratron types CX1140 and CX1159 were replaced by ceramic envelope tubes, CX1180 and CX1154, in many radar and linear accelerator modulators. The crowbar ratings for glass tubes were optimistically proposed for the ceramic range where equivalence occurred, but for several years no requirements arose where ceramic tubes were used to these ratings. When a requirement did arise, it occurred in an application using single ended multigap ceramic thyratrons for the beam dumping magnets of the S.P.S. at Cern, Geneva and problems of quenching due to gas starvation appeared. It was realised that arc extinction was occurring in the grid/anode region of the ceramic tubes. At this stage the single ended ceramic tubes had to be de-rated for peak current by a factor of 2 and for amp. second rating by a factor of 10. The double cathode range of ceramic tubes eventually satisfied the S.P.S. requirement (Ref. 2).

FIG.4 CX1154 QUENCHING AT THE END OF 1500 AMP 60 MICROSECOND PULSE. (Scale: 10 microsecs and 800 Amps per division)

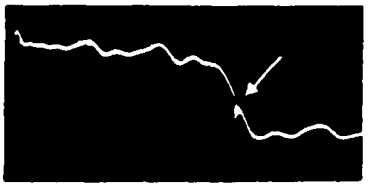


Fig. 4 shows the current waveform of a CX1154 thyratron under quenching conditions in the 60 μs, 2 Ω modulator. Quenching occurs at the end of a 1500 A pulse. Fig. 5 shows the current waveform of a CX1559 thyratron at over 6,000 A in the same modulator, without any signs of quenching.

FIG.5 CX1559 PASSING 6 KA FOR 60 MICROSECS WITHOUT QUENCHING (Scale: 10 microsecs and 2.4 KA per division.)



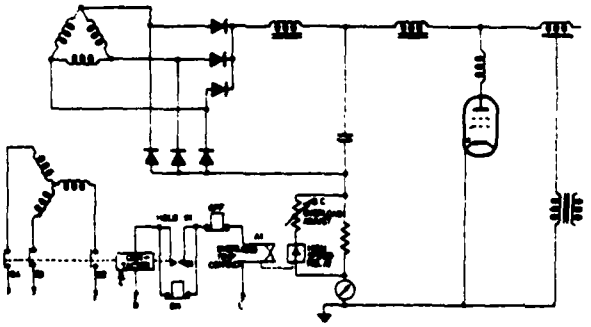
Overload Protection

A second tube limitation is apparent when a modulator fault causes the hydrogen thyratron switch tube to act as its own crowbar until the protection and overload circuits operate. In many equipments designed to use glass tubes these protection circuits were relatively slow and the thyratron had to withstand a large amp. second rating. Replacement of glass tubes by their ceramic equivalents in such modulators resulted in premature tube failures. Thus, the flange mounted glass tube is a more satisfactory alternative for medium and higher power radars between 2 and 20 MW.

It is important, however, to give detailed attention to the protection

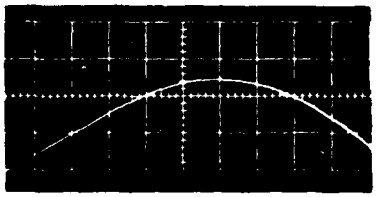
circuits, where speed of operation and performance of the overload detector are critical. The need for a fast breaker is obvious and the performance of solid state systems is usually superior to that of mechanical systems. Should a mechanical system be used, a fast operating, low inertia breaker is essential and its 'hold on' coil should be interrupted directly by the contacts of a high speed relay. The positioning of this relay is of paramount importance to the speed of fault detection. It must be placed where it can receive the initial surge of current from the reservoir capacitor (Fig. 6) as current levels in the rectifier and transformer circuits rise so slowly that sensing these currents cannot prevent tube damage.

FIG.6 MODULATOR CIRCUIT SHOWING FAST-TRIP OVERLOADS



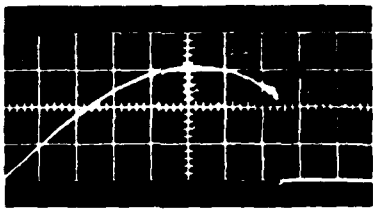
The average current value should also be monitored as it is possible under certain circumstances to suffer a 'slow arc' condition, which although causing severe overloads, never reaches a peak value sufficient to operate the 'peak' detector circuit.

FIG.7 CX1154 QUENCHING AT 300 AMPS 7.5 MILLISECS.
(Scale: 100 Amps and 1 millisec per division)



In order to investigate thyratron operation under equipment fault conditions, a single shot 10 millisecond half sine wave pulser was commissioned. Fig. 7 shows the CX1154 ceramic tube quenching at 7.5 ms, 300 A peak pulse. The quenched current was diverted into high power surge arrestors for circuit protection. Fig. 8 shows the CX1559 passing a current of 500 A peak for 10 ms without quenching.

FIG.8 CX1559 PASSING 500 AMPS FOR 10 MILLISECS WITHOUT QUENCHING (Scale: 200 Amps and 1 millisec per division)



Conclusion

When a modulator trips and the switch tube is forced to crowbar the power supply it has the worst of 'all worlds'. It has to be able to cope with high peak currents from the pfn, in normal pulsing and also to discharge the reservoir capacitors, and handle the longer duration power supply short circuit follow on current under fault conditions.

Thus to survive without damage to itself a thyratron modulator switch tube must be able to pass both high current short pulses and low current long pulses. It has been demonstrated that the flange mounted glass thyratron adequately fulfils these requirements.

References

(1) High Rate of Rise of Current Pulse Generation using Low Cost Glass Envelope Thyratrons. R. L. Snelling Et. al. Intl Pulsed Power Conference Lubbock, 1976.

(2) Generation of High Current Long Durations Rectangular Pulses, P. E. Faugeras Et. al. - Cern 11th Modulator Symposium.

Acknowledgements

The writers wish to thank the directors of the English Electric Valve Co. Ltd. for permission to publish this paper.

DOUBLE ENDED HYDROGEN THYRATRONS FOR CROWBAR PROTECTION OF HIGH POWER TWT SYSTEMS

N. S. Nicholls
RSRE, Malvern, England

H. Menown & R. J. Wheldon
English Electric Valve Company Limited
Chelmsford, Essex.

Summary

The double ended multigap ceramic thyratron is a versatile switch for crowbar applications. It will provide protection over a very wide range of H.T. voltages and will operate within a submicrosecond time delay. Since the tube operates in a normal nondestructive 'thyratron mode' it will fire reliably for many millions of shots. Practical crowbar conditions can be complex, in particular with floating deck modulators where stray capacitance and inductance can cause the H.T. voltage to ring and sometimes completely reverse. In the event of voltage reversal the double ended thyratron conducts smoothly in the reverse direction as the circuit requires.

The paper describes a new range of compact double ended thyratrons specifically designed for crowbar use up to 100 kV with an auxiliary power consumption of only 75 W. A dynamic test arrangement is described which demonstrates the tube's capability of discharging 0.75 μF charged to 60 kV, the current rising to 5000 A at a rate of 50 kA/μs, with an anode delay time of 200 ns. The test equipment simulates either grounded cathode or floating deck operation under conditions where a flash arc fault occurs. The efficiency of the protection is evaluated by monitoring the "let through current" (i), charge (it) and energy (i^2t). Coincidence counters register faulty operations. A compact auxiliary supply module makes these tubes especially attractive to aerospace systems engineers.

Introduction

Gridded-gun klystrons and T.W.T.'s working at voltages between 30 kV and 100 kV are employed in the transmitters of compact radars. Such tubes frequently need protection against damage during a flash arc by means of an electronic crowbar. The circuit condition and performance requirements for the crowbar in a typical radar transmitter call for device parameters which are difficult to meet. Because the T.W.T. is connected more or less directly across a large reservoir capacitor, crowbar action is required within a few hundred nanoseconds in order to limit the energy "let through" into the transmitting tube to a safe value. For a fault arc duration of a few microseconds it is likely that the very high current densities in the molten and solid material of the forming arc spot will be resistive and therefore the amount of material vapourised will be dependent on $\int i^2\,dt$. This integral may either be calculated from the current waveform or determined from the temperature rise in a resistor in the fault tube circuit. When the arc is established and has a voltage drop independent of current, then the energy into the arc will be dependent on $\int i.dt$.

The voltage across the crowbar device at the time of firing will usually be much less than the voltage during normal transmitter operation; in an extreme case it will even be reversed. Also, crowbar protection is usually required over a wide range of H.T. voltage. Thus the minimum firing voltage of the device should be as low as possible, and at most a few percent of the maximum operating voltage. The rate of change of voltage across the crowbar at the time of firing may have a high negative value which could cause a problem due to capacitive coupling to the triggering electrode. The requirements on the crowbar system are complicated by the wide variations observed in the rate of build-up of arc current in the transmitting valve. After the reservoir capacitor has been discharged, there will often be a follow-through current from the short-circuited power supply sufficiently large to damage the transmitting valve unless it is diverted by the crowbar. The crowbar current will pass through a low value immediately after the capacitor discharge, so that a device with a low holding current is required if conduction is to be maintained. These requirements on the crowbar device are discussed in more detail in subsequent sections.

A number of different types of device have been used as the crowbar tube such as: ignitrons, thyratrons, triggered spark gaps, triggered vacuum gaps, and cadmium surge diverters. All of these, except the thyratron, are different forms of cold cathode device and appear attractive to the user in that they do not require auxiliary supplies other than the trigger. It will emerge during the subsequent discussion that the cold cathode devices have certain drawbacks on electrical performance which leave the thyratron, in particular the double ended version, as the most versatile, reliable and the fastest operating crowbar.

CH1371-4/78/0000-0105$00.75 ©1978 IEEE

The ignitron and the cadmium tube are limited to less than 20 kV for reliable hold-off voltage, so that for the voltage range with which we are concerned, a number of devices must be connected in series. These devices are relatively slow to turn on and the ignitron requires a large trigger power. The triggered spark gap has a limited voltage working range and requires a high trigger voltage. The triggered vacuum gap requires a high trigger energy and fires much more slowly than the thyratron (this will be illustrated later).

Both the T.S.G. and the T.V.G. operate in a spark mode where the electrodes are sputtered with every shot, and arc extinction occurs if the current falls below a few amperes. The double ended thyratron will continue to conduct even at a current of a few milliamps and is, therefore, unlikely to extinguish during any period of power supply follow-on current. The thyratron has an adequate follow-on current capacity.

The thyratron operates from its hot cathode in a non destructive mode, particulatly since the emissive source is separated from the high voltage gaps. Thyratrons will work over an extremely wide voltage range, with a submicrosecond delay time and with a minimal triggering signal. In order to achieve reliable voltage hold-off any number of high voltage gaps may be put in series in the same tube, with little change in triggering requirements, delay time or minimum working voltage. Thyratron lives of between 10^4 and 10^8 shots have been achieved depending on the energy passed.

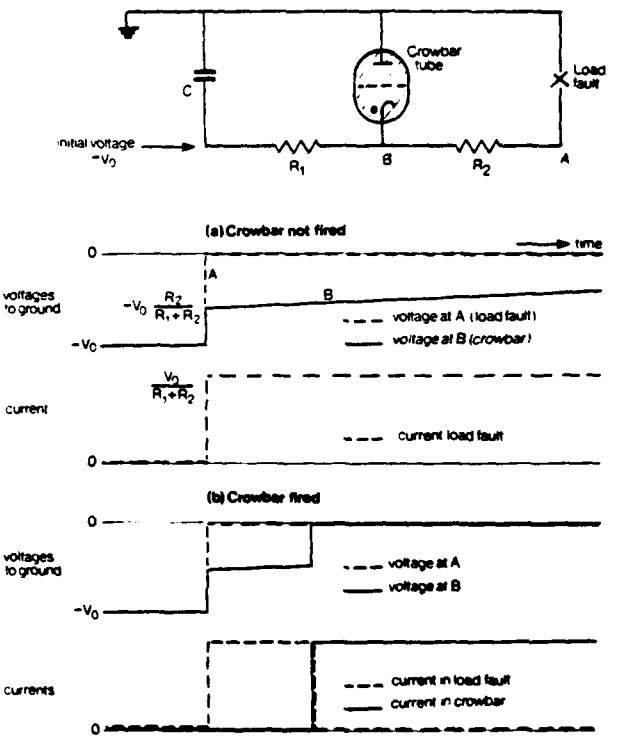
An important advantage of the double ended thyratron is that it will continue to conduct current in either direction, as the circuit demands, until all stored energy has been removed. It does this as a hot cathode discharge at all times and therefore is not subjected to arc back damage.

ANALYSIS OF TRANSIENTS IN H.T. SUPPLY CIRCUITS

The waveforms observed following a T.W.T. arc in a typical transmitter circuit containing a crowbar are complex, due to the numerous significant stray inductances and capacitances. These waveforms must be taken into account, not only when specifying the characteristics required of the crowbar device, but also when designing the trigger circuits for it.

There is some evidence that the rate of build-up of arc-current in a T.W.T. transmitter can assume a wide range of values. From the point of view of the demands it makes on the performance of a crowbar, a rapid fall in voltage on the T.W.T. is likely to be the worst case. This is because the minimum of anode delay time is then allowable and because the disturbance of the voltages in the H.T. supply circuit will be greatest. As we shall see, these disturbances tend to greatly reduce or even reverse the voltage on the crowbar tending to increase firing delay. In this section we will, therefore, assume an infinite rate-of-fall of voltage across the T.W.T., leaving the problems of protection of fault, and the problem of diverting follow-through current from the power supply, to be considered in a later section.

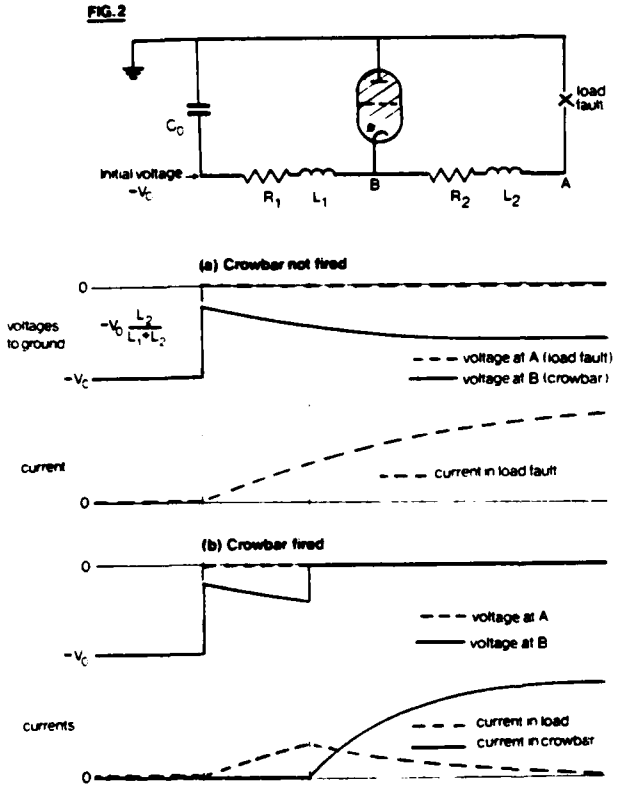
FIG.1



To build up an understanding of the waveforms, it may be useful to start by considering calculated waveforms for simple idealized circuits and then examine the effect of progressively adding various circuit strays. In the absence of any stray capacitance or inductance the simplified circuit and the significant waveforms are as shown in Fig, 1. The voltage on the crowbar, immediately after the load arc, is reduced by the factor $R2/(R1 + R2)$. The rapid drop in voltage at the crowbar may in some crowbar devices tend to interfere with firing due to capacitance coupling to the trigger electrode. When the drop in voltage at the crowbar is large, multi-gap thyratrons may need to be fitted with grading capacitors to prevent

over-stressing, and possible damage, to individual gaps due to a temporary departure from correct voltage sharing. The current in the T.W.T. drops instantaneously to zero as the crowbar fires. The crowbar current leaps to its maximum value and dies away exponentially as the reservoir capacitor discharges. Fig. 2 shows the effect of the stray inductances L_1 and L_2 which are inevitably significant in a high-voltage circuit. The voltage on the crowbar, immediately after a load arc, is reduced in the ratio $L2/(L1 + L2)$. With typical values, this voltage may be less than that determined by the resistance ratio.

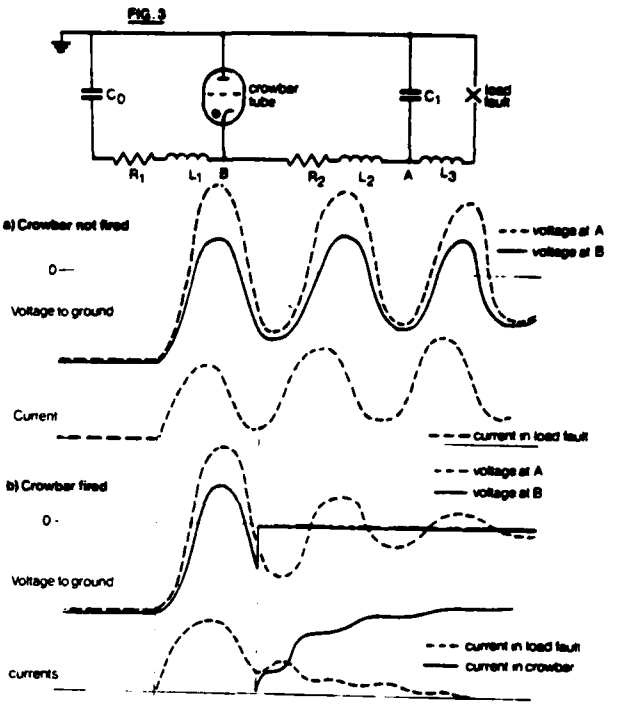
FIG.2



The crowbar is likely to fire before he current in the T.W.T. reaches its maximum value, but the current continues for some time afterwards as the energy stored in L2 is dissipated in R2. This contributes substatially to the "let-through". To minimise this, either L2 must be made small, when the voltage on the crowbar at firing will be reduced (L1 + L2 being fixed by transmi ter layout) or R2 must be made large, with consequent high power-loss during normal transmitter operation.

Fig. 3 shows a typical effect of the inevitable stray capacitance associated with power supplies and grid-driving equipment for the T.W.T. The effect on the

FIG.3



voltage at the crowbar before the crowbar fires is to produce a period of reversed voltage on the device. Typically this occurs at about, or just before, the time when the crowbar might otherwise be expected to fire.

To ensure reliable operation of a triggered spark-gap under these conditions would be difficult, since the gap voltage may be low or reversed when trigger-gap breakdown occurs. A T.V.G. or thyratron might be expected to start conducting as forward voltage reappears.

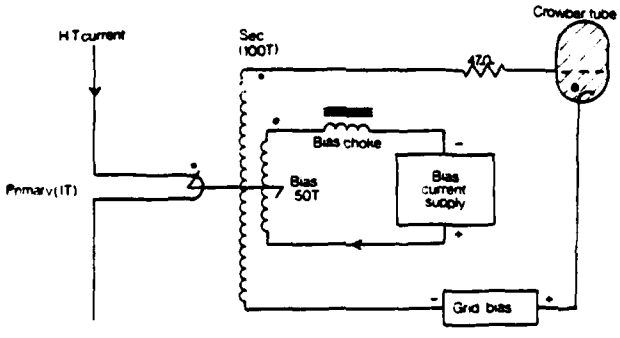
Addition of the stray capacitance associated with the power supply and trigger circuits for a thyratron crowbar modifies the waveforms in detail but without altering their general character. The discharge of this capacitance through the inductance of the crowbar tube and its connections will, however, contribute a component of reverse current through the crowbar tube.

It may not be easy to eliminate the reversals of voltage and current in the crowbar by altering circuit constants or by the addition of damping components without significantly increasing the size, weight and power loss of the transmitter. The 'let-through' will also in general be increased. Thus a crowbar device capable of operating satisfactorily under conditions of voltage and current reversal facilitates optimum design of other parts of the transmitter.

OTHER ASPECTS OF CROWBAR SYSTEM DESIGN

It is necessary in the design of crowbar systems to cover the possibility of slow-growing arcs in the transmitting tube. Such an arc may absorb a large amount of energy by the time that the H.T. current reaches its normal peak operating value, so that the threshold at which the crowbar is fired should not be too far above this. To obtain good current descrimination it will generally be necessary to add an auxiliary switching device in the crowbar trigger circuit. This must be robust and reliable, but must not introduce a time delay which would be unacceptable in the fast-arc case.

FIG.4



Crowbar trigger transformer with current threshold

A technique which has been found suitable for use with thyratrons uses a magnetic switch (fig. 4). The primary winding, which consists of a single turn, carries the H.T. current. A suitable secondary winding is connected between the grid of the thyratron and its grid-bias supply. A tertiary winding carries a biassing current. This has a magnitude and direction such as to oppose the H.T. current and to hold the core in a state of saturation until the H.T. current exceeds the required threshold, when a positive voltage appears on the thyratron grid. Further increase of the H.T. current provides grid-current to fire the thyratron. The biassing current must be supplied from a source of high impedance at high frequencies such as the choke illustrated. The energy which must be stored in this choke is about an order of magnitude greater than the triggering energy delivered to the thyratron. A low minimum triggering energy for the crowbar device keeps the components small and power consumption low, and in this respect a thyratron is much superior to a T.V.G.

The electrical isolation possible with transformer-coupled triggering gives freedom to insert the device at any point in the H.T. circuit. To deal with fast arcs, a point near the T.W.T. appears advantageous because it would give earlier warning of a fault. However, tests in this position have shown no improvement, possibly due to the oscillatory nature of the fault current at this point, which could result in the thyratron grid being driven negative at a critical time. Also, during the period when the voltage across the crowbar has fallen to a low value, the precise time at which it fires will have little effect in the subsequent current waveforms. A more significant advantage may be taken of the electrical isolation of the grid circuit by firing the crowbar from the T.W.T. body current. This is particularly easy when, as is usually the case, separate capacitors are employed for the T.W.T. body and collector. The threshold current may then be reduced by about an order of magnitude, giving earlier detection of slow arcs and also making the circuit sensitive to a variety of other transmitter faults, hazardous to the T.W.T. There are a number of these faults which may be most easily detected at ground potential. If it is deemed necessary to protect against these with the crowbar, it is convenient to communicate the trip signal to the crowbar deck by means of a light-link. After amplification, the triggering signal may be applied to the thyratron grid through a diode. If the trigger power required is sufficiently small, a transistor may be employed to drive the grid. This is simpler to use than a thyristor, which requires additional circuits to secure turn-off under all conditions.

The low power, relatively low voltage trigger required by a crowbar thyratron makes it much preferable to other devices when this facility is required.

A further problem may arise in transmitters lacking fast trip circuit breakers for interrupting the supply of H.T. current within a few tens of microseconds of an arc occurring. For instance, if after the initial discharge of the reservoir capacitors, the current in the crowbar device should dip below its holding current, the device will turn off, and voltage will begin to reappear across the T.W.T. If this has not recovered from the effects of the initial arc, it could break down again before the voltage is reached at which the crowbar is able to fire in the presence of a T.W.T. arc. After an arc restrikes in the T.W.T. under these conditions, the crowbar voltage will be reduced below its take-over voltage. Then the crowbar will be unable to refire and the T.W.T. arc will carry the whole of the follow-through current of the power supply, which is disastrous. To reduce this risk, the holding current of the crowbar device

should be low, since there may not be any prior load current in the circuit when the initial arc occurs; the current minimum may be a fraction of an amp. This favours a thyratron in comparison with a T.V.G. If crowbar extinction does occur, the safest course is to refire it as soon as its anode take-over voltage is reached. This must be done by an auxiliary electronic firing circuit, the energy for which is kept to a minimum if a thyratron crowbar is used.

It is concluded that a much more effective and compact crowbar system is possible, particularly in transmitters with follow-through current, if a thyratron is used for the crowbar, rather than any of the alternative devices.

NEW COMPACT CROWBAR THYRATRONS

The foregoing section has shown the need for the crowbar to be able to operate under a wide variety of circumstances depending upon the detail of the particular crowbar circuit.

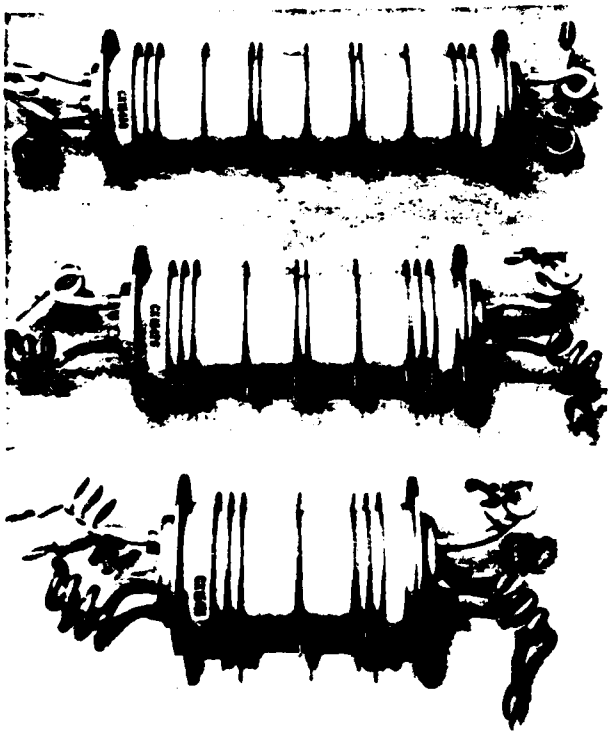
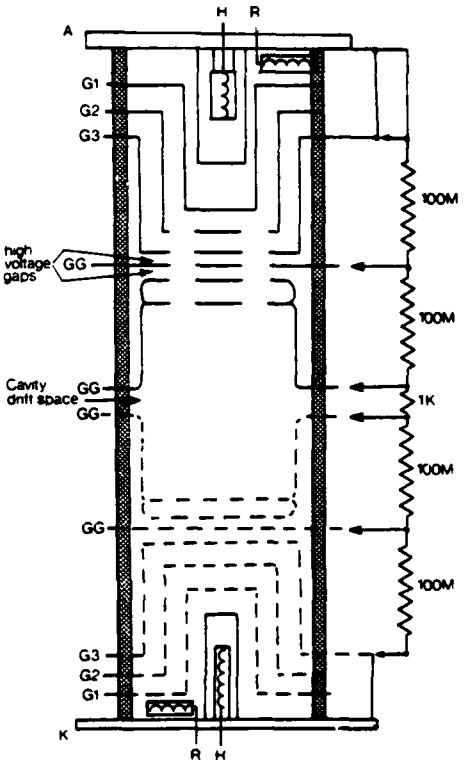


Fig. 5

A new range of compact double ended thyratrons has been developed which require only a small amount of auxiliary power. Fig. 5 shows a photograph of 3 of these tubes, the CX1541B, CX1542B and CX1543B rated for 35 kV, 65 kV and 100 kV respectively. They are designed for operation under insulating liquid for compactness. Fig. 6 is a diagrammatic representation of the CX1542B, the dotted section indicates how the basic two gap unit is repeated for additional sections. The two gap unit consists of two closely spaced gradient grids and these are joined by a cavity drift space in the higher voltage tubes.

FIG. 6 Schematic of CX1542B



The tube is quite symmetrical and has similar cathode, priming grid G1, triggered control grid G2 and shield grid G3 at each end. The G3s are connected to their adjacent cathodes and therefore act as virtual anodes for the collection of electrons. They also shield the control grids against the capacitive coupling of fast rates of voltage change across the tube. Such effects could either cause spurious voltage hold-off failure or, even inhibit triggering. The high voltage gaps are stressed at less than 20 kV per gap and therefore give very reliable voltage hold off.

The cathodes are compact, rugged, but low wattage, and rely on the hollow cathode structures within the surrounding heat shields to enable them to pass the high peak current and coulomb ratings. A small reservoir at each end of the tube supplies sufficient gas for a long life.

Tube ratings and characteristics are given in table 1.

TABLE 1

TUBE RATINGS AND CHARACTERISTICS

	CX1541B	CX1542B	CX1543B
Maximum Forward Anode Voltage	35 kV	65 kV	100 kV
Minimum Working Anode Voltage	1 kV	2 kV	3 kV
Peak anode current (max)	5000 A	5000 A	5000 A
Rate of Rise of current (max)	50 kA/μs	50 kA/μs	50 kA/μs
Peak discharge (max)	0.05 C	0.05 C	0.05 C
Peak follow on current (max)	10 A	10 A	10 A
Follow on discharge (max)	1 C	1 C	1 C
G1 priming current	10 mA	10 mA	10 mA
G2 trigger pulse voltage	500 V	500 V	500 V
G2 trigger pulse current	5 A	5 A	5 A
Heat power (each end)	35 W	35 W	35 W
Anode delay time (5 kV upwards)	200 ns	200 ns	200 ns
Diameter	3.25 inches	3.25 inches	3.25 inches
Length	4.5 inches	6.75 inches	9.0 inches
Weight	1.87 lbs	2.68 lbs	3.4 lbs

A CROWBAR TEST CIRCUIT

A test circuit for crowbar tubes must have two functions: firstly to measure some basic parameters of the tube under test; secondly, to show that the tube will operate fast and reliably (when the circuit reactance causes the anode voltage to ring) in a simulated floating deck circuit. In the latter situation, current, charge and energy 'let through' into the fault are monitored.

FIG.7 Static test circuit

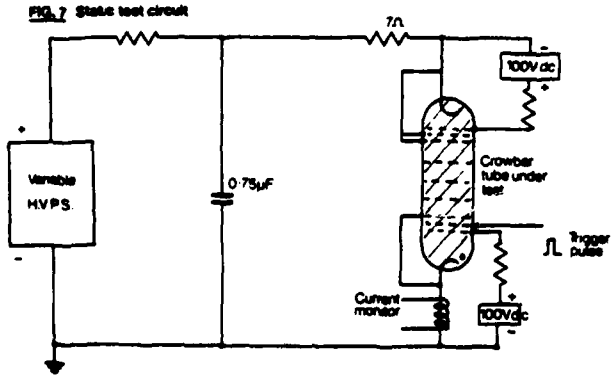
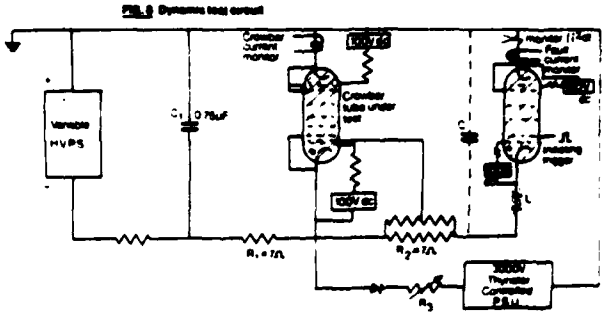
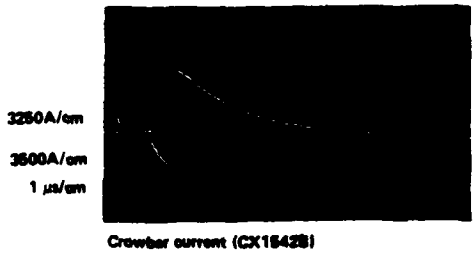


Fig. 7 shows a simple capacitor discharge circuit with positive H.T. where voltage hold-off tests can be carried out on the crowbar tube and anode delay time measurements can be made with a well defined trigger pulse. Fig. 8 shows a dynamic test circuit where a simulated fault is generated



and the response of the crowbar tube is measured. The test sequence is initiated by triggering the fault tube, which starts to discharge the 0.75 μF capacitor C1 charged to 65 kV through R1 and R2. A trigger for the crowbar is derived from the growth of current in R2 or from a current transformer in the fault tube line. The fault tube is a multigap thyratron which has a fast current rise time and therefore supplies sufficient signal to trigger the crowbar within tens of nanoseconds. After a further interval, which is the anode delay time of the crowbar tube, it starts to conduct and divert the energy. Stray reactances of the fault tube filament supply may be comparable with that of a T.W.T. floating deck or can be adjusted by adding L & C. Fig. 9 shows typical current waveforms through the fault tube and the crowbar tube. The current through the fault rises until the crowbar conducts and then dies away exponentially discharging the energy stored in the inductances of the crowbar/fault tube loop. The area under the fault current curve is a measure of the possible damage which could take place when a fault occurs in a T.W.T., i.e. the energy transferred into an arc. The fast rise time of the thyratron fault tube gives a top limit for 'let through' current.

FIG.9



Crowbar current (CX1542B)

Fault current (CX1171B)

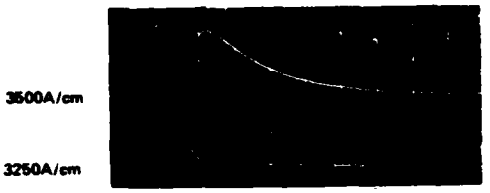
FIG.10



Crowbar current (CX1542B)

Fault current (T.V.G.)

FIG.11



Crowbar current (T.V.G.)

Fault current (CX1542B)

If a device with a slower rise time, such as a triggered vacuum gap, is used as the fault tube then the 'let through' is reduced, see waveform Fig. 10. Fig. 11 shows the 'let through' current and crowbar current when a thyratron is used as a fault tube and a triggered vacuum gap as a crowbar tube. The greater 'let through' in this case is due to the longer anode delay time and slower current rise of the T.V.G. Comparing $\int i^2\,dt$ in Figs. 9, 10 and 11, they are 3.2, 1.05 and 27.5 $A^2.s$ respectively and $\int i\,dt$; 1.8, 1.3 and 7.4 mA.s. Faulty operations, such as spurious breakdown or failure to fire, of the crowbar tube are registered by coincidence counters. The test circuit also has the facility to subject the crowbar tube to a simulated follow through current pulse. A thyristor controlled power supply and resistor R_3 allow the fault current amplitude and duration to be varied.

THE INTERFACE BETWEEN TUBE AND CIRCUIT

The use of a multigap device with hot cathodes necessitates the following associated components:-

1) Sharing resistors and capacitors to divide the voltage equally between the gaps under all circumstances.
2) Heater supplies for both ends of the tube, one end usually at ground potential, the other at positive or negative H.T.
3) D.C. priming supplies for G1 at each end of the tube.

The sharing resistors can be of high value, 100 MΩ across each gap, hence their wattage dissipation is low. Single resistors which connect between the terminal tabs on each electrode have been found entirely satisfactory and only dissipate about 2.5 W each. (Fig. 12). Compact ceramic sharing capacitors of about 100 pF, each with a small series resistance (500 Ω) are connected across each high voltage gap. These ensure equal sharing under transient conditions.

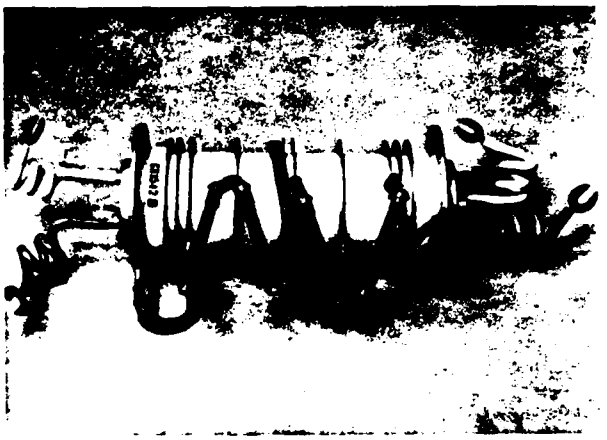


Fig. 12

A compact method of providing the heater and priming supplies for both ends of the tube is from an encapsulated transformer driven by an inverter (at say 20 kHz). The transformer is a cylindrical column of similar size to the crowbar thyratron itself, with secondary windings for both heaters and grid 1 priming supplies. The total power used by the crowbar tube is about 75 watts. If indirect triggering of the high voltage end of the thyratron is required, the small amount of power for a trigger submodulator can also be derived from the same transformer.

LARGER DOUBLE ENDED CROWBAR THYRATRONS

There are two ranges of larger multigap double ended thyratrons which have been described at previous Modulator Symposia, and are suitable for crowbar use. References 1), 2), 3) and 4). The CX1168B, CX1171B and CX1199B are rated for 1.0.A.s peak discharge at 60 kV, 90 kV and 120 kV respectively and the CX1175B, CX1192B and CX1193B for 2.0 A.s peak discharge at 60 kV, 90 kV, and 120 kV.

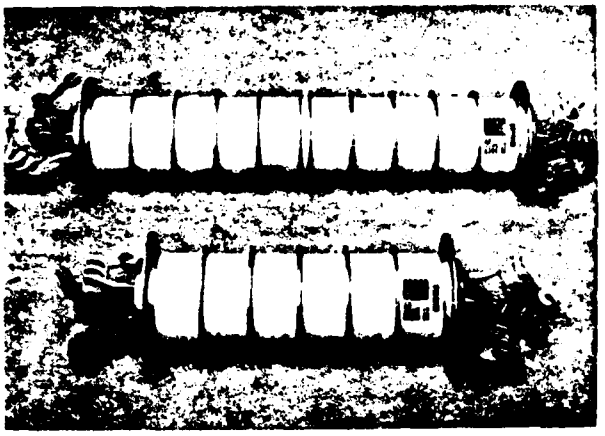


Fig. 13

Two new tubes CX1544B and CX1545B have recently been introduced, see Fig. 13. These are more compact versions of the 1.O.A.s range with 8 gaps and 4 gaps respectively and are for use under insulating liquid. Brief characteristics of these tubes are given in Table 2.

TABLE 2

	CX1544B	CX1445B
Maximum Forward Anode Voltage	200 kV	100 kV
Minimum Working Anode Voltage	5 kV	2 kV
Peak Current	15,000 A	15,000 A
Peak Discharge	1.0 A.s	1.0 A.s
Heater Power (each end)	180 W	180 W
Trigger Pulse Voltage	500 V	500 V
Diameter	4.5 inches	4.5 inches
Length	17.5 inches	10.5 inches

CONCLUSION

It has been shown that of all the crowbar devices which might be employed in compact radar transmitters, a double ended hydrogen thyratron is the only device which completely fulfills the performance requirements in every case.

References

(1) A Multigap, Double Ended Hydrogen Thyratron, H. Menown, B.P. Newton Eleventh Modulator Symposium 1973 p. 232.

(2) Hydrogen Thyratron Preamble p.p. 32 & 41. Hydrogen Thyratrons and Pulse Amplifier Tetrodes. English Electric Valve Co. Ltd. Chelmsford, U.K.

(3) The Use of a Double-Ended Hydrogen Thyratron for Crowbar Applications. W. E. Hannant, C. Rowe and H. Menown. Twelfth Modulator Symposium 1976 p. 231.

(4) Symmetrical Double-Ended Thyratrons in Pulse Modulators. R. B. Molyneaux-Berry. Twelfth Modulator Symposium 1976 p. 30.

Acknowledgements

The Authors wish to thank the directors of the English Electric Valve Co. Ltd. for permission to publish this paper.

Acknowledgements are also given to the Ministry of Defence (Procurement Executive) who have given support for this work.

DOUBLE GAP METAL ENVELOPE THYRATRONS

R. J. Wheldon
English Electric Valve Company Limited
Chelmsford, Essex.

Summary

The metal envelope thyratron has established itself as a versatile switch capable of high power service over a wide range of duties. The compact barium aluminate cathode used in these tubes gives a long life at both high peak and high average currents and the metal envelope provides efficient electrode cooling under these conditions. A compact high content gas reservoir system allows direct switching at high current without gas starvation. A 'boxed in' anode with the high voltage insulator behind the anode prevents material sputtered by ion bombardment in the presence of inverse voltage from degrading the insulation. This range of tubes now includes two new higher voltage versions.

The paper describes the CX1525 which is capable of switching 3500 A at 70 kV and the CX1536 10,000 A at 70 kV at 5 and 10 A continuous average current respectively. It describes the grids and gradient grids which enable very short recovery times for tubes of their size (of the order of 25 µs), allowing operation at prfs in excess of 10 kHz. An alternative method of tube operation is described, as a single gap triple grid tube, which further improves the recovery time and screens the control from fast rates of change of anode voltage.

Introduction

The metal envelope thyratrons were described at the Modulator Symposium of 1973, Ref (1). The most recent additions to the range have been two double gap tubes, capable of higher voltage hold-off.

The metal envelope thyratron differs from the ceramic envelope tube in that the thermal conduction paths from the active regions of the tube, (anode, gradient grids and the grids) to the external cooling surface, have a much lower thermal impedance. This is achieved by the use of thick copper electrodes and a copper envelope. Insulators are used in the envelope only where voltage isolation is required. This design philosophy has lead to compact tubes capable of high average power dissipation. Heat is removed efficiently from the envelope by fitting fins and applying either forced air or liquid cooling. Fig. 1 shows the single gap versions of these tubes CX1526, CX1527, CX1528 and CX1529. The first two have short anode insulators and are designed specifically for liquid cooling, the last two for air cooling.

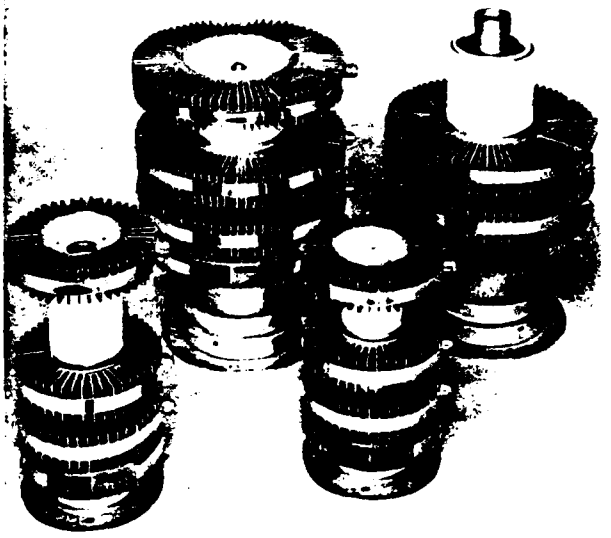


FIG.1

The double gap tubes CX1525 and CX1536 are shown in fig. 2 and illustrated diagrammatically in fig. 3.

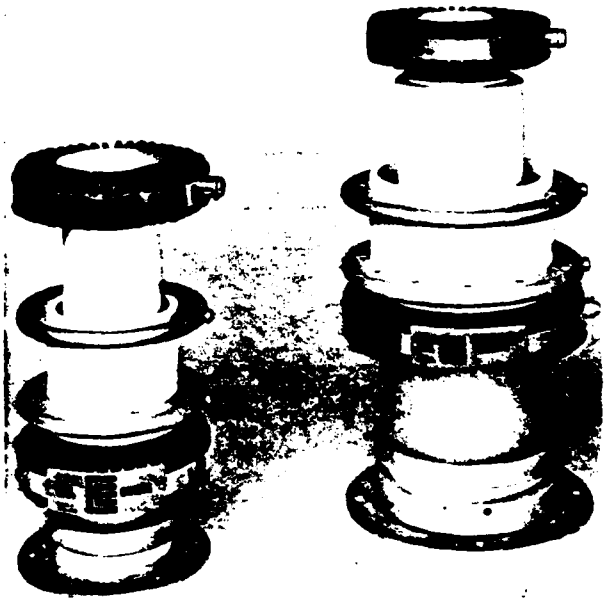


FIG.2

DESIGN OF HIGH VOLTAGE GAPS

There are two approaches to multigap thyratron design:- one is the iterative cavity design illustrated in fig. 4, the

CH1371-4/78/0000-0113$00.75 ©1978 IEEE

other is the single or two layer gradient grid design as shown in fig. 3. The advantage of the former is that it can easily be extended to additional gaps but has the disadvantage that the drift space contains a large volume of ionisation during a pulse and therefore takes a relatively long period to recover. The design of fig. 3 is limited to two or possibly three gaps before the conductive paths from the electrode apertures to the envelope become long and begin to restrict the heat flow, but it has the advantage that the volume of ionisation is small and faster recovery can be achieved.

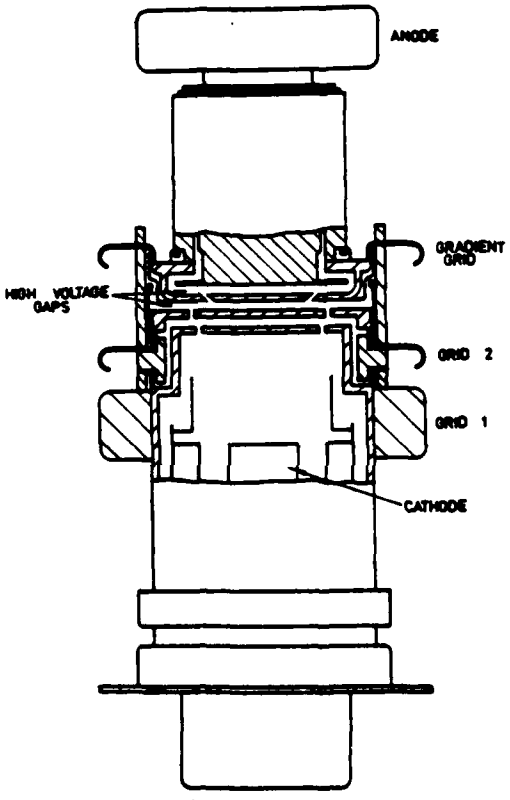


FIG. 3 SCHEMATIC OF CX1536 DOUBLE GAP METAL ENVELOPE THYRATRON

In fig. 3 the anode to gradient grid gap is a 'boxed in structure', that is, the gradient grid forms a box round the anode plate and the high voltage insulator is behind the anode, therefore shielding it from metal sputtered from the electrodes during pulsing. The gradient grid itself consists of a single layer of thick copper with angled slots through it. The lower gap between gradient grid and control grid is conventional and closely fills the bore of the high voltage insulator. Overlapping molybdenum shields protect the insulator from sputtered material. The thermal paths are all short.

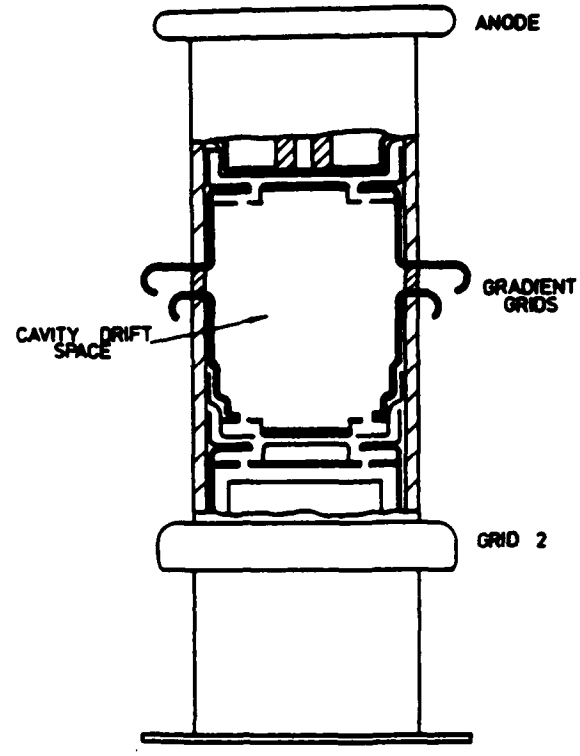


FIG.4 SCHEMATIC OF CERAMIC ITERATIVE DOUBLE GAP THYRATRON

In order to achieve a short recovery time the volume of plasma between G1 and anode has been kept small. The two grids and gradient grid are therefore close together.

THE CATHODE

Barium aluminate impregnated tungsten cathodes are used in this range of tubes. It has been shown that they will give a good life at high average currents for both high and low duty ratio applications. The design of the hollow cathode structure surrounding the cathode is important since it contributes significantly to the high pulse current capability. The solid tungsten matrix and large reserve of emissive material held by the cathode makes it less prone to permanent damage due to sparking and ion bombardment than the oxide cathode.

THE RESERVOIR SYSTEM

The reservoirs are compact, of relatively low thermal mass, and are well isolated thermally from the body of the tube. The gas content in the reservoir is high and, therefore, to give the required pressure stability, the current is controlled by a rugged barretter mounted within the base of the tube. The reservoirs are constructed so as to respond very quickly to transient gas pressure changes. These features enable

the tube to be directly switched at very high peak and average powers without gas starvation of the discharge occurring.

POWER HANDLING CAPABILITIES OF METAL ENVELOPE TUBES

Continuous Operation

The average power which a thyratron can handle is dependent upon the duty ratio under which it is made to operate. If the duty ratio is low, i.e. high peak current and short pulse, the tube will only handle a fraction of the average power that it is capable of at a high duty ratio; i.e. low peak current, long pulse. This is due to the additional dissipation associated with the leading and trailing edges of a high peak current pulse. For many years now the CX1527 has been operated in medium frequency intertors. In these applications the tube has to hold-off 30 kV forward voltage and pass continuous average currents of up to 60 amperes. The duty ratio is high (0.5) and the prf is a few kilohertz. A pair of tubes produce a megawatt average continuous medium frequency power with lives of many thousands of hours.

ADIABATIC OPERATION

If a tube is operated in an adiabatic mode, i.e. a short on period with a longer off period, it is possible to increase the average power during the on period significantly above the continuous average tube ratings. The uprating will depend on several factors:-

1) The repetitive duty ratio. (This includes pulse amplitude, width and prf).

2) The duration of the operational and off periods.

3) The thermal stabilisation and thermal recovery time of the electrodes, which will depend on their mass, thermal conductivity and external cooling.

Some adiabatic operation tests have been carried out on metal envelope tubes. Since the maximum pulse power available was 200 MW pK - 350 kW average, with an r.ms current of 420 amperes, tests were carried out on the smaller metal envelope tube (the CX1526) operating in oil with a 30 sec on period followed by a 4½ min off period. A similar electrode temperature was reached for 350 kW average as for 100 kW continuous operation. Three of these small tubes discharging separate pfns into a common load would, therefore, handle about 1 MW average power under adiabatic conditions. It would be expected that the CX1527, which will operate at 300 kW continuously would switch about 1MW adiabatically. The CX1525 and CX1536 might be expected to switch similar average powers to CX1526 and CX1527 respectively but at 50% higher voltages.

OIL COOLING OF THYRATRONS

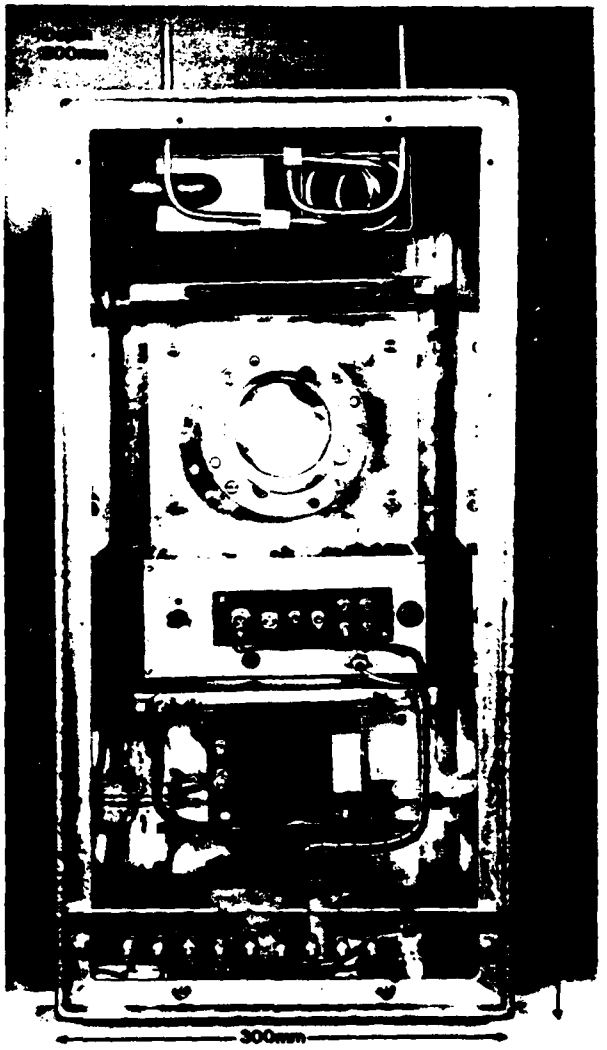


FIG.5

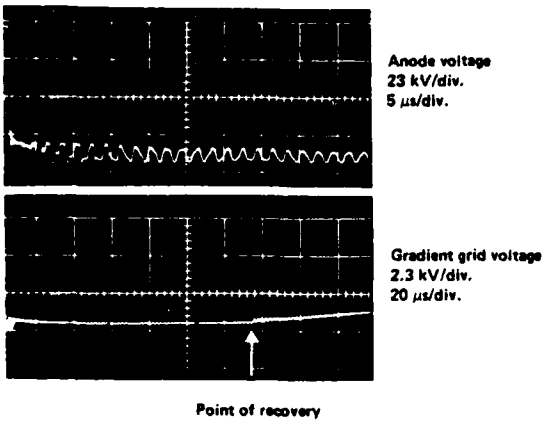
The CX1526 and CX1527 are designed for operation under oil, similarly the CX1525 and CX1536 can, with advantage, be operated in the same manner. Fig. 5 shows a tank housing which is capable of operating any of these thyratrons in oil. This unit contains all the auxiliary, priming and bias supplies, and gradient grid resistors, for the thyratron along

with a water cooled heat exchanger complete with oil circulation pump. For high rates of rise of current where low inductance is important, an oil filled coaxial housing should be considered.

Oil cooling is a simple and efficient way of removing heat from the metal envelope and enhances many of the tubes' power ratings. (Ref (2)).

RECOVERY TIME

FIG. 6 ANODE AND GRADIENT GRID VOLTAGE WAVEFORMS FOR A CX1168



The long recovery time of double gap ceramic thyratrons with cavity type gradient grids is due to the slow recovery of the cavity. Fig. 6 shows the anode and gradient grid voltage waveforms of a CX1168 ceramic thyratron. The point at which the gradient grid recovers is indicated by the start of oscillations on the gradient grid waveform and is over 100u. Before this time, the full inverse voltage is across the top gap.

FIG. 7 ANODE AND GRADIENT GRID VOLTAGE WAVEFORMS FOR A CX1525

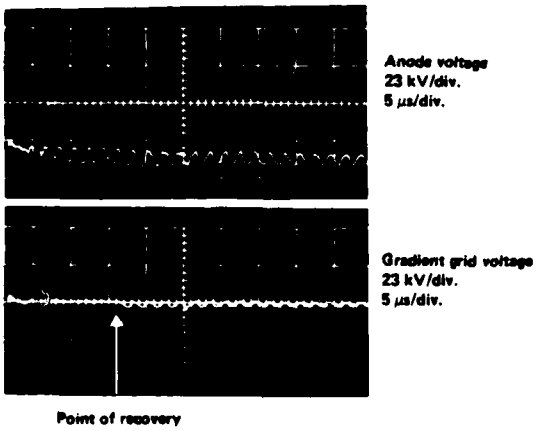


Fig. 7 shows the anode and gradient grid waveforms of a CX1525 operating under the same conditions. It will be seen that the gradient grid recovers within 20 μs.

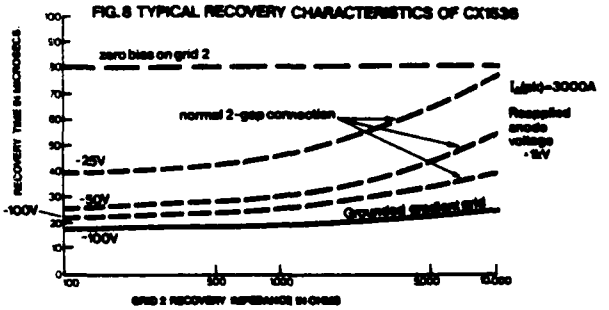
PRINCIPAL RATINGS AND CHARACTERISTICS OF THE CX1525 AND CX1536

	CX1525	CX1536
Peak anode voltage	70 kV	70 kV
Peak anode current	5 kA	10 kA
Rate of rise of anode current	10kA/μS	10 kA/μS
Average anode current	5 A	10 A
Heating factor	100×10^9	300×10^9
Peak power (continuous)	100 MW	300 MW
Average power (continuous)	150 kW	300 kW
Recovery Time	20 μs	25 μs

TRIPLE GRID OPERATION

The construction of the CX1525 and CX1536 lends itself to an alternative mode of operation. The gradient grid may be connected to cathode instead of to the potential divider. The tube then becomes single gap with half the voltage hold-off rating. The grounded "third" grid will further improve the recovery characteristic (see fig 8) and will also screen the control grid from fast rates of change of anode voltage. In circuits where the anode voltage is rising fast, (as in high rep. rate charging), or falling fast, (as in a crowbar) capacitive coupling between anode and grid 2 can cause a tube to prefire. The "third" grid used as a screen reduces the coupling capacity by more than an order and thus eliminates these effects.

FIG.8 TYPICAL RECOVERY CHARACTERISTICS OF CX1536



References

(1) Development of Deuterium Thyratrons for Operations at High Duty ratios and High Average Currents. R. J. Wheldon, N. S. Nicholls. 11th Modulator Symposium, p. 239.

(2) Cooling of Oil Filled Electrical Equipment with special reference to High Power Line type Pulse Generators. G. Scoles, International Pulsed Power Conference, Lubbock, Texas 1976.

Acknowledgements

The Author wishes to thank the directors of the English Electric Valve. Co. Ltd. for permission to publish this paper.

DEVELOPMENT OF A HYDROGEN THYRATRON HAVING A LONG PULSE CAPABILITY

D. Dolbear, D. Fleischer, S. Merz, R. Plante and D. Turnquist
EG&G, Inc., Salem, Massachusetts

N. Reinhardt
Consultant, Lexington, Massachusetts

Summary

A hydrogen thyratron is being developed which is capable of switching 80 amperes at 100 kilovolts with the additional and unusual requirement that the pulse width be as long as 30 seconds with a 10 percent duty cycle. Thyratron operation under these relatively long pulse conditions at moderate current levels represents a unique class of thyratron service, requiring significant departures from standard thyratron design practices.

Radical departures from standard cathode design are necessary to ensure effective utilization of the cathode at the required cathode current on the long time scales involved. In addition, energy losses which occur both in the cathode plasma and at the grid structure integrate over the duration of the current pulse, and the resulting high transient heating must be considered and controlled.

The need for a conservative 100-kilovolt anode holdoff capability necessitates the use of a multiple-section high voltage holdoff structure, and this need is complicated by an additional requirement that high voltage recovery be achieved within 100 microseconds.

The various aspects of the overall tube design are reviewed and the design approach is discussed. Experimental results are presented and consideration is given to the external circuitry associated with the tube in its intended environment, a neutral beam power supply for a magnetic plasma confinement fusion application.

Introduction

The design of a high voltage, long pulse thyratron was undertaken in response to a need for the switching of a neutral beam sustainer source for testing high power neutral beam plasma heating. The basic switching requirement is to deliver an 80-kV, 80-ampere pulse to the modulator load, with a pulse width variable between 0.5 and 30 seconds, once every 5 minutes.

The essentials of the modulator circuit are shown in Figure 1. In this circuit, the thyratron is used as a series switch, triggered on to start the current pulse. The inductor L2 limits the thyratron di/dt to 200 a/μs. To end the pulse, an L-C ring-around circuit is used. To turn off the thyratron, the vacuum spark gap, SG1, and V2 are triggered. C1 rings through L1, and then reverses through D1 and D2, to commutate V2 and SG1. During this entire period, the thyratron anode is held below ground by C2, to allow the thyratron to recover. At the end of this period, the thyratron anode is recharged to 80 to 100 kV, with a dV/dt somewhat less than 3 kV/μs. The requirements for the thyratron in this circuit are given in Table 1.

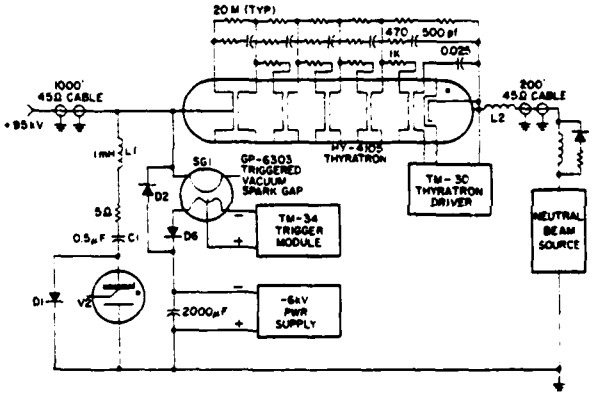


Figure 1. Basic modulator circuit.

Table 1. Thyratron requirements.

Forward Holdoff Voltage, epy (kV)		100	
Peak Current, ib (a)	150	85	80
Pulse Width, tp (sec)	5×10^{-6}	0.5	30
Pulse Repetition Rate		1 pulse/5 minutes	
Recovery Time (μs)		100	
Recharge Rate (kV/μs)		3	
Anode Inverse Voltage, epx (kv)		0-6	

The major design considerations resulting from these requirements are:

- The cathode design must differ significantly from that of standard thyratrons, since the low peak current prevents utilization by the plasma of the usual vertically extended cathode vane structure. The very high average current during the long pulse does, however, produce high power dissipation in the cathode structure, due to the voltage drop in the cathode plasma sheath and adjacent plasma, as well as rms heating of the cathode structure.

CH1371-4/78/0000-0117$00.75 © 1978 IEEE

- The need for reliable 100 kV static holdoff in air requires the use of a conservative, multiple section thyratron with low voltage stress per section. The design of the grid-anode structure must also be compatible with high power dissipation during the pulse, must not allow current quenching during the long 30-second pulse, and must recover in less than 100 microseconds.

- The external trigger circuit, divider string, and auxiliary components must all be integrated with the tube to give reliable triggering, good recovery, and immunity from false triggering during recharge.

- The entire system must be tolerant of faults, arcs, and other mishaps in a very high power environment.

In order to accomplish this task, we were fortunately able to draw heavily on our experience with adiabatic mode thyratron design[1,2,3] for both high voltage structures and for design information to accommodate high current burst heating effects.

Thyratron Design

Cathode Design

In most thyratron applications, the peak current is hundreds or thousands of amperes, and the pulse widths are of the order of tens of microseconds, or much less. Even in rectifier or induction heating applications, the pulse widths do not approach the requirements of this application. The direct implications of the very long, 0.5 to 30 seconds, pulse widths or cathode design are:

1. The allowable cathode current density at the emissive surface is considerably less than that for short pulses but may still be higher than those permitted for continuous duty in vacuum tubes. For pulse widths of this magnitude, in low pressure hydrogen, arc limits for various cathode types are not well established.

2. In most thyratron designs, the cathode structure takes advantage of the ability of the discharge plasma to penetrate and envelop complex extended structures and shapes. By using vanes or coaxial structures, large cathode areas may be contained in relatively small volumes. The penetration of the plasma into these structures, and hence the utilization of the cathode area, is for most structures proportional to the square root of the peak current.[4] At 80 amperes peak, consideration of the cathode utilization factors requires that the cathode surface be nearly planar, or a hollow spherical sector with only a very shallow vane structure.

3. The cathode-plasma sheath and adjacent plasma will give a cathode power dissipation of at least 2000 watts and possibly more, depending on plasma loss to other nearby structures. In addition, there will be resistive losses in the cathode structure and coating that may approach a kilowatt. Over a 30-second pulse, the total energy absorbed may thus be in excess of 100 kilojoules.

In the worst case condition, all of this energy must be absorbed and dissipated over the 4-1/2- to 5-minute inter-pulse interval.

Oxide Cathode: The first type of cathode tested for this program was based on a standard production HY-5 thyratron cathode. This cathode is of a triple oxide, indirectly heated vane design, of approximately 500 sq. cm. This type of cathode is used in the HY-5001 and 5002 thyratrons, which have been tested at up to 9 ka peak and 30 amperes average, in a 30-second burst.[1,3]

The high rms current (520 Aac) and significant average current in these tests indicated that the basic cathode structure might at least be adequate for short pulses in the 80-ampere condition. Accordingly, the vane structure was altered to allow better utilization at low currents, and is shown in Figure 2. The total emissive area is in excess of 150 sq. cm., but only a little more than the projected area of 20 sq. cm. is available to the 80-ampere discharge. Three such cathodes have been built and tested, first in a bell jar test, then in an HY-5001 standard triode thyratron structure, and finally in a full scale HY-4105 thyratron. In this final version, the high purity nickel used in the vane structure was replaced by nickel coated molybdenum for improved thermal conductivity and arc resistance. These tests showed that at cathode temperatures in excess of 760°C (brightness):

1. With a 1/2-second pulse, the arc limit is between 120 and 135 amperes.

2. With a 30-second pulse, the cathode could deliver 80 amperes without arcing, but overheating and consequent metal vapor deposits would substantially impair the high voltage holdoff of the tube.

3. At 80 amperes, a pulse length of less than 8 seconds results in no apparent damage to the tube.

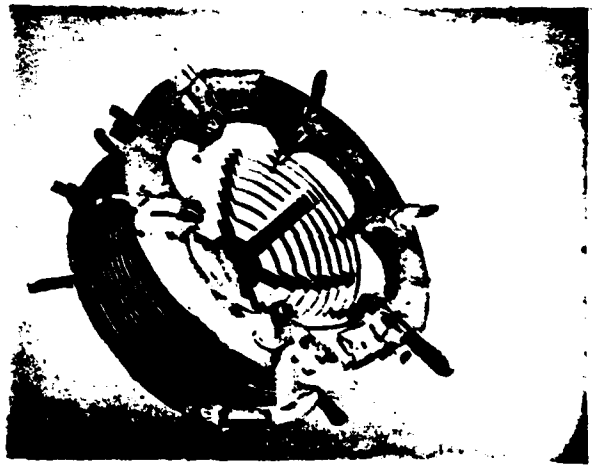
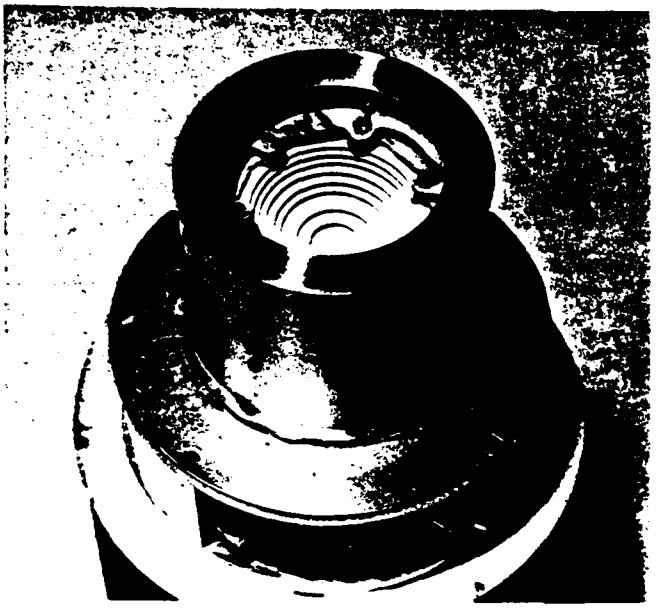


Figure 2. Triple oxide cathode vane structure (wrap-around heater not shown).



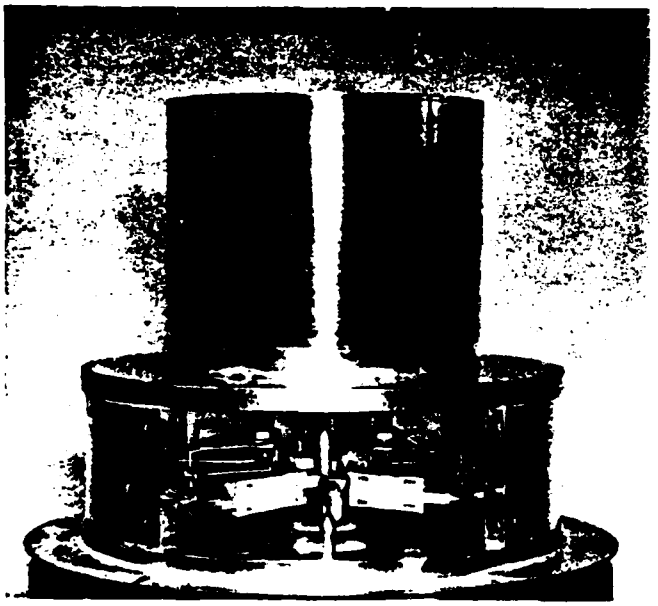


Figure 4. Cathode and reservoir mount.

the titanium weight is 100 grams, with a gas exchange area of 2000 sq. cm. and a heat exchange area of 100 sq. cm. The titanium strips and heater are confined by molybdenum liners, screens, and plates. The entire structure is supported by a Hastelloy frame.

Grid-Anode Design

To operate successfully, the design of the grid and anode high voltage structures must provide for several crucial factors:

1. 100-kV holdoff: To achieve reliable 100-kV static holdoff in air requires a multiple holdoff section structure, with relatively long insulators. The entire structure must be long enough to accommodate the necessary corona shields. With a conservative 20-kV per section holdoff, a reiterated cavity type grid-anode structure is favored, with relatively tight grid baffling.

2. Grid quenching and gas flow: Although the 80-ampere peak current is low, the very long pulse length of 30 seconds presents a possibility for severe gas starvation and grid quenching. The likelihood of quenching is expected to be high for long structures, and therefore the use of a relatively large diameter tube, with large grid aperture area is favored.

3. Grid dissipation with the 80-ampere current pulse is significant, both from the voltage drop in the discharge column (originally estimated to be of the order of 10-29 v/cm, giving 800-1600 w/cm) and possibly from the formation of Langmuir double sheaths at the grid baffle entrances. If such sheaths are present, another voltage drop of the order of 30 volts is expected, giving another 2400 watts per sheath. The high dissipation favors the use of relatively massive grid structures.

4. Recovery time of less than 100 μs, followed by a voltage rise at a rate of 3 kV/μs without retriggering of the tube, would not be a problem for standard, fast recovery, single section thyratrons, with measured recovery of 1 to 10 microseconds. The large cavity type grids used for this design, however, are known to have slow recovery. Since de-ionization is by ambipolar diffusion to the wall, followed by wall recombination, a partial solution is to reduce aperture, baffle, and intracavity spacings. Unfortunately, any structural changes which enhance recovery are liable to cause triggering difficulties.

The design chosen for the high voltage structure was largely based on the earlier HY-5001 and HY-541/MAPS-250 designs.[1,2,3] These tubes have demonstrated:

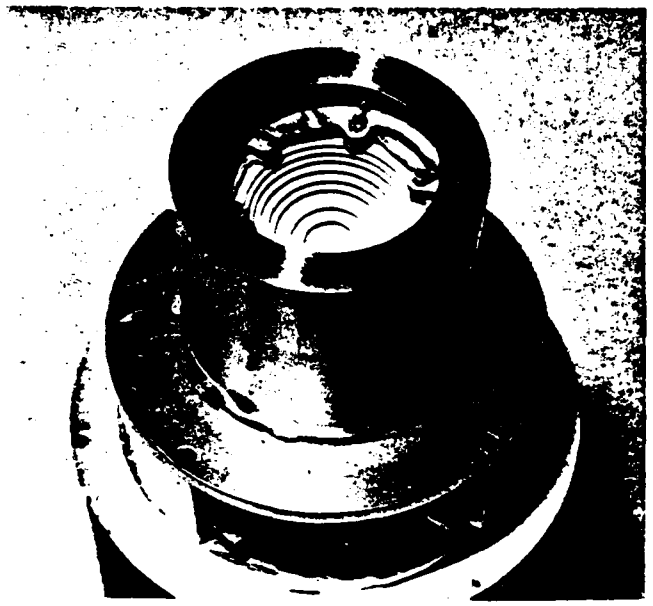
1. 30-ampere average, 30-second burst condition in a single section thyratron.

2. 215 kV holdoff and operation in a 10-section, cavity type thyratron.

Figure 5 shows the essentials of the design used for the first HY-4105. A five-section design is used, with the cavities partitioned by heavy copper plates, both to reduce recovery time, and to absorb power dissipation in the structure.

The external high voltage ceramic spacers are convoluted to provide long creepage path, and glazed for ease of cleaning.

The fourth, uppermost cavity insulator is extra long, to prevent external flashover of this spacer when the tube is triggered. External breakdown of the upper cavity occurs because the voltage cascades up the high voltage stack when the tube is triggered, redistributed capacitively as each grid and anode element sequentially collapses to cathode potential. The upper cavity is therefore exposed to as much as half of the 100-kV holdoff voltage, for some 10's of nanoseconds. External breakdown or puncture of the



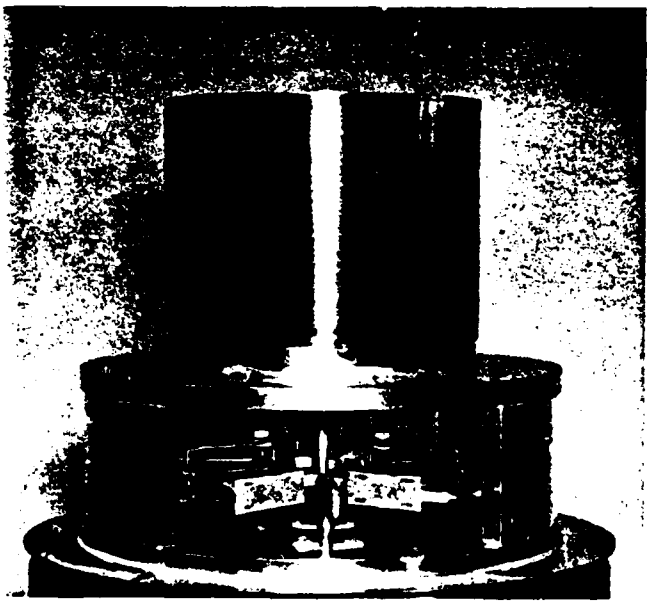


Figure 4. Cathode and reservoir mount.

the titanium weight is 100 grams, with a gas exchange area of 2000 sq. cm. and a heat exchange area of 100 sq. cm. The titanium strips and heater are confined by molybdenum liners, screens, and plates. The entire structure is supported by a Hastelloy frame.

Grid-Anode Design

To operate successfully, the design of the grid and anode high voltage structures must provide for several crucial factors:

1. 100-kV holdoff: To achieve reliable 100-kV static holdoff in air requires a multiple holdoff section structure, with relatively long insulators. The entire structure must be long enough to accommodate the necessary corona shields. With a conservative 20-kV per section holdoff, a reiterated cavity type grid-anode structure is favored, with relatively tight grid baffling.

2. Grid quenching and gas flow: Although the 80-ampere peak current is low, the very long pulse length of 30 seconds presents a possibility for severe gas starvation and grid quenching. The likelihood of quenching is expected to be high for long structures, and therefore the use of a relatively large diameter tube, with large grid aperture area is favored.

3. Grid dissipation with the 80-ampere current pulse is significant, both from the voltage drop in the discharge column (originally estimated to be of the order of 10-29 v/cm, giving 800-1600 w/cm) and possibly from the formation of Langmuir double sheaths at the grid baffle entrances. If such sheaths are present, another voltage drop of the order of 30 volts is expected, giving another 2400 watts per sheath. The high dissipation favors the use of relatively massive grid structures.

4. Recovery time of less than 100 μs, followed by a voltage rise at a rate of 3 kV/μs without retriggering of the tube, would not be a problem for standard, fast recovery, single section thyratrons, with measured recovery of 1 to 10 microseconds. The large cavity type grids used for this design, however, are known to have slow recovery. Since de-ionization is by ambipolar diffusion to the wall, followed by wall recombination, a partial solution is to reduce aperture, baffle, and intracavity spacings. Unfortunately, any structural changes which enhance recovery are liable to cause triggering difficulties.

The design chosen for the high voltage structure was largely based on the earlier HY-5001 and HY-541/MAPS-250 designs.[1,2,3] These tubes have demonstrated:

1. 30-ampere average, 30-second burst condition in a single section thyratron.

2. 215 kV holdoff and operation in a 10-section, cavity type thyratron.

Figure 5 shows the essentials of the design used for the first HY-4105. A five-section design is used, with the cavities partitioned by heavy copper plates, both to reduce recovery time, and to absorb power dissipation in the structure.

The external high voltage ceramic spacers are convoluted to provide long creepage path, and glazed for ease of cleaning.

The fourth, uppermost cavity insulator is extra long, to prevent external flashover of this spacer when the tube is triggered. External breakdown of the upper cavity occurs because the voltage cascades up the high voltage stack when the tube is triggered, redistributed capacitively as each grid and anode element sequentially collapses to cathode potential. The upper cavity is therefore exposed to as much as half of the 100-kV holdoff voltage, for some 10's of nanoseconds. External breakdown or puncture of the

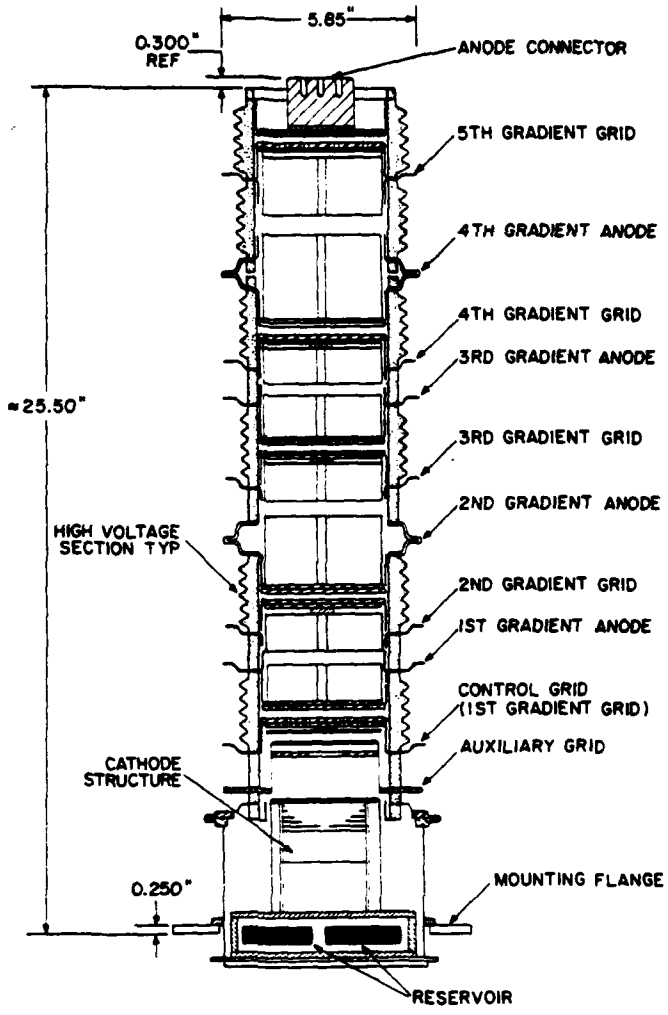


Figure 5. Thyratron design.

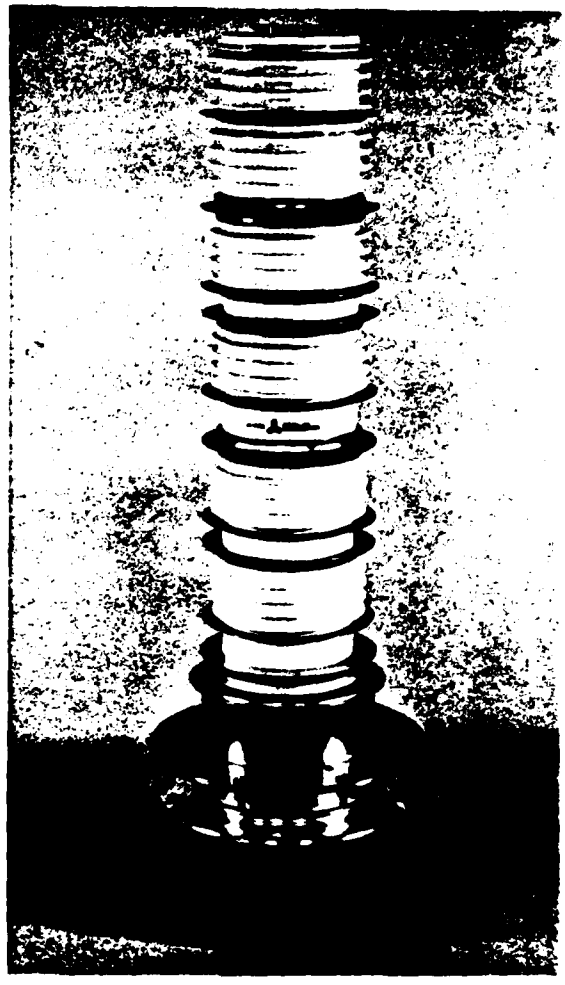


Figure 6. HY-4105 thyratron.

ceramic thus limits the minimum length of the upper cavities in this type of design.

In order to aid the triggering process, an auxiliary grid was included.

Since the severe damage effects of high current arcs on conventional copper elements have been seen in both the experimental testing done for this tube and in other high power tube development, special measures were taken to ensure tube survival under fault conditions. All of the surfaces exposed to the high voltage, or likely to be the site of an arc, are molybdenum. The auxiliary grid, control grid, gradient grids, and gradient anodes were all made of molybdenum-copper-molybdenum sandwich structures to provide both arc resistance and high thermal conductivity. The grid baffles, inner cavity structures, and support caps were made of copper, for thermal conductivity and high specific heat.

Figure 6 shows the final tube, resting on its base fins.

Testing

Full scale testing has not yet been done on the tube, although operating conditions have been simulated in two types of test, first in testing the cathode structure by drawing a current pulse from an arc welder and/or a battery bank, and second, in a series of triggering and recovery tests.

The triggering and recovery test circuit consisted of two parts, a current pulse generator protected from the high voltage by a diode string, and a 100-kV step function generator with a controlled dV/dt (set to 3 kV/μs). The voltage ramp could be triggered on at a variable time after the current pulse termination. Using this circuit, an extensive series of tests was performed to determine the best arrangement of divider elements for reliable operation.

In the type of tube tested, the stray capacity between each anode-grid pair is about 30-40 pF, and that of the cavities is about 15-25 pF.

The two major problems encountered in achieving the required 100 μs recovery were:

1. Non-uniform voltage distribution on the holdoff sections during recharge, requiring use of a particular compensating network, and

2. Cavity recovery, requiring low tube operating pressure.

High Voltage Divider

A number of high voltage divider and compensating networks were tried:

1. With only resistor dividers as in Figure 7a, or with symmetric compensation, as in Figure 7b, the lower sections charge much faster than the upper ones, receiving almost all of the anode voltage, and limit the tube to 50-60 kV before self-firing occurs.

2. If in the circuit of Figure 7b the lowest divider capacitor, C1, is made 1/3 the value of the others, and the auxiliary and control grids are severely clamped (with 0.025 μF), the tube no longer self-fires but is very hard to trigger. With an additional 20-kV trigger pulse applied to the second or third section, the tube could be triggered with 7 kV on the anode. Figure 7c shows that the compensation is not quite correct, either.

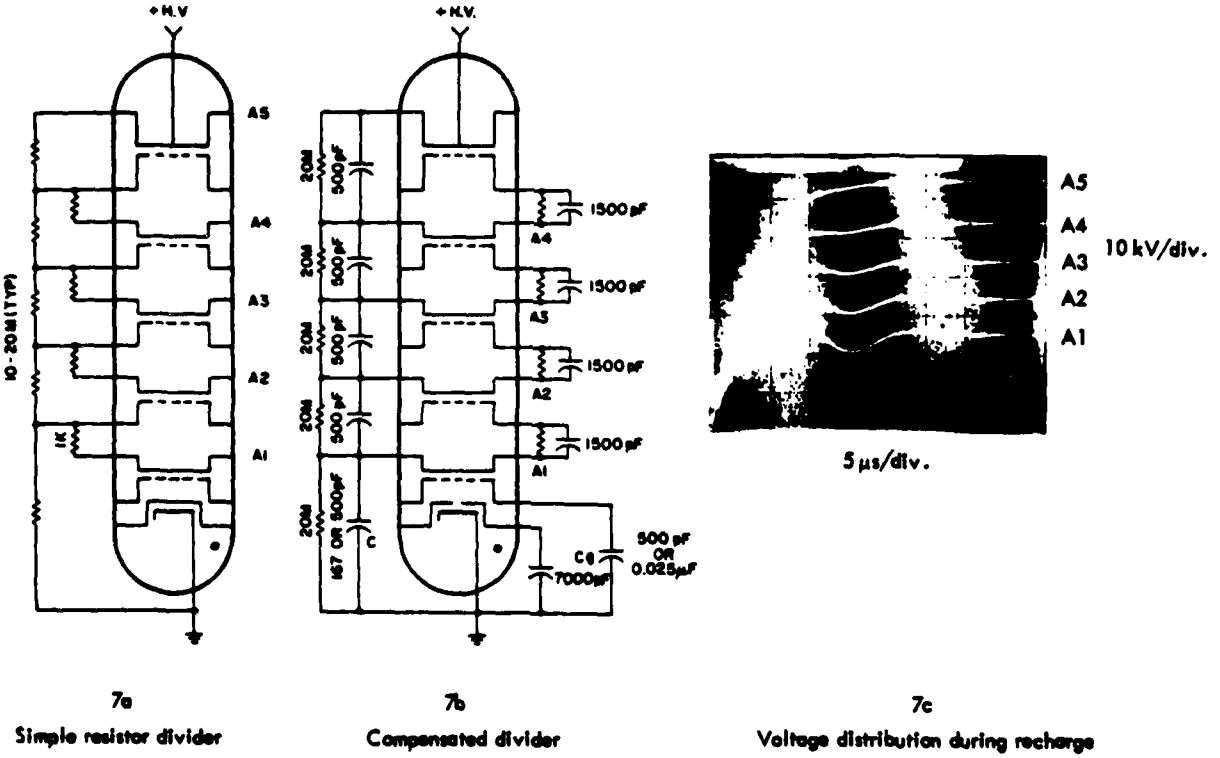
3. Figure 8 shows the correct compensation network, which gives uniform voltage division. In this circuit, the minimum anode voltage required is 12 kV. The required grid drive is 2 kV open circuit, from a 50-ohm source.

Recovery Time

Prior to construction of the full scale tube, a number of triode, tetrode, and single cavity gradient grid tubes were tested for recovery time. A current pulse of 80 to 160 amperes was first applied to the tube under test and then, after a variable time delay, a 3-kV/μsec voltage ramp was applied. During the recovery period, a predetermined inverse anode voltage was applied to the tube. These tests demonstrated several important facts:

1. The use of negative control grid bias reduces the effective recovery time by a factor of 3 or more, and is particularly effective if the inverse anode voltage is sufficiently high. In all cases, a bias voltage of -50 Vdc produced the maximum result observed.

2. Inverse anode voltages applied to all tube types were found to be somewhat marginal at -500 volts and adequate at -1 kV. Further increases in inverse to -2-1/2 kV produced no further observable reduction in recovery time.



7a Simple resistor divider

7b Compensated divider

7c Voltage distribution during recharge

Figure 7. Anode voltage dividers.

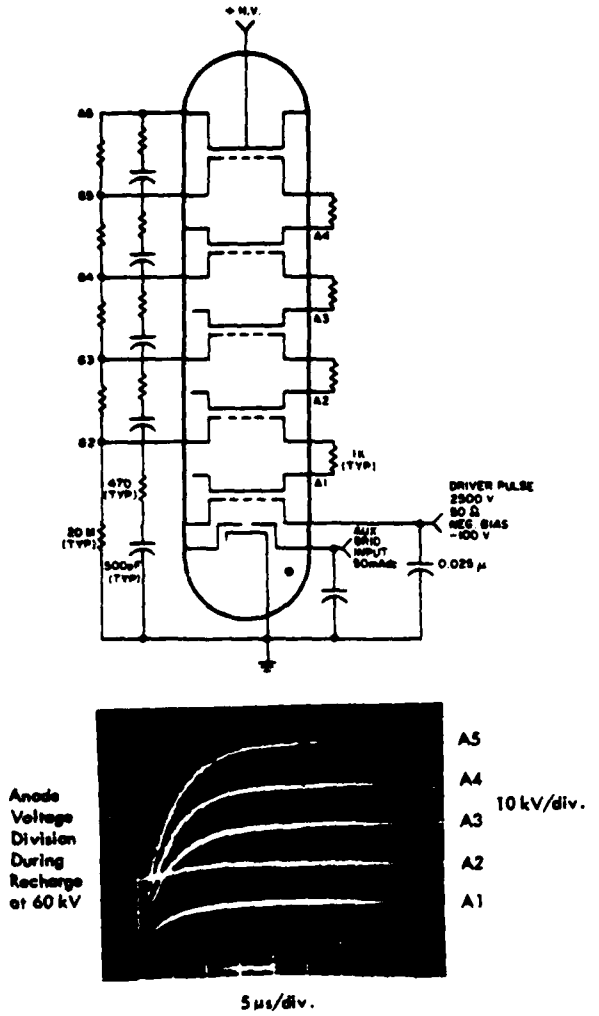


Figure 8. Optimum divider configuration.

3. *In large cavity type tubes the cavity dominates the recovery process, giving recovery time 3 to 10 times that of related large tube types except at very low pressures.*

The results of these tests were used to guide the design of the full scale tube. The HY-4105 was tested for recovery after the conclusion of the divider experiments.

In the configuration of Figure 8, *a number of experiments were made to determine recovery time.*

1. Varying the tube current from 45 to 150 amperes increased recovery time by 50%.

2. Varying the applied anode voltage from 50 to 90 kV increased recovery time by about 20%.

3. Adding a negative bias of -9 to -22 volts had no effect until a number of factors were changed, resulting in recovery times less than 80-100 μs. In this range, cavity bias and cavity recovery time dominate the recovery time behavior.

4. Tube pressures above 0.15 torr give recovery times of 250 to 325 μs, and below 0.1 torr give an abrupt change to 50-75 μs.

Tube Drop

Anode-cathode tube drop during conduction was found to be 600 to 700 volts, or 12-13 v/cm overall average.

Cavity Delay Time

A series of tests to observe the voltage distribution during triggering showed that the voltage was almost redistributed uniformly in the time between the voltage collapse of successive sections. This time was of the order of 100 *nanoseconds* per section at a tube pressure of 0.1 torr pressure, and about 50 nanoseconds per section at 0.18 torr.

Ancillary Equipment Requirements

With the various compensation network requirements established, the final drive and heater requirements for the HY-4105 were defined. These are:

Control Grid Drive —	2000 volts open circuit, 50-ohm source impedance, 1 μsec minimum voltage and current pulse widths.
Auxiliary Grid —	50 to 100 mAdc from a 300 Vdc source.
Control Grid Bias —	-50 to -150 Vdc.
Cathode Heater —	6.3 ±0.5 Vac, 30 Aac *max.*
Reservoir Heater —	Variable 6 to 16 Vac, 25 Aac max.

Conclusion

Further testing at high power is needed. The tests currently underway, however, have shown that several improvements are possible, particularly to extend the pulse width capabilities of the tube, and to further reduce its recovery time. The performance of various critical tests, *and the construction and* preliminary testing of the HY-4105 have demonstrated the basic feasibility of the design of thyratrons for high power, long pulse applications.

References

1. J. Creedon, J. McGowan, and A. Buffa, "Adiabatic Mode Operation of Thyratrons for Megawatt Power Applications," IEEE Conference Record of 1976 Twelfth Modulator Symposium, pp. 46-50.

2. W. Wright, A. Buffa, and S. Schneider, "A Blumlein Modulator for a Time-Varying Load," IEEE Conference Record of 1976 Twelfth Modulator Symposium, pp. 163-167.

3. J. Creedon and S. Schneider, "Megawatt Average Power Adiabatic Mode Thyratrons," Proc. Int. Pulsed Power Conference, Lubbock, Texas, 1976, pp. 1B4-1 - 1B4-6.

4. S.T. Martin and S. Goldberg, "Research Studies on Hydrogen Thyratrons," Final Report, Signal Corps Contract DA36-039sc-15372, 1953.

THYRATRONS FOR SHORT PULSE LASER CIRCUITS

H. Menown & C.V. Neale
English Electric Valve Company Limited
Chelmsford, Essex.

Summary

The conventional thyratron is a unidirectional switch; therefore when circuit design demands large current reversals (as in many short pulse laser drivers) arc back, or positive ion sweeping of the anode surface, causes metallic sputtering which soon leads to a degradation of forward voltage hold-off.

A new range of tubes is described which is designed to accommodate this circuit requirement by storing plasma produced during the forward pulse within a hollow annular apertured anode structure. It is shown that by careful design of the grid/anode geometry, a form of bi-directional operation, without loss of forward voltage hold-off, can be obtained. Information is given concerning circuits suitable for operating these thyratrons, principally in order to avoid problems associated with recovery time.

Introduction

The advent of the pulsed gas discharge laser has opened up an entirely new field for the application of hydrogen thyratrons. Due to the nature of the laser as a load, however, the conventional radar modulator optimised thyratron has some shortcomings. The radar modulator is designed to have a suitably matched line and load with controlled inverse voltage, whereas the laser discharge cavity, being a time varying load, demands high rates of rise of current allied with the ability to withstand rapid rates of application of inverse voltage on the anode.

Experience of operating gas discharge laser circuits has shown that merely applying a high voltage across the laser cavity does not necessarily result in instantaneous conduction, as the actual breakdown time is dependent upon gas pressure, electrode surface condition and residual ionisation from the previous pulse. Any substantial delay in breakdown will lead to inverse voltages appearing on the thyratron anode after a delay equal to the transmission time of the laser energy storage system. With the current amplitudes and time scales involved, the use of a conventional thyratron will often result in reverse arcing of the tube causing severe loss of condition and irreversible damage.

A new range of tubes has now been developed to operate under these demanding conditions in a reliable manner without introducing circuit complications. (See fig. 1). The new feature, incorporated in these tubes, is in the anode design which is a hollow box with an aperture facing the main discharge region. When inverse voltage appears on the anode, some plasma formed during the forward pulse is available for reverse conduction. Hence the reverse arc drop is kept mainly in the glow/arc mode of conduction which prevents sputtering of the anode, and the tube operates as a bi-directional conductor after switching. The duration of reverse conduction is limited by the amount of plasma stored during the forward pulse, as, unlike the double cathode thyratron which has an ionising source built into the anode, plasma is not readily replaced during reverse conduction.

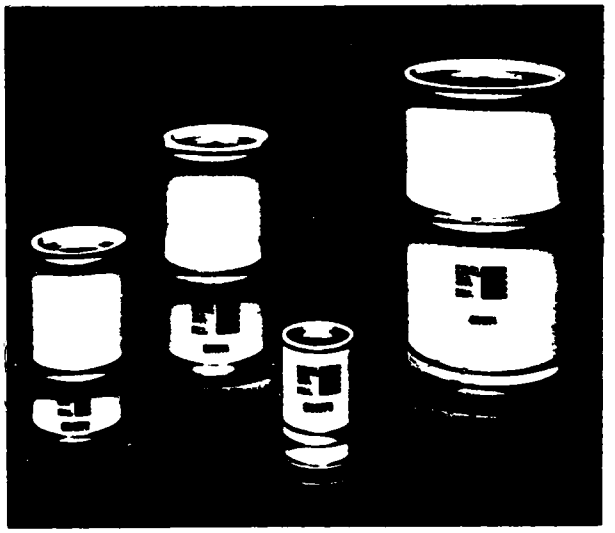


Fig. 1

Tube Design

It became obvious early in 1976 that laser drivers of all types then available, e.g. spark gaps, conventional thyratrons and grounded grid thyratrons, left much to be desired as far as operating life was concerned.

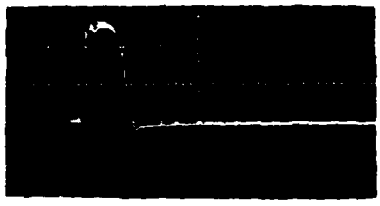
The last tube appeared promising but experiments at our Chelmsford Plant proved that if it were used in the grounded grid/spark gap mode, lives of only a few hours could be obtained. Investigation revealed

CH1371-4/78/0000-0125$00.75 ©1978 IEEE

that the switch tube was being subjected to a very high inverse voltage immediately following the current pulse. In some cases, especially when the laser did not break down, this inverse voltage equalled the forward voltage.

The solution to this problem was suggested by the results obtained from experiments on a two gap thyratron (CX1168) when operated as a single gap tube with the gradient grid electrodes shorted to the anode. This produced a plasma containment volume in the gradient grid cavity and it was observed that when run in the normal mismatched test modulator, forward current conduction was followed by reverse current conduction. (See fig. 2a & b).

FIG.2 CX1168 EXPERIMENTAL CURRENT WAVEFORMS



a) Operated as normal CX1168 (note small clean up current).



b) Operated with anode short circuited to gradient grid (note large current reversal).

Operation in this mode over an extended period of time did not cause any damage to the tube, even though it appeared to be arcing back. It was realised at this stage that the 'arc back' was in the glow/arc discharge mode and not in the destructive metal vapour mode which characteristically destroys voltage hold-off. As a result the thyratron developed for laser circuit driving has a hollow box anode.

Fig. 3 shows diagrammatically the general principle adopted for the anode structure as a plasma containment box. The annular hole in the control grid aperture is mirrored by a similar hole in the anode. The Paschen breakdown distance between the electrodes has, therefore, been increased. As a result the voltage hold-off may be reduced slightly compared with a similar conventional tube filled to the same gas

FIG.3 HOLLOW ANODE THYRATRON

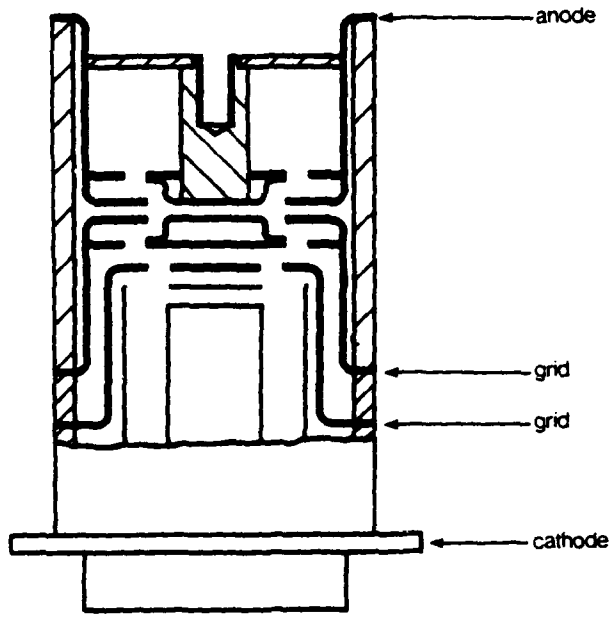


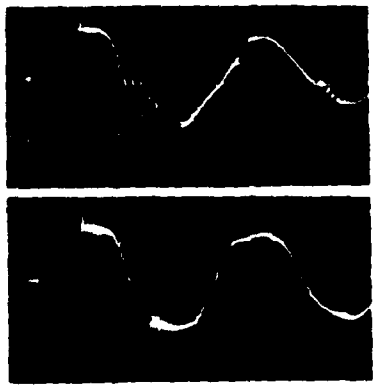
FIG.4

Solid anode thyratron	Hollow anode derivative	Voltage rating	Typical peak current
CX1157	CX1570	16 kV	3,000 A
CX1530	CX1571	20 kV	4,000 A
CX1180	CX1572	25 kV	5,000 A
CX1154	CX1573	35 kV	7,500 A
CX1174	CX1574	35 kV	15,000 A

pressure.
Fig. 4 lists the hollow anode derivatives of the EEV range of ceramic thyratrons with their voltage hold off and peak current ratings.

Fig. 5(a) shows the current pulse through a CX1157 at 15 kV when the test modulator load is short-circuited. The tube is being forced into a sparking arc back condition due to the imposition of the inverse voltage at the end of the pulse.

FIG.5 CURRENT WAVEFORMS WITH SHORT CIRCUITED LOAD

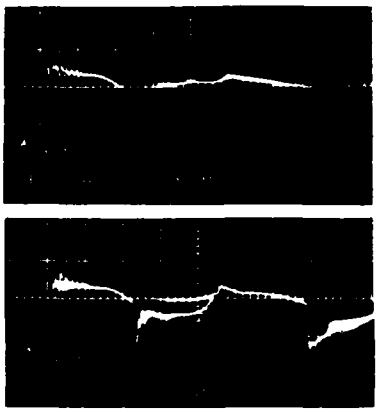


a) CX1157

b) CX1570

Fig. 5(b) shows the current pulse through a hollow anode CX1570 at 15 kV in the same modulator under the same conditions. It will be noticed that the pulse current reverses with an acceptable amount of commutation loss and comparison of the voltage waveforms substantiates this. (Fig. 6a & b).

FIG.6 ANODE VOLTAGE ARC DROP WAVEFORMS WITH SHORT CIRCUITED LOAD.



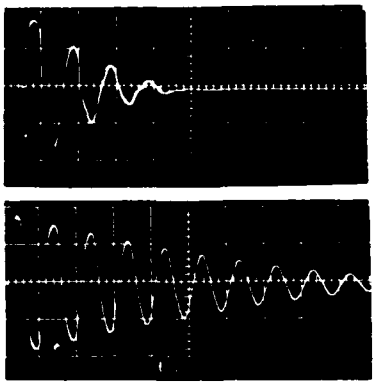
a) CX1157

b) CX1570

COMPARISON WITH DOUBLE CATHODE THYRATRONS

Figs. 7 & 8 show a CX1573 and a CX1154B double cathode tube operating under the same short circuit load conditions in the same modulator. The commutation arc drop losses of the hollow anode tube should be noted and compared with those of the double cathode tube, also the number of voltage and current reversals for each type as these show the fundamental differences between the two types. Therefore, for circuits where commutation losses are important, e.g. beam bending magnets for high energy nuclear particle accelerators or for high power laser driving, the double cathode tube is preferred. For pulsed lasers originally driven by triggered spark gaps the hollow anode tubes have distinct advantages especially for higher prf operation. They have the same outline dimensions as the solid anode tubes and do not require any extra circuitry.

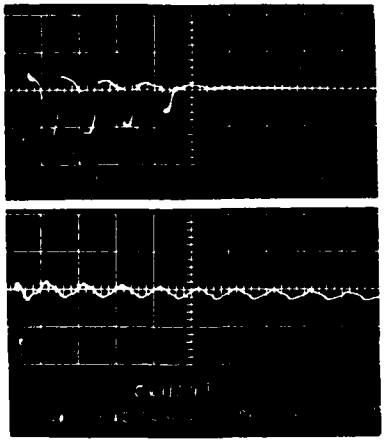
FIG.7 CURRENT WAVEFORMS WITH SHORT CIRCUITED LOAD



a) CX1573

b) CX1154B

FIG.8 ANODE VOLTAGE ARC DROP WAVEFORMS WITH SHORT CIRCUITED LOAD



a)

b)

Their higher reverse arc drop in some ways is an advantage since the oscillatory currents which maintain conduction in the tube die away more rapidly. Tube recovery is therefore not as great a problem as for the double cathode tubes and it has been found in practice that normal modulator circuit precautions are all that are necessary. Recovery time measurements so far made at EEV have shown that hollow anode tubes recover within a microsecond or so of the recovery time (measured from the point of current extinction) of the solid anode tube.

LASER OPERATION

FIG.9 LASER DRIVE CIRCUIT

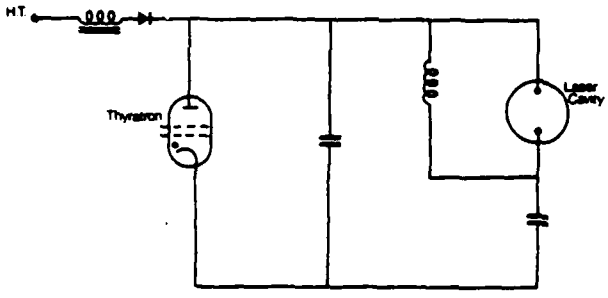


Fig. 9 shows a typical pulse nitrogen laser circuit. The capacitors are charged to double H.T. voltage by a resonant choke charging circuit. When the thyratron is triggered the voltage on the adjacent capacitor is rapidly reversed resulting in four times the H.T. voltage appearing across the laser cavity. Ideally the laser discharge takes place just before maximum voltage is achieved and the energy stored in the capacitor is rapidly dissipated in the cavity. As in many practical circuits there is a formative time lag for cavity breakdown and the thyratron will see an inverse voltage of the same order as the forward voltage.

FIG.10 OPERATION IN NITROGEN LASER CIRCUIT

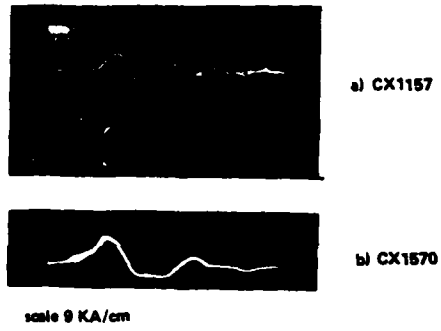


Fig. 10a shows the unstable sparking arc back of a solid anode CX1157 which can be compared with fig. 10b showing the more stable glow/arc discharge of the hollow anode CX1570. A nitrogen laser is being driven by a CX1570 at EEV as a life test. To date it has achieved 200 hours continuous running at 100 pps and is still operating satisfactorily.

Acknowledgements

The Authors wish to thank the Directors of English Electric Valve Co. Ltd. for permission to publish this paper.

MULTI-GIGAWATT HYDROGEN THYRATRONS WITH NANO-SECOND RISE TIMES

S. Friedman, S. Goldberg, J. Hamilton, S. Merz, R. Plante, and D. Turnquist
EG&G, Inc., Salem, Massachusetts

Summary

A new and advanced class of high-power hydrogen thyratrons is being developed which is capable of switching very short and ultra fast-rising multi-gigawatt pulses. The effort underway is to extend the operating range of thyratrons to values of di/dt and current rise time an order of magnitude faster than heretofore achieved, and to do so at high voltages, peak currents, and repetition rates. Immediate goals are di/dt = 10^{12}a/s with a 5-20 ns rise time, peak currents of up to 75 ka, pulse repetition rates of 1 kHz, and forward voltage holdoffs of 50 kV for a single section tube and up to 250 kV for a gradient grid tube. Retention of the usual advantages of thyratron switches (stable operation, fast recovery time, and long life), is required in addition to meeting various other requirements imposed on these tubes in these applications. This paper describes some of the problems we have encountered and the progress we have made in this previously uninvestigated regime of thyratron operation.

Thyratron Design Requirements

Thyratron tubes of existing design are capable of meeting the objective high-voltage, peak-current, and repetition-rate requirements.

A 10-section gradient grid tube capable of switching 215 kV and 20 ka has been constructed.[1] The HY-7 operates at a peak current of 40 ka and can switch 40 kV at megawatt average power.[2] It is the high di/dt and short rise time that pose the greatest challenge, especially in conjunction with high voltage holdoff. This is because fast switching requires very low inductance and hence short tubes and compact systems, while good holdoff has, in the past, required long gradient grid designs and long external breakdown paths. The major portion of our effort has been accordingly directed in two primary areas: discharge propagation and growth in the thyratron, and the high-voltage structure.

di/dt

Thyratrons are usually operated in a regime where the current rise time is much longer than the breakdown time (anode fall time) of the tube. When the rise time reaches the 10-ns range this is no longer the case, and di/dt is influenced by the manner in which the discharge in the tube forms and spreads. We therefore constructed a number of specially modified thyratrons that enabled us to independently control the formation of the grid-cathode discharge and the moment of commutation. Most of the di/dt experiments to date have been carried out using design based on standard 1802/7322 tubes fitted with an auxiliary grid between the control grid and the cathode. The structure of these tubes, designated as HY-3004, is shown in Figure 1. The density of the grid-cathode discharge is controlled by the voltage on the auxiliary grid, and is spread prior to commutation by the bias on the control grid.

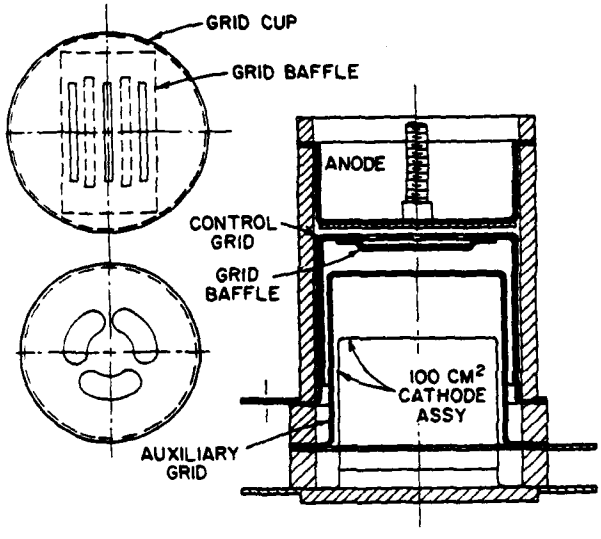


Figure 1. Experimental HY-3004, modified 1802/7322 thyratron.

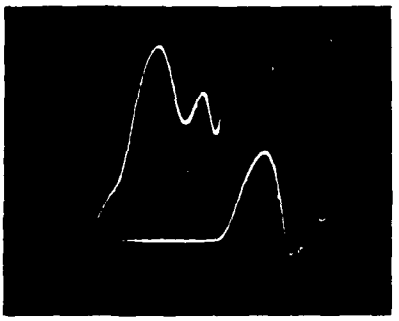
Figure 2 compares the tube operation in low and high di/dt regimes with both grids triggered simultaneously. The pulse forming network (PFN) consists of a single capacitor and inductor, and di/dt is varied by changing the inductor. Note that at high di/dt the anode fall time is equal to the current rise time, and is much longer than in the low di/dt case. This illustrates the point made above; the current rise time and the measured anode fall time are interrelated, and cannot be treated separately as in the low di/dt regime. In this latter case the anode fall time is only a function of pressure, and the current rise time depends only on PFN capacitance and inductance.[3] At high di/dt, inductance within the tube causes the anode fall time, which would otherwise be a measure of the breakdown time of the tube, to contain a significant di/dt term.

Several interrelated factors influence the discharge growth and di/dt. Our current results are summarized below.

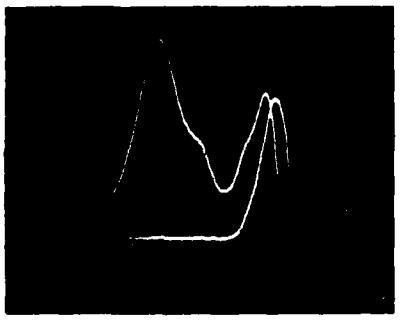
Grid-Cathode Breakdown

di/dt is significantly higher when the auxiliary grid (the grid closest to the cathode) is used to trigger commutation than when the control grid is triggered. Figure 3 shows this effect. In each case the untriggered grid has a high impedance to ground. Note that when the auxiliary grid is triggered, grid-cathode breakdown is more developed at the instant of commutation.

CH1371-4/78/0000-0129$00.75 © 1978 IEEE



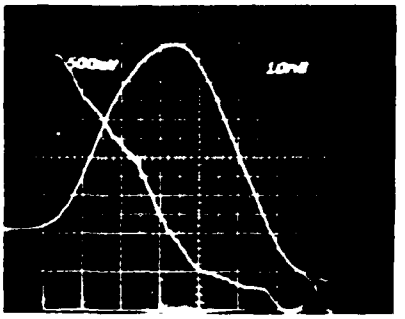
(a)



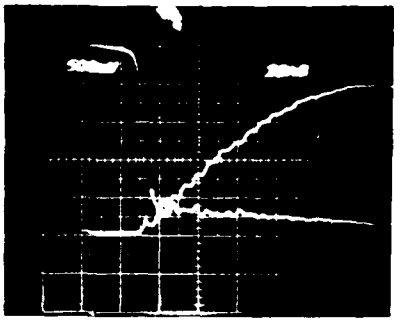
(b)

Figure 2. Anode fall and anode current.

Pressure = 400 millitorr.
a) High di/dt
b) Low di/dt
Voltage: 500V/minor div.
Current: a) 200A/minor div.
b) 40A/minor div.
Time: a) 10 ns/minor div.
b) 20 ns/minor div.



(a)



(b)

Figure 3. Grid voltage and anode current.

a) Control Grid Triggered
b) Auxiliary Grid Triggered
Voltage: 200V/minor div.
Current: 200a/minor div.
Time: 20 ns/minor div.
epy = 15 kV
Driver source impedance, zg ~2 ohms.

di/dt also increases substantially if a DC discharge of about 100V and 100 ma (not enough to cause commutation) is established in the auxiliary grid-cathode region prior to triggering the control grid, as shown in Figure 4. Further increases in auxiliary grid drive produce further, though diminishing, results. For example, a change from 1 amp to 200 amps produces a change of about 10% in di/dt.

Discharge Spreading

The inductance of the tube depends in part on the degree to which the discharge fills the volume. Discharges tend to begin from one spot on the cathode, and spread laterally. To study the effect of spreading on di/dt, the control grid was biased negative to delay commutation while a 2 kV pulse was applied to the auxiliary grid. Figure 5 shows the resulting auxiliary grid voltage and anode current waveforms for zero and -100V control grid bias, corresponding to a variation of over two orders of magnitude in delay time. No effect on anode current rise is seen. This

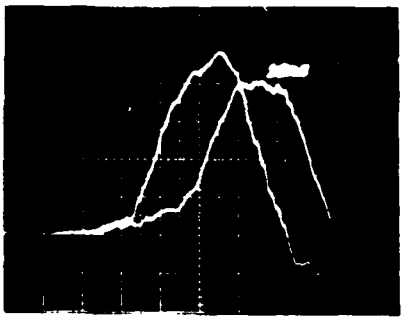
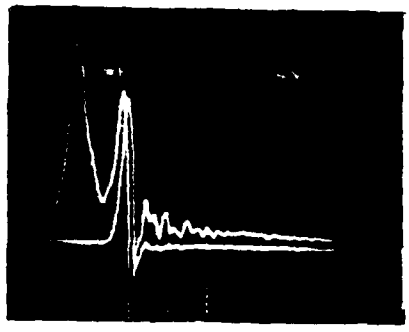
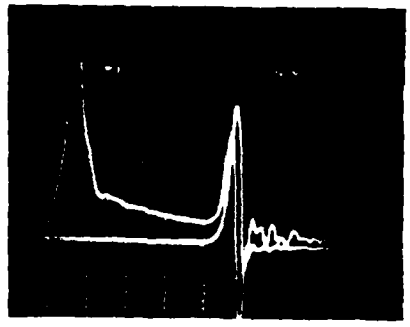


Figure 4. Anode current 500a/minor div.

epy = 10 kV.
Pressure = 400 millitorr.
Control Grid Triggered.
With (left) and without (right) 100V, 40ma, DC discharge between auxiliary grid and cathode.



(a)



(b)

Figure 5. Grid voltage and anode current at zero (a) and -100V (b) Control grid bias (Ecc).

epy = 15 kV.
P = 400 millitorr.
Voltage: 200V/minor div.
Current: 200a/minor div.
Time: 50 ns/minor div.

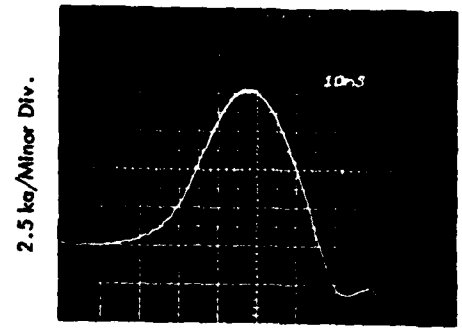
negative result is contrary to what we expected from the grid-cathode breakdown experiments, and is not yet understood. Experiments are continuing, and a number of tubes fitted with Langmuir probes are being constructed so that discharge propagation can be measured directly.

Pressure

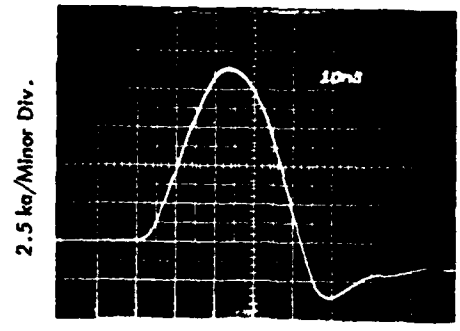
Tube breakdown time varies inversely with pressure because the electron-neutral collision frequency increases. Figure 6 shows anode current pulses at three different pressures. Note that most of the increase in amplitude results from a steepening of the early portion of the pulse, indicating a decrease in the resistive phase rise time. No significant increase in di/dt is observed at pressures beyond 500 to at least 800 millitorr, suggesting limitation by inductive effects in this region.

Tube Geometry

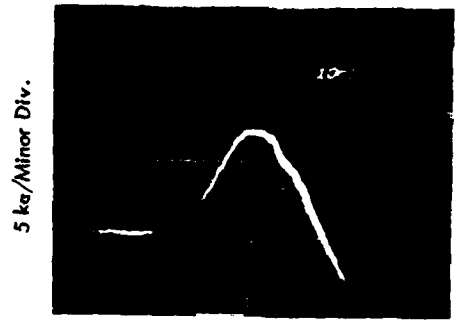
di/dt should increase if the inductance of the thyratron decreases. The inductance of the thyratron can theoretically be reduced by making tubes that are



(a) Eres = 6.0V



(b) Eres = 7.2V



(c) Eres = 8.0V

Figure 6. Risetime variation with pressure.

(Hydrogen reservoir voltage as a parameter)
(epy = 25 kV, E_F = 5V)
Time: 10 ns/minor div.

shorter and/or wider, and we are presently doing both. The HY-3004 tubes presently in use are 3 in. in diameter and 5 in. long, and together with their return current shroud are calculated to have an inductance of 40 nh. (This is in good agreement with measurements of anode voltage divided by di/dt.) We are constructing a 2-1/2 in. long 1802/7332 type tube, and also a 4-1/2 in. diameter HY-53 having an anode-to-cathode distance of 1-1/2 in. (The standard HY-5 distance is 5 in.) Close fitting current return structures have also been made, and the calculated inductances of the new 1802/7332 and HY-5 assemblies are approximately 20 and 13 nh, respectively.

di/dt Results

The attainment of high di/dt required grid currents of several amperes. High di/dt is sensitive to trigger location, making it better for auxiliary grid triggering.

The highest value of di/dt attained to date is 5×10^{11} a/s at epy = 25 kV, ib = 13.5 ka, and 500 millitorr pressure, with the auxiliary grid triggered and the control grid floating (Figure 6c). The trigger impedance was 1 ohm and the trigger voltage 1 kV. The PFN consisted of thirty 30-ohm cables in parallel. The calculated inductance of the tube and shroud was 40 nh, assuming the discharge filled the tube to the outer diameter of the auxiliary grid slots. This assumption is supported by observed uniform anode damage patterns in a tube operated at a high pulse repetition rate (prr). Since di/dt was found to vary linearly with epy, this is an encouraging result. However, the early part of the pulse still needs steepening if a 20-ns rise time is to be achieved.

High Voltage Holdoff and Repetitive Pulse Operation

Designing and constructing reliable, high-voltage, very low inductance switches requires a systems approach that simultaneously takes into account several normally separate elements. The charging method, the coupling of circuit components, the distribution of electric fields both inside and outside the tube, the choice of dielectric materials, and the overall system geometry are all being carefully studied.

Repetitive Pulse Operation

Breakdown tests with the HY-3004 (modified 1802/7322) attained better than 40 kV forward holdoff (the limit of the test system used) at 800 millitorr pressure using command charging at a rate of 10 kV/μsec. With conventional resonant charging this tube operates at only 25 kV, at 400 millitorr pressure. We have therefore proceeded with the construction of a 50 kV, 1 kHz modulator circuit and load using an HY-3004 variant and command charging (Figure 7). The tube is operated at 400-500 millitorr pressure, and is immersed in silicone oil for electrical insulation. The dielectric strength of the oil immersed cable end was tested successfully to 30 kV DC across a 1/4 in. gap. The tube anode is water-cooled. The PFN is a 15-ohm Blumlien consisting of two groups of four 30-ohm cables. The load is an acid bath and has an impedance of approximately 15 ohms. We have presently attained 25 kV and 3.2 ka at 1 kHz and are systematically eliminating various problems associated with higher voltage operation. Figure 8 shows load current waveforms in this system, at two levels. In these photographs the bandwidth of the measuring equipment is exceeded.

Recovery time of the command charge triode imposes a limit on the minimum obtainable time at high voltage. We are now operating at dwell times of about 20 μs.

In general, the average heating of thyratron anodes is a function of di/dt x prr x epy, designated by us as the π_b factor (by analogy with the old plate breakdown factor, Pb). For most thyratrons we

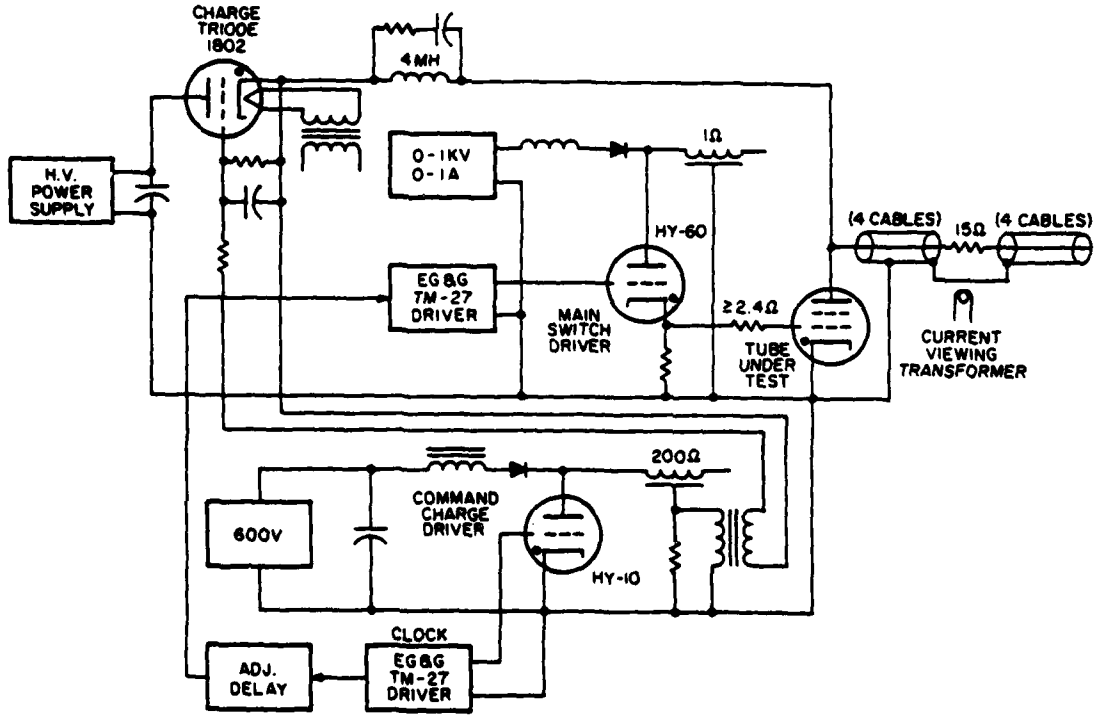


Figure 7. Schematic of 1 kHz modulator.

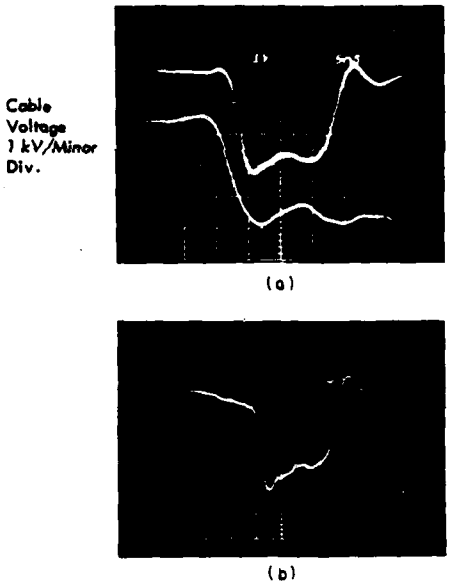


Figure 8. Low level (a) and high level (b) Blumlien load current pulses.

HY-3004, Pressure = 500 millitorr.
prr = 1 kHz.
Load resistance: approximately 15 ohms.
Time: 5 ns/minor div.

are able to clearly distinguish several levels of anode heating:

$\pi_b > 1 \times 10^{17}$	Amp x Hertz x volts/sec. Air cooling needed, hot anode.
$\pi_b > 3 \times 10^{17}$	Red hot anode in air, liquid cooling needed.
$\pi_b = 250 \times 10^{17}$	Present limit of experience.

Inadvertent destruction of one tube in this circuit by anode overheating reemphasized the need for proper cooling and anode design for operation at high di/dt and high prr.

High-Voltage Holdoff

Requirements for the 250 kV gradient grid tube are much more severe, and a major effort is being directed toward solving many interrelated problems stemming from conflicting demands of high di/dt and high voltage. The major problems and the methods we are using to solve them are summarized below.

High di/dt requires high pressure, short tubes, and close-fitting current return paths. High pressure lengthens the recovery time, and degrades forward holdoff. However, high voltage becomes an especially severe problem when the tube is switched, since an ever-greater fraction of the total forward voltage will appear across the tube sections closer to the anode as the preceding sections break down, placing extreme stress on the ceramics and other dielectrics. The shorter the sections and the smaller the current return path spacing, the greater the stress.

Our approach to these problems involves three areas of investigation.

Pulse Charging: This will improve forward holdoff both internally and externally. The required charging rate might well be several 10's of kV/ sec. Our present approach uses total charge times less than 20 μs.

Studies of Electric Field Distribution: Knowledge of the transient internal voltage distribution among the tube sections is critical in determining the minimum number of sections required to withstand the stress. Figure 9 shows the calculated capacitive transient voltage distribution for different numbers of grids. For the assumed capacitance ratio shown, it appears that five grids represent the point of diminishing returns. (This ratio is determined in part by the external dielectric fluid, as well as by grid geometry.)

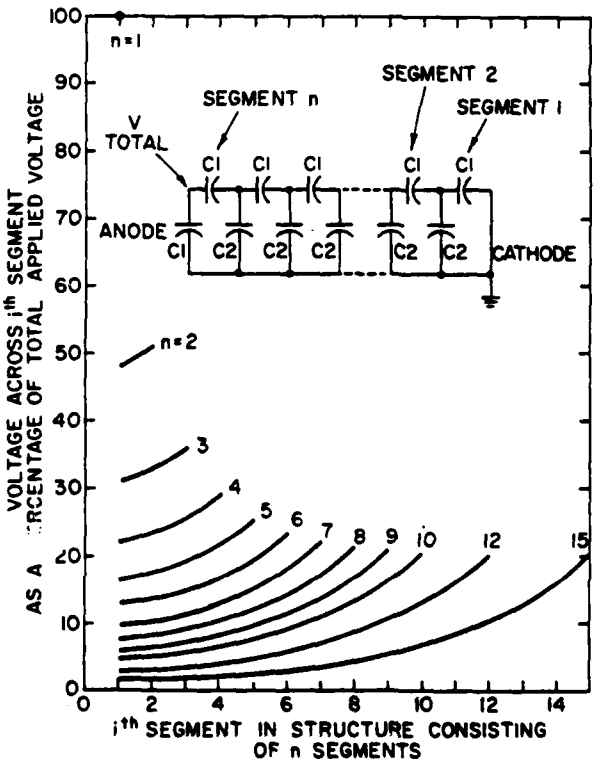


Figure 9. Capacitive transient distribution of multi-segment structure, fixed capacitive ratio C1/C2 = 20.

Computer calculations of the external electric fields have also been made. Results for a 5-section tube are shown in Figure 10. These computations are being used to design insulator and electrode shapes that minimize the voltage stresses, as shown in Figure 11.

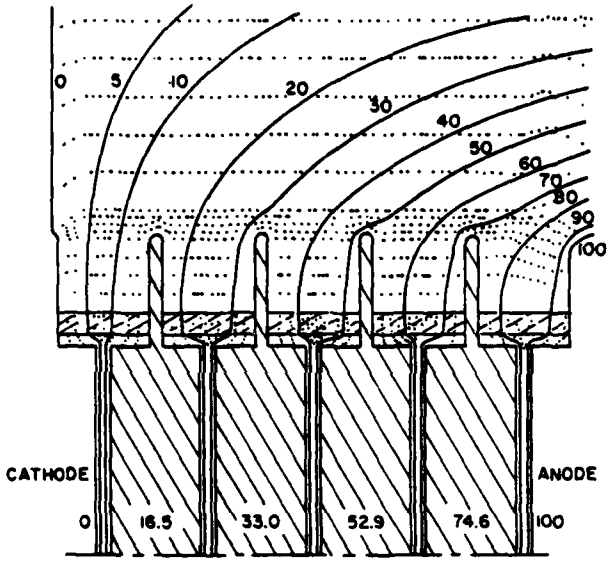


Figure 10. 5-segment tube structure under capacitive distribution.

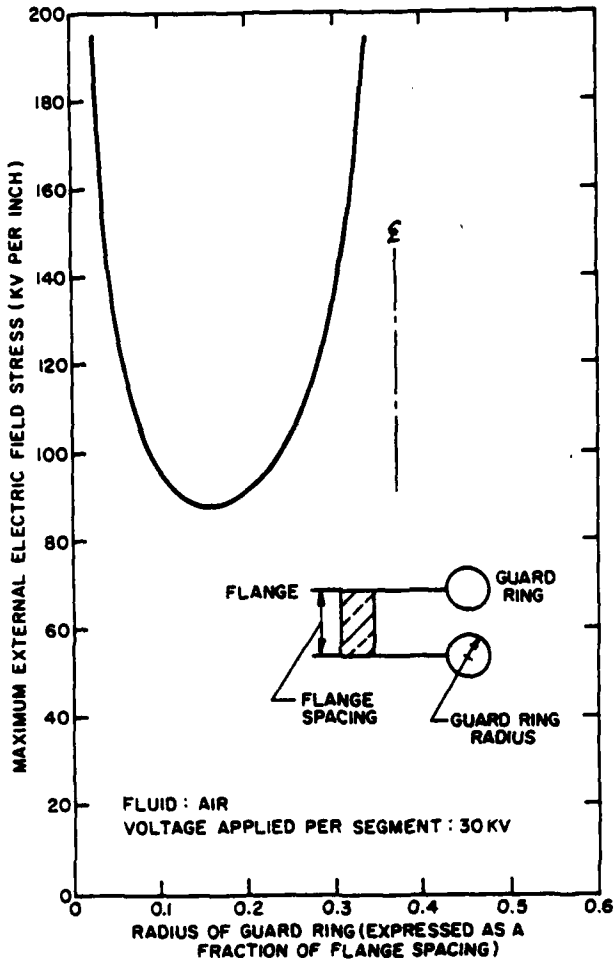


Figure 11. Maximum external field stress as a function of guard ring radius.

Materials Studies: High stress levels require careful selection of ceramic and dielectric materials. The ceramic must also withstand ion bombardment, x-rays, and thermal stress, over a reasonable life. Experimental testing of several different insulating materials is being conducted. Special attention is being given to the effects of flaws, small defects, and other non-uniformities in composition. It is also important to consider machining properties and availability of standard sizes and shapes in selecting materials and designing system parts.

The results of these calculations and investigations will be tested on a 5-section tube now under construction.

Conclusions

Modest extrapolation of present di/dt and voltage holdoff data show that the attainment of 10^{12} a/s at greater than 50 kV at a prr of 1 kHz awaits only the completion of the required circuitry. Extension to compact gradient grid tubes and higher voltages is moving from the theoretical into the experimental stage. Several factors influencing current rise time have been identified, and experiments aimed at gaining a better understanding of the basic breakdown mechanism and discharge spread are continuing.

References

1) J. Creedon and S. Schneider, Megawatt Average Power Adiabatic Mode Thyratrons, Proc. Int. Pulsed Power Conf., Lubbock, Texas, 1976, pp. 1B4-1 - 1B4-6.

2) J. Hamilton, S. Merz, R. Plante, D. Turnquist, and N. Reinhardt, Development of a 40 kV Megawatt Average Power Thyratron, 13th Pulse Power Modulator Symp., Buffalo, New York, 1978.

3) S. Goldberg and J. Rothstein, Hydrogen Thyratrons, Advances in Electronics and Electron Physics, Vol. XIV, New York, Academic Press, 1961, pp. 207-264.

Acknowledgments

This work is supported in part by the Naval Surface Weapons Center, Dahlgren, Virginia, under Contract No. DAA807-77-C2725, and in part by the Los Alamos Scientific Laboratory, under Contract No. EN-77-C-04-4047.

DEVELOPMENT OF A FORTY KILOVOLT MEGAWATT AVERAGE POWER THYRATRON (MAPS-40)

J. Hamilton, S. Merz, R. Plante, and D. Turnquist
EG&G, Inc., Salem, Massachusetts

N. Reinhardt
Consultant, Lexington, Massachusetts

J. Creedon and J. McGowan
ETDL, USA ERADCOM, Fort Monmouth, New Jersey

Summary

The thyratron which resulted from the MAPS-40 Megawatt Average Power Switch development effort achieved switching of 40 kV and 40 ka with a pulse width of 10 microseconds and a repetition rate of 125 Hz. Operation was in 10- to 15-second bursts at the 1-megawatt average power level.

The MAPS 40 embodies new engineering solutions to the problems encountered in high power thyratrons. In this development, careful attention had to be given to the control of operating dissipations, to the storage and dispersal of heat, to the strength and protection of internal tube structures, and to the special requirements of tube and circuit operation at the megawatt level.

In the first phase of the program, eight thyratrons were constructed, five of which were delivered to Fort Monmouth for evaluation. Four of these prototype tubes were tested to the specified objectives in short-burst operation, and were subjected to further tests to explore their nominal design capabilities. Seven more tubes have since been built, all of the same design, all of which have met the specified objectives.

Introduction

The MAPS-40 megawatt average power thyratron program is an outgrowth of the earlier MAPS-70 project, in which operation at several hundred kilowatts was achieved.[1,2] The work performed in this development relied heavily on advances made in earlier programs in extending operation to the present megawatt power level.

Specified objectives for the MAPS-40 thyratron are listed in Table 1. The operating condition features:

1. Operation at an epy level of 40 - 44 kilovolts.
2. Peak current of 40 kiloamperes.
3. Average current of 50 amperes.
4. An rms-equivalent current of 1480 amperes.
5. Repetitive burst mode operation, with "on" cycles of 3 to 30 seconds at the 1-megawatt average power level.
6. Restrictions on the number of missing pulses or kick-outs experienced during extended burst-mode operation.
7. A 48-hour standby requirement (heaters only).

Major problems were forward and inverse holdoff capability, aggravated by the standby requirement, and the thermal and mechanical design of heavy internal structures.

Table 1. Major specification objectives for MAPS-40 thyratron.

Parameter (Units)	Rating	Operation (1)	Operation (2)
epy (kV)	40	44	44
ib (ka)	40	44	11
egy (kV)	1.5-4.0	--	--
tp (μs)	--	10	20
prr (Hz)	500	125	250
Ib (A dc)	50	50	50
Ip (kA ac)	1.48	1.48	0.74
Pb (10^9 va/s)	400	242	121
dik/dt (ka/μs)	20	20	20
tad (μs)	--	0.2	0.2
Δtad (μs)	--	0.1	0.1
tj (μs)	0.02	--	--
Ef=Eres (Vac)	15±1.5	--	--
If (A ac)	70	--	--
Ires (A ac)	40	--	--
tk (sec)	900	--	--
Life (pulses)	--	$5x10^6$	$5x10^6$

Principal Design Considerations

A conventional external-anode, planar-electrode, ceramic-metal tube design was chosen to meet the basic design considerations for the MAPS-40 thyratron as outlined in Table 2. To obtain reliable, kick-out free operation at 40 - 44 kV, the use of a gradient grid was necessary. To prevent quenching, a large total grid-slot aperture area was required, implying an 8-inch diameter tube design. An auxiliary grid was necessary to obtain good triggering characteristics. To handle the operating dissipations at the cathode, a novel open-work type of vane structure was proposed.

CH1371-4/78/0000-0135$00.75 ©1978 IEEE

Table 2. Principal design considerations.

Design Parameter	Area of Principal Concern	Design Decision
Electrical		
40 kV operation	Forward voltage hold-off, reliable operation.	Use gradient grid and tight baffling.
40 ka peak current	Grid aperture quenching.	Use 8-inch diameter tube.
High di/dt; low tad, Δtad and jitter.	Conflict with tight baffling of grids.	Incorporate auxiliary grid; use "keep-alive" bias.
1480a rms current.	Current distribution; ohmic heating in the cathode structure.	Careful attention to feeds and connections.
Burst-mode operation	Transient hydrogen cleanup.	Use fast-response reservoir.
High average power	Overheating.	Use composite construction of adequate thermal mass and conductivity: low thermal resistance from grids to external flanges.
Survival under arc-fault conditions	Melting of tube elements.	Molybdenum high-voltage surfaces: anode, grids, and shields.
Thermal and Mechanical		
8-inch diameter seals	Thermal stresses arising from bimetallic electrode construction.	Use compensation and stress relief techniques.
Burst-mode operation	Thermal runaway.	Absorption of heat followed by dispersal during "off" periods.
Deuterium Pressure Stability	*Titanium reservoir* temperature and rate of response.	Isolate reservoir from thermal surges in rest of tube; design for fast response.
Sagging, creep, warping	Complex and heavy mechanical parts made of ductile materials in grids, cathode, reservoir.	Brace structures with stiff framework of refractory metals.
Environmental		
Survival under shock and vibration	Tube envelope and structures.	Design for strength and stiffness.
Field Handling	Shipping, mounting, connecting.	Handling features planned as integral part of tube.

The most difficult design problems arose in the thermal and mechanical design of the tube structures. Massive internal structures were needed to carry currents and to absorb and distribute operating dissipations. These had to function without warping, local melting, or causing electron emission to occur in undesirable places.

The grids, for example, were designed as thick copper-molybdenum sandwiches to resist arc damage and to spread heat away from the grid slots and conduct it to the tube exterior. These sandwiches had to be prevented from warping, or from exerting powerful expansion forces on the ceramic-to-metal seals.

The cathode required that a kilogram of dead-soft nickel be supported well enough to prevent sagging, creep, or deformations from g-forces (all problems experienced in the earlier MAPS-70 cathodes). The early tubes in the MAPS-40 program were built with what was basically a structurally augmented MAPS-70 cathode; later tubes incorporated an entirely new design in which operating dissipations were minimized and the structure integrally braced.

The reservoir, designed for rapid response to pressure or heater power changes, likewise had to be protected against deformation and heater shorts, and it had to be isolated from thermal surge in the rest of the tube.

The tube envelope, used to transfer the grid-dissipation heat loads efficiently to the surrounding air, was designed to employ butt-seals to heavy 1/8-inch thick copper flanges and to nickel-iron alloy flanges. Figure 1 shows the external appearance of the finished tube.

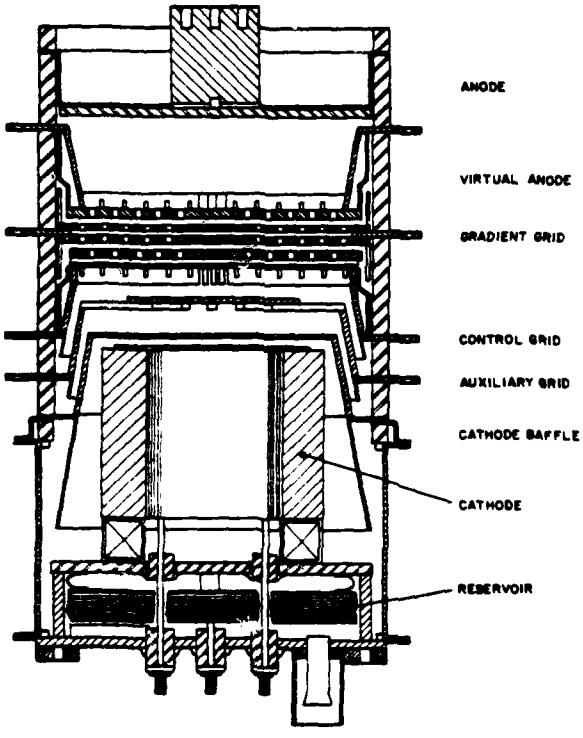


Figure 1. External view of MAPS-40 thyratron.

Significant Design Details

In tubes of this size and power level, it is necessary to carefully engineer many details of construction which can be left uncritically over-designed in smaller tubes. In the MAPS-40, many details were significant design problems, requiring that the tube electrodes and components be individually developed and tested separately to assure proper functioning as part of the complete tube.

Anode

Anode dissipation was assumed to be roughly 60% of that of the gradient grid, or about 1200 watts maximum. Its surfaces had to withstand potential arc damage and be suitable for maintaining high voltage holdoff.

In the MAPS-40 tube, inverse voltage holdoff was expected to be poor due to large peak currents and high di/dt required by the operating conditions. The use of a "virtual" anode, employed elsewhere and believed to act as its own inverse clipper, as well as to improve quenching characteristics, was considered as shown in Figure 2, and was tried on preliminary evaluation samples and on one actual early 8-inch diameter tube. Despite much effort, results proved negative or inconclusive, and this approach to the inverse holdoff problem was shelved. The virtual anode concept may offer some advantages, but its use was not pursued further in this program. The final tube design employs a conventional anode as shown in Figure 3. In this structure, a 3/16 in. thick molybdenum disk is supported by a tapered cup made from Driver Harris No. 146 alloy. A stepped shield of molybdenum surrounds the anode to prevent damage to the cup caused by discharges going up the side wall.

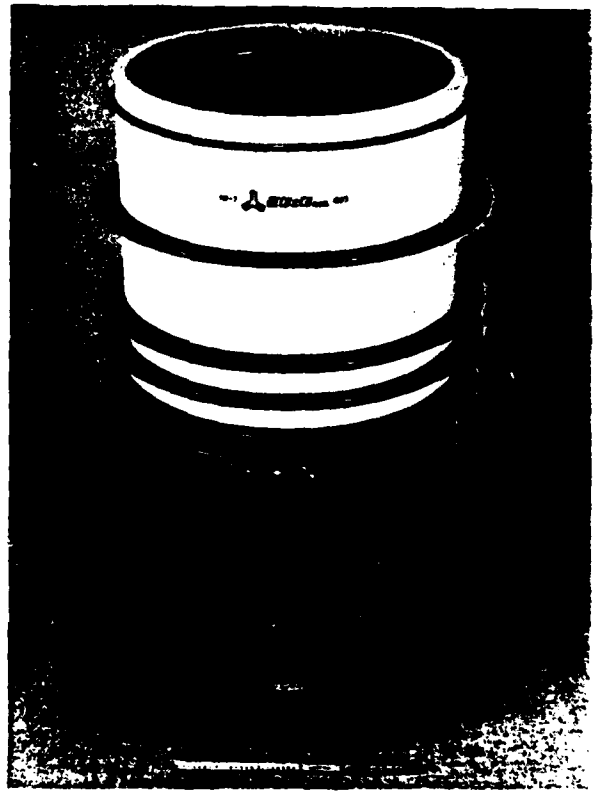


Figure 2. Trial version of MAPS-40 with virtual anode.

Gradient Grid

Of the alternative cavity and box-type grid designs depicted schematically in Figure 4, the box type was chosen because of its compact structure. Cavity-type grids imply longer, heavier structures and tend to exhibit poor recovery time.

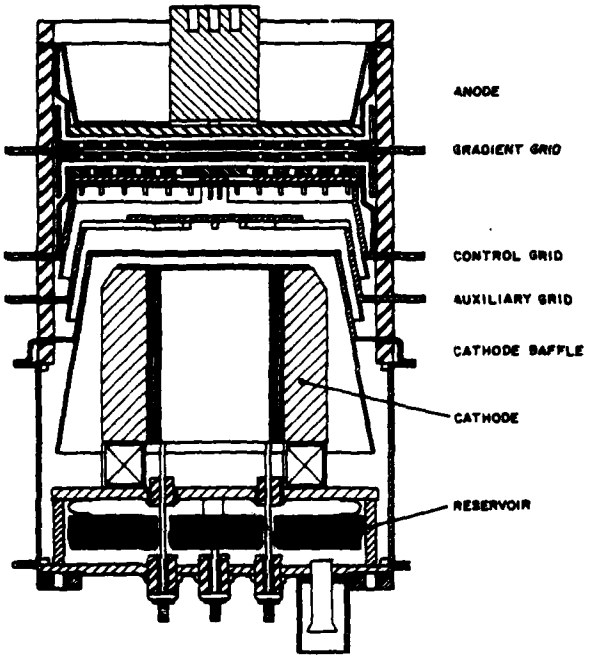


Figure 3. Cross section view of MAPS-40 with conventional anode.

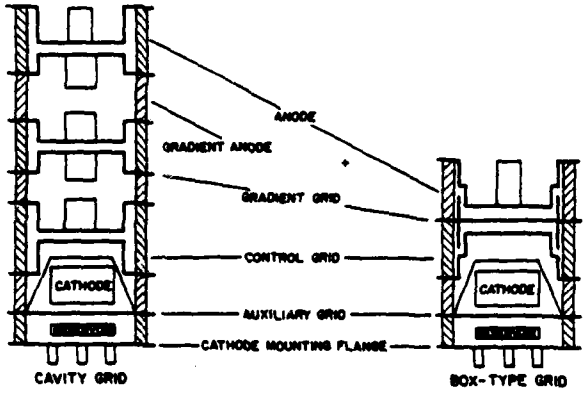


Figure 4. Comparison of cavity- and box-type grids.

Tight grid baffling was used to promote good forward holdoff. Molybdenum wall shielding was used to improve inverse holdoff capability and to increase quenching limits. For additional holdoff capability, the use of deuterium as planned in place of hydrogen as a fill gas. Gradient to control grid aperture offset was 0.110 in. Gradient grid to anode spacing was 0.125 in. Total grid aperture area was about 7.5 square inches, large enough to avoid quenching at the typical limit of 10 to 11 kiloamperes per square inch, a value confirmed experimentally early in this program. The aperture slots themselves were 0.155 in. wide, arranged as a concentric circular pattern of arc segments, a configuration found to give less heat buildup at the grid slot edges than a radial-slot layout with the same total aperture.

The mass and thermal conductivity of the grid were chosen so that the worst-case calculated grid dissipation (approximately 2000 watts) could be sustained for 30 seconds without causing more than a 250°C rise in average temperature. Overall grid thickness was 3/8 in., posing a formidable problem in accommodating differential thermal expansions. Strain-relief cuts and the use of deformable copper protect the ceramic-metal seal from failure due to these expansions.

Control Grid

Control grid dissipation was assumed to be higher than that of the gradient grid, to a maximum of about 3000 watts, due to power lost in the vicinity of the control grid baffle from the 30- to 50-volt Langmuir double-sheath drop to be expected where the discharge constricts. Copper bars were attached to the underside of the grid to increase its mass and to assist the radial heat flow, with the object, again, of restricting the operating temperature rise to 250°C. Slots were cut in the copper bars to provide strain relief. The conical control grid support was also made of copper.

The aperture pattern used for the control grid was identical to that employed in the gradient grid. Control-grid to grid-baffle, and control-grid to gradient-grid aperture offset was 0.110 in. Control-grid to gradient-grid spacing was 0.140 in.

Auxiliary Grid

The tight baffling of the gradient and control grid sections, used to promote forward holdoff and retard migration of emissive material from the cathode, was expected to have an adverse effect on triggering characteristics. Accordingly, it was decided to use an auxiliary grid, which could be supplied with "keep-alive" bias to shorten time of anode delay from hundreds to tens of nanoseconds, to stabilize delay-time drift, and to suppress jitter. The presence of the auxiliary grid would also aid recovery, help suppress cathode material migration, and most significantly, lower the heat load of the control grid by the interception and reflection of cathode power.

The auxiliary grid is a molybdenum plate connected by heavy copper heat-conducting bars to a copper support cone. A skirt keeps evaporated material off the ceramic insulator ring. The auxiliary grid is spaced from the control grid by about 5/8 in.

Cathode Baffle

The cathode baffle is basically a heat shield which intercepts power and evaporated material from the cathode. It is heavily constructed at the top to resist damage. Currently a single-layer structure, its dimensions are chosen to obtain a nominal cathode heater power requirement of 800-1000 watts. Its upper surface is spaced 1 in. away from the auxiliary grid, and about 1/4 in. away from the cathode vanes.

Cathode

The 5000 cm^2 cathode used in the earlier MAPS-70 program, suitably braced and provided with extra current feeds as shown in Figure 5, was used for the early tubes in the MAPS-40 program. While this cathode was capable of supplying the necessary peak current, completion of an entirely new design (Figure 6) was necessary. Its design objectives were:

1. Improved utilization.
2. Improved storage and distribution of the operating dissipations.
3. Better thermal efficiency.
4. Prevention of thermal runaway through careful design of welds and current feeds.
5. Mechanical ruggedness.
6. Independence of the cathode from all mechanical and electrical connections to the heater.

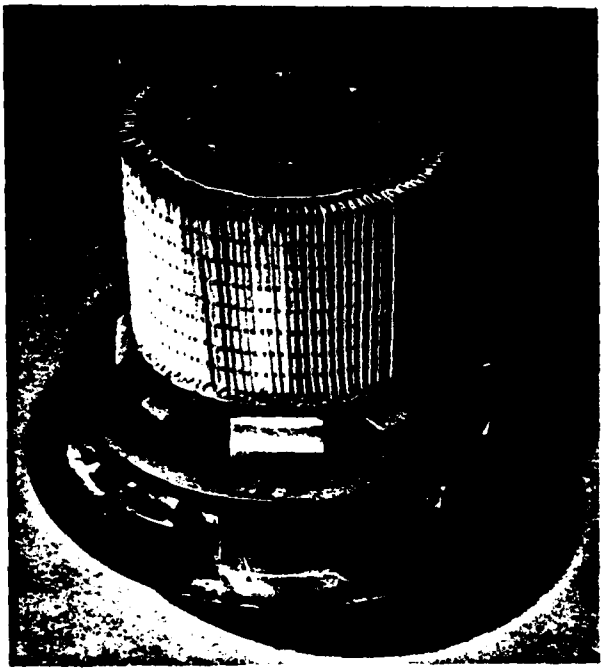


Figure 5. Early MAPS-40 cathode structure.

The thermal mass of the cathode, together with its radiative and conductive properties, allows it to absorb the high operating dissipations encountered during "on" cycles and to disperse them to the surrounding structures and tube exterior during "off" cycles. Vanes covering the upper face and the sloped contour are intended to improve cathode utilization. The vanes are held and spaced by slots in both the support structure and the circumferential band, made of Hastelloy B. Figure 7 shows the nickel vanes fitted to the Hastelloy support structure. No baseplate or cylinder is used between the vanes and the central heater: heat transfer is by direct radiation and gas conduction from the heater to the emitting surfaces of the vanes, an arrangement which allows both efficient use of a cool-running heater, and the prompt redistribution of possible localized heat buildups due to operating dissipations. Individual welding of each vane, illustrated in Figure 8, to the annular current-feed ring assures uniform electrical current distribution, while the stiff cylindrical understructure provides support and restricts conducted heat losses to a tolerable level.

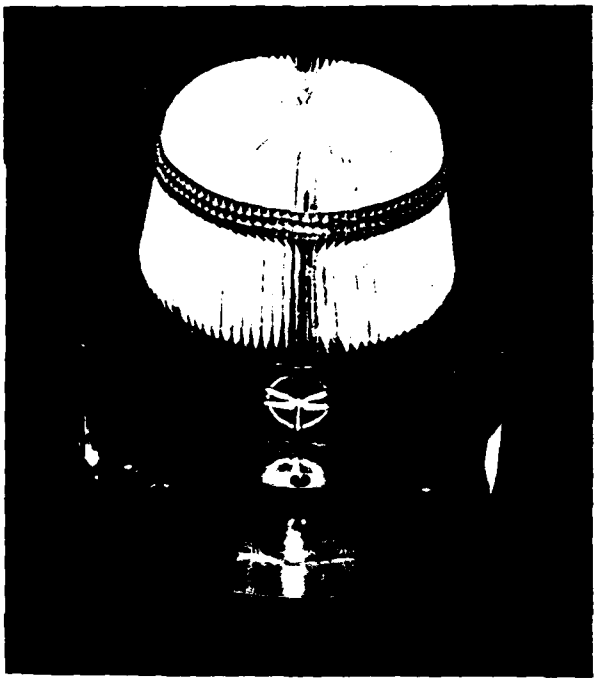


Figure 6. Cathode design developed for MAPS-40.

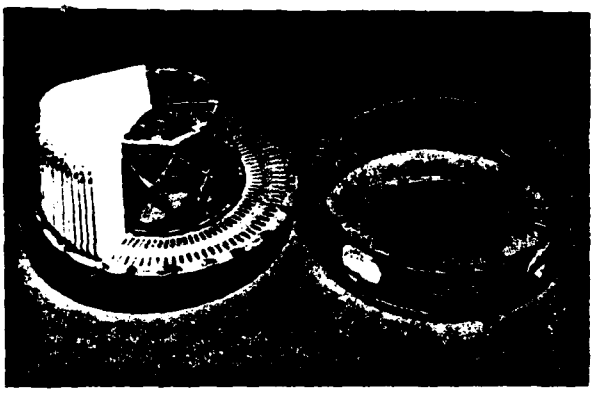


Figure 7. MAPS-40 cathode support structures.

As a bell-jar test, a one-eighth pie-wedge sector of the cathode was isolated electrically and heated to the estimated maximum operating temperature in vacuum by means of the cathode heater. The output of a 200-ampere arc-welder was then connected across it through a current distributing harness. An examination was made for hot-spots or signs of thermal

runaway, a test equivalent to 1600 amperes rms-equivalent through the complete cathode. No signs of distress were observed.

As an environmental test, the entire cathode structure, thoroughly annealed by prolonged test runs at operating temperature, was bolted to a test bed and subjected to 10-g vibration at 50-2000 Hz, and to 100-g shocks in the axial and orthogonal planes. No major resonances were observed and no deformation took place, a distinct advance over the earlier MAPS cathode structures.

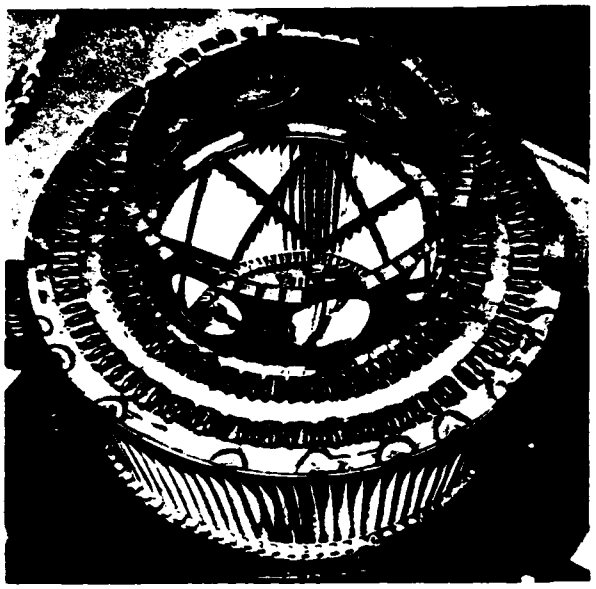


Figure 8. Cathode vanes individually welded to current feed ring.

Heater

Previous experience indicated that it was best to run the heater at a relatively low temperature, and to separate it mechanically and electrically from the cathode structure. The area available for heat transfer inside the cathode vane structure is small; therefore, severe demands are made on the design of the heater.

The heater shown in Figure 9 is a cylinder of vertically pleated molybdenum mesh, assembled from four quadrants, each with its own head and tail current feeds, which are connected down at the bottom of the structure, well away from the hot-zone. Toothed "gears" made of ceramic-covered molybdenum support the pleats both internally and externally, preserving their spacing and bracing them against lateral and torsional vibration.

This heater has withstood 75 cycles at three times the design power, followed by pounding on the bracing structure with a hammer and further cycling, without shorting or fracture. Its net emissivity to the surrounding vane structure at operating temperature is 0.78.

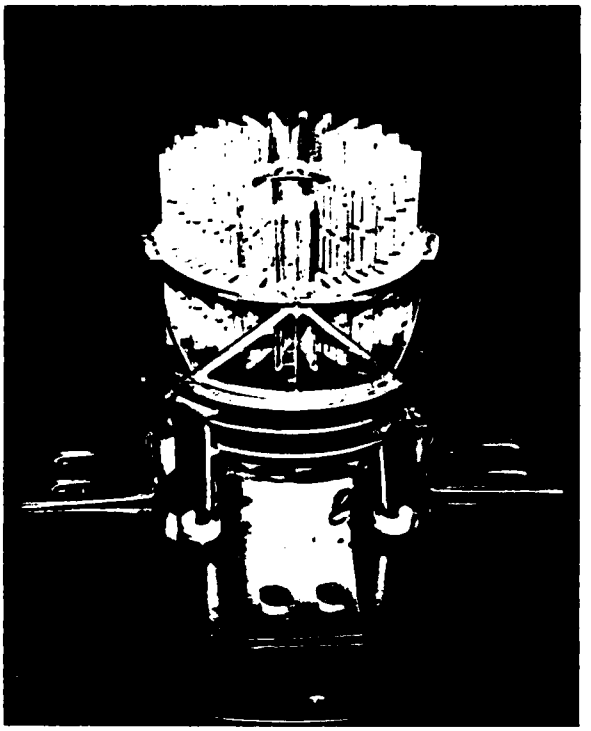


Figure 9. MAPS-40 cathode heater.

Reservoir

Transient cleanup was suspected to be a problem during burst-mode operation, with very little time available to readjust the pressure. A fast-acting reservoir able to respond quickly to pressure and heater-power changes was required. The reservoir used in the MAPS-70 had these desirable characteristics, but it was fragile and unstable. After much effort, the reservoir was redesigned.

The MAPS-40 reservoir shown in Figure 10 consists of a flat serpentine heater flanked by two sets of titanium strips stacked edgewise. The resulting sandwich is packaged in a lightweight, open frame, where it loses heat primarily by radiation and gas conduction. Run hot, at a relatively low specific loading, the reservoir responds quickly to changed conditions at a rate determined only by power, mass, and specific heat considerations. A complete reservoir consists of four of the units shown, a total mass of 400 grams of titanium loaded to approximately 500 liter-torr total of deuterium at 0.3 torr equilibrium fill pressure.

The reservoir is isolated from the cathode heater and tube operating dissipations by suspending it beneath a heavy sole-plate, a "false-bottom" connected to the tube base by massive copper bus bars. The sole plate also serves as the current feed and mechanical support for the cathode, which is bolted to its upper surface. All heat reaching the sole plate is promptly conducted out through the base of the tube.

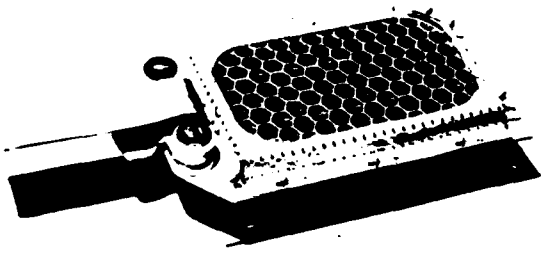


Figure 10. MAPS-40 reservoir.

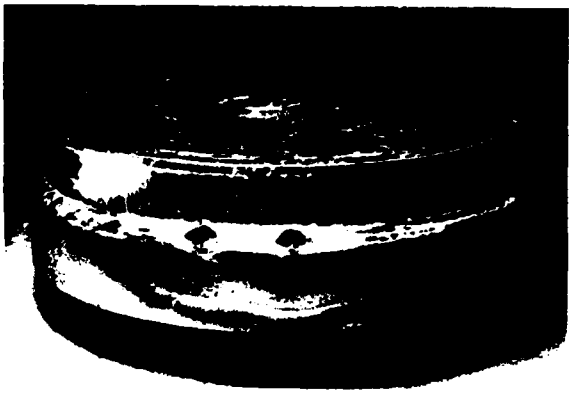


Figure 11. Damage to anode shield.

Aging and Testing

After assembly and processing, the tubes were given a preliminary aging and test at EG&G in Salem, Mass. They were then shipped to the high power test laboratory of the US Army Electronics Command, in Fort Monmouth, New Jersey, for further aging and final testing.

In the first phase of the program, of five tubes shipped, four were selected for full power test and evaluation. The procedure consisted of bringing the tubes up to the 40 kV, 40 ka operating level, and then increasing the repetition rate in stages to give successively higher average power levels. Sufficient time was allowed at each stage for the tube to stabilize and adapt itself to the increased demands made upon it. The aging time per tube varied between four and ten hours, while the number of kick-outs ranged from a low count of two to about thirty.

Aging and running-in proved to be a critical process, due to the prevalent possibilities for sudden catastrophic failure in both tube and test circuitry at the power levels involved. Here, phenomena such as anode overheating or glow-spots could rapidly assume serious proportions when the energy responsible for them became concentrated in one spot. Protecting the test instrumentation from conducted spikes and stray fields was a critical problem. As experience was gained in getting the tubes to run, the final tubes in the series became relatively easy to bring up to full power.

The following necessary precautions were taken:

1. Careful monitoring of the tube anode, envelope, and seal temperatures, and use of adequate and symmetrical forced air cooling.

2. Visual observation of the anode and the entire 360° of envelope circumference to catch sudden overheating, glow-spots, and other troubles before they became severe.

3. Attention to tube pressure to avoid catastrophic tube failure from hydrogen starvation. Figure 11 shows a hole burned through the anode shield by excessive dissipation due to low deuterium pressure.

4. The use of a distributed-current feed, as shown in Figure 12A, was essential to keep magnetic fields from pushing the internal tube discharge into the walls and structures,

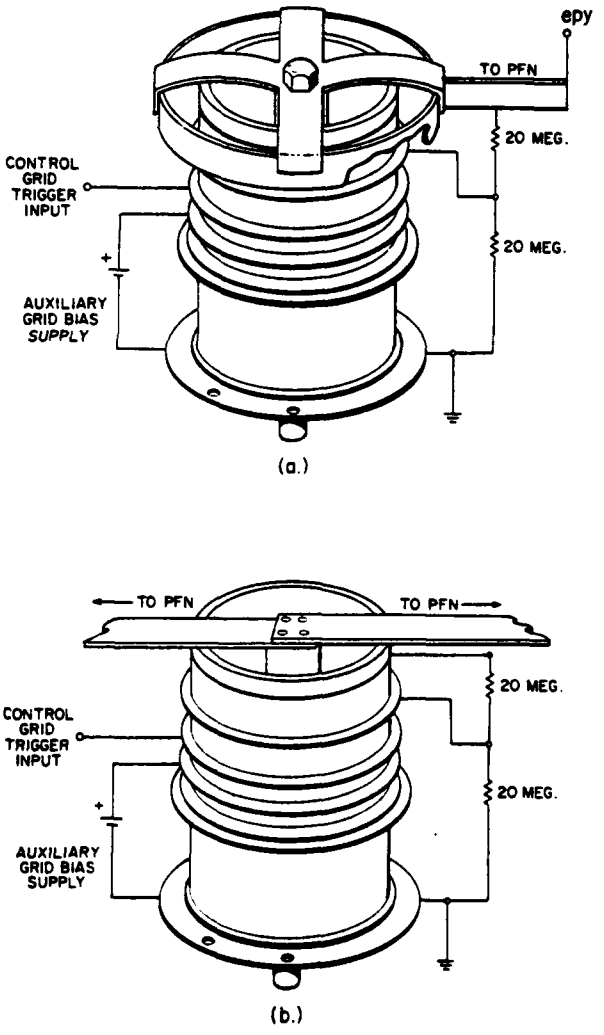


Figure 12. Distributed and symmetrical current feed.

where it could degrade holdoff and cause considerable damage. The problem is now avoided entirely by use of a symmetrical feed from the pulse forming network (PFN) as shown in Figure 12B.

5. Use of inverse clippers. As expected, the tube did not display any inverse holdoff capability. Figure 13 shows inverse breakdown occurring at only 2 kV.

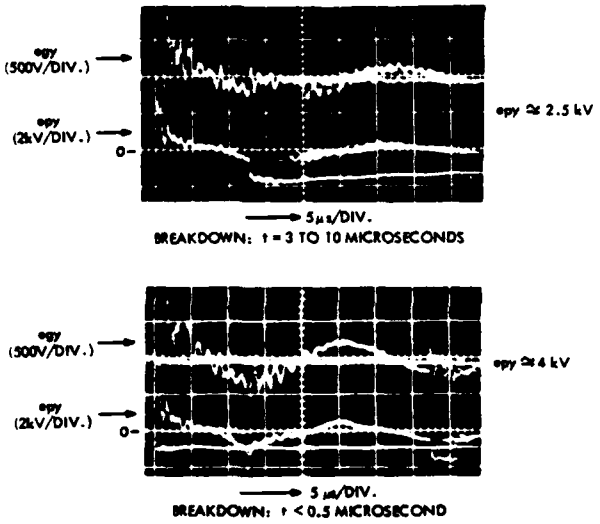


Figure 13. MAPS-40 inverse breakdown voltage.

6. Allow generous warmup time to help overcome an initial tendency to kick-out when first starting up.

7. Monitor the temperature and resistance of the copper solution used as a load to maintain the proper ratio of load to PFN impedance during tube operation.

8. Use of thyrites in the cathode heater and control grid leads to prevent spikes from getting into the filament and trigger supplies.

9. Presence of keep-alive current in the auxiliary grid circuit was essential in reducing tad and jitter.

Operation at the full megawatt power level produces brilliant red bands of hydrogen Balmer-alpha light which encircles the tube envelope, accompanied by a heavy hammering at the repetition rate. It is obvious that much is being demanded of both tube and test circuit at this power level.

Test Results

Specification Objective Tests

Representative test results for the first four tubes evaluated at the full megawatt average power condition at Fort Monmouth are indicated in Table 3, which compares the original specified objectives with observed performance.

Once aged in and running, both the original four tubes tested and the subsequent seven tubes built under this program operated within specified limits. Trigger voltage was typically 2000 volts, well within

Table 3. Representative performance of developmental MAPS-40 thyratrons.

Parameter (Units)	Specification Objectives		Representative Performance			
	Rating	Operation (1)	Full Power Test	Special Tests (1)	(2)	(3)
epy (kV)	40	44	44	40	36	50
ib (kA)	40	44	44	75	36	50
egy (kV)	1.5 to 4.0	–	2	–	–	–
tp (μs)	–	10	10	–	–	–
prr (Hz)	500	125	125	–	77	50
Ib (A dc)	50	50	50	–	20	24
Ip (kA ac)	1.48	1.48	1.48	–	0.85	1.1
Pb (10^9 va/s)	400	242	242	–	–	–
dik/dt (kA/μs)	20	20	20/40	75	36	50
td (μs)	–	0.2	<0.2	–	–	–
Δtad (μs)	–	0.1	<0.1	–	–	–
tj (μs)	0.02	–	<0.02	–	–	–
Ef (Vac)	15±1.5	–	–	–	–	–
Eres (Vac)	15±1.5	–	–	–	–	–
If (A ac)	70	–	66	–	–	–
Ires (A ac)	40	–	40	–	–	–
tk (sec)	900	–	1200	–	–	–
Life (pulses)	–	5×10^6	*	Highest Peak Current	Continuous Operation	Highest Voltage

*0.3×10^6 pulses achieved to date without discernible change in performance.

the specified range. The anode delay time of 0.2 microsecond was met with the aid of an auxiliary keep-alive current of 50 ma. (Measurements indicate a tad of much less than 0.2 microsecond.)

Due to temporary test equipment limitations, none of the existing tubes has been tested to the full thirty seconds of "on" time in burst mode at 40 kV. They have been repeatedly run, however, at this voltage for "on" cycles of 10 and 15 seconds, and in other tests, they have been subjected to a full 30 seconds at 30 kV and 0.56 megawatt, and have also been run for 10 seconds at 45 kV and 1.27 megawatt. The capability shown so far augurs well for success in the full 30-second burst at 40 kV and 1.0 megawatt.

Representative values for temperature rise during burst-mode operation are shown in Table 4. The relatively modest temperatures reached and the small spread between them shows that the thermal loads are well balanced and not excessive.

Table 4. Temperature rise at megawatt average power MAPS-40 Tube No. 10 — 10 second "On" cycle.

Temperature Probe Location	Temperature, °C Start	Finish
Cathode Enclosure	120	210
Cathode — Auxiliary Grid	135	255
Auxiliary Grid — Control Grid	100	220
Control Grid — Gradient Grid	65	150
Anode (avg.)	35	180
Final Temperature Spread	—	15

Other Tests

Additional information was obtained in the course of exploratory tests of the nominal design limits.

In a peak current test, the thyratron was operated into a 0.25-ohm load at 40 kV, switching a peak current of 75 ka. The 70- to 80-ka ultimate design limit due to quenching was confirmed.

In an average current test, the thyratron was subjected to continuous operation for 30 minutes at 40 kV and a pulse repetition rate of 50 Hz, giving an average current of 20A. The thyratron operated well throughout this interval, but additional cooling was required. While incapable of confirming the expected 30A average current capability for continuous operation, this 20-ampere, 30-minute run established a benchmark for high average current operation.

In a high voltage test, one tube was run at 50 kV at the 0.5 megawatt power level without difficulty, showing that the single gradient grid will allow higher voltages to be reached at these power levels.

Warm-up behavior was explored in a separate test wherein a tube was operated in a standard 2.5-microsecond, 7-ohm, 400-Hz thyratron test set. A standard 2400V, 50-ohm driver was used, with the auxiliary grid tied to ground through a 30K ohm resistor. The following results were obtained:

	Ef (Vac)	If (Aac)	Eres (Vac)	Ires (Aac)	epy (kV)	Elapsed Time (min.)	tad (μsec)
Run 1	15	63	12	37	15	15 (T_k)	3.0
	15	63	13	39	40	25	1.3
	15	63	14	43	40	50	0.14
Run 2	16	68	14	43	25	7 (T_k)	0.8
	16	68	14	43	40	8.5	0.72

Minimum Ebb was 4kV.

Conclusions

Of the eight thyratrons constructed in the first phase of the MAPS-40 project, four were tested successfully against the specification objectives at the megawatt power level. Seven additional tubes have been constructed and tested, all of which met the specification objectives at this power level. While further exploration of the design limits needs to be done, including a full 30-second run at 40 kV, it is already apparent that the MAPS-40 can be rated for burst-mode applications at the megawatt average power level, and for high power continuous repetition-rate operation as well. The tube is producible, and the thermal and mechanical features are capable of extension to still higher power levels. The MAPS-40 gives the pulse power circuit designer the option of employing the well-known advantages of the hydrogen thyratron for switching at megawatt power levels.

Acknowledgment

The work presented in this paper was supported, in part, by the following government agencies under Contract No. DAAB07-76-C-1352:

ERADCOM, Ft. Monmouth, New Jersey
AFAPL, Dayton, Ohio
NSWC, Dahlgren, Virginia
MIRADCOM, Redstone Arsenal, Alabama.

References

1. J.E. Creedon, et al, Adiabatic Mode Operation of Thyratrons for Megawatt Average Power Applications, IEE Conference Record, Twelfth Modulator Symposium, February 1976.

2. J.E. Creedon and S. Schneider, Megawatt Average Power Adiabatic Mode Thyratrons; Proceedings, Int'l Pulsed Power Conference, Texas Tech University, Lubbock, November 1976.

3. J.J. Hamilton and D.V. Turnquist, Forty Kilovolt Megawatt Average Power Thyratron, Final Report No. ECOM-76-1352-F, October 1977.

DOUBLE-ENDED THYRATRONS IN HIGH POWER BURST MODE PULSE MODULATOR APPLICATIONS

R.B. Molyneux-Berry

Marconi Research Laboratories, Chelmsford, U.K.

Summary

The use of four-gap double-ended thyratrons in a 30 to 100 μS pulse modulator is described. The PFN-type modulator operates at 105 kV peak, charged from the 11 kV public supply, and powers an ill-matched and potentially unreliable load directly at 30 to 70 kV without a pulse transformer. The maximum repetition rate is 200 pulses per second. The completed modulator has been delivered to the customer and successfully re-commissioned.

Satisfactory operation is reported with 200 MW 6 kJ pulses in bursts of average power up to 400 kW; this is well in excess of the published ratings of the tubes employed. The methods used to obtain this performance are discussed and the main details are given of pulse discharge, energy dump and switched charge circuits appropriate to the thyratrons used.

The possibility of uprating the modulator is mentioned, and certain recent developments in large thyratrons are discussed. These include larger diameters, increased numbers of gaps and a new pentode-type electrode system which should give improved performance with simpler deck circuitry. For extended bursts at long pulse lengths the realistic maximum capability of single tubes in current production seems to be about 1 GW peak at 2 MW average power. *Tubes at present being developed hold the promise of* at least doubling these powers.

Introduction

An earlier paper described work to determine the performance of double-ended thyratrons in a range of pulse modulator circuits.[1] No attempt was made to explore the very high power performance of which the tubes are capable. Further work has now been completed, using multi-gap double-ended thyratrons in PFN modulator circuits up to 400 kW burst average power level, in excess of published ratings. From the results, the highest burst ratings practicable with the present generation of tubes have been deduced, and the performance of a new series of double-ended tubes, at present still being developed, estimated.

Modulator Development

The work reported was undertaken in connection with the development and manufacture of a burst-rated power system which included a pulse modulator. The nature and purpose of this equipment are described in a companion paper[2].

In addition to prototype work, and the series of measurements and tests essential to the modulator development programme, a special programme of tube testing was carried out to determine the optimum operating conditions for double-ended thyratrons in burst mode and the maximum performance that could reliably be achieved without tube damage or reduction of useful life. The results of these tests have been confirmed by the reliable operation of the equipment for the past year with the three tubes originally fitted.

Modulator Load

The modulator is designed to power a load whose impedance is complex and varies widely, being only partially under operator control. The real part of the load impedance, under specified burst running conditions, is predictable only to within a factor of 2:1 error either way, and the actual load impedance tends to vary progressively during each pulse, and throughout a burst. The modulator is therefore required to deliver a specified minimum of 330 kW average burst power into any load impedance whose real part lies between 7.5 and 90 ohms; this is sub-divided into three overlapping ranges by adjustment of modulator tappings to match the coarse degree of operator control of load impedance. The 330 kW burst must be sustained for at least 0.3 seconds (100 kJ delivered) with the capability of extending this to 400 kW for 1 second (0.4 MJ) when favourable load conditions are maintained.

The load is liable to erratic malfunctions resulting in its becoming open-circuit or short-circuit for part or all of a pulse duration. The two extreme conditions may both occur within a single pulse. The modulator is required to maintain uninterrupted burst operation in spite of sporadic malfunctions of this sort, and to absorb all excess energy within itself without overvolting the load or *affecting the accuracy of succeeding pulses. The* modulator is in fact capable of safely absorbing the full burst energy, though in practice the modulator control system is normally programmed to discontinue a burst in the event of severe load malfunction, in order to minimise risk of damage to the load.

Basic Modulator Circuit

Each of the switches shown in Figure 1 represents a four-gap double-ended thyratron. This circuit arrangement has been chosen for reasons given in previous paper and further discussed elsewhere.[1,2] The composite pulse forming network (PFN) shown consists of three identical units each of 42 ohms impedance (Zo), 30 μS pulse width, storing 2 kJ of energy

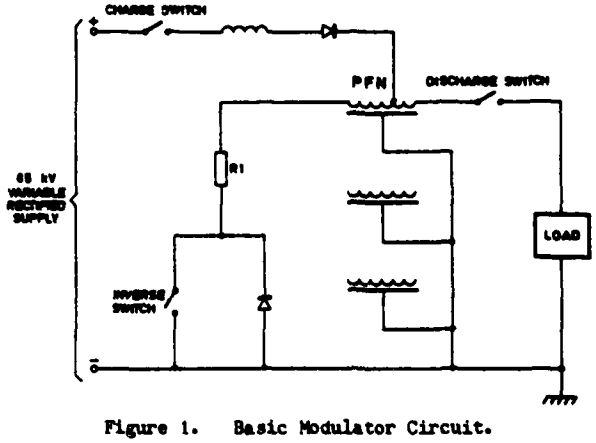


Figure 1. Basic Modulator Circuit.

CH1371-4/78/0000-0144$00.75 © 1978 IEEE

at 105 kV peak charge voltage. These may be combined in five series or parallel arrangements to ensure that at least 330 kW can be delivered to the load over the full range of load impedance. A choice of pulse lengths (30, 60 or 90 μS) is available; these may be varied by using the inverse switch as a pulse shortener. The principal use of this switch is to enable the matched inverse load, R_I, to absorb positive polarity PFN mismatch energy after each modulator pulse. This enables the modulator to accept load impedances greater than the Zo of the composite PFN.

Maximum Ratings

Pulse of 6 kJ can be delivered to the load. At 30 μS pulse width this represents 200 MW at match and requires about 4 kA peak pulse current in the discharge circuit. Adverse match conditions can increase this to 5 kA, while the peak short-circuit current is 7.5 kA. These currents must be switched repetitively by the discharge tube. The average tube current under these conditions can reach 8A depending on pulse repetition frequency (PRF). The maximum rated PRF depends on pulse energy and is 67 Hz with 6 kJ pulses, rising to 200 Hz at 2 kJ. The peak pulse voltage applied to the load normally lies between 36 kV and 72 kV, according to match.

Discharge Switch Thyratron

The discharge thyratron has the most arduous duty of the three switch tubes (Figure 1) since, under negative mismatch conditions ($R_{LOAD} < Zo$), it carries the sum of the average currents in the other two tubes. The maximum peak and average currents under these conditions have been quoted above. In addition, the discharge tube must be completely reliable in withstanding 105 kV peak working voltage in order to protect the load from being directly fed from the rectified supply. Fault current under these conditions can reach 100A for 40 mS (4 coulombs). The English Electric Valve Company (EEV) recommended the standard 3-inch 4-gap double-ended thyratron type CX1199B for this duty although it meant burst operation of the tube well beyond its continuous rating of 3A average current. This rating is principally due to thermal limitations. It was considered that if suitable conditions were established in the tube prior to each burst, it would behave satisfactorily in an adiabatic mode, and that the large reserve of hydrogen available within the grid/cathode/reservoir structure at each end of the tube would flow through the grid apertures to prevent quenching (metal arc), voltage breakdown, or other undesirable effects due to ion transportation. Moreover, the reverse conduction capability of the double-ended type of tube removes the risk of tube damage due to high-voltage arc-back.

Preliminary Tube Testing

A test programme was carried out jointly by Marconi Research Laboratories, by the tube manufacturers, and by R.S.R.E., Great Malvern, in order to determine the optimum running conditions for double-ended tubes in burst duty. It was determined that:

(a) The tube cathode heater voltage could, with advantage, be increased by about 8% to allow for the lack of self-heating by the anode current between bursts.

(b) Three-inch double-ended tubes would carry the full current required by the modulator specification at normal gas pressure without quenching though with only a small margin under worst-case conditions.

(c) Three-inch tubes had a good current margin at increased gas pressure but with slightly reduced voltage hold-off capability.

(d) The larger 4½-inch tubes were completely satisfactory at all duties up to the maximum capability of the test modulator.

(e) Voltage hold-off degradation which occurred when a quench was deliberately forced could be corrected, in situ, by simple reconditioning techniques without overall ill effect; a reliable electronic means to detect quenching was developed.

(f) Very high reliability of voltage hold-off could be ensured by operating the tubes in a 'screen grid' mode, i.e. with g_2 connected to cathode at each end. This arrangement also minimised 'dark current', simplifying the static sharing of applied voltage between gaps, and prevented self-triggering on rapidly-applied voltage.

(g) Trigger sensitivity in the 'screen-grid' mode was quite adequate, using g_1 only: a few amps ensured rapid turn-on while a few hundreds of milliamps of steady positive bias served to hold each of the cathodes ready to conduct even in the temporary absence of anode current.

(h) Tubes run in the 'screen-grid' mode would hold off maximum voltage with zero bias on both grids, and were best triggered sharply on both g_1's simultaneously to initiate conduction. (Low-level forward bias should be continued at both ends until major currents in the anode circuit have ceased; the tube will then turn off and recover quickly and reliably as soon as the forward g_1 bias is discontinued).[3]

(j) A simple and convenient arrangement of small passive components arranged on a 'bandolier' around each tube gap would ensure static and pulse sharing of the applied voltage, and also serve to force reliable sequential breakdown of all gaps when the tube is triggered, even when the total applied voltage is as low as 3 kV.

(k) Four-gap tubes would operate satisfactorily in air up to 60 kV. A higher voltages there was a tendency to external flash-over when the tube was triggered due to the sequential nature of gap breakdown. Operation in oil was entirely satisfactorily up to the maximum voltage tested (110 kV).

(l) No external X-radiation was detectable, either statically or when triggered, up to 60 kV in air or at full voltage in an oil-filled steel tank.

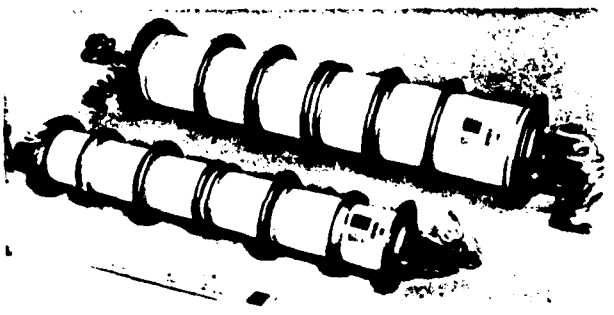


Figure 2. Four-Gap Double-Ended Thyratrons.

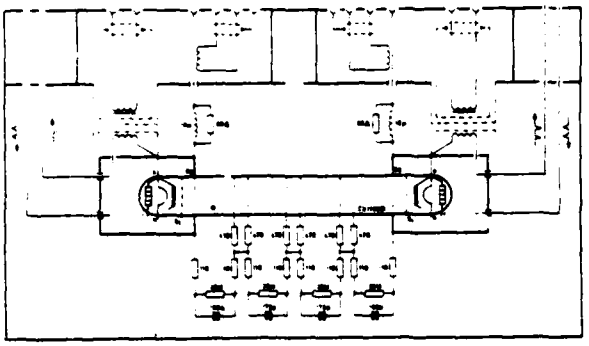


Figure 3. Circuit of Thyratron Switch in Tank.

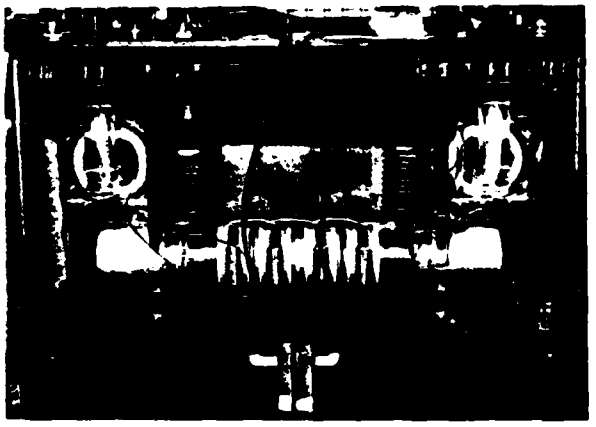


Figure 4. Mounted Thyratron Raised from Tank.

Tube and Tank Assembly

Figure 3 shows the circuit of the tube in its tank, and Figure 4 shows a tube raised from its tank for inspection. The tank was designed so that, if necessary, the CX1199B 3-inch thyratron could be directly replaced by the larger CX1193B 4½-inch type. Tube heaters, gas reservoirs and all trigger and control circuitry within the can-shaped decks are powered via the polymer-insulated filament transformers. These transformers, which operate at 2.4 kHz, are rated at 400 watts each to allow for the use of a 4½-inch thyratron; typical power consumption is only half this with a 3-inch tube. The tank is naturally cooled by free oil circulation guided by a funnel system.

The tube layout within the tank, like the tube itself, is completely symmetrical and the whole system may be used in reverse polarity if required. To limit the initial rate of rise of current the anode inductor is divided symmetrically between the two cathodes. The resonant frequency of the tube within its tank is damped by resistances within the anode inductors, assisted by the CR sharing network on the 'bandoliers'. High-voltage coaxial sockets and cables are used for the main connections, and all other connections (filament supplies and current transformers) are double screened. Triggering and monitoring are carried out via optical fibre links. These precautions have eliminated any tendency for tubes to trigger due to external interference; the shielding of the tubes is sufficient to enable the widespread use of sensitive analogue and digital circuitry for modulator monitoring and control. This is assisted by the use of H.V. coaxial cable throughout the modulator to define and enclose high-current paths.

In order to maintain the insulating properties of the oil filling under direct voltage stress, the thyratron tanks are hot-vacuum processed and sealed under a positive pressure of dry nitrogen. The thyratrons can satisfactorily withstand repeated processing cycles.

The Inverse Circuit

The inverse circuit (Figure 1) consists of a high energy carbon-ceramic block resistor bank which can be accurately matched to each of the five possible PFN arrangements, with an inverse semiconductor diode stack and a double-ended thyratron switch. The inverse circuit is located at the end of the PFN remote from the charge and discharge circuits. The inverse diode is redundant since its function may be performed by the thyratron across it. It was provided for the development and commissioning phases of the modulator, before the inverse thyratron was available in a fully manufactured and tested state - the semi-conductor diode stack was subsequently retained as it gives useful back-up protection to the PFN under unexpected short-circuit conditions, being independent of external triggering and the state of readiness of the thyratron.

Because the forward characteristics of the diode and the thyratron differ slightly, and to assist the thyratron to conduct in parallel with the diode, the inverse resistor is subdivided and tapped. This ensures the best possible match between the inverse circuit and the PFN, and therefore the complete absorption of unwanted energy of either polarity within a single PFN pulse duration. A small CR network is provided to damp fast transients associated with thyratron turn-on and diode snap-off.

In normal use the inverse thyratron is always triggered just before the mid-point of the PFN discharge pulse so that it conducts first in the positive direction and then, almost immediately, reverses to conduct in parallel with the diode if the main load is undermatched ($R_L < Z_o$). This tailbiting mode gives a useful improvement in pulse fall time. If the main load is overmatched ($R_L > Z_o$) the thyratron continues to conduct in the positive sense until the remaining PFN energy has been absorbed.

The inverse thyratron may be triggered earlier (up to half a pulse before the discharge switch) to obtain any desired degree of pulse shortening. The inverse tube and load are rated to absorb the full burst energy.

Under severe fault conditions the inverse tube may be triggered to discharge the PFN and divert current from the rectified supply. The protective action is not instantaneous because of the delay of the intervening PFN. This allows sufficient time for the modulator control system to detect the fault and trigger the inverse tube before the fault condition robs the tube of initial hold-off voltage essential to turn-on. The discharge wavefront travelling down the PFN from the inverse switch will usually provide sufficient current reversal at the fault to permit the arc to extinguish, leaving the inverse circuit to absorb up to 100A of rectified supply current until the primary circuit-breakers have acted.

A further function of the inverse switch tube is to remove unwanted initial charge from the PFN

immediately before the start of a modulator power burst. Due to conduction through the voltage sharing network across the charge switch tube the PFN can slowly charge to a significant voltage when the rectified supply remains energised between bursts. The discharging action of the inverse tube ensures that this does not result in the amplitude of the initial output pulse being incorrect.

Because the inverse tube must withstand the full system voltage and, when pulse shortening or with an overmatched load, carry peak currents approaching those in the discharge tube, the same CX1199B type has been used in both positions. For convenience both switches are mounted with identical circuitry into identical tanks and are fully interchangeable.

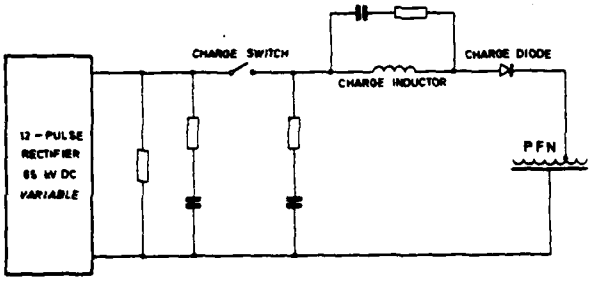


Figure 5. Basic PFN Charging Circuit.

Charging Circuit

When using a double-ended thyratron as a charge switch, the tube will conduct backwards immediately after peak charge, discharging the PFN again unless it can be quickly turned off when the current reaches zero. This is difficult at high voltage, so a separate semiconductor charging diode is used in the normal position following the resonant charging inductor (Figure 5). The charging thyratron is permitted to conduct backwards in order to discharge stray energy associated with the inductor. This overcomes the arc-back troubles commonly associated with thyratron charge switches, and results in a reliable circuit.

Although the lower forward voltage and small peak currents in the charging circuit seem to indicate that a smaller thyratron is adequate, consideration of transient voltages at the rectifier output makes the use of a 4-gap tube desirable, while the relatively high average current (up to 5A) requires the use of at least the 3-inch size; therefore the same CX1199B type, in another identical tank, has been used here too. It has proved most convenient to have all tubes immediately interchangeable.

Although the charge tube is fitted with the standard CR voltage-sharing network, which ensures rapid and reliable breakdown of all gaps when triggered, the rate of rise of current through the external charging circuit can be very low (especially at reduced HT and PRF) so that means must be provided to ensure that the tube reaches and maintains latching current, about 100 to 200 milliamps depending on gas pressure. It is insufficient merely to use long trigger pulses as these cannot maintain conduction in the central gaps once the local CR networks have discharged. It is also important to control and damp out stray circuit oscillations initiated by triggering in case the associated current reversals (which the double-ended tube will pass without harm) upset the latching process.

These requirements have been met by the careful choice and placing of a number of CR networks, the principal ones being shown in Figure 5. The optimum CR necessary to control charge inductor internal oscillations is insufficient to guarantee latching, so an additional CR network from tube 'cathode' to ground makes up the difference and ensures that the mean tube current does not fall below 200 mA under worst-case conditions until charge is complete. Energy loss in the resistors is small under burst conditions. The CR networks also control H.T. circuit oscillations, and define and damp inductor oscillations at the end of charge.

To limit fault currents, and to avoid H.T. droop at the beginning of each power burst, the H.T. rectifier has no significant reservoir capacitor. The half-sines of charging current are delivered by the transformer directly from the 11 kV input. A 12-pulse rectifier is used to reduce H.T. ripple. Additional CR networks (and a surge clipper) have therefore been fitted to the rectifier output to damp oscillations associated with transformer leakage and H.T. cabling. Sufficient bleed is provided to prevent these components charging up to overvoltage when the rectifier is off load between bursts.

Commissioning

The thyratrons and the H.T. circuits of the modulator fully achieved the design aims during the commissioning period. Full power burst operation has been demonstrated into loads ranging from a direct short to an open circuit. No serious troubles or faults were encountered. The tubes have shown no signs of quenching and, although one of the three took longer than the others to condition to achieve stable and reliable voltage hold-off, commissioning to all essentials of the specification was completed without any tube damage. A CX1193B (4½-inch) held in reserve during commissioning was not required - if used, the modulator would probably have reached a full power burst of 10 seconds.

Ultimate Tube Performance

The performance achieved into a reasonably matched load (about 200 MW pulse at 400 kW mean burst) is probably not far short of the realistic capabilities of the present 3-inch tubes, though under optimum conditions they should be capable of perhaps 250 MW, 500 kW. Further increases in power may be expected if pulse and burst lengths were to be significantly reduced, but operation in this region has not been explored in detail. The short-pulse, higher-PRF region seems particularly favourable to the tubes with respect to both maximum current and voltage hold-off, but the relatively poor deionisation time of multi-gap tubes limits their useful PRF to about 2 kHz.

Under crowbar conditions the 4½-inch tubes are rated at four times the peak current of the 3-inch types, due to their substantially enlarged grid apertures. It is therefore to be expected that the CX1193B tubes will handle up to 1 GW peak pulse output power at 2 MW average into the load, and burst lengths comparable with those reported above. Verification of this must await the construction of a sufficiently powerful modulator.

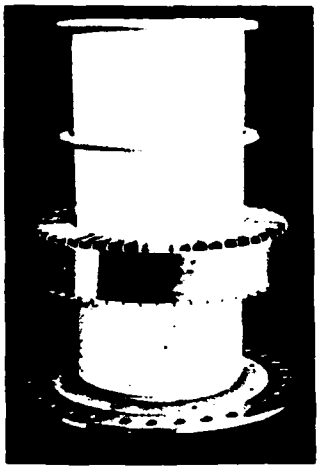


Figure 6. Six-inch Multi-gap Thyratron

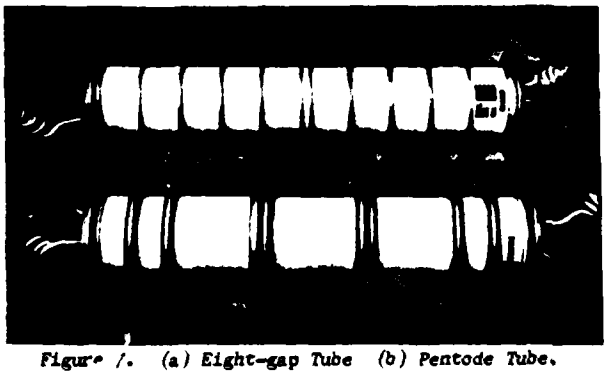


Figure 7. (a) Eight-gap Tube (b) Pentode Tube.

Tubes for Higher Power

Experimental 6-inch thyratrons have been manufactured but not double-ended versions (Figure 6). Further increases in burst power may be achieved by paralleling tubes and there seems no reason why techniques successful with normal thyratrons should not be used.[4] Recently, however, an experimental 3-inch thyratron has been made with 8 gaps giving the option of approximately doubling the power by increasing the voltage (Figure 7 - upper tube). Experience with 4-gap tubes has been most safisfactory and there seems no reason to suppose that eight (or more) gaps would prove unmanageable in practice. A $4\frac{1}{2}$-inch version is not available.

Double-ended Pentode Thyratron

Double-ended multigap thyratrons having an extra grid at each end (Figure 7 - lower tube) are now available. The tube corresponding to the CX1199B is designated the CX1199BC. The $4\frac{1}{2}$-inch version CX1193BC is also available.

The extra grid is created, in effect, by replacing g_1 in the tetrode version by two grids. The tetrode g_2 remains unchanged but is re-numbered g_3 in the pentode. This arrangement permits tetrode bias and triggering techniques on g_1 and g_2 while g_3 is used as the screen grid, connected to cathode. A constant positive bias may be used on g_1 to give a continuous plasma around the cathode, ensuring ion protection and very rapid triggering by g_2 which can carry the usual bias and trigger waveforms. The g_1 bias level may be used to monitor the state of readiness of the tube.

The chief differences in performance are that, with the pentode tubes, g_2 recovery is improved, and protective g_1 to cathode bias can be applied without affecting hold-off voltage. The pentode tube can have a much simpler check circuit as it is not necessary to use time-sharing methods to combine bias, monitoring, triggering and recovery-control circuits on a single grid. If these tubes had been available earlier, they would have been chosen in preference to the tetrode version.

Conclusions

It has been established that multi-gap double-ended thyratrons will perform reliably to maximum ratings in the major switch positions of PFN modulators. With pulse lengths in the region 30-100 μS, they will switch up to three times rated average power for bursts of a few hundreds of milliseconds. No special or unexpected difficulties have been encountered.

The maximum power available with single current-production tubes is probably about 1 GW at 2 MW average burst power for pulse and burst lengths comparable with those reported here. Tubes which might achieve twice these powers are being made. Further increases in pulse power would, at the present time, require multiple switch tubes.

Acknowledgements

This work has been carried out with the support of the Procurement Executive, Ministry of Defence, U.K. *The author wishes to thank the Technical Director,* GEC-Marconi Electronics Ltd., for permission to publish this paper. The helpful collaboration with the sponsors must be acknowledged, also the contribution to the tube test programme made by Mr. N.S. Nicholls of R.S.R.E., and by E.E.V. engineers.

Further acknowledgement is made to the author's colleagues in the High Power Systems Group, Marconi Research Laboratories, who contributed to the overall success of the project.

References

1. R.B. Molyneux-Berry, "Symmetrical Double-ended Thyratrons in Pulse Modulators". IEEE 12th Modulator Symposium, 1976.

2. T.H. Robinson, "Power System for a High-power Burst-mode Pulsed Load". IEEE 13th Modulator Symposium, 1978.

3. British Patent 1517846; U.S. Patent 4081719.

4. R.L. Snelling & G.J. Scoles, "Operating Hydrogen Thyratrons in Parallel". IEEE 13th Modulator Symposium, 1978.

COMPLETE CHARACTERIZATION STUDIES VERIFY RBDT-RSR RELIABILITY

J. B. Brewster
Westinghouse Electric Corporation
Pittsburgh, PA (R&D Center)

G. F. Sherbondy
Westinghouse Electric Corporation
Youngwood, PA (Semiconductor Div.)

SUMMARY

This paper presents the latest characterization information available for a two terminal, high speed, solid state switch previously called the RSR (Reverse Switching Rectifier) but presently referred to as the RBDT (Reverse Blocking Diode Thyristor). Studies of the RBDT have been continuing, leading to broader pulse loss characterization than had previously been available. Loss characterization and trigger studies were made concurrently, and the results show that with proper triggering, the RBDT will function reliably and with minimum loss. New test equipment, which tests to customer specified load conditions is described. The paper concludes with a summary of field originated life data, which supports the conclusion that the RBDT may be effectively and reliably applied for short pulse, high current, high rate-of-rise duty.

INTRODUCTION

During the last 10 years, a solid state switch called the Reverse Swtiching Rectifier (RSR) was developed for short, high current pulse duty. Using IEEE nomenclature, the device has now been renamed the Reverse Blocking Diode Thyristor (RBDT). The meaning of the RBDT acronym is as follows:

R)
B) Reverse Blocking
D) Diode or Two Terminal
T) Thyristor or Four Layer

The first fully characterized RSR-RBDT was a device of 3/8" diameter, called the T40R RBDT, which is available in a 1/4" stud or DO5 package. In the initial application of the T40R-RBDT, 20 modulator modules were paralleled to obtain full rated modulator output. The T62R-RBDT, a device of similar voltage capability but capable of carrying a much higher current due to the use of a larger fusion diameter (.91 inch) was then developed to reduce the amount of paralleling required. The T62R device is available in a standard T62 type (two terminal) flatpack. See Figure 1.

Both the T40R and the T62R RBDT's are used as radar modulator switches in systems presently functioning or under construction. When devices first became available, a few early failures were encountered. This indicated the need for more RBDT characterization and for a testing program to weed out infant mortality failures. This paper describes current characterization study results and testing techniques designed to make RBDT application easier and more reliable due to an improved testing program. The intent of the most recent characterization is to make available needed data to circuit designers so that the RBDT may find its way into a variety of applications not presently served by the device.

Of particular interest is the power handling capability of the RBDT and the optimum triggering levels necessary to reliably achieve the best device performance. Watt second per pulse loss curves have been determined for various trigger voltage rates so that a variety of pulse widths can be accommodated and proper heat sinking may be determined. Some field results are included to demonstrate that characterization data and reliability goals were achieved.

Mechanical Configuration

Comparative two dimensional drawings are shown in Figure 2 of a standard thyristor structure and of an RSR-RBDT. Fundamentally, both devices are four-layer in structure, and both are fabricated by existing reliable and reproducible all-diffused-design techniques. The thyristor requires a gate lead for triggering, but the RBDT is turned-on by application of a trigger voltage between anode to cathode. The recommended RBDT trigger voltage is large and tightly specified, but no other solid state switch of this size can exhibit comparable switching speed, excluding solid state switches triggered with laser light.

Electrical Characterization

The RBDT was originally designed for use as a solid state radar modulator switch. It has been, and is now being applied for that purpose.

In this application, it is necessary to characterize the RBDT in terms of more than one parameter. As an example, a thyristor used for 60 Hz applications may simply be rated in terms of maximum half-wave average 60 Hz rectified current, but thyristors rated for narrow pulse width applications require concurrent characterization where peak current, pulse width, losses, etc., must be simultaneously specified for proper circuit design and realizable device performance.

Similarly, the RBDT must be characterized using several parameters to define its permissable operating region, the principal ones being peak current and pulse width. The peak currents are in excess of those normally associated with 3/8" or .9" fusions, and the pulse widths are smaller than those associated with high speed chopper thyristors. As an example, most high speed chopper thyristors are characterized for pulse widths no less than 50 microseconds, whereas the RBDT is not characterized for pulse widths higher than 30 microseconds. Also, a six-sized chopper thyristor is rated at a peak current of approximately 1000 amperes, whereas the T62R device (six-sized RBDT) is rated to 3000 amperes. Although RBDT's are rated using techniques previously associated with high speed thyristors, the rated values are specified using higher peak currents and narrower pulses than similar sized thyristor devices.

For a particular combination of peak current and pulse width, measurements were made of RBDT switching losses on a watt-sec/pulse basis. A rating approach paralleling gated thyristor rating procedures and also adopting thyristor derating techniques allows determination of permissible maximum pulse rate levels.

CH1371-4/78/0000-0149$00.75 © 1978 IEEE

Triggering

Early work with both the T40R and T62R RBDT's demonstrated the need for very precise trigger levels. Before complete and thorough trigger studies were made, some applications were troubled with unexplained device failures. These difficulties were initially attributed to inadequacies in two areas. (1) Full and complete RSR trigger characterization requirements were lacking, and (2) adequate device test results at full load levels were also lacking. As a result, a program was initiated to study RBDT trigger requirements in detail.

Forward Characteristic Response

The characteristics of the RBDT when a forward voltage is applied between anode to cathode may be divided into three regions. These are as follows:

1) DC voltages applied at levels less than the forward hold-off voltage rating.

2) Transient voltages applied at less than the forward hold-off voltage rating.

3) High speed transient voltages which exceed the forward blocking voltage.

The response to a dc voltage applied to the RBDT less than its rated blocking voltage is similar to the response of other four layer thyristor-like devices. Some small forward leakage current will flow and at maximum leakage current, rated blocking voltage is defined. Early in RBDT development, latching and holding currents were tested by breaking over RBDT devices under dc or near dc conditions. This resulted in a substantial number of failures, and the technique was abandoned. For this reason RBDT's should never be turned on with less than minimum recommended trigger drive.

The RBDT response to transient voltages less than rated forward blocking voltage is similar to that of the gate triggered thyristor. Turn-on will occur by dv/dt at some level. During in-circuit operation, transient voltages should not exceed maximum rated data sheet dv/dt's to avoid false triggering.

The response of RBDT's to high speed triggering is not as expected. Most thyristors will be found to respond similarly, but most will be found to fail with any appreciable load current. The RBDT has been designed and tested to accept a high speed trigger and respond with broad turn-on. The response of any four layer device to a transient voltage with rate-of-rise at least an order of magnitude higher than its transient rated dv/dt and an open circuit level at least 2.5 times higher than rated blocking voltage is to support this transient for a short time, then turn-on broadly as in the RBDT case, or turn-on destructively as in the gate triggered thyristor case. The high speed transient voltage supported by the four layer device will be greater than rated blocking voltage for an instant.

Trigger Response

A normal RBDT trigger response is shown in Figure 3. The peak RBDT trigger voltage will always exceed the RBDT rated blocking voltage. In the range of rated trigger voltage rate-of-rise, the response of the RBDT is slow, and peak trigger voltage (a) exceeding the rated breakover voltage will be supported by the device. Thereafter, a trigger current will begin to flow which will exist while substantial voltage is still across the device (b). Finally, voltage collapse will result in switch turn-on (c). From turn-on considerations, all current existing after voltage collapse is not useful trigger current. All current occuring during and before voltage collapse is considered a dv/dt inspired current, which is accountable for broad RBDT turn-on area.

Because RBDT junction capacity varies little between devices, trigger current is completely defined by a specified rate-of-rise of voltage (dv/dt) during the trigger period. The rate-of-rise of trigger voltage must be linear up to the peak trigger voltage, since it has been shown that it is the margin of trigger voltage in excess of hold-off voltage which accounts for fast RBDT triggering. Figure 3a shows trigger voltage across the RBDT without the holdoff voltage which produces the main current pulse. Holdoff voltage will be less than rated RBDT blocking voltage; this is required for more than blocking voltage considerations. See Figure 3b for a typical trigger-load circuit arrangement.

An RBDT voltage waveform showing combined trigger and hold-off voltage is shown in Figure 4. With the presence of hold-off voltage, trigger current begins to flow only after trigger voltage exceeds hold-off voltage. Recommended trigger rate-of-rise values given in data sheets apply between points (d) and (e) in Figure 4. As hold-off voltage approaches rated blocking voltage, the differential transient voltage (e-d) is reduced, as is trigger current. For optimum operation, hold-off voltage should be no more than 2/3 of rated blocking voltage.

Any means which allows the device to operate with a wide differential transient voltage (e-d) improves RBDT turn-on. It has been repeatedly demonstrated that two devices in series have lower switching loss per device than a single device switching the same hold-off voltage. This is a direct result of creating a larger differential transient voltage per device, more trigger current, and less switching loss per device. We do not recommend that two RBDT's be used to switch a hold-off voltage where one device will be adequate. This result merely illustrates the character of RBDT switching. It has been found that two devices switching the same voltage as a single device exhibit reduced switching losses of about .15 per unit, so that two devices show a combined loss of $(.85 \times 2) = 1.7$ p.u., as opposed to the 1.0 p.u. loss in a single device. If absolute loss levels are unimportant, then it may be generally stated that the RBDT works best when differential transient voltage is maximized, however this occurs.

Early RBDT circuit failures were eliminated by determining experimentally the minimum recommended trigger pulse voltage rate-of-rise. For the two types of devices available, these are:

Device	Minimum Differential Transient dv/dt (Holdoff Voltage $\leq .66\ V_{DRM}$)
T-40R	5,000 volts/us
T-62R	15,000 volts/us

Optimized RBDT Triggering

The minimum differential transient trigger voltages as tabulated were initially determined by trial and error over an extended period, but a carefully planned experiment was undertaken to determine optimum trigger drive. A large number of switches were tested using a short 3 microsecond pulse of 2000 ampere peak. Current rate-of-rise for the test pulse was 2500 A/us. All test results were obtained when switching a hold-off voltage of 600 volts, and all results are presented for a test system using one RBDT test device to produce the test current pulse. (Some previously published RBDT results presented loss data for two devices in series which was averaged to determine the losses per single switch.) A typical load current pulse is shown in Figure 5.

Watt-second per pulse loss data for a sample group of devices is shown in Figure 6. Single device losses are shown here as a function of trigger voltage rate-of-rise, in volts per micro-second using a type

T62R RBDT test device. Trigger voltage rate-of-rise was altered by changing the open circuit trigger voltage, and the most general trend in the results is a decrease of switching loss as trigger dv/dt is increased. In the region of 25,000 volts per microsecond, losses for most devices appear near minimum, and for this reason this point is taken as the optimum suggested working point. For least switching stress, it is recommended that the T62R RBDT be driven with no less than a trigger dv/dt of 25,000 volts per microsecond.

Trigger responses for this lowest loss condition are shown in Figure 7 and Figure 8 for the condition of zero holdoff voltage. Figure 7 shows a unique photograph in that two sweep speeds are presented simultaneously. The first portion of the sweep showing trigger voltage occurs at a speed of .1 μsec/div, while the trigger current, in the right hand portion of the trace is shown at a speed of 1 μsec/div. Hence, the most interesting features of each response may be viewed simultaneously, but not simultaneously in time frame. Simultaneous presentations of trigger current and voltage are shown in Figure 8 for the recommended 25000 volt per microsecond trigger speed. Similar photographs for the minimum recommended trigger (15000 volts per microsecond) are shown in Figures 9 and 10 for comparison. All responses are for zero hold-off voltage.

For the optimum recommended trigger situation, RBDT loss performance data has been measured to cover an operating spectrum of pulse conditions as indicated in the following tabulation.

Pulse Widths	Peak Current
3 μsec	5000 A
10 μsec	5000 A
20 μsec	5000 A
30 μsec	5000 A

Full Load Testing

The second feature of RBDT characterization lacking in early development was full load testing. A test system has been devised and constructed such that RBDT fusions may now be full load tested to customer specifications before encapsulation. As a result, the RBDT product leaving the factory will have been tested at a desired switching level before shipment.

The full load level testing subjects the test RBDT to the dynamic pulse conditions expected to be encountered by a customer, but at reduced pulse rate. High pulse rate effects are simulated by elevation of fixture temperature anywhere in the temperature range of 25°C to 100°C. Since the RBDT fusion is small, it will quickly assume the temperature of the more massive fixture, showing that the customer specified pulse width and peak current may be tolerated, at worst case junction temperature conditions.

Photographs of the test system are shown in Figures 11 and 12, as well as block and power component diagrams in Figures 13 and 14 respectively. The important parameters of the test system are:

1) Trigger rate-of-rise control
2) Peak current and pulse width control
3) Turn-off time measurement run concurrently with selected peak current
4) Average junction temperature selection

Trigger voltage rate-of-rise may be selected over the range of 5000 to 40,000 volts per microsecond. In most cases the recommended trigger is applied and devices are classified by peak trigger voltage.

Peak load current and pulse width are determined by the design of the pulse forming network used. RBDT's in fusion form are load tested at the customer selected level resulting in elimination of some seldom occurring infant mortality failures. Although this test has not been designed to determine pulse switching losses, measurements have been made of dynamic forward conducting voltage, and correlation obtained between this parameter and pulse switching loss. Means are then available to select devices of better than average switching capability, if this should be necessary.

During testing at full load current and maximum junction temperature, a turn-off time test is performed at customer required reapplied blocking voltage. RBDT in-circuit simulation and maximum load current testing is complete. In effect, a single RBDT is given an effective in-circuit test to give every assurance of switching tolerance and forthcoming in-circuit reliability.

Reliability

As a result of this complete and extensive test programming, RBDT reliability in initial applications has been reasonable and acceptable. The types of applications served by the RBDT are demanding of system reliability. The need for extreme reliability in radar tracking systems is unquestionable. The thorough testing schedule described in this paper, as well as additional environmental testing have improved RBDT reliability over that existing ten years ago. The most convincing and meaningful testimonial to system and device reliability is the accumulation of operating device hours in a variety of pulse applications. At the present time, pulse power modulators used in radar transmitters and laser systems now utilize parallel combinations of RBDT's with a wide spectrum of pulse widths, peak currents, and frequencies. Of those systems using the T40R device, some 340,000 device hours have been logged for a variety of pulse conditions. These include peak currents of 100 to 550 amperes, di/dt's up to 2000 amperes per microsecond, and pulse widths from a fraction of a microsecond up to 55 microseconds. These applications of the T40R include operating pulse rates of from 15 to 1000 pulses per second. For the larger disc type T62R device, over 300,000 device hours of operation have been logged. Operating conditions include peak currents to 5000 amperes, at 2500 amperes per microsecond, and pulse widths of 3 to 20 microseconds at frequencies up to 365 pulses per second.

Additional long term reliability runs are presently in progress in order to generate quantitative data under controlled conditions to support the incoming field originated data. For the long term reliability runs, voltage stress levels on both device types are typically 75 to 80% of maximum on a per device basis. Formal, finalized data indicating RBDT life and reliability will then be available at the highest working stress level.

In addition to electrical testing, environmental tests have also been conducted at temperatures ranging from 10°C to 50°C ambients while operating a modulator at full load. These types of information have resulted in a calculated system MTBF of over 17,000 hours.

CONCLUSIONS

Early applications of the RBDT, a solid state switch designed for radar modulator duty, lacked complete trigger characterization and adequate fusion testing at full load levels. Recently completed RBDT characterization studies now indicate the existence of optimum triggering levels. Recently constructed RBDT test equipment allows full load level testing of unencapsulated devices resulting in the exclusion of marginal devices before final encapsulation. Accumulated device operating time indicates that the RBDT testing program and characterization studies are yielding

improved reliability and better service life than was attainable using earlier devices.

REFERENCES

1. "Solid State Modulator Loss Performance Characterization", J. B. Brewster, R. A. Hill, 1976 Twelfth Modulator Symposium (IEEE).

2. "A New Solid-State Switch for Power Pulse Modulator Applications, The Reverse Switching Rectifier", J. B. Brewster, P. F. Pittman, 1973 Eleventh Modulator Symposium (IEEE), pp. 6-11.

3. "1000 Volt and 800 Amp Peak Reverse Switching Rectifier", C. K. Chu, J. B. Brewster, 1973 IEEE - IAS Meeting, pp. 267-282.

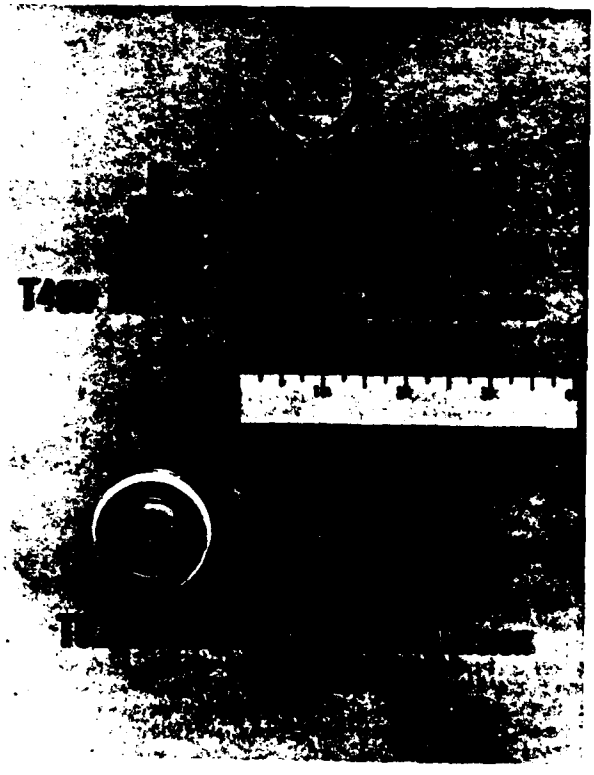
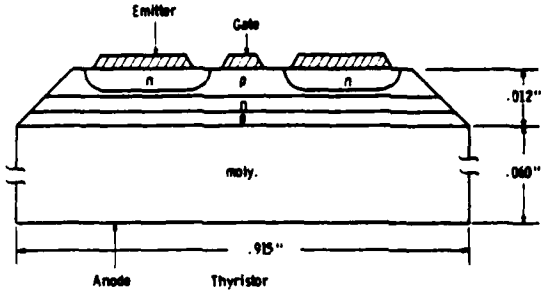


Fig. 1 - T40R and T62R RBDT fusion and package.



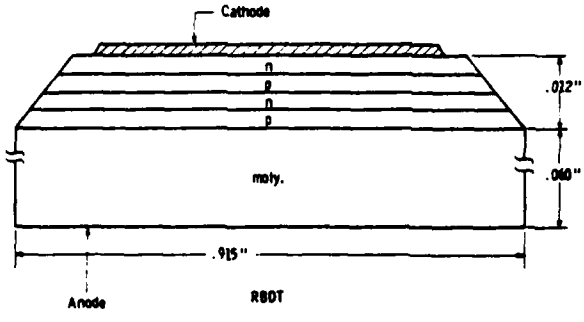


Fig. 2 - Two dimensional thyristor and RBDT structure.

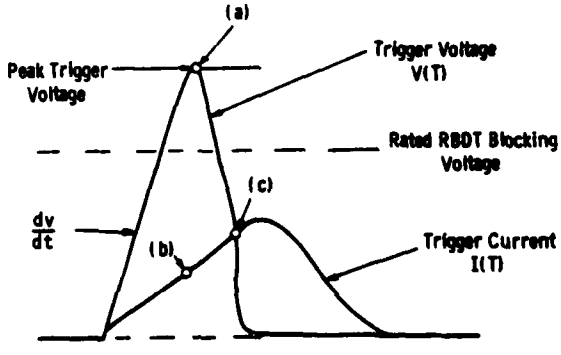


Fig. 3a—Normal RBDT trigger response

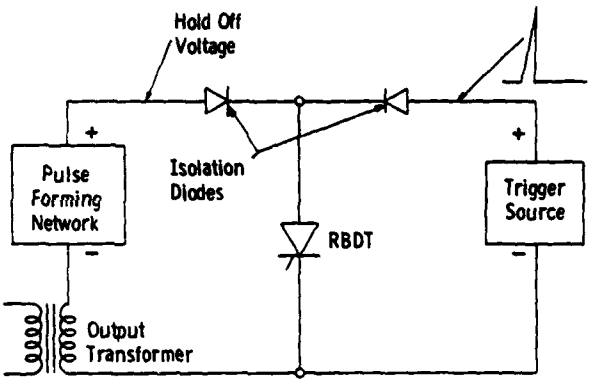


Fig. 3b – Symbolic RBDT typical trigger and load circuit

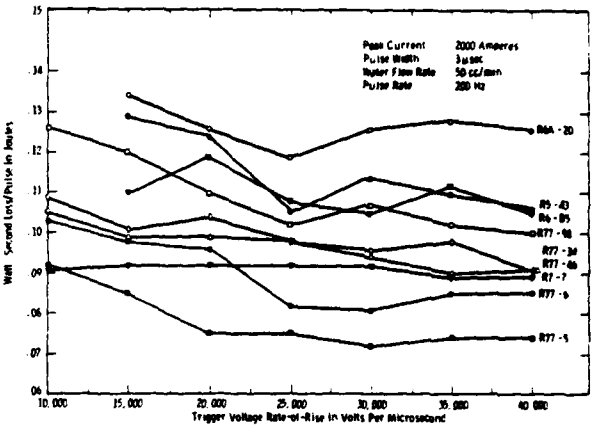


Fig. 6—Loss per pulse versus trigger voltage rate of rise

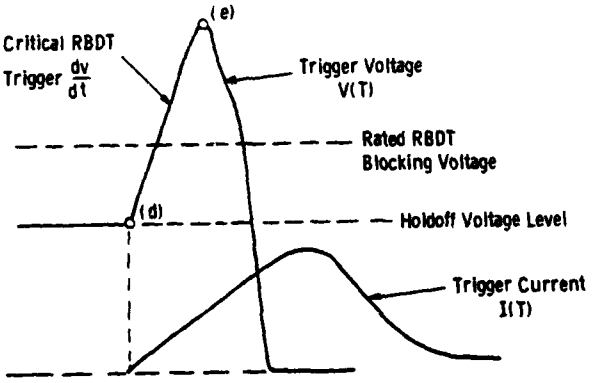
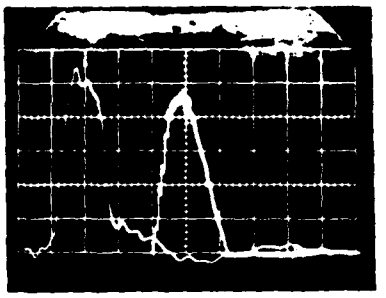


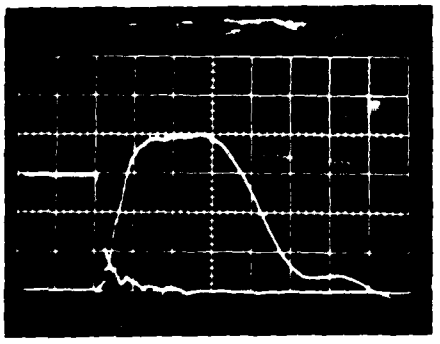
Fig. 4 —RBDT trigger with holdoff voltage



Hor
.1 usec/div: 1 usec/div

Vertical
200 volts/div
20 amps/div

Fig. 7 - RBDT trigger voltage and trigger current for trigger dv/dt = 25,000 volts/usec.



Hor
1 usec/div

Vertical
200 volts/div
500 amps/div

Fig. 5 - Typical RBDT load current and anode voltage pulse.



Hor
.1 usec/div

Vertical
500 volts/div
20 amps/div

Fig. 8 - RBDT trigger voltage and trigger current for trigger dv/dt = 25,000 volts/usec.

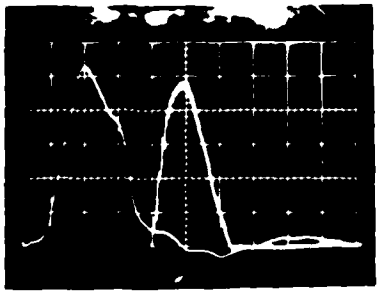


Fig. 9 - RBDT trigger voltage and trigger current for trigger dv/dt = 15,000 volts/μsec.

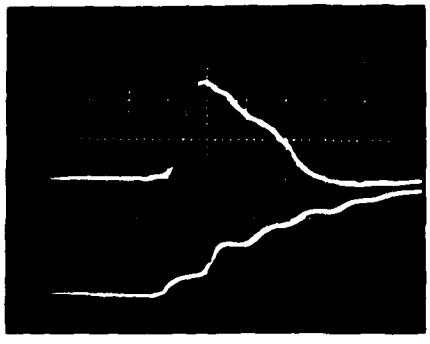


Fig. 10 - RBDT trigger voltage and trigger current for trigger dv/dt = 15,000 volts/μsec.



Fig. 11 - RBDT full load current and tq tester, front view.

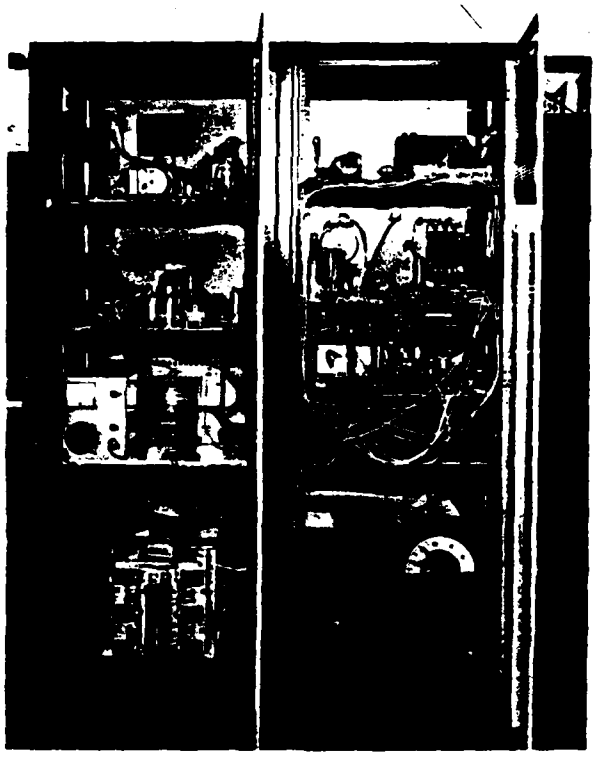


Fig. 12 - RBDT full load current and tq tester, rear view.

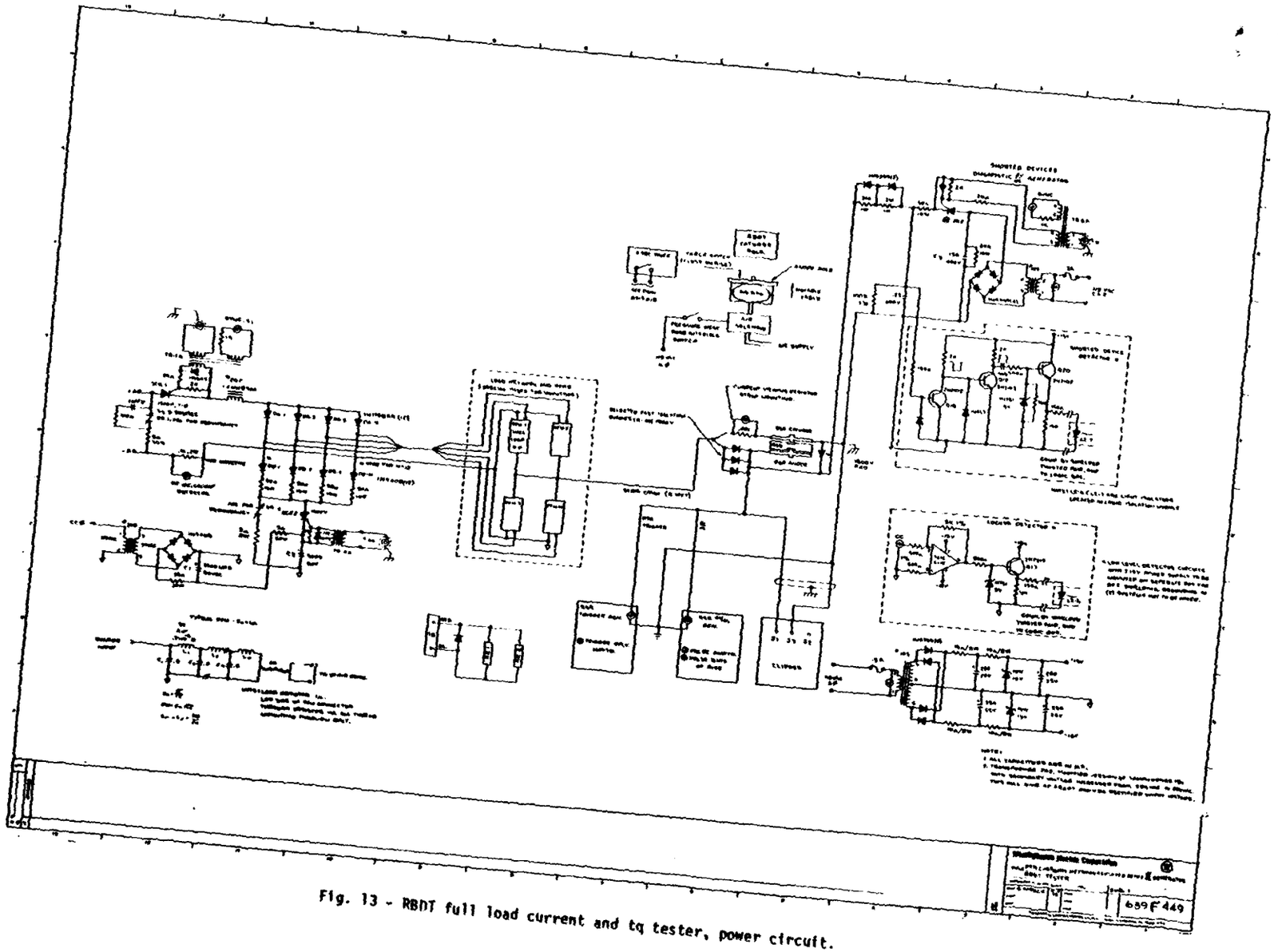


Fig. 13 - RBDT full load current and tq tester, power circuit.

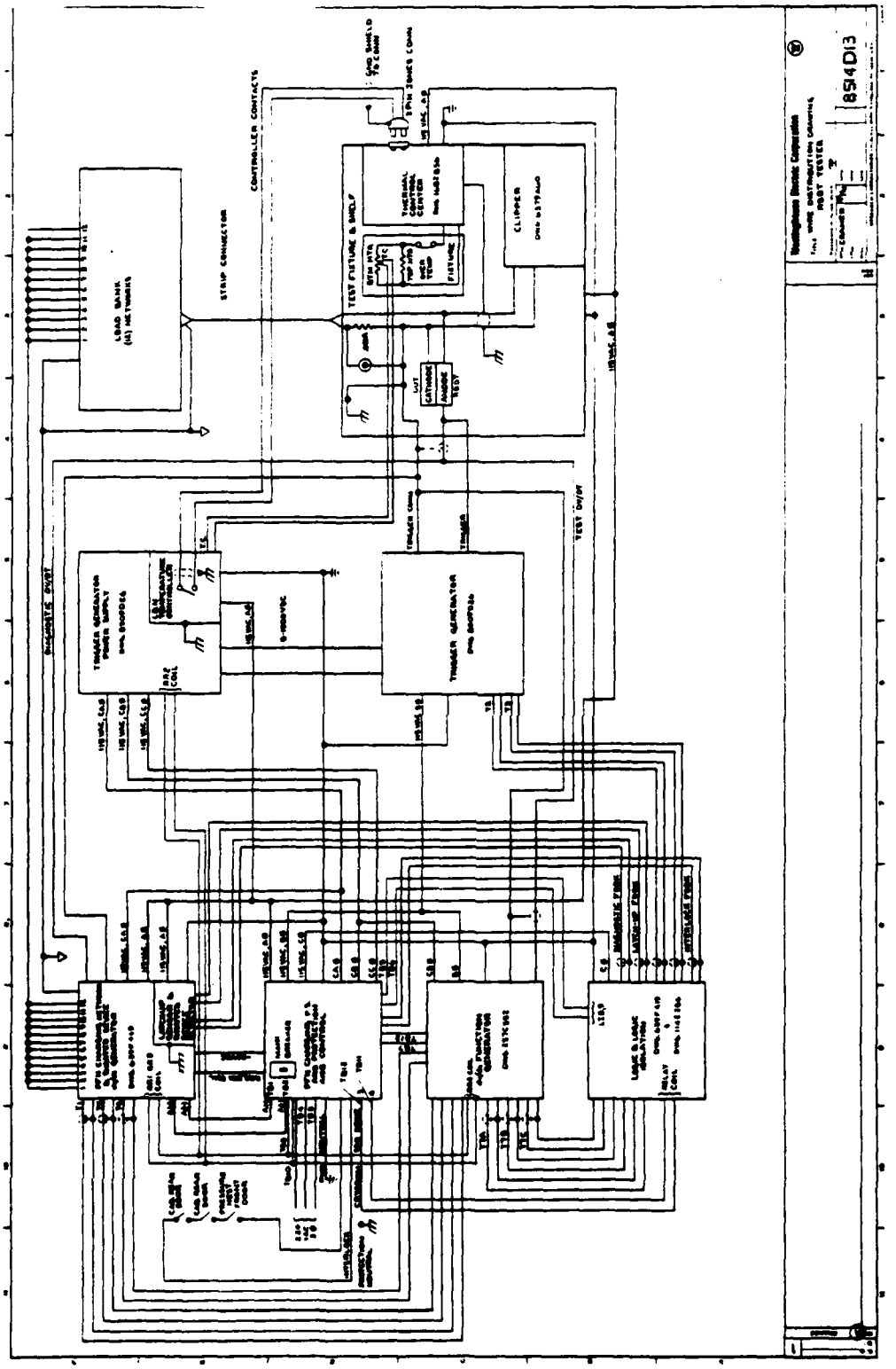


Fig. 14 - RBDT full load current and tq tester, wiring diagram.

HYBRID SCR SWITCH

D. L. Pruitt
RCA Government Systems Division
Missile and Surface Radar
Moorestown, New Jersey 08057

Abstract

Hybrid solid state switches were designed and constructed using SCR (silicon controlled rectifier) chips on a beryllia substrate. Peak pulse currents of up to 6000 A with 2 μs rise time, or up to 3000 A with 1 μs rise time, were achieved. A series stack was constructed to produce a 10 kV air cooled switch.

Introduction

High power pulse switches, using parallel/series arrangements of small SCRs, were designed and constructed at RCA in the 1973-75 time frame. These efforts were reported in a paper delivered at the Twelfth Modulator Symposium in 1976.[1]

Early in this program, the use of hybrid circuit techniques was recognized as offering a potential dramatic reduction in size and weight for the parallel SCR switch module. When glass passivated chips of an appropriate size became available in 1975 (Unitrode Corporation), plans were made to initiate a hybrid circuit development at RCA in 1976.[2]

Hybrid Circuit Design

A 40-ampere (rms rating) 600-volt chip (R044060) was chosen. This chip is 5 millimeters (0.2 inch) square. The concept involves attaching, by reflow soldering, 20 main switch SCR chips in a 10 parallel/2 series configuration, plus two trigger (or pilot) SCR chips, on a beryllia substrate. Beryllia was chosen for its excellent thermal properties - high conductivity and high specific heat.

Figure 1 is a schematic diagram of the resulting circuit.

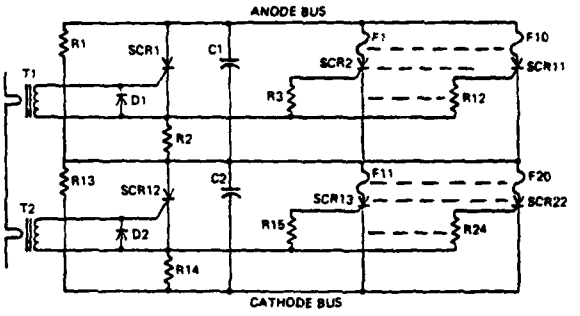
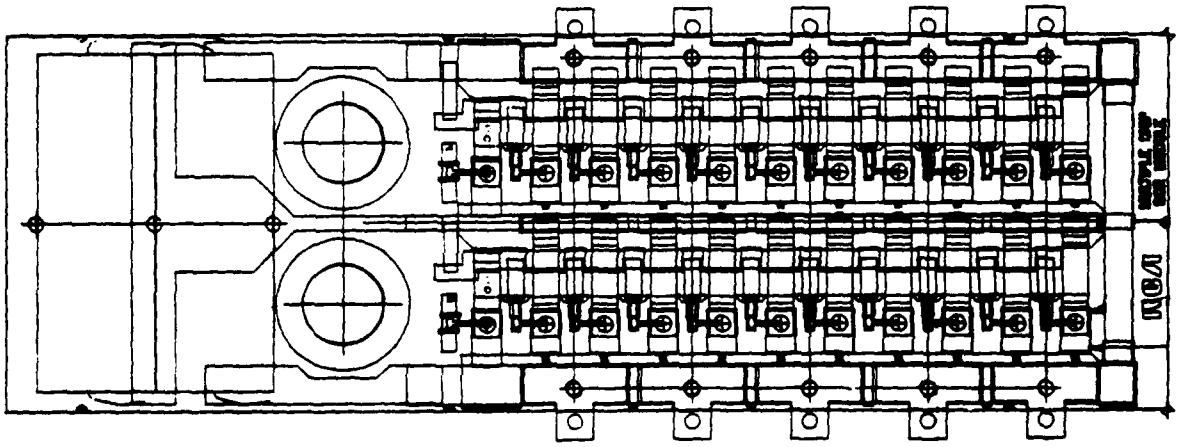


Figure 1. Hybrid SCR Chip Switch

The circuit of Figure 1 operates in essentially the same manner as the parallel/series SCR switches described in the Twelfth Modulator Symposium. Briefly, a sharply rising current pulse (50 amperes typical) in the primary loop of Pulse Current Transformers T1 and T2 provides "hard" triggering (1 ampere peak) trigger pulses to pilot thyristors SCR1 and SCR12. SCR1 and SCR12, in turn, switch the voltages on capacitors C1 and C2 onto the main trigger buses, resulting in "hard" triggering (2 to 3 amperes peak) for main SCRs SCR2-SCR11 and SCR13-SCR22 and establishing a conduction path from anode bus to cathode bus.

Several trial layouts were generated and discarded in arriving at the current hybrid circuit layout shown in Figure 2. Because of the high currents involved (40 amperes rms per chip), the SCR chips are not soldered directly to the substrate metallization, but are soldered to copper contact



LAYER	1	2	3	4	5	6	7	
REV	-	-	-	-	-	-	-	
ITEM NO.	-	-	-	-	-	-	-	

SCR CHIP SWITCH
DATE 4-38-76
LOGIC REV. 1
DWG REV. 4
H.F.S.8-9-76
COMP.8-9-76

Figure 2. Hybrid Circuit Layout

CH1371-4/78/0000-0157$00.75 © 1978 IEEE

pads which are in turn reflow-soldered to the metallization pattern. The printed circuit resistors (gate resistors and bleeder resistors) add negligible weight to the hybrid circuit. The trigger transformers (T1 and T2) and the circuit capacitors (C1 and C2), contribute significant (but not major) weight to the hybrid module.

The completed module weighs 190 grams without cooling fins, and 235 grams with cooling fins attached.

Figure 3 is a photograph of a completed hybrid circuit thyristor switch module.

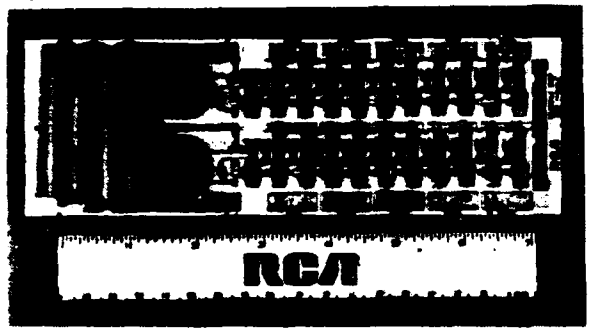


Figure 3. Hybrid SCR Chip Switch Module

One of these hybrid circuit modules was pulse tested, with forced air cooling, to the following maximum conditions:

- Peak Voltage 600 V
- Peak Current 6 kA
- Pulse Width 20 μs
- Current Rise Time 2-1/4 μs
- Repetition Rate 100 pps
- Duty Cycle 0.002
- Peak Power 1.8 MW
- Average Power 3.6 kW
- Length of Run 1 Hr

This rigorous test provides confidence that the modules can reliably achieve air cooled objectives as follows:

- Peak Voltage 1 kV
- Peak Current 3 kA
- Pulse Width 10 μs
- Current Rise Time 1 μs
- Repetition Rate 100 pps
- Duty Cycle 0.001
- Peak Power 1.5 MW
- Average Power 1.5 kW

Ten hybrid SCR modules were connected in series to obtain a 10 kV (nominal) air cooled switch (shown in Figure 4. Objective rating for the air cooled switch was as follows:

- o Peak Voltage 10 kV
- o Peak Current 3 kA
- o Pulse Width 10 μs
- o Current Rise Time 1 μs
- o Repetition Rate 100 pps
- o Duty Cycle 0.001
- o Peak Power 15 MW
- o Average Power 15 kW

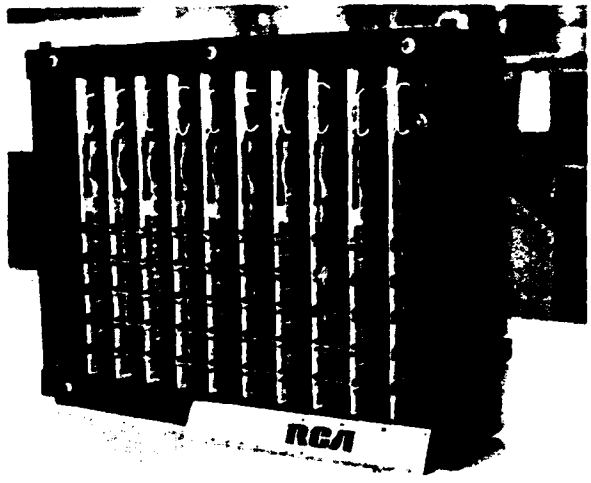


Figure 4. 10 kV Air Cooled SCR Switch

The 10 kV hybrid SCR switch was installed in a test modulator. In initial testing, some difficulty was experienced with module voltage sharing, resulting in device failure. After repairs, maximum voltage was limited, resulting in the following maximum operation:

- Peak Voltage 8.9 kV
- Peak Current 3 kA
- Pulse Width 10 μs
- Current Rise Time 1 μs
- Repetition Rate 100 pps
- Duty Cycle 0.001
- Load Resistance 1.2 ohms
- Peak Load Power 10.8 MW
- Average Load Power 10.8 kW

Conclusions

The work performed on thyristor switching has shown that series/parallel arrangements of relatively small thyristors can be effectively utilized in super-power, artificial line type pulse modulators. A lightweight, compact, air-cooled hybrid SCR switch attained 10 megawatts peak and 10 kilowatts average load power in an aritifical line type modulator.

Acknowledgement

This work was sponsored by the Air Force Systems Command's Rome Air Development Center, Griffiss AFB, N.Y., under Contract F30602-76-C-0197.

References

1. D.L. Pruitt, "Multi-Megawatt Solid State Switch," Conference record of 1976 Twelfth Modulator Symposium, February 4-5, 1976, pp. 62-66.

2. "Final Report, Multiple Chip SCR," Contract F30602-76-C-0197, RCA 6T0062A1.

OPTICAL DRIVE REQUIREMENTS FOR LASER ACTIVATED SEMICONDUCTOR SWITCHES*

P. G. McMullin and L. R. Lowry
Westinghouse R&D Center
Pittsburgh, PA 15235

Summary

Laser activated semiconductor switch (LASS) devices of the thyristor type exhibit three regimes of operation. At low optical drive, optical triggering is obtained with delay time before conduction and relatively low current rise rates. At intermediate drive levels, fast switching is obtained with no appreciable delay time and fast current rise rates (greater than 10^9 A/S) but with substantial power lost in the switch element. At higher optical drives saturated switching is observed with the rise rate and power loss relatively independent of the optical drive level.

LASS thyristors of 1 kV and 4 kV operating voltage ratings have been characterized in the lossy fast switching regime. For pulses of 100 ns duration, the devices act as resistive elements. The magnitude of the resistance varies inversely with the optical drive, and can be understood as conductivity modulation of the conduction path by the photogenerated carriers.

Such characterization allows switch system design tradeoff between the required optical drive level and the tolerable power loss in the switch elements.

Introduction

Laser activated semiconductor switch (LASS) systems combine the proven power handling capabilities of solid state switching elements with the short pulse durations obtainable from Q-switched lasers to attain power switching at very high current rise rates. A LASS comprised of a silicon thyristor driven by an optical input from a neodymium-YAG laser has achieved current rise rates of 10^{12} A/s at current levels of 1000A.[1] Other work has demonstrated 20000A pulses of 40 μs duration switched from a 2 kV supply with 0.5 μs risetime.[2] The rise rate has been limited by the inductance in the external circuit, and the power by the available pulse sources. The limits of the LASS system capability in terms of maximum current rise rate or maximum power handling have not yet been established.

Reliability of the LASS system depends on the functioning of both the solid state and optical parts of the system. Silicon thyristors are well known to be very reliable within the operating range encountered in electrically triggered operation. The very high current rise rates possible with optical drive pose more stringent operating conditions, but no particular problems are expected given a good device design for distributing the current flow and maintaining adequate heat sinking.

As for the optical source, Nd-YAG lasers are used in production facilities for scribing, trimming, and welding operations with low failure rates and low maintenance requirements. Nevertheless, the bulk of the cost and complexity of the LASS system lies in the optical source and delivery subsystem. Therefore, important design considerations are (1) how much optical drive is needed for a given switching function, and (2) how can one trade off switch performance for optical drive.

This paper concerns efforts to come up with a relatively simple device model to use in preliminary system design. It is well known that thyristor modeling is a difficult task. Electrical regeneration built into the two-transistor combined structure means that the electrical properties governing behavior are not subject to external control or even measurement. High current operation implies high injection conditions. A two-dimensional structure is inherent in view of the spreading of the current from the illuminated region and in view of the built-in gain structure. Also, heating is an important variable.

Previously Davis developed a model to calculate the instantaneous temperature rise in the silicon structure and the corresponding voltage drop across the switch element for a given initially illuminated area and a given current waveform.[3] This work was extended and confirmed experimentally for long (~ 40 μs) pulses by Davis and Roberts.[4] Although many simplifying assumptions were made to make this calculation possible on a reasonably sized computer, a large body of input data to the program is required and no explicit connection is established between the intensity of the optical drive and the impedance of the switch.

This paper presents recent experimental results for LASS system performance in a limited range of operation. The pulse width is limited to 100 ns. This time scale is suitable for short pulses or for the initial portion of a longer pulse. Also, the current density is assumed to be limited to about 10^4 A/cm^2. Although this current density is high when compared to transistors or the conventional operating limits of thyristors, it is a reasonable level for short pulses where heat will not build up excessively. An empirical model has been developed to describe LASS operation under these conditions. This model is approximated by a simple conductivity modulation calculation that can be used for preliminary system designs.

Experiment

Pulses of 100 ns duration were generated by a pulse forming network composed of several 50 ohm coaxial cables connected in parallel. The number of cables was changed from one to ten to adjust the system impedance from 50 to 5 ohms, respectively. The charged cables were switched into a matched load by the LASS device under test. The load was composed of the proper number of 50 ohm terminations connected in parallel. Some measurements were taken of the voltage across the LASS device by means of probes placed at the terminals of the device, connected to differential inputs of an oscilloscope. The oscilloscope display verified that the voltage across the device collapsed rapidly to a low value under the drive conditions for lossy fast switching. Most of the measurement data were taken by observing the voltage across the load. This presented the advantage that precise measurements of small changes in the peak voltage could be taken using a null offset procedure with a Tektronix 7A13 module as the input part of the oscilloscope. A further advantage of this procedure is that it directly measures the power delivered to a load which is the principal performance figure for any switch system. The sample holder is a

CH1371-4/78/0000-0159$00.75 ©1978 IEEE

stripline configuration for low inductance. Test pulse response measurements show response times in the ns range for this structure.

The optical drive for the LASS switch element was provided by an ILS LL-103 Nd-YAG laser. Depending on the laser alignment and on the operating conditions, the laser output pulse duration ranged from 22 to 50 ns, full width at half maximum. The laser output was adjusted in steps by Schott glass attenuators, and continuously by a Glan prism polarizer. Apertures were used to confine the region illuminated by the laser beam to areas ranging from 1 to 8 x 10^{-3} cm^2. The laser pulse energy was measured at the position of the test sample by a Scientech absorbing calorimeter or by ballistic thermopile. It is assumed that 30 percent of the incident energy is reflected at the uncoated silicon surface. All optical energy measurements refer to the transmitted energy that actually enters the silicon wafer.

System Model

The measurement data was treated on the basis of the system model shown in Figure 1. The load resistance is denoted by R, and the switch impedance by S. The resistor Z represents the impedance of the charging line and incorporates also any resistance in the

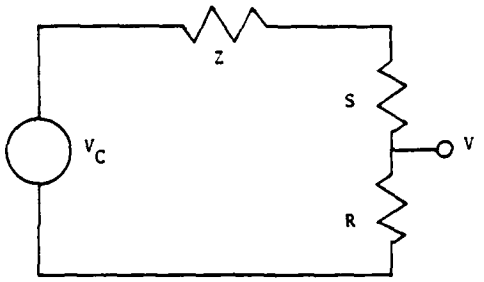


Figure 1. Equivalent circuit of LASS test system.

switch device which is not modulated by the optical drive. For a given charging voltage V_c, the voltage V observed at the load during pulse is given by

$$V = V_c \times \frac{R}{S + R + Z} \qquad (1)$$

As the optical drive is increased to reduce S to a minimum, the maximum voltage observed at the load is Vm;

$$V_m = V_c \times \frac{R}{R + Z}$$

Then the switch impedance can be expressed by

$$S = (R + Z) \times (V_m - V)/V \qquad (2)$$

In practice, V_m is established by increasing the optical drive until the observed voltage no longer changes. A very definite saturation in output voltage is observed for which increases in optical drive of two orders of magnitude do not increase Vm.

Results

As the optical drive is varied, three regimes of operation can be seen as shown in Figure 2. At low drive, the LASS element switches on relatively slowly

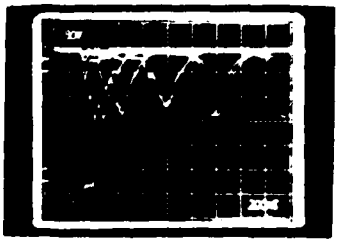


Figure 2. Waveshapes for six optical drive levels. At lowest optical drive, there is a 1.6 µs delay before the thyristor turns on. At higher drive levels there is less delay, and at the highest level the waveform is a sharply defined pulse of 100 ns duration.

after a substantial delay. This corresponds to electrical gate drive of a conventional thyristor in which the switching process is due to the regenerative gain of the thyristor structure. As the optical drive is increased, the delay time shortens until conduction occurs during the drive pulse. However, the device is not completely turned on, so although the switching is fast it is also lossy. Finally, as the drive is increased still further, the switch loss reaches a minimum value which is insensitive to further changes in optical drive. This is saturated fast switching, and represents the best electrical performance, but at the expense of high optical drive. By reducing the optical drive to a tolerable loss level in the switch, the switch system design can be optimized.

In the lossy fast switching regime the wave shape of the output pulse at the load is practically identical to the saturated output pulse, but the amplitude is reduced. When the switch resistance is calculated according to expression (2), the device resistance can be plotted against the optical drive as shown in Figure 3. These data were taken with device 4J10 which is rated for 1000 volts forward operating voltage. The observed resistance is relatively independent of applied voltage, system impedance, and size of aperture, depending mainly on the optical drive. As seen in the Figure, the device resistance and the optical drive input pulse energy are linearly related in the log-log plot over a range of two orders of magnitude. The slope and intercept for the best straight line fit to the data are given in Table 1.

TABLE 1

REDUCED DATA ON TWO LASS UNITS

Device	Voltage Rating	Log Plot Parameters		Experimental c Ω x µJ	Theoretical c' Ω x µJ
		Slope	Intercept		
4J10	1 kV	-.953	.6001	3.98	1.2
N2	4 kV	-.993	1.218	16.5	5.2

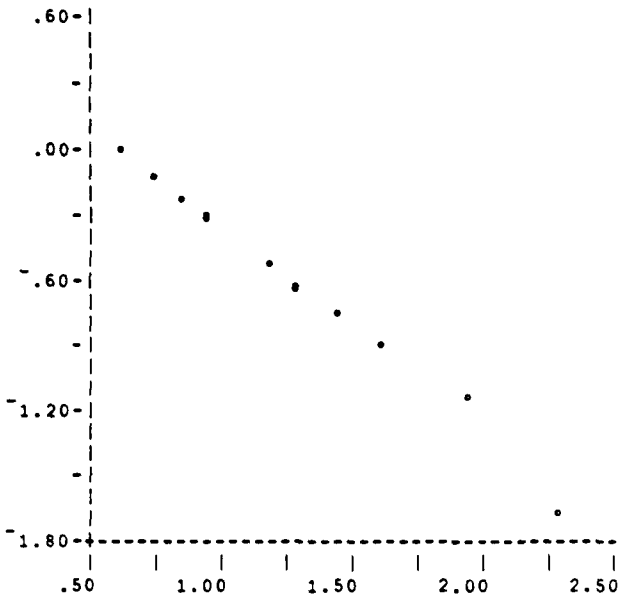


Figure 3. Device resistance S vs. optical drive pulse energy E for device 4J10. The vertical axis is log S in ohms, and the horizontal axis is log E in μJ.

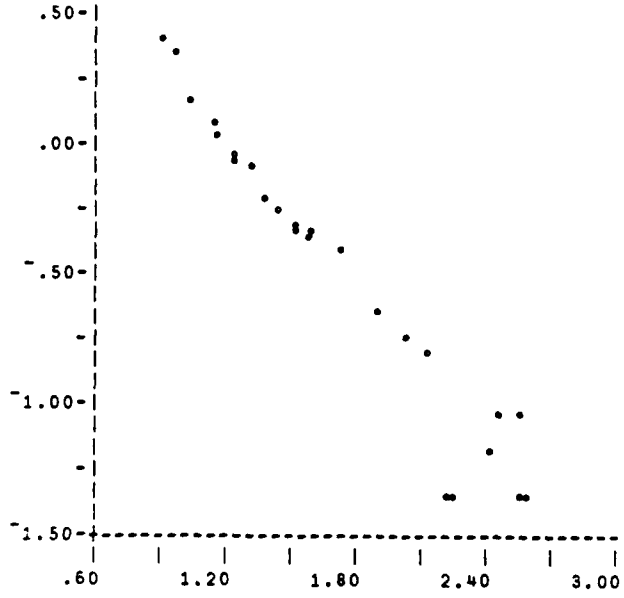


Figure 4. Device resistance S vs. optical drive pulse energy E for device N2. The vertical axis is log S in ohms and the horizontal axis is log E in μJ.

Since the slope is very nearly equal to -1, the data are well described in this range of operation by the expression

$$S = C/E \qquad (3)$$

where E is the energy of the optical drive pulse that enters the silicon, and C is constant. The magnitude of the constant C is also shown in Table 1.

The resistance data for another device are shown in Figure 4. This device, designated N2, is rated for operation at 4000 volts forward operating voltage. The measurements were made with a 5 ohm test system impedance at a voltage of 1000 volts, limited by breakdown in the connectors of the coaxial cables in the charging lines. Within the limits of the lossy fast regime, this device is also well described by expression (3). The linear best fit parameters and the scaling constant C are listed in Table 1.

Device Model

The simplicity of the relation (3) suggest a straightforward physical mechamism domimating device characteristics in the lossy fast switching regime. The required form is obeyed by conductivity modulation. To calculate the magnitude of this effect, we assume that the current is restricted to a cylindrical region of circular cross-section defined by the aperture in the laser beam path. The resistance of this path is given by

$$S = \frac{1}{A} \int \rho \, dx$$

where A is the area of the wafer surface illuminated by the laser and ρ is the resistivity of the silicon as a function of the distance x from the surface. For carrier concentrations below 10^{18} cm^{-3}, the resistivity can be written as

$$\rho = 1/q \, \mu g$$

Where q is the electron charge, μ is the sum of hole and electron mobilities since both contribute to the current, and g is the density of hole-electron pairs produced by the laser drive pulse. If the total optical energy entering the wafer is E, then g is given by

$$g = E \, \alpha \, e^{-\alpha x}/E_o A$$

where E_o is the energy of a single photon, and α is the absorption constant for the laser light in silicon. Here it is assumed that each photon absorbed in the wafer creates a hole electron pair, a valid approximation when free carrier absorption is low as it is at carrier densities below 10^{19} cm^{-3}. Taking the integral over the length L of the path where conductivity is modulated, we obtain

$$S = \frac{E_o \, (e^{\alpha L} - 1)}{\mu \, \alpha^2} \times \frac{1}{E} \qquad (4)$$

where E_o is expressed in electron volts. It can be seen that the switch resistance has the expected form of expression (3), is independent of the area of the illuminated region, and depends only on the material constants μ and α and the length L which described the device structure. To evaluate this expression for comparison with the experiments, the low concentration mobility, μ = 2000 cm^2/VS, the optical absorption, α = 20 cm^{-1}, and the photon energy 1.16 eV were used.

The lengths L were taken as the entire thickness of the device, 300 μm for device 4J10 and 760 μm for device N2. The results are listed in Table 1. The model also neglects the effects of the two forward biased junctions in the thyristor structure and the stored charge at the reverse biased center junction.

Discussion

Several LASS devices characterized in the same way have shown a similar reciprocal relation between optical drive and device resistance as described by expression (3). This relation has important implications for switch system design. The main point of this relation is that the device resistance depends mainly on the total energy input into the wafer and not on the way it is distributed. In the measurements described here, the optical drive is confined to a region much smaller than the total area of the wafer. If the optical drive is divided among several equivalent areas, and the resistances described individually by expression (3) are combined in parallel, it can be seen that the total resistance depends only on the total energy input. Dividing the optical drive in this way to create a number of parallel paths will decrease the circuit inductance and improve the thermal performance by distributing the heat. In addition, performance for long pulses will be improved by reducing the time necessary to reach full conduction by spreading of the plasma.

As seen in Table 1, the agreement between the experimental number for the constant C is not as close as desirable to the model prediction C'. The most major likely factor contributing to this discrepancy is scattering of the input light at the rough surface of the silicon. Qualitative optical views of scattering in similar wafers with both surfaces exposed shows that most of the input light remains an approximately collimated beam so this effect by itself is not likely to be the full explanation. Other factors are free carrier absorption in the highly doped emitter region at the surface, carrier-carrier scattering and Auger recombination. None of these effects is expected to change the result by more than about 15%. It is likely that complete agreement will come only after more detailed study of device characteristics.

Acknowledgements

The authors wish to express their appreciation to E. S. Schlegel for providing the 4 kV device, and to D. J. Page and J. R. Davis for helpful discussions.

*This work was partially supported by the Dept. of Energy, Oak Ridge Gaseous Diffusion Plant through Union Carbide.

References

1. O. S. F. Zucker, J. R. Long, V. L. Smith, D. J. Page, and P. L. Hower, "Experimental Demonstration of High-Power Fast-Rise-Time Switching in Silicon Junction Semiconductors," Applied Physics Letters, Vol. 29, pp. 261-263, 1976.

2. L. R. Lowry and D. J. Page, "Light Activated Semiconductor Switches," Proceedings of 1977 National Aerospace and Electronics Conference, pp. 616-622.

3. J. R. Davis, "A Theoretical Model of Light-Fired Thyristors," Power Electronics Specialists Conference Record 1975, pp. 305-312.

4. J. R. Davis and J. S. Roberts, "Ultra-Fast, High-Power Laser-Activated Switches," Power Electronics Specialists Conference Record, 1976, pp. 272-279.

IMPROVEMENTS ON TRANSMISSION LINE PULSERS

R. Dollinger and C. Scheffler

Laboratory for Power and Environmental Studies
Department of Electrical Engineering
State University of New York at Buffalo
Amherst, New York 14226

Summary

A series of pulsers have been built that produce up to 10 kV pulses into 1 to 100 Ohm loads with rise time of 1/2 to 1 ns, durations of $\lesssim$ 1 ns to $\sim$ 100 ns and repetition rates in excess of 10 kHz (or several megahertz if transmission line reflection techniques are used). Most of the advantages without the difficulties of mechanical and solid state switches can be obtained by using a stream of mercury globules to bridge the gap between the two electrodes which are used to discharge the transmission line into the load or by having a charged mercury globule discharge into the load.

Introduction

A common solution to the problem of generating pulses with nanosecond rise times has been to discharge a transmission line into its characteristic impedance. The method of operation is quite simple and is shown in Figure 1. Initially (t<0), the left piece of coaxial cable is charged to the voltage V (see the top graph). At t = 0, the switch is closed and a voltage pulse of 1/2 V propagates toward the load and another one to the left which partially discharges the initially charged line (see the middle graph). The last pulse reflects from the open circuited left end of the cable and travels to the right (see the bottom graph). This pulse finishes the discharging of the originally charged line and forms the trailing edge of the output pulse. Thus, the output pulse has at most an amplitude of 1/2 V and a duration equal to 2L divided by the wave velocity. The actual output voltage and the rise and fall times of the pulse as well the case of unmatched cables and load will be discussed later.

Historically, mechanical switches with metal contacts can discharge a transmission line into a matched load and produce a pulse with $\lesssim$ 1 ns risetime. However, such a switch has inherent characteristics that limit its performance such as: contact erosion (i.e. short lifetime), slow moving contacts (i.e. low repetition rates), limited travel (i.e. low voltage), and sticking and bouncing contacts (i.e. prefiring and non-uniform voltage pulses). These difficulties have been substantially reduced by using mercury globules as the switching medium.

Mercury wetted reed relays were often used as the switch for discharging the line because of their availability and durability but their low repetition rates ($\gtrsim$ 30 Hz) and voltage ratings ($\sim$ 100 V) are rather low[1]. Triggerable pulsers can be made using avalanche transistors[2,3]. However, they are relatively expensive, hard to find and require 12 transistors in series to produce 1 kV pulses[2]. By using mercury globules as the switching medium, pulsers are obtained with essentially all of the above advantages that can also operate at higher voltages into lower resistance loads at high repitition rates with little switch erosion.

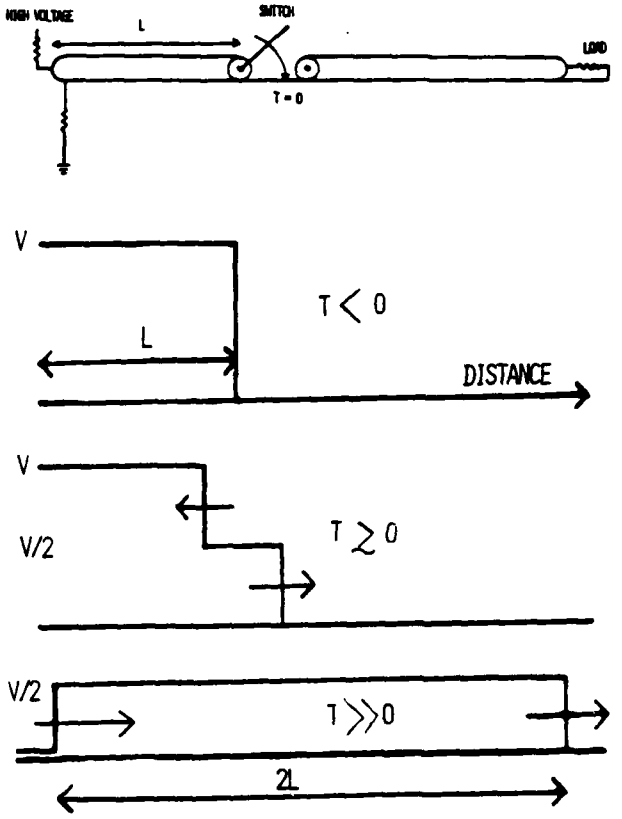


FIGURE 1. Schematic of transmission line pulser and waveforms corresponding to the operation of the pulser.

Subnanosecond pulses can be obtained by making the initially charged line very short[4,5,6,7]. The first pulser referenced uses a hydrogen spark to discharge a stray capacitance of 2 pF to produce 20 to 400 V pulses from a supply of 500 to 2000 V at repetition rates up to 80 kHz.

CH1371-4/78/0000-0163$00.75 © 1978 IEEE

The next two pulsers referenced use a small metal ball or cylinder as the charged line. The ball is electrostatically attached to the charging lead and is then electrostatically repelled toward another lead which is attached to the load, where it discharges. This pulser is designed so that the electrostatic forces are aided by the bouncing of the ball off the surface of each lead. Using nitrogen pressurized to ∿ 25 atmospheres, this bouncing ball generator can produce ∿ 200 ps wide pulses of ∿ 2 kV into a 50 Ohm load with repetition rates of several hundred Hertz. The last pulser uses a metal ball that is alternately rotated past the charging and discharging lead by an insulated paddle. The advantages of this rotating-ball generator is that almost any size ball can be used and that the repetition rate is variable.

Similarly, a charged mercury globule is used to produce subnanosecond pulses. The main advantage of this pulser over a hydrogen discharge and the ball generators is the reduced electrode erosion because a new globule is used everytime and the increased operating voltage because of the velocity with which the globules move. The repitition rate is controlled by the rate at which the mercury globules impinge on the discharge leads. The maximum rate is limited by the velocity, diameter and spacing of the globules in order to insure sufficient insulation for the switch.

Construction of Pulsers

The pulsers that were used can be classified by output pulse characteristics into the three groups.
1) long duration (∿ 100 ns) pulses into a high impedance (50 to 125 Ohms),
2) long duration pulses into a low impedance (1 Ohm), and
3) subnanosecond pulses.
Of all the pulsers that were built only the construction details of the three pulsers that were used to obtain the reported data will be given.

The first pulser uses a ∿ 6 m length of RG-63 B/U coaxial cable as the initially charged line (see Figure 1). This line was discharged into another length of cable terminated in 50 Ohms.

The second pulser used a parallel plate transmission line with a characteristic impedance of 1 Ohm (See Figure 2). The line consisted of 2 strips of aluminum foil each 5 cm wide and 6.3 m long that were separated by 2 layers of (4 mil ≈ 100 μm) polyethylene film. The 1 Ohm load was made of ten 10 Ohm, 2 W carbon resistors in parallel and was located at the end of a 10 cm, 1 Ohm line. In order to reduce the inductance of the load, the loop formed by every other resistor was twisted so that the direction of the magnetic field of each loop was in the opposite direction of the magnetic field of the adjacent loops. To conserve space, the assembly was wound in an evenly spaced helix on an insulated cylinder 33 cm in diameter and 69 cm in length. The pulser was triggered using mercury droplets dropped or injected between the electrodes.

The third type of pulser had a charged, ∿ 2 cm diameter sphere that comes into contact with the center conductor of a piece of 50 Ohm coaxial cable (see Figure 3). Also sketched in this figure are the electric field lines from the sphere to either the outer (ground) or the inner conductor of the terminated, 50 ohm, coaxial cable. In order to obtain the maximum output voltage (1/2 V in Figure 1), it is necessary that the electric field be between the sphere and the outer conductor only. This is because the electric field to the inner conductor represents charges on the inner conductor that are neutralized when the sphere discharges. These neutralized charges can not produce an output pulse. Typically, the magnitude of the output pulse is

∿1/2 V for V $\lesssim$ 100 volts and ∿ 1/5 V for V $\gtrsim$ 1 kV.

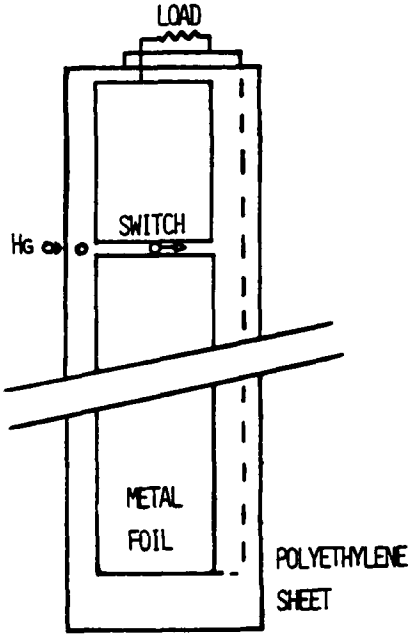


FIGURE 2. One Ohm transmission line pulser.

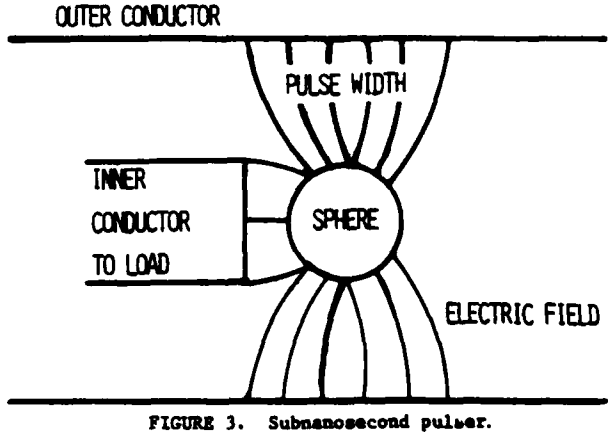


FIGURE 3. Subnanosecond pulser.

As the sphere comes closer to the inner conductor the unwanted charge on the inner conductor can be so large that there is essentially no pulse produced. Thus, it it important for a "spark" to discharge the sphere before these charges build up. This "spark" should not be confused with the gas breakdown that can occur

between the sphere and inner conductor if the charging voltage is too high. The "spark" results in a desireable pulse with a fast risetime. It is unclear why the gas breakdown does not always occur before the sphere comes close enough to spark. This is especially puzzling when one considers the low velocity ($\sim$ 1 m/s) at which the sphere's move. If the unwanted gas breakdown does occur it can be stopped by either increasing the velocity of the sphere or by pressurizing the switch. Typically, mercury globules with a velocity about 1 m/s are sufficient to produce 3 kV pulses and 10 m/s globules for 10 kV pulses.

Results

Typical output pulses of the three pulsers just described are shown, respectively, in Figure 4,5 and 6. The oscilloscope traces were all taken with a Tektronix 519 oscilloscope and wideband attenuators (DC to 10 GHz). The rise and fall times, the charging voltages, the pulse amplitudes and the pulse widths are given in the following table.

Figure Number	Rise Time 10 to 90% (ns)	Charging Voltage V (Volts)	Pulse Amplitude (Volts)	Pulse Width (ns)	Fall Time 10 to 90%
4	$\lesssim$ 1	45	20	125	< 5
5	0.5(10)	1800	400	45	15
6	0.4	16 k	3000	1	0.4

It was found that the location of the power supply connections to the line to be charged is not critical but it is often necessary to have a large resistor in each lead of the power supply as close as possible to the line in order to obtain a zero level following the pulse. A better but more difficult way to accomplish this is to use optical or mechanical techniques to electrically charge the line between pulses.

For the longer transmission lines the pulse length is just twice the length of the charged line divided by the propagation velocity. This no longer holds true for the subnanosecond pulsers because of the fringing field between the sphere and the outer conductor (see Figure 3). In this case, the characteristic length of the induced charge on the outer conductor is used instead of the length of charged line for calculating the pulse width.

This was qualitatively demonstrated experimentally by using three different locations of the end of the outer conductor in relation to the ball. In the first location, the outer conductor was two centimeters short of the end of the inner conductor. In the second position, the outer conductor was even with the center of the sphere. In the last location, the outer conductor extended several centimeters beyond the sphere. For the first case, there was no output pulse, because the electric field was small between the sphere and the outer conductors. For the second location, the output pulse was less than the width of the output pulse corresponding to the last location, because the width of the fringing electric field region (to the outer conductor) was less in the former than the latter.

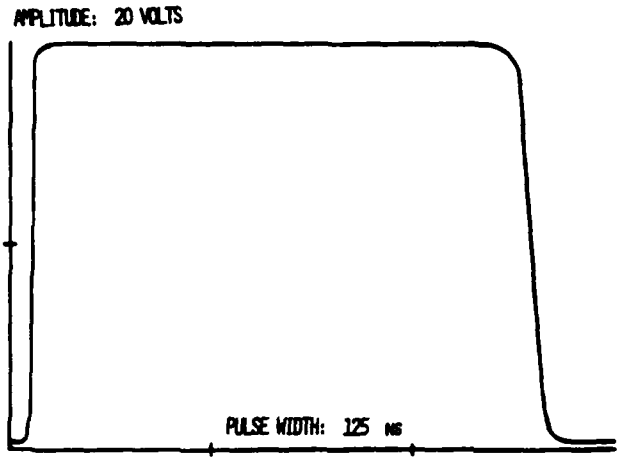


FIGURE 4. Oscilloscope trace of output pulse from RG-63 B/U pulser.

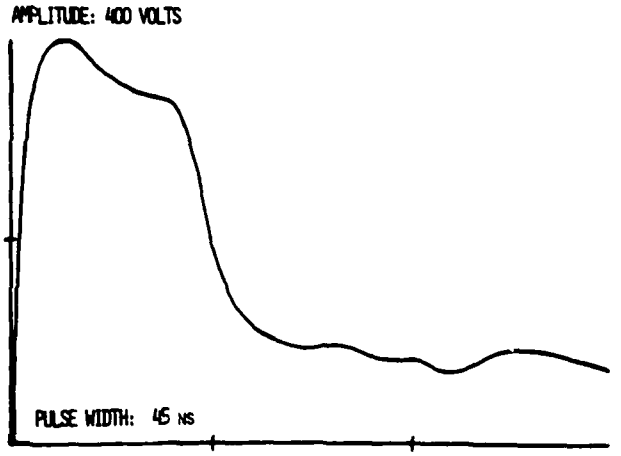


FIGURE 5. Oscilloscope trace of output pulse from the one Ohm pulser.

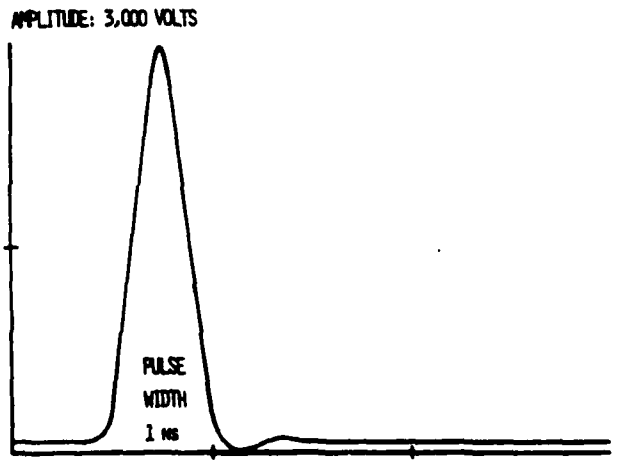


FIGURE 6. Oscilloscope trace of output pulse from the subnanosecond pulser.

The fall times should be as short as the rise time but can be much longer if the load is not matched to the cable. An example of this can be seen in Figure 5. The unmatched load was also responsible for the overshoot in Figure 5 and resulted in the two values given in the table for the risetime of this pulser. The 0.5 ns risetime was for the main pulser, without overshoot, and the 10 ns value includes the effect of the overshoot. Thus, it should also be possible to tailor the waveform of the pulse by suitably designed mismatching. For example, the load was removed from the coaxial pulser used for Figure 4. This resulted in a pulse repitition rate of 13 MHz.

Conclusion

The transmission line pulsers described in this paper produce up to 10 kV pulses into 1 to 100 Ohm loads with rise times of 1/2 to 1 ns, durations of $\lesssim$ 1 ns to $\sim$ 100 ns and repetition rates in excess of 10 kHz (or several megahertz if transmission line reflection techniques are used). These pulsers use a stream of mercury globules to the gap between the two electrodes which are used to discharge the transmission line into the load or by having a charged mercury globule discharge into the load.

References

1 William P. Robbins, Robert M. Lantz, and Betsy Ancker-Johnson, "Nanosecond Risetime, High Power, Variable Delay Double Pulser with Application to Electron-Hole Plasmas", Boeing Scientific Research Laboratories Document D1-82-0628, August 1967

2 Arvid Lundy, Joseph R. Parker, James S. Lumsford, and A. Don Martin, "Avalanche Transistor Pulser for Fast-Gated Operation of Microchannel Plate Image-Intensifiers", IEEE Trans. on Nuclear Science NS-25, No. 1, pp 591-597, February 1978.

3 Branko Leskovar and C. C. Lo, "Time Resolution Performance Studies of Contemporary High Speed Photomultipliers", IEEE Trans. on Nuclear Science, NS-25, No. 1, pp 582-590, February 1978.

4 H. S. Caplan, and D. T. Stewart, "Simple Millimicrosecond Pulse Generator", Jour. of Scientific Instruments, Vol. 38, pp 133, April 1961.

5 J. B. Gunn, "Bouncing-Ball Pulse Generator", Electronics Letters, Vol. 2, No. 5, pp 172-173, May 1966

6 E. Kunhardt, J. Tardiff and B-R Cheo, "The Bouncing Conductor Generator", Proc. International Pulsed Power Conference, paper VIIID7 pp 1-5, November 9, 10 & 11, 1976.

7 E. Kunhardt and R. Dollinger, "Rotating Ball Generator", Rev. Sci. Instrum, Vol. 48, No. 12, pp 1676-1677, December 1977.

TIME RESOLVED RESISTANCE DURING SPARK GAP BREAKDOWN

William K. Cary, Jr.
John A. Mazzie
Naval Surface Weapons Center
Dahlgren, Virginia 22448

Summary

The breakdown voltage and the time derivative of the current through a spark gap terminating a transmission line were measured as a function of 4 gas species, 3 gap pressures and 2 gap spacings. From these measurements, the time varying channel resistance, the power, and the energy dissipated in the discharge can be determined for the first 1500 ps of breakdown.

Data were obtained with a 74 cm long transmission line, open at the charging end, and terminated by a spark gap at the other end. The line was pulse charged with a 2 microsecond risetime pulse having a maximum voltage of 3kV. The breakdown voltage was determined by monitoring the charge voltage waveform while a di/dt probe close to the spark gap provided a sampling oscilloscope with the other desired signal. The latter waveform was then digitized and the data reconstructed using Fourier techniques on a computer to account for the frequency response of the required signal delay line.

Introduction

The mathematical theory for the underdamped response of an RLC circuit was first advanced by Lord Kelvin in 1853[1]. It neglects the resistance of the spark compared to the load, and predicts a logarithmic decrement in which the ratio of the amplitudes of consecutive oscillations is a constant. In 1914 John Stone[2] pointed out that the energy transfer in a high frequency discharge is less than a low frequency discharge because the capacitance used is much smaller. He argued, therefore, that as one goes to higher and higher frequency oscillations, the resistance of the spark should become more and more important in the behavior of the circuit. To illustrate the point, he assumed the resistance of the arc inversely proportional to the amplitude of the oscillatory current, and showed that this led to a linear rather than logarithmic decay.

Typical LC generators capable of producing a transient discharge ringing at 200 MHz have characteristic impedances of 1 to 5 ohms, and a time to quarter cycle of 1.25ns. With limited energy storage, efficient operation would therefore require the resistance of the spark to fall to a value less than the characteristic impedance on a time scale short compared to 1.25ns. But except for the pioneering work of Sorensen and Ristic[3] who investigated nitrogen and helium, there is a dearth of experimental data on the resistive phase of a gaseous discharge during breakdown. We have therefore built on their work to measure time resolved resistances for a number of other gases during breakdown, and this paper reports on those experiments.

Experimental Methodology

Setup

Data were obtained with a 74cm long transmission line open at the charging end and terminated by a spark gap at the other end. The line was pulse charged with a 2 microsecond risetime pulse having a maximum voltage of 3kV. The breakdown voltage was determined by monitoring the charge voltage waveform, while a di/dt probe close to the spark gap provided a sampling oscilloscope with the other desired signal. The latter waveform was then digitized and the data reconstructed using Fourier techniques on a computer to account for the frequency response of the required signal delay line.

A drawing of the transmission line terminated with the spark gap is shown in Figure 1. Castall 300 was employed as the dielectric material. A two component ceramic epoxy resin with very low shrinkage upon curing, it possesses both a high dielectric strength and dielectric constant.

The dielectric was poured in place between the copper pipe and the brass electrode, the latter being centered by a mold at the gap end. This mold also served to offset the electrode (1mm) and to shape the dielectric in the gap area. When cured, a gas tight seal was obtained. Because the other electrode was adjustable, a means of shorting it to the housing through a low inductance, low resistance path was required. This was obtained by using a ring of copper braid with a brass foil insert as shown in Figure 1.

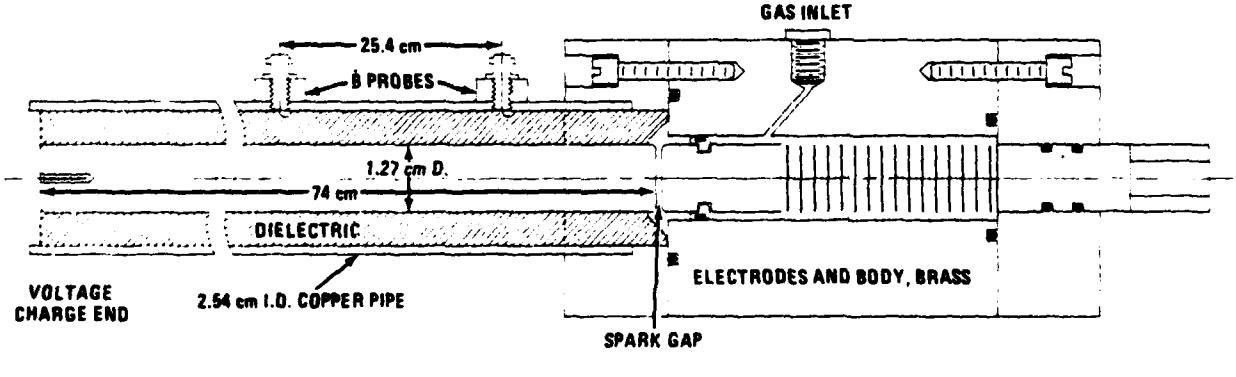


FIGURE 1. Transmission line terminated by spark gap.

U.S. GOVERNMENT WORK NOT PROTECTED BY U.S. COPYRIGHT.

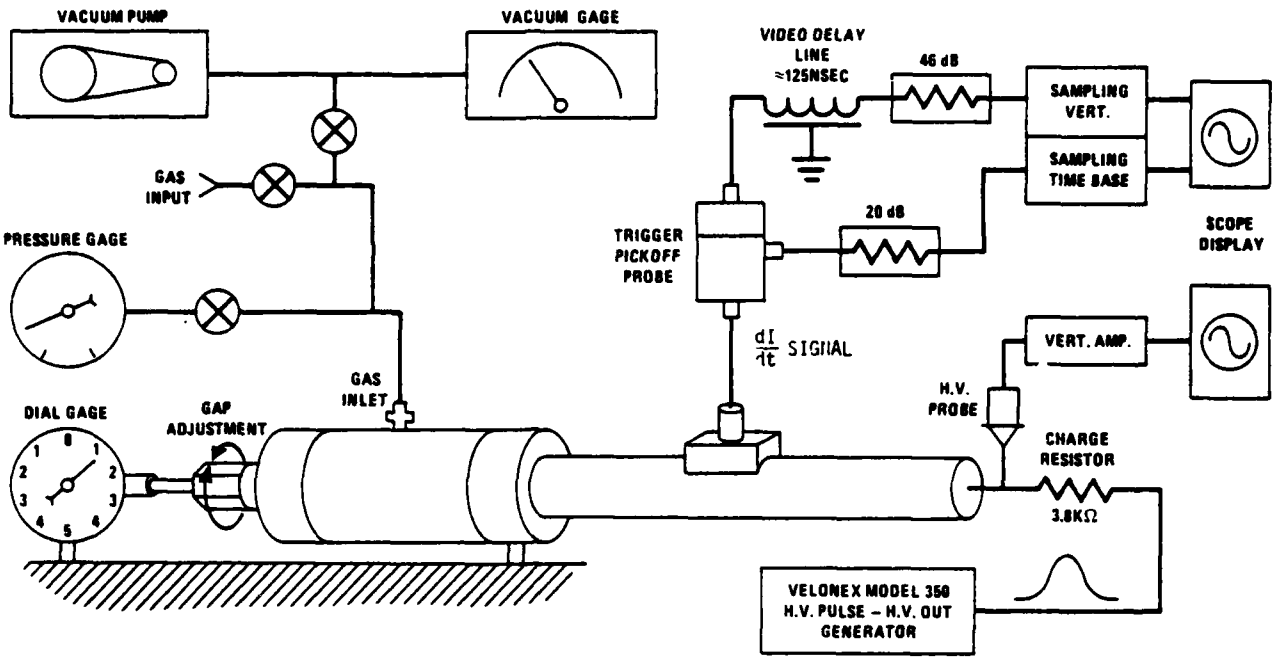


FIGURE 2. Experimental Set-Up.

Brass was chosen as the electrode material because it is commonly used in spark gaps and the experimental results will then be readily available in an appropriate form for spark gap designs.

Figure 2 shows the experimental setup. The transmission line is charged through a resistor with a voltage pulse from a high voltage pulse generator. The charging voltage is monitored with a Tektronix P6015 high voltage probe. When the spark gap at the other end reaches breakdown voltage, typically 2 microseconds after the start of the charge pulse, a di/dt wave is launched towards the $\dot{B}$ probe from the gap.

The output of this probe is useful only for about 4.8 ns, which is the one way transit time of the line. To display this $\dot{B}$ signal, it is first used to trigger a Tektronix 7T11 sampling time base, and subsequently delayed by 32 M of cable (so the scope is on) before reaching a Tektronix 7S11 sampling vertical amplifier. A 25 ps Tektronix S-4 sampling head used in the vertical channel provided the risetime resolution. The pulse generator is necessary to provide a fixed repetition rate which allows relaxation of the gap so the amplitude variations (jitter) of the displayed signal are a minimum. This repetition rate was 500 hertz.

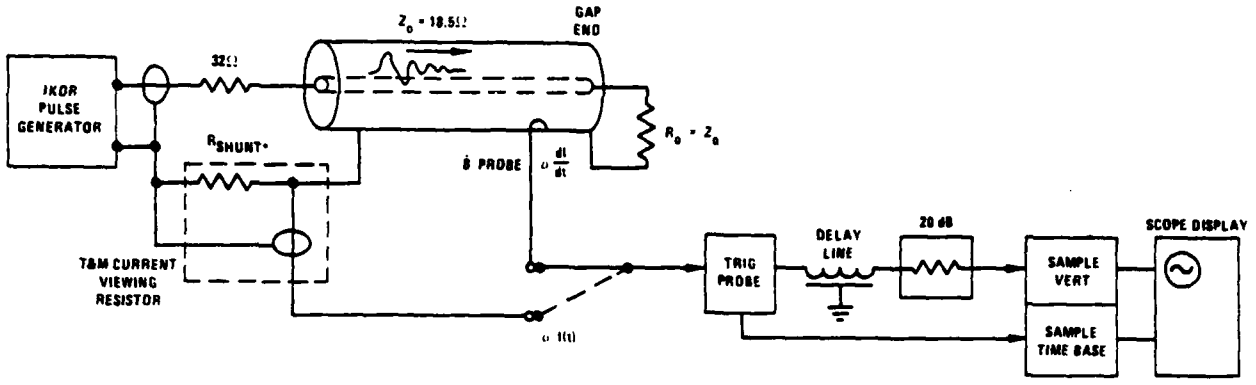
The propagation velocity in the transmission line was measured by injecting a voltage impulse from an Ikor impulse generator and noting the time required for the impulse to pass between the two $\dot{B}$ probes. The Ikor generator impulse has a frequency content similar to the experimental data, and in fact, a similar waveform. This velocity was determined to be 44.6% the velocity of light in vacuum, which yielded a relative dielectric constant of 5.03, as compared to a manufacturer's specification of 6.0 @ 100 KHz. The velocity and the physical dimensions of the transmission line give a characteristic impedance of 18.53 ohms for the frequencies of interest and a line capacitance of 286pF. The gap capacitance as a function of gap setting was determined by measuring the differential capacitance with an impedance bridge.

Figure 3 shows the setup used to determine the $\dot{B}$ probe constant k, where:

$V_{PROBE}(t) = k \frac{dI}{dt}$. Again, an Ikor pulse generator impedance matched to the terminated transmission line provided a $\frac{dI}{dt}$ signal to the probe, while the actual transmission line current was determined with a 300 ps risetime coaxial current viewing resistor. Knowing I and integrating V, the ratio of the two yielded a k value of 2.13×10^{-10} ohm-seconds for the approximately 3mm diameter semicircular probe. With these parameters known (k, Z_0, C, V_{break}), the probe signal $V_{probe}(t)$ measured in a given breakdown allows determination of the time dependent channel resistance via the equation[3]

$$R(t) = \frac{V_{brk}\, k - Z_0 \int_0^t V_p(t)\, dt}{C\, Z_0\, V_p(t) + \int_0^t V_p(t)\, dt} \quad . \qquad (1)$$

Because the probe signal is so important, and because that signal is delayed by 32 M of cable which acts as a low pass filter, the attenuation as a function of frequency of both this cable and its ancillary cables and connectors was measured using standard microwave techniques. As described later, this attenuation was then used in a computer program to correct the probe signal for its frequency dependence. Measurements also showed there were no dispersive effects from 100 MHz to 2.5 GHz, beyond which the CW phase measurement became difficult. The manufacturer claims negligible dispersion thru 9 GHz.



*WHEN Ḃ PROBE OUTPUT WAS MEASURED, R_{SHUNT} WAS SHORTED

FIGURE 3. Determination of Ḃ probe constant.

Procedure

The spark gap was conditioned for 3 hours at approximately 1 KHz with a 2 mil gap filled with nitrogen at 38 psig. Strict gas tight integrity was maintained throughout the gas handling system. Before and after a run with a given gap pressure, spacing, or gap species, a vacuum of 20 millitorr was pulled on the system, and repeated flushing were performed when switching gases. The narrow gap spacings used for this experiment, 1 and 3 mils were chosen because of power supply voltage limitations. For valid results, these spacings required accurate adjustment. This was done to $\pm$3μm using a dial guage on the adjustable electrode with the gap pressurized to the pressure of interest. The closed gap zero from which the distance measurement was made was determined by monitoring the charging end voltage when a pulse was applied. Repeated excursions about this zero point showed some slight hysteresis on the order of $\pm$2μm. The dial guage zero thus set, the gap was opened to the desired setting, and the H. V. pulse generator output set such that breakdown occurred typically at the 2 microsecond point on the charge curve. After the gap parameters stabilized (about 3 minutes), voltage and Ḃ probe readings were taken. Figure 4 shows a Ḃ probe signal as seen by the sampling scope for nitrogen gas at 50 psig and a 3 mil gap.



FIGURE 4. Ḃ probe signal; nitrogen gas, 3 mil gap, 50 psig.

Data Reduction

The software schematic in figure 5 shows those steps used to process the experimental data of which the previous figure is typical. After photographic enlargement of the oscilloscope trace to 8x10 inch size, its information content is entered into the computer program by manually digitizing closely spaced sequential points along the wavefrom to produce an ordered set of digital x, y coordinates. Figure 6 shows a data picture with significant amplitude jitter which had to be manually smoothed so it could be entered for data reduction.

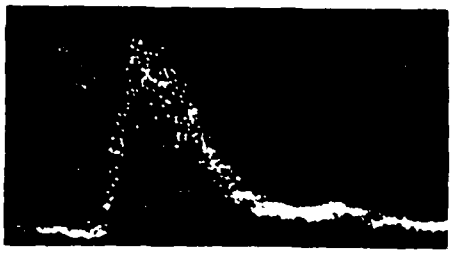


FIGURE 6. Ḃ probe signal, Hydrogen gas, 3 mil gap, .5 psig.

To sample the digitized data at precise intervals for Fourier transforming, a sliding linear averaging and interpolation algorithm was written. It determines the time location of each sampled data point and then determines the height of each point by looking at the two adjacent existing data points on each side. By projecting straight lines from a combination of these points through the sampled point time coordinate and taking an average, the sampled point height coordinate is calculated.

At this stage, the sampled data represents the measured Ḃ probe signal. To remove the delay line effects, the measured probe signal is FFT'D, combined with the time invariant delay line characteristics to remove the line's frequency dependent attenuation effects, and then inverse transformed to reconstruct a corrected Ḃ probe signal.

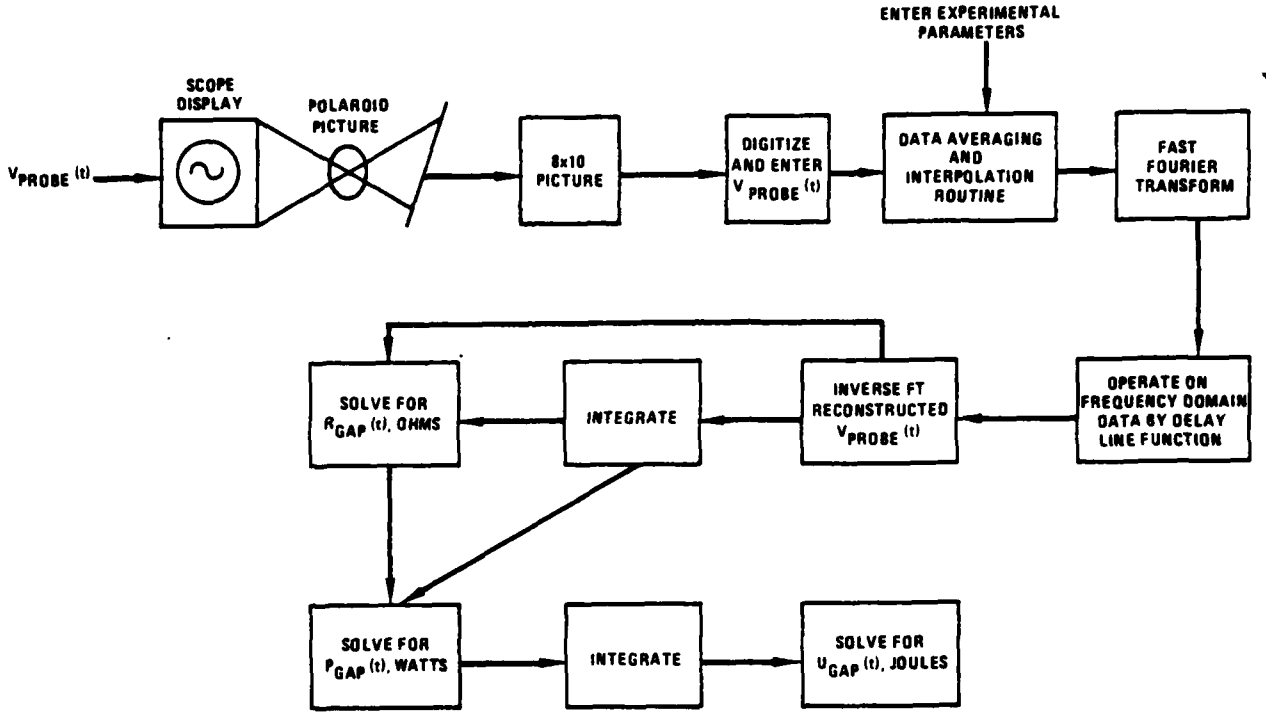


FIGURE 5. Software Schematic.

To avoid aliasing, the Nyquist frequency of 10 GHz was chosen, mandating a sampling interval of 50 ps. A total of sixty-four sampling points was chosen to give sufficient data sampling and accuracy without an excessive number of data points to be plotted. Frequency leakage effects, caused by non-zero data at the start and end of the sampling period[4] were eliminated by the manner in which the experimental data was entered, namely zero fill.

With the measured data FFT'D, the real and imaginary amplitude components were next corrected by accentuating them the same amount they were originally attenuated at each frequency. From 100 MHz to 4.5 GHz, that attenuation was basically linear with frequency and the VSWR was low, so that the correction was essentially a real function. Above 4.5 GHz, the VSWR was high and the attenuation became much higher.

Since the inverse FFT operation is of the same form as the forward one[5], the same FFT subroutine was then used to construct a resultant time ordered $\vec{B}$ waveform from its corrected frequency ordered components. Using the trapezoidal rule, the reconstructed $\vec{B}$ signal is next integrated and equation (1) subsequently evaluated to determine the time dependent spark gap resistance.

Results

The results presented are from an ongoing research program. There is a general agreement with other published work, but there is also some deviations. These are now being investigated. Time resolved resistances during the first 1500 ps of breakdown were determined as a function of 4 gas species, 3 gas pressures, p, and 2 gap spacings, d. The gases were nitrogen, argon, hydrogen and a mixture of 95% argon 5% hydrogen. For each of the gases, measurements were made (i) with the gap spacing set to 1 mil and to 3 mils, and (ii) with the gap pressurized to .5, 25, and 50 psig. Resultant pd's in the gap ranged from 2 to 25 torr-cm, while the electric fields, E, ranged from 158 to 669 kV/cm, and E/p varied from 0.05 to 0.85 kV/cm torr.

The measurements in nitrogen were made to check agreement with the data of Sorensen and Ristic[3], but an important difference was evident between the two sets of data. Their results, published for a 3.94 mil gap pressurized to 94 psi in which $\frac{E}{p} = 0.08$ kV/cm-torr show a time dependence which is inversely proportional to time cubed. Limitations of our high voltage pulse generator precluded breaking down such a gap so pressurized, and we were forced to work with a 3 mil gap pressurized to 50 psig, for which the corresponding $\frac{E}{p}$ number was 0.092 kV/cm-torr. While these $\frac{E}{p}$ numbers are comparable, our gaps withstood a slightly higher field.

If the resistance R during breakdown varies with the time t as Rat^{-m}, then a plot of the data on log paper should produce a straight line with a slope equal to the exponent m, or a series of straight line segments having differing slopes which are indicative of changes in that exponent corresponding to changes in the time dependence. On such a plot, the data of Sorensen and Ristic would appear as a straigt line with a slope of 3 over the time scale of interest. For comparison, our results in nitrogen are shown in Figure 7.

The topmost of two curves in that figure correspond to .5 psig of nitrogen in a 1 mil gap (dots) and in a 3 mil gap (squares). The lower two curves in that same figure correspond to 50 psig of nitrogen in the 1 mil gap and the 3 mil gap. The curves suggest that the higher pressure discharges approach the milliohm levels more rapidly than the lower pressure discharges. The curves also indicate that a number of different time dependences are operative in the discharge over the time scale shown. It is not known why this result differs from that of Sorensen and Ristic below 800 ps, but the agreement afterwards suggests at least some degree of consistency. The non-identical pressure and spacing, however, hinder direct comparison.

New data were acquired in other gases. For clarity a number of curves which would otherwise overlap have been omitted. Figure 8 shows the resistance versus time curves for Argon in a 1 mil gap at 25 psig and in a 3 mil gap at 1 psig and 50 psig. The corresponding $\frac{E}{p}$ value is 0.534 kV/cm torr. For a given pressure and gap spacing, it would appear that argon approaches the milliohm level more rapidly than nitrogen.

The resistance curves for hydrogen in a 1 mil gap pressurized to 1/2 psig and in a 3 mil gap pressured to 25 psig are shown in figure 9. The corresponding $\frac{E}{p}$ values are 0.826 kV/cm-torr and 0.076 kV/cm-torr, respectively. Figure 10 shows the resistance curves when argon is mixed with hydrogen in a 95%/5% ratio. The curve for a 3 mil gap at 25 psig (not show) is virtually coincident with the lower curve.

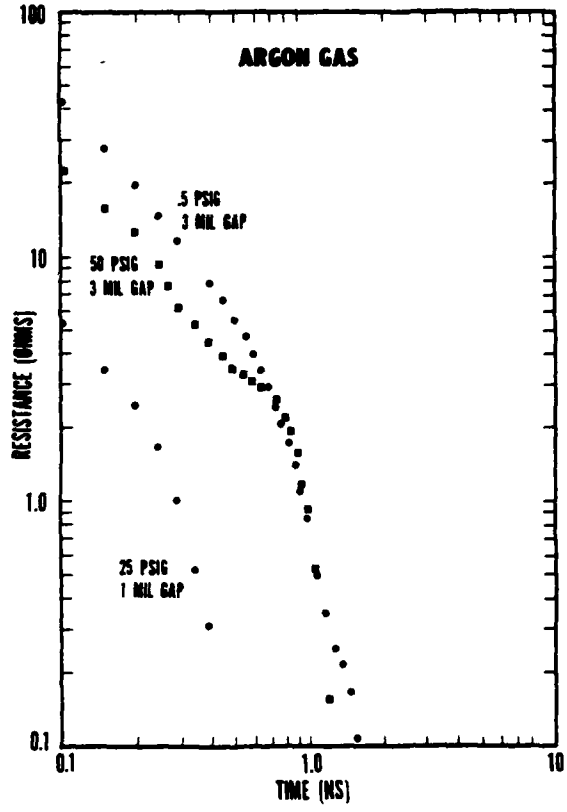


FIGURE 8.

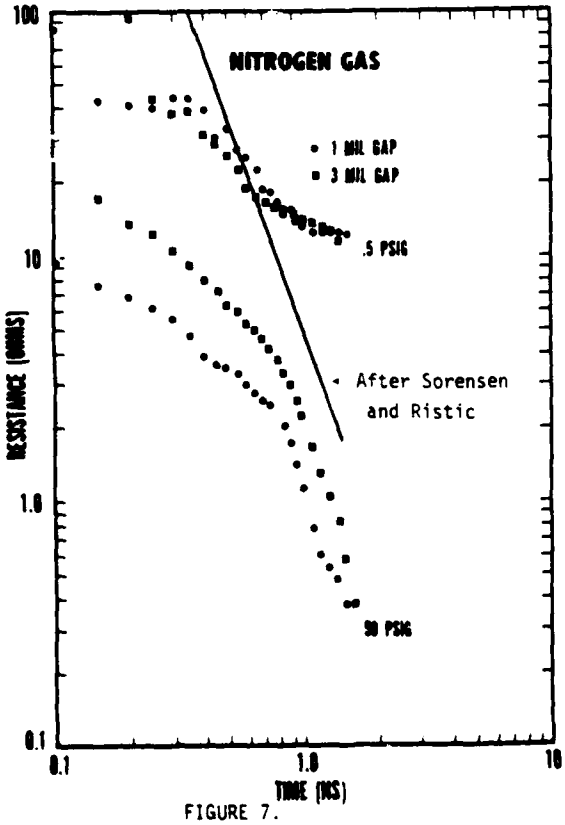


FIGURE 7.

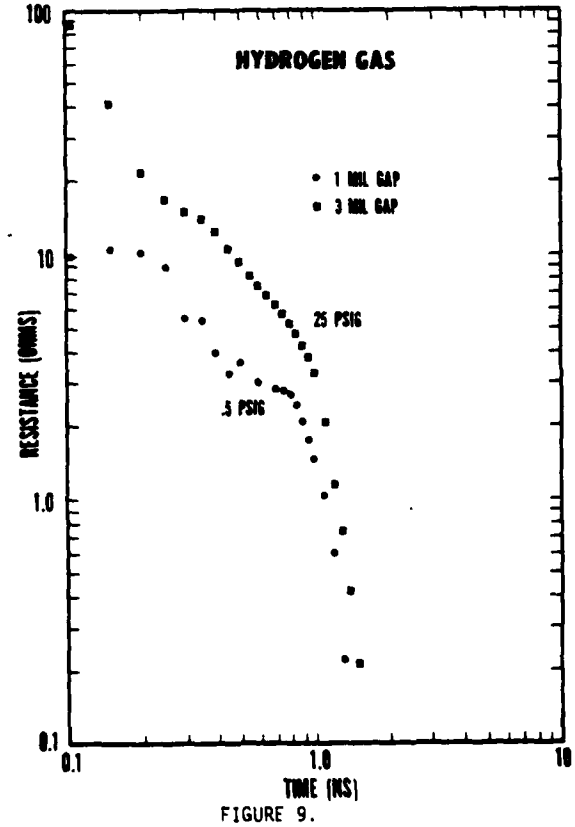


FIGURE 9.

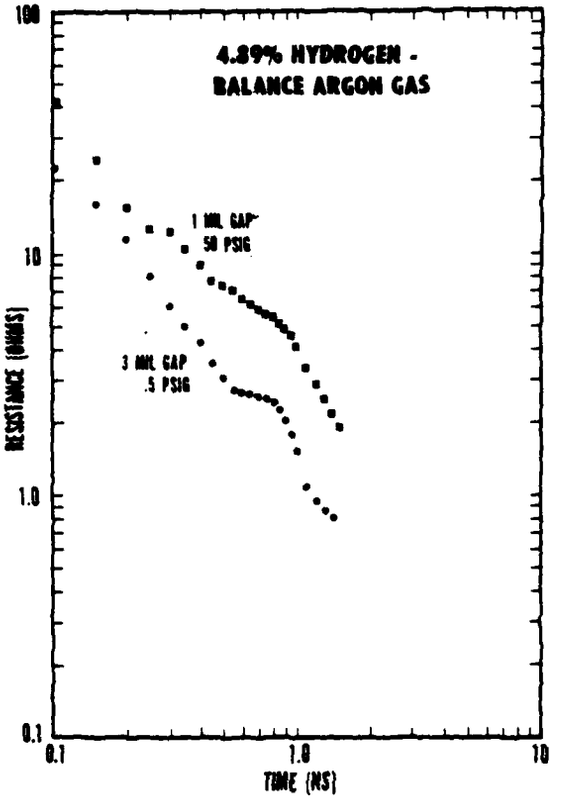


FIGURE 10.

References

1. Philosphy Magazine, series 4, Vol. V, p. 393.
2. Proc. Inst. Radio Engr., Vol. 2, No. 4, p. 30.
3. J. Appl. Phy., Vol. 48, No. 1, p. 114.
4. Brigham, E. O., The Fast Fourier Transform, Section 9-5, p. 140; Prentice-Hall, 1974.
5. Ibid, section 10-10, p. 163.

HIGH POWER SWITCHING CAPABILITIES

T. Burkes, M. Kristiansen, W. Portnoy and M. Hagler

Department of Electrical Engineering
Texas Tech University
Lubbock, Texas 79409

Summary

Various high power switches are compared with regard to their capabilities in terms of maximum hold-off voltage, peak current, pulse repetition rate, current risetime, coulomb handling capability and lifetime. The specific switches considered are thyratrons, silicon controlled rectifiers (SCR's), vacuum tubes, ignitrons and spark gaps. Information for this study was obtained from the open literature.

Emphasis is placed on a switches capability to handle rated voltage and current simultaneously. The resulting repetition rate and etc. imposed by operation at maximum voltage and current forms the basis for comparison. If incomplete information was available to allow calculation of the comparison parameters, those parameters were simply deleted. In some cases, data describing an experiment or test was used. The accumulated performance of the particular switch under test is utilized even though the life data may be incomplete.

The results indicate spark gaps, an expected, are capable of greater voltage and current than other types. Solid state devices have more coulomb handling capability because of their high average current capability and long life expectancy. Vacuum tubes and thyratrons also move large amounts of charge throughout their limited life but at high currents, high rates of rise and significant pulse repetition rates. The capabilities of ignitrons in short pulse service is not well established.

Introduction

New developments in high-technology areas, such as lasers and fusion, often require electrical switching capabilities beyond what are currently available. Each new requirement may result in new switch studies and development programs devoted to a particular application and consequently to a narrow region in parameter space. Few studies however, have considered broad areas of high power switching and the general comparison of various switching technologies. This paper is a partial summary of a study effort currently under way at Texas Tech University to define and evaluate the state-of-the-art for high power switching in general.

The types of switches described here are limited primarily to thyratrons, spark gaps, ignitrons and silicon controlled rectifiers (SCR's). (Other switching concepts, not as mature as the aforementioned ones, will be discussed in a later, more complete report.) The emphasis is on "closing" rather than "opening" switches. The vacuum tube is the only concept discussed which clearly qualifies as an "opening" switch. Also, operation under "square pulse" conditions is utilized where data is available. Data on operation as phase control devices are not included in this evaluation.

A meaningful and fair comparison of competing switch technologies is difficult. The meaning of the expression "the state-of-the-art" varies with the user. The achievement of a particular voltage and current combination may serve to define the state-of-the-art if this happens to be the first time this particular data point is achieved. However, for mature switching technologies, the extension of a particular parameter(s) must be balanced against others so that a certain overall level of performance is achieved. For instance, in thyratrons, the switch parameters (peak current, peak voltage, repetition rate, etc.) are balanced so that a certain life expectancy can be achieved. Thus, it is necessary to choose a consistent set of operating conditions (where possible) in order to compare the date. The rational used to obtain the data in this report is described in the next section.

Only the information found in the open literature and manufacturers' data sheets is utilized (except in some spark gap cases) in the present report even though the authors are aware of experiments in various laboratories that have not yet been published. Although, it is unlikely that all available literature data has been found, sufficient information seems to have been gathered to define the state-of-the-art in high power switching in a reasonable way.

Data Base Rationale

The set of parameters chosen for evaluation here are maximum rated voltage, peak repetitive current, current rate of rise (di/dt), pulse repetition rate, Coulomb transfer per shot, total number of shots in expected life, and the total Coulomb transfer throughout the expected life. The data used in this evaluation is presented in Tables 1-5. Each entry represents a particular device performance under a specitic set of operating conditions. Note that not all parameters were available for each entry.

Because switches can be operated to enhance one particular parameter at the expense of others, it seems reasonable to choose a common set of parameters and operating conditions were possible for all switch types so that easy comparisons can be made. For instance, life expectancy in spark gaps and ignitrons is usually stated as a number of operations or shots under some set of conditions (voltage hold-off voltage, peak current, and Coulomb transfer) whereas the life of vacuum tubes and thyratrons is usually expressed as a number of operating hours (usually 10^4 hours) and the life of solid state devices in years. In all these devices the life expectancy can be increased by reduction of the operating stress, i.e., lower voltage and current and Coulomb transfer or pulse width, as well as a reduced rate of current rise. This is generally true because of lower energy dissipation in the switch.

For thyratrons, the set of operational conditions are simultaneous operation at rated

CH1371-4/78/0000-0173$00.75 ©1978 IEEE

voltage and pulsed current, operation at rated average current and pulse repetition rate determined by the anode heating factor and a 10,000 hour life. From this set of data it is relatively easy to calculate the required set of parameters (Table I). In some cases, it was found that this procedure resulted in inconsistencies with other operating parameters such as the rms current, etc. However, sufficient consistent data were found for the present purposes.

Vacuum tubes are somewhat more difficult to evaluate. Little information was, for instance, found on di/dt. This is because di/dt is a function of the drive power one is willing to invest for a particular tube. A pulse width limitation was stated in several cases. The data shown in Table II were derived by postulating operation at rated voltage and current, maximum pulse width and rated anode dissipation. A 10,000 hour life was assumed. Some of the tubes are developmental types and only incomplete data were available (Table II).

Ignitrons are mostly rated for crowbar and ringing capacitor discharge service. A very limited life results from such operation (1000's of shots) and manufacturer's data tend to be very conservative. It is well known that the ignitron life in rectifier service is many years. However, this type of operation is not within the present meaning of "high power switching." Some data are available on operation of ignitrons in high repetition rate, square pulse service and these data were included. Otherwise, the data supplied by manufacturers on the crowbar or capacitor discharge operation form the data base (Table I).

Spark gap data (Table IV) are particularly difficult to compare since most spark gaps are individually designed and built by the user for a particular application. As a result the gaps are also usually tested in a limited parameter range for the given application. Many lifetests for instance, have been terminated before the device actually failed because there was no need at the time for longer life or because there was no funding for continuing the test. As a result it is felt that the indicated lifetimes for spark gaps are quite conservative. The few manufacturer's specifications that exist for spark gaps are generally uninteresting in that they usually describe rather low performance devices. The information used in this paper was gleaned mostly from conference papers and technical reports supplemented by interviews were obvious holes in the data base existed.

The SCR data (Table V) were obtained from manufacturers' data sheets for high power inverters; phase control devices are not included. V_T represents the repetitive forward or reverse blocking voltage. The peak current, I_p, is the maximum peak current obtained for a trapezoidal pulse with a leading edge ramp of 100 A/usec. The maximum values of dI/dt (shown in parenthesis in Table V) for these inverters are based on dissipation constraints, and, except for the lowest value, which was obtained repetitively (a European test condition), are non-repetitive values. The remaining data were obtained from the open literature. V_T for the RSR is the forward breakover voltage; the values for the LASS devices are conventional SCR blocking voltages. Pulse shapes for these data were more or less rectangular. dI/dt for the RSR was measured repetitively, and is related to the turn-on efficiency of the device. The dI/dt value for the LASS devices were obtained from pulse risetimes and peak currents. No lifetime data were available for any of the tabulated devices, but it is to be expected that they will have the very long lifetimes (in the order of 20 years) generally associated with semiconductor power devices.

Results

Figure 1 shows data from Tables I-V on rated hold-off voltage versus peak forward current at that voltage. As expected the maximum values occur for spark gaps. It also shows that spark gaps ignitron and SCR's tend to be lower impedance devices than vacuum tubes and most thyratrons. Figure 2 shows the total Coulomb transfer through the switch versus life time expressed as the total number of shots obtainable. The best device in this regard is the SCR but little data are available and the expected life is so great in comparison to the other devices as to be off scale in Fig. 2. After SCR's come vacuum tubes in their ability to transport charge. Thyratrons can be expected to transport 10^8 to 10^9 total Coulombs with greater than 10^{10} shots. Spark gaps and ignitrons are next. Ignitrons are not usually operated in a manner similar to thyratrons but when they are, respectable performance is obtained. Notice that, as expected, devices with longer lifetimes transfer the most total change.

The total Coulomb transfer capability shown in Fig. 2 gives, of course, no inclination of the rate of charge transfer. Thus, the charge transfer per pulse versus pulse repetition rate is shown in Figure 3 and the peak repetitive current versus repetition rate is shown in Fig. 4. The general fall-off in charge transfer per pulse at high rep-rates results from device heating limitations and for the reduced pulse width possible at high rep-rates. Figure 4 would be identical to Fig. 3 if the pulse lengths were the same for all devices. Notice that vacuum tubes are capable of considerable Coulomb transfer per pulse but the repetition rate is low (Fig. 2) and a low peak current (Fig. 3) implies long pulse operation. By reducing the pulse width or Coul/shot much higher repetition rates can be achieved.

Figure 3 shows only a modest Coulomb/shot capability for thyratrons because operation at maximum current (Fig. 4) is assumed. Reduction of the peak current will allow a considerable increase in pulse width allowing for a much greater Coulomb/shot capability.

The di/dt versus the peak current and maximum hold-off voltage for the various switches are shown in Figs. 5 and 6. The characteristic turn-on time, $\tau = I_p/(dI/dt)$, for the devices described in Fig. 5 generally seems to decrease as the peak current capabilities increases. Although vacuum tubes seem capable of reaching their peak rated current somewhat faster than the other devices, spark gaps show the greatest capability for combined speed and peak current. Little data were found on di/dt capabilities or limitations of ignitrons. Also, the di/dt capabilities of vacuum tubes is a function of the drive capabilities as previously mentioned and little actual data were found.

The di/dt limitation of thyratrons is to a degree, determined by the application. At

high repetition rates and high di/dt operation, considerable tube heating may occur and the life of the tube is thus reduced. However, sufficient data was found to say that reliable operation from 10^4 to 10^5 amperes/microsecond can be expected for most commercially available devices.

Spark gaps have been tested in short-circuit discharges and shown to have extremely high di/dt. Generally, spark gaps can be designed with multichannel discharges to provide such a low inductance that the current risetime is limited by the load rather than the switch itself. Many spark gaps with liquid or solid dielectric media also have spectracular performance characteristics in single shot service but it is difficult to envision how one can extrapolate these parameters to rep-rated service. The data presented here are, therefore, mostly for gas filled gaps except for one vacuum gap listed in Table IV.

Conclusions

This paper presents data for thyratrons, SCR's, vacuum tubes, ignitrons, and spark gaps operating at maximum hold-off voltage and the maximum rated current under that condition. Generally, spark gaps permit larger hold-off voltages and higher peak currents than other devices. Spark gaps, SCR's and ignitrons seem to offer the lowest impedance ($V_{hold\text{-}off}/I_p$). Vacuum tubes, thyratrons and SCR's presently last longer than the other devices and hence provides a larger total Coulomb transfer. Spark gaps and SCR's usually provide the largest charge transfer per pulse for repetition rates greater than 100 per/second while thyratrons seem to offer higher peak currents under these conditions. Vacuum tubes currently have the shortest turn-on time ($\approx I_p/(dI/dt)$). The relative merits of these devices are likely to change as a result of further development in device technology.

Acknowledgement

This work is funded by the Naval Surface Weapons Center/Dahlgren Laboratory, Special Applications Branch, through the Post Doctoral Program at the Air Force Aero Propulsion Laboratory Wright-Patterson AFB.

Bibliography

General:
"Proc. Workshop on Switching Requirements and R&D for Fusion Reactors," EPRI ER-376-SR, July, 1977, M. Kristiansen, editor.

"Proc. 1st. IEEE International Pulsed Power Conf.," Lubbock, Texas, Nov. 1976, (IEEE Conf. Proc. No. 76CH1147-8 REG 5).

Sparkgaps:
"High Power Spark Gap Switch Development," Maxwell Lab. Rept. MLR-484, May 1975 (Final Rept. to AFAPL)

"High Power Spark Gap Optimization," Maxwell Lab. Rept. MLR-670, June 16, 1977 (Final Rept. to NSWC).

"Investigation of the Erosion Phenomenon in High Current, High Pressure Gas Discharges," J. E. Gruber and R. Suess, Proc. 6th Symp. on Fusion Tech, Aachen, FRG., Sept. 1970.

"A 250 Coulomb 40 kV Spark Gap," E. E. Bishop and G. D. Edmonds, Proc. 5th Symp. on Fusion Tech, Oxford, U.K., 1968.

"Arc Voltage of Pulsed High Circuit Spark Gaps," T. E. James and J. L. Browning, Proc IEE Gas Discharge Conf., Sept., 1970.

"Statistical Performance Data for a High Current 60 kV Spark Gap Switch," R. A. Burder and T. E. James, Proc. 7th Symp. on Fusion Technology, Grenoble, Oct., 1970.

"Gas Cooling and Electric Strength Recovery After a Spark Discharge," E. P. Bel'kov, Soviet-Phys.-Tech. Phys., 16, 1321 (1972).

"Multimegavolt Modular Study," J. J. Moriarty, H. I. Milde, J. E. Hipple, RADC-TR-70-107.

"Multichannel Spark-Gap Technology for Staged Theta Pinch Machines," W. H. Borkhagen, et. al.

"Explosive Erosion in stromstarken Funkonentladunge, K. Schonbach, Zeitsch Angew. Phys., 32, 253 (1971)

Ignitrons:
"Professional Electron Tubes," Abridged Data, G.E.C. Electronic Tube Company Limited, 1976/77.

Fred Vorwerk, "Evaluation of the Z-5233 Ignitron," Technical Report. ECOM-2512.

G. Gronner, J. Murray and S. Duritt, "Ignitron Long Pulse Testing," MATT-1104 Jan. 76, Plasma Physics Laboratory, Princeton University.

A. Booth and J. Holliday, "High-Voltage Mercury-Arc Switch for Heavy Current Pulse Duty," Proceedings of IEE, Vol. 110, Nov. 63.

D. Cummings, "Development of Switching Tubes for Controlled Fusion Research," Electrical Engineering, 79, 1960.

H. Knight, L. Herbert and R. Maddison, "The Ignitron As A Switch In High-Voltage Heavy-Current Pulsing Circuits," IEE, April 59.

D. Cummings, "Ignitron Discharge Growth During High Current Pulses," IEEE Transactions on Communication and Electronics, 68, 514 1963.

"Ignitron Excitation Circuits and Their Requirements," G-E Power Tube Department Publication PT-50, Dec. 60.

"Ignitrons, Capacitor Discharge and Crowbar Service," G-E Tube Products Department Publication M-1256, Nov. 74.

E. B. Forsyth, "A General Purpose Hundred Kilojoule Pulser," Proceedings of the Ninth Modulator Symposium, May 66.

J. Romanelli, "Pulse Characteristics of A GL-5630 Ignitron," Proceedings of the Eighth Symposium on Hydrogen Thratrons and Modulators, May 64.

T. F. Turner and H. S. Butler, "Performance of

Ignitrons in Pulse Service," Proceedings of Seventh Symposium on Hydrogen Thyratrons and Modulators,

P. Faugeras, H. Kuhn and J. Zanasco, "Generation of High Current, Long Duration Rectangular Pulses," Conference Record of Eleventh Modulator Symposium, Sept. 73.

"Electronic Control Devices for Industry," National Electronics, Inc., Geneva, Illinois.

Vacuum Tubes:
H. D. Doolittle, H. Langer, J. A. Randmer and B. Singer, "A Sixty-Megawatt Hard-Tube Modulator," Proceedings of Eighth Symposium on Hydrogen Thyratrons and Modulators, May 1964.

L. J. Fox, "Development of a 325-Kilovolt, High-Vacuum Switch Tube," Proceedings of the Eighth Symposium on Hydrogen Thyratrons and Modulators, May 1964.

Philip A. Ingwersen, "A 200-MW Hard-Tube Modulator," Proceedings of the Ninth Modulator Symposium.

George W. Taylor, "Drive Requirements for High-Voltage Low-Grid-Current Tubes," Proceedings of the Ninth Modulator Symposium.

Glenn Grotz, "Design Consideration for 180 KV Floating Deck Modulator," Proceedings of the Ninth Modulator Symposium.

J. J. Tritchler and W. L. Wills, "Development and Test of a 50-Megawatt High-Vacuum Pulse-Modulator Tube, Proceedings of the Tenth Modulator Symposium, May, 1968.

D. H. Preist, "High Voltage Switch Tubes for Neutral Beam Injectors-A New Design Approach," Conference Record of the 12th Modulator Symposium, Feb., 1976.

Rudolf A. Ecken and Leonard Genova, "600 kW Peak High Repetition Rate Hard Tube Modulator," Conference Record of the Eleventh Modular Symposium, Sept., 1973.

R. E. Byram and J. T. Mark, "Long Pulse Switch and Power Amplifier Tubes for Phased Array Radar," Conference Record of Eleventh Modular Symposium Sept., 1973.

Paul Byran and Howard Beard, 4CW 100,000 Tetrode Pulse Tests at RADC, Conference Record of the Eleventh Modular Symposium, Sept., 1973.

Bobby R. Gray, "Long Pulse Switching of High Power Tetrodes," Conference Record of the 12th Modulator Symposium, Feb., 1976.

Thyratron:
Professional Electron Tubes, Abridged Data, G.E.C. Electronic Tube Company Limited, 1976/77.

H. Menown, "Gaseous Switches: The Past and Present State of the Art," Proceedings IEEE International Pulsed Power Conference, Nov. 1976.

Bobby R. Gray, "Evaluation of State-of-the-Art Hydrogen Thyratrons at Extended Ratings, Hqs. Rome Air Development Center, Conference Record of Eleventh Modular Symposium Sept., 1973.

J. Hamilton, D. Turnquist, "Forty Kilovolt Megawatt Average Power Thyratron (MAPS40)," Technical Report ECOM-76-1352-F, U.S. Army Electronics Command, Fort Monmouth, N.J., July 77.

"Hydrogen Thyratron Tubes," Electron Tube Division of ITT, Easton, Pennsylvania.

"Ceramic-Metal Hydrogen Thyratrons," Electro-Optics Division of EG&G, Salem, Mass.

SCR's:
"Advanced Reverse Switching Rectifier Modulator," E. H. Hooper and B. L. Jordan, Air Force Weapons Laboratory Report AFWL-TR-75-100, Kirtland Air Force Base, New Mexico, October, 1975.

"Light Activated Semiconductor Switches," L. R. Lowry and D. J. Page," 1977 NAECON Record.

"Megawatt Nanosecond Switching of High Power Laser Activated Silicon Switches," O. S. Tucker, J. R. Long, U. L. Smith, D. J. Page and J. S. Roberts, 12th Modulator Symposium, New York, February, 1976.

"Silizium-Thyristoren," Siemens Datenbuch, 1967, 77.

"Electronic Control Devices For Industry," National Electronics, Inc., Geneva, Illinois.

G.E. Semiconductor Data, Semiconductor Products Department, Syracuse, N.Y.

Ed. Hooper and B. Jordan, "Advanced Reverse Switching Rectifier Modulator," Final Report, AFWL-TR-75-100, Oct. 75.

TABLE I. Thyratron Data

V_T kV	I_p kA	di/dt A/μs	Q_T Coul	N_T	Q_s Coul/shot	f_r pps
50	80	$2(10^5)$	$9(10^8)$	$1.35(10^{10})$	$6.67(10^{-2})$	375
50	5	10^4	$2.88(10^8)$	$5.76(10^{10})$	$5(10^{-3})$	$1.6(10^3)$
80	12	10^4	$4.32(10^8)$	$1.0(10^{10})$	$2.06(10^{-2})$	291
120	6	10^5	$2.16(10^8)$	$0.7(10^{10})$	$3.0(10^{-2})$	194
160	6	10^5	$2.16(10^8)$	$0.52(10^{10})$	$4.1(10^{-2})$	146
40	10	10^4	$5.4(10^8)$	$1.8(10^{10})$	$3(10^{-2})$	500
25	1	$5(10^3)$	$4.5(10^7)$	$7.2(10^{11})$	$6.2(10^{-5})$	$20(10^3)$
44	44	$2(10^4)$	$2.2(10^6)$	$5(10^6)$	.44	125
44	11	$2(10^4)$	$1.1(10^6)$	$5(10^6)$	.22	250
260	2	10^4				

TABLE II. Vacuum Tube Data

V_T kV	I_p Amp.	di/dt Amp/.5sec.	Q_T Coul	N_T shots	Q_s Coul/shot	f_r pps
40	350	$1.1(10^5)$	$1.44(10^9)$	$4.1(10^{11})$	$3.5(10^{-3})$	$1.14(10^4)$
200	225					
65	800	$1.5(10^5)$	$2.88(10^9)$	$3.6(10^{11})$	$8(10^{-3})$	10^4
75	2 KA	$1.5(10^50$	$7.2(10^8)$	$3.6(10^8)$	2	10
65	1.2KA		$2.6(10^7)$	$2.16(10^5)$	120	.006
320	30					
200	200					
100	90				90	D.C.

TABLE III. Ignitron Data

V_T kV	I_p kA	di/dt A/μs	Q_T Coul.	N_T	Q_s Coul.	f_r pps
25	300		$2(10^5)$	10^3	200	2/min
50	15		$.15(10^5)$	10^3	15	2/min
50	65			10^3		
25	100				400	
75	60				120	
75	150				45	
35	1.1		$1.26(10^6)$	$4.5(10^8)$	$2.78(10^{-3})$	360
30	75		$2.25(10^5)$	$2(10^5)$	11.25	
25	80	200			400	.2
	21	$1.7(10^4)$				
35	7.4		$2.86(10^6)$	$1.3(10^8)$	.0222	60

TABLE IV. Spark Gap Data

V_T kV	I_p kA	di/dt A/us	Q_T Coul.	N_T	Q_s Coul.	f_r pps
120	25	$25(10^3)$	$>.14(10^6)$	$2.6(10^6)$	$53(10^{-3})$	2 - 5
54	1	$200(10^3)$	$>10^3$	$>10^5$	.1	(10^3) *
100	100	$10(10^3)$	$\sim 10^8$	10^6	100	$5(10^3)$ *
90	4.5				$240(10^{-3})$	250 ++
1 MV	500	$5(10^7)$			$50(10^{-3})$	single shot
240	43					**
60	330	(10^9)				
60	140		$4.5(10^4)$	$5(10^3)$	9	
60	60	$2.1(10^4)$	$.7(10^6)$	$2(10^6)$	.35	.1
125	500	$4(10^6)$	$5(10^3)$	$5(10^3)$	1	
60	6				$360(10^{-3})$	250 ++
80					1.2	100 ++
80					.56	200 ++
80	.4				.28	400 ++
80					.24	500 ++
20					.56	500 ++
60	400	$\sim 2(10^5)$	$1.3(10^6)$	$1.6(10^5)$	8	.13
60	10^3				50	
45	400		$\sim 4(10^5)$	$13(10^3)$	30	1/60
40	750			10^3	50	

*(single shot di/dt)
+ vacuum gap with replaceable electrode
** (di/dt and I_p under short ckt conditions)
++ synthetic testing

TABLE V. SCR Data

V_T kV	I_p kA	di/dt A/usec	Q_T Coul	N_T shots	Q_s Coul/shot	f_r pps
1.3	1.8	100(200)			18	50
1.3	10.0	100(800)			0.5	218
2.1	10.0	100(800)			2.1	60
1.2	5.0	2500			0.1	250
2.0	10.00	$1.1x10^6$			0.001	1000
2.0	24.0	$4.0x10^4$			.96	1000

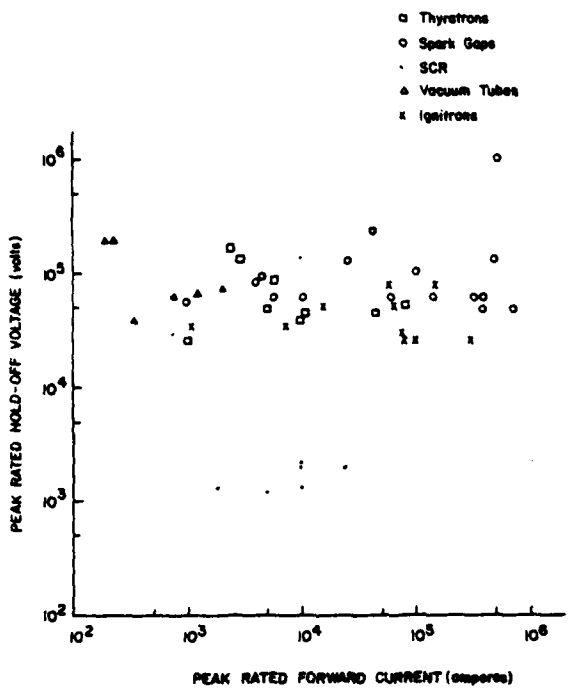


Figure 1. Peak Hold-off Voltage vs Peak Forward Current

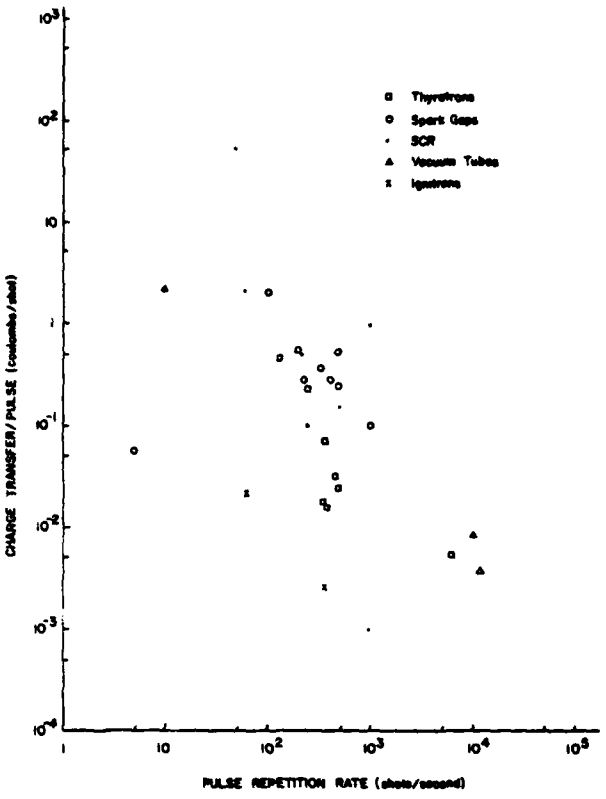


Figure 3. Charge Transfer per Pulse vs Rep-rate

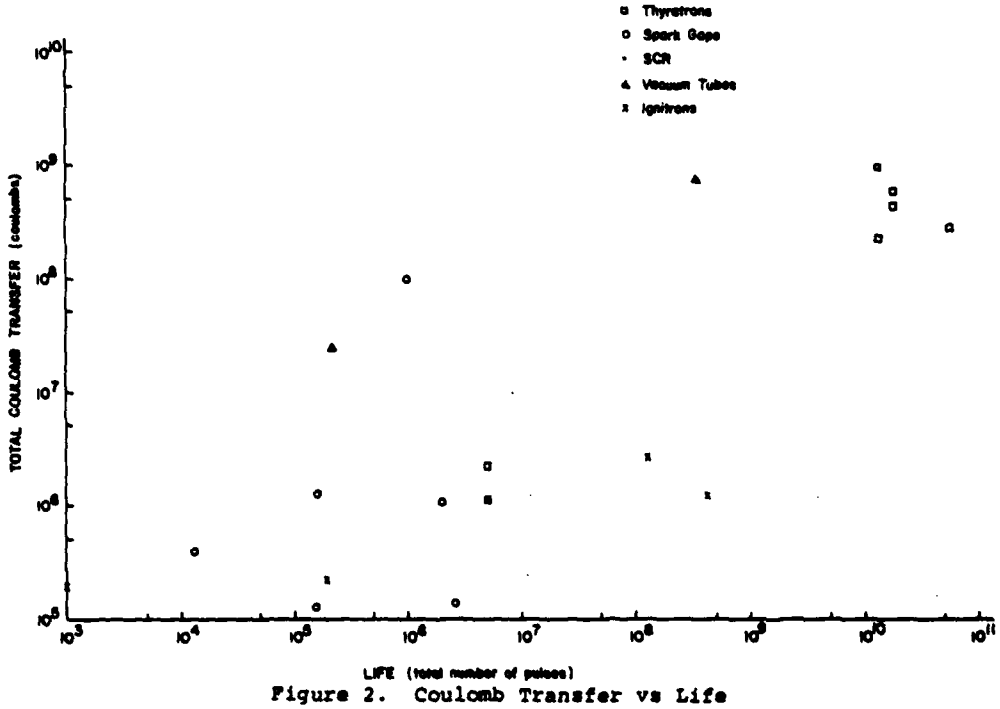


Figure 2. Coulomb Transfer vs Life

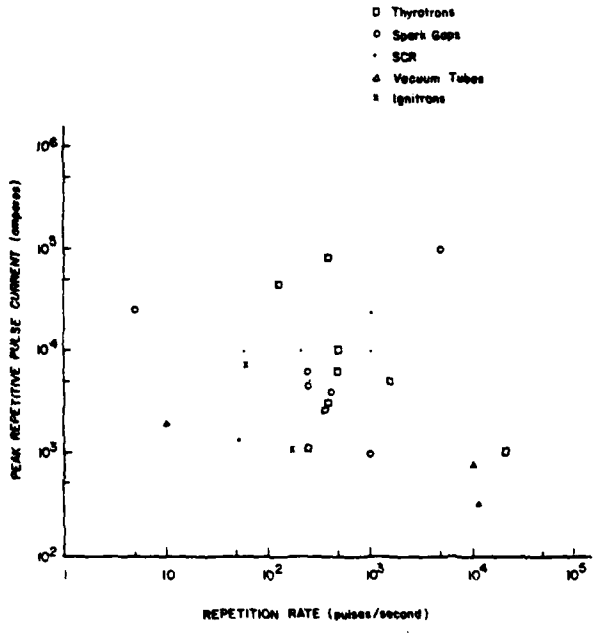


Figure 4. Peak Pulse Current vs Rep-rate

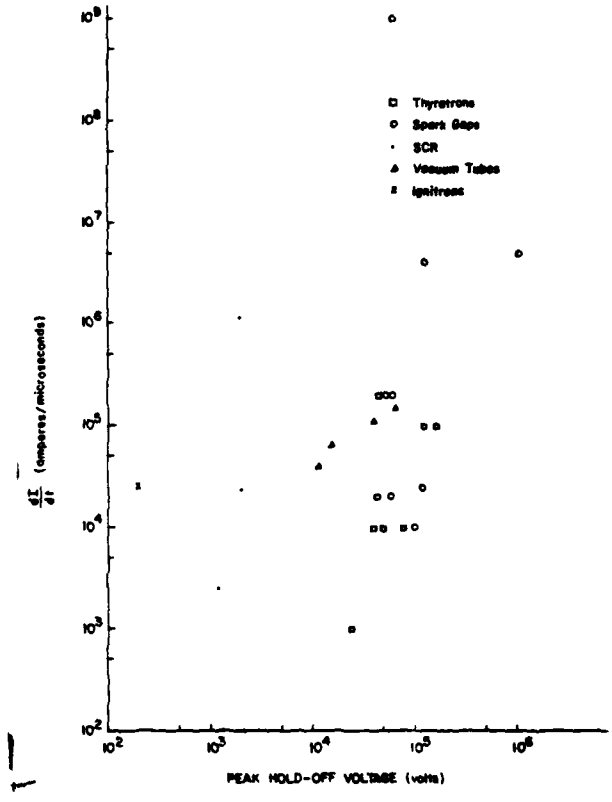


Figure 6. Current Rise Time vs Peak Hold-off Voltage

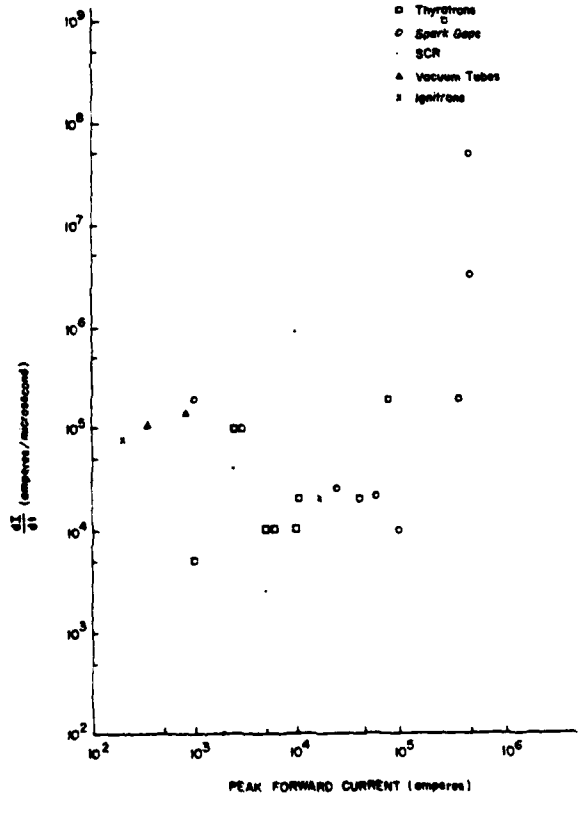


Figure 5. Current Rise Time vs Peak Current

A 100 KV, 80 AMP. LONG PULSE SWITCH TUBE

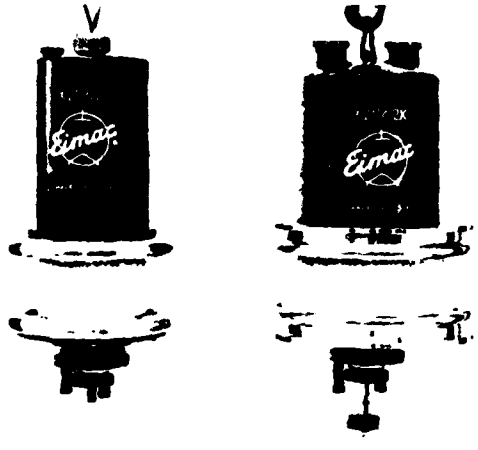
Sterling G. McNees
Varian EIMAC Division
San Carlos, CA. 94070

A high power vacuum grid tube has several characteristics which make it ideally suited for repeated DC high voltage, high current, interrupt applications. It has no moving parts, no arc quenching problems, adjustable current limiting in the case of a shorted load, and the ability to dissipate power. This latter feature can be used to advantage to pre-program any desired di/dt during the turn "on" or turn "off" interval. The ability to handle large amounts of dissipation during the "on" cycle permits the high vacuum power grid device to be used as a voltage regulator; a very attractive feature when constant voltage over the load is required as in neutral beam sources.

The power grid tubes described here have 100 KV and 80 Amps. DC ratings and typically operate at 97 to 98 percent efficiency. They require approximately 25 KW of auxilliary power for filament and driver circuits.

The design of a power grid vacuum tube involves many compromises between many more or less independent variables. In the case of a switch tube this means increased spacing between plate and screen for voltage holdoff, an output seal which minimizes voltage stresses across the ceramic, and a long pump and age schedule to clean up and condition the many surfaces within the tube.

The X2062J and K described here are water cooled power grid tetrodes. These tubes are part of the 4CV250,000 family and there are over 120 active operating sockets. The tubes are shown in Figure 1.



The X2062J is approximately 30" long and 14" in diameter and weighs 100 lbs. The X2062K is 36" long, 17" in diameter and weighs 180 lbs.

The electrical ratings are given in Figure 2 and the characteristics curves in Figures 3 and 4.

Electrical Ratings

	X2062J	X2062K	
Pulse Modulator			
Filament Voltage	12	12	V
Filament Current	660	660	A
Interlectrode Capacitance			
Cin	770	770	pf
Cout	75	65	pf
Cgp	4	3	pf
Csk	40	40	pf
Csg	480	480	pf
DC Plate Voltage	100,000	120,000	V
DC Plate Voltage During Conduction Phase	3,000	3,500	V
DC Screen Voltage	2,500	2,500	V
Peak Cathode Current	90	90	A
Plate Dissipation (Average during Pulse)	300,000	400,000	W
Screen Dissipation (Average during Pulse)	* 3,500	3,500	
Grid Dissipation (Average during Pulse)	1,500	1,500	W
Pulse Length	Infinite	Infinite	

*For long pulse, screen dissipation is usually the limiting factor.

Note that the only major difference in characteristics between the two tube types is the point where Plate Current saturation occurs. At 80 amperes this is at 1.5 KV Plate Voltage for the X2062J, but for the "K" with it's increased anode spacing, this voltage is increased to 2.2 KV. The lower this voltage the more efficient the switch tube. Unfortunately, lower voltage means closer spacing and thus a lower voltage rating. The output spacing for the X2062J is 2.3 cm and for the X2062K 3.3 cm.

FIGURE 2.

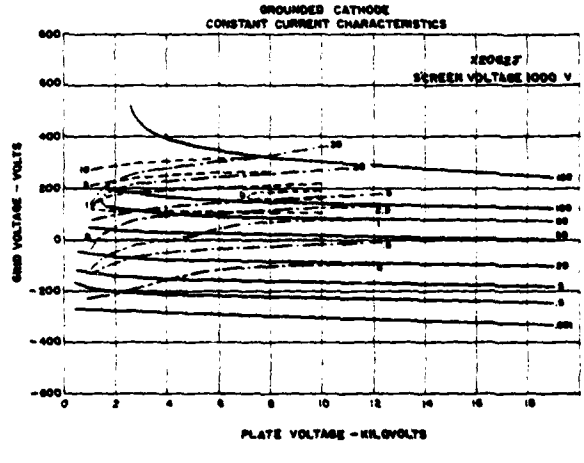


FIGURE 3.

CH1371-4/78/0000-0180$00.75 © 1978 IEEE

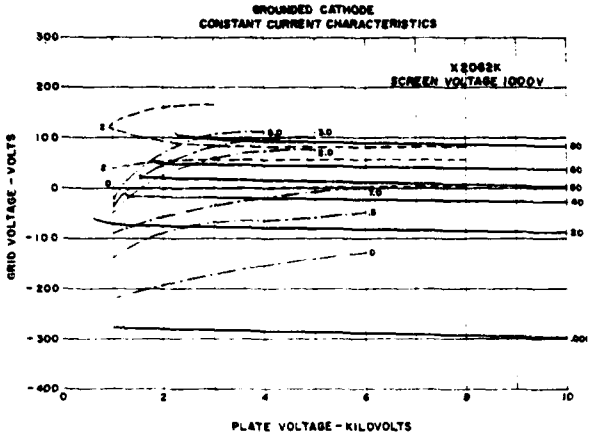


FIGURE 4.

One of the nice features of a tetrode is the fact that plate current is substantially independent of voltage drop. This means that in the event of a load arc the current will increase only about ten percent above what the switch tube was programmed to pass. With this characteristic minor vacuum arcs will clear without recourse to an interrupt.

Looking at the characteristic curves observe that screen dissipation increases with increased screen voltage and a given plate current. In general, for long pulses in particular, the screen voltage should be so adjusted as to give the required plate current at zero grid voltage.

Since the X2062J and "K" are derived from tubes intended for RF communications the turn "off" and "on" can be done in nanoseconds if necessary, but in general much slower rise and fall times are dictated in order to avoid ringing and the danger of tube overvoltage.

Both the X2062J and "K" can be used as programmable power resistors. The X2062J has a continuous 300 KW dissipation rating and the X2062K 400 KW. These are average ratings for short pulses - the peak power may be much higher. The dissipation ratings give the circuit designer flexibility in the event that pulse shaping or voltage regulation are design requirements.

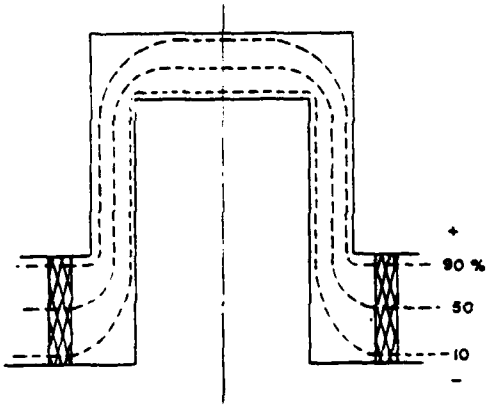
Finally, no section on ratings and performance is complete without mentioning tube arcs. Any high voltage, high vacuum device will generate an arc sometime and if damage to the tube is to be avoided then special provisions are required. It is convenient to divide arcs into two classes - those generated by a malfunction within the tube and those simply caused by serious overvolting, such as caused by ringing. Fault detection usually depends on a current sensing device sometimes augmented with a differentiating device for high rates of current changes. If a tube arc occurs it is mandatory that the voltages be removed quickly. If this is done within 20 usec then there is usually no physical damage or gassing in the switch tube and operation can resume immediately.

The vacuum and aging processes are perhaps the most important operations in guaranteeing reliability in the user equipment. Vacuum pumping is a lot more than just removing the gas. All surfaces tend to give up or absorb gases. During the pumping process conditions are set up so as to favor quick desorbtion of gases and since different gases behave differently this is not a straightforward procedure.

The finished switch tube has a vacuum of 10^{-9} Torr. If the finished tube is to have long life with few arcs, there are theoretical calculations which indicate the partial pressure of CO_2, CO, H_2O and CH_4 should be less than 10^{-20} and 02 less than 10^{-40} Torr. Although the literature is voluminous the nature of voltage breakdown in vacuum is, at best, poorly understood. It is reasonable to assume that as we learn better processing techniques the voltage ratings of switch tubes will increase without increase in size or cost.

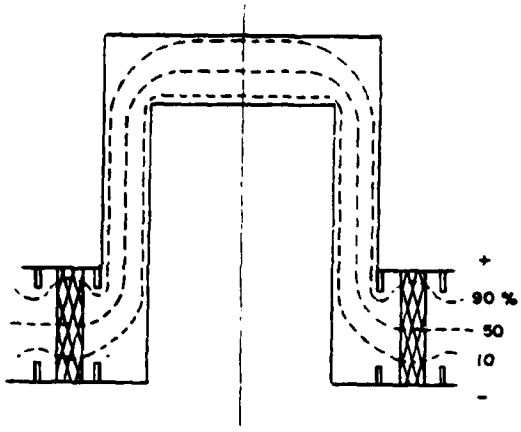
So far, the remarks have applied mostly to points inside the tube. another area which needs special attention is the insulator and vacuum seal, usually called the output seal. One solution for the output seal problem is to make it big, but, for a number of reasons, such as expansion and tolerances, this is not practical.

In Figure 5 an output seal typical of what is used in small tubes is shown. This is unsatisfactory for high voltage. The voltage gradient tends to be concentrated at the plate or high voltage end a problem made worse when the effect of the dielectric constant of the ceramic is considered. By adding the corona rings, Figure 6, the concentration of the field at one end is corrected but a new problem is created. The equal potential lines are now no longer normal to the ceramic surface. This is dangerous because of the low voltage gradient along the surface of the ceramic which makes an ideal place for the buildup of a negative charge. This charge comes from stray electrons emitted from the negative surface and when it gets large enough a punctured ceramic results.



TYPICAL CERAMIC SEAL
FOR LOW VOLTAGE TUBE

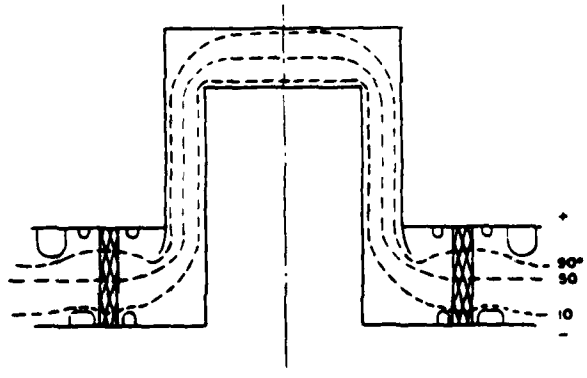
Fig. 5



TYPICAL CERAMIC SEAL
DESIGN FOR HIGH POWER TUBE

Fig. 6

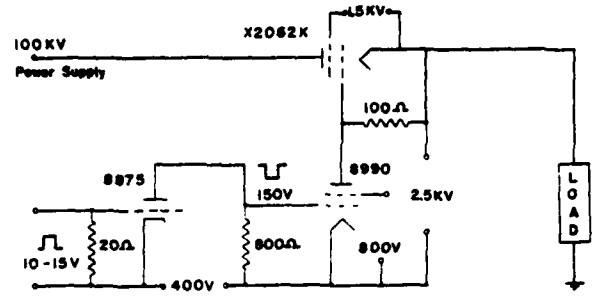
In Figure 7 the ceramic is moved out and a double corona ring arrangement is used at the positive voltage end. The larger spacing keeps the equal potential lines near normal to the ceramic surface. The small corona rings close to the ceramic serve the purpose of shielding the metalized edge of the ceramic - a region that often has sharp points. The external corona ring spacing is such that in the event of an arc the breakdown is between them and not across the ceramic surface. Designs of this type have been successfully used up to 200KV.



CERAMIC SEAL DESIGN
FOR HIGH VOLTAGE
SWITCH TUBE

Fig. 7

The switch tube requires a driver and since it is usually located at high potential it is desirable that it be as compact as possible. A possible driver circuit is shown in Figure 8. The low value of 100Ω for the X2062K grid is for stability. Such a value will make oscillations difficult and minimize ringing. The driver tube should have a high transconductance. The 8990 meets this requirement. An 8875 is used to drive the 8990. It is operated in a zero bias mode requiring a 10-15 V pulse. At this point solid state and electro-optical isolators can take over.



DRIVER CIRCUIT
FOR
X2062K

Fig. 8

This direct bootstrap circuit required four floating power supplies. The plate supplies must be suitably bypassed for the shortest rise and fall time desired. Fall times are dictated by the characteristics of the load. A fast turn off of the switch tubes does not necessarily mean fast removal of voltage from the load.

The X2062J and "K" are vacuum tubes which are available today to solve the problems of switching off and on high voltage DC quickly and frequently, as well as providing regulation. We do not feel that this is the end of the switch tube design, but rather a beginning and future tubes will have both higher voltage and current ratings.

LONG PULSE HIGH EFFICIENCY SWITCH TUBE DEVELOPMENT

Albert F. Morreall

Thermionics Section

Surveillance Technology Branch

Surveillance Division

Rome Air Development Center

Griffiss AFB, New York

Summary

A high power linear beam tetrode switch tube was tested and evaluated at RADC's High Power Laboratory. Utilizing the device as a series modulator for a klystron amplifier, parameters attained were 120 KV video output at 0.05 duty cycle with pulse lengths up to 300 microseconds. Measurements of efficiency, collector depression, perveance, control grid interception, anode (screen grid) current and collector dissipation were performed. The ability to control the pulse width and shape was demonstrated at a variety of voltage and power levels. These results indicated that operation at 140 KV, 100 amperes at 0.06 duty could be achieved with an appropriate load tube.

This switch tube was designed and fabricated by Varian Associates under RADC sponsorship. Details of the advantages of this device and of Varian's preliminary testing are covered, in addition to RADC's extensive evaluation.

Background

During the mid and late 1960's, efforts were pursued by the Department of the Air Force to develop a super-power beam type switch tube. This work was performed by Varian Associates and was supported primarily by RADC and MIT. Early models of this device were capable of 200 KV hold-off voltage and could provide 140 KV, 95 amp pulses at approximately 20 usec. Favorable measurements of grid emission, field emission, arcing, grid interception and cathode activity demonstrated the feasibility of operating a gridded gun in a high voltage environment. However, the electronic performance of the gridded gun was below expectations in terms of gain, and beam transmission through the anode was only about 80 percent. Later versions of the tube exhibited increased gain but were still severely limited in efficiency and duty cycle (approximately 80 percent and 0.001 respectively). Reports of this early work are available from DDC to qualified requestors.[1]

By 1972, a linear beam tetrode switch tube was developed which had a peak video output power of 14 megawatts producing 140 KV pulses at 100 amperes with a pulse duration of 25 microseconds and a duty of .005. This device featured a "100 percent" depressible collector and provided efficiencies in the 90 percent area.[2]

Theory of Operation

The long pulse high efficiency switch tube utilizes a modified Pierce-type electron gun. The concave nickel cathode button contains 125 dimples which provide the emitting surface for the beamlets that form the electron beam. A nickel shadow grid is aligned with the dimples to mask the emission directly behind the control grid wires in order to minimize grid interception. The electron beam converges and flows through the anode hole as in a gridded klystron gun. When the beam traverses the anode to collector space, the collector is depressed toward cathode potential causing an equivalent current to flow in the diode load. (Earlier work had established that the optimum anode-collector configuration was a mirror image of the electron gun-to-anode region. A central probe was placed in the collector to compensate for the absence of the cathode button. Also, the collector is fly-trapped to capture a portion of the returned electrons that otherwise would flow to the anode).

For maximum efficiency it is necessary that the load impedance be slightly less than the impedance formed by the electron gun in order that the voltage on the collector is slightly less than the beam supply voltage. The perveance of the electron gun is variable with grid drive in the region between 1.5 and 2.0 x 10^{-6}. A thermionic diode load is ideal since the constant perveance feature makes the load impedance match the switch tube impedance at any voltage up to the rated limits. The degree of collector depression allowable without reflecting electrons to the anode determines the switch tube drop and therefore, the efficiency of the modulator.

Advantages

The unique features of this device are:

(a) the non-intercepting control grid.

(b) the convergent beam passing through a single hole in the anode.

(c) the high efficiency made possible by the controlled spreading of the electron beam.

(d) the rise time of the load voltage follows closely the rise time of the grid drive voltage because the total capacitance of the switch tube collector, the load tube gun and the filament transformer is about 90 pf. This capacitance can be charged by the beam current in 100 nanoseconds.

U.S. GOVERNMENT WORK NOT PROTECTED BY U.S. COPYRIGHT.

(e) the load tube is fully protected from damage in the event of an internal arc since it is isolated from the dc power supply by the massive anode which is at ground potential. The maximum arc current in the load is limited to the switch tube current.

(f) the ability to control the pulse shape (minimization of droop and ripple) will in turn minimize distortion effects in the rf output of the load tube which will enable optimized performance in highly sophisticated pulse compression radar systems where extreme precision in phase and amplitude control is of prime importance to the functioning of the signal processing system.

(g) the ability to change pulse width permits variations in average power which can yield a "burnthrough" capability in ECM environments.

Objectives

The goal of this program was to develop a linear beam hard tube switch capable of operation at the following parameters:

Hold off	165 KV
DC operation	155 KV
Video output	140 KV, 100 amperes
Load impedance	1.6 to 2 uk(perveance)
Pulse length	up to 300 usec
Duty cycle	.03 min., 08 goal

Emphasis was placed on the ability to control the pulse shape, particularly at the longer pulselengths. Also important was the design of the cathode in order to provide sufficient current at 300 usec pulses. Probably the most difficult problem to be overcome was the design of the collector-probe system so that sufficient power could be dissipated to permit operation at the desired duty cycle.

Figure 1 is a photograph of the switch tube which is approximately four feet long and eighteen inches in diameter. Figure 2 shows a schematic diagram of the tube as a series modulator. Figure 3 is a sketch of the collector-probe region while Figure 4 depicts a simplified modulator layout sketch.

Testing at Varian's Facility

Varian's testing was limited primarily by the capacitor ratings of their power supply. They were able to operate very briefly at 100 KV at a 0.03 duty cycle before successive failure of capacitors made operation at lower power levels necessary. The majority of their testing was limited to a maximum supply voltage of 88 KV at a duty cycle of 0.01. Although operation at 300 usec pulse lengths was demonstrated, most of their data was taken with a pulse length of 125 usec at 80 pps.

The load device was an S-band microwave tube with a perveance of about 1.9×10^{-6}, which provided an excellent match for the switch tube. As Figure 5 illustrates, the switch tube is virtually cut off at a positive drive of 1.0 KV while 45.3 amps peak was attained at a drive of 3.8 KV. Figure 6 illustrates an interesting and important characteristic of the switch. As the grid drive is increased, the current to the collector increases creating a corresponding rise in collector depression. Above about 60 percent depression the efficiency of the tube increases rapidly to a point where the electric field strength is insufficient to collect the majority of the electrons. Many of the electrons are returned towards the gun and are collected on the body (anode) which accounts for the sudden increase in body current. The most favorable area of operation is at about 95 percent collector depression which results in an overall tube efficiency of approximately 90 percent.

Testing at RADC

Testing at RADC was performed in the Arthur J. Frohlich High Power Laboratory. The switch tube and grid pulser were immersed in an oil pit which is eight feet deep, therefore, no meaningful photographs could be taken. Due to the fact that no thermionic load tube was available which could operate at the goals of the switch tube (140 KV, 100 amps at pulse lengths up to 300 usec), a water load was utilized. This load is a closed system device with flow rates up to about 50 gallons per minute and is capable of removing 300 KW of average power per minute. The resistance of the load can be altered by adding or removing small quantities of copper sulphate. Figures 7 and 8 are photographs of the load and heat exchanger respectively.

Initially, serious problems were encountered with arcing and outgassing. Although Varian had hi-potted the tube to 165 KV, this was performed with a cold cathode. At RADC, a significant rise in pressure was noted with a hot cathode, grid bias and the grid pulser in operation without any voltage applied to the cathode. This indicated the presence of grid current and considerable time was required to outgas the control grid. Similar problems occurred when cathode voltage was applied with a hot cathode, the grid biased but with no grid pulse. The cathode voltage had to be raised very slowly in order to keep the tube pressure low and minimize arcing. Eventually a cathode voltage of 145 KV was attained.

Actual operation was first performed at 20 usec pulse width at 30 pps (0.0006 duty cycle). With a load resistance of 4000 ohms, 65 KV was applied to the cathode which resulted in a collector output of 62.5 KV at 16 amps. Then the PRF and pulse width were gradually increased to 60 pps and 60 usec respectively which increased the duty cycle to 0.0036. Outgassing occurred but the pressure gradually decreased to about 10^{-6} Torr. At this point the collector depression was 96% and tube efficiency 91%. Power output was 1 MW peak and 3.6 KV average.

With the duty cycle set at 0.0012 and the cathode voltage at 135 KV, the output was 130 KV at 30 amps. Anode current had now reached 2.5 amps which resulted in further outgassing. Depression and efficiency percentages remained essentially the same but the output power had increased to 3.9 MW peak and 4.7 KW average.

At a pulse width of 300 usec and duty at 0.018 favorable results were attained up to about 75 KV cathode potential, i.e, 70 KV and 20 amps output. Further increases in cathode voltage did not result in the expected increases in collector voltage and current. Also increasing the drive amplitude resulted in no apparent change. After reducing the load to 2000 ohms the following was attained with 300 usec pulses at 0.018 duty:

Ebb (KV)	E Coll. (KV)	I (A)	I coll. (A)	Depress (%)	Efficiency (%)
75	60	1.5	28	80	75
90	62.5	1.7	30	69	64
115	65	1.8	31	56	50

Although the maximum positive grid drive required was expected to be 3.5 KV, increasing the drive to 5.0 KV had no apparent effect. By disconnecting a diode clipper in the pulser circuitry, a positive drive of 7.5 KV was attained. This resulted in the following:

Ebb (KV)	E Coll. (KV)	I (A)	I coll. (A)	Depress (%)	Efficiency (%)
62	50	1.2	24	80	75
90	72	1.9	36	80	75
100	77.5	2.0	39	78	73

At this point the reasons for low collector depression and efficiency were evaluated. The possible problems were that the cathode was incapable of producing sufficient current, or the pulser voltage was too low, or the pulse voltage was reduced at the grid because the grid interception current was too high. In similar devices which used the same type and size cathode, 100 amps were reached so the cathode does not appear to be the problem. Also, in these earlier tubes, a positive grid drive of 5.5KV was more than sufficient. Therefore, the problem is most likely associated with grid current. The grid interception current is approximately 5% of total tube current so that at 20 amps tube current the grid current would be about 1.3 amps. The grid pulser uses an Eimac 4PR65A tetrode which is rated at 1.3 amps *maximum*. Obviously the driver tube needs to be replaced with a tube with current ratings of at least 5 or 6 amps. Time did not permit this change to be made at this point.

The only other meaningful testing that could be performed at this time was to increase the duty to evaluate the dissipation of tube electrodes. At a PRF of 120 Hz and a pulse width of 400 usec, the tube was operated at 60 KV cathode potential with a load at 2000 ohms. Although the collector depression (83%) and the efficiency (78%) were comparatively low as expected, operation at this duty cycle (0.048) was successful with only a slight rise in tube pressure. The average output power was about 50 KW with approximately 11 KW collector dissipation, 1.1 KW probe dissipation and 1.5 KW dissipated in the tube body. Insulation oil was used as the coolant and was calculated to be about 20% as efficient a heat remover as water.

Perveance measurements were made at all test points and were quite constant varying between 1.5 and 1.9 x 10^{-6}. Pulse shape presented no problems. The collector pulse was always very similar to the grid drive pulse. Figures 9 and 10 show representative pulse shapes. In both cases, the horizontal dimension is 50 usec per division. In Figure 9, the upper trace is the collector current pulse at 20 amps per division, the center trace is the body current at 1 amp per division and the lower trace is the collector voltage at 50 KV per division. Figure 10 is the same except that the collector current setting is at 50 amps per division and the body current is at 2 amps per division. The droop in the collector current pulse is believed to be caused by the current viewing transformer which is approaching saturation. The droop in the collector voltage is accurate and is identical to the drive pulse.

Conclusions

The long pulse high efficiency switch tube represents an advance in the state of the art of linear beam series switching for radar modulator and linear accelerator applications. Operation at 145 KV was demonstrated and it is believed that this could be increased to 165 KV with proper aging. Pulse widths of 400 usec at a duty cycle of 4.8% were achieved. With water cooling it is expected that the duty could be increased by one or two percentage points. Efficiencies of about 91% were attained at moderate current levels. The goal of 100 amps was not met but this limitation was probably due to the insufficient current capabilities of the driver. Within the next few weeks this problem will be rectified and RADC will publish a final report on this effort in September.

The author would like to express his appreciation to the High Power Laboratory personnel who assisted in this work: Edgard I. Biondi, Joseph N. Favata, Airman Paul J. Grassel, Bobby R. Gray and Anthony J. LoVaglio.

References

1. Super Power Beam Type Switch Tube

   RADC-TR-66-494 September 1966

   RADC-TR-67-494 July 1967

   RADC-TR-69-208 July 1969

2. Long Pulse High Efficiency Switch Tube Development

   RADC-TR-77-319 September 1977

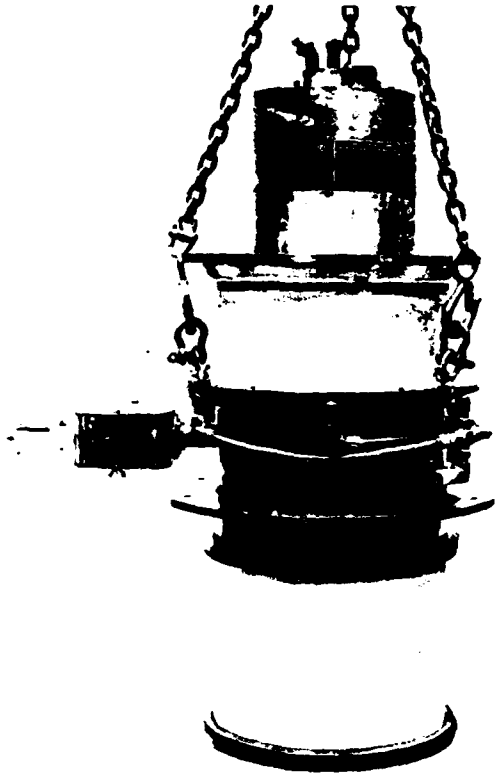


Figure 1. Long Pulse High Efficiency Switch Tube

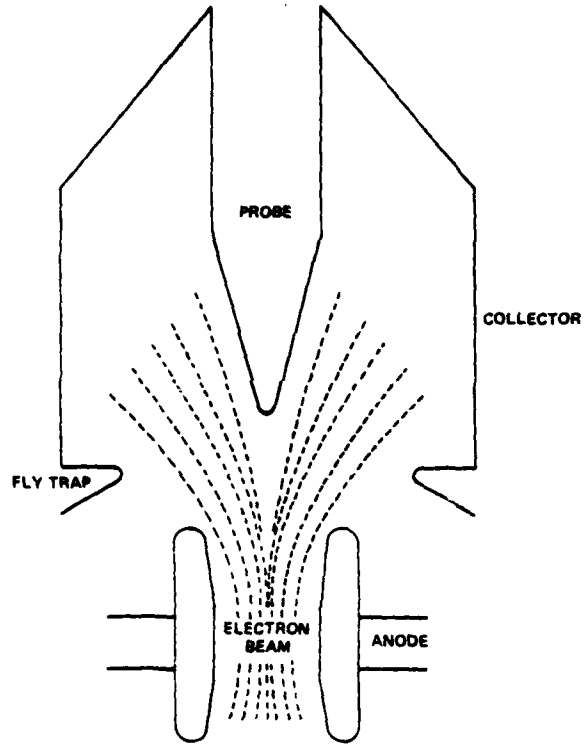


Figure 3. Sketch of Collector-Probe Region

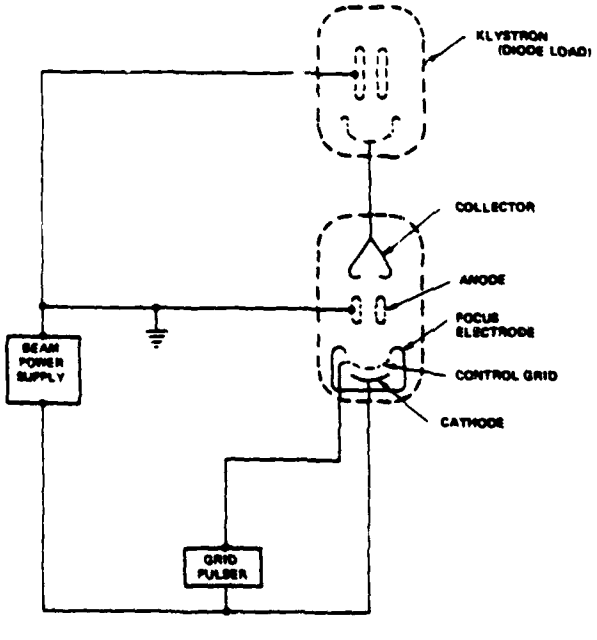


Figure 2. Schematic Diagram Tetrode Switch Tube Series Modulator

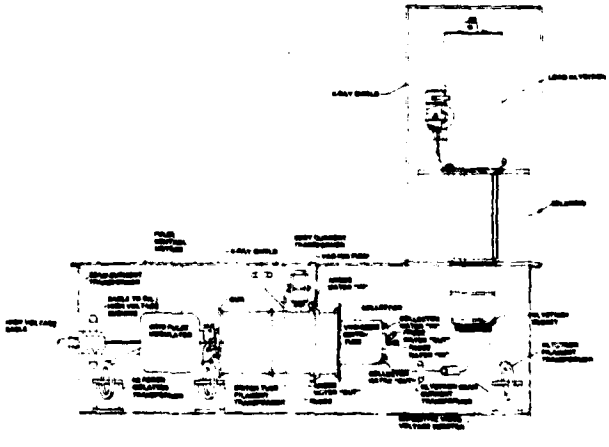
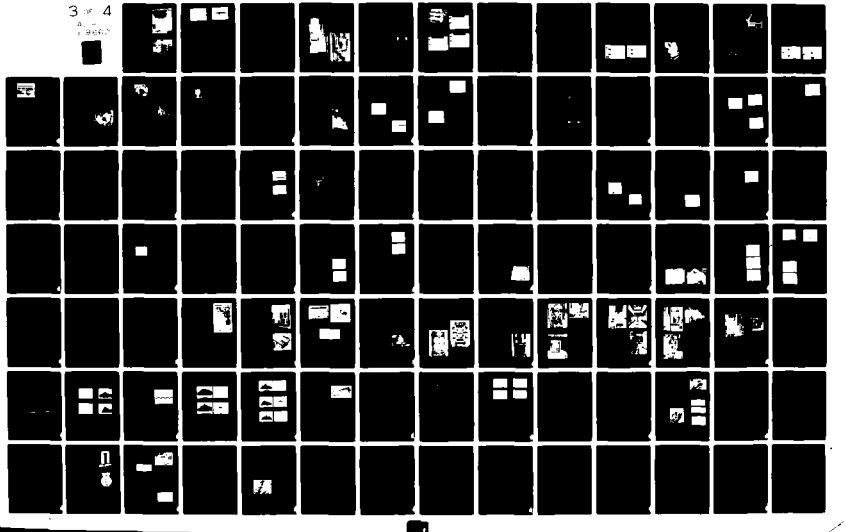


Figure 4. Simplified Modulator Layout Sketch

AD-A119 662 PALISADES INST FOR RESEARCH SERVICES INC NEW YORK F/G 9/5
IEEE CONFERENCE RECORD OF 1978 THIRTEENTH PULSE POWER MODULATOR--ETC(U)
1978
UNCLASSIFIED 78-CH-1371-4-ED NL

3 OF 4



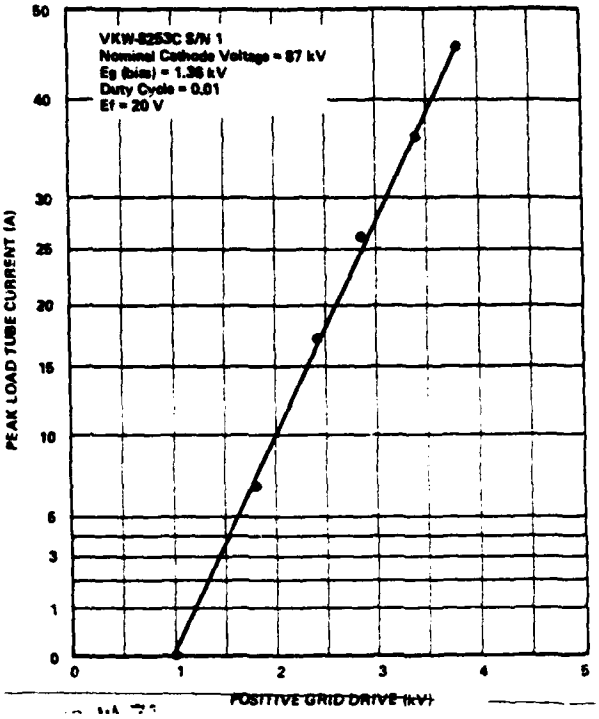


Figure 5. Load Tube Current Versus Grid Drive at 87 KV

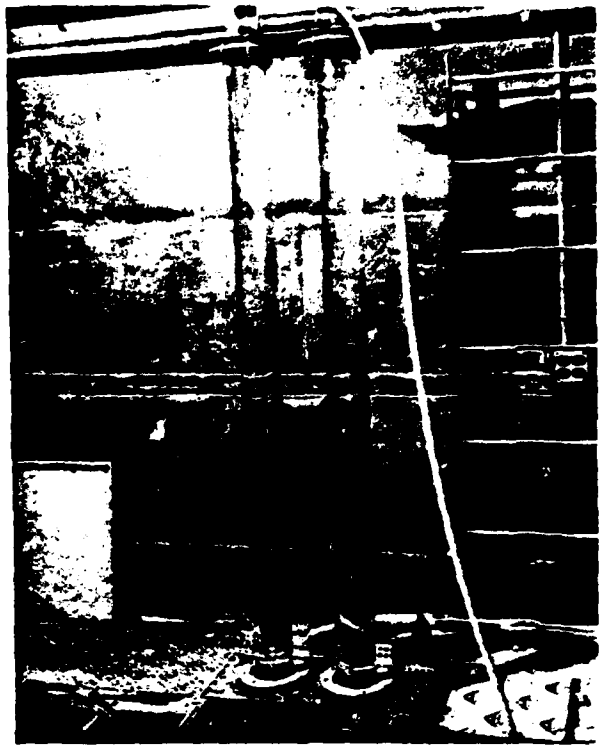


Figure 7. Water Load

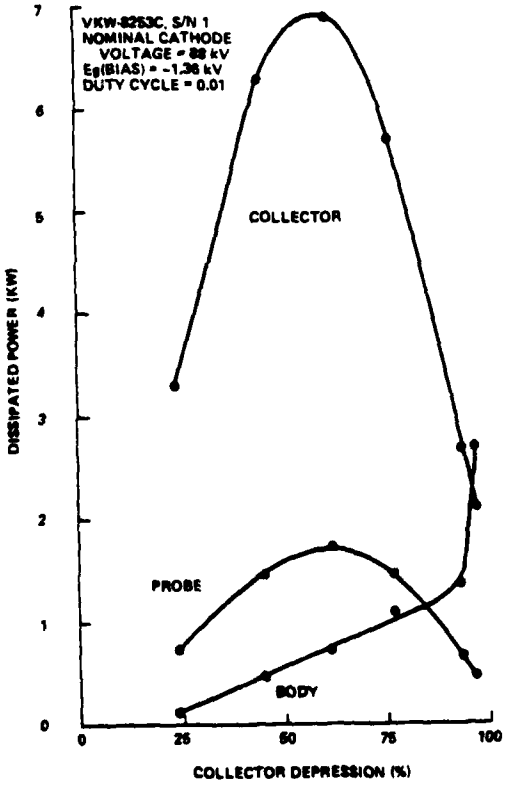


Figure 8. Collector, Probe and Body Power Versus Collector Depression

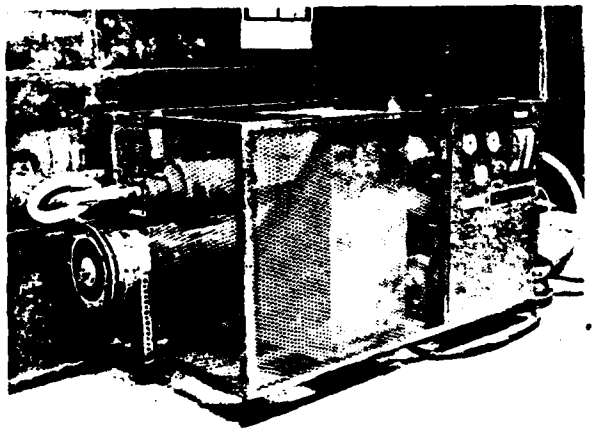


Figure 6. Heat Exchanger

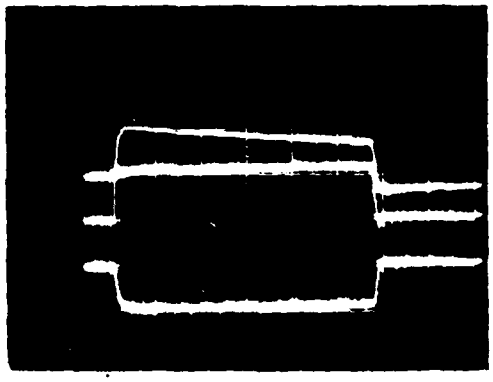


Figure 9. Pulse Shapes at 62 KV

Horizontal - 50 usec per division
Upper Trace - Collector current at 20 amps per division
Center Trace - Body current at 1 amp per division
Lower Trace - Collector voltage at 50 KV per division

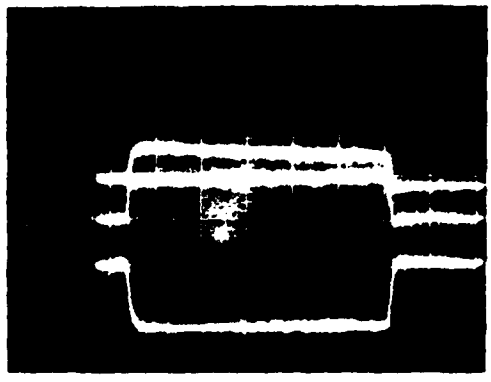


Figure 10. Pulse Shapes at 88 KV

Horizontal - 50 usec per division
Upper Trace - Collector current at 50 amps per division
Center Trace - Body current at 2 amps per division
Lower Trace - Collector voltage at 50 KV per division

THE USE OF VACUUM INTERRUPTERS AT VERY HIGH CURRENTS

by

R. W. Warren* and E. M. Honig
Los Alamos Scientific Laboratory
of the
University of California
Los Alamos, New Mexico 87545

Introduction

There is a slowly growing, widely based need for switches which can be used to interrupt dc currents. In recent years the demands of fusion devices such as tokamaks have overshadowed all others and have illuminated the need for conventional switches with vastly improved performance or for better entirely new kinds of switches. Switches presently being developed for tokamak uses must interrupt 25 kA at 25 kV with a reliability of 99% or so for a total of many thousands of cycles.[1] Next generation tokamaks may operate at 100 kA and 100 kV and require switches with a reliability of 99.9% and a much longer life. No existing switch can meet these requirements.

A promising approach to these goals is based upon a vacuum interrupter used in conjunction with a commutation or counterpulse capacitor bank. This bank is used to create a forced current zero at which interruption can occur. Tests have been performed at the Los Alamos Scientific Laboratory (LASL) to determine the feasibility of this approach by using conventional commercially available interrupters. These tests have established the limits of current and voltage at which interruption can be achieved and determine the reliability and life time of the interrupter under this duty. This work has been presented in earlier reports.[2] Its major conclusions are presented in Fig. 1 which shows that the interruption limit of conventional interrupters increases roughly linearly with the electrode diameter and that the largest interrupter available can interrupt a maximum current of about 25 kA.

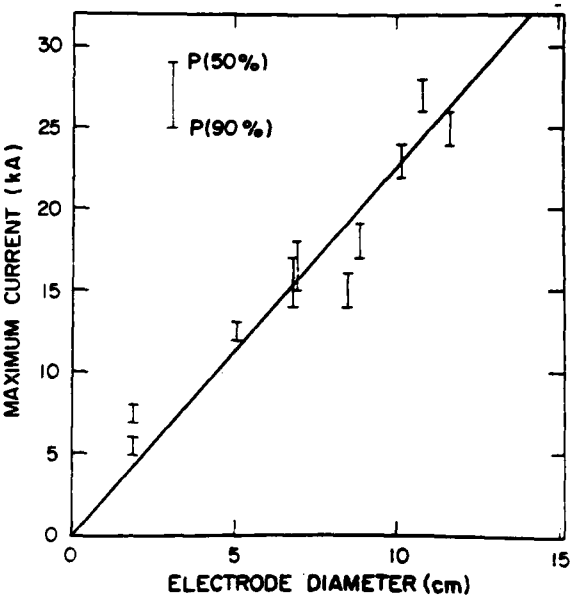


Fig. 1.

Maximum Interruptible Current vs electrode diameter.

This report also mentions other techniques being tested which have promise of increasing these limits. It is the purpose of this paper to present in greater detail the work done at LASL with some of these novel approaches. In particular, we shall discuss in some detail experiments with axial magnetic fields, experiments performed by connecting two identical interrupters in parallel, and in less detail, investigations with interrupters employing a novel geometric construction or novel electrode materials.

Axial Magnetic Fields

Experiments by Kimblin et al.[3] and others[4] have shown that axial magnetic fields can have important effects upon vacuum arcs. The field modifies the tendency of the arc to constrict at high current levels. It causes a marked reduction in arc voltage and in the characteristic noise commonly observed in the arc voltage.

An axial field has been impressed upon the arc in three different ways: 1) by using a solenoid which surrounds the interrupter and is supplied from a separate power source, 2) by using a similar solenoid which is supplied by the current passing through the interrupter, and 3) by employing a compact solenoid which is inserted inside the vacuum interrupter and supplied by the current passing through it. Each of these techniques has particular advantages and disadvantages. The first, for example, generates a field which is essentially dc and which can be varied independently of the current to be interrupted. It involves a relatively large power supply and certain timing and insulation problems. The second, avoids the power supply but suffers the inflexibility that for a given solenoid the field strength is proportional to the current to be interrupted. Another disadvantage involves the partial shielding of the arc region by the electrode structure. How rapidly, for example, does the field at the arc position rise and fall when the interrupter current is turned on and off? The third technique suffers from both disadvantages of the second technique but has two advantages. The field is concentrated near the electrodes where it is needed, and the solenoid and interrupter are connected within the bottle. This eliminates all special wiring peculiar to the axial field and makes possible the direct substitution of an axial field interrupter for a conventional one. A special disadvantage of the third technique is related to the form of solenoid required. It is normally split into two coils, one directly connected behind

*Westinghouse Research Laboratory Industrial Staff Member.

CH1371-4/78/0000-0189$00.75 ©1978 IEEE

each electrode. This arrangement requires that one of the coils moves very fast with its electrode during each interruption cycle. The stresses on this coil and the disadvantage introduced by its extra mass become especially serious when very fast actuation is required.

Figure 2 shows the solenoid used with the first technique. It is composed of 39 turns of 4-0 cable wound on an insulating spool. It has a resistance of about 10 mΩ and is normally driven by a dc power supply with a maximum rating of 10 V and 1 kA. At

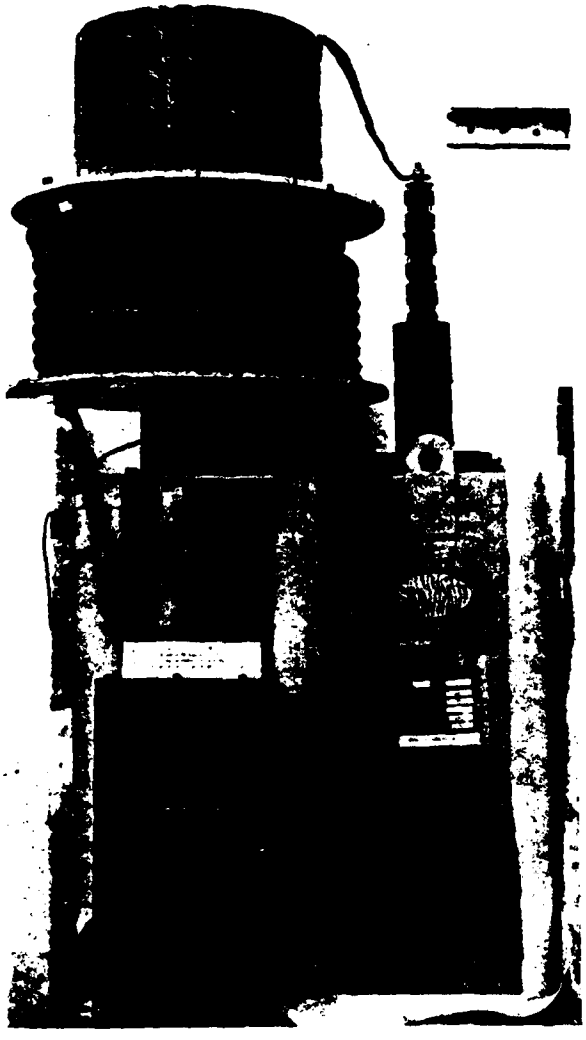


Fig. 2.

Axial field solenoid using external power supply.

this value of current the field generated between the electrodes is 0.13 T. When this solenoid is used its current is turned on several seconds before an interruption. Measurements are made of arc voltage and interruption reliability versus field strength with the interrupter current held as a parameter. Both polarities of field have been used with no apparent difference. Figure 3 shows data of this kind found for a typical interrupter. Clearly the arc voltage drops significantly with increasing field.

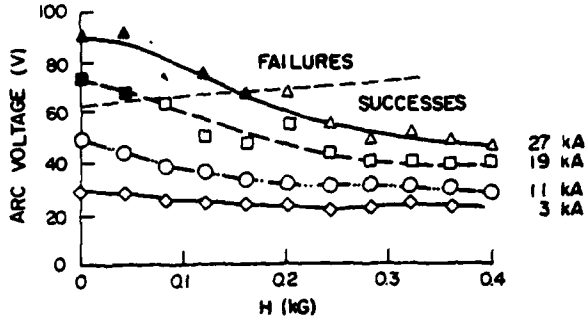


Fig. 3.

Arc voltage and reliability vs field strength.

The experimental points above the dotted line are mostly failures; those below are mostly successes. At the highest field used, the interruption limit is well in excess of 27 kA; with no field it is 15 kA. This improvement of about a factor of 2 is typical for the 7-in. interrupters examined. Smaller interrupters show a smaller improvement. The best performance found with commercially available 7-in. interrupters is a maximum interruptible current of 36 kA with 90% reliability at a field of 0.11 T.

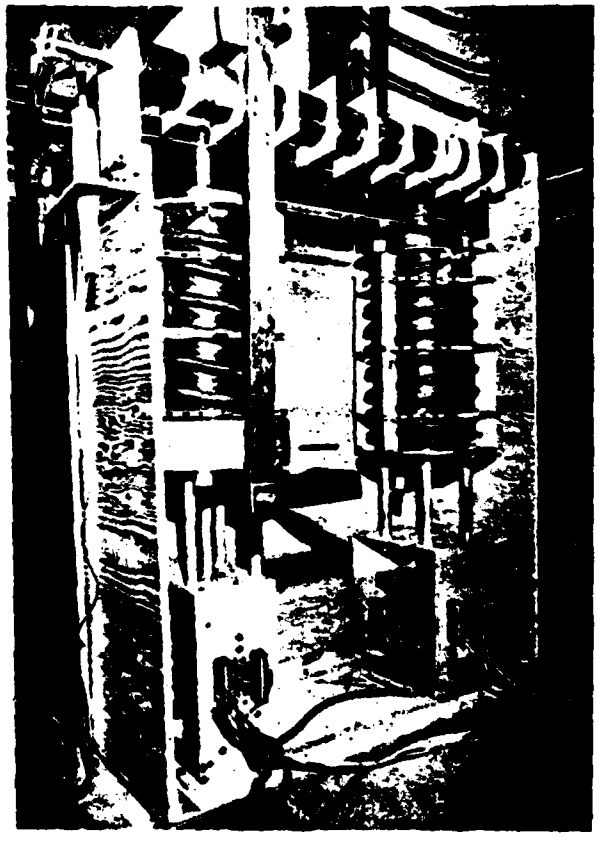


Fig. 4.

Axial field solenoids driven by interrupter current.

Figure 4 shows two coils used with the second technique. Each is a 4-turn solenoid, wound with two parallel 4-0 conductors. Parallel conductors are used to reduce the force on each one and to smooth out field variations caused by the coarse pitch of the windings. When carrying 20 kA, the field produced by this solenoid at its center is 0.17 T. This solenoid was placed directly in series with the interrupter. With this connection and our standard test circuit, the solenoid current turned on about 3 to 4 ms before interruption and turned off exactly at the time of interruption. A discussion of the test circuit and facilities used in these experiments is given by Honig.[5] The components and techniques used with this circuit are given by Warren.[1] The solenoid could have been inserted elsewhere in the circuit so that its current would continue for several hundred microseconds after interruption, but the connection was made as described because of the opportunity it afforded to investigate the more severe duty in which the field is reduced at the same time as the arc current.

Measurements were made on the same interrupter tested under conditions of the first two techniques. The maximum interruptible current was the same in each case even though the field was larger by a factor of about 3 for the second technique. Thus both techniques differ in detail but are equally successful in increasing the interruption limits of conventional interrupters. The interrupter used to investigate the third technique was specially built by Westinghouse.[6] It contained two half-turn coils capable of generating 0.2 T at a 20 kA interrupter current. This device was able to interrupt 42 kA with a 90% reliability. Since the electrode's geometry and mass were different from those used in techniques 1 and 2, we cannot easily draw a comparison of the effectiveness of the third technique relative to the others.

Within the range of fields investigated, larger fields have always given better performance. This suggests testing with fields even larger than those presently used. This has proved to be difficult, however, because of the extra mass and inductance introduced by the larger field windings and because of their additional heating. The second technique appears to be the most appropriate for higher fields; so we intend to use it in this way soon.

Parallel Interrupters

If two interrupters are connected in parallel, their combined interruption limit could be as high as twice their separate rating. This would occur only if the current split evenly between the two. Examinations of the fluctuations in the arc voltage of a typical interrupter and of the variations between different interrupters makes one doubt that this even split would occur naturally. Placing balancing impedances in series with each interrupter seems to be a necessary step. If resistors were used, their power losses would be excessive for most applications. Separate inductors or a single balancing transformer is to be preferred.

Accordingly, tests with paralleled interrupters were performed using the circuit of Fig. 5. The saturable reactors, L_{SR}, are used to assist interruption. Their inductance when saturated is about 1 μh and when unsaturated is much larger, as discussed elsewhere.[1] The resistors, R, are used to balance the current division during the long time when the interrupters are closed and carrying current. The resistance of the closed interrupters is about 100 μΩ and that of the connections and leads of each actuator

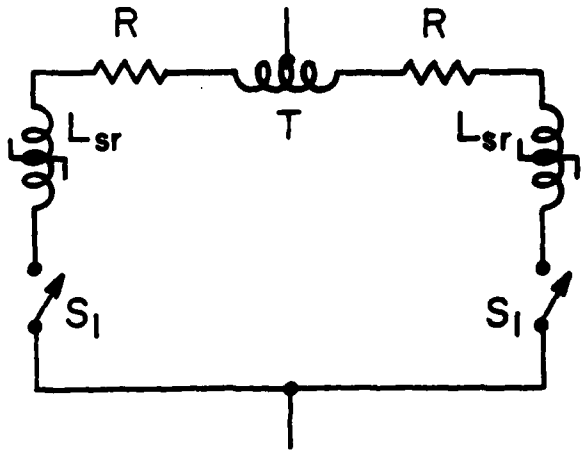


Fig. 5.

Circuit used for parallel connection.

assembly about 450 μΩ. Taken together, these resistances are large enough and, usually, well enough balanced so that any additional resistors R can be set equal to zero. T is the current balancing transformer. It is composed of a number of cores wound from 4-mil-thick silicon-steel tape and provided from an adjustable air gap. Thicker laminations cannot be used because of excessive eddy current losses. These cores are threaded with two 4-0 cables as shown schematically in Fig. 6.

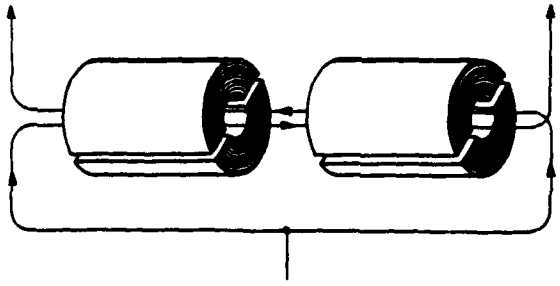


Fig. 6.

Schematic diagram of transformer.

Figure 7 shows a photo of this transformer that functions by generating a voltage which is applied in series with the interrupters. This voltage cancels the difference in the arc voltages of the interrupters and thus keeps the total current evenly split between them. The flux rating of the cores must be chosen large enough. Its minimum value is proportional to the difference that exists between the two arc voltages and to the length of time that this difference must be cancelled. Typically these values are 50 V and 4 ms. Thus the flux rating of the cores must be about 50 V x 4 ms = 0.2 Vs. Each core used in T is rated at 0.006 Vs. Thus about 30 cores are needed. A total of 36 was used in T, as shown in Fig. 7.

If the currents through the two interrupters are balanced only moderately well, i.e., within 1% or so, gapless transformer cores will saturate before the interrupters are opened and be unavailable for their balancing role. If the gaps are too large, the



Fig. 7.

Thirty-six-core balancing transformer.

transformer inductance will be so small that the individual interrupter currents will become significantly unbalanced during the arcing interval. Calculations show that gaps of 10 mil or so are optimum. Experiments were performed to verify these conclusions and to choose the best gap and total flux value for the core.

Figure 8 shows typical traces of the currents through each interrupter when the balancing transformer T is not used. The traces are 15 ms long. R was chosen equal to 250 μΩ bringing the total resistance in each interrupter leg to about 800 μΩ.

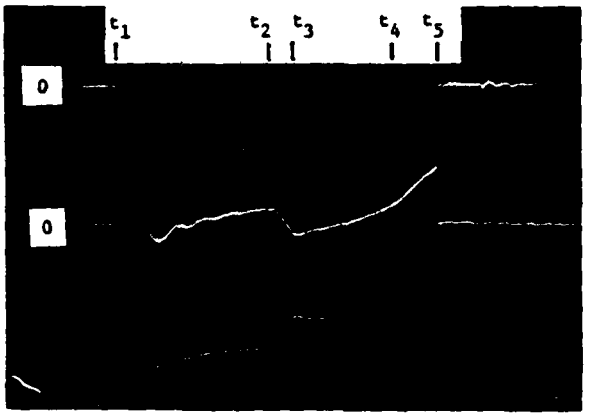


Fig. 8

Currents when transformer is not used.

These 250 μΩ resistors are current shunts which provide the signals of Fig. 8. On Fig. 8 several particular times are worth noting. At t_1 the current is established in each closed interrupter. The current traces are essentially identical showing that the balance is good. At t_2, interrupter number 1 opens; the arc voltage forces the current to begin to transfer to interrupter number 2. At t_3, interrupter number 2 opens, stopping the rapid transfer to it. At t_4, the arc voltage (not shown) of interrupter number 1 undergoes a spontaneous upward fluctuation and transfers current to interrupter number 2. At t_5, the counterpulse is fired and successfully interrupts both currents. At t_5, about 10 ms after t_1, the two currents are seriously unbalanced, roughly in the ratio 2:1.

Figure 9 shows what happens when no changes are made in the circuit other than the introduction of gapless transformer T. Clearly the current sharing is nearly ideal at all times. Curves like Fig. 9 are seen only when the initial current balance is very good. If it is not, curves like that shown in Fig. 10

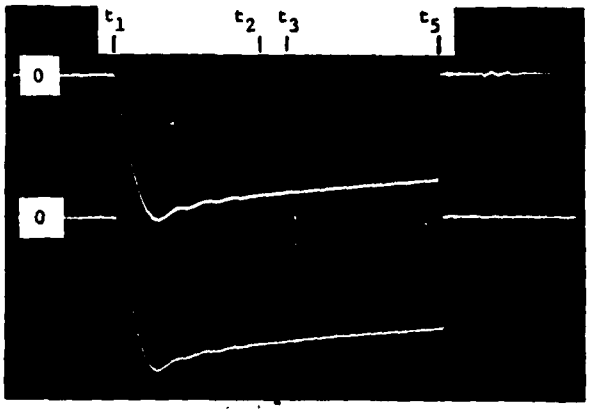


Fig. 9.

Currents with a gapped transformer--initial balance is good.

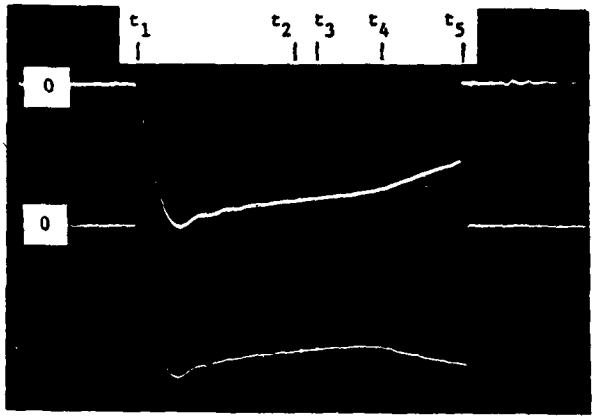


Fig. 10.

Currents when initial balance is not good.

are seen instead. In this case the initial unbalance caused the cores to be nearly saturated. The correction of the further unbalance, which occurred after arcing starts, forced them completely into saturation at t_4. After t_4, the unbalance increased without control until a 2:1 ratio in currents occurred at interruption. This saturation effect can be cured by opening gaps in the cores. In agreement with our calculations, a 5- to 10-mil gap was found to be optimum. With this arrangement we have successfully tested two paralleled 7-in. interrupters to 29 kA, the limit of our facility at the time of the testing. With our upgraded facility we plan to test parallel interrupters beyond the anticipated limit of twice the single interrupter limit, i.e., 2 x 21 kA = 42 kA. We also plan to test three or more interrupters connected in parallel.

Interrupters With Novel Geometric or Metallurgical Arrangements

Conventional vacuum interrupters have electrodes which are made of Cu-Bi or CLR.[7] Such electrodes display roughly equal interruption ability but differ in other respects such as their contact erosion rates. Special interrupters have been tested which have special configurations of CLR contacts. These include cup-like electrodes with slots in their sides and plain unslotted disk electrodes with raised contact rings. From our limited number of samples it appears that the simplest disk electrodes out perform the more complicated ones with respect to their interruption limits.

An unconventional geometry soon to be tested is that developed by Rich.[8] His interrupter is composed of small disk electrodes surrounded by parallel rods. The arc initially formed between the disk electrodes is rapidly transferred to the rods. Their much larger area allows the arc to burn in a diffuse mode. This is expected to provide higher interruption limits and reduced erosion.

Another interrupter, which has been tested, employs "Amsler" contacts.[9] These unconventional electrodes are in the form of a copper cup containing radial iron vanes oriented parallel to its axis. The arc initially forms between the copper cups, but is rapidly transferred to the iron vanes.[10] Due to a combination of the unique geometry and the magnetic and resistive properties of the iron, the arc voltage is unusually low, e.g., 47 V at 20 kA, and free of noise. The limit to interruption at 90% reliability is 34 kA for this 7-in. interrupter. This is about 1.5 times better than conventional interrupters for the given set of parameters. This limit is insensitive to magnetic field, i.e. no further improvement is noted when an axial field is applied.

Further Improvements in Ratings

Interrupters with axial magnetic fields have arc voltages which are low and reproducible. Paralleling such interrupters should be easier than with conventional ones. We will shortly pursue this subject. Early counterpulsing operation in conjunction with very fast actuator opening has been discussed previously.[1] This largely-untried technique should allow very large currents to be interrupted with negligible arc currents and erosion. An unsolved problem is the large "popping" force found under such conditions. The popping force, caused by magnetic repulsion of the electrodes at the current-constricting contact points, is typically 500 N for a current of 25 kA. It will require large counterforces to hold the contacts closed and will make the design of a fast actuator difficult. We believe that further improvements in the ratings of vacuum interrupters will be made by combining these three improvements--early counterpulse, axial magnetic fields, and parallel interrupters.

Conclusions

An unconventional interrupter has been tested which can interrupt 34 kA without an impressed magnetic field. The use of axial fields extends the rating of conventional interrupters to 36 kA and special interrupters to 42 kA. These ratings are 1.5 to 2 times that achieved with conventional interrupters used in a conventional manner. Techniques for paralleling interrupters have been developed which work well with two conventional interrupters and should be easily applied to unconventional ones, to axial field interrupters, and to combinations of more than two interrupters. With these techniques, the limit of interruption should increase linearly with the number of interrupters connected together. Great promise is found in early counterpulse techniques, although the fast actuator problems appear to be severe.

References

1. R. W. Warren, "Experiments with Vacuum Interrupters Used for Large DC-Current Interruption," Los Alamos Scientific Laboratory report LA-6909-MS.

2. R. W. Warren, "Vacuum Interrupters Used for the Interruption of High DC-Currents," Proc. of the Seventh Symposium on Eng. Problems of Fusion Res, Knoxville, Tennessee, October 1977, IEEE Pub #77CH1267-4-NPS, pg. 1774.

3. C. W. Kimblin, "The Effect of Axial Magnetic Fields on Vacuum Arcs," 10th International Conference Phenom. Ionized Gases, Oxford, England, 1971, p. 215; C. W. Kimblin and R. E. Voshall, "Interruption Ability of Vacuum Interrupters Subjected to Axial Magnetic Fields," Proc. IEE, Vol. 119, No. 12, pg. 1754, 1972.

4. O. Morimiya, S. Sohma, T. Sugawara, and H. Mizutani, "High Current Vacuum Arcs Stabilized by Axial Magnetic Fields," Trans. IEEE PAS-92/5, pg. 1723. (1973).

5. E. M. Honig, "Dual 30-kA, HVDC Interrupter Test Facility," Proc. Seventh Symp. on Eng. Prob. of Fusion Res, Knoxville, Tennessee, October 1977, IEEE Pub #77CH1267-4-NPS, pg. 1071.

6. Westinghouse Industrial and Govt Tube Division, Horseheads, New York.

7. Proprietary contact material used by Westinghouse, Ref. 6.

8. J. A. Rich and C. P. Goody, Abstract of IEEE Int. Conf. on Plasma Sci, Troy, New York, May 1977, pg. 179, conf. record.

9. J. Amsler, Sprecher and Schuh, Switzerland Characteristics of the Vacuum Arc with Various Electrode Designs. (In German). Bull SEV/VSE 65, 16 pp. 1209-1215 (Aug. 1974).

10. R. Dethlefsen, Gould, Inc., Greensburg, Pa., Personal Communication.

THE USE OF VACUUM INTERRUPTERS AND BYPASS SWITCHES TO CARRY CURRENTS FOR LONG TIMES

by

E. M. Honig and R. W. Warren*
Los Alamos Scientific Laboratory
University of California
Los Alamos, New Mexico 87545

INTRODUCTION

Vacuum interrupters are normally designed for use in ac utility circuits where they typically carry a maximum continuous current of 2 kA but must interrupt fault currents well in excess of 25 kA. Vacuum interrupters are also used[1] to carry and interrupt the large dc currents found in fusion devices such as tokamaks. In contrast to ac uses, however, these dc applications usually require that the continuous current limit be the same as the interruptible current limit. In a previous paper[2] we have reported tests performed at the Los Alamos Scientific Laboratory (LASL) which show that the interruption ability of standard vacuum interrupters used with dc currents is satisfactory for currents in excess of 20 kA. Little, however, is known about the ability of standard interrupters to carry such large currents for long times.

It is the purpose of this paper to describe measurements which determine the period of time conventional interrupters can carry currents as large as 20 kA without compromising their interruption ability; describe special interrupters which should extend this period; describe a bypass switch we have built and two ways of using it to relieve the vacuum interrupter of its heating load; describe the bypass switch experimental setup and test results; and discuss ways to extend the life of the bypass.

CURRENT CARRYING LIMITS OF VACUUM INTERRUPTERS

The limit to the continuous current which a switch can carry is set by problems encountered near the contacts due to heating. This limit can be increased by decreasing the resistance of the contacts and by improving their cooling. Practical techniques for standard vacuum interrupters include cooling the electrode stems, increasing the contact force, and choosing interrupters which have soft, high conductivity contact surfaces.

Cooling the stems is effective only if current is being carried long enough so that a significant amount of heat can migrate from the contacts to the stem. This critical time is of the order of several minutes. For current pulses shorter than this time, the temperature of the electrodes becomes independent of cooling and, for a given interrupter, depends only upon the contact force and $\int I^2\,dt$ taken over the conduction interval.

It is this "short pulse" situation which is important to present day tokamaks and other fusion devices. They are typically used in a pulsed mode with a conduction time of 1 s or less. This is the situation for which we have performed the experiments discussed below.

*Westinghouse Research Laboratory Industrial Staff Member

Circuit Arrangement

Our experiments were carried out with a synthetic circuit which is able to heat the electrodes with one apparatus and then connect the interrupter to another apparatus which can test its interruption ability.

This arrangement is shown schematically in Fig. 1, where HP, the electrode heating source, is a homopolar generator capable of generating up to 30 kA for a minute. Its maximum terminal voltage is 6 V, but it can reach this voltage only after several seconds. It is connected in series with identical vacuum interrupters VI1 and VI2 by means of a low-resistance bus. CVR is a .25-mΩ current-viewing resistor.

The top terminal of VI1 is shown connected to the "normal interruption test circuit," (NITC). This circuit is shown schematically in Fig. 2 and is described in detail elsewhere.[2,3] Capacitor C_{ST}, used in conjunction with switches S_1 and S_2 and inductor L, establish an exponentially decaying current in L_{SR} and the interrupter under test. A few milliseconds later capacitor C_{CP} and switch S_3 generate a very rapid, opposite polarity counterpulse current through this same leg. If the interrupter is open and arcing, the counterpulse can force its current to zero and achieve the interruption of its arc.

Interrupter VI2 is used to isolate VI1 from the homopolar generator when NITC is to be used. This isolation and transfer operation takes place in a few milliseconds and is accomplished by opening VI2 and by using the exponentially decaying current from NITC to counterpulse and extinguish the arc in VI2. In this way the initiation of the "normal interruption test sequence" automatically and rapidly disconnects VI1 from the homopolar circuit and connects it to NITC.

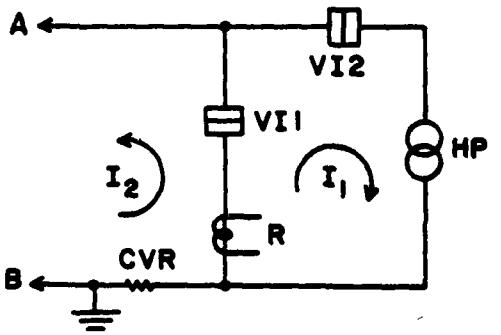


Fig. 1.
Heating test circuit.

CH1371-4/78/0000-0194$00.75 ©1978 IEEE

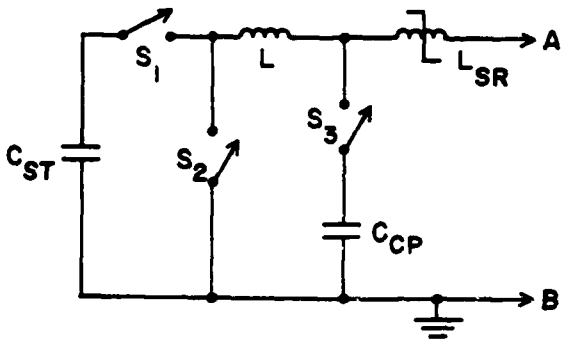


Fig. 2
Normal interruption test circuit.

This sequence is illustrated in Fig. 3 which shows oscilloscope traces of the current through resistor CVR (upper trace) and the current through VI1 (lower trace). The current through CVR is the exponentially decaying current pulse generated by NITC. The current through VI1 includes this NITC current and the homopolar current. Its baseline in Fig. 3 is somewhat distorted because a Rogowski coil and an RC integrating circuit were used to generate this waveform. This also causes trace B to be inverted with respect to A.

Several important times can be noted on Fig. 3. Before t_1 the tail of the homopolar current pulse can be seen flowing through VI1. At t_1, VI2 is opened. Its arc voltage drives the homopolar current to zero at t_2 so that VI2 interrupts at this time. At t_3, S_1 is closed, generating the exponentially decaying current pulse in CVR and VI1. At t_4, VI1 is opened and arcs. At t_5, S_3 is closed, successfully interrupting the current in VI1. In some cases, as shown in Fig. 4, the timing is changed so that the current through VI1 does not fall completely to zero before t_3. Figure 4 also shows an interruption failure.[3] These traces are 20 ms long.

This synthetic circuit has proved to be reliable and flexible. Its only deficiency is the existence of that short interval near time t_3 when the interrupter current momentarily drops well below its average value. This dip occurs several milliseconds before interruption. Separate experiments with NITC alone have shown that the interruption ability depends only upon the gross heating of the electrodes and is insensitive to short dips of the nature discussed above.

Experimental Procedure and Results

A conventional 7-in. vacuum interrupter with CLR[4] contacts was tested with a spring applied contact force of 80 lbs. With this force, these contacts had a resistance of about 100 μΩ. The homopolar current was increased steadily for several seconds so that I^2 increased approximately linearly and the final current I_m equaled the current at which interruption was then tested. The ramp time was as long as 20 s and I_m as high as 20 kA. Under these maximum conditions, $\int I^2 dt = 4 \times 10^9$ A^2s.

A thermocouple mounted on one stem of the interrupter showed a temperature rise of 130°C following this maximum pulse. Internal temperature changes were clearly much larger. A period of 10 to 15 minutes was used between shots to allow the stem temperature to return to 40°C.

A series of ten shots was performed in this way at each value of I_m and $\int I^2 dt$. Figure 5 shows the results of these tests, where P_I is the fraction of successful interruptions during each set of ten shots, $\int I^2 dt$ is shown on the x axis, and separate curves are shown for the three largest values of I_m tested. From Fig. 5 it can be seen that $\int I^2 dt$ values as high as 4×10^9 A^2s have no effect upon the success of interruptions at 10 kA, but reduce the probability of interruption to 80% at 15 kA, and to 30% at 20 kA. At

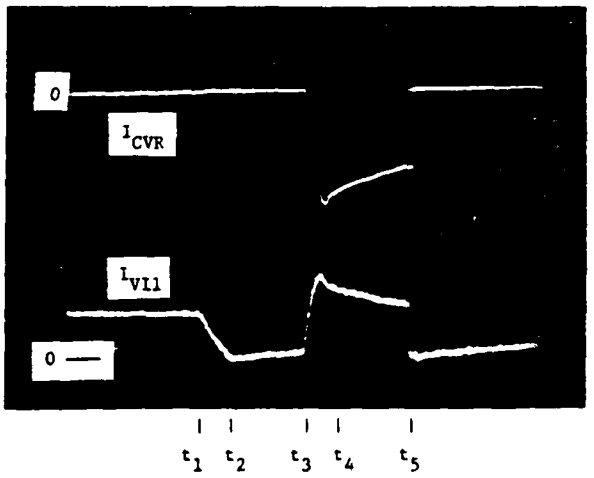


Fig. 3
Current waveforms of I^2t test.

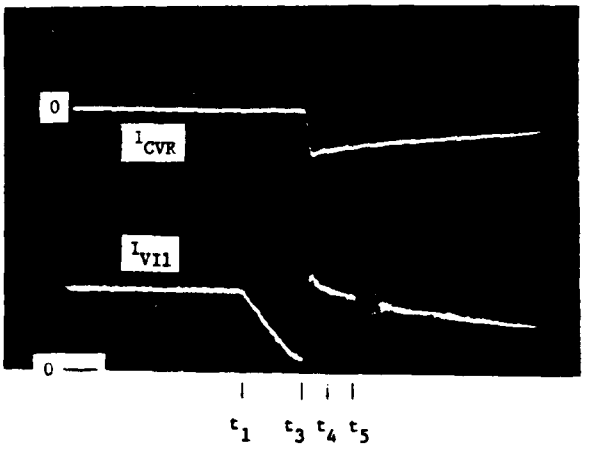


Fig. 4.
Current waveforms of I^2t test with interruption failure.

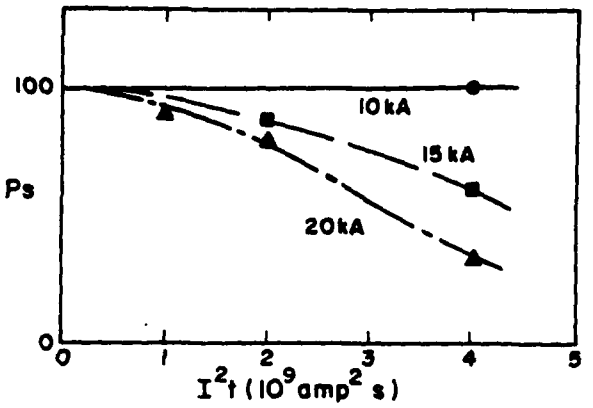


Fig. 5.
Probability of interruption vs I^2t.

20 kA, the reliability of interruption is high only for values of $\int I^2$ dt less than 1 x 10^9 A^2s.

The interrupter was disassembled at the conclusion of the tests. Figure 6 shows a photograph of one of its electrodes. Indications of gross melting are obvious. One of the spiral fingers was broken and adhered to its opposite member; large "flanges" of melted material formed between the spiral fingers; and a general bending of the fingers occurred. Clearly at the maximum $\int I^2$ dt values used, much of the electrode had been raised up to or beyond its melting point. It is remarkable that the interruption ability of the interrupter was maintained so well up to this limit.

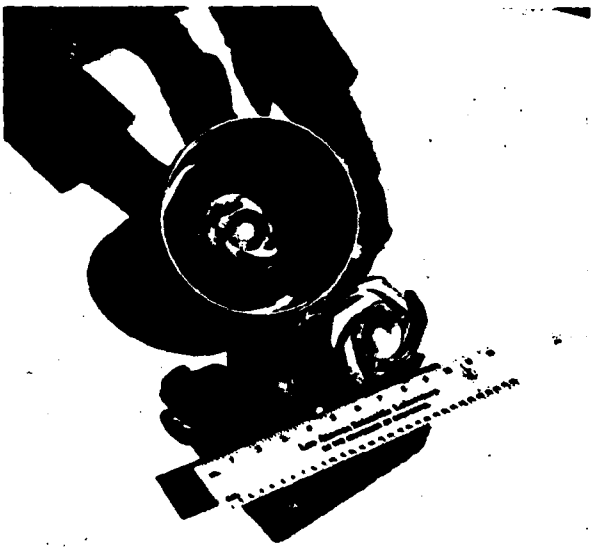


Fig. 6.
Electrodes of vacuum interrupter after overheating.

NEW INTERRUPTER TYPES WITH HIGHER I^2t RATINGS

Improved cooling of the electrode surfaces should allow higher values of I^2t to be realized. The cooling must be applied very close to the contact surfaces to be effective. Figure 7 shows a modified interrupter design which employs forced flow of cooling water immediatly behind the contact surfaces. With this design a continuous current of 10 to 30 kA should be possible as well as much higher $\int I^2$ dt ratings for long pulse use. We have acquired an interrupter built to this design[5] and will test its performance soon.

BYPASS SWITCHES

Switching conditions which exceed the I^2t limits of a vacuum interrupter require the use of a parallel bypass switch. The continuous current rating of the bypass should match the interruption limit of the vacuum interrupter. The bypass switch must carry the current under continuous duty, open to transfer the current to the vacuum switch, and after interruption withstand the same recovery voltage as the vacuum interrupter. In addition to meeting the standoff voltage and continuous current requirements, it would be desirable for the bypass switch to complement the

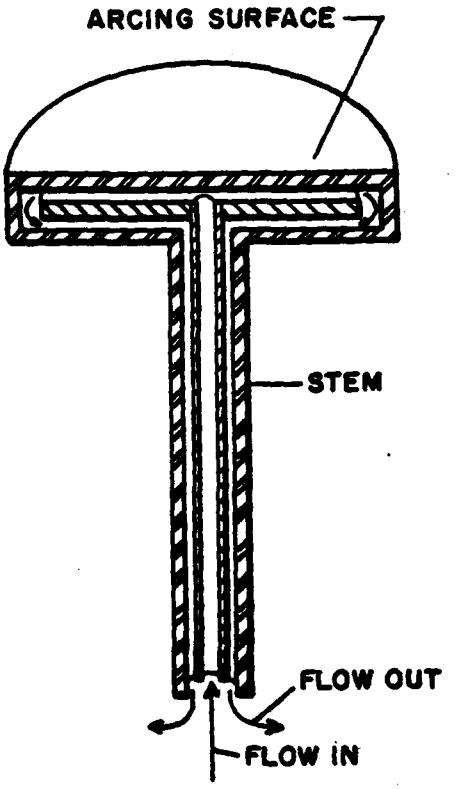


Fig. 7.
Water-cooled electrode design.

vacuum interrupter by having about the same size, cost, and life.

Construction

Since no switch meeting these requirements was available, a prototype was designed, built, and tested at LASL. A commercial high-current, low-voltage switch, Fig. 8, was modified to withstand high voltages by installing nonconducting structural support members and using oil insulation. A movable contact bridging the gap between the two stationary contacts provides the switching action. Figure 9 shows the modified switch in the open position. A conventional pneumatic actuator operating at 150 psi can open the switch in 30 ms. In the closed position its resistance is 6 μΩ.

Modes of Operation

Under conditions requiring a bypass switch, the vacuum interrupter can be either open or closed during the continuous current period. If initially open, the vacuum interrupter must be closed to accept the current transfer from the bypass switch just prior to interruption. If initially closed, the vacuum interrupter will carry some current, but it must not exceed its continuous-duty rating. Since the resistance of the bypass switch is 6 μΩ and that of the vacuum interrupter is 100 μΩ, the current in the vacuum interrupter remains safely below its 2-kA continuous rating for total currents below 35 kA due to current sharing.

Experimental Procedures and Results

The bypass switch was tested for its dc voltage and current performance, its current transfer and recovery voltage characteristics, and its erosion performance. Limits of the test facilities dictated that these characteristics be investigated in separate tests.

A voltage standoff test was conducted by applying high voltage across the switch 100 ms after opening with no-load. The switch successfully held off voltages up to 90 kV.

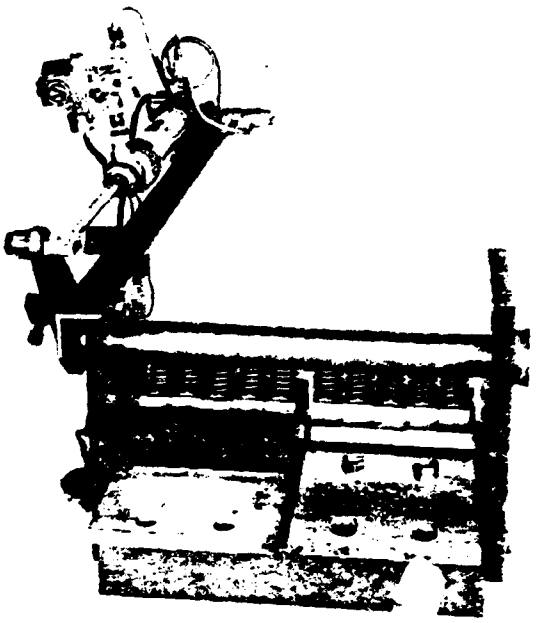


Fig. 9.
Prototype bypass switch.

Heating of the switch in oil was tested by passing 10 kA through one half of the switch. As shown in Fig. 10, the switch temperature rose only 45°C after 15 minutes. Using both sections of the switch in parallel and oil cooling should allow 25 kA to be carried continuously.

The crucial transfer and interruption operations of the bypass switch in parallel with a vacuum

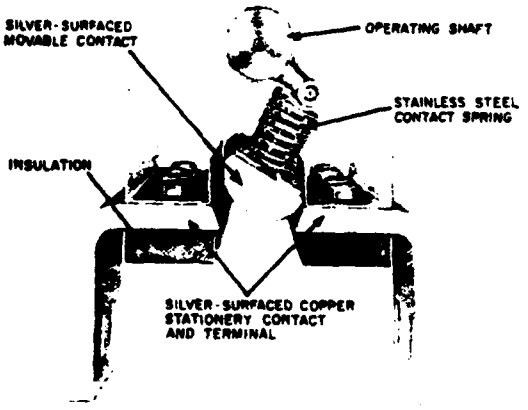


Fig. 8.
High-current, low-voltage commercial switch.

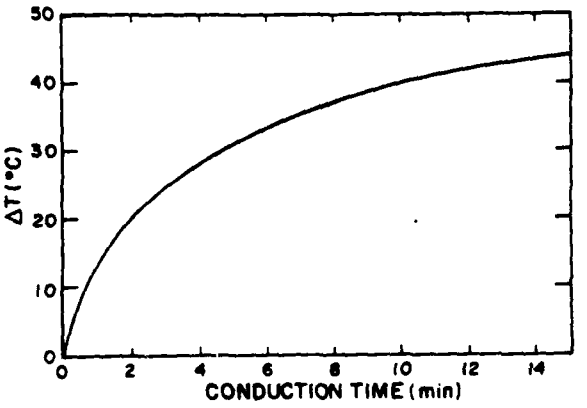


Fig. 10.
Heating of bypass switch.

interrupter were tested in the pulsed switch test facility[2,3] (the NITC described earlier) under the two modes of operation described above. The circuit of Fig. 11 was used to test the vacuum interrupter-closed mode of operation. VI is a vacuum interrupter, BP is the bypass switch, R is a Rogowski probe, and CVRs 1 and 2 are 1- and 0.25-mΩ current-viewing resistors, respectively. CVR1 was included in the VI leg to monitor the current and to achieve proper current sharing under the pulse conditions of the test. Figure 12 shows the current waveforms for the bypass switch and vacuum interrupter (upper and lower traces, respectively). The traces are 51 ms long. Both VI and BP are closed at t_0, the beginning of the current pulse. Resistive current sharing is achieved by t_1. When BP is opened at t_2, an arc develops which forces the current to transfer into VI until the arc extinguishes itself. The arc in BP lasts longer than normal because the voltage developed across CVR1 opposes the transfer. Interruption of the current in VI was delayed until t_3 to give BP time to open far enough to withstand the recovery voltage.

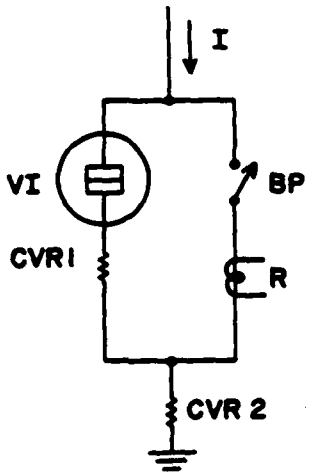


Fig. 11.
Bypass switch/vacuum interrupter test circuit.

The VI-open mode of operation was tested with the same circuit configuration as shown in Fig. 11 except that CVR1 was removed. Figure 13 shows the waveforms for the current in the bypass switch (upper trace) and the total current in both switches (lower trace). Since VI was open at t_0, BP initially carried all the current. VI closed just after t_0, and current sharing took place until t_1, when the contacts of VI unavoidably bounced open again. The contacts of VI closed without further bounce just prior to t_2, when BP opened and all the current transferred to VI. The elimination of CVR1 allowed the transfer to occur more rapidly and at reduced arc voltage. Interruption occurred normally at t_3. The unavoidable contact bounce caused by the VI actuator was undesirable, but it was reproducible enough not to interfere with the transfer operation.

Contact erosion was investigated by installing new copper contacts in the bypass switch and performing 100 VI-closed transfer operations at 28 kA. From these tests, a life of about 1000 operations was estimated for copper contacts. A set of contacts with silver-tungsten arcing surfaces was then installed. Figure 14 shows the erosion of these contacts after 100 transfer operations at 28 kA. A life of 5,000 to 10,000 operations was estimated for the silver-tungsten contacts.

The problem of reduced VI life resulting from erosion of the contacts while bouncing and arcing could be serious. If the VI-open mode is used, a bounce-free actuator or a saturable reactor which would prevent current flow in VI during the bounce period might be required. Contamination of the oil was another problem. Sufficient arc products were produced in the oil to indicate the need for an oil

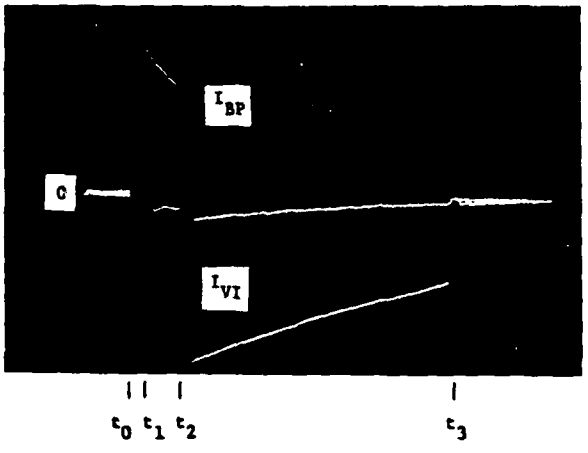


Fig. 12.
Current waveforms of VI-closed mode.

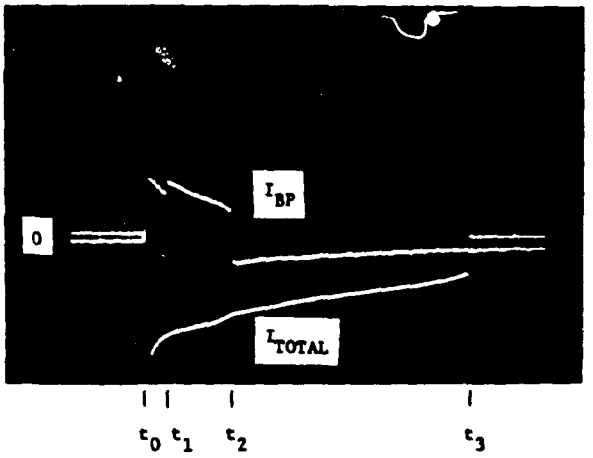


Fig. 13.
Current waveforms of VI-open mode.

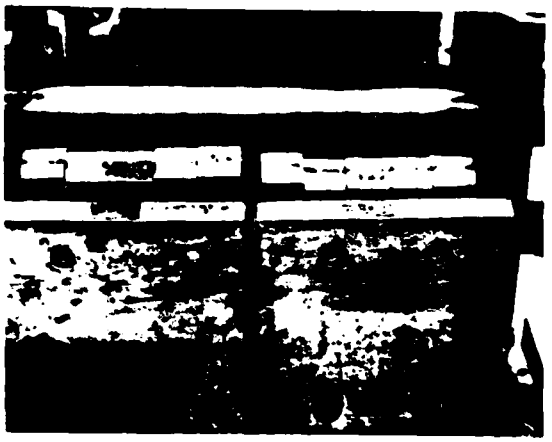


Fig. 14.
Erosion of silver-tungsten contacts.

recirculation and filtering system. One restrike occurred in very contaminated oil at 32 kV.

The bypass switch performed well in these tests. It carried and transferred up to 28 kA to a vacuum interrupter and withstood 51 kV after a 10-kA transfer. The VI-closed mode of operation seems to be the better mode since the natural current sharing is well within the VI limits, no VI contact bounce occurs, and the timing of events is easier.

Extending Switch Life

While the bypass switch built and tested at LASL has a life comparable to present vacuum interrupters, longer life bypass switches may be needed for use with improved vacuum interrupters. Since the erosion of the bypass switch depends primarily upon the current being transferred and the stray inductance of the BP-VI loop, not much improvement would be obtained with other designs. Two methods of extending the bypass switch life are proposed, both depending upon reducing the arcing current. One method is to add a resistor in series with the bypass switch and use the VI-open mode of operation. Upon closing VI, this resistance would force much of the current into VI before BP is actually opened. However, the voltage drop and energy loss produced by the resistor might be unacceptable. A more promising method is to use an auxiliary circuit to counterpulse the bypass current to zero, forcing the current into the vacuum interrupter and allowing the bypass switch to open under no-load.

CONCLUSIONS

Tests of vacuum interrupters show that they can safely carry continuous current to the I^2t limit of 1×10^9 A^2s. This is equivalent to carrying 25 kA for 1.6 s or 20 kA for 2.5 s. A bypass switch is needed for conditions exceeding this I^2t limit. A bypass switch with a 25-kA continuous current limit and which is comparable to vacuum interrupters in size, cost, and life has been built and tested successfully. Methods of extending the bypass switch life are being pursued.

References

1. A. N. Greenwood, P. Barkan, and W. C. Kracht, "HVDC Vacuum Circuit Breakers," IEEE Trans. PAS Vol. 91, pp. 1575-1588 (1972).

2. R. W. Warren, "Vacuum Interrupters Used for the Interruption of High DC Currents," Proc. 7th Symp. Engr. Prob of Fus. Res., Knoxville, Tennessee, October 1977, IEEE Pub. No. 77CH1267-4-NPS, pp.1774-1778 (1977).

3. E. M. Honig, "Dual 30-kA, HVDC Interrupter Test Facility," Proc. 7th Symp. on Engr. Prob. of Fus. Res., Knoxville, Tennessee, October 1977, IEEE Pub. #77CH1267-4-NPS, pp. 1071-1075 (1977).

4. Proprietary contact material, Westinghouse Industrial and Govt Tube Division, Horseheads, New York.

5. Westinghouse Industrial and Govt Tube Division, Horseheads, New York.

6. E. M. Honig, C. E. Swannack, R. W. Warren, and D. H. Whitaker, "Progress in Switching Technology for METS Systems," IEEE Trans. Plasma Science, Vol. PS-5, No. 2, pp. 61-65 (June 1977).

7. ITE Imperial Corp, Greensburg, Pennsylvania.

8. Gould Inc., Greensburg, Pennsylvania.

HIGH REPETITION-RATE, HIGH POWER PULSE TESTS OF VACUUM ARC SWITCHES*

by

R. N. Miller, R. Dollinger and A. S. Gilmour, Jr.
Department of Electr' ·l Engineering
Laboratory for Power and Environmental Studies
State University of New York at Buffalo

Summary

Research has been proceeding at the State University of New York at Buffalo on developing vacuum arc switches that can be operated in a pulsed mode[1,2,3]. These switches have been demonstrated to have turn-on and turn-off times in the order of microseconds, and recent tests now show that the vacuum arc switch exhibits significant potential for high frequency pulsing applications. These new tests, which have been conducted on vacuum arc switches employed in a series inverter circuit, show that the switches can be reliably turned on by kilovolt-level triggers having a rise time on the order of one microsecond. They also show that the switches can be reliably self-commutated to a turned-off mode by the operation of a series resonant circuit placed in series with the load. Combining these two techniques provides reliable pulsing of the vacuum arc switches if the resonant frequency of the resonant circuit is higher than the pulsing rate of the switches. Using this procedure, repetition rates in the five to eight-kilohertz range have been reached.

Introduction

The earlier work devoted to the adaptation of the vacuum arc switch to power conditioning applications, particularly in inverter circuits, is well documented[1,2,3]. Since this early work the advances made by that work have been consolidated, and expanded facilities[5] have made possible continued refinements of the vacuum arc switch in inverters[4]. Many of the techniques and refinements employed in the construction and use of this switch in inverters make this device potentially more desirable in other pulse power applications. It is the purpose of this paper to document these techniques and refinements, as well as to point out limitations that have been learned in later work. In this pursuit, the following paragraphs describe the evolution of the vacuum arc switch and its application since the earlier work.

Initial Problems Encountered in Operating the VAS in a Pulsed Mode

Operation of the vacuum arc switch in the continuously cycling inverter circuit has revealed several problems in the switches that were not earlier apparent. Attempts to alleviate these problems have resulted in the evolution of the switches to their present form.

The initial problem encountered was loss of high vacuum under repetitive firing conditions. This resulted in a loss of ability to stand off high voltages, and severe internal arcing in the switches resulted. At first this was felt to be an out-gassing problem, and particular efforts were then employed to insure that the switch components were clean when assembled. Extensive bake-out procedures and discharge cleaning were then employed to condition the switches prior to firing. These procedures helped but did not eliminate the problem. Continued efforts to discover the source of the gas led to the discovery that nitrogen appeared to be evolved from the boron nitride insulator between the cathode and igniter electrode when the switch was triggered. Because of this, it was decided to re-design the cathode-igniter electrode configuration to change the igniting mechanism to one that would not cause evolution of gas from the boron nitride insulator. The early igniting mechanism being used[4] can be envisioned by examining the cathode-igniter electrode assembly shown in Figure 1. In this figure the center piece is the chromium cathode, and the small ring surrounding it is the boron nitride insulator. The large ring that appears next is the copper igniter electrode, and the final ring is a stainless steel retaining device for the igniter electrode. When the switch is fired, a thin layer of cathode material is deposited on the insulator. To ignite the switch for the next firing, a pulse having approximately 0.1 joule of energy is flashed across the surface of the insulator, blasting part of the deposited layer off, forming a plasma which initiates conduction through the switch.

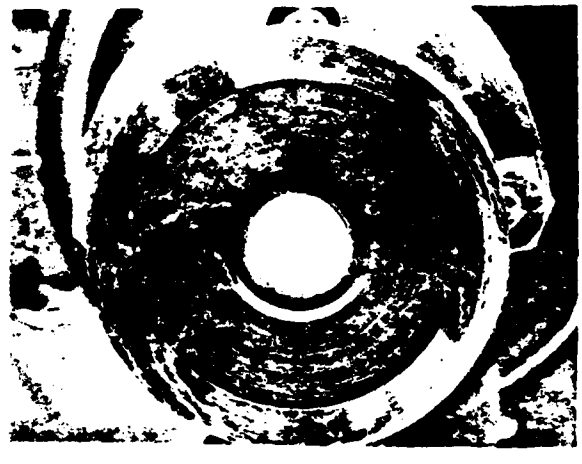


FIGURE 1. Early Cathode-Igniter Electrode Assembly.

The new cathode-igniter electrode assembly designed to change the igniting mechanism is shown in Figure 2. In this device the center piece is still the cathode, and the smooth, rounded ring on the outside is the trigger electrode. To ignite the switch, a 6-10 kV pulse is applied across the 0.020" (1/20 cm) gap between the igniter electrode and the cathode. This pulse causes an arc to form between the two electrodes, and along with the arc a small cloud of plasma is evolved from the cathode. This plasma initiates switch conduction. Thus, this new igniting mechanism does not depend on conduction across

* This work is being supported by the Air Force Aeropropulsion Laboratory, Wright-Patterson Air Force Base, Ohio.

CH1371-4/78/0000-0200$00.75 ©1978 IEEE

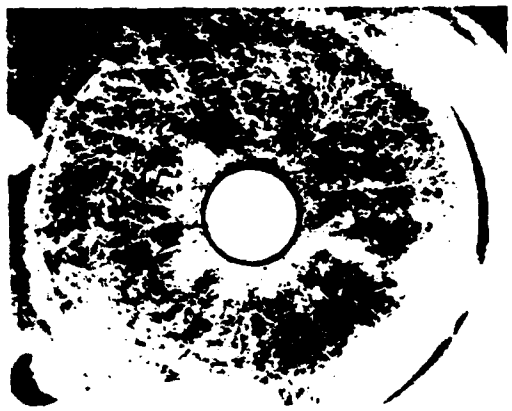


FIGURE 2. Redesigned Cathode-Igniter Electrode Assembly.

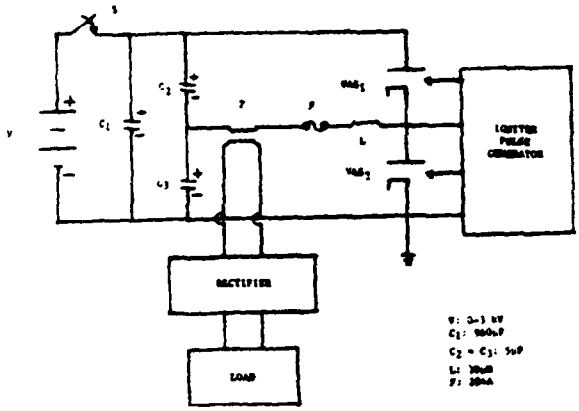


FIGURE 3. Series Inverter Circuit Schematic Diagram.

the surface of the boron nitride to achieve ignition. The important point here, however, is that the loss of vacuum problems experienced before were eliminated by this change.

Two side effects from this change are important to mention. The first is that since this change was made it has been discovered that the extended bake-out procedures do not appear to be necessary. The normal cycle of achieving a vacuum in the order of 10^{-7} - 10^{-8} Torr seems to be sufficient so that the first few firings of the switch after pump-down take care of any out-gassing problems. These initial firings after pump-down result in harder vacuums. It appears that the "gettering" action of the chromium on firing plays a large part in eliminating the necessity for bake-out.

The second side effect is that extensive conditioning of the cathode-igniter electrode assembly is necessary before reliable ignition is achieved. This conditioning seems to be a conditioning of the gap and is evidenced by material being splattered radially outward and upward on the igniter electrode and away from the gap. This splattered material, which consists of both cathode and igniter electrode material, can be seen in Figure 2.

A second problem which appeared simultaneously with the one just discussed was an internal arcing of one of the switches from the anode to the stainless steel envelope. The inverter circuit being used when this arcing occurred is shown in Figure 3. This problem occurred in VAS_1 of that circuit. As can be seen in the steady state, the voltage with respect to ground at the node between VAS_1 and VAS_2 is essentially equal to V when VAS_1 is conducting and equal to 0 when VAS_2 is conducting. If a nonconducting period exists between alternations of the inverter[4] the voltage at this node is either + QV or - QV, where Q is the Q of the resonant circuit, depending on whether VAS_1 or VAS_2, respectively, has just completed its conduction time. The key voltage relationship causing the problem exists just as VAS_1 begins conduction. At this time the anode of VAS_1 is at V with respect to ground and the cathode is at - QV. In the original inverter configuration, the envelope of VAS_1, shown in Figure 4, was connected to ground through the connecting vacuum plumbing. This condition

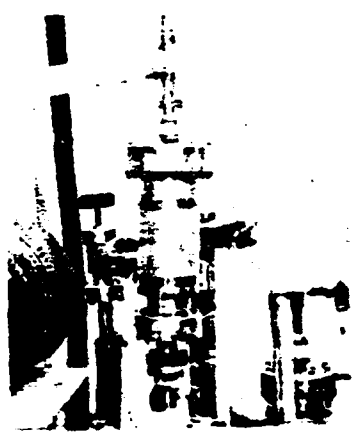


FIGURE 4. VAS_1 of the Inverter Circuit.

made the envelope QV volts positive with respect to the cathode and, upon ignition, a conduction path was established through the plasma from both the anode and the cathode to the envelope, the anode-envelope path being the more important because this path shorts across the terminals of the power source V.

Three actions were taken to eliminate this problem. First, a section of the stainless steel vacuum plumbing was removed and replaced with a piece of rubber vacuum hose. This can be seen below the valve in Figure 4. The envelope was then electrically connected to the cathode.

Second, a glass shield, shown in Figure 5, was inserted between the envelope and the conducting elements of the VAS to eliminate the possibility of direct arcing from the anode to the envelope. Third, the anode was made to fit down over the cathode-igniter electrode assembly like an inverted cup. This step was taken to insure that the plasma resulting from conduction would be contained in the inter-electrode space of the anode and cathode. The spacing between the cathode and the bottom of the anode cup is approximately three-eights of an inch (1 cm), and between the igniter electrode and the



FIGURE 5. The VAS Glass Shield.

sides of the anode cup the spacing is approximately one-half inch (1.3 cm).

These three actions have effectively isolated the active elements of the switch from the envelope, and no further internal arcing has been experienced. Successful high repetition-rate pulse testing of the switches was now possible.

High Frequency Pulse Testing of the VAS

High frequency testing of the inverter circuit is detailed in reference 4, but, to summarize, the three modes used to test the inverter were 1) single-cycle, unloaded, 2) multiple-cycle, unloaded, and 3) multiple-cycle, loaded. Testing in the two unloaded modes revealed that the vacuum-arc-switched inverters can be operated at power levels of at least 2.5 MVA and at frequencies of at least 1 kHz. Testing in the loaded mode indicated that these inverters can be operated at power levels of at least 200 kVA and at frequencies of at least 5 kHz. These tests demonstrate the potential of the vacuum arc switch in high frequency pulse power applications, but several other important characteristics of the vacuum arc switch were revealed by these tests. These characteristics are device characteristics, and can be divided into two general groups, switch turn-on characteristics and switch turn-off characteristics. It is important to note that these characteristics are for vacuum arc switches conducting into series resonant circuits, and operation with any other load impedance would require appropriate adjustments.

Vacuum Arc Switch Turn-On Characteristics

The inverter tests revealed that supplying an ignition pulse to the switch is a necessary but not necessarily a sufficient condition to establish conduction through the switch. Although the mechanism which is used to establish the proper conditions for conduction is not fully understood, two basic parameters of the ignition pulse which does cause conduction are known. These parameters are 1) the minimum voltage amplitude required for the pulse and 2) the minimum energy required in the pulse. These two parameters can be combined into one if properly used. This one parameter is called the device minimum igniting energy rate $\bar{\epsilon}_i$. The proper use of this characteristic is dependent upon a second device characteristic, minimum switch ignition current, I_o. Further discussion about the switch-load circuit relationship is now necessary to establish the usefulness of $\bar{\epsilon}_i$ and I_o.

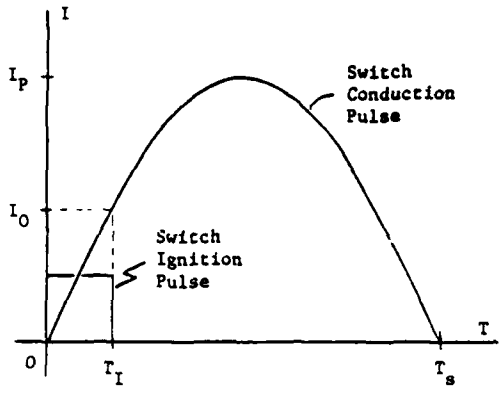


FIGURE 6. Vacuum Arc Switch Ignition Pulse and Conduction Pulse Relationships.

As previously pointed out, in the inverter tests the vacuum arc switch conducted into a series resonant circuit, so the conduction current waveform is a single, half-wave sinusoidal pulse as shown in Figure 6. This restriction requires that the switch current start at zero sometime during the ignition pulse. This ignition generates the initial plasma for switch conduction, and then the switch current must be high enough to maintain the plasma until the end of the switch current pulse. Thus, the ignition pulse must generate a burst of plasma of sufficient density not only to start switch conduction, but also of sufficient quality to support conduction until the switch current is high enough to sustain the plasma. (Many test cases were observed in which an ignition pulse occurred, but conduction was not established.) It was found that the switches conducting into a 10-ohm resistive load required ignition pulses at least 250 volts in amplitude to break down the cathode-igniter electrode gap. After gap break-down, these pulses furnished an average of 0.03 joules for one microsecond. These pulses reliably established conduction, so $\bar{\epsilon}_i$ was taken to be 250 volts, 0.03 joules/microsecond for the inverter switches.

The duration of the ignition pulse, or how long the minimum igniting energy rate must be supplied to the switch conducting into a series resonant circuit, can be determined through the use of the second turn-on characteristic, I_o. An explanation of I_o, its use, and its relationship to $\bar{\epsilon}_i$ follows.

In the inverter tests, the width T_i of the ignition pulse was about 1.5 microseconds, and the resonant frequency of the loading series resonant circuit was 10 kHz. As can be seen from Figure 6, the most ideal situation for establishing switch conduction is for conduction to start at the beginning of the ignition pulse. This arrangement would put the switch conduction 5.4° into its sinusoidal current pulse at the termination of the ignition pulse. At this time, the value of the inverter current pulse is 0.09 times the anticipated peak value. The minimum peak value of switch current achieved in the inverter testing was approximately 400 amps. Using this value for the peak current in the

analysis indicates that a maximum of 38 amps was flowing through the switch at the end of the 1.5 microsecond ignition pulse. Refering to Figure 3, the second vacuum arc switch turn-on characteristic, minimum ignition current, is defined to be

$$I_o = \frac{T_i}{T_s} I_p, \quad T_i < 0.1\ T_s$$

where T_i is the duration of the ignition pulse and T_s and I_p are, respectively, the duration and the peak value of the switch conduction pulse.

Thus, if T_i and I_o are determined for a particular electrode configuration in a vacuum arc switch and if the switch is to conduct into a series resonant circuit having known parameters, then the duration of the ignition pulse required is established and the design parameters of the igniter pulse generator are thus determined.

Vacuum Arc Switch Turn-Off Characteristics

The voltage rate of recovery is the primary vacuum arc switch turn-off characteristic of interest in vacuum arc switch inverter circuits because it determines how much delay must be maintained between alternations of the inverter output. No inverter tests were conducted to determine the minimum delay possible, but in some single-cycle, unloaded tests this delay was reduced to 4 microseconds with successful recovery. In this case the voltage rate of recovery was at least 1.5 kV per microsecond. This compairs conservatively with the 8 kV per microsecond determined in earlier work[2].

Conclusions

The triggered vacuum arc switch has undergone a period of both operating and application refinement, and it is apparent after extensive tests in an inverter circuit that the switch has significant potential in many high frequency pulse power applications. This potential justifies the continuing study and development, of the triggered vacuum arc switch, especially to increase ignition reliability and to determine switch operating characteristics with other loads.

References

1 A. S. Gilmour, Jr. and D. L. Lockwood, "Pulsed metallic-plasma generators", Proc. IEEE, Vol. 60, pp. 977-991, August 1972.

2 A. S. Gilmour, Jr. and D. L. Lockwood, "Vacuum arc inverter switch development program", Proc. IEEE 1975 NAECON, pp. 281-288, June 1975.

3 A. S. Gilmour, Jr. and D. C. Hopkins, "Recent results of vacuum-arc switched multi-megawatt inverter tests", Proc. IEEE International Pulse Power Conference, Texas Tech University, Lubbock, Texas, November 1976.

4 R. N. Miller, D. C. Hopkins, C. J. King, A. Pedano, R. Dollinger and A. S. Gilmour, Jr., "A multi-megawatt, vacuum arc switched inverter for airborne applications", Proc. IEEE Pulse Power Modulator Symposium, State University of New York at Buffalo, Amherst, New York, June 1978.

5 R. N. Miller, P. T. Glinski, and A. S. Gilmour, Jr., "A facility for testing high power dc, ac, or pulsed devices", Proc. IEEE International Pulse Power Conference, Texas Tech University, Lubbock, Texas, November 1976.

A MULTI-MEGAWATT, VACUUM ARC SWITCHED INVERTER FOR AIRBORNE APPLICATIONS*

by

R. N. Miller, D. C. Hopkins, C. J. King, A. Pedano,
R. Dollinger and A. S. Gilmour, Jr.

Department of Electrical Engineering
Laboratory for Power and Environmental Studies
State University of New York at Buffalo

Summary

In previous papers[1,2] the single-cycle tests of the operation of a vacuum arc switched inverter have been reported. Now, the High Power Test Facility at the State University of New York at Buffalo has reached a sufficient state of completion to permit more advanced testing of the inverter than has previously been reported. Several of these tests have been completed in which many cycles having peak voltage amplitudes up to 1.6 kV and peak current amplitudes up to 1.8 kA were produced. The switches used in this advanced inverter embody several new refinements in the evolution of electrically controlled vacuum arc switches. The inverter employing these new switches is also refined, with special care being taken to reduce internal power losses in the circuit elements and leads. These tests and refinements emphasize the usefulness of vacuum arc switches in high power inverter applications.

Introduction

High-frequency, high-power inverter circuits employing vacuum arc switches as the switching elements have been under development at the State University of New York at Buffalo (SUNYAB) for some time.[1,2,3] The circuit employed in this development is the series inverter shown schematically in Figure 1 and pictorally in Figure 2. The igniter pulse generator has been developed to properly synchronize the conduction of the vacuum arc switches, and three types of tests have subsequently been conducted with the inverter.

The first two types of tests were made with the circuit unloaded; that is, the transformer, T, was removed from the circuit and the primary was replaced with a short circuit. The third type of test was conducted with the circuit connected as in Figure 1. The following paragraphs describe the operation of the inverter circuit during each of the three test modes, and results of these tests are discussed.

Unloaded, Single-Cycle Testing

After the inverter circuit was assembled the initial tests made were single-cycle, unloaded tests. Figure 3 shows the inverter in the unloaded configuration. In this mode, the three capacitors are precharged to the desired initial values, after which VAS_1 and VAS_2 are each triggered one time sequentially. Figure 4 shows an oscillograph of the current through L resulting from one such test firing. For this test, C_1 was initially charged to positive 300

* This work is being supported by the Air Force Aeropropulsion Laboratory, Wright-Patterson Air Force Base, Ohio.

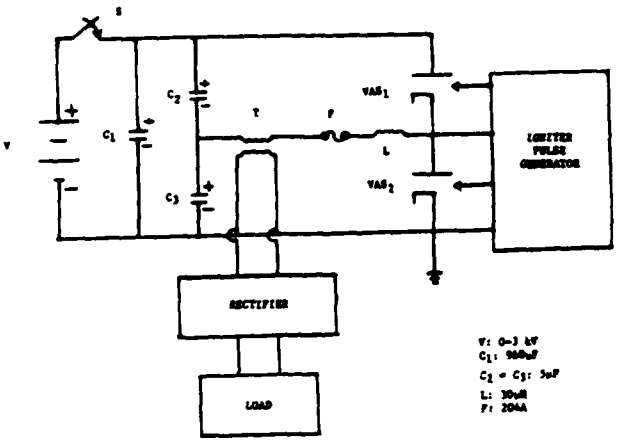


FIGURE 1. Series Inverter Circuit Schematic Diagram.

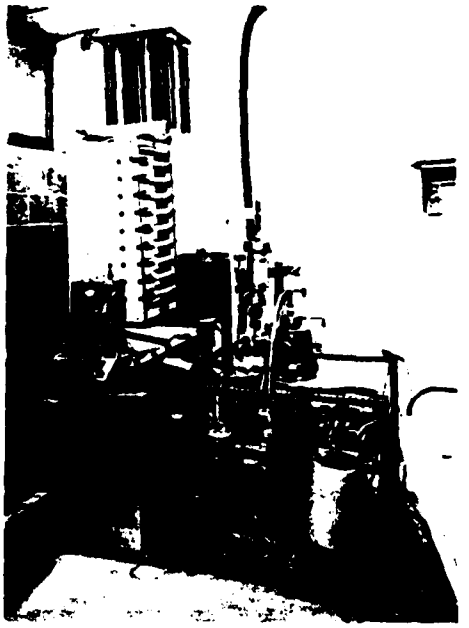


FIGURE 2. Inverter test circuit. The ladder-shaped device is the fuse F, the box to the left of the fuse is the transformer T and the rectifier, and the power resistors mounted on top of the fuse comprise the 3.2 kΩ load resistance. To the right of the fuse is the inductor L, VAS_1, and VAS_2. Below the fuse is C_3 (front) and C_2 (rear). To the left and below the fuse is C_1. The plumbing and devices below VAS_2 constitute the vacuum system for the VAS's.

CH1371-4/78/0000-0204$00.75 ©1978 IEEE

volts, C_2 charged to positive 3 kV, and C_3 charged to negative 2.7 kV. Triggering VAS_1 and VAS_2 95 microseconds apart produced the 1750 amp peak waveform shown.

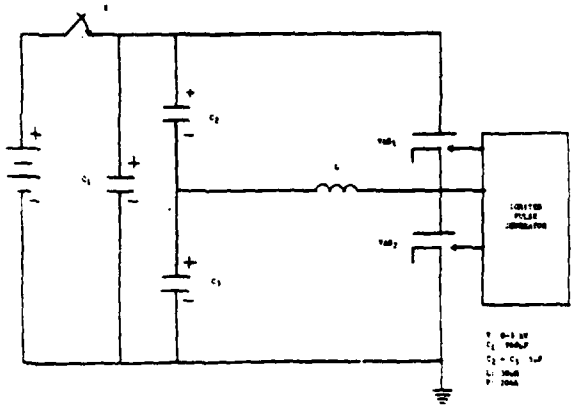


FIGURE 3. Unloaded Series Inverter Circuit.

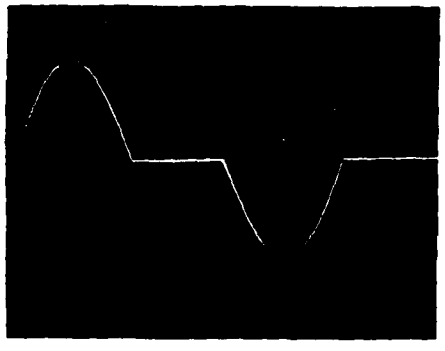


FIGURE 4. Oscillograph of the inductor current during single-cycle testing. Vertical calibration: 800 amps per cm; horizontal calibration: 20 microseconds per cm.

The results of this and other similar single-cycle tests produced several significant results, three of which stand out as being most important. First, power levels of at least 2.5 MVA are demonstrated to be feasible using the vacuum arc switches. Second, at the conduction levels achieved in this experiment, the vacuum arc switch losses are approximately five joules each for each cycle of operation, and third, the spacing between the alternations of a cycle can be at least as small as four microseconds. This first result is viewed as being important because it shows that the switches as designed are capable of standing off the voltages and conducting the currents necessary to achieve multi-megawatt inverting. Additionally, it appears from other tests [5] that single-cycle current levels of at least an order of magnitude higher are possible with properly designed switches.

The second result mentioned provides an indication of the cooling problem to be encountered in sustained operation of the inverter over many cycles. As has been previously discussed,[1] the large majority of the losses in the vacuum arc switches take the form of heat in the cathode. Therefore, cathode cooling will become a particular problem to be solved before continuous inverter operation at higher power levels can be achieved.

The third result is important because it provides an indication of the upper bound to be encountered in the plasma dispersal time in the vacuum arc switches used. The importance of this characteristic is easily seen if one imagines the firing of one vacuum arc switch in Figure 3 before the other switch has completely "shut off", that is, before the plasma density in the switch completing conduction has been reduced to the point where that switch will no longer support conduction. In such a circumstance, both switches would then be conducting simultaneously, providing a short circuit path to the power source V. At high power levels such operation clearly creates a situation earmarked for disaster. Thus, if the two alternations are to be brought close together to approximate sinusoidal operation, a highly reliable technique must be developed to insure conduction of only one of the VAS's at any one time.

Unloaded, Multi-Cycle Testing

The second mode of testing was essentially identical to the first except that sustained operation over many cycles was attempted. The voltage wave form developed across C_3 during such a test is shown in the oscillograph of Figure 5. In this test C_1 was precharged to a positive 200 volts, C_2 to positive 1.2 kV and C_3 to negative 1 kV. The vacuum arc switches were triggered at a 1 kHz rate, and the shape of the waveform envelope is due to the Q of the series resonant circuit and to the exhausting of the energy prestored in the capacitors. The peak value of the initial alternations is 1.1 kV, and the peak value of the last alternation before erratic ignition occurs is 700 volts. Thus, for this test the inverter operated at an average power level in excess of 200 kVA, at a frequency of 1 kHz for 7 milliseconds. Several other tests yielded similar results, the maximum continuous operating time being approximately 10 millisconds. It is important to note that the operating time was not limited by the device, but was the result of the energy stored in the three capacitors being expended in the circuit resistance. Only when the voltages on C_2 and C_3 dropped below 700 volts did the vacuum arc switches begin to operate erratically.

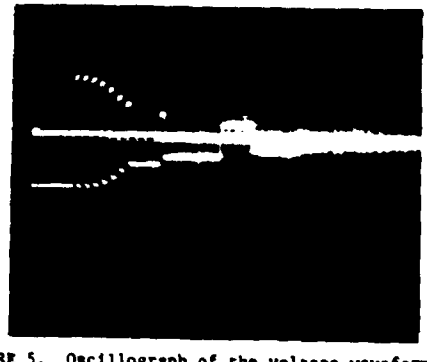


FIGURE 5. Oscillograph of the voltage waveform developed across C_3 during multi-cycle, unloaded testing. Vertical calibration: 1 kV per cm; horizontal calibration: 1 millisecond per cm.

The series of tests in this mode of operation also uncovered two particular problem areas. The first of these problems was that for voltages on C_2 and C_3 in excess of 1.6 kV, VAS_1 arced internally from the anode to the stainless steel envelope[6]. It was determined that the solution to this problem was to electrically connect the envelope to the cathode. This solution was realized by removing a section of the stainless steel vacuum line to the switch and replacing that section with a piece of insulating hose. Insulation was also inserted between the envelope and its support. VAS_1 has since been operated successfully for several cycles having peak values up to 4 kV.

The second principal problem, one that has been more persistant, is that when a switch is triggered and ignites, a signal of sufficient strength to disrupt the operation of the igniter pulse generator is coupled back along the trigger leads. Extensive grounding the shielding efforts have reduced this problem, but not eliminated it.

Loaded, Multi-Cycle Testing

As indicated in the Introduction, the third mode of inverter testing has been conducted with the transformer, rectifier and load resistance connected as in Figure 1, and sustained operation over many cycles was again attempted. Because of the increase in the rate of input energy consumption caused by the addition of the load, a different scheme for precharging the capacitors was employed for these tests: C_1 was charged to positive 1.2 kV, C_2 to positive 1.6 kV, and C_3 to negative 400 volts. The inverter was then triggered as before, except at various frequencies up to 8 kHz.

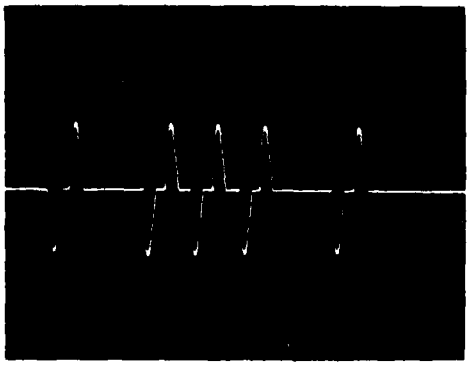


FIGURE 6. Oscillograph of the Primary Current during Multi-Cycle, Loaded Testing. Vertical calibration: 400 amps per cm; horizontal calibration 0.2 millisecond per cm.

Figure 6 shows an oscillograph of representative results of testing in this mode. This oscillograph displays the current through the transformer primary while the inverter is being triggered at a 5 kHz rate; the peak current is approximately 550 amps. This oscillograph also reveals one example of the triggering problems mentioned in the last section, and which continued into this mode of testing. The oscillograph of the primary current shown in Figure 7 presents another aspect of the triggering problem. In the test from which this oscillograph was made, the irregularities in the third alternation are caused by VAS_2 erroneously beginning conduction while VAS_1 is conducting. The cause of this occurence is not yet fully understood, although it appears that coupling through the interelectrode capacitances and through the common anode-cathode connection between the two switches has a contributing effect. This possibility is currently under investigation.

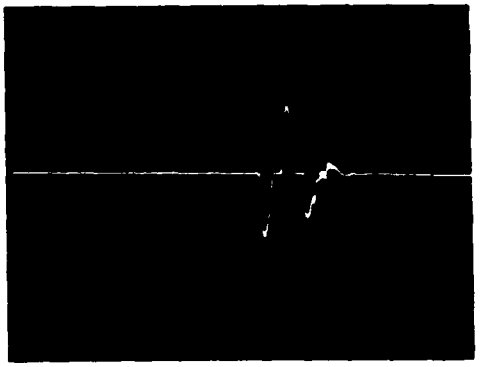


FIGURE 7. Oscillograph of the Primary Current during Multi-Cycle, Loaded Testing. Vertical calibration: 400 amps per cm; horizontal calibration 0.2 millisecond per cm.

Conclusions

The inverter has been operated in both a single-cycle mode and a multiple-cycle mode in an unloaded configuration and in a multiple-cycle mode in the loaded configuration. These tests indicate that the presently used vacuum arc switches have both the current carrying capacity and the reverse voltage stand off ability to enable the inverter to operate at 2.5 MVA for about 10 milliseconds at 1 kHz in a multiple cycle, unloaded mode. Similarly, the multiple-cycle, loaded tests indicate that the inverter will operate for several cycles at 5 kHz and higher and at power levels of 200 kVA. However, vacuum arc triggering problems indicate the need for further study of the vacuum arc switch, particularly the triggering mechanism and the effects of the interelectrode capacitances on the dynamic operation of the switches in the inverter circuit.

References

1 A. S. Gilmour, Jr., and D. L. Lockwood, "Vacuum Arc Inverter Switch Development Program", Proc. IEEE 1975 NAECON, pp 281-288, June 1975

2 A. S. Gilmour, Jr., and D. C. Hopkins, "Recent Results of Vacuum-Arc-Switched Multi-Megawatt Inverter Tests", Proc. IEEE International Pulsed Power Conference, Texas Tech University, Lubbock, Texas, Nov. 1976

3 R. N. Miller, P. T. Glinski and A. S. Gilmour, Jr., "A Facility for Testing High Power DC, AC, or Pulsed Devices", Proc. IEEE International Pulsed Power Conference, Texas Tech University, Lubbock, Texas, Nov. 1976

4 D. C. Hopkins, "Construction and Energy Loss of a Vacuum Arc Switched Series Inverter:, MSEE Thesis, State University of New York at Buffalo, Amherst, New York, February 1978

[5] C. D. Bowman, A. S. Gilmour, Jr., D. P. Malone, and R. Dollinger, "Energy Considerations in Pulsed Operation of Vacuum Arc Current Limiter", Proc IEEE Pulse Power Modulator Symposium, State University of New York at Buffalo, Amherst, N.Y., June 1978.

[6] R. N. Miller, R. Dollinger, and A. S. Gilmour, Jr., "High-Repetition-Rate High-Power Pulse Tests of Vacuum Arc Switches," Proc. IEEE Pulse Power Modulator Symposium, State University of New York at Buffalo, Amherst, New York, June 1978.

MAGNETIC FLUX CONCENTRATION WITH THE ANODE IN A VACUUM ARC SWITCH*

Y. Swen and A. S. Gilmour, Jr.

State University of New York at Buffalo

Summary

The anode of a vacuum arc switch may be used as a magnetic flux concentrator. This is done to permit the use of a large diameter field coil, perhaps located outside the vacuum envelope, for generating large magnetic flux densities in the anode-cathode interelectrode region. The time required for the magnetic flux to decrease substantially in density because of diffusion through the anode is of interest in switch applications where it is necessary for the arc interruption process to be relatively slow. In this paper measured flux diffusion speeds through a vacuum arc switch anode are compared with those calculated using the diffusion equation subject to boundary conditions in two limiting cases.

Introduction

The configuration of the vacuum arc switches being investigated [1,2] at the State University of New York at Buffalo is shown in Figure 1. A vacuum arc is ignited on the surface of the cathode with a pulse of energy applied to the igniter electrode. Conduction through the ensuing vacuum arc plasma is interrupted by applying a pulsed magnetic field to the device. As is shown in Figure 2, the anode of the vacuum arc switch may be used as a magnetic flux concentrator. This makes it possible to generate a large magnetic flux density in the interelectrode space between the cathode and the anode with a magnetic field coil having a relatively large inner diameter. The large coil diameter is necessary in some cases to make possible the location of the field coil outside the vacuum envelope. In other cases, when the coil is located inside the vacuum envelope, it is necessary to use a large coil diameter so that the coil and its supporting insulators, etc. can be adequately shielded from the metallic plasma generated by the vacuum arc.

In most applications of the vacuum arc switch the magnetic field is applied so rapidly that there is essentially no diffusion of the magnetic flux through the anode and so the desired field concentration effect is achieved. In other applications of the switch the rate of change of current during the interruption process must be relatively low and so the magnetic field must be applied gradually. In these cases the diffusion of the field through the anode may have a substantial effect on the magnitude and/or the variation with time of the field in the interelectrode space.

The objective of the study reported in this paper was to determine, analytically and experimentally, the diffusion properties of the field through the annular anodes of vacuum arc switches.

* Supported by the Air Force Aero Propulsion Laboratory and the Electric Power Research Institute.

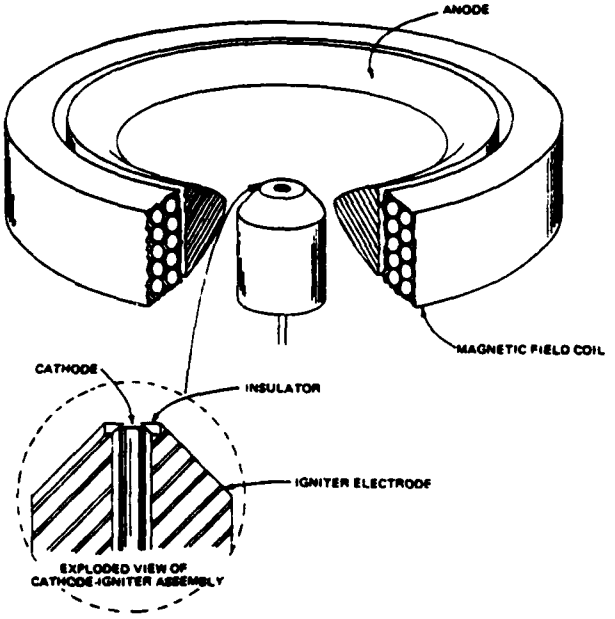


Figure 1. Vacuum Arc Device Capable of Current Limiting or Interruption

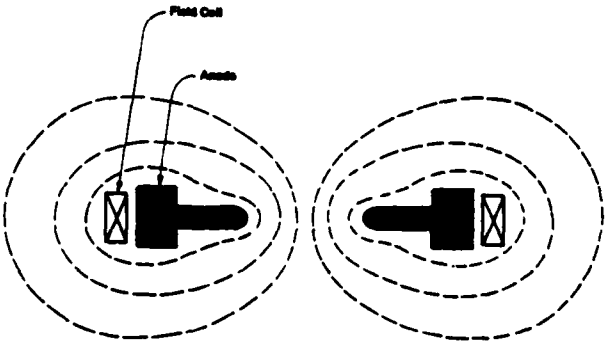


Figure 2. Concentration of Magnetic Flux by Anode

Analysis

When a slotted** anode of a vacuum arc switch is placed concentrically in a field coil, as is shown in Figure 3, and a time varying current is passed through the coil there is an induced current in the anode as is shown by the dashed line.

** The slot is necessary to prevent the anode from acting as a shorted single-turn secondary winding on a two-winding transformer.

CH1371-4/78/0000-0208$00.75 © 1978 IEEE

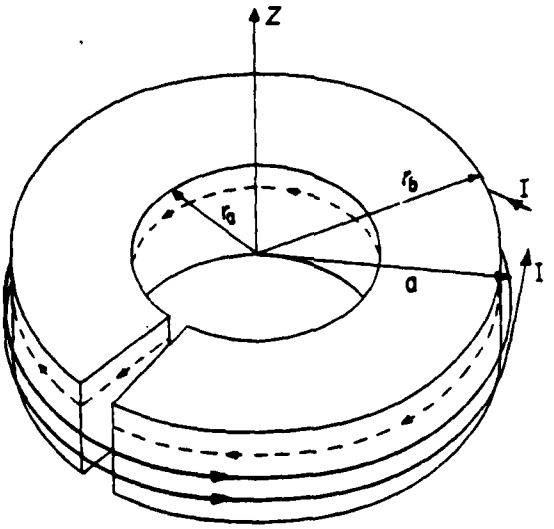


Figure 3. Induced Current in Magnetic Flux Concentrator

With the assumption that the induced current in the slot does not affect the magnetic flux density in the axial direction at the center, the magnetic flux density due to the induced current at the outer edge of the anode is in the reverse direction and is almost o the same magnitude as the magnetic flux density due to the field coil. Therefore, these two magnetic flux components nearly cancel each other. The remaining magnetic flux density is due to the induced current at the inner edge of the anode. The magnitude of this flux density can be several times the magnitude of the flux density in the absence of the anode if the inner radius of the anode is substantially smaller than the outer radius. Thus the slotted anode functions as a magnetic flux concentrator.

The magnetic flux diffusion equation is

$$\nabla^2 B - \frac{1}{K}\frac{\partial B}{\partial t} = 0 \qquad (1)$$

Where $$K = \frac{1}{\mu\sigma} \qquad (2)$$

and where B = magnetic flux density
μ = permeability
σ = conductivity

The solution can be divided into the steady state solution B_o, and the transient state solution B_t, as is shown in Eq.3. The coordinates are as shown in Figure 4.

$$B(r,z,t) = B_o(r,z) + B_t(r,z,t) \qquad (3)$$

The initial condition is

$$B(r,z,o) = 0 \qquad (4)$$

The diffusion equation will be solved subject to the boundary conditions of two limiting cases.

For case I, it will be assumed that the flux density at the surfaces of the anode is the steady state value, B_o, and that the initial flux density within

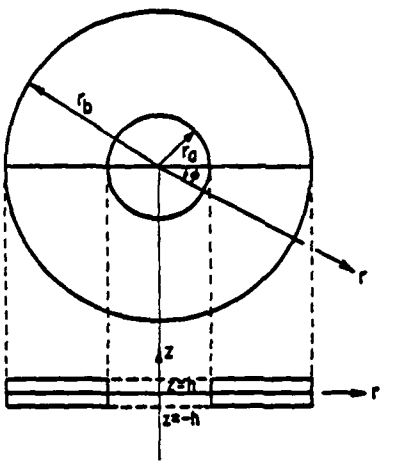


Figure 4. The Anode in Cylindrical Coordinates

the material of the anode is zero. For this case, the assumed flux density at the surface of the anode is always smaller than the actual value. (The actual value is higher because of the concentration effect.) As a result, the calculated time required to reach a specific flux level is longer than the actual time.

For case II, it will be assumed that the flux density at the inner surface of the anode ($r = r_a$) is the peak concentrated value. Again, the initial flux density within the material of the anode is zero. For this case, the assumed flux density at the surface of the anode is always larger than the actual value. As a result the calculated time required to reach a specific flux level is shorter than the actual time.

Solution of Case 1:

The steady state solution can be found by using the Biot-Savart Law.

The transient solution can be obtained by solving

$$\frac{\partial B_t}{\partial t} = K\nabla^2 B_t \qquad (5)$$

By separating the variables, the solution is

$$B_t(r,z,t) = \sum_{n=1}^{\infty}\sum_{m=1}^{\infty} C_{mn} U_o(\alpha_n r)\cos(\beta_m z)$$

$$e^{-k(\alpha_n^2+\beta_m^2)t} \qquad (6)$$

where $$U_o(\alpha_n r) = J_o(\alpha_n r)Y_o(\alpha_n b) - J_o(\alpha_n b)Y_o(\alpha_n r) \qquad (7)$$

and α_n is the nth root of

$$J_o(\alpha_n a)Y_o(\alpha_n b) - J_o(\alpha_n b)Y_o(\alpha_n a) = 0 \qquad (8)$$

β_m is the mth root of

$$\cos(\beta_m h) = 0$$

$$\beta_m = \frac{2m-1}{2h}$$

Combining the steady state solution and transient solution, the complete solution is obtain as follow:

$$B(r,z,t) = B_o(r,z) + \sum_{m=1}^{\infty}\sum_{n=1}^{\infty} C_{mn}\, U_o(\alpha_n r)\cos(\beta_m z)$$

$$e^{-k(\alpha_n^2 + \beta_m^2)t} \qquad (9)$$

where C_{mn} can be determined by the orthogonal properties of $U_o(\alpha_n r)$ and $\cos(\beta_m z)$.

where the $C_{mn}U_o(\alpha_n r)\cos(\beta_m z)$ are the weighting factors for the attenuation terms.

Solution of Case 2:

The steady state solution is separated into two parts

$$B_o(r,z) = B_o(r)\, B_o(z) \qquad (10)$$

B (z) can be approximated by a straight line since the thickness of the anode is small compared with the diameter of the anode. B (r) can be solved by the method of separating variables subjected to the boundary conditions in 5-5.

Thus

$$B_o(r,z) = \left| \frac{B_o(r_a,z)\ln(b/r)+B_o(r_b,z)\ln(r/a)}{\ln(b/a)} \right| \left| 1 + \frac{m}{B_o(r)}\, z \right| \qquad (11)$$

where m = -256 is the slope of B (z) at r=2.83 in. (7.2 cm).

The complete solution of case 2 is of the same form as in Eq. (9) of case 1, except that the steady state solution is changed to (11) instead of being obtained directly from the Biot-Savart Law.

The curves of magnetic flux density versus time can be plotted from the solutions of the diffusion equation subjected to these two boundary conditions and are shown in Figure 5.

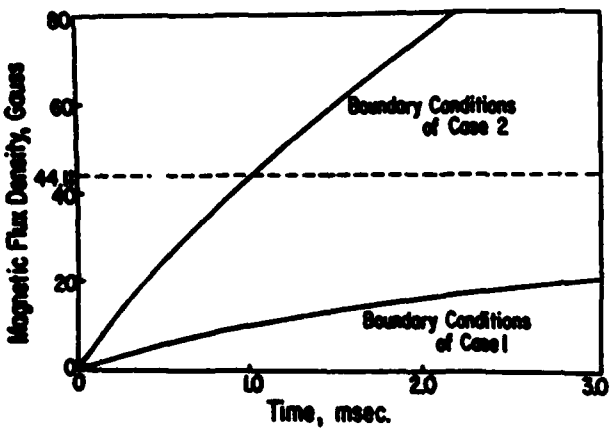


Figure 5. Results of Flux Density Calculations for Limiting Cases

Measurement of Diffusion Speed

The rate at which the magnetic flux diffuses into the anode can be measured by observing the transient response of the magnetic flux density to a step current in the field coil.

The induced voltage of an n-turn sensing coil in a magnetic field is

$$V(t) = -\, n \frac{d\phi}{dt} \qquad (12)$$

where

V(t) = the induced voltage

n = number of turns

ϕ = total flux in the coil

And the magnetic flux density is

$$B = \frac{\phi}{A} = -\frac{1}{n}\frac{\int_0^T V(t)dt}{A} \qquad (13)$$

where A is the area of the sensing coil and this area is so small that flux density is approximately uniform in this coil.

Figure 6 shows how the induced voltage is taken from the coil, then displayed on an oscilloscope after amplification and integration. The oscilloscope is triggered externally at the instant that the field current is switched on.

According to Eq. (13), the waveform which appears on the oscilloscope is proportional to the magnetic flux density versus time.

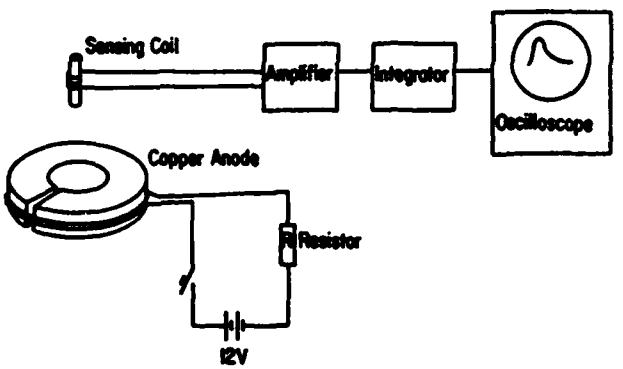


Figure 6. Technique for Measuring Diffusion Speed

A Gauss meter was used for calibrating the output signal from the integrator.

The steady state magnetic flux density in this experiment was 29.47 Gauss. The magnetic flux density can be increased either by increasing the field current or by increasing the number of turns. As the number of turns is increased, the rise time will be increased due to the increase of inductance. An excessive number of turns could not be used because it was necessary to keep the rise time of the step current in the microsecond range. As the field current is increased, the resistance of the field circuit will be increased due to the temperature rise resulting from joulean heating.

In this experiment, the number of turns n, was 2, the field current I, was 265 amperes, the radius of the current loop was 4.45 in (11.3 cm) and the voltage of the batteries was 12 volts. A magnetic flux density of 29.47 Gauss was generated at the center of the current loops.

The inductance of the two turn current loops was about 1.84 μH, the total resistance of the field circuit was 45.3 mΩ and so the rise time constant of the step input current, which is the ratio of inductance to resistance, was about 40 microseconds.

Shown in Figure 7 is the magnetic flux density versus time at the center of the current loop in the absences of the anode. This is also, of course, the current waveform in the field circuit.

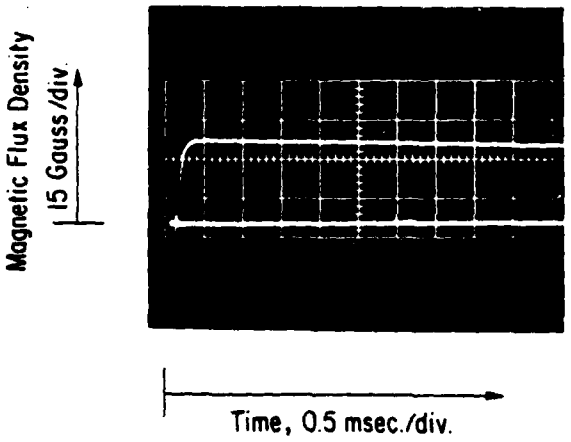


Figure 7. Output From the Integrator Without an Anode in the Current Loop

A slotted copper anode of 1.417 in (3.6 cm) inner radius, 4.25 in (10.8 cm) outer radius and 1 in (2.54 cm) thickness as shown in Figure 8, was placed concentrically within the field coils.

The magnetic flux density versus time, as shown in Figure 9 was taken from a sensing coil of 7 turns which was placed at the center of the anode. From the picture, it can be seen that the magnetic flux density can reach about 105 Gauss initially which is about 3.5 times the steady state magnetic flux density, then it decays to the steady state because the magnetic flux diffuses into the anode.

In section One, it was predicted that the peak flux density would be about three times the steady state value or about 90 Gauss. The higher value actually observed (105 Gauss) resulted from the noise introduced at the switch and by the shape of the anode.

The experiment described in the proceding paragraphs was repeated with the anode slot shorted by two copper plates. The result is shown in Figure 10. Initially the magnetic flux density was zero at the center since there was no induced current at the inner edge of the anode. However, the magnetic flux density at the center of the anode increased to the steady state value when the magnetic flux diffused through the anode.

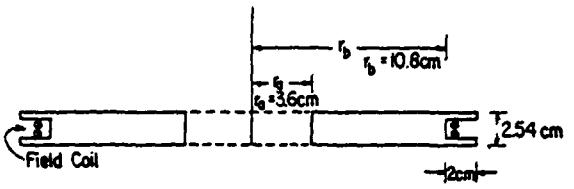


Figure 8. Cross-Section of the Anode in this Experiment

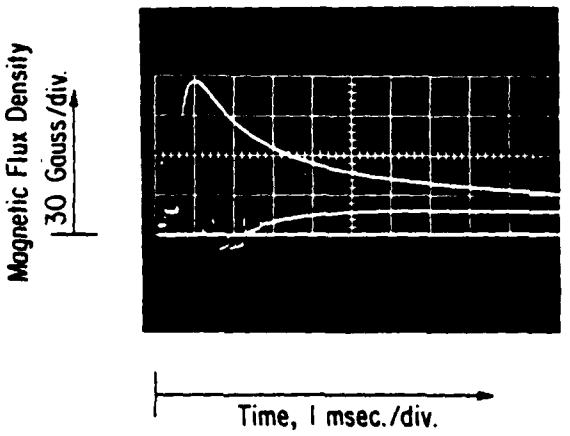


Figure 9. Output From the Integrator with an Anode in the Current Loop
The Lower Trace Was Due to the Induced Current Introduced as the Field Circuit Was Turned Off.

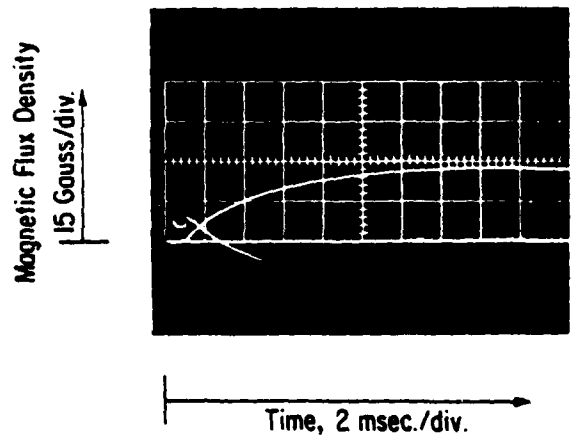


Figure 10. Output From the Integrator When the Slot in the Anode is Shorted

A hole of 0.2 in (0.5 cm) diameter was drilled at the position 2.83 in (7.2 cm) from the center of the anode. A sensing coil containing 20 turns was placed in the hole and flux density measurements were made with the slotted anode. Figure 11 shows that the magnetic flux density increased from zero to the steady state value as the mangetic flux diffused into the anode from both the outer and the inner edges.

Shown in Figure 12 are the experimental results, compared with the theoretical results from Figure 5. Note that the experimental curve initially follows the calculated curve for Case II. This is to be expected because the initial flux density at the surface of the anode is the concentrated value used for the calculations of Case 2. As expected, the experimental curve then approaches the same asymptotic value as is calculated for Case I. Note that the effective flux concentration time is on the order of one millisecond.

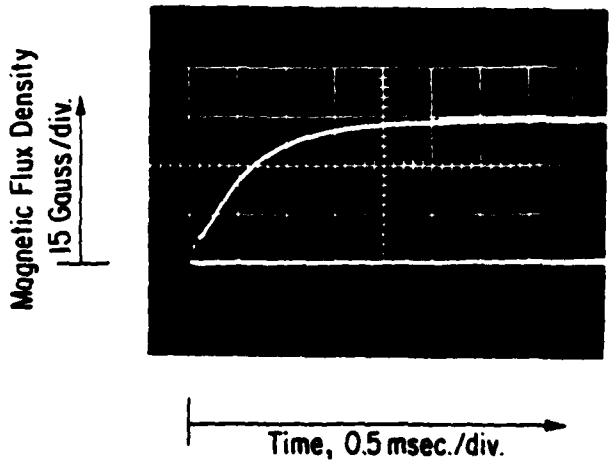


Figure 11. Magnetic Flux Density vs Time at the Position R=7.2 CM, Z=0 CM. Steady State Magnetic Flux Density = 44.11 Gauss.

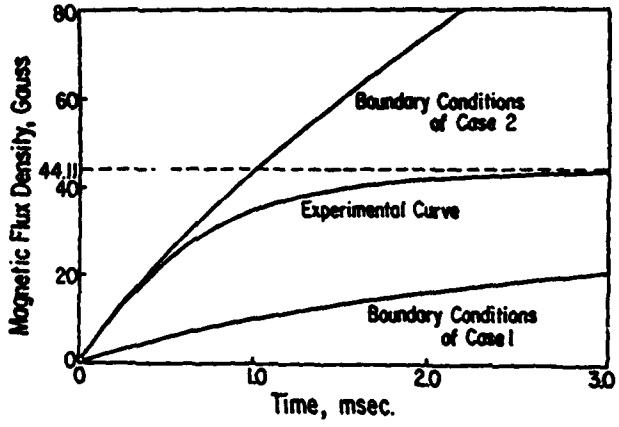


Figure 12. Measured Flux Density Compared with Calculated Values for Limiting Cases.

Summary and Conclusions

An experimental and theoretical study has been carried out to determine the magnetic diffusion properties of the anodes of vacuum arc switches. From the analysis of two limiting cases, an effective magnetic flux concentration time on the order of one millisecond is calculated for one particular anode under consideration. This time agrees well with the measured diffusion time.

References

1 A. S. Gilmour, Jr. and D. L. Lockwood, "Pulsed Metallic-Plasma Generator," Proceedings IEEE, Vol. 60, No. 8, pp. 977-991, Aug. 1972

2 A. S. Gilmour, Jr. and D. L. Lockwood, "The Interruption of Vacuum Arcs at High DC Voltage," IEEE Trans. Electron Devices, Vol. ED-22, No. 4, pp. 173-180, April 1975

ENERGY CONSIDERATIONS IN THE PULSED OPERATION OF A VACUUM ARC CURRENT LIMITER*

by

C. D. Bowman+, A. S. Gilmour, Jr., R. Dollinger
and D. P. Malone

Laboratory for Power and Environmental Studies
Department of Electrical Engineering
State University of New York at Buffalo
4232 Ridge Lea Road
Amherst, New York 14226

Summary

It has been demonstrated at SUNYAB that current peaks as high as ~ 120 kA can be limited to ~ 1 kA using a vacuum arc current limiter (VACL). During current limiting a large voltage is developed across the VACL and so a very large impulse of energy is applied to the anode. This paper describes the results of a study that has calculated the current amplitudes with and without the VACL in the system. The resulting energy impulses applied to the device were determined and a transient analysis of the temperature distribution within the anode was made.

Introduction

The work discussed in this paper resulted from interest in the possibility of using a vacuum arc device to limit fault currents to a value which power supplies can easily handle. The use of such a device in the system would result in a smaller power supply and reduced cost because the cost of a power supply that had to withstand the maximum fault current would be considerable. Limiting fault currents to low values would also limit the degree of damage to the load by preventing a high current failure in the load. The VACL is also a triggerable vacuum arc so it can be used as a turn-on switch.

The operation of a VACL depends on the characteristics of vacuum arcs. A vacuum arc is a plasma discharge established between two electrodes in a vacuum as shown in Figure 1.[1,2] The cathode material is vaporized and ionized by arc spots to provide the conducting medium. A vacuum arc discharge is a good switching medium as it makes possible a high vacuum device having excellent insulation properties when nonconducting and it becomes a plasma drop during normal conduction.

For current limiting to occur, the electrodes must be of coaxial geometry (see Figure 1)[3,4]. The cathode is a relatively small electrode placed on the axis and the anode is an annulus surrounding the cathode. The arc current may be limited by applying a coaxial magnetic field in such a way that the field lines are essentially perpendicular to the paths of the electron current from cathode to the anode. The effect of the field is to increase the voltage drop across the arc (increase plasma resistance) and therefore decrease the current. If enough current is sent through an additional magnetic field coil, the vacuum arc can even be turned off. Thus, the VACL can act as a opening switch as well as a closing switch.

* This work was supported by the Electric Power Research Institute and Sandia Laboratories.

+ Present Address: Ontario Hydro, 700 University Avenue, Toronto, Ontario

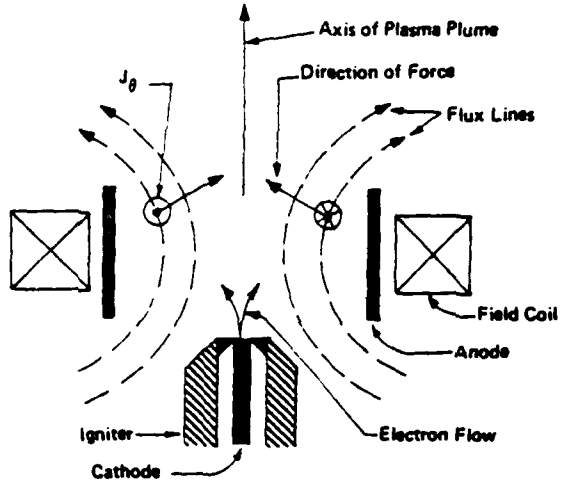


FIGURE 1. Vacuum arc current limiter.

Transient Current Analysis

The current limiting device can either be put in series with the 60 Hz power line to the power supply or in series with the unipolar output of the power supply. The present configuration of the VACL is similiar to a diode in that it conducts in one direction only. Thus, if the current in the 60 Hz power line is to be limited, two VACL's are needed for each current direction and they must be alternately triggered on each half cycle. Of course, only one VACL is needed in the output of a unipolar supply. At first sight, the latter location for the VACL might seem to be better than the former location because only one device and turn-on trigger is needed. However, the former position has the advantage that the fault current can be terminated at any of the 60 Hz current zeroes by merely not triggering the VACL which is necessary for current flow in the next half cycle. For this reason, the work presented here will assume the current limiting is done in the 60 Hz power line. Thus, the current limiter, CL in Figure 2, is actually two VACL's in anti-parallel.

The circuit under analysis is shown in Figure 2. The circuit elements are identified as:

V_S = source voltage (kV rms);

L_S = source inductance (Henrys);

CH1371-4/78/0000-0213$00.75 © 1978 IEEE

R_S = source resistance (Ohms);

R_L = load resistance;

L_L = load inductance;

I = fault current (kA);

and $V_{arc} = V_{arc}(0)\ (1 + K^2 I^2)$.

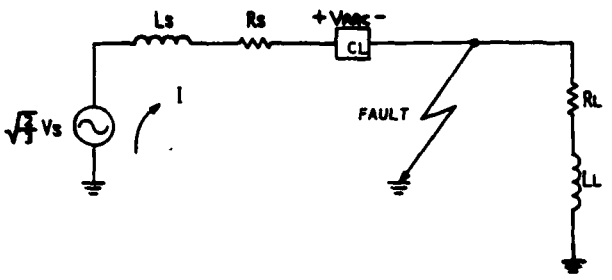


FIGURE 2. Circuit Model.

The last equation is the model for the VACL where $V_{arc}(0)$ is the arc voltage with zero magnetic field[3]. This is essentially the cathode fall potential and is assumed to be 20 V. The K^2 is a device constant[3]. The anaylsis presented uses the following values for the circuit elements.

V_S = 38 kV

L_S = 23.3 mH

$K^2 = 10^{-5}$

The greatest heating of the anode occurs when the fault current is the largest. Only the worst case is considered. Therefore, it is assumed that the fault occurs at a voltage zero, because this results in the largest fault current. The current as a function of time without the CL satisfies the equation:

$$\sqrt{\frac{2}{3}}\, V_S \sin(\omega t) = R_S\, I(t) + L_S \frac{dI(t)}{dt}$$

With the CL, the current satisfies the equation:

$$\sqrt{\frac{2}{3}}\, V_S \sin(\omega t) = R_S\, I(t) + L_s \frac{dI(t)}{dt} + V_{arc}(0)\ (1 + K^2 I^2(t)).$$

the resultant fault current with and without the CL is shown in Figure 3.

Heat Transfer in the Anode

The equation for the temperature in the anode as a function of time and distance into the anode may be obtained by solving the heat equation:

$$\frac{\partial T}{\partial t} = \alpha \nabla^2 T,$$

where

T = temperature, a function of space and time;

t = time;

α = diffusivity = $\frac{k}{\rho C_V}$;

k = thermal conductivity of anode material (copper);

ρ = density of anode material

and C_V = heat capacity of anode material.

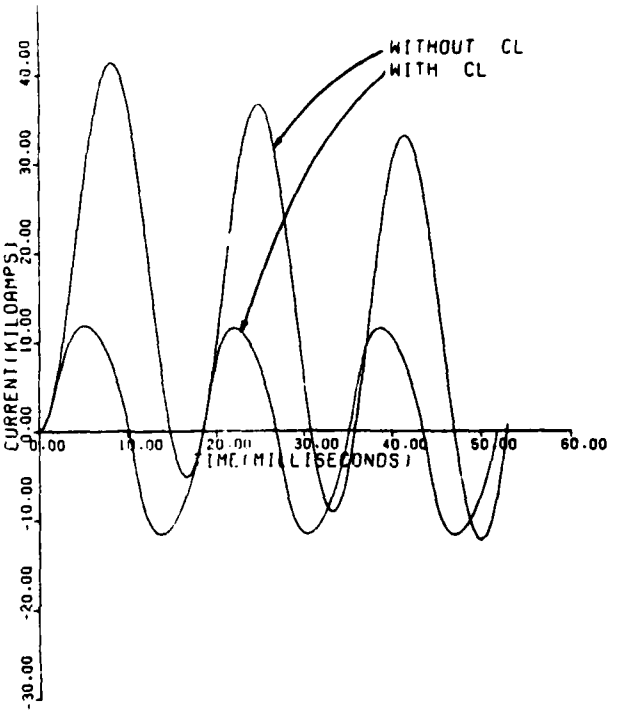


FIGURE 3. System current with and without CL.

As can be seen in Figure 1, the arc strikes the anode surface uniformly and perpendicularly, so it is assumed that the flow of heat is radially only. Because the anode diameter is much larger than the depth of heat penetration, the cylindrical anode is modelled as a one dimensional (z) heat flow problem with rectilinear symmetry. Therfore, the heat equation becomes:

$$\frac{\partial T(z,t)}{\partial t} = \frac{\alpha \partial^2 T(z,t)}{\partial z^2}$$

with the conditions:

$T(z,0) = 0$
$T(\infty,t) = 0$

and $\frac{\partial T(0,t)}{\partial z} = \frac{-D(t)}{k}$

where D(t) is the power density incident on the anode and is equal to $V_{arc}(t)\ I(t)/(\text{Anode Area})$ in watts/cm^2 D(t) is graphed in Figure 4 where the positive and negative values correspond to the power density incident on the respective anode of one VACL (i.e. one current direction) and the other VACL (i.e. the other current direction). It can be shown that the temperature distribution is given by:

$$T(z,t) = \frac{1}{k}\sqrt{\frac{\alpha}{\pi}}\int_0^A D(t-\lambda)\lambda^{-\frac{1}{2}} \exp\left(\frac{-z^2}{4\alpha\lambda}\right) d\lambda,$$

which is solved by numerical techniques.

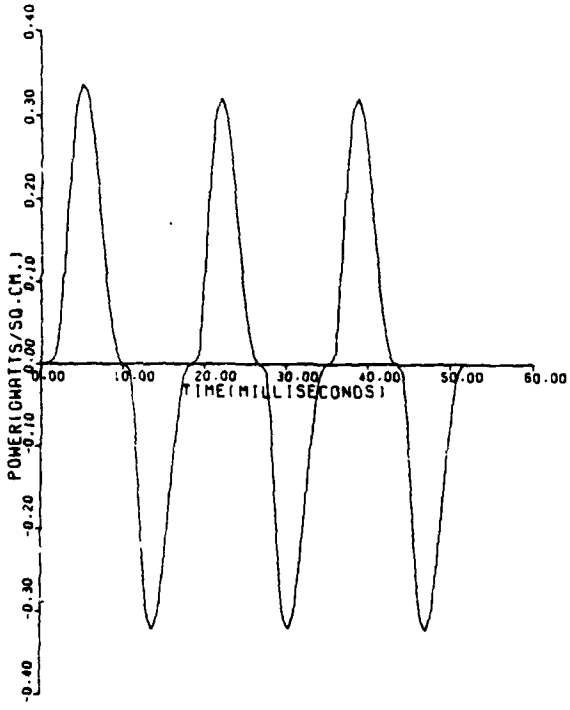


FIGURE 4. Power density incident on the anode, D(t).

The temperature distribution versus time and distance into the copper anode of the VACL which carries the first positive current pulse is shown in Figure 5. The temperature has been normalized with respect to the anode surface area. The temperature distribution curves are not given at the surface of the anode because it is not clear what is happening at or near the surface of the anode as several phenomena, such as ion implantation and radiation, which cannot be representated in this simple model are taking place. Thus, this model holds only for depths just inside the surface and farther on inward.

Anode Design

From an examination of Figure 5, one can see that the required thickness of the anode wall is small compared to its overall dimensions because the depth of heat penetration is small. Thus, the overall anode dimensions are dictated by the maximum temperature, because the dimensions must define a surface area which would limit the maximum anode temperature value less than its melting tempeature (T_m = 1083°C). For design purposes, an area which would limit this maximum temperature (T_S) to 1/2 T_M or even 1/4 T_M might be necessary. These areas are tabulated below. The corresponding minimum depths for these areas which would keep the outer surface of the anode at a temperature (T_o) less than 100°C are also shown.

	Inside Anode Surface Area	Minimum Depth into Anode such that T_0 <100°C
T_S = 1/2 T_m	10,720 cm^2	0.3 cm
T_S = 1/4 T_m	21,440 cm^2	0.6 cm

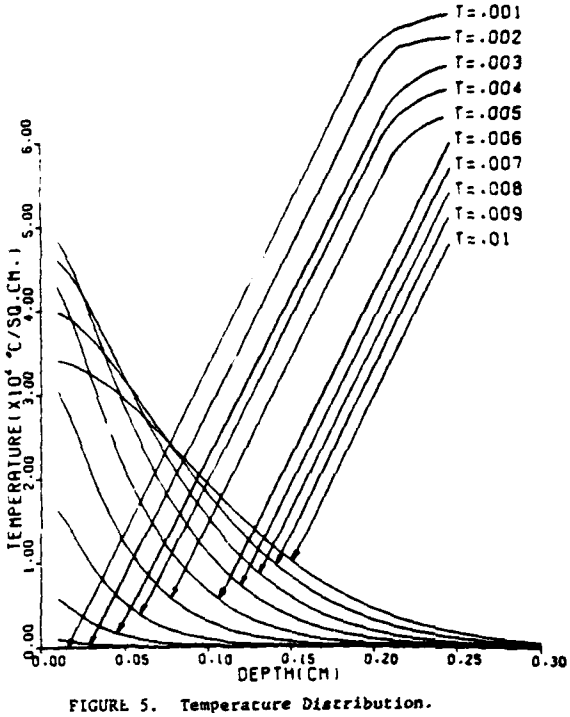


FIGURE 5. Temperature Distribution.

Conclusion

It has been shown in the preceding analysis that the anode of a VACL would have to be fairly large if the current in a 38 kV system is to be limited to 10 kA in the case of a load fault. The large dimensions are necessary in order to achieve the large anode surface areas that are needed to prevent the surface from melting. However, the model studied does not take many possibilities into account such as corrugated anode surfaces, alloy anodes, multi-layer anodes, parallel commutation resistors, etc. Whatever course is chosen, it must be kept in mind that enormous amounts of energy must be dealt with and research and development are needed if a VACL is to be feasible.

References

1 G. A. Farrall, "Vacuum Arcs and Switching", IEEE Proc. Vol. 61, No. 8, p. 1113, August 1973.

2 Amos Selzer, "Switching in Vacuum: A Review", IEEE Spectrum, June 1971.

[3] A. S. Gilmour, Jr., and D. L. Lockwood, "Pulsed Metallic Plasma Generators", Proceedings of the IEEE, Vol. 60, #8, August 1972.

[4] A. S. Gilmour, Jr., and D. L. Lockwood, "Interruption of Vacuum Arcs at High DC Voltages", IEEE Transactions on Electron Devices, Vol. ED-22, No. 4, pp. 173-180. April 1975

RELAXATION PULSING WITH A VACUUM ARC DEVICE*

by

A. S. Gilmour, Jr., R. Dollinger, C. N. Manikopoulos, P. Schwartz, M. Rosenfeld

Department of Electrical Engineering
Department of Engineering Science
Laboratory for Power and Environmental Studies
State University of New York at Buffalo

Summary

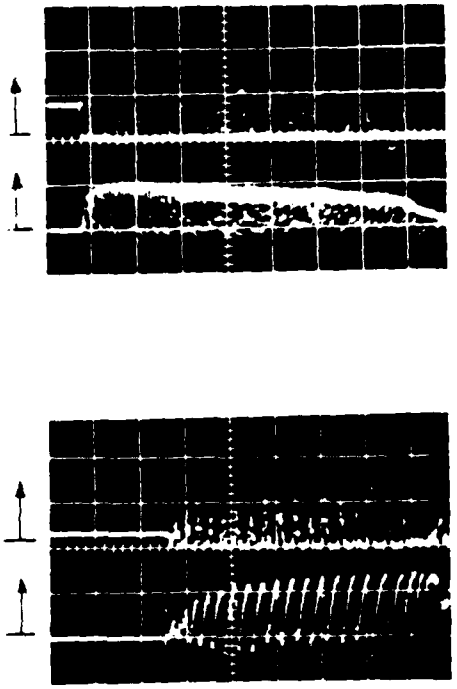
In some configurations of a vacuum arc device with a cylindrical anode and an axially positioned cathode, high-repetition-rate relaxation pulsing occurs. Narrow, repetitive voltage spikes occur with amplitudes well in excess of several kilovolts. Each voltage pulse is accompanied by a rapid "chop" in the current through the arc from a level as high as 10 kA to zero. The repetition rate for this phenomenon is approximately 30 kHz. Such a repetitive, opening switch could be very useful if its pulse characteristics could be controlled. An intensive, experimental and diagnostic effort to understand this phenomenon has been in progress for some time now. This paper will present the results that have been obtained to date concerning the spiking phenomenon.

Introduction

The type of relaxation pulsing, voltage spiking, being reported is shown in Figure 1[1]. These pulses were observed during some of the previous work on the DC vacuum arc interrupter using ring anodes and magnetic fields from external coils[2,3]. Since then, the authors have demonstrated that the magnetic field from an external coil is not necessary but that the ring anode is necessary. The following brief description of these devices and vacuum arc discharges in general is given to orient the reader.

A vacuum arc is a plasma discharge between two electrodes in a vacuum[4]. The constituent material of the negative electrode is vaporized and ionized by the arc spots to provide the conducting medium[5]. A vacuum arc discharge is an almost ideal medium for use in switching because it makes possible a high vacuum device having excellent insulation properties when nonconducting and it becomes a plasma discharge device which, depending on the configuration of the electrodes, has a low voltage drop[6,7] during conduction.

Shown in Figure 2 is a drawing of a vacuum arc device capable of producing the relaxation oscillations of the type shown in Figure 1. A vacuum-arc discharge between the cathode and anode is initiated by the use of a third electrode called an igniter. The igniter electrode is separated from the cathode by an insulator on which the metallic vapor from the arc can deposit forming a conductive thin film. To ignite the arc, a current pulse is passed through this film causing a portion of it to vaporize. The resulting plasma burst quickly fills the inter-electrode space allowing the main arc current to pass between the anode and cathode with a rise time on the order of one microsecond. During the ensuing discharge, the metallic film is regenerated, preparing the system for the next ignition pulse.



Top: 2000 V/div.

Bottom: 4000 A/div.

Time: 0.1 ms/div.

FIGURE 1. Relaxation oscillations occurring in current limiter.

As shown in Figure 2, the cathode is a relatively small electrode placed on the axis and the anode is a annulus surrounding the cathode. Only if the electrodes are of the coaxial geometry shown, can the arc current be controlled by applying a coaxial magnetic field to the device in such a way that the field lines are essentially perpendicular to the paths of the electron current from the

* This work was supported by the Electric Power Research Institute and Sandia Laboratories

CH1371-4/78/0000-0217$00.75 ©1978 IEEE

cathode to the anode. The effect of the field is to increase the voltage drop across the arc and thereby decrease the discharge current.

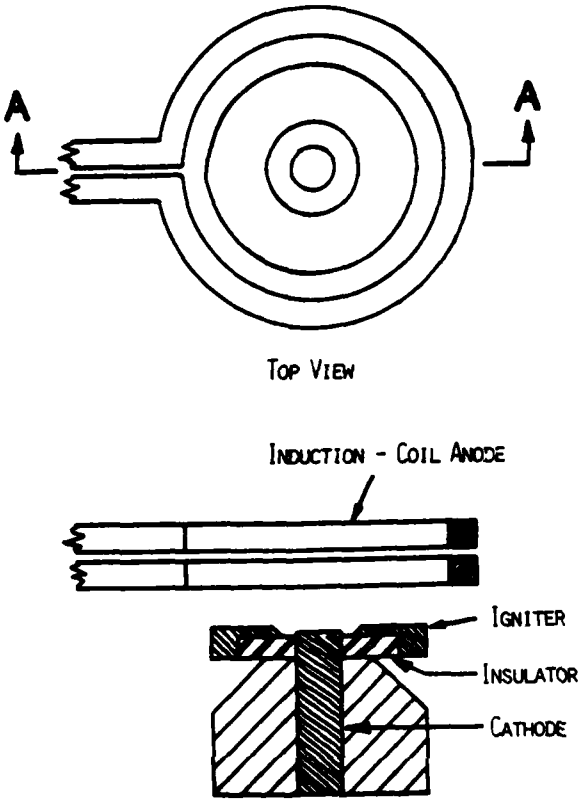
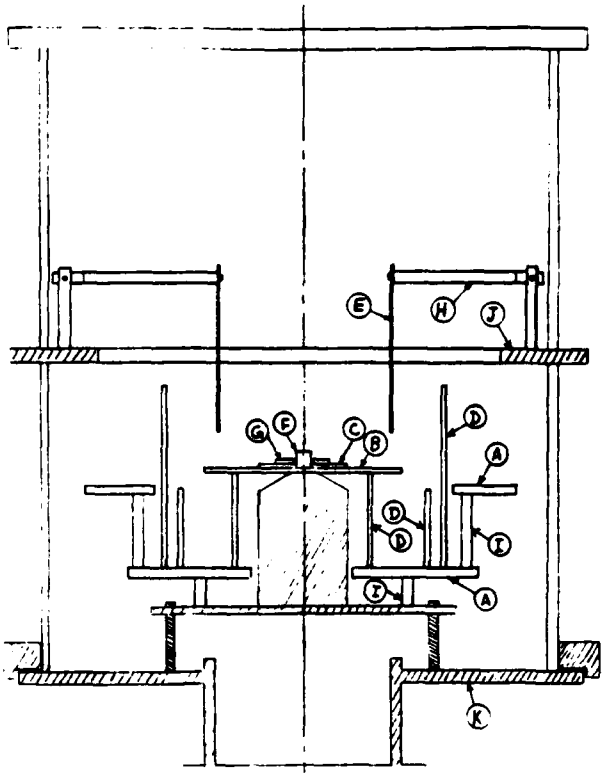


FIGURE 2. Vacuum arc device used to demonstrate the relaxation oscillation.

The vacuum arc device shown in Figure 2 can operate in the self excited mode, in that the anode current is made to flow in the magnet coil that is used to produce the axial magnetic field previously described. This can be accomplished by using the magnet coils as the anode and by suitable electrical connections of the ends of the two, single-turn induction coils shown in the figure. In the self-excited mode, this vacuum arc device becomes a current limiter which has experimentally limited fault currents to 1 to 10 kA from 3 kV sources. (The reader is referred to the literature for more details[1,2].)

It was during investigations of the vacuum arc current limiter that the relaxation pulses were seen. The unexpected occurred, however ,when these pulses were still observed when the coil ends where shorted together so that the anode current in the coils were thought to produce no net axial magnetic field. The experimental arrangement, however, was asymmetric so current flows could exist which have produced magnetic fields that might be the cause of the pulses. In order to reduce these asymmetries, the vacuum arc device drawn in Figure 3 was constructed.



A. Glass Barrier
B. Glass Plate
C. Boron Nitride Disk
D. Glass Cylinder
E. Anode Cylinder (Copper)
F. Cathode Material
G. Ignitor Ring
H. Anode Support Post
I. Ceramic Spacer
J. Anode Feedthrough Ring (Stainless Steel)
K. Cathode Base (ground)

FIGURE 3. Vacuum arc device that is presently being used to investigate the relaxation oscillation.

The key features of this device are that:

- the anode is a continuous ring,
- the electrical connections to the anode and cathode are cylindrically symmetric,
- the machine is easily accessible for the performance of diagnostics and
- the internal, structures are easily changed as required for the parameter studies.

The vacuum feedthrus for the anode and cathode are respectively the stainless steel ring separating the two glass cylinders of the vacuum chamber and the metal baseplate to the Vac Ion pump. In the scale drawing, the anode is a cylinder 10 cm high and 18 cm inner diameter. After these major constructional changes in geometry and dimensions, not only did the relaxation pulses still exist but even the repetition rate was the same (30 kHz)!

The remainder of this paper outlines the intensive experimental and diagnostic effort to understand this pulsing phenomenon+.

Parameter Studies

A series of parameter studies were initially begun not only to improve the operating characteristics of the device depicted in Figure 3 but also to help explain the phenomena. The following is a partial list of these parameter studies.

List of Parameter Studies

1) Effects of various series and parallel impedances external to the device; on the repetition rate, pulse width and amplitude of the pulses.

2) The correlation of current limiting to the occurrence of the pulses.

3) Effects of dimensions:
   a) anode height and diameter,
   b) spacing between andoe and cathode and
   c) relative location of the stainless steel ring feed thru and the anode.

4) Effects of 13 different cathode materials on 7 different characteristics of the voltage and current traces. These results were then correlated to 30 physical properties of each cathode material. Combinations of physical properties are also being studied.

5) Effects of an externally produced, DC magnetic field.

6) Effects of different vacuum chambers:
   a) Materials (glass or metal or combinations of both),
   b) volume and
   c) relative placement of internal parts.

7) Effects of different capacitor bank:
   a) capacitance,
   b) inductance,
   c) physical arrangements and
   d) voltages

8) Effects of shielding:
   a) materials (glass or metal or combinations of both),
   b) geometry (rings, cylinders, plates, washers, etc.),
   c) dimensions,
   d) general location and
   e) necessary clearances.

9) Effects of ignitor trigger:
   a) exploding thin film versus vacuum gap,
   b) waveform,
   c) duration,
   d) amplitude,
   e) polarity,
   f) energy in pulse,
   g) dimensions of ignitor,
   h) relative placement of ignitor to the cathode and anode and
   i) power source.

10) Effects of:
   a) background pressure,
   b) cleaning techniques (discharge cleaning and electrochemical polishing,
   c) material purity of the various parts and
   d) conditioning.

11) Effects of cathode spot and cell characteristics for multi-cell, multi-spot vacuum arcs.

12) The effects of new current distributions by the insertion of additional electrodes.

13) Correlation of arc turn-on to ignitor plasma, voltage, current and energy with such parameters as thin film thickness, resistance, material, cleanliness, etc.

The performance of these parameter studies did lead to improved operating characteristics and an intuitive understanding of device operation. However, it became apparent during these studies, that only a series of plasma-type diagnostics would lead to a better understanding of the relaxation pulsing phenomena.

Probable Plasma Theories

It is now believed that the relaxation pulsing is a plasma phenomena and not an electrical circuit effect primarily because a capacitor in parallel or an inductor in series with the vacuum arc device does not change the repetition rate of the relaxation pulsing. There are many possible plasma effects that could be causing the pulsing. Some of the theories are listed below.

List of Plasma Theories

1) Formation of double sheath (caused by density gradients which in turn might be caused by magnetic fields generated by arc currents).

2) Anode sheath formation.

3) The anode partially intercepts the axial ion jet generated by the cathode spots.

4) Rotating plasma spoke.

5) Magnetic field blowout of a plasma spoke.

6) Turbulent heating.

7) Standing plasma wave.

8) Plasma instability such as a repetitive "sausage" or "kink" instability.

The results available from the parameter studies are inconclusive if not contradictory, as to which theory (or theories) might be applicable. Therefore, the performance of plasma diagnostics is essential.

+ It should be noted that there is insufficient space in this paper to discuss the motivation and results of most of the various efforts being carried out and many require individual independent reports. Therefore, even though all the efforts are listed, only a few will be discussed further.

Diagnostics

There are many factors involved in the selection of just which diagnostics should be performed. Some of the more important factors are:

- The diagnostic must provide data that can be interpreted.
- The performance of a diagnostic can not interfere with the mechanism producing the pulses.
- The diagnostics should be applicable to several different theories in order to provide duplicate information in case a particular diagnostic cannot be done for some unforeseen reason.
- The necessary physical constants must be available.
- The resources (such as equipment, expertise, access to plasma, cost, personnel, time, etc.) should be available.

After many trade-offs, the following diagnostics are presently being performed.

List of Diagnostics

1) Capacitive probes to detect plasma potentials, sheaths and plasma concentrations.
2) High speed framing photography.
3) Microwave emission, reflection and interferometry.
4) Spatially resolved but time integrated spectroscopy for determing the temperature and *density of Cu I electrons.*
5) Faraday cup measurements.
6) Fast voltage and current measurements.
7) Single and double electric probes.
8) The plasma theory which is chosen from the interpretation should be consistent with the results of the parameter studies.

The interpretation of the available information is discussed in the following paragraphs.

Results

Data from the parameter study using 13 different cathode materials show that some elements produce the repetitive voltage spiking while others show very little spiking. Furthermore, the occurrence of spiking is dependent on the capacitor bank voltage prior to the ignition of the vacuum arc discharge. This can be seen in Figures 4, 5 and 6 where arc current is graphed versus the initial voltage on the capacitor bank. The straight line is the current that would flow in the 1/4 Ohm series limiting resistor if the arc voltage is zero. The other curve is experimental. Any large divergence of the two curves indicate voltage spiking (i.e. an increased averaged arc voltage that causes a reduced current flow). A small divergence represents only a small arc voltage and no significant spiking. Thus, chromium (see Figure 4) produces negligible spiking; aluminum (see Figure 5) exhibits spiking at low bank voltages and vanadium (see Figure 6) causes spiking at all bank voltages. Typically, the amplitude of the voltage spikes is in excess of 60% of the bank voltage.

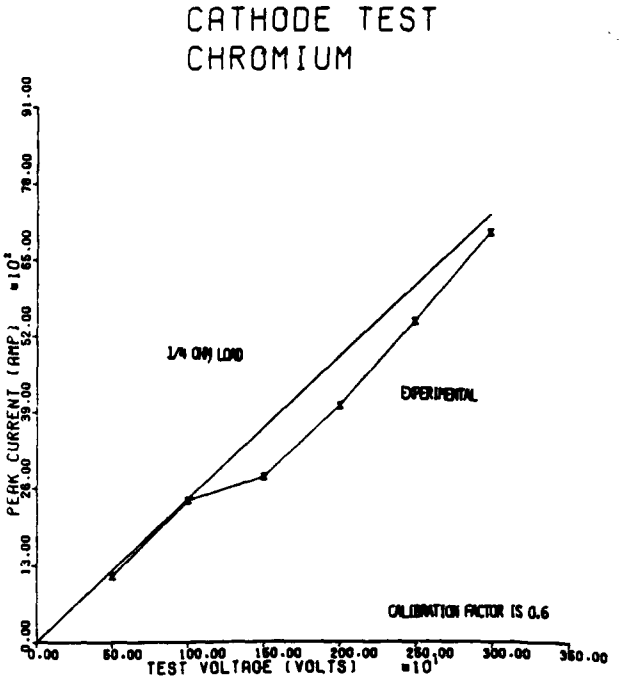


FIGURE 4. Arc current versus initial voltage on capacitor bank which shows that chromium produces negligible voltage spiking.

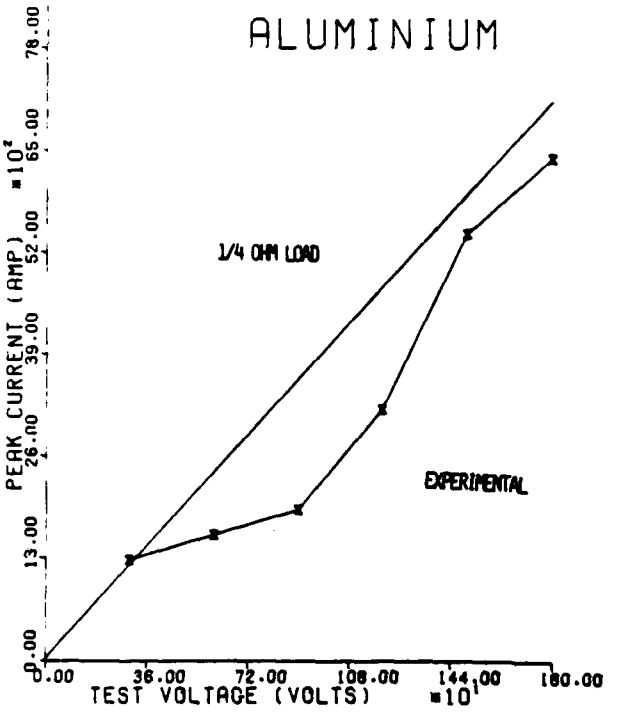


FIGURE 5. Arc current versus initial voltage on capacitor bank which shows that aluminum produces spiking only at low bank voltages.

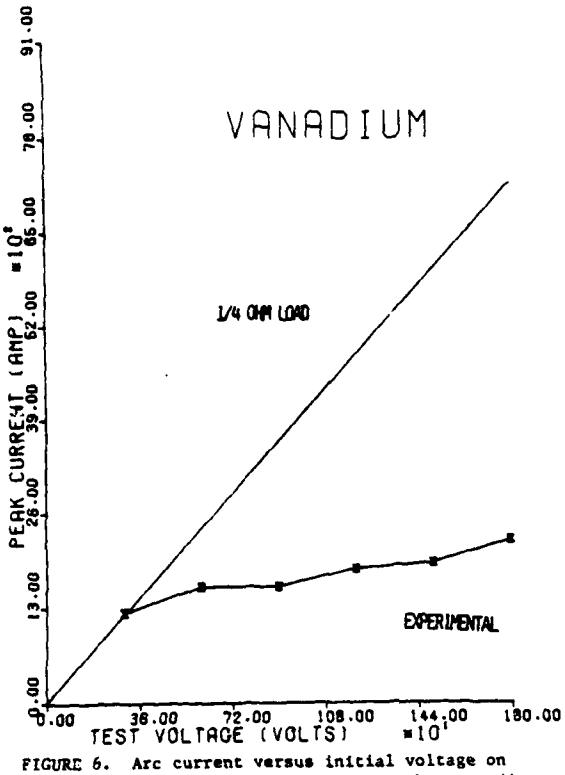


FIGURE 6. Arc current versus initial voltage on capacitor bank which shows that vanadium produces voltage spikes at all bank voltage.

Conclusion

The spectographic study shows that copper ions are found only in the axially oriented plasma plume which is ejected by the cathode spots. The results of 10 GHz microwave interferometry and reflection measurements correlate in showing a decrease in electron density during spiking.

Most of the completed diagnostics give more of an indication of which theories are not applicable than those which are applicable. In this regard, it seems that a rotating plasma spoke, the magnetic field blowout of a plasma spoke, turbulent heating, standing plasma wave and a repetitive sausage or kink instability are unlikely in this vacuum arc device. They do indicate that the plasma energy is being uniformly deposited on the anode surface. This is desirable because it means that the dimensions of a high power vacuum arc relaxation pulser could be kept to a minimum.

Acknowledgements

The authors wish to acknowledge the efforts of D. Benenson, D. Malone, R. Bennett, C Bowman, W. Crompton, D. Dettman, J. Lee, D. Huang, G. Smith, J. Sullivan, P. Tam and F. Yao for their work on this project even through there was insufficient space in the paper to give the results of their work.

References

1 Electric Power Research Institute EL-276-SR, "Symposium Proceedings New Concepts in Fault Current Limiters and Power Circuit Breakers", A. S. Gilmour, Jr., pp 17-1 thru 17-18, April 1977.

2 A. S. Gilmour, Jr. and D. L. Lockwood, "Pulsed metallic-plasma generators," Proc. IEEE, vol. 60, pp. 977-991, August 1972.

3 A. S. Gilmour, Jr. and D. L. Lockwood, "The Interruption of vacuum arcs at high dc voltages," IEEE Trans. on Electron Devices, vol. ED-22, no. 4 pp. 173-180, April 1975.

4 G. A. Farrall, "Vacuum arcs and switching," IEEE Proc. vol. 61, no. 8, pp. 1113, August 1973.

5 A. E. Gile, "Arc electrode phenomena," Proc. Inst. Elec. Eng. (IEEE Review) vol. 118, pp. 1131-1154, September 1971.

6 A. Selzer, "Switching in vacuum: a review," IEEE Spectrum, vol. 8, pp. 26-37, June 1971.

7 M. P. Reece, "The vacuum switch," Proc. Inst. Elec. Eng., vol. 110, pp. 793-811, April 1963.

MAGNETICALLY MODULATED VACUUM ARC FOR DC SWITCHING

Rolf Dethlefsen and Justus Mylius
Gould Inc., R&D Division
P. O. Box 98, Greensburg PA 15601

Summary

Experiments are reported on vacuum arcs in a magnetron-type discharge geometry. Magnetic fields up to 0.6 Tesla are applied. Various de-gassed cathode materials are tested at currents up to 10 kA.

Depending upon geometry, the magnetic field can raise the vacuum arc voltage from typically 150 V to several kV. The probable cause is an electron space charge current limitation in front of the ring shaped anode.

Dependent upon parallel capacitance, strong oscillations are excited by the magnetic field. Application of the magnetic field can reduce the arc current from several kA to the current chopping level, where circuit interruption is followed by rapid dielectric recovery. High repetition rates in the kHz region appear feasible.

INTRODUCTION

The term vacuum arc is used for discharges conducted in a vacuum ambient through a medium of ionized electrode material which is usually eroded by the arc attachment from the cathode. The arc voltage is in the range from about 15V to 100 V for electrodes with opposing surfaces.

Higher arc voltages can be observed if a line of sight connection does not exist between cathode and anode, because the arc plasma requires a supply of positive ions which are emitted at high velocity from the cathode spots.

A. S. Gilmour[1,2,3] showed in 1967 that a vacuum arc in a coaxial geometry could be switched off by the application of an axial magnetic field. 800 A interruption at a recovery voltage of 25 kV and also a repetition rate of 1 kHz at reduced power levels were demonstrated. From the development of AC vacuum circuit breakers, it is known that a vacuum arc in suitably processed and degassed hardware allows circuit interruption following a current zero with high intrinsic values of di/dt and du/dt.

The possibility of magnetically modulating a vacuum arc to the point of discharge extinction allows new applications to emerge. DC circuit breakers or fast acting commutation switches are conceivable. A magnetically controlled high power, high repetition rate modulator could allow continuously variable pulse length. A weight reduction may result in comparison with the pulse forming network - thyratron systems. Other uses for high power, high repetition rate ON-OFF switches exist in the general area of power conversion and inductive energy storage.

Gould Inc. is involved in protective switching for electric power systems. Following A. S. Gilmour's work, magnetically modulated vacuum arcs have been investigated with respect to the development of a fast acting commutating switch. A progress report is given about work that is proceeding under EPRI sponsorship.

The objective is to increase the interruption ability while using realistically sized vacuum envelope hardware for the experimentation in order to insure practical applicability of the results.

Experiments

Standard vacuum interrupter materials are used for construction of the experimental devices. The cathode consists of various vacuum degassed metals. The ring shaped anode surrounds the central cathode coaxially. The anode constitutes a part of the vacuum envelope. The test chamber is demountable for a quick change of the experimental variables. Vacuum in the 10^{-7} Torr range is provided by an ion pump with sorption rough pumping.

The vacuum arc is initiated by a trigger discharge which is established by a voltage surge between an auxiliary trigger electrode and the cathode (see Fig. 1).

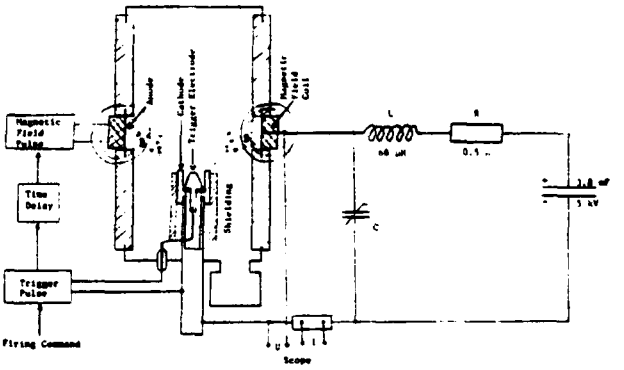


Fig. 1. Test setup for the Magnetically Modulated Vacuum Arc. Power is provided by a Discharge Capacitor Bank.

The current is fed coaxially to the test device in order to minimize the magnetic effect of the current return path.

The resulting vacuum arc discharge burns with about 150 V arc voltage until the stored charge is drained from the discharge capacitor bank which serves as a convenient supply of test power. Application of a magnetic field raises the arc voltage substantially. Circuit interruption results if the experimental parameters are chosen properly. Residual voltage

CH1371-4/78/0000-0222$00.75 © 1978 IEEE

remains on the capacitor bank if a circuit interruption is performed.

The magnitude and shape of the discharge current and the transient circuit recovery voltage following an interruption are controlled by air core inductor L and resistor R. Further capacitance C is placed in parallel to the discharge device as an experimental variable. The pulse shape of the test current is determined by the total circuit inductance, resistance and the 3.8 mF capacitance of the capacitor bank. The frequency of the recovery voltage oscillations is determined by the parallel capacitance C and the circuit inductance L. Capacitance C is charged in parallel with the capacitor bank. Upon triggering of the vacuum device, an oscillatory inrush current is created which is determined by capacitor C and the distributed inductance between C and the vacuum device. (About 2.0 μH). The inrush current often crosses the zero line which can lead to premature recovery of the vacuum gap. In this case only a short pulse of current is conducted. This problem is overcome by extending the length of the trigger pulse.

Magnetic switching is initiated after the oscillatory inrush current has been damped out. A typical switching operation is shown in Fig. 2. 0.4 msec after initiation of the 4.5 kA vacuum arc, a magnetic field is applied which drives the arc current toward zero. The peak transient recovery voltage is 9.5 kV.

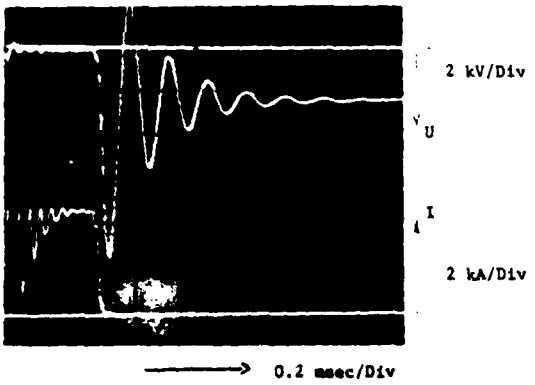


Fig. 2. 4.5 kA Vacuum Arc switched off by the application of a 59 mT magnetic field pulse. Copper Cathode. 11.4 μF of capacitance parallel to the vacuum device.

Magnetic Control Field

The magnetic control field is generated by discharging a capacitor into a winding of about 10 turns of solid core automotive ignition wire which surrounds the anode. This wire provides sufficient high-voltage insulation and high temperature capability.

The anode acts as a partial short circuit winding to the pulsed magnetic field coil. The magnetic field pulse diffuses through the anode as described in the following partial differential equation.

$$\nabla^2 \vec{B} = \mu \sigma \frac{\partial \vec{B}}{\partial t}$$

with $\vec{B}$ = magnetic field strength

μ = magnetic permeability

σ = electrical conductivity

t = time

The associated time delay τ can be estimated by inserting characteristic variables.

$$\tau = \mu \sigma d^2$$

with d = anode wall thickness

τ = typical time delay of the magnetic pulse diffusing through the anode metal, flat plate approximation

An example of a magnetic field calibration is shown in Fig. 3. The lower trace is obtained from a calibrated search coil placed inside the anode. The upper trace shows the exciting current flowing through the winding on the outside of the anode. Diffusion delays the peak of the magnetic field by about 0.3 msec beyond the peak of the current.

The time delay can be varied over a wide range by properly choosing the anode wall thickness, conductivity and permeability of the material.

The magnetic field can either be excited from a separate power supply with electronic control for timing or from the anode current through a series connected winding. In the latter case the diffusion time delay can replace the electronic timing control. Anode geometry and material can be designed for a time delay up to a millisecond. The series connected winding simplifies the system considerably.

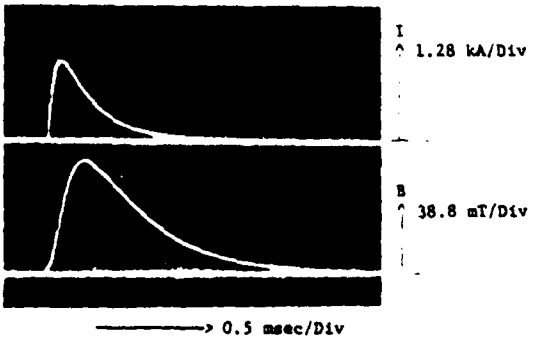


Fig. 3. Magnetic Field Pulse inside the ring anode and excitation current in 8 turn coil surrounding the anode

PARAMETRIC STUDIES

1. Discharge Geometry

Magnetic modulation of vacuum arcs requires the application of a magnetic field rectangular to the flow of arc current. Most effective is an axi-symmetric electrode arrangement where a closed-ring Hall-current can be established.

Coaxial cylinder and parallel disc-electrodes were tried. These were found to be less effective than the geometry of Fig. 1, which is detailed in the cross section drawing of Fig. 4. A metallic section of the vacuum envelope acts as the vacuum arc anode, thus eliminating any possible problems with separate anode feedthrough connections. The cathode is mounted on axis with an offset. The counter plate to the cathode is kept electrically floating in order to eliminate spurious cathode spot attachment. The trigger electrode is mounted inside of the cathode.

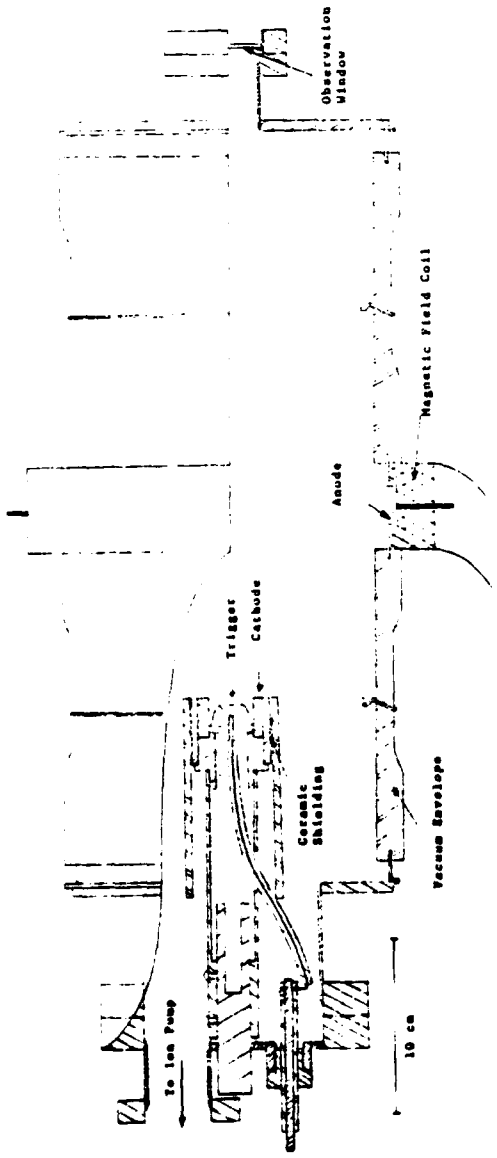


Fig. 4. Coaxial discharge geometry with axially offset cathode

High speed ion and neutral jets are emitted at right angle from the cathode spot attachment area. Elevated arc voltage results if the anode is shielded from impingement of these jets. Elevated arc voltage is also associated with high frequency oscillations on the current and voltage trace.

2. Pressure

The demountable test facility is not baked after assembly. The interior surfaces are therefore loaded with surface gases. Initial discharges result in gas bursting. The initial switching ability is impaired. It appears that a low plasma density in front of the anode is essential to attaining high arc voltage and switching ability in the presence of a magnetic field.

3. Magnetic Field Strength

The stated magnetic field strength applies to the inside of the ring-shaped anode. The value on the axis is about 37% lower.

Magnetic modulation of the vacuum arc impedance is demonstrated in Fig. 5. 0.7 msec after start of the discharge, a magnetic field pulse of 0.54 Tesla peak magnitude is applied to a 4.5 kA vacuum arc. For the duration of the magnetic field pulse, the arc voltage is raised from 300 V to a peak of 1,700 V. Oscillations of about 40 kHz frequency are introduced if the parallel capacitance is 7.6 μF. Shut-off does not occur with this particular test shot.

The magnetic field strength determines the magnitude, but not the frequency of the oscillations during the magnetic modulation.

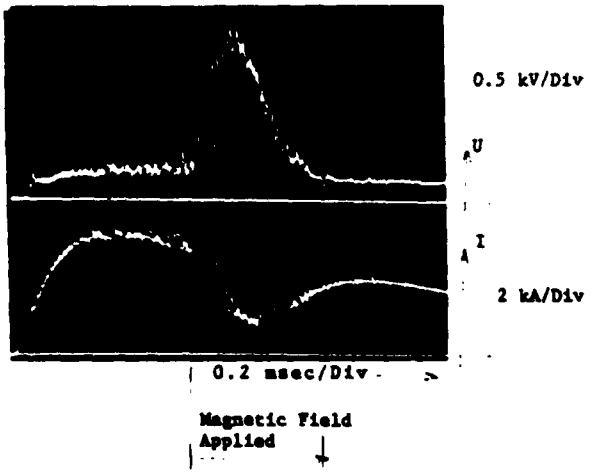


Fig. 5. Elevation of arc voltage due to an applied magnetic field of 0.54 T peak magnitude. Aluminum cathode, parallel capacitance 7.6μF

This observation rules out a rotating current spoke as the source of oscillation. The frequency of a rotating instability would grow with the magnetic field strength.

A summary of magnetic modulation data is shown in Fig. 6. The vacuum arc impedance as derived from noise averaged values of arc voltage and arc current is shown as a function of the instantaneous magnetic field strength. The data are derived from oscillograms similar to Fig. 5. Parameter is the arc current.

The voltage - current characteristic of the vacuum arc is positive without applied magnetic field. The value is near 0.04 Ω.

The voltage current characteristic changes to negative when sufficient magnetic field is applied. Progressively larger magnetic fields are required to achieve magnetic modulation at higher arc currents.

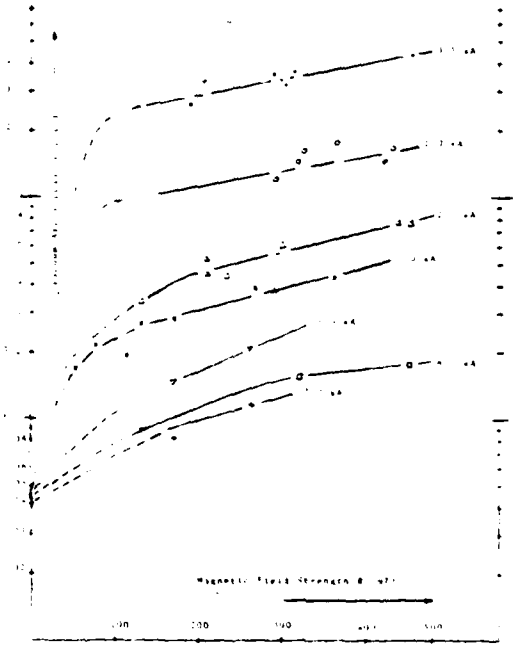


Fig. 6. Increase of vacuum arc impedance due to applied magnetic field. Parameter is the arc current. Molybdenum cathode with ring anode of 330 cm^2 area. Pressure 10^{-7} Torr range.

4. Shunt Capacitance C

The magnetic field increases the arc voltage and excites oscillations which are identical in frequency with the inrush oscillations. This frequency scales approximately with the shunt capacitance to the $-\frac{1}{2}$ power.

The observed oscillations exchange energy between the vacuum device and the shunt capacitor. It is suggested that this is related to an oscillating electron space charge sheath in front of the anode.

DC circuit switching can be obtained when the magnetically induced oscillations bring the arc current toward zero. For a clean vacuum system, dielectric recovery will follow with a high du/dt capability. Adding 15μF of shunt capacitance to the vacuum device increases the dc switching ability by a factor of about two.

For low values of shunt capacitance, it takes many oscillations until the arc current is forced to zero. With shunt capacitance over about 10 μF, the arc current can be brought to zero within the first oscillation (see Fig. 2). An example of 13 hKz oscillations excited by a 0.54T magnetic field is shown in Fig. 7.

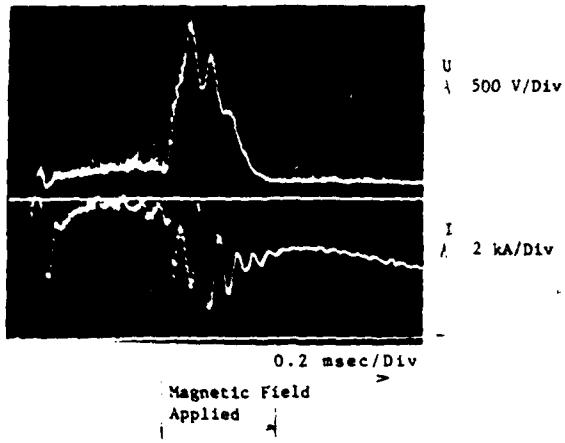


Fig. 7. Elevated arc voltage and oscillations excited by a magnetic field of 0.54T peak magnitude. Aluminum cathode, parallel capacitance 60 μF.

5. Cathode Materials

Magnetically modulated vacuum arcs can be operated with either a liquid or solid cathode of sufficiently low vapor pressure. Fourteen solid cathode materials were tested with respect to trigger and switching ability. These were in the shape of a 1 cm diameter cylinder surrounded by a trigger electrode. The ring-shaped anode had an area of 330 cm^2. The parallel capacitance was 0.04 μF. Arc voltage was measured as a function of current and magnetic field strength. High frequency noise of about 100 to 200 V amplitude is superimposed on the voltage traces. High arc voltage is associated with high noise amplitude.

Average values of arc voltage are shown in Table I. The strongest magnetic modulation of arc voltage is obtained for molybdenum, vanadium, titanium and aluminum. The amplification factor appears to be related to a low atomic weight and a high melting point of the cathode material.

The following materials were found easy to trigger:

Aluminum, silver, titanium, graphite and molybdenum, vanadium only if a graphite trigger electrode is used.

The switching ability with 134 mT of magnetic field applied during the cathode study was over 3 kA for the following materials: Aluminum, titanium, nickel, copper and tungsten.

TABLE I

Cathode Material	Average Arc Voltage at 3 kA for Magnetic Field Strength of 0	19 mT	57 mT	96 mT	134 mT	Amplification Factor
	Volt	Volt	Volt	Volt	Volt	
Aluminum	200	330	500	600	800	4
Silver	150	180	300	400	520	3.46
Titanium	200	320	500	700	900	4.5
Iron	200	240	500	480	500	2.5
Nickel	200	270	480	800	820	4.1
Copper	250	300	500	500	760	3.04
Molybdenum	160	240	500	680	800	5
Graphite	200	200	280	400	550	2.75
2% Thoriated Tungsten	170	180	300	430	580	3.4
Tungsten	200	260	400	560	700	3.5
Vanadium	140	200	400	450	680	4.85
Tantalum	170	320	500	420	600	3.5
Niobium	200	500	500	600	760	3.75
Chrome	200	240	400	560	680	3.4

The lowest switching ability was shown by: Silver (2.4 kA) thoriated tungsten (2 kA) and graphite (below 2 kA).

6. *Potential Distribution*

The floating potential was measured on several metallic inserts in the vacuum envelope in order to locate the potential drop region which is associated with elevated vacuum arc voltages. The arc current was 3 kA. It was found that either with or without magnetic field, the major potential drop occurs in the anode area.

The floating potential at any position measured a minimum of 55 to 60 volt positive in relation to the cathode. Application of the magnetic field does not raise the potential in areas which are remote from the anode.

DISCUSSION

Commonly cathode and anode oppose each other in vacuum interrupters. The high velocity plasma jets originating from the cathode impinge on the anode where they lead to relatively high local plasma densities.

The present coaxial electrode geometry is such that the cathode jets do not directly reach the anode.

It is postulated that the plasma in front of the anode becomes too tenuous to maintain charge neutrality. A space charge layer forms which requires a large potential drop in order to provide continuity for the arc current. A plasma sheath usually assumes the width of about 10 times the Debye Length.

The voltage - current relation of a space charge layer can be calculated from the Child-Langmuir relation (4). The observed anode current density and potential drop indicate a space charge layer of a few mm thickness. This is in a reasonable relation to the Debye Length as calculated from plasma parameters known from the literature.

The theory of operation is not sufficiently developed. Work is proceeding in cooperation with Prof. Gilmour at the State University of New York at Buffalo.

The highest switch-off ability so far attained was 9 kA with a peak recovery voltage of 6 kV. The parallel capacitance was 157 µF with a magnetic field strength of 97 mT applied, using a molybdenum cathode.

The highest arc voltage amplification factor due to a 0.6 T magnetic field applied to a 2 kA arc on a molybdenum cathode was 22.5. The cathode material study indicated that high melting point and low atomic weight lead to a high amplification factor. This suggests that beryllium might be a superior cathode material. Beryllium has not been tested due to its toxic nature.

A high level of current chopping is expected to aid the switching ability. A vacuum arc cathode of molybdenum shows the highest current chopping level (1). Molybdenum is therefore a preferred cathode material.

The present design using a magnetic field coil outside the vacuum envelope leads to a relatively slow rise of the magnetic field strength. Nevertheless current switch-off with a rate of fall of current between 100 and 200A/µsec has been attained.

ACKNOWLEDGMENT

The skillful laboratory work of Norm Oswalt, Dave Moreno and Joe DeSalvo is gratefully acknowledged.

REFERENCES

1. A. S. Gilmour, D. L. Lockwood
The Interruption of Vacuum Arcs at High DC Voltages. IEEE Trans. on Electron Devices Vol. ED-22 No. 4 pp. 173-180 (1975)

2. A. S. Gilmour, D. L. Lockwood
Pulsed Metallic - Plasma Generators
Proc. IEEE Vol. 60 pp. 977-991 (1972)

3. U. S. Patent No. 3,396,264 (1972)
Magnetically Modulated Vacuum Arc Diode

4. J. D. Cobine
Gaseous Conductors p. 125
Dover Publications, 1958

ADVANCES IN THE DEVELOPMENT OF A GAS DISCHARGE SWITCH HAVING A REPETITIVE CURRENT INTERRUPTING CAPABILITY

R.F. Caristi, R.P. Simon, and D.V. Turnquist
EG&G, Inc., Salem, Massachusetts

Summary

The practical applications of a repetitively openable and closable high current, high voltage switch have resulted in considerable interest in the phenomenon of current interruption in a conducting gas by the application of a transverse magnetic field to a gas discharge channel. Such a switch is useful as a series-connected protective device, a controllable charging diode, a mechanism for the generation of variable width pulses at high power levels, and as a regulating device for high power, high voltage sources.

The physical basis for magnetic current interruption has been shown to be the action of the $J\times B$ force on the gaseous conductor. This force serves to drive the gas against a suitably chosen channel sidewall such that the impedance of the discharge rapidly increases as recombination takes place. The geometry of the discharge channel is thus important in the design of a practical magnetic interrupter.

The parameters of principal interest are the current being interrupted, the voltage level of the interruption, the voltage drop across the switch when it is fully conducting, and the magnetic field energy necessary to achieve the interruption.

A practical gas discharge switch has been developed which contains a unique "chuted-wall" discharge channel. This geometry allows reliable interruption of high current at high voltage with readily achievable magnetic fields. Nevertheless, the switch operates with a reasonable voltage drop when in the closed state. Based on hydrogen thyratron technology, the device is scalable to high power levels, operates at usefully high pulse repetition rates, and exhibits an economically feasible life time.

The interruption of 600 amperes at 20 kilovolts has been achieved with a magnetic field energy of less than 8 joules. The interruption of 1 to 2 kiloamperes at 50 kilovolts is anticipated using comparable magnetic fields in a device operating with a total drop of 1400 volts when in the closed state. A life of 10,000 hours including 20,000 interruptions at full power is projected.

Introduction

The interruption of a gas discharge current by the application of a transverse magnetic field has been the subject of considerable study in recent years. Various workers have considered the phenomenon as a potential mechanism for developing an openable switch for use in a variety of applications including the protection of microwave tubes against internal arc-overs[1-6], a triggered charging tube with magnetic protection[5], and the generation of variable-width, high power pulses[5]. Other applications include arc protection for high power gas lasers, and command-charge/stop-charge service in high energy modulators and pulse generators.

The physical basis for magnetic interruption is the action of the $J\times B$ force on a gaseous conductor such that upon application of the magnetic field, the conducting gas is driven against the sidewall of the gas discharge channel[4-5]. Recombination then rapidly ensues, and the impedance of the discharge column increases accordingly. If the magnetic field is established at a level insufficiently high to provide a complete interruption, the discharge can be constrained to function as a variable impedance, the value of which can be controlled via the intensity of the applied magnetic field.

A practical mechanism for utilizing the magnetic control of a gas discharge is to incorporate a discharge channel into a hydrogen thyratron. In the absence of any magnetic field, the resultant device operates substantially as a standard hydrogen thyratron. It will thus function as a closable switch upon application of a suitable triggering pulse to the grid, and may be maintained in the conducting state with a keep-alive current if desired. Upon application of a magnetic field, the switch current can be interrupted wholly or partially as desired. Permanent interruption can be achieved, even with a pulsed magnetic field, if the keep-alive is removed upon application of the field, and the device is equipped with a holdoff section capable of gaining control during the period over which the pulsed field is impressed. The discharge will not restrike, and the switch will remain open until it is retriggered and the keep-alive is reapplied. Such a device thus operates as a uni-directional switch, capable of operation in either the normally open or normally closed states. Alternatively, the device can be made to function as a variable impedance, the value of which may be controlled by the magnetic field independently of the system voltage or impedance level.

The parameters of principal concern in the development of such a switch are the current to be interrupted, the voltage level of the interruption, the voltage drop of the device when it is in the fully conducting state, and the magnetic field intensity necessary to achieve interruption. This discussion addresses the relationships existing among these parameters for a class of practical and efficient switches designed to interrupt currents of at least 300 amperes at voltages in excess of 15 kilovolts.

Discussion

Types of Interrupters

Figure 1 illustrates in schematic form several variations of the magnetically controlled interrupter concept. In Figure 1a, no provision is made for voltage holdoff after the removal of the magnetic field, but such a capability is possible if a regular thyratron is used in series with the discharge channel[6]. Figure 1b shows a scheme where the magnetic field is applied to a specially designed multi-grid structure built into a standard hydrogen thyratron. Such a device is capable of permanent

CH1371-4/78/0000-0227$00.75 ©1978 IEEE

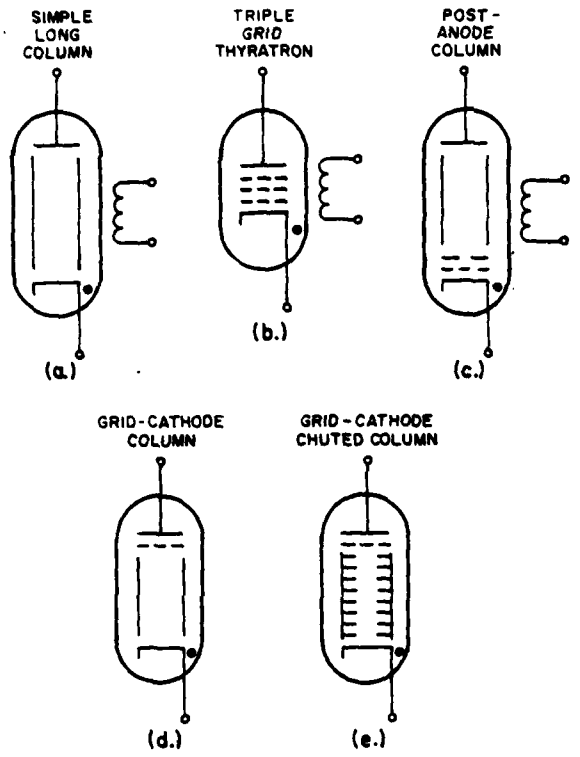


Figure 1. Examples of magnetic interrupters.

interruption and is reported to have operated with a low total tube drop, but reliable interruption of currents greater than about 15A could be achieved only at very low voltages (5-7 kV)[5].

Figure 1c shows an interrupter of the "post anode" type, wherein the discharge channel is appended to a thyratron having a perforated anode. Such four-element tubes provide permanent interruption, but exhibit very poor triggering characteristics[6]. Figure 1d shows a tube where the discharge channel is located in the grid-cathode space. Although large triggers are required, triggering stability is acceptable, and discharges of the order of 200A at 10 kV have been interrupted in tubes of this type using magnetic fields of about 10 kilogauss peak[6]. Figure 1e shows an interrupter similar to that of Figure 1d except that the geometry of the discharge channel has been specifically chosen to facilitate the interruption process. Discharge currents as high as 600A at 20 kV have been interrupted in such tubes with magnetic fields of less than 6 kilogauss peak (magnetic field energy of less than 8 joules), and the nature and performance of such devices form the basis for the discussion which follows.

Typical Interrupter Waveforms

Ideal Case

In the circuit of Figure 2a, assume that an ideal magnet pulse could be generated as shown. A total tube drop, etd, total grid and column drop, egk, and a holdoff section deionization time, td, are assumed for the interrupter, as is an effective grid-to-ground stray capacity, Cg. If the tube is triggered at t=0 and the magnet current, im, exceeds the level required to achieve interruption, the circuit waveforms will be as shown in Figure 2b. (Note that the grid is lifted to Ebb upon interruption.) Also, if tm2-tm1 is greater than the sum of td and 5RgCg, the grid will be at ground at the end of the magnet pulse. Permanent interruption will have been achieved.

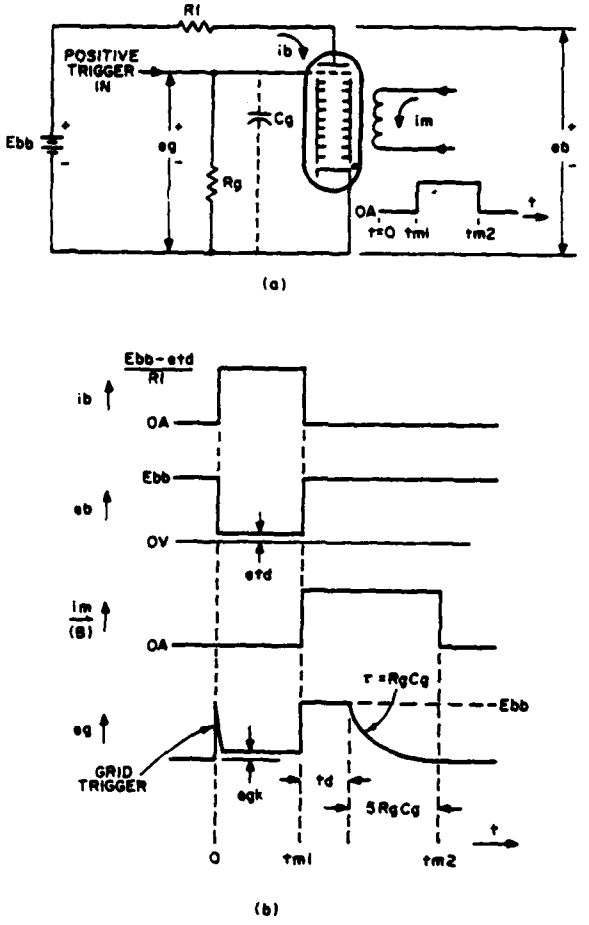
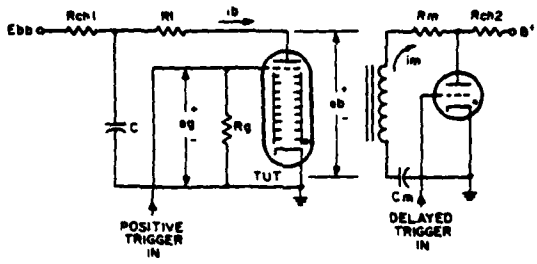


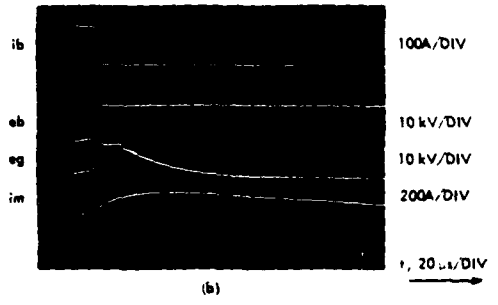
Figure 2. Interrupter circuit and ideal waveforms.

Practical Case

A practical magnet circuit is shown in Figure 3a. Rm is chosen to provide a critically or slightly underdamped im, and the magnet pulse is electronically delayed. As seen in the oscillogram of Figure 3b, the anode drops to etd as the current rises to its peak value. The grid trigger is too narrow to be visible in the waveform of eg, but the grid-to-ground drop, egk, which includes the drop of the discharge channel, may be clearly seen. When the magnet current reaches



(a)



(b)

Figure 3. Interrupter test circuit and waveforms.

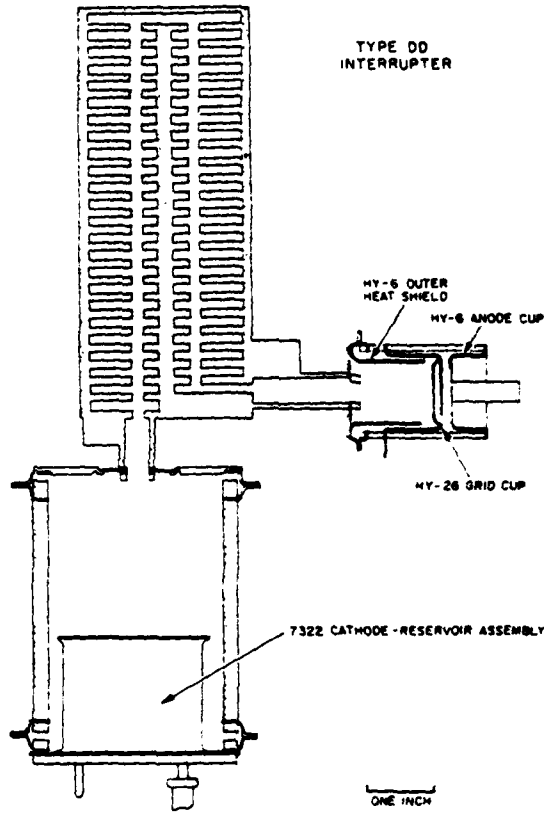


Figure 4. Construction details — Type DD interrupter.

the appropriate level, interruption rapidly ensues. The anode returns to high voltage (some charge has been removed from C by ib), ib drops to zero, and the grid follows the anode to the capacitor voltage, at which level it remains until deionization of the holdoff section occurs. Thereupon the grid decays exponentially to ground. Since eg=0 well in advance of im=0, restriking does not occur. Figure 3b is a time exposure showing about 10 interruptions at 2 Hz to indicate the voltage and timing stability of the device.

Practical Interrupters

Construction of a Typical Tube

Figure 4 shows the construction details of an interrupter of the type shown in Figure 1e. The discharge column is of a relatively narrow bore, but is fitted with a plurality of "plasma chutes" of rectangular cross-section, the axes of which are normal to that of the bore. The tube is positioned within the air gap of the magnet core such that the JxB force is directed into the chutes of choice. Either short or long chutes may be selected depending on the direction chosen for im. Upon triggering the magnet circuit, the discharge in the interrupter is driven against a relatively large surface area and the discharge column length is materially increased, both to the benefit of reducing the magnetic field required to interrupt a given discharge.

Variations in Channel Geometry

Six "chuted" tubes have been built, each with one of the channel geometries shown in Figure 5. Types A, B, and C have a common bore diameter, which is twice that of Types D, E, and DD. Types A through E are rated at 15 kV. Type DD is a double-length tube, designed to operate at 30 kV, and folded at mid-length to fit within the magnet core and fully utilize the available magnetic field energy. Test results for the chuted tubes are discussed later in this paper.

Self-Quenching in a Thin Discharge Channel

Effect of Quenching on Magnetic Field Required for Interruption

Self-quenching of the tube current at the grid aperture of a hydrogen thyratron is a widely observed phenomenon[7]. At normal tube pressures and pulse widths (400 microns, 10 microseconds), a quenching level of 10,000 per square inch has been empirically determined. This level holds over a wide range of aperture sizes. In thyratron design, the grid aperture is often a free parameter, and current-time and current-pressure relationships exist such that self-quenching of the tube current can generally be avoided.

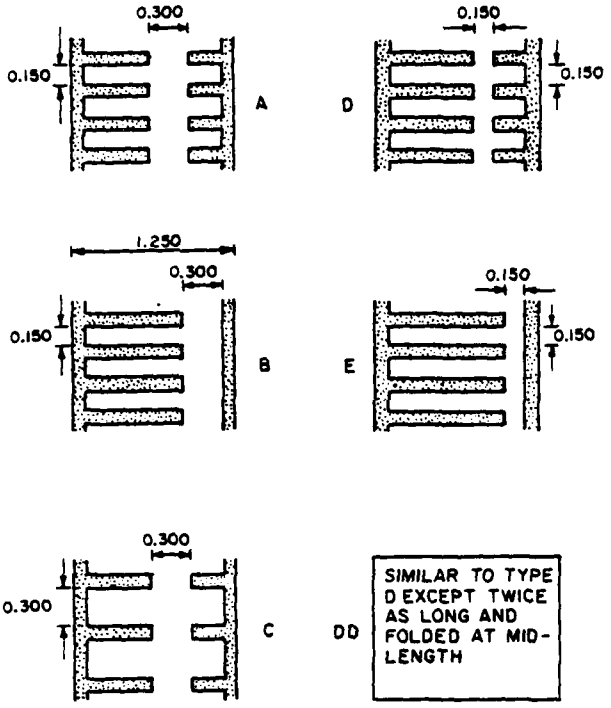


Figure 5. Discharge channel geometries.

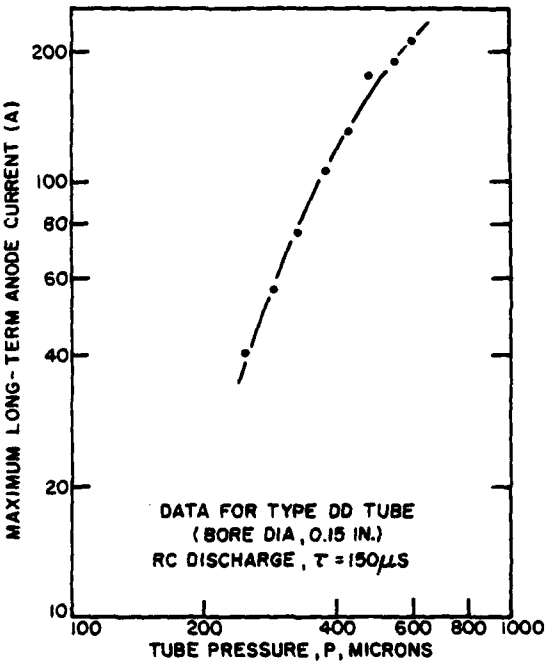


Figure 6. Maximum quench-free current vs. tube pressure.

In interrupter design, self-quenching can be used to advantage to reduce the magnetic field required for interruption. This is most likely to occur in protective applications where the tube need only interrupt fault currents, which may be many times the normal peak tube current.

Self-quenching effects were investigated for the Type DD tube of Figure 4. It was determined that the magnetic field required for interruption was reduced by a factor of three when quenching was allowed to occur, and that this factor of three prevailed over a factor of five in tube current (40 to 200A).

Quench-Free Operation at Long Pulse Widths

When a thin channel device such as an interrupter is to be operated at long pulse widths, it is necessary to ensure that self-interruption will not occur at the required normal current level, and the tube pressure and diameter must be adjusted accordingly. Figure 6 shows the quench-free long term current level as a function of pressure for the DD tube. With a normal thyratron operating pressure of 400 microns, one calculates that self-quenching will occur at ib=177A. From Figure 6, the observed value is 115A, an agreement sufficiently close to indicate that chuted interrupter discharge channels behave in the same fashion as do normally constricted regions within standard thyratrons. It should be emphasized that Figure 6 applies only for long-pulse operation. The DD tube easily passed a 300-ampere, 1-microsecond current pulse at pressures as low as 150 microns.

Interruption Characteristics of Chuted Tubes

The interruption characteristics of the Type B tube are shown in Figure 7. This tube was chosen for discussion because its overall performance is typical of the several different modes of interrupter operation commonly observed. For the 1000-ohm load resistance, the tube current never approaches the calculated self-quenching level of 380A, and the magnetic field required for interruption, B, varies substantially in direct proportion to Ebb. When the load resistance is reduced to values such that the quenching level is approached (100 ohms and less), it is seen that a current dependence exists for B with higher currents more easily interrupted for a given Ebb. Finally, at ib equal to 160A (one-half the calculated self-quenching current), B increases rapidly with increasing Ebb. The processes underlying tube behavior in this latter regime are not yet understood.

Figure 7 shows two curves for a load resistance of 60 ohms. In one case, $J\times\bar{B}$ is directed into the chuted surface, and in the other, into the unchuted (smooth) surface. The chuting is seen to aid in the interruption process, and for tubes equipped with both short and long chutes (such as Type DD), directing $J\times\bar{B}$ into the short chutes generally provided the lower B. The present theory is that the existence of a relatively large volume of plasma behind the driven discharge serves to provide a "plasma reservoir" which functions either to supply plasma to the interrupting discharge or to inhibit the self-quenching process.

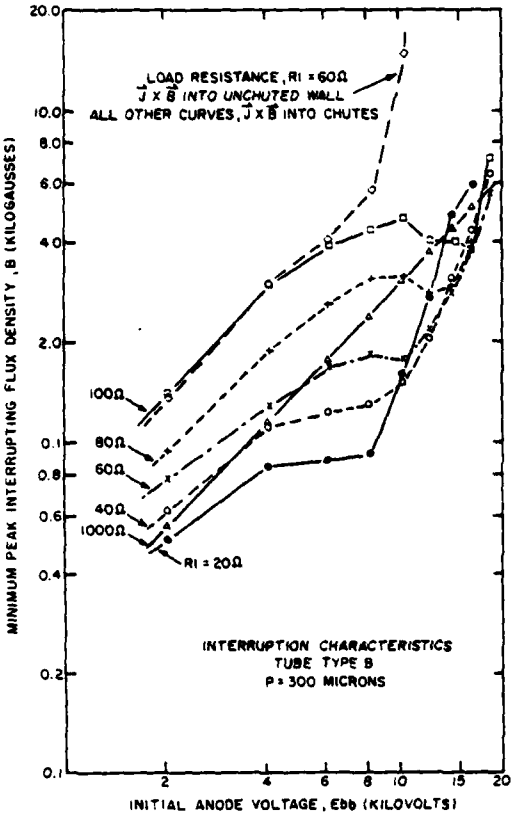


Figure 7. Interruption characteristics — Tube B.

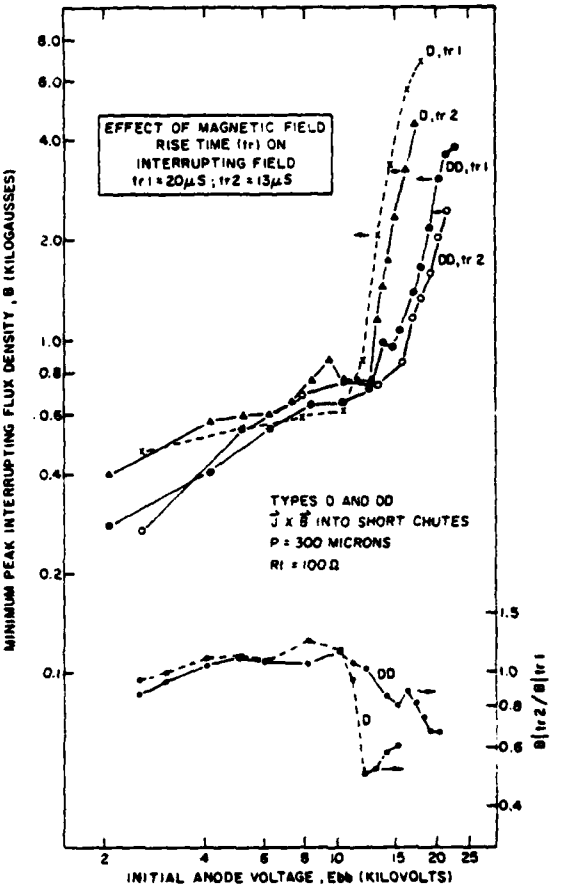


Figure 8. Effect of magnetic field risetime on interruption.

Figure 8 presents the interruption characteristics for the D and DD tubes at fixed pressure and load resistance, but with differing magnetic field rise times. Two observations are made: first, the double-section DD is by far the more efficient tube at high Ebb; and second, both tubes perform better at high Ebb with faster magnetic field rise times. The DD presents double the surface area and path length to the discharge and better utilizes the magnetic energy available in the air gap, but of course, operates with twice the channel drop. The basis for the rise time relationship is not clear since field penetration times into the plasma may be calculated to be of the order of one microsecond.[1,8].

Figure 9 shows the interruption characteristics for the six tubes at high current (low load resistance). The DD tube is clearly superior. Next best are the B and the E, tubes having a smooth wall, and thus no "plasma reservoir." Narrow-bore tubes work well at low Ebb where self-quenching effects are known to predominate.

Tube Drop

Relationship Between Average Column Drop and Peak Forward Anode Voltage

The design trade-offs between average column drop and magnetic field intensity have been previously investigated[4,6]. For the chuted tubes, the column drop is relatively insensitive to pressure over the desired range of 150 to 600 microns. At pressures less than 150 microns, the tubes are difficult to trigger. At pressures in excess of 600 microns, the holdoff capability of the grid-anode space is severely limited.

The five single-section, 15 kV tubes typically operated with a drop of 400 volts across their 15.5 cm-long interaction columns; that is, 26 volts/cm. The double-length column of the 30 kV tube typically operated at 800 volts. No arcing was observed during interruption for any of the tubes when operated at

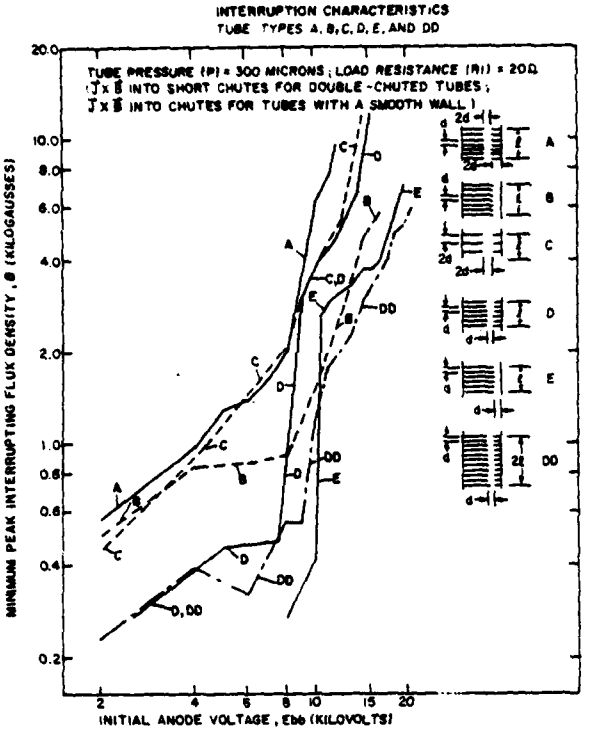


Figure 9. Interruption characteristics of chuted tubes.

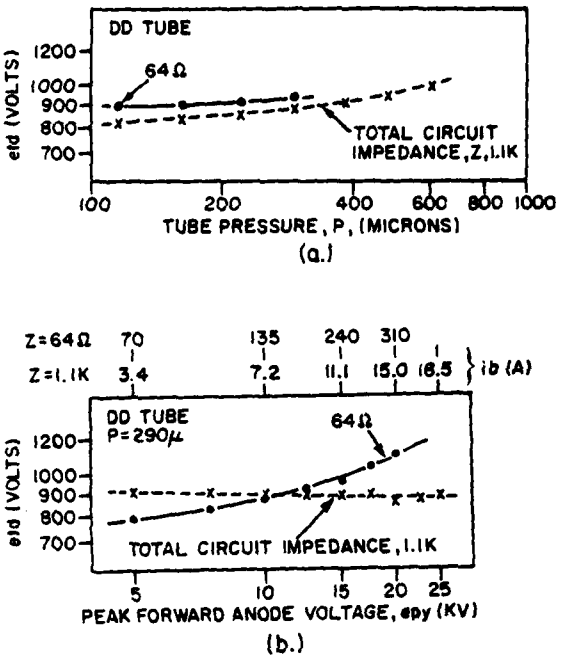


Figure 10. Steady-state tube drops.

rated maximum voltage. To a first approximation, for columns of the general design and dimensions investigated, the column length, l, adequate for interruption at a voltage level, E, is conveniently given by l(in cm)=E(in kV). When operated at currents of about 5 to 50A, the column drop, ecd, is roughly ecd (in volts)= 26 E(E in kV).

Tube Drop as a Function of Pressure and Current

Figure 10a shows the total drop, etd, of the DD tube as a function of pressure for high and low current cases. The tube drop is not a strong function of pressure. Figure 10b shows the total tube drop as a function of peak forward anode voltage at a typical pressure of 290 microns. From Figure 10b one assumes an optimum ib for minimum etd lying somewhere between about 20 and 70A. Figures 11a and 11b show the grid-to-ground drop (essentially the column drop) when the tube is subjected to RC discharges of differing peak currents. In both cases, minimum drop is seen to occur at 25 to 30A.

If epy is defined as the peak forward anode voltage of a non-conducting interrupter, then the ratio etd/epy serves as a measure of the interrupter's effectiveness as a closed switch.

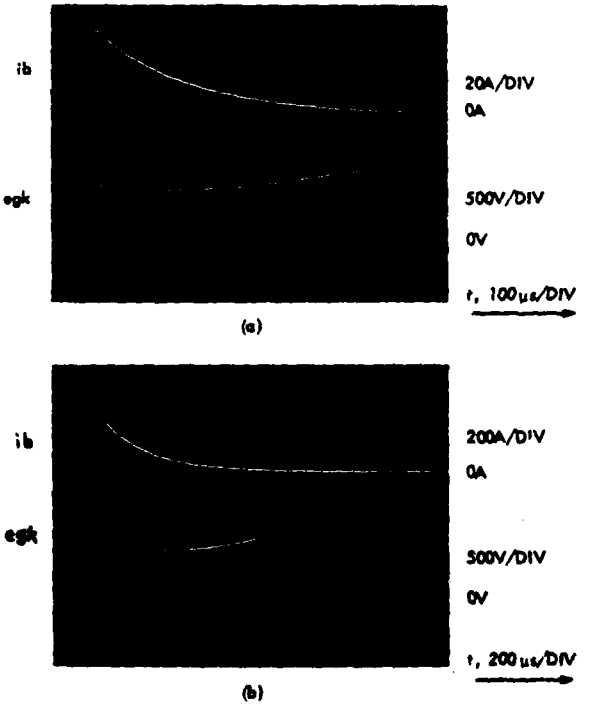


Figure 11. Instantaneous tube drop.

Figure 12 shows the ratio etd/epy for the DD tube as a function of epy for both high and low current cases. The increase in etd at high currents is reflected in the curve of Figure 12 which applies to the high current case; but in the low current case, which case is pertinent to tube operation as a protective device, etd is still in the current regime where increased ib reduces etd. Hence, etd/epy continues to decrease with increasing epy. The conclusion is that total tube drops of only a few percent are feasible for high voltage operation at moderate tube currents.

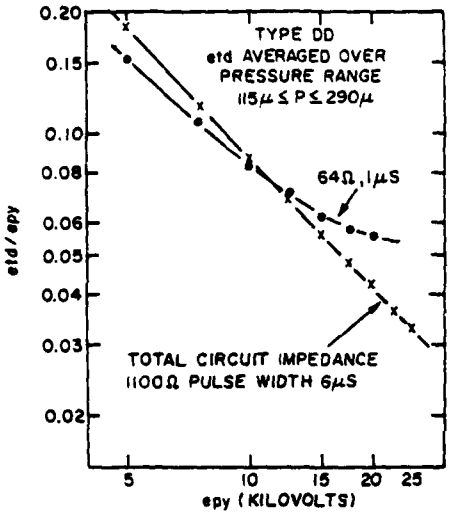


Figure 12. Ratio of total tube drop to peak forward anode voltage.

Repetition Rate, Column Dissipation, and Life

Figure 3b shows a total deionization and grid decay time of 60 microseconds, implying a maximum pulse repetition rate of 16 kHz at the 100A, 10 kV level. Data exist which show that at least twice this pulse rate should be readily achievable. Permanent interruption of 200A at 20 kV has been accomplished with a total grid decay time of about 400 microseconds (implying a pulse rate of 2.5 kHz) in a circuit not optimized for high pulse rates.

Interaction columns capable of dissipating 2 to 3 kW or more per section can be readily manufactured, which suggests that average tube currents of up to 7A are feasible.

Figures 13a and 13b give results of an interruption life test performed on the DD tube. The pulse rate and power levels were limited by considerations other than the tube's capabilities. The test was intentionally terminated after 100,000 interruptions with no apparent damage to the tube or change in its characteristics.

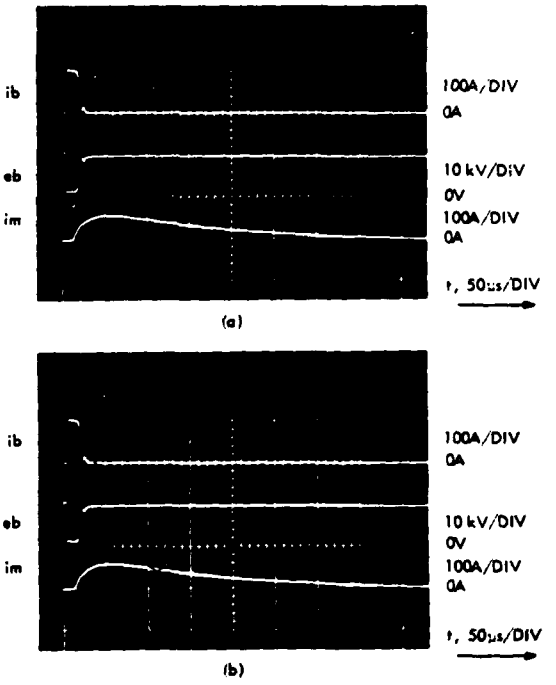


Figure 13. Life test waveforms — Type DD interrupter.

Design Goals

Present work is directed toward the development of a tube capable of interrupting at least 1 kiloampere at 50 kV. Extrapolation of existing data shows that with the proper channel geometry, 50 kV, 1 kA interruptions should be achievable with a magnetic field energy of the order of 10 joules and a total tube drop of 1400 volts.

A closure efficiency for interruptible switches may be defined as $\eta_c = 1 - V/E$, where V is the total drop of the conducting switch and E is the voltage level of the interruption. An interruption quotient may be defined as $\eta_Q = EI/W$, where E is the voltage level as before; I is the interrupted current; and W is the magnetic field energy necessary to achieve the interruption. A map of η_c and η_Q appears as Figure 14, where the performance of the projected device, the DD tube, and results typical of an unchuted tube are shown[6].

On the basis of present data, it should be possible to develop a 50 kV tube capable of operating at an average current of several amperes and at pulse repetition rates of 10 kHz or higher. An operating life of 10,000 hours including 20,000 interruptions at full power should be achievable.

Conclusions

Practical gas discharge switches utilizing the phenomenon of magnetically controlled interruption of

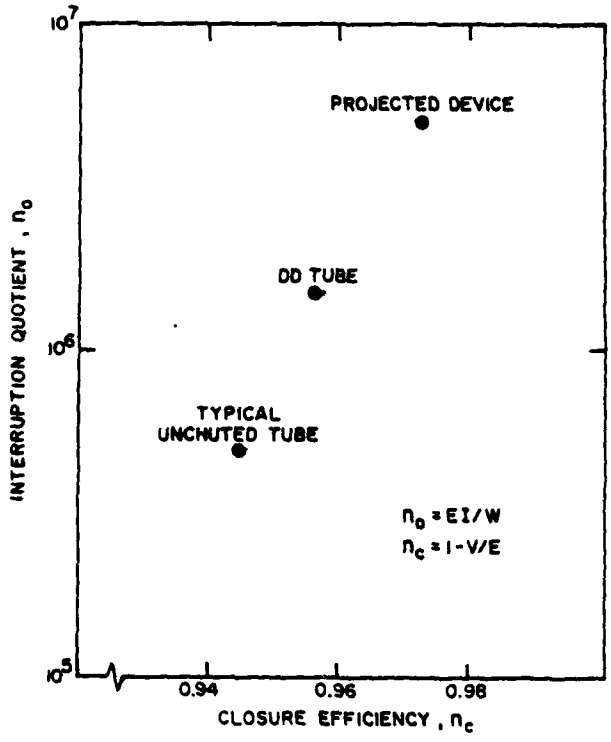


Figure 14. Map of interruption quotient and closure efficiency.

high current at high voltage presently exist at the 20 kV/600A level, with every indication that operation at 50 kV and 1-2 kA can be achieved with magnetic field energies of the order of tens of joules. Such devices can be made to function as normally open or normally closed switches, or as independently controllable impedances. The current within the device follows the command of the magnetic field, and does so on essentially an instantaneous basis. The maximum achievable pulse repetition rate is limited principally by the recovery time of the holdoff section, and secondly by the heating associated with high average currents. The device is scalable and amenable to the application of standard thyratron engineering technology. Operation at 50 kV, several kiloamperes peak, and several amperes average should therefore be achievable.

Acknowledgment

The work described herein was conducted at EG&G, Inc., Technical Products Group, Salem, Massachusetts, and was sponsored by the U.S. Army Electronics Technology and Devices Laboratory (ERADCOM), Fort Monmouth, New Jersey, under Contract DAAB07-76-C-1301.

References

1. Thomas, J., Vanden Brink, H., and Turnquist, D., "New Switching Concepts," Technical Report ECOM 00123-F, 1967.
2. Taylor, G.W., and Schneider, S., "Energy Control for Microwave Amplifier Arrays," IEEE Trans. on Aerospace and Electronic Systems. 4.5. 1968.
3. Shackleford, C.L., "Repetitive Series Interrupter," R&D Technical Report ECOM-73-0320-F, 1974.
4. Weiner, M., "Repetitive Series Interrupter," Proc. IEEE Twelfth Modulator Symposium, 1976.
5. Wheldon, R.J., "A Thyratron with Magnetic Interruption," Proc. IEEE Twelfth Modulator Symposium, 1976.
6. Turnquist, D.V., and Simon, R., "Repetitive Series Interrupter II," R&D Technical Report ECOM-76-1301-6, 1978.
7. Goldberg, S., and Riley, D.F., Research Study on Hydrogen Thyratrons, Volume III, EG&G, Inc., Boston, 1957.
8. Turnquist, D.V., "Magnetic Control of a Gas Discharge Switch," Proc. Ninth Modulator Symposium, 1966.

A MODULATOR FOR THE SEASAT-A RADAR ALTIMETER

K. Y. Ishikawa, C. T. McCown, G. E. Stronks

Hughes Aircraft Company
Electron Dynamics Division
Torrance, California 90509

Summary

This paper describes the modulator for the Seasat-A Radar Altimeter. The unit, which consists of a grid modulator, power supply and traveling wave tube (TWT), has been delivered to the Applied Physics Laboratory for their altimeter system in the Seasat-A Global Weather and Ocean Survey satellite.

The TWT power supply develops 12 kilovolts at an average power of 90 watts and peak power of 18 kilowatts during pulse operation.

The grid modulator which operates at the TWT cathode potential swings the grid voltage over a 350 volt range with rise and fall times of less than 80 nanoseconds to gate the TWT RF signal on and off. Transition times of approximately 13 nanoseconds are realized for the RF output pulse. During the pulse operation the cathode voltage is held to within 2 volts by the wide bandwidth cathode voltage regulator.

System Description

The modulator system consisting of the grid modulator, power supply and traveling wave tube is shown in Figure 1. Figure 2 is the actual modulator hardware with the cover removed.

A more detailed block diagram of the modulator is shown in Figures 3 and 6. Figure 3 contains the high voltage power supply and the cathode regulator. The heater voltage output is supplied by a series regulator followed by a static inverter. This heater supply also provides the floating deck modulator bias at the cathode potential.

The TWT cathode voltage is provided through two stages of regulation. The first stage of regulation is a pulse width modulating switching regulator followed by a linear regulator. Other blocks indicated in the diagram are the control logic/timing and protection/fault circuits.

Figure 6 is the Grid modulator block diagram. Starting with the pulse gate input an emitter coupled logic line receiver provides the interface. The line receiver then drives the pulse conditioner, which forms a turn on signal coincident with the input signal followed by a turn off signal immediately following the falling edge of the turn on signal. This doublet signal not only provides the required signals for the pull up and pull down grid modulator circuits but provides volt-second balance for the pulse transformer. This doublet signal drives the transformer driver which provides power gain to drive the pulse transformer. The pulse transformer provides the high voltage isolation and also provides the signals for the pull up and pull down switches. The pull up and pull down switches are normally off and the TWT grid bias is set to a cutoff voltage by the grid bias resistor. When the pulse gate is received by the pull up switch the grid is pulled up for the duration of the switch and the pull down switch pulls the grid negative at the termination of the pulse gate.

For protection, a fault circuit is provided that monitors the average voltage of the TWT grid and sends a fault signal to the power supply when the average grid voltage becomes more positive than is safe.

Interface Requirements

The interface requirements for the modulator are presented in two parts: Spacecraft to modulator and modulator to TWT. The spacecraft to modulator interface is summarized in Table 1 and the modulator to TWT interface in Table 2. The heater and grid voltages are referenced to the cathode voltage. Additional interface requirements include: input overcurrent, cathode overvoltage, and line undervoltage protection, built-in time delay, and arc protection for the modulator and TWT.

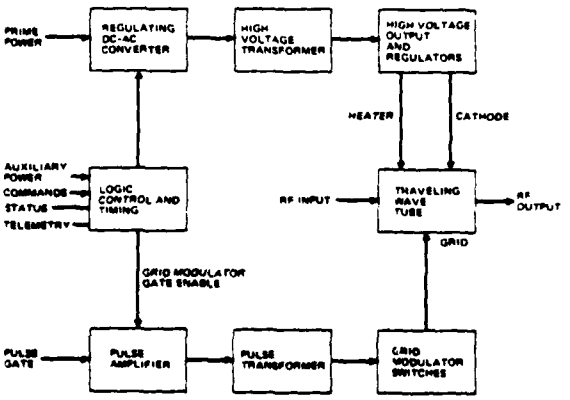


Figure 1 Block diagram - TWT amplifier.



Figure 2 Modulator with cover removed.

CH1371-4/78/0000-0235$00.75 © 1978 IEEE

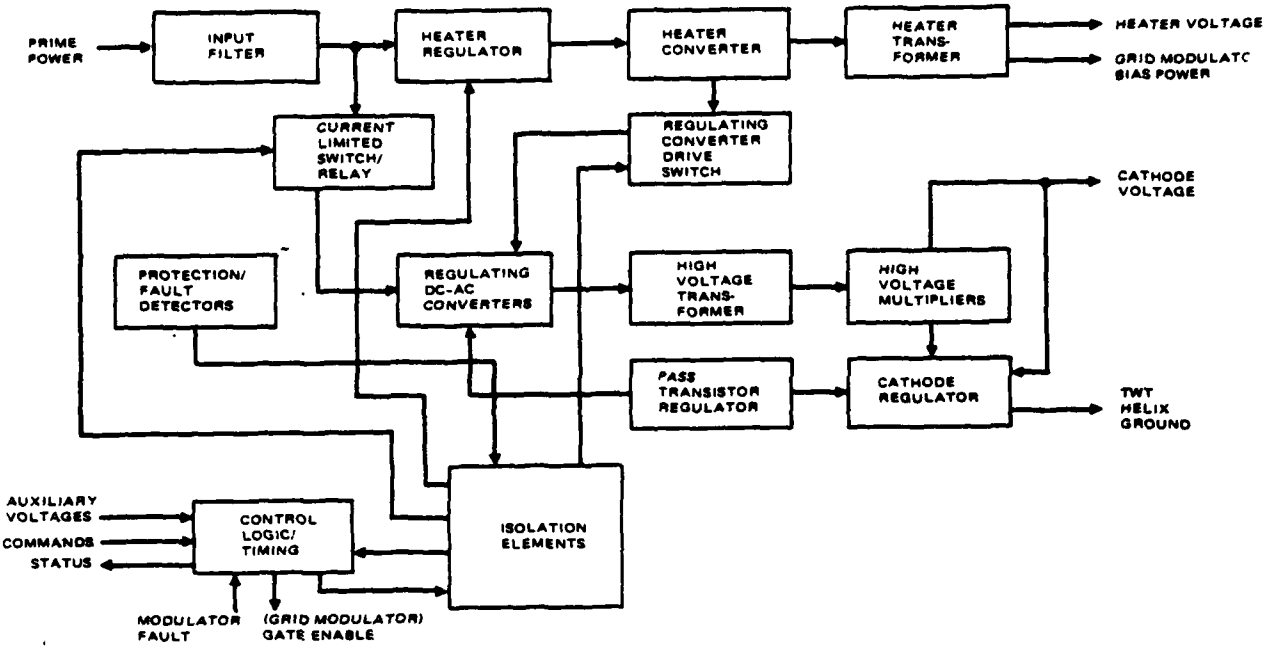


Figure 3 Block diagram - TWT power supply.

Power Supply Description

High Voltage Power Conversion Circuits

The main purpose of the high voltage power supply is to power the TWT. The primary regulating DC-AC converter, the high voltage transformer and high voltage multipliers as shown in Figure 3 make up the high voltage power conversion circuits. The regulating converter is the Hughes patented Venable Converter.[1] This converter, see Figure 4, was selected for this application for the following desirable features.

1. For high voltage applications and for the power level needed it has higher efficiency than the conventional circuit arrangement of switching regulator followed by a DC to DC converter.
2. All the switches are inductively fed, thus minimizing switching current transients and reducing power switch stress.
3. The pulse width modulated converter produces a square wave output with continuous load current thus reducing load filtering problems.
4. The duty ratio transmission function, has both a corner frequency, fo, and damping, Q, independent of the dc duty ratio.
5. The duty ratio transmission function has no left or right halfplane zero.

The high voltage multiplier circuit is shown in Figure 5. One significant advantage is that it simplified the high voltage transformer. Its major disadvantage is a relatively high output impedance for its size. Due to this disadvantage a pass transistor regulator is required to adjust the primary regulating converter for load changes. The primary regulating converter and the pass transistor regulator act only to compensate for average load and line changes.

Grid Modulator

The grid modulator switches the TWT grid to gate the RF output power. The elements which make up the grid modulator as shown in the block diagram in Figure 6 are described. Difficulties in the design of the grid modulator included:

1. Packaging the circuit boards to withstand a 12 kV potential.
2. Switching the TWT grid voltage from -150 to +200 volts with less than 80 ns rise and fall times.
3. Maintaining a grid pulse flatness to within ±2 volts.
4. The necessity of adjusting the output pulse voltage after the circuit boards have been potted.
5. The design and fabrication of a 12 KV isolating pulse transformer with excellent pulse transfer qualities.
6. The requirement that the modulator withstand repeated high voltage arcs.

The packaging of the two high voltage circuit boards is a can within a can concept with the high voltage insulating material in between. The inner can is at cathode potential and the outer can is at ground potential. The two high voltage circuit boards prior to the first potting step are shown in Figure 7. A two step potting procedure is used with conductive paint applied after the first potting to achieve an

TABLE 1
SPACECRAFT TO MODULATOR INTERFACE

Input Voltages	
Power Buss	24-33 Vdc
Auxiliary Voltages	+5 Vdc +15 Vdc + 28 Vdc
Input Power	95 watts maximum
Inrush Current	10A maximum
Commands	
Heater ON/OFF	TTL
HV ON/OFF	TTL
Fault Reset	TTL
TWT Gate	ECL
Status	
HV Ready	TTL
HV ON	TTL
Fault	TTL
Telemetry	
Cathode Voltage	1 volt per 3KV
Beam Current	1 ampere per volt
Weight	30 pounds
Size	5.5" width x 15" length x 6.25" height
Temperature Range	-10°C to 50°C
EMI Requirements:	
Conducted Susceptibility	1V pp
Conducted Emission	0.1A pp at TWT modulation rate

TABLE 2
MODULATOR TO TWT INTERFACE

Cathode Voltage	-12 KV DC
Cathode Pulse Current	1.5A peak for 3.2 μs
Cathode Droop	5 volts maximum
Cathode Regulation	1% (line, load, temperature)
Heater Voltage	6.0 VAC
Heater Current	2.5 amps
Grid Voltage:	
Off	-150V
On	+200V
Grid Current	200 mA
Rise/Fall Times	<200 ns
Grid Droop Across the Pulse	<2V

equipotential surface at 12 kilovolts and the second potting is in the grid modulator outer case.

The TWT grid pulse requirement of 350 volts, rise and fall times of 200 ns and flatness of less than ±2 volts resulted in a solid state modulator switch design. The reasons for the selection of the solid state switch approach are described. The output switches Q1 and Q2 in Figure 8 are a push pull design in which the output transistors are operated

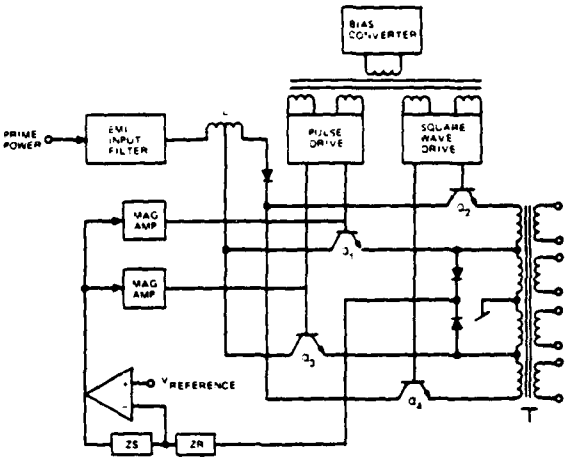


Figure 4 Simplified Venable regulating DC to AC converter.

in a clamped common base configuration. The switches are clamped with diodes D1 and D2 against a regulated voltage to achieve the required switching speed and pulse flatness. The pull up switch is clamped to an adjustable regulated voltage to achieve a pulse flatness of less than 2 volts.

Further, the design goals were achieved using approved JANTXV output transistor switches. The transistors that were finally used were the 2N5157. These devices are, in terms of switching speeds,

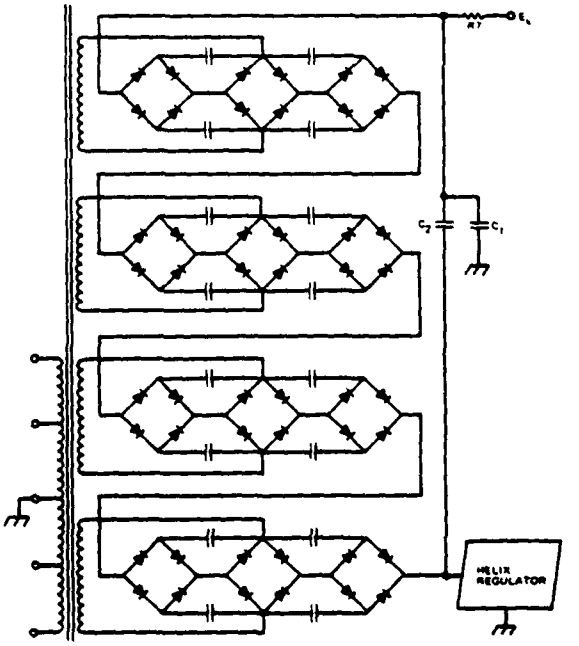


Figure 5 High voltage multiplier stage.

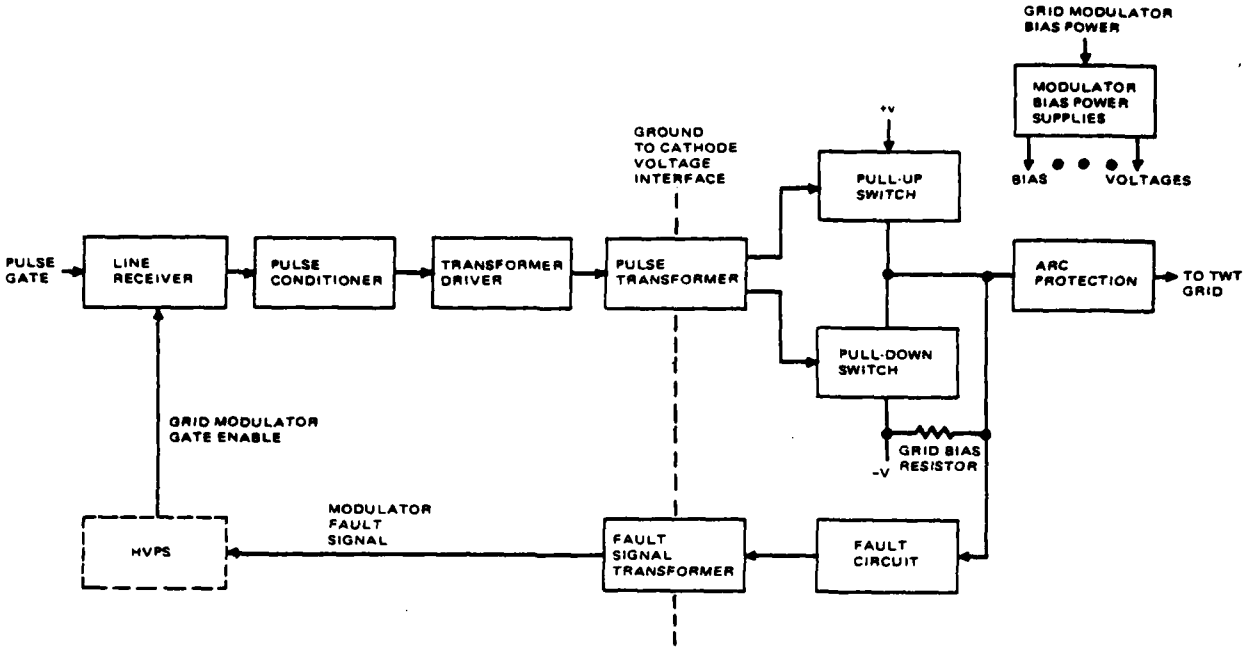


Figure 6 Block diagram - grid modulator.

relatively slow, but in the particular configuration that was used, transition times of less than 80 ns were achieved.

The grid voltage rise and fall times are shown in Figure 9. During Breadboard experiments using faster transistor devices, rise and fall times of less than 30 ns were obtained.

One of the required adjustments of the grid modulator is the output amplitude voltage swing. This voltage adjustment requirement is the result of differences in the TWT characteristics. Therefore, the grid voltage must be adjusted for each TWT to obtain the required RF output power. This adjustment of the output voltage in the 12 KV potted grid modulator is accomplished external to the potted assembly when the grid modulator and TWT are assembled.

To provide a pulse signal to drive the push-pull grid modulator switches, a transformer with excellent pulse qualities were required. This pulse quality requirement indicates close coupling between primary and secondary. Normally this coupling requirement would not be a problem if the spacing between primary and secondary could be close. However, the voltage between primary and secondary is 12 KV and the ability to provide close coupling between the primary and

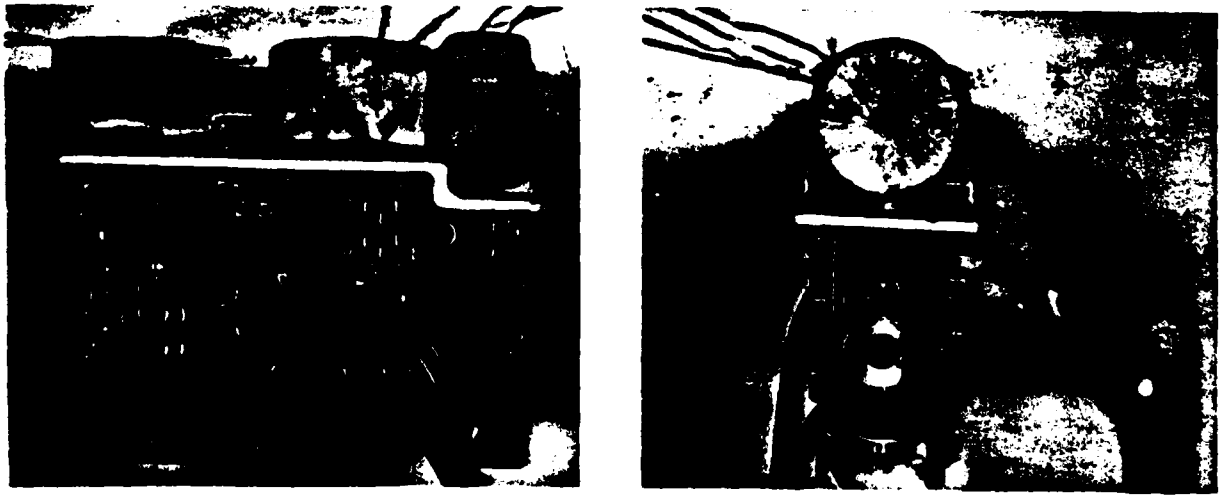


Figure 7 Grid modulator circuit boards.

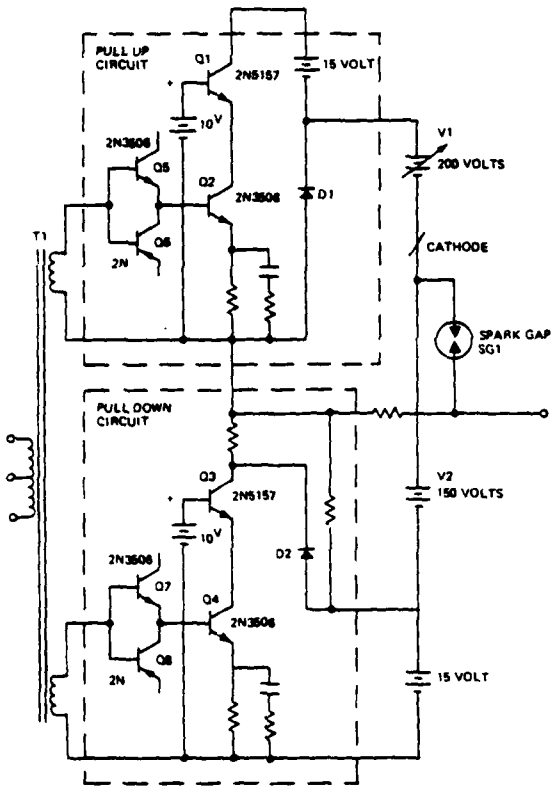


Figure 8 Simplified schematic of the grid modulator pull up and pull down circuit.

secondary is more difficult. The successful solution involved the design and fabrication of a hard potted, coaxial wound pulse transformer using a Ferrite core.

The design approach using solid state switches has many advantages in achieving good performance. However, it has the disadvantage of making the grid modulator susceptible to arcs. The solution to making the grid modulator arc immune was to direct the arc current along paths which bypassed sensitive parts of the circuit without compromising the performance of the grid modulator. The grid modulator was subjected to over one thousand grid to ground arcs without degredation in performance. Further, the arc protection not only had to protect the grid modulator, but provided the required protection for the TWT.

As an example of the overall modulator and TWT performance, Figure 10 shows the time delay from the emitter coupled logic input to RF output, and Figure 11 shows the RF rise and fall times of approximately 13 nanoseconds.

The Cathode/Helix Regulator

In order to provide the DC and pulse regulation requirements of the TWT a wide band cathode regulator is used. This regulator is designed to regulate the DC cathode voltage and the cathode voltage during the 1.5 ampere TWT load pulse. Figure 12 is a photograph of the cathode voltage during a load pulse. The pulse droop is less than 2 volts and the passive filtering used in the high voltage is a 0.16 uf, 18 KV capacitor. If the cathode regulator was not designed to regulate the load pulse a 2.4 uf, 18 KV capacitor would be required to achieve the same regulation. This additional capacitance represents greater high voltage stored energy, size, and increased inrush energy from the power line.

During linear operation the cathode regulator loop is basically all feedback controlled and has a 100 KHz bandwidth. Additionally, with the high DC gain and input characteristic of amplifier U_3 the cathode DC regulation is less than 0.2% over line, load, and temperature. When the TWT is pulsed by the grid modulator and beam current is drawn, a voltage step occur across R_7. Figure 13 This voltage step if fed into preamplifier U_3. The output of U_3 is large enough to initiate the feedback damping network

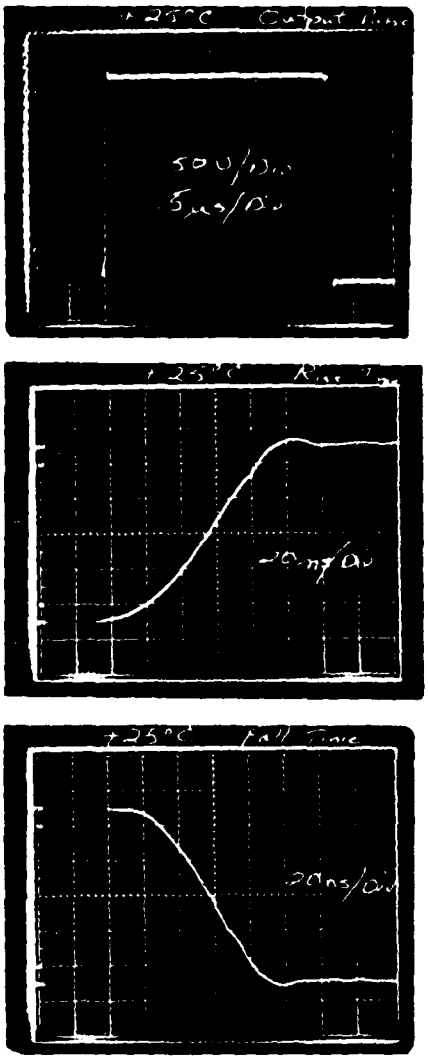


Figure 9 Grid pulse characteristics.

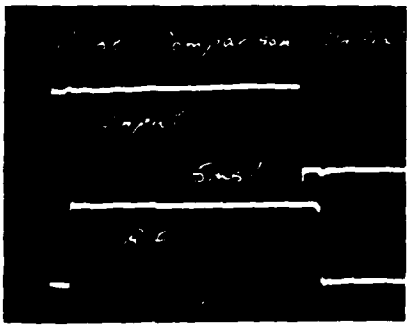
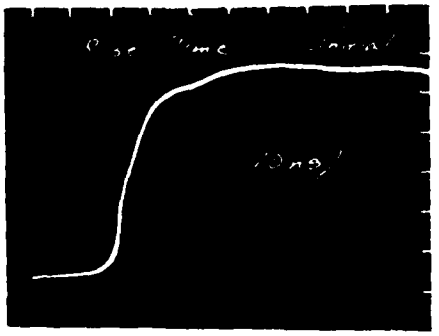


Figure 10 ECL input to RF output delay.

of U_1 and Q_1 to form a current source which is matched to the TWT beam current. During the 1.5 ampere beam current the voltage across Q_1 changes to force current through C_2 to maintain the voltage across C_1 constant.

The linear operation of the circuit is fairly straight forward in that most of the internal operational blocks are feedback controlled. Referring to Figure 12 the regulator output push-pull stage transistors Q_1 and Q_2 vary the voltage of the near ground side of the high voltage output to maintain a constant cathode voltage. Amplifiers U_1 and U_2 are drivers for the output stage transistors and provide power gain from the output of amplifier U^1. Amplifier U_1 is the error amplifier and compares the cathode voltage, through a resistive divider, with a reference voltage. All the amplifier stages are capable of linear operation at up to the saturation level of the output transistors. Thus, the power bandwidth of the circuit should approach the small signal bandwidth.



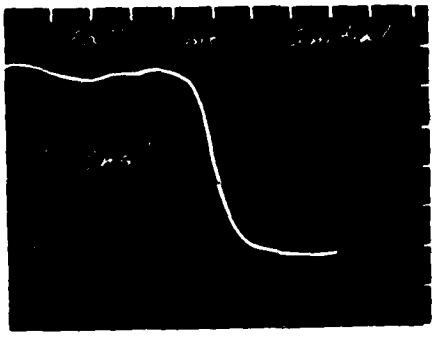


Figure 11 RF rise and fall.

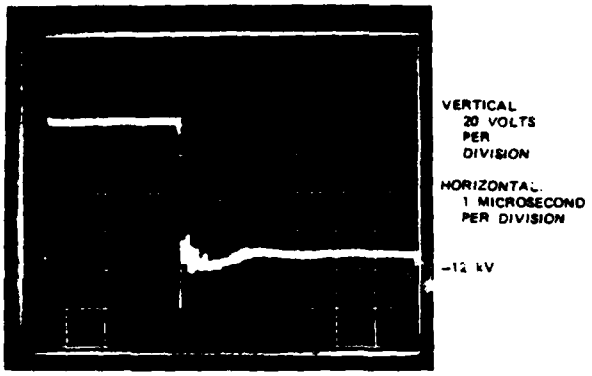


Figure 12 Cathode voltage during pulse load.

In addition, when the output at Q_1 and Q_2 is switching from one transistor to the other or when the output of U_1 is zero, the feedback at the output stage of U_1, Q_1 and U_2, Q_2 use resistors R_9 and R_{10} to provide idle current in the output transistors Q_1 and Q_2 to prevent crossover distortion.

Test Results

The performance of the modulator was obtained from the engineering and flight models over line, load and temperature. The results are given in Table 3.

Conclusions

The design of the modulator for the Seasat-A Global Weather and Ocean Survey Satellite resulted in the development and integration of circuits, components and packaging concepts. A new cathode regulator with sufficient high frequency response to control the cathode voltage droop during the load pulse was designed. A grid modulator capable of modulating the grid voltage 350 volts in less than 80 nanoseconds was developed. The grid modulator required the design of a 12 KV isolating coaxial wound ferrite pulse transformer with excellent pulse characteristics. Careful design and corona testing proved solid encapsulation of 12 KV components feasible. The modulator was tested to be arc protected.

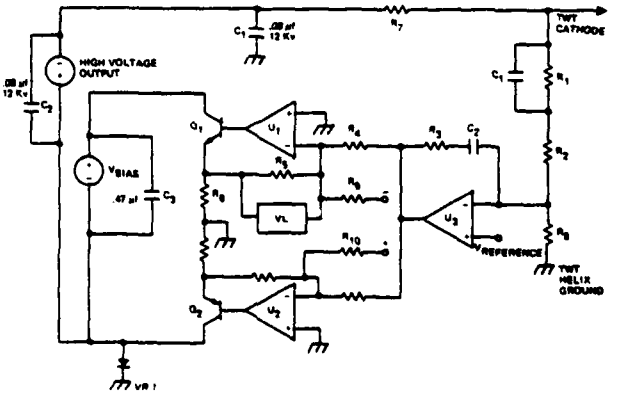


Figure 13 Simplified cathode regulator.

TABLE 3
TEST RESULTS

Characteristic	Specification	Measured Performance
Power input	95 W max.	92.4 watt max.
Inrush transient at H.V. turns on	10 Amp PK	8 Amps PK
Delay time from H.V. command to RF power out on input voltage range	1 second max.	0.6 sec max.
Input voltage range	24 - 34 volts DC	22 - 35 Vdc
Cathode regulation	1%	0.2%
Cathode droop across the pulse	<5 volts	2 volts
Conducted susceptibility	1 vpp	5 vpp
Conducted emissions	0.1A pp at 1 KHz	10 ma at 1 KHz
Grid rise and fall times	200 ns max.	80 ns typical
Grid droop across the pulse	2V max.	1V typical

Reference

1. R. Hayner, T.K. Phelps, J.A. Collins, and R.D. Middlebrook, "The Venable Converter: A New Approach to Power Processing," IEEE Power Electronics Specialists Conference Record, 107-111, 1976.

AN ALL SOLID-STATE MODULATOR FOR THE ARSR-3 TRANSMITTER

Edward H. Hooper
Stephen R. Bird

Westinghouse Electric Corporation
Systems Development Division
Baltimore, Maryland 21203

SUMMARY

This paper describes an all solid-state, high power pulse modulator used in the ARSR-3 system (an FAA air route surveillance radar system). The modulator, the culmination of a number of years of both device and circuit development, uses fast switching Reverse Blocking Diode Thysistors (RBDT's) to directly switch 14 MW, three microsecond video pulses at high current without the use of magnetic switching aids.

The modulator consists of five identical PFN modules, a trigger amplifier, and a pulse transformer which matches the modulator output to the beam characteristics of a klystron. Each module contains its own pulse forming network, discharge RBDT switch assembly, and associated circuitry. This modulator is the first production equipment to use the new Westinghouse T62R RBDT devices. The devices switch 2200 amp pulses with a turn on rate of rise of up to 3000A/microsecond.

INTRODUCTION

The ARSR-3 system is a new high performance, air route surveillance radar system which incorporates the most advanced aspects of modern radar technology. Among these is a high power modulator which has demonstrated the reliable performance available in an all solid-state system.

The ARSR-3 modulator is a modularized, all solid-state, line type pulser which provides the required video pulse power to the cathode of the transmitter klystron final power amplifier. Nominal operating parameters of the modulator are as follows:

Modulator Peak Pulse Power	14 MW
Modulator Average Power	15.3 KW
Pulse Repetition Frequency	365 pps
Video Pulse Width	3 uSEC
Klystron Beam Voltage	130 KV
PFN Storage Voltage	3200 V

Note particularly that the modulator operates at substantially lower PFN voltage than do conventional line type modulators of similar power levels.

The modulator is packaged in a cabinet assembly shown in Figure 1, which is designed to provide utmost maintainability. The plug-in modulator modules can easily be replaced, or completely removed from the cabinet for operation of the modulator with reduced power capability.

Performance of the modulator has been verified through a comprehensive series of tests and the demonstration of an entire ARSR-3 diplex radar system which has been in operation at a Westinghouse test site. Reliability demonstration tests have just been completed with over 1000 hours of operation on the system, which includes two modulators, with no modulator failures. In addition, the ARSR-3 transmitter has completed environmental tests per FAA-E-2483b.

BLOCK DIAGRAM

Figure 2 is a block diagram of the modulator. Five PFN modules, each comprising a pulse forming network and a solid-state switch make up the body of the modulator. Outputs of the five modules are combined and coupled to the klystron cathode through a high turns ratio pulse transformer. A trigger amplifier unit provides the necessary trigger pulse to turn on the solid-state switches.

The PFN's are charged to their nominal operating voltage of 3200 volts by a precision charging system[1] which controls the PFN voltage to better than 0.05% pulse-to-pulse. Upon discharge, each of the five modulator modules deliver a 2200A, 3 microsecond pulse to the HV transformer primary. The resulting composite primary current is 11,000A.

The pulse transformer is a foil wound transformer having a step up turns ratio of 93:1 to step up the nominal 1400 volts pulse on the primary to 130 KV on the secondary. The transformer is mounted in an oil tank together with the klystron socket and filament transformer located directly behind the electronics cabinet. Connections to the transformer from the modules utilize multiple twisted pairs of high voltage insulated wire to minimize inductance between the modules and the pulse transformer primary.

The trigger amplifier is essentially a switch system which arms itself by charging trigger energy capacitors in each of the PFN modules. Operation of this switch then simultaneously dumps these capacitors to provide the trigger energy required to operate the PFN modules.

SOLID-STATE SWITCH

The problem of switching short high power pulses with solid-state devices is answered in the ARSR-3 with the Westinghouse type T62R Reverse Blocking Diode Thyristor (RBDT). The RBDT[2,3] is a four layer thyristor type device which holds off voltage in the forward direction until switched on. When properly turned on, it conducts very high current with low

CH1371-4/78/0000-0242$00.75 ©1978 IEEE

forward voltage drop. Furthermore, the turn-on mechanism is such that in a properly triggered device, the junction is fully on within one microsecond of triggering. This means that the device is ready for full current almost immediately without the need for magnetic switching aides.

The RBDT is a two terminal device related to the SCR thyristor. It differs primarily in the turn-on mechanism and the absence of a gate lead. The internal structure of the four layer device is optimized for turn-on by the action of displacement current through the blocking junction capacitance as shown in Figure 3. The source of this trigger current is a high dv/dt impulse across the device from a trigger generator.

In the ARSR-3, five Westinghouse T62R RBDT devices, each having a rated hold off voltage of 800 volts are connected in series to give a total switch assembly hold-off voltage of 4000 volts. The turn on trigger is applied across the string of five devices, causing the turn-on displacement current to flow through the five devices in series. The result is that all five turn on simultaneously. With the trigger applied in the ARSR-3, the RBDT "stack" switches a nominal pulse current of 2200A with a di/dt of up to 3000A per microsecond from turn on.

The required trigger for this operation is a voltage impulse above the voltage hold off level which has a rate of rise sufficient to cause 20A of switching current to flow. In the stack of five devices used in the ARSR-3 switch a trigger voltage with 25 KV per microsecond rate of rise to at least 6500 V ensures this trigger current.

Figure 4 illustrates schematically the utilization of the five RBDT devices in each ARSR-3 module and the technique used for triggering the five modules. Fundamentally, each PFN module is configured as a conventional line type modulator. Five such circuits are operated in parallel. Each module contains its own pulse forming network, RBDT switch assembly, trigger transformer, and trigger energy storage capacitor. All five switch assemblies are triggered from a common trigger amplifier. When the trigger amplifier switch is closed, trigger energy, stored in a capacitor in each module, is applied through the trigger transformer to the stack of five RBDT devices. The resulting voltage impulse causes sufficient displacement current to flow through each device to cause dv/dt across each stack to reach at least 25 KV per microsecond, which satisfactorily turns the devices on. The diodes in series with the RBDT devices are to isolate the trigger impulse from the PFN.

Provisions are made in the transmitter control system to guarantee adequate trigger by monitoring the voltage on the trigger storage capacitors just prior to trigger operation. If for some reason this voltage is not sufficient for proper device triggering, the trigger amplifier is inhibited and modulator operation is interrupted.

Further test provisions provide a means for assessing the state of the RBDT devices in each module. The design margin is such that in the unlikely event that one of the RBDT's should fail, the module will continue to operate with only four good devices. Device failure does not mean immediate shut down of equipment. It only means that the failed device should be replaced at the next maintenance period.

EQUIPMENT

Figure 5 is a photograph of the transmitter modulator cabinet with protective doors and covers opened. The five visible modules at the lower right are the five PFN modules. The trigger amplifier module is the horizontal module to the left of the PFN modules. The total volume occupied by these units is 8 cu. ft. The high voltage pulse transformer, is in an oil tank immediately behind the PFN modules. The volume occupied by the pulse transformer is 4.7 cu. ft.

Figure 6 is a photograph of a PFN module. The RBDT switch assembly which includes backswing and trigger blocking diodes is in the center portion of the module. The large block is the pulse forming network. The modular concept for solid-state modulators has demonstrated not only reliable operation but has proved to be extremely easy to maintain. The peak pulse power capability of a single module is over 3.5 MW. This means that one module may be removed if necessary and peak RF pulse power may be maintained. Current and voltage detectors are incorporated into each module to provide fault isolation to the module level and removal of the module, after opening the key interlocked safety door, is accomplished by simply pulling out the plug-in module. This type of construction is possible since each PFN module is operated with only 3 KV stored on the pulse forming network.

Figure 7 is a side view of the solid-state switch assembly showing the five RBDTs and six isolation diodes stacked in series. Also pictured are the heat sink fins utilized for cooling purposes. Copper plates are used for interconnections to the switch assembly to minimize inductance in all pulse current conductors.

Figure 8 is a photograph of a modulator trigger amplifier. The RBDT switch assembly is in the back right portion of the unit. The remainder of the modulator trigger amplifier is comprised of a trigger switch driver, and all the fault logic functions for modulator protection.

MODULATOR PERFORMANCE

The solid-state modulator has performed well in various ARSR-3 transmitter tests performed over the past year. These include environmental tests in accordance with FAA-E-2483b and a 1000 hour life test for a diplex transmitter system.

Environmental tests were completed successfully on two transmitters last fall. These tests consisted of subjecting the transmitter to operation from -10°C to +50°C with up to 90% relative humidity and concluded with an extended operating period at 25°C.

The 1000 hour life test followed construction of a test site in which an entire diplex radar system was placed in operation. As of the writing of this paper the 1000 hours has been exceeded with no failures in either of the two modulators in the system.

Performance wise the modulator fully meets the system requirements for a range of 200 nautical miles and an MTI Cancellation factor of 40 dB. Figure 9 is a photograph of the modulator output (pulse transformer secondary current). The slight rounding of the pulse is due to inductance of the transmission system between the PFN's and the klystron cathode.

Jitter and delay measurements were made on the video pulse under various operating conditions. Under uniform PRF conditions, pulse-pulse jitter was less than 4 nanoseconds rms. Under stagger pulse conditions this increased to 10 nanoseconds. Delay time, measured as the time between the leading edge (70% amplitude) of the input trigger timing pulse and the 70% point of the modulator video pulse to the klystron was measured at 2.5 microseconds nominal.

Efficiency of the modulator from energy stored in the PFN to pulse energy supplied to the klystron is 81% for 5 MW RF operation (13.9 MW peak video power to the klystron). Of the total power loss, slightly less than half (1200 watts) is in the diodes and RBDT devices in the switch stack assemblies.

As a result of the success in the test and evaluation of the ARSR-3 equipment five dual channel systems have already been shipped to the FAA. This includes one system currently in use by the FAA for training purposes.



Figure 1. ARSR-3 TRANSMITTER CABINET

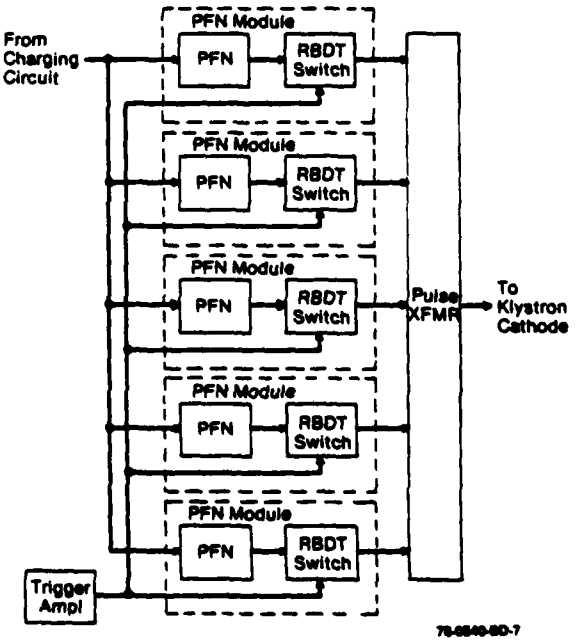


Figure 2. MODULATOR BLOCK DIAGRAM

ACKNOWLEDGEMENTS

This modulator, produced as part of the ARSR-3 system under FAA contract DOT-FA75WA-3641 is the most recent result of several years of work at Westinghouse on Thyristor type devices for pulse modulator switches.

FOOTNOTES AND REFERENCES

1. C.A. Corson, "Precision Regulated, 20 KW Modulator PFN Charging System", 1978 Thirteenth Pulse Power Modulator Symposium, June, 1978.

2. P.F. Pittman and J.B. Brewster, "A New Solid-State Switch for Power Pulse Modulator Application; "The Reverse Switching Rectifier," IEEE Conference Record of 1973 Eleventh Modulator Symposium, Sept., 1973, pp 6-11.

   Note that the Reverse Switching Rectifier (RSR) is an earlier name given to the Reverse Blocking Diode Thyristor. Both names refer to the same device.

3. J.B. Brewster and G.M. Sherbondy, "Complete Characterization Studies Verify RBDT-RSR Reliability;" 1978 Thirteenth Pulse Power Modulator Symposium, June, 1978.

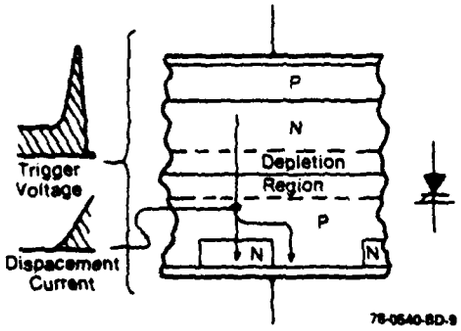


Figure 3. RBDT DEVICE CROSS SECTION AND TRIGGER CURRENT

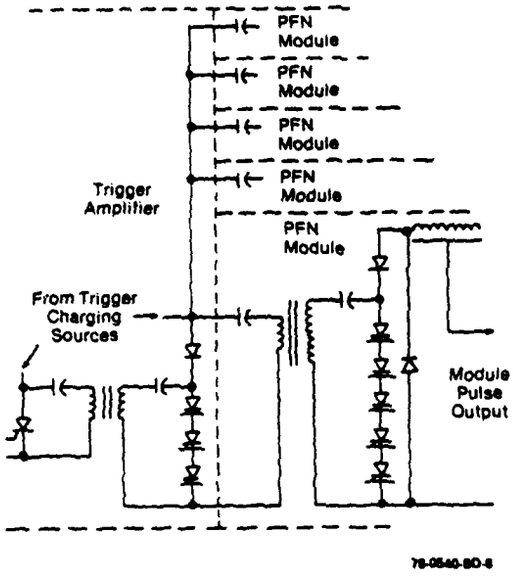


Figure 4. SOLID-STATE MODULATOR TRIGGER SYSTEM

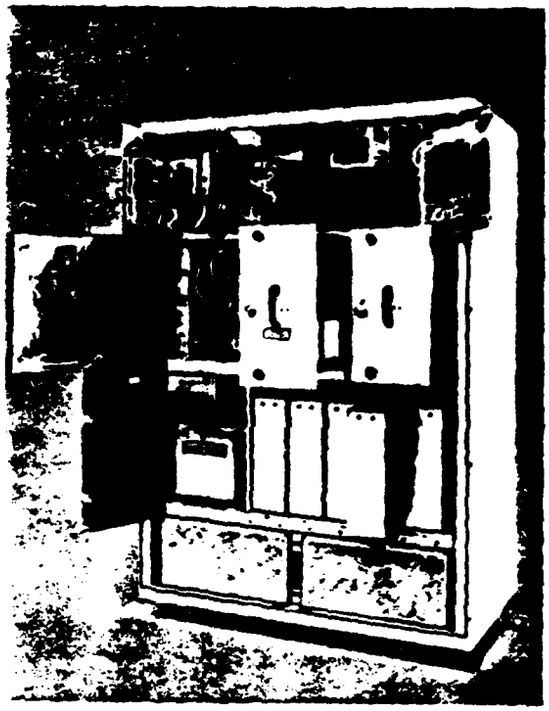


Figure 5. TRANSMITTER CABINET WITH DOORS OPENED TO SHOW MODULES

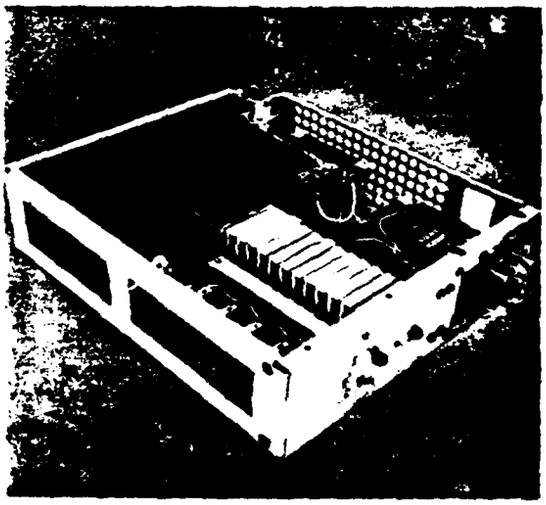


Figure 6. PFN MODULE

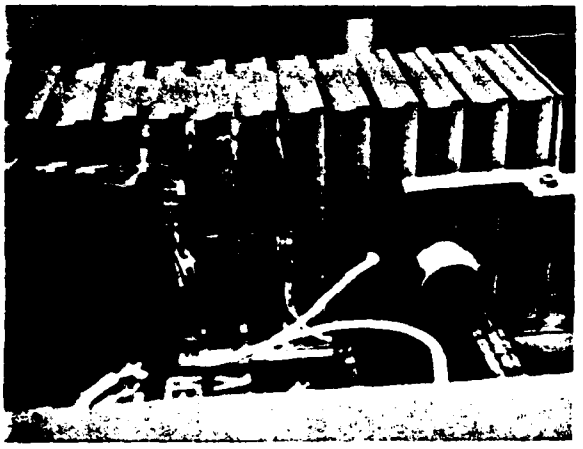


Figure 7. SOLID-STATE SWITCH ASSEMBLY

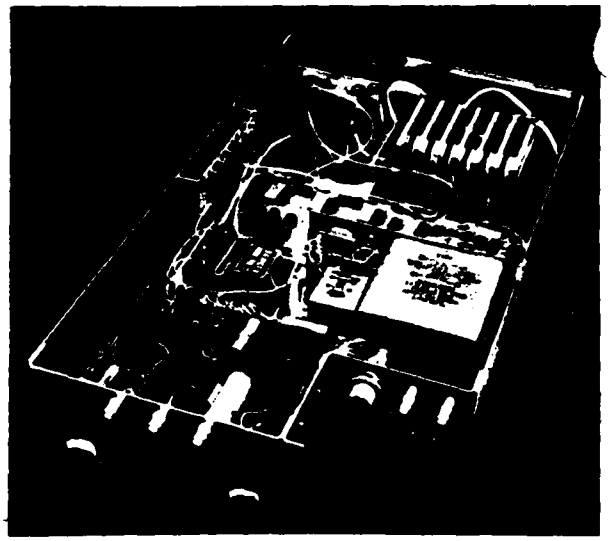


Figure 8. MODULATOR TRIGGER AMPLIFIER

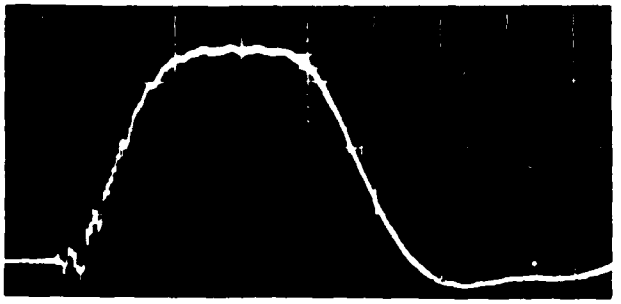


Figure 9. PULSE TRANSFORMER SECONDARY CURRENT
0.5 μS/DIV, 30 A/DIV

HAYSTACK HILL LONG-RANGE IMAGING RADAR TRANSMITTER*-

William North

GTE Sylvania, Electronic Systems Group
Needham Heights, Mass. 02194

*This work was sponsored by the Department of the Air Force under a subcontractor of M.I.T. Lincoln Laboratory. "The views and conclusions contained in this document are those of the contractor and should not be interpreted as necessarily representing the official policies, either expressed or implied, of the United States Government."

HAYSTACK HILL LONG-RANGE IMAGING RADAR TRANSMITTER

By

William North

GTE SYLVANIA, INC.
Electronic Systems Group
77 "A" Street
Needham Heights, Massachusetts 02194

ABSTRACT

TITLE: The Haystack Hill Long-Range Imaging Radar Trainsmitter

AUTHOR: William North

(Contracted by Lincoln Laboratory to work on system developed by Lincoln Laboratory)

PROFESSIONAL AFFILIATION: GTE Sylvania, Electronic Systems Group

LOCATION: Needham Heights, Mass.

The Long-Range Imaging Radar (LRIR), developed by MIT Lincoln Laboratory for the USAF, is presently installed at the Haystack Hill NEROC radiotelescope facility, in Westford Mass, and uses its 120-foot diameter parabolic reflector antenna. Its transmitter is designed around the Varian VTX-5681 TWTA, which was developed specifically for this application under the sponsorship of MIT Lincoln Laboratory.

Each state-of-the-art VTX-5681 has a peak power of 100 kW, average power of 50 kW, pulse duration of 50 milliseconds, and instantaneous 1-dB bandwidth from 9.5 to 10.5 GHz. The LRIR transmitter uses four of them in its FPA; the RF outputs of which are combined in pairs, split, and cross-combined, to present signals to the inputs of the high-efficiency feed which are equi-phase and equi-amplitude despite individual tube dissimilarities.

TWT beam voltage is 42 kVdc at 10 amperes, which is gated by means of the output of a direct-coupled floating deck modulator connected to the unity-mu modulating anode of each parallel-connected TWT. The modulator, which uses Eimac 8960 switch tubes, is capable of pulse durations of from less than 10 microseconds to CW, and PRFs up to 2000/second. Output amplitude control is accomplished by a diode-coupled grid-catcher circuit applied to the upper switch tube grid. Low-level signal coupling is by means of a balanced, capacitively-coupled 10 MHz links, using microcircuit components.

Maximum use was made of the existing 58 kVdc, 21-ampere HVPS and the 80 kV, 156 mF capacitor bank and crowbar. It was necessary, however, to augment them with a 20-ampere electronic current regulator, between rectifiers and capacitor bank, and a 40-ampere electronic voltage regulator, between capacitor bank and TWT beam input, and an output buffer capacitor bank and separate crowbar. Both regulators use Eimac 4CW250,000 tetrodes.

Introduction

The LRIR was installed at the NEROC Haystack Hill Radiotelescope facility early in 1977, taking maximum advantage of its considerable facilities. Foremost of these, shown in Figure 1, is the 120-foot diameter, Cassegrain optics, parabolic reflector antenna, dimensionally accurate for operation beyond 35 GHz. At the 10-GHz center frequency of the LRIR the antenna beamwidth is only 3 minutes of arc.

Of the total complement of transmitter equipment the entire high-level RF chain and the floating-deck modulator are housed in an environmental enclosure or "T/R box," 12 feet long and 8 feet square in cross-section. This box, as shown in Figure 1, can be hoisted from floor level to a position at the focal point of the approximately 9-foot diameter subreflector. The high-efficiency multimode antenna feed protrudes from the front of the T/R box through a hole in the back of the primary reflector. The remainder of the transmitter equipment is located in a high-voltage vault at ground level.

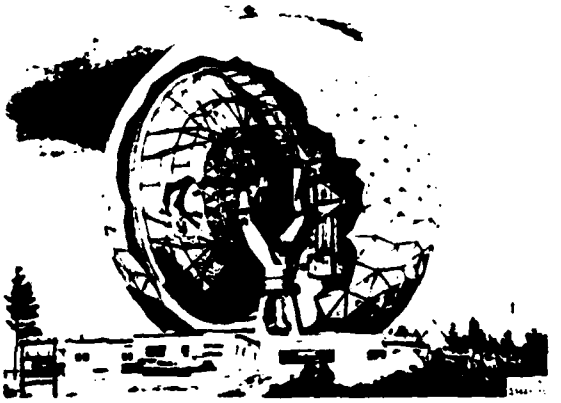


Figure 1. Haystack Hill Radiotelescope Facility

RF Chain

The LRIR transmitter was designed around the capabilities and requirements of the state-of-the-art Varian VTX-5681, which was developed under contract from MIT Lincoln Laboratory specifically for this application. Each of these coupled-cavity tubes is capable of peak power of 100 kW, over an instantaneous 1-dB bandwidth from 9.5 to 10.5 GHz, for pulse durations up to 50 milliseconds and duty factors up to 50 percent, with a saturation RF drive power of nominally 1 watt.

The transmitter uses four of the VTX-5681 TWTs, as shown in Figure 2. The tubes are combined in pairs and the combined signals are re-split, cross-coupled and recombined, so as to produce equi-phase

and equi-amplitude signals, irrespective of individual TWT phase delay and amplitude dissimilarities, at the inputs of the binary hybrid splitter tree which ultimately produces the eight inputs to the antenna feed.

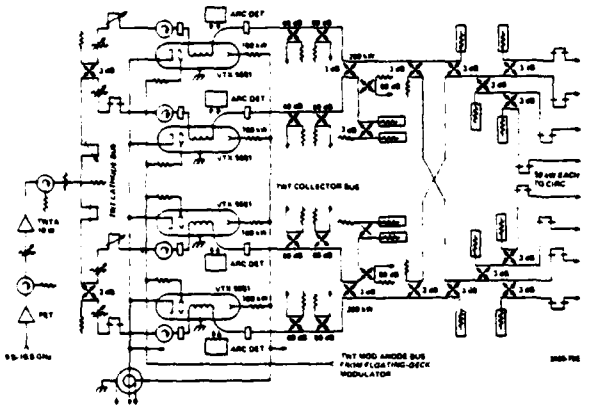


Figure 2. Simplified Schematic of RF Chain

All of the output waveguide components are in nonstandard water-cooled WR-102 waveguide, using stainless-steel flanges and soft copper gaskets. The highest waveguide power levels, 200 kW peak and 100 kW average, are handled by integrated waveguide assemblies consisting of cascaded short-slot, 3-dB, quadrature hybrids. All waveguide components were tested to a least full operating power before system installation in a resonant ring driven by a 10 kW X-band klystron.

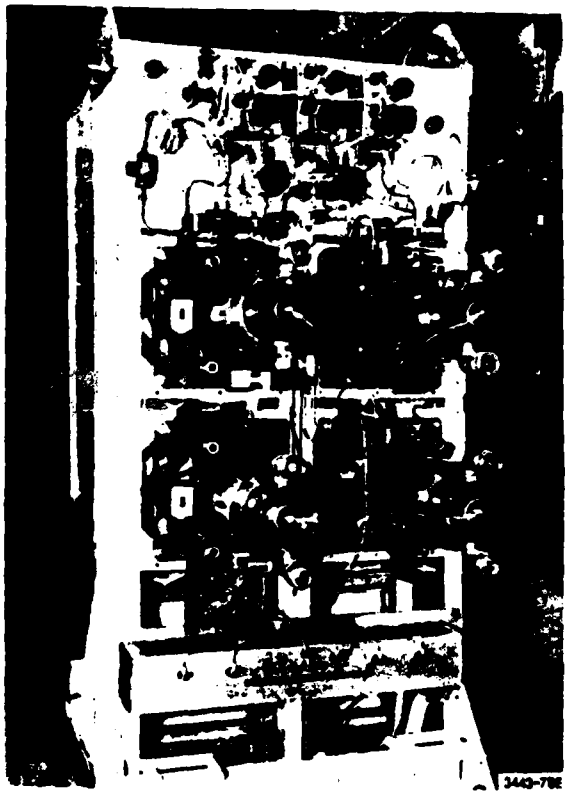


Figure 3. TWT Assembly

Figure 3 shows the TWT assembly, looking at the output end. The four TWTs are horizontally mounted in mirror image. The four water-cooled, 5 kW focus solenoids are mounted within the support structure. The TWT collectors are seen protruding toward the viewer. The WR-102 output waveguide flanges of the two left-hand tubes are visible to the left of the tube centerlines. The WR-90 input waveguide connections to the TWTs are visible above the upper tubes and below the lower ones. The semirigid coaxial low-level input circuitry, including the four manually-adjustable attenuators and the three remotely controlled, motor-driven line-length adjustors can be seen above the tubes. The line-length adjustors are used to maximize the combined signal (minimize hybrid waster-load power) for pairs of tubes and for the cross-coupled recombination. Note that the waster loads for TWT pair power combination is actually a hybrid-combined pair of water loads. This higher power capability is required in situations where one of a pair of tubes is inoperative for any reason, in which case half of the output power of the remaining tube must be dissipated in it.

Figure 4 shows the same aspect as Figure 3 but with the waveguide components up to the ferrite circulator assembly attached. Also visible are two of the four wheels which permit the TWT and modulator assembly (Figure 3) to be rolled out of the T/R box for TWT replacement. To effect TWT removal and replacement, the framework is rotated 90 degrees in a special handling jig so that the tubes can be handled with their major axes vertical.

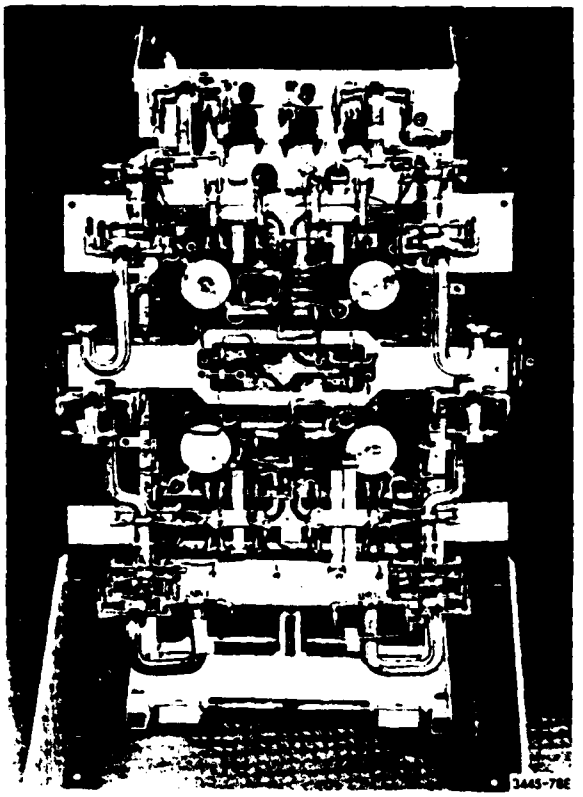


Figure 4. TWT Assembly with Waveguide Attached

Antenna duplexing is accomplished by an assembly of eight high-power ferrite circulators. Additional transmit signal attenuation is provided for the receiver front-end by gas-filled receiver protectors.

At the front-end of the transmitter RF chain, preamplification is provided by an FET amplifier which drives a packaged X-band TWTA with 10-watt rated output.

Floating-Deck Modulator

The VTX-5681 TWT operates at a beam voltage of 41 to 42 kV with a peak pulse beam current of 10 amperes. Beam current is controlled by a unity-mu modulating anode. As shown in Figure 5 the modulating anodes of the four TWTs are driven in parallel from the output of a floating-deck modulator, using EIMAC type 8960 tetrode switch tubes.

The minimum operational pulse duration in the LRIR waveform repertoire is the 250-microsecond wideband ramp, which is linearly frequency modulated from 9.5 to 10.5 GHz. This waveform can recur at PRF up to 2000/second. At the other extreme is the long pulse, which can extend for 50 milliseconds at a rate of 10 per second. To accommodate the range of waveform characteristics, the modulator was designed to produce a minimum pulse duration of approximately 10 microseconds, with a rise time of approximately 5 microseconds and a maximum pulse width of CW.

The modulator output voltage varies from a level approximately 500 volts negative with respect to the TWT cathode voltage during the interpulse interval to a level which is adjustable between approximately 100 volts negative with respect to ground and 15 kV negative with respect to ground. The total output pulse, therefore, is adjustable in amplitude from approximately 26 to 42 kV. At the lower value the individual TWT beam current is 7 amperes, reaching its nominal value of 10 amperes 1 or 2 kV below maximum.

As can be seen from Figure 5 the amplitude control is accomplished by means of a grid-catcher circuit applied to the "on" tube of the modulator. A 0 to -15 kVdc bias voltage is injected into the grid circuit by means of an 8020 (100R) thermionic diode. A number of different types of solid-state diode stacks were used in this application, all of which performed satisfactorily during normal operating conditions. None of them, however, would continually survive the transient conditions resulting from TWT internal arcs and crowbar discharges. The 8020 has proven quite forgiving.

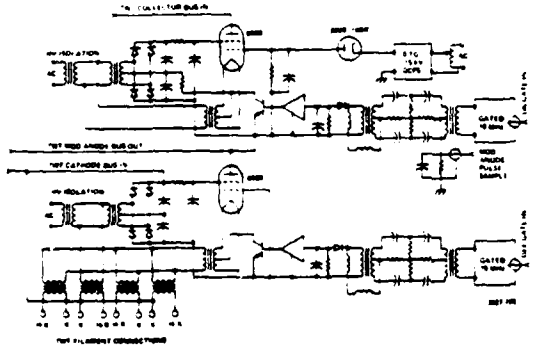


Figure 5. Simplified Schematic of Floating-Deck Modulator

The grid-catcher circuit functions in the following way. An "on" pulse is initiated by gating a 10 MHz signal, derived from an integrated-circuit computer clock-pulse generator, into the primary of a balun transformer; the secondary center-tap of which is referenced to ground. The balanced 10-MHz signal is transmitted to the floating deck by means of a balanced, capacitively-coupled transmission line, each leg of which consists of 10 capacitors in series, each rated at 100 pF, 6 kV, shunted by 1000 megohm voltage equalization resistors. The capacitance of each leg is 10 pF and the video currents which flow in each, as a result of the rise and fall transitions of the output pulse cancel in the secondaries of the transmitter and receiver balun transformers. The output of the receiver balun transformer, after detection by the diode rectifier, is applied to a transistor amplifier which causes saturation of the transistor in the cathode circuit of the 8960, resulting in zero-bias current flow in the 8960, producing a 5 microsecond transition to the intrapulse output voltage level. When the rising output voltage becomes less negative than the intra-pulse bias voltage the 8020 diode conducts, rapidly developing cutoff bias across the 8960 grid-leak resistor, clamping the output voltage at approximately the bias voltage. The 10 MHz burst is terminated 5 microseconds prior to the desired end of the modulator "On" pulse to compensate for storage time in the saturated transistor amplifier and preclude simultaneous conduction of both the on and off switch tubes.

The negative-going transition to the intrapulse output voltage condition is accomplished by a similar sequence of events applied to the off switch tube, except for the grid-catcher feature.

Due to an unusual problem encountered with the VTX-5681 it became necessary to drive the off deck during the entire interpulse interval in order to provide a low impedance path to the interpulse bias voltage. The problem manifested itself in high (as much as 5 mA) leakage current between body and modulating anode with 40 kV between them. The passive pull-down resistors originally used could not be made low enough in resistance to ensure beam-current cutoff during the interpulse interval without prohibitive power dissipation, due to the 50-percent duty factor of the modulator. Note that the TWT cathode bus is connected to the screen supply voltage of the off tube. With no more than 5-mA interpulse current and zero bias, the plate drop of the off tube during the interpulse interval is less than 200 volts. The modulating anodes of the TWTs, therefore, are biased some 500 volts negative with respect to their cathodes by a 700-volt screen supply voltage.

Figure 6 shows the modulator end of the TWT assembly (the other end of Figure 3) with the doors closed. Figure 7 shows it with the doors open and the lower access panel removed. The gun bushings of the four TWTs are seen protruding about halfway up the cabinet. In the upper left-hand corner is the "on" deck, with its low-capacitance ac isolation transformer to its right. The 8020 diode is mounted, upside-down, behind the 8960 switch tube. In the center is the common point of the mod-anode bus, with the individual isolating resistors fanning out from it. On either side, between upper and lower tubes, are enclosures for the ferro-resonant filament transformers, each of which is rated at 7 Vac, 10 amperes. They provide regulated filament voltage and, more importantly, limit cold-filament inrush current to less than 15 amperes, less than twice the hot value of current, 8 amperes. There are two transformers in each box. Note that mod-anode, cathode and filament/cathode connections to the tubes are made with jumbo banana plugs and jacks, which has proven quite successful in accomplishing fast disconnection of an inoperable or troublesome tube. In the lower middle is the "off" deck, below which is its power-isolation transformer, which is of standard capacitance. In front of the transformer is the pot-head cable connector termination for the TWT beam voltage.



Figure 6. Floating-Deck Modulator Enclosure

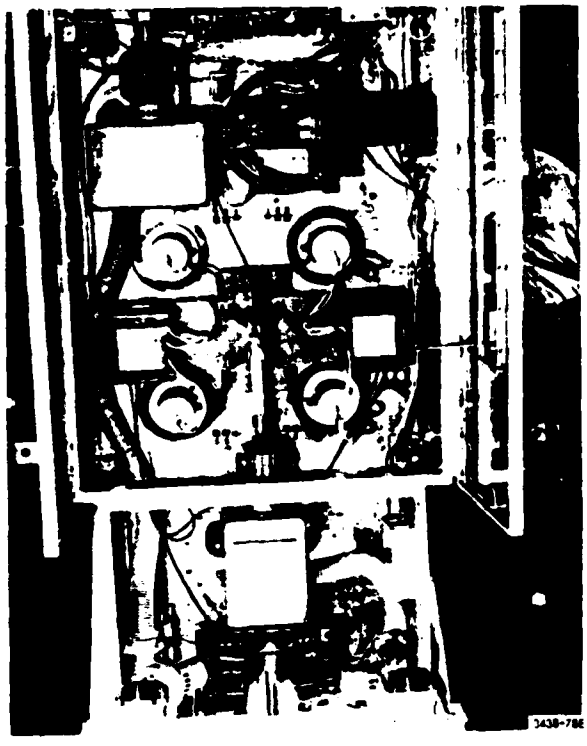


Figure 7. Floating-Deck Modulator

Figure 8 shows the interior of one of the decks and Figure 9 is a close-up of a balanced 10-MHz up-link.

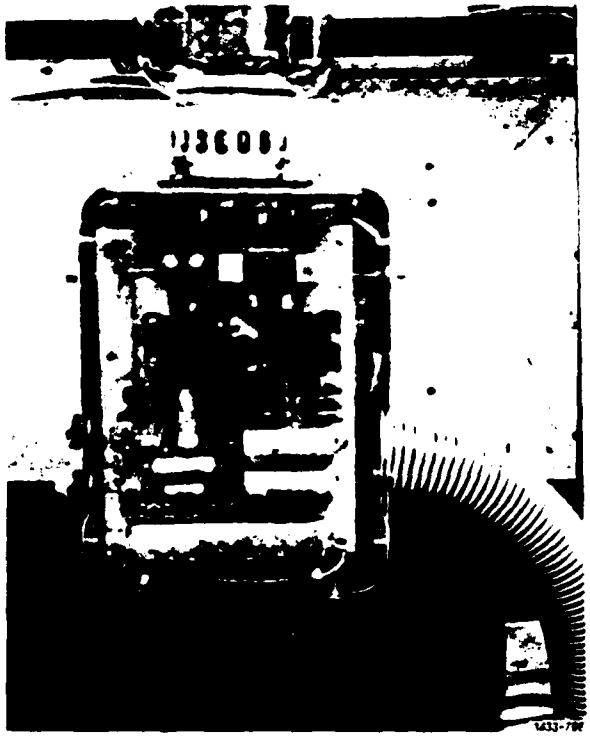


Figure 8. "On" Deck of Modulator

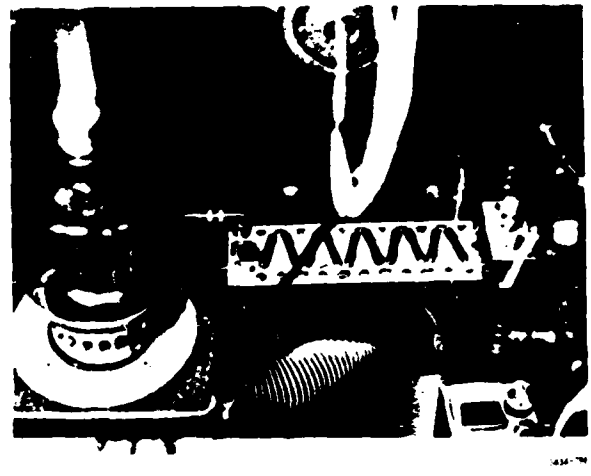


Figure 9. 10 MHz Up-Link of Modulator

High-Voltage Power Supply and Energy Storage System

The fundamental high-power, high-energy system, consisting of the 2.06 MVA, 4160 Vac, 3-phase Inductrol input regulator; the dual 29.1 kV, 20.5 amperes (per secondary winding) rectifier transformers, capable of being connected in either delta or wye, and the winding sets connected either in parallel or series; the dual 3-phase, full-wave bridge rectifiers, having a total, series-connected PIV rating of 75.6 kV at 8.3 amperes average per leg; the energy storage capacitor bank, consisting of 372 capacitors, each rated at 1.68 mF, 40 kV, and each having two parallel 1000 ohm resistors in series; and the infinite-voltage range, needle firing-gap, air-gap crowbar discharge switch were in existence at Haystack Hill as part of the original Planetary Radar System.

For the purposes of the LRIR, the rectifier transformers were connected delta-delta, with each secondary feeding one of the full-wave bridge rectifiers, which were series connected, as shown in Figure 10. Figure 11 shows the transformer terminals as they penetrate the vault wall (both the Inductrol and the rectifier transformers are located outdoors) and two of the upper three of the rectifier legs. The capacitor bank, which is in two rows, stacked three capacitors high, was connected as shown in Figure 12, to yield an equivalent of 156 mF at 80 kV. Figure 13 is a view between the two rows of the capacitor bank. Figure 14 shows the main crowbar, which was moved from its original location to atop the crowbar trigger rack so that the high-current crowbar discharge loop would not encircle newly installed low-voltage circuitry. The main crowbar discharge current reaches a peak value of slightly less than 2000 amperes.

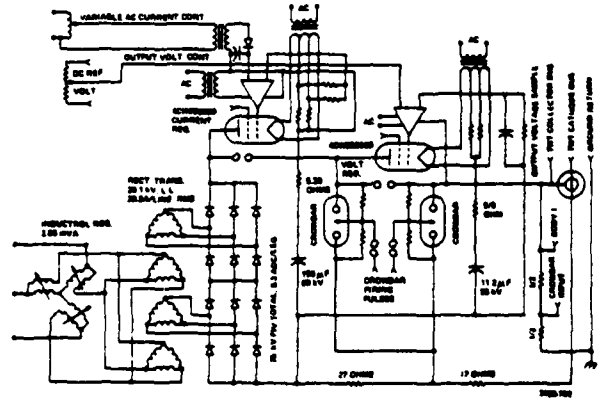


Figure 10. Simplified Schematic of High-Voltage Vault



Figure 11. Rectifier Transformer Terminals and Two of Three Upper Rect. Legs

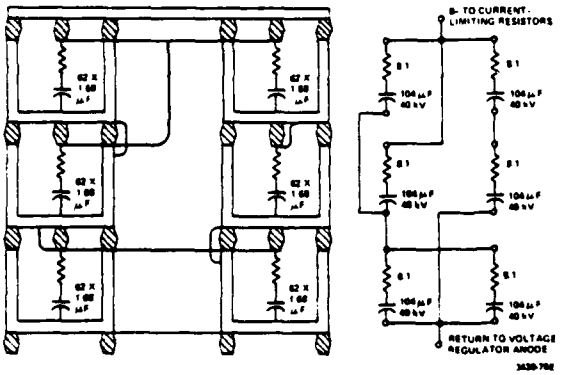


Figure 12. Capacitor Bank Connections for 15 μF, 80 kV

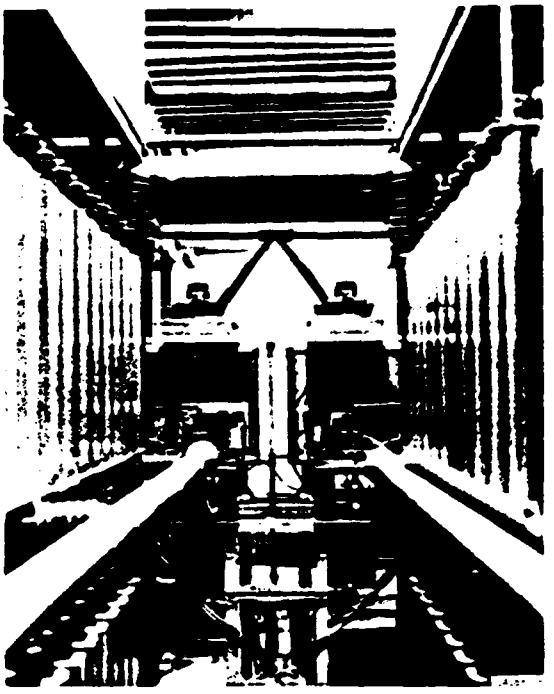


Figure 13. Capacitor Bank

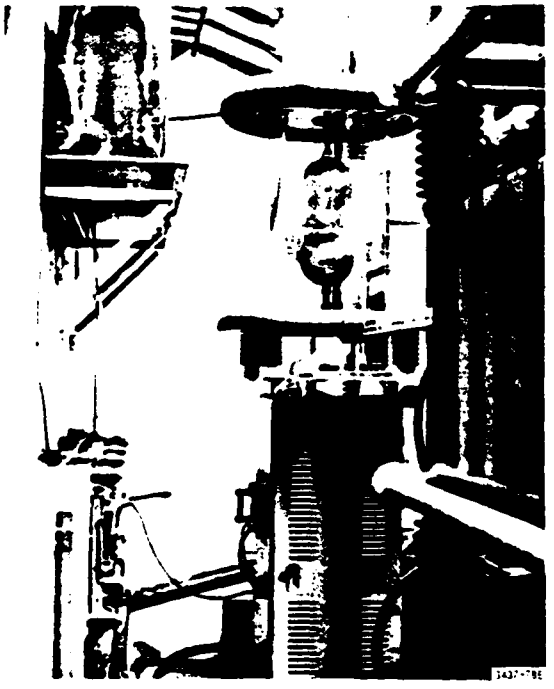


Figure 14. Main Crowbar

Electronic Voltage and Current Regulators

The requirement for pulse durations up to 50 milliseconds at PRFs up to 10/second, places unusual demands upon the high-energy system. With a total of 40-ampere TWT beam current during the pulse, half of which can be expected to be supplied by the rectifiers at 50-percent duty, even a capacitor bank as prodigious as this one will suffer a voltage decrement of 6.4 kV over a 50-millisecond pulse. With the tolerable voltage variation between TWT cathode and ground, during a pulse limited to something less than 100 volts, a form of voltage regulation is obviously called for.

An electronic voltage regulator, as shown in Figure 10, was developed, using an EIMAC 4CW250,000 pass tube and a solid-state error amplifier. No-load screen voltage of approximately 1.3 kV was used, obtained from a simple single-phase, full-wave supply with capacitor filter; which however, was fed from a ferro-resonant constant-voltage transformer which limited screen current and power to well below rated dissipation limits during the time when the beam power supply

voltage was below the point of regulation. Figures 15 and 16 show the electronic voltage regulator circuitry. The 4CW250,000 can be seen with its water jacket pointed down and its filament transformer to the left (Figure 15).

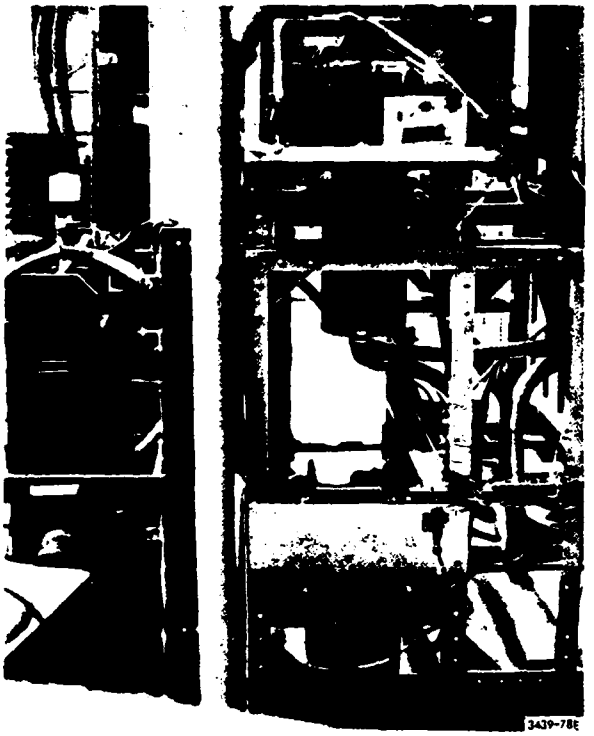


Figure 15. Electronic Voltage Regulator

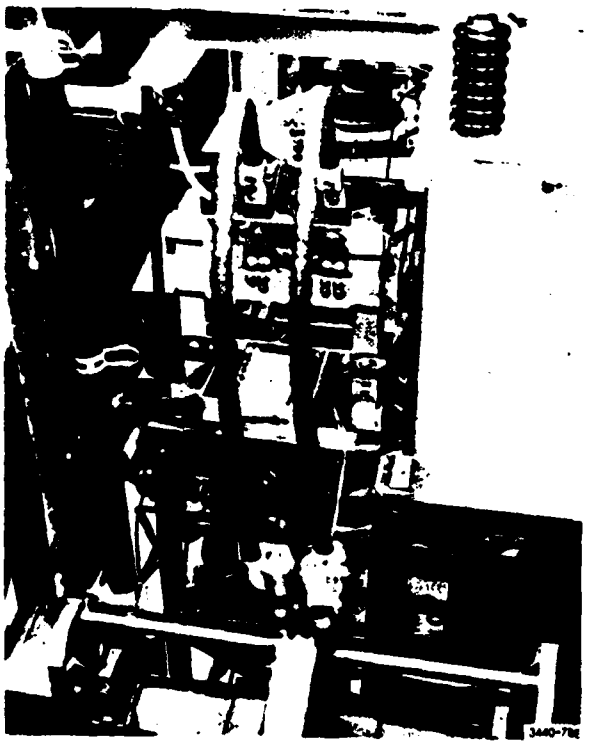


Figure 16. Electronic Voltage Regulator

An 11.2-μF buffer capacitor bank was connected to the output of the regulator, with its own smaller crowbar, of the same type as the large one. This equipment can be seen mounted on the wall behind the large crowbar in Figure 17.

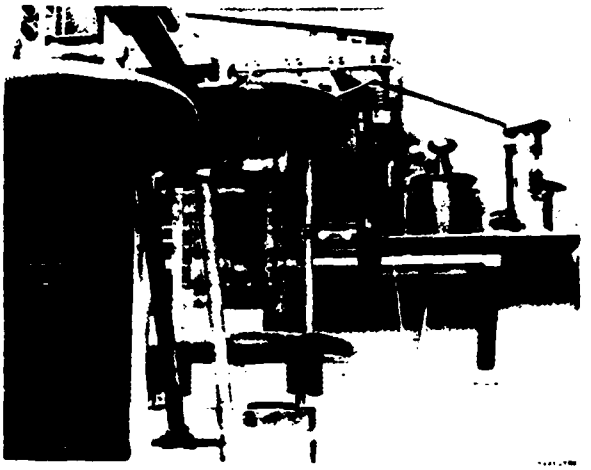


Figure 17. Buffer Capacitor Bank and Secondary Crowbar

The voltage regulator solved only half the problem. Without something to limit rectifier current during the pulse the rectifiers would tend to deliver all of the 40-ampere pulse current. Even though the average current ratings of the rectifiers would not be exceeded, the rms current rating of the transformers would be. Moreover, the impulsive load, at a recurrence rate of 10/second, could be expected to produce quite objectionable lighting flicker for those sharing the 4160-volt feeder.

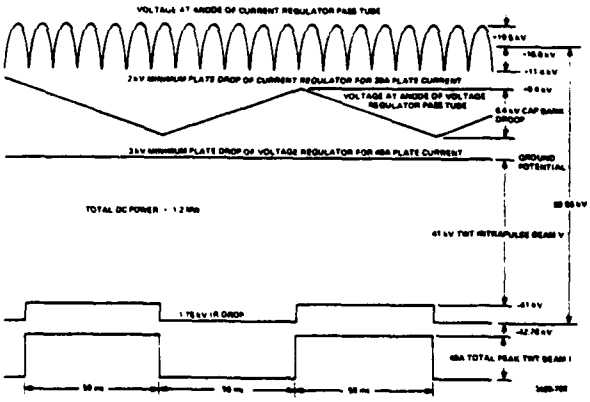


Figure 18. Profile of Voltages and Current Throughput High-Energy System

An electronic current regulator, also using a 4CW250,000 tetrode pass tube, a solid-state error amplifier, and a constant-voltage screen supply of only 800 volts, however, was developed, as shown in Figure 10. The profile of voltages and currents throughout the regulator chain is shown in Figure 18. The pulsed output current is shown at the bottom. Above it is the most negative voltage, approximately -42.6 kV, which exists during the interpulse interval. During a 40-ampere pulse the voltage is less negative by the 1.76-kV drop in the 44-ohm current-limiting resistance. The TWT collector voltage, which is the output of the voltage regulator, is off ground potential only by the flow of total TWT body current through the 1-ohm sampling resistor (except during TWT internal sparks to body, where fault current is limited to 1000 amperes and collector voltage to ground is limited by protective diodes shunting sampling resistor). The minimum plate drop of the voltage regulator pass tube for 40 amperes is 3 kV. Added to this is the 6.4-kV peak capacitor bank droop. The sum is the

voltage at the junction of current and voltage regulators. The minimum plate drop required for the current regulator to pass the maximum average current of 20 amperes is 2 kV, added to which is the rectifier ripple voltage. The total average voltage, therefore, is 59.56 kV.

Figure 19 shows the current regulator circuitry.

The high-voltage connections are made from the high-voltage vault to the T/R box by means of a three-conductor coaxial cable. The TWT cathode bus is carried by the center conductor, the TWT collector bus, which is isolated from ground, is carried by the inner outer conductor and the T/R box chassis connection, which is common to TWT body, is made via the outer outer conductor.

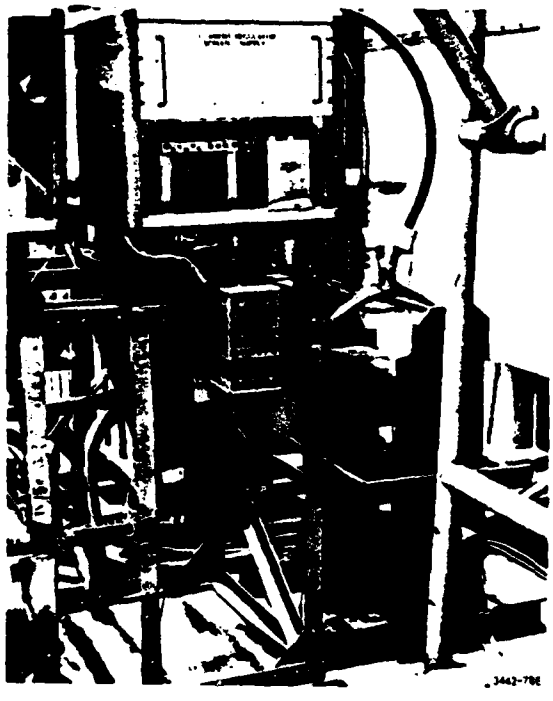


Figure 19. Current Regulator

Control Console

The transmitter control console is shown in Figure 20. RF chain conditions are indicated by lamps located at key points throughout a "road-map," similar to Figure 2, located on the center and right-hand sloping panels. The indications of normal and overload conditions are telemetered from the T/R box, where the primary sensors, such as the photoelectric arc detectors and the excess reverse power monitors are located, to the control console via a time-division-multiplexed serial digital data stream, in order to conserve conductors in the interconnecting cable-wrap.

Control of the TWT operating voltage is accomplished at the left-hand sloping panel where the control voltage for the electronic voltage regulator can be adjusted and the raise-lower control for the 100-percent buck and boost Inductrol line regulator is located. Digital meters on this panel display average body current, average beam current, TWT cathode voltage and average regulator drop, for either voltage or current regulator. A circuit monitors TWT cathode voltage and produces an output which inhibits on-gate pulses to the modulator for voltages between -10 and -40 kV, which encompasses the range of voltage within which dangerous TWT self-oscillation is possible.

Located above voltage control panel are the TWT collector-current monitor scope, the test waveform generator, and the slow-speed interlock status panel; which includes such functions as water-flow, door interlocks, etc.

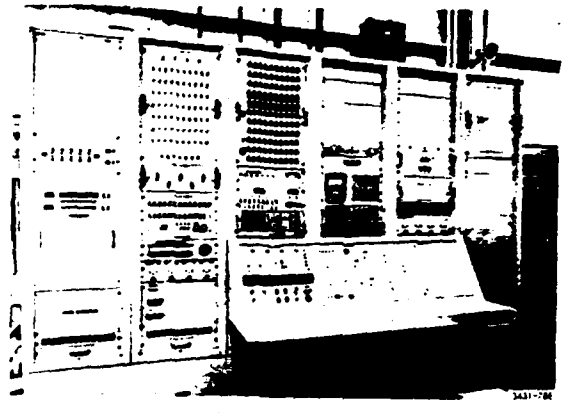


Figure 20. Transmitter Control Console

Conclusions

As of the time of presentation of this paper the LRIR transmitter will have been in operation for almost a year and a half and has proven remarkably reliable for such an ambitious undertaking.

Acknowledgements

The author would like to thank all those of MIT Lincoln Laboratory and NEROC who were also a part of this program, either technically or managerially, for providing an environment of competence and enthusiasm that is seldom matched, and, in particular, Clarke Heon and Lou Rainville, of NEROC, Clarence Jones, of MIT Lincoln Laboratory, and Bill James, of Varian Associates, without whom the job might have been possible but it certainly would have been nowhere near as much fun.

HIGH REPETITION RATE LC OSCILLATOR

Stuart L. Moran
Naval Surface Weapons Center
Dahlgren, Virginia 22448

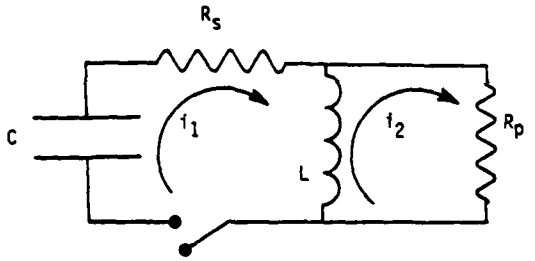
Summary

L-C oscillators have been built which can produce multikilowatt RF pulses in the megahertz frequency range with repetition rates of tens of kilohertz. The L and C for these oscillators can be determined from the frequency requirement and the high Q requirements. The high repetition rates are achieved using a high pressure spark gap switch together with a DC to AC inverter power supply. Closely spaced antenna elements can be used to increase the Q of the radiated waveforms.

Introduction

The inductance capacitance (L-C) oscillators described in this paper place an emphasis on high frequency and high repetition rate. These oscillators store millijoules of energy and can produce multi-kilowatt radio frequency (RF) pules in the megahertz frequency range with repetition rates of tens of kilohertz.

The oscillator consists of an inductor (L) and a capacitor (C) in series with a spark gap switch as shown below.



R_s represents the series losses in the system and R_p represents the parallel losses or the load. The oscillator produces a damped sinusoid with a center ringing frequency of $(2\pi\sqrt{LC})^{-1}$.

The energy storage in the capacitor is given by $\frac{1}{2} CV^2$ where C is the capacitance and V is the voltage between the capacitor plates. It will be shown that C is relatively fixed for a given frequency so that V is the only variable for control over the energy storage.

Spark Gap Switch

A spark gap switch is used in these oscillators. It consist of two Rogowski electrodes (1 cm in diameter) which are overvolted to close the switch. To minimize the inductance and resistance, the gap spacing is small (5-10 mils). To maintain a high standoff voltage with narrow gap spacings the gas between the electrodes is pressurized.

The switch handles currents of about 1,000 amps and stands off several thousand volts. It should be noted that there is no distinct anode or cathode since the current reverses direction during each RF cycle. For high efficiency, the switch must be able to close quickly compared to a quarter cycle of the RF and must open quickly compared to the repetition rate. This requires closing times of about one nanosecond and opening times of a few microseconds. To meet the ionization and de-ionization requirements, the type of gas used in the spark gap is important. The narrow gap spacing precludes the use of any gas which is corrosive or forms deposits, such as air or oxygen. Other gases, such as nitrogen, do not work well at high repetition rates. Above one kilohertz it has been emperically determined that a mixture of 95% argon and 5% hydrogen gives satisfactory results. This is the gas mixture currently being used.

Maximizing the Q

For an oscillator with series and parallel losses the damped sinusoid wave will consist of a continuous range of frequencies in the neighborhood of the undamped ringing frequency $(2\pi\sqrt{LC})^{-1}$. In general it is desirable to maximize the Q of the circuit to concentrate the energy in a narrow frequency range. If the characteristic impedance ($\sqrt{L/C}$) of the oscillator is too low, the series losses will severely damp the device. If the characteristic impedance is too high, the parallel losses caused by the load will severely damp the device. The characteristic impedance which will maximize the Q can be obtained by solving the LC circuit shown in figure 1. Expressions for the currents i_1 and i_2 are given by[1]:

$$i_1(t) = \alpha \left(\frac{\frac{2R_p + R_s}{Z}\frac{Z}{R_p}}{\sqrt{4 - \left(\frac{Z}{R_p} - \frac{R_s}{Z}\right)}} \sin \beta\omega t + \cos \beta\omega t \right)$$

$$i_2(t) = \alpha \left(\frac{-\frac{R_s}{Z} - \frac{Z}{R_p}}{\sqrt{4 - \left(\frac{Z}{R_p} - \frac{R_s}{Z}\right)}} \sin \beta\omega t + \cos \beta\omega t \right)$$

where

$$\alpha = \frac{V_0}{R_s + R_p} \exp - \left[\frac{Z + \frac{R_s R_p}{Z}}{2(R_s + R_p)} \omega t \right]$$

and

$$\beta = \frac{R_p}{2(R_s + R_p)} \sqrt{4 - \left(\frac{Z}{R_p} - \frac{R_s}{Z}\right)^2}$$

U.S. GOVERNMENT WORK NOT PROTECTED BY U.S. COPYRIGHT.

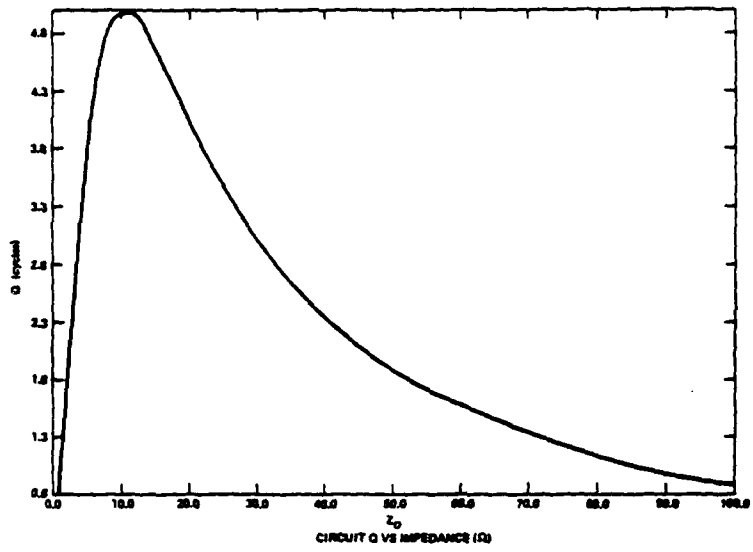


Figure 2. Theoretical Q as a function of oscillator characteristic impedance where the series loss is one ohm and the parallel load is 100 ohms.

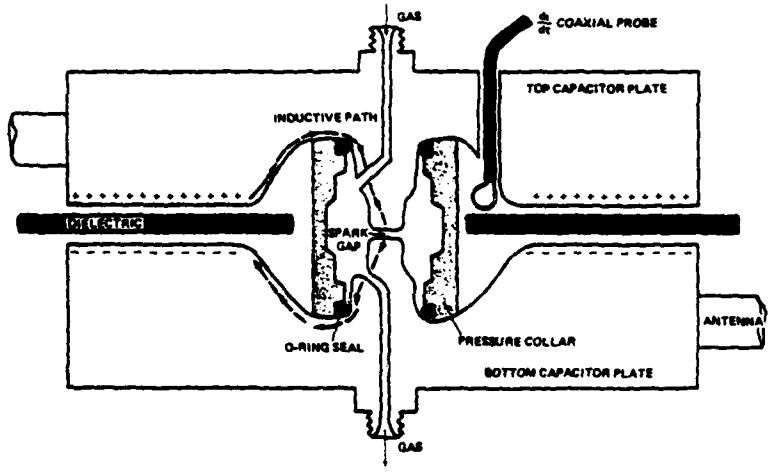
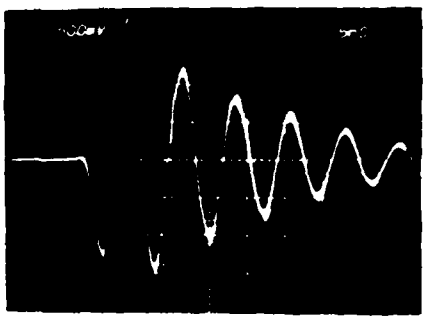
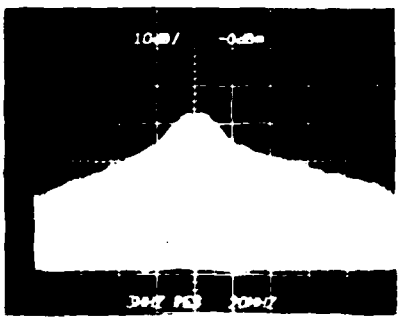


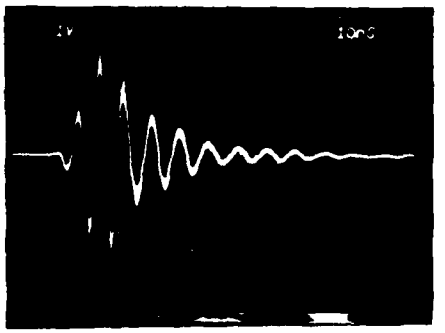
Figure 3. Cross section of a 150MHz LC oscillator.



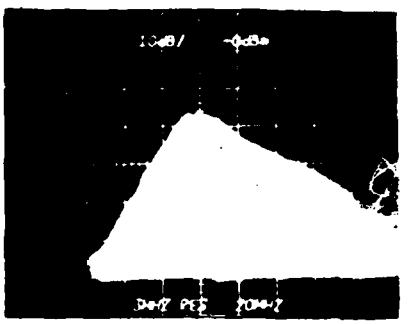
di/dt Waveform Using a Magnetic Pickup Probe Inside the Device--5 ns/div. Without Transmit Antenna



Frequency Spectrum Using a Magnetic Pickup Probe. 150 MHz Center Frequency. 10 dB/div. Log Scale Vert.-- 20 MHz/div. Horiz. Without Transmit Antenna



Receive Signal Time Trace Using a Cross Dipole Receive Antenna --10 ns/div.



Receive Signal Frequency Spectrum Using a Cross Dipole Receive Antenna. Same Scale as Above.

Figure 4. Signals produced by an LC oscillator.

The exponential decay term can be used to find the time (t) for the peak amplitudes to drop to 1/e of their initial value. The period of the damped sine wave will be $T = 2\pi/a_\omega$ and therefore the Q of the circuit will be $\pi t/T$ which gives:

$$Q = \frac{\sqrt{4 - (Z/R_p - R_s/Z)^2}}{2(Z/R_p + R_s/Z)}$$

where $Z = \sqrt{L/C}$
R_p = parallel losses (antenna)
R_s = series losses.

The oscillator will not ring unless the Q is real. Maximizing the Q gives:

$$Z \text{ (for maximum Q)} = \sqrt{R_p \times R_s}$$

Therefore,

$$Q \text{ max} = \frac{1}{2}\sqrt{R_p/R_s}$$

From this it can be seen that for a reasonably high Q (5 or more) the condition $R_s << Z << R_p$ must hold.

The series and parallel losses can be estimated by varying Z and observing the change in Q. Our experiments indicate that for an unpressurized spark gap firing at low repetition rates with RF frequencies in the megahertz range, the effective series losses are about 1 ohm and the effective parallel load using a half wave dipole antenna is about 100 ohms. Therefore, the optimum oscillator characteristic impedance is about 10Ω. A graph of the Q versus oscillator impedance is shown in figure 2.

Design and Performance of the Oscillator

Using the two equations Z=10 and $f=(2\pi\sqrt{LC})^{-1}$ both L and C can be obtained. A frequency of 150 megahertz was chosen as a convenient size. This gives L = 10nH and C = 100pF. Several oscillators have been built with approximately these parameters. The design is shown in figure 3. Each capacitor plate includes a spark gap electrode and is machined from one piece of metal. Brass, copper and aluminum have been used with very little observed difference. The capacitance depends on the surface area, dielectric material, and dielectric thickness. The inductance is given by the geometry of the plates and is roughly proportional to the charge-flow path-length from one side of the capacitor to the other. The diameter of the capacitor is roughly 10 cm. A pressure collar of plexiglass seals the electrodes with O-rings to allow the spark gap to be pressurized to several hundred psi. Signals obtained from these devices are shown in figure 4. A di/dt probe consisting of a half centimeter loop of wire can be placed inside the inductive channel surrounding the electrodes. Signals from such a probe show that the first peak of the waveform is low indicating that the spark is significantly resistive during the first half RF cycle. A half wave dipole can be connected to the oscillator as shown in figure 3. Figure 4 shows the receive signals obtained from this configuration using a standard gain receive antenna in an anechoic chamber at a distance of 70 feet. The receive spectrum is narrower than the di/dt spectrum due to the frequency response of the transmit and receive antennas. The oscillators perform as expected. They will run many hours before there is detrimental wear or erosion of the spark gap electrodes.

Power Supply

The power supply used to power the oscillator is a DC to AC power inverter which converts 24 volts DC to 5,000 volt pulses at the desired repetition rate. The major advantage of this type of power supply over resistive charging is that voltage is not re-applied to the capacitor immediately after discharge. The "dead time" between charging allows for better de-ionization of the spark gap. Figure 5 shows the charging waveform produced by the power supply while running the oscillator. The discontinuities are points where the spark gap fires. Note the zero voltage (dead time) following each spark gap firing.

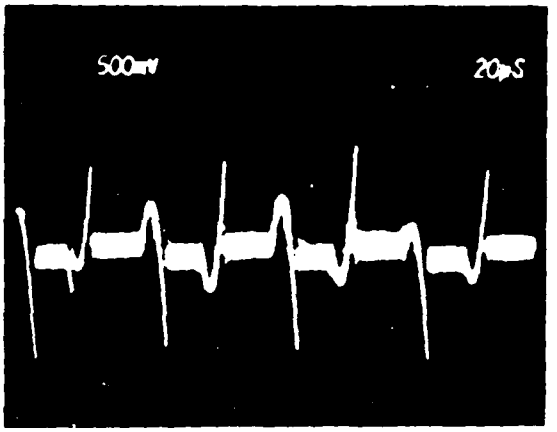


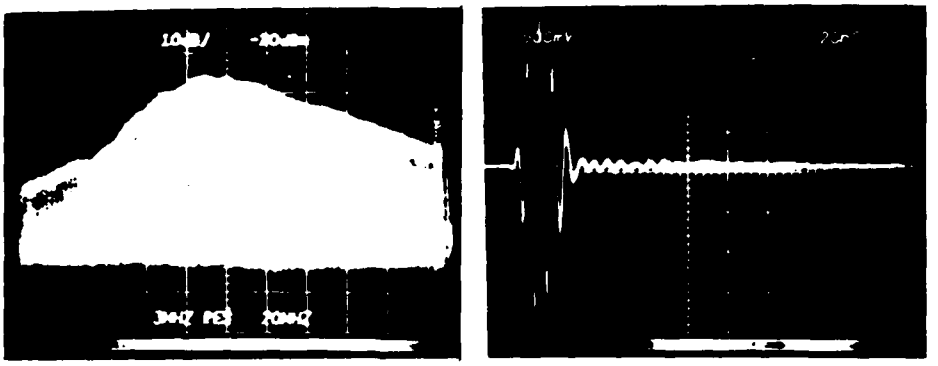
FIGURE 5. Charging waveform produced by a DC to AC inverter while operating an LC oscillator.

Antennas

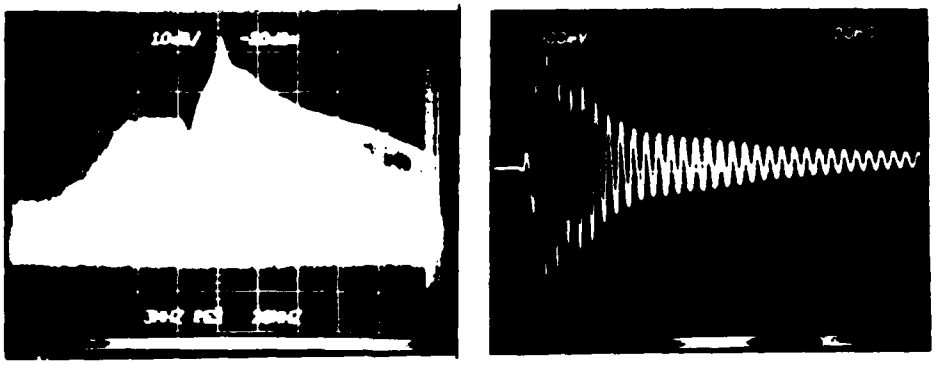
Emperical studies done with dipoles and yaggi arrays indicate that the antenna pattern at a particular frequency produced by the L-C oscillator pulses is not significantly different from the antenna pattern produced by a CW signal at the same frequency. Attempts have been made to increase the Q of the transmitted waveform through antenna design. It has been found that one particular type of antenna gives a substantial increase in the radiated Q as observed from a receive antenna. It consists of an element about one half wavelength long and place approximately λ/10 behind an oscillator with a standard dipole attached. The close arrangement of the elements causes a large increase in the radiated Q and an alteration in the spectrum shape (see figure 6). A variation of the element spacing or element length and the use of several elements can all be used to vary the output waveform and spectrum. Figure 7 shows some examples. Note the amplitude modulation in the waveforms and the creation of substantial peaks and notches in the spectrum shape.

Reference

1. Moran, Stuart L., "High Repetition Rate LC Oscillator", Naval Surface Weapons Center Technical Report TR3656, December 1977, Appendix C.

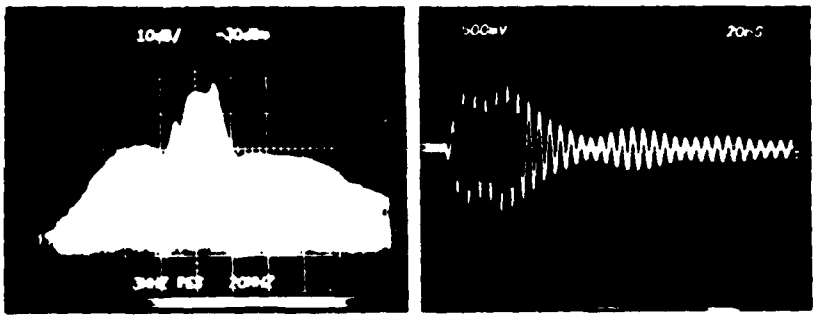


STANDARD DIPOLE

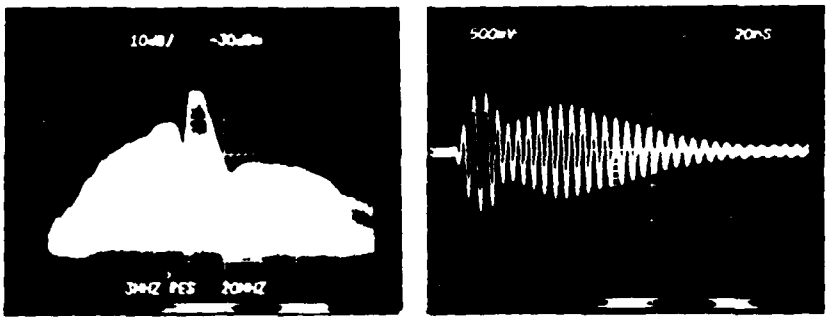


36 INCH ROD PLACED 3 INCHES BEHIND A STANDARD DIPOLE

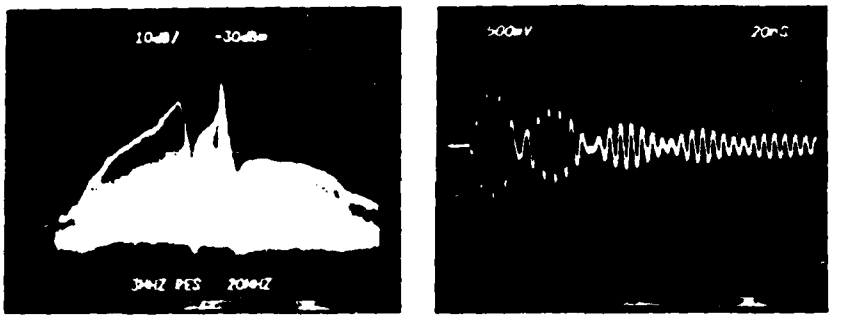
Figure 6. Receive signals at a distance of 70 feet showing the effects of placing a half wavelength element close to the standard-dipole transmitting antenna of an LC oscillator. Note the 10db increase in the spectrum peak at the center frequency and the increase in the Q of the time waveform. Spectrum photographs are 10db/division vertical and 20 MHz/division horizontal with 150 MHz center frequency.



40 inch reflector 3 inches behind dipole and 34 inch director 9 inches in front of dipole. Dipole length is 38 inches tip to tip.



40 inch director 5 inches in front of dipole and 34 inch director 10 inches in front of dipole.



40 inch director 10 inches in front of dipole and 34 inch director 5 inches in front of dipole.

Figure 7. Some examples of received waveforms and spectra from an LC oscillator with closely spaced parasitic elements. Center frequency is 150MHz.

A 1200 MEGAWATT VAN-MOUNTED LINE-TYPE MODULATOR

P. A. Corbiere, R. E. Kolibas and J. J. Moriarty

Raytheon Company, Missile Systems Division
Bedford, Massachusetts 01730

Summary

A line-type modulator is described which operates from a 4160 V ac source and delivers repetitive 12 kJ pulses to a remote load. The module and its controls are self-contained in a 45 foot long environmentally controlled, trailerable van. The pulser is comprised of fourteen thyratron-switched modulators, command-charged from a common source and coupled to the load by means of a single output transformer and cable.

Test equipment has been developed which provides system shutdown and fault identification in the event of thyratron malfunction, load fault or charging imbalance.

The module has been operated into a resistive load at the following levels:

Output Voltage	165 kV
Energy per Pulse	12 kJ
Pulse Repetition Rate	Single Shot to 25 pps
Burst Duration	15 s
Pulse Duration	10 μs and 20 μs

Design Considerations

The simplified circuit diagram of the dc-resonantly-charged line modulator is shown in Figure 1. Equipment layout is shown in the artist's conception in Figure 2. Prime power at 4160 V ac is brought directly into the rear of the van through a commercial air-breaker to an air-insulated transformer-rectifier. Auxiliary power at 480 V ac and 208 V ac for lighting, environmental control, and cathode heaters is brought through weather-tight connectors on the road side of the van to the power distribution and control rack which also contains trigger, command charge and fault monitoring functions as well as interlocks to maintain personnel and system safety.

A command-charge gate is generated, amplified and applied to the grids of a bank of ML8773 triode switch tubes. The duration of the charging gate can be adjusted to vary the final pulse-forming network (PFN) voltage from the fixed-voltage dc source by stopping the resonant charge prior to its completion.

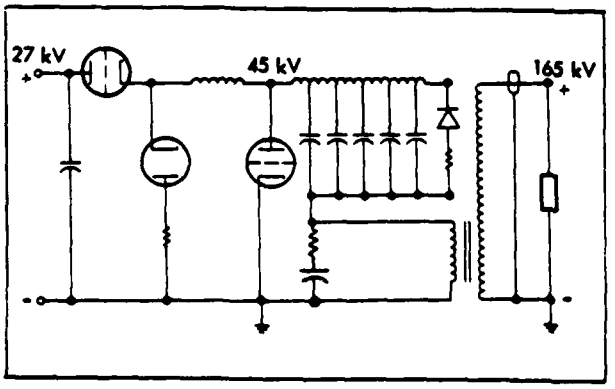


Figure 1 - Command-Charged Line Modulator Circuit

Energy stored in the charging reactors at the time of interruption is diverted to the PFNs through the free-wheeling diode at the cathode of the series triode bank.

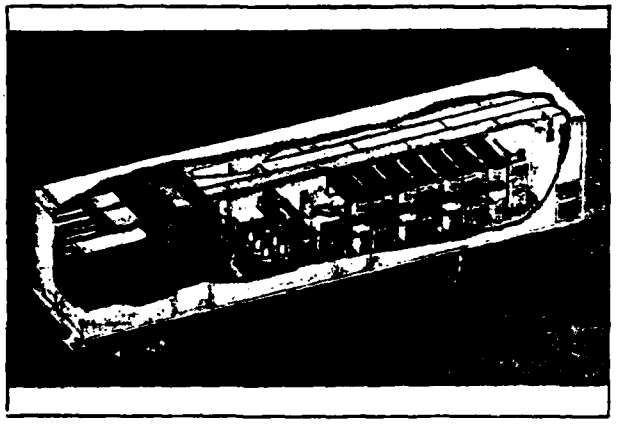


Figure 2 - Van-Mounted Line Pulser

The primary pulse forming circuit is made up of fourteen, parallel 10 μs PFNs, each charged to 45 kV and switched by means of an air-cooled CX1175 thyratron. A clipper diode and resistor are connected across the end of each pulse forming line. Each of the seven charging reactors is connected to a pair of PFNs in the 10 μs mode of operation. A simple mechanical adjustment allows one to interconnect the PFNs in series pairs for 20 μs pulse duration. In either connection, all fourteen thyratrons are triggered from a common pulse generator package which also supplies the negative grid bias voltage.

A 7.5:1 step-up pulse transformer combines the outputs of all the PFNs and is connected to the load by means of a single 250-foot coaxial cable which is fitted with a plug-in connector mated to an oil-insulated receptacle on the secondary of the transformer. A cross section of this 40 Ω cable is shown in Figure 3.

Active resetting of the pulse transformer core is required only in the 20 μs case and is provided by means of an inductively isolated dc power supply which delivers approximately 50 A at 2 V dc.

The single-point grounding philosophy applied to this system is shown in Figure 4. Care was taken to isolate the ground plane carrying pulse currents from the van frame except at the single point where all pulse grounds, power line grounds and chassis grounds are tied together, just forward of the wheels. The ground plane is constructed of 3/8-in. aluminum with all joints welded over their full length.

The secondary winding of the pulse transformer has been electrically isolated from the trailer and system ground plane to avoid ground loops between the van and its load. A spark gap is provided in case the fluctuations exceed the 5 kV hold-off rating of the secondary-low bushings.

CH1371-4/78/0000-0260$00.75 © 1978 IEEE

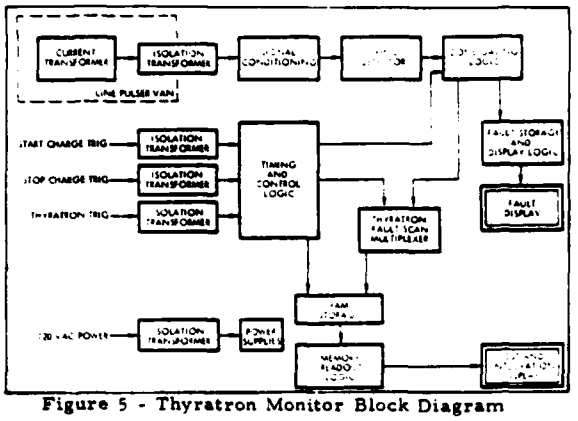


Figure 5 - Thyratron Monitor Block Diagram

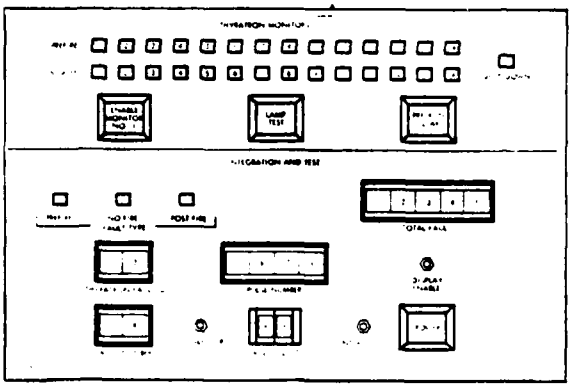


Figure 6 - Thyratron Monitor Display Panel

Since a "misfire" failure displayed on the upper front panel could refer to either a "no-fire" or "post-fire", further fault encoding is performed and the information stored in a random access memory (RAM). The lower front panel provides access and information display to identify which thyratrons have faulted, their fault mode and the number of the pulse within a single burst on which the fault occurred.

Despite careful grounding and shielding it was not possible to find a logic series with both adequate noise immunity and the more complex large-scale-integration (LSI) capabilities. Therefore, a high noise immunity (HINIL) bipolar logic series has been used as the protective interface logic in combination with a buffered complementary metal oxide semiconductor (CMOS) series which performs the higher level logic and memory storage functions.

The resulting noise immunity for the buffered CMOS logic is more than six times greater than that of the standard transistor-transistor logic (T^2L). The HINIL bipolar logic achieves a noise immunity of more than nine times better than the T^2L series by using the basic T^2L configuration modified with a zener diode to increase its input threshold level.

Test Results

Testing was performed at Raytheon's 500 kVA test facility in Bedford, Massachusetts. The load consisted of a copper-sulfate-enclosed termination at the end of a 250-foot output cable. Two separate load solutions were used to vary the impedance from 22.7 Ω for the 10 μs pulse to 45.4 Ω for the 20 μs pulse.

In the 10 μs case the mismatched output cable increased the effective leakage inductance by 6 percent, thereby increasing the risetime. The observed risetimes were 3.5 μs and 1.6 μs for the 10 μs and 20 μs modes, respectively, compared with calculated values of 3.1 μs and 1.6 μs. The risetime calculations, based on transformer and cable leakage inductance and measured PFN risetime, are summarized in Table 1.

TABLE 1. RISETIME CALCULATIONS

	10 μs	20 μs
LOAD IMPEDANCE R_L	22.7 Ω	45.4 Ω
CABLE IMPEDANCE	40 Ω	40 Ω
LEAKAGE INDUCTANCE ΔL		
PULSE TRANSFORMER	51 μH	51 μH
OUTPUT CABLE (250 FT)	8.7 μH	----
TRANSFORMER & CABLE RISETIME		
$T_{TC} = 2.2\ \Delta L/2R_L$	2.9 μs	1.2 μs
PFN RISETIME T_{PFN}	1.1 μs	1.1 μs
SYSTEM RISETIME $T = \sqrt{(T_{TC})^2 + (T_{PFN})^2}$	3.1 μs	1.6 μs

The addition of an RC despiker across the primary of the pulse transformer actually improved the risetime somewhat by providing a path around the load leakage inductance and allowing the thyratrons to turn on more rapidly. Current traces for the two conditions are shown in Figures 7 and 8.

The current pulse was measured by viewing the return current in the output cable shield with a Pearson Model 1040 current transformer. Voltage was observed at the primary of the pulse transformer by means of a Tektronix Model P6015 probe. Secondary voltage was derived from the measured transformer turns ratio of 7.5:1.

The load impedance was varied about the nominal values such that output voltages in the range of 140 kV to 180 kV were observed and secondary currents were observed over the range of 3 kA to 7.5 kA. Energy delivered to the load, as calculated from the current and voltage, was varied between 10 kJ and 12 kJ depending on load impedance and input voltage.

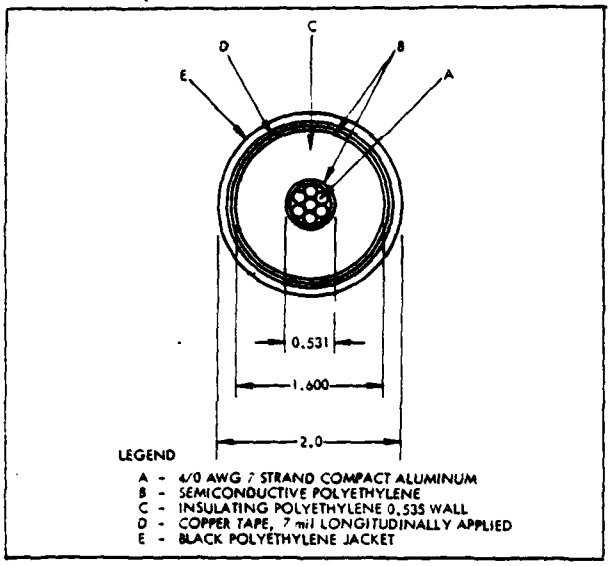


Figure 3 - Output Cable Cross-Section

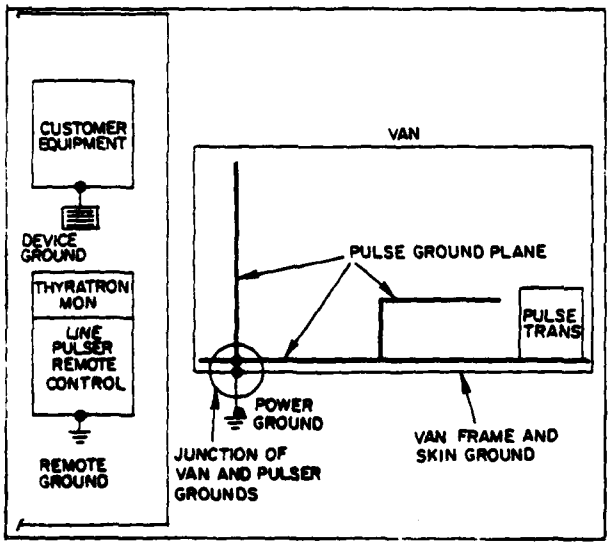


Figure 4 - Grounding Philosophy

Fault Monitoring Apparatus

Although faults which draw excess prime power current will trip the main circuit breaker, several potential malfunctions are monitored by means of circuitry which will initiate a controlled shutdown of the system in the event of

- Uneven PFN charge
- Free-wheeling diode short
- Load fault
- Thyratron misfire or prefire

Monitoring of the first three fault types is provided in a single chassis which is an integral part of the van control rack. The thyratron monitoring function is provided by a separate chassis which can be located remotely and which is applicable to a variety of systems containing multiple thyratron switches.

The PFN fault charge monitor compares the voltages on each of seven pairs of PFNs by means of resistive dividers on the thyratron gradient resistors. If the voltage on any pair does not rise at the same rate as the others, or if one pair goes to a higher than specified value, the charging cycle will be interrupted and subsequent charge and trigger signals will be inhibited.

Current through the free-wheeling diode at the series switch cathode is monitored by means of a current transformer. Observation of excessive diode current, indicative of a shorted diode, will cause the charging cycle to be stopped and will inhibit further charge and trigger signals.

A fault at the load will be detected by sensing excessive current through one of the end-of-line clippers due to an abnormal reflection. Since it may be desirable to continue pulsing through an occasional fault, an adjustable counter is provided to allow up to nine successive load faults before system shutdown.

Thyratron Monitor

The cathode current through each thyratron is monitored by means of a current transformer near the base of each tube. This signal is then analyzed to determine whether the thyratron has fired early, late, or not at all. In the event of a prefire or repeated misfires the system will receive a shutdown signal which can be used either to inhibit the charging and triggering signals or to open the main circuit breaker. A display panel will then identify the faulty thyratron and will store a limited amount of information concerning the number and type of faults encountered.

A block diagram of the thyratron monitor subsystem is shown in Figure 5. The sensitive logic circuitry of the monitor was protected from electromagnetic interference, ground voltage transients and electrostatic coupling between cables by the use of shielded-twisted-pair signal cable (RG108) and balanced-line isolation transformers.

The interconnection from the van to the monitor is also through shielded-twisted-pair cable in which the isolated signal and signal return from the balanced line isolation transformer are referenced to the monitor's signal ground, and the shield is referenced to the monitor's power ground. The shield is isolated from the van ground to avoid coupling of transients into the monitor. In addition, the 120 V ac input power to the monitor is transformer-isolated from the rest of the system.

The thyratron current signal received by the monitor is signal-conditioned and threshold-level detected to determine whether a thyratron fired. Data processing proceeds through the timing and control logic which develops the prefire zone, valid fire zone and misfire zone from the system start charge trigger, stop charge trigger and thyratron trigger. Valid fire zone resolution is 2 μs or less.

This zone timing information is then fed to the zone gating logic which compares the output of the firing detector with these zones in real-time. When a failure occurs, it is defined and isolated as to fault type and then stored and displayed on the upper front panel (See Figure 6). After each pulse the timing and control logic also commands the multiplexer logic to check each of the fourteen separate detector channels for failures. The shutdown signal is generated during this scan sequence once it is determined that a prefire has occurred, or that the same thyratron has misfired more than once, or that more than one thyratron misfired during the same pulse.

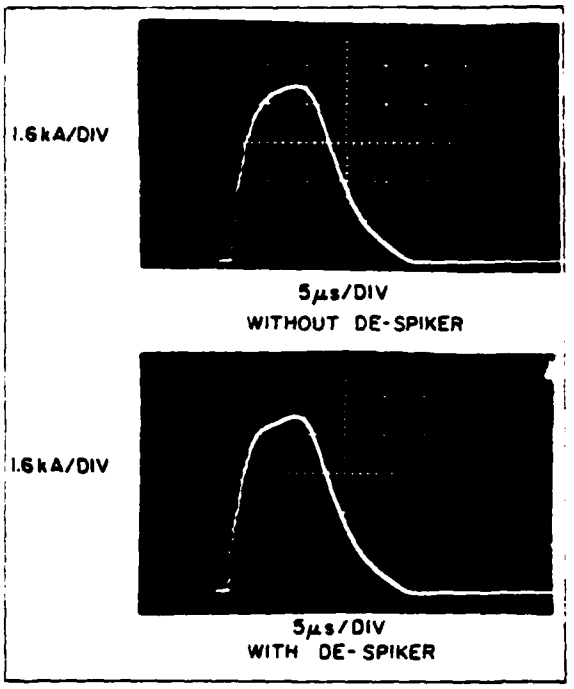


Figure 7 - Current Pulses - 10 μs Case

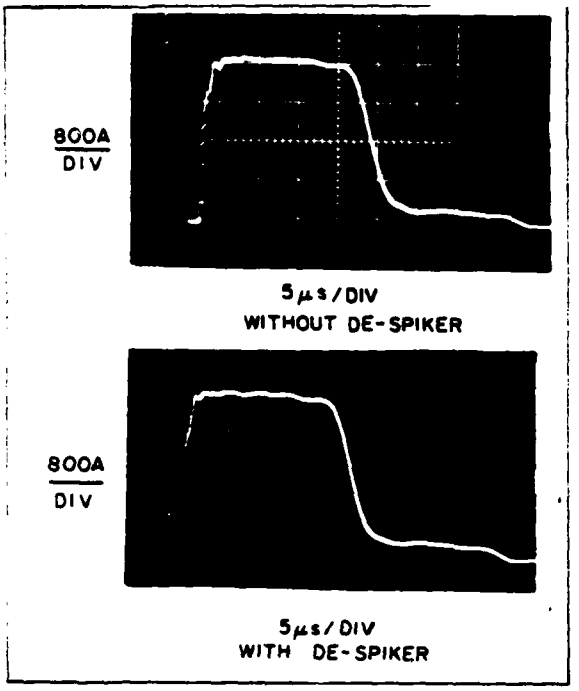


Figure 8 - Current Pulses - 20 μs Case

Acknowledgements

The authors are pleased to acknowledge the many contributions to the electrical design and test of this equipment which were performed by Mr. Gordon K. Simcox* while he was with the Raytheon Company.

We acknowledge also the prior development of the basic command-charged circuit by Mr. James F. O'Loughlin**. Thanks are also due to Mr. Robert M. Feinberg of AERL and Mr. John E. Creedon of ERADCOM for sharing with us their knowledge and experience with high power switches and modulators.

*Present Address: Physics International Company, San Leandro, California

**Present Address: Air Force Weapons Laboratory, Kirtland AFB, New Mexico

COMPACT MEGAWATT AVERAGE POWER PULSE GENERATOR*

By

J. E. Creedon, J. Mc Gowan, A. J. Burfa, and S. Schneider
Electronics Technology and Devices Laboratory
USA Electronics R&D Command
Fort Monmouth, New Jersey 07703

Summary

A compact, lightweight, burst mode pulse generator has been designed and evaluated at a megawatt of average power. The modulator, occupies a volume of 0.81 cubic meters (m^3) and weighs 225 kilograms (kg). The recently developed MAPS 40 thyratron[1] and two high energy density pulse forming networks[2] (PFN) are used as the switch and energy store. A solid state end of line clipper circuit is included and was found to be essential at high average power loadings. The modulator has been evaluated using a copper sulphate load at 40 kilovolts (kV) peak voltage, 40 kiloamperes (kA) peak current, 10 micro-second (μs) pulse width, 40 kA per μs rise time, and 50 amperes (A) of average current at a repetition rate of 125 hertz (Hz). Repeated burst on times of 5 seconds in a 35 second time period have been demonstrated.

Introduction

During the past few years, ERADCOM has been developing technology aimed at reducing the size and weight of line type modulators for high average power burst mode applications. In a typical burst mode system the on-time is relatively short, of the order of tens of seconds, while the off-time is from one to two hours. Since the on-time is short, the internal heat capacity of a component can be used as a heat sink and then normal conduction and convection cooling can be used during the off-period to remove the stored heat. Thus, an increased dissipation density in a low mass device can be sustained allowing the device momentarily to operate at higher energy and average power loadings than it would normally be rated for. This assumes that the device is otherwise designed for the voltage stress and can provide the peak, average and root mean square currents. While a detailed discussion of the pros and cons of various power conditioning approaches is not considered appropriate for this paper, it can be readily argued that the most feasible approach to high energy/high average power conditioning with moderate repetitive rate capabilities is that of a line type modulator circuit. Figure 1 shows the circuit. Although many factors influence this conclusion, the most important are system efficiency, high repetition rate capability and state-of-the-art component technology. Of these, the recent availability of high power thyratrons and high energy density pulse forming networks now gives a high probability of success with respect to achieving compact, lightweight megawatt (MW) pulse generators. The purpose of this paper is to demonstrate the availability of this new technology.

Megawatt Pulse Generator Design

The MW pulse generator is designed to be consistent with the performance characteristics of the MAPS-40 thyratron and the 4 kilojoule (kJ) PFN. Although the design was principally aimed at generating a 10 μs pulse the pulser is easily modified to produce a 20 μs pulse. Table 1 summarizes the basic electrical characteristics while Table 2 lists the overall mechanical characteristics and auxiliary requirements.

Table 1

Basic Characteristics of Compact Megawatt Pulse Generator

	Cond. A	Cond. P
Peak Voltage (kV)	40	40
Energy (kJ)	8	8
Peak Current (kA)	40	20
Peak Power (MW)	800	400
Average Current (A)	50	50
Average Power (MW)	1	1
Pulse Width (μs)	11	22
Rise Time (μs)	1	< 1
Pulse Repetition Rate (Hz)	125	125
Anode Delay Time (μs)	< 0.2	< 0.2
Anode Delay Time Drift (μs)	< 0.1	< 0.1

Table 2

Mechanical Characteristics and Auxiliary Requirements

Total Weight	225 kg
Volume	0.8 m^3
Grid Driver	2 kV, 50 ohm, 0.5 joules
Heater Power	1 kW at 15 volts ac
Reservoir Power	0.5 kW at 10-12 volts ac
Blower	50 watts

Figure 2 shows the layout of the PFN and switch. The switch, the MAPS-40 thyratron is located between the two PFNs. The thyratron cathode is electrically connected to the aluminum ground plate by four 2 x 15 centimeter (cm) posts spaced 90° apart. The thin cylindrical metal housing surrounding the base of the switch is a plenum wherein there is an ambient air flow around the base which is then directed onto the lower ceramic. Although this air flow is not essential for operation, it reduces the rate of oxidation at the heater and reservoir connections. In addition, on-time reliability is improved by keeping the ambient temperature of the ceramic envelope below 200°C.

A side view of the modulator, shown in Figure 3, shows the end of line clipper circuit. This circuit consists of a solid state diode[3] in series with a matched load. The series combination is connected in parallel with the end capacitors of the PFNs. The diode is made up of 40 each Westinghouse compensated diodes, type 1N4594. These diodes are rated for 1000 V peak inverse voltage at 150 A. The value of the resistor is 0.5 ohms, obtained by

* This work was partially supported by US Army Missile Research and Development Command, Air Force Aero Propulsion Laboratory, and Naval Surface Weapons Center, Dahlgren Laboratory.

U.S. GOVERNMENT WORK NOT PROTECTED BY U.S. COPYRIGHT.

parallelling two one ohm resistor stacks, and it matches the impedance of the parallelled networks. Four Carborundum washer resistors (0.25 ohms each), type No. 916WSR25L, are stacked in series and then parallelled with an identical configuration to give the 0.5 ohms.

Not visible in the photograph are the filament and reservoir transformers which are mounted between the PFNs. For convenience, 60 Hz heater power was used. We have used 400 Hz power on another system which uses the MAPS-40 and in that case the combined weight of the filament supplies was reduced by a factor of two. External variacs are presently used to adjust heater power although ultimately it is expected that they will not be required.

The grid drive for the MAPS-40 is obtained from a EG&G TM30 which dimensionally is 14 x 10 x 30 cm and weighs approximately 7 kg. It provides a 3 us wide 2 kV pulse from a 50 ohm source and its designed to operate up to 250 Hz. It also provides a negative bias of 125 volts to the control grid and a keep alive supply of 160 volts at 50 milliamperes (mA) to the auxiliary grid. The negative bias is not necessary for recovery at the 125 Hz rate, but the auxiliary keep alive discharge is necessary to assure achieving the anode delay time and anode delay time drift values listed in Table 1.

The sizes and weights of the various components making up the megawatt pulse generator are listed in Table 3. The dimensions include mounting structures when used.

Table 3

Size and Weight of Components

Component	Dimensions cm	Volume m^3	Weight kg
MAPS-40	23 Diam x 37	0.015	20
PFN (1)	53 x 16 x 88	0.075	57
PFN (2)	53 x 16 x 88	0.075	57
Clipper Diode	53 x 32 x 11	0.019	11.4
Clipper Load	27 x 29 x 13	0.010	9.1
Plenum	31 Diam x 15	0.011	3.9
Blower	9 Diam x 10	0.0006	1
Filament Transformer	17 x 15 x 20	0.005	15
Reservoir Transformer	12 x 24 x 14	0.004	6.5
Base	137 x 92 x 1	0.012	19
Totals		0.215	200*

* This weight does not include the lucite sides and top, wiring, and mounting hardware.

The aluminum base and lucite sides and top comprise the housing. It is planned to use external shielding which would be attached to the housing to reduce EMI. Overall dimensions of the pulse generator are 137 x 92 x 64 cm. Inside the housing, a conservative voltage stress of 4 kV/cm was used which permits operation in normal air environment. The resulting packing factor is 0.27 could be increased by 20-30 percent by employing more plane to plane surfaces in the high voltage areas or by the use of atmospheres such as sulphur hexafluoride. Both approaches would permit a higher voltage stress to be used thereby reducing the overall volume of the housing.

Performance Characteristics

Full power testing of the MW pulse generator was done using a 30 kV - 50 A dc power supply, operating with burst on times of up to 5 seconds. A 0.75 henry inductor was used to resonantly charge the networks to 40 kV while a liquid load[4] was used to terminate the pulser. The liquid load was a copper sulphate-sulphuric acid mixture contained in a low inductance assembly and it was adjusted to have an impedance of 0.45 ohms at room temperature.

Peak current/voltage waveforms under condition A are shown in Figure 4 (a) and (b), respectively which were taken during a one MW average power run. Figure 4 (a) shows peak current at 1 and 2 μs/cm. The peak current waveform was obtained using a Pearson current transformer. The vertical sensitivity is 20 kA/cm. The pulse width at the 70 percent value is 11 μs and the rise and fall times measured between the 10-90 percent values are 0.9 μs and 2.9 μs, respectively. The load voltage waveform shown in Figure 4 (b) was obtained using a resistance divider having a ratio of 10,600:1. PFN lifetimes in excess of 0.8×10^6 pulses have been demonstrated. One MW pulse generator has operated for over 300,000 pulses without a component failure.

Acknowledgements

The authors would like to acknowledge the contributions of V. Newman and C. Paduano with respect to the mechanical design and construction of the pulse generator.

References

1. J. Creedon, S. Schneider, "Megawatt Average Power Adiabatic Mode Thyratrons," Proceedings International Pulsed Power Conference, #76CH1147-8 REG 5, Nov 1976.

2. J. Creedon, ERADCOM, R. Fitch, Maxwell Labs, "A Half Megawatt Pulse Forming Network (PFN)," Proceedings International Pulsed Power Conference, #76CH1147-8 REG 5, Nov 1976.

3. S. Levy, J. E. Creedon, "Solid-State Clipper Diodes for High-Power Modulators," 13th Pulse Power Modulator Symposium, June 1978. Buffalo, N.Y.

4. W. Wright, Jr., "Low Inductance Low Impedance Megawatt Average Power Load," 13th Pulse Power Modulator Symposium, June 1978, Buffalo, N.Y.

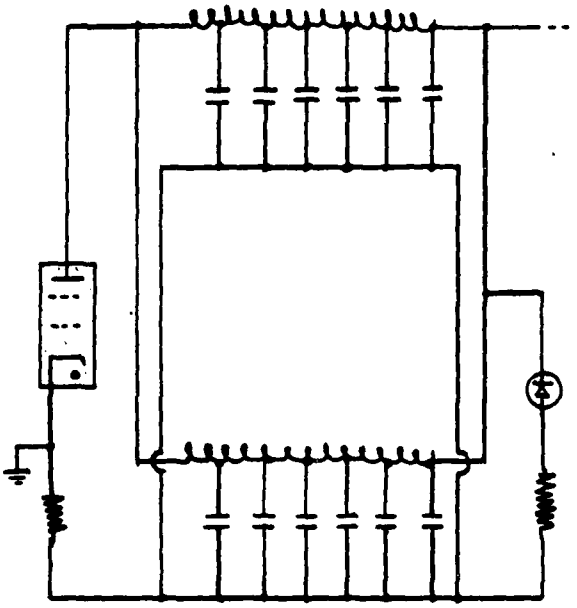


Fig. 1 Line type modulator, R_L = 0.5 ohms, R_C = 1.0 ohm, C_N = 5 μf, each individual capacitor equals 0.84 μf.

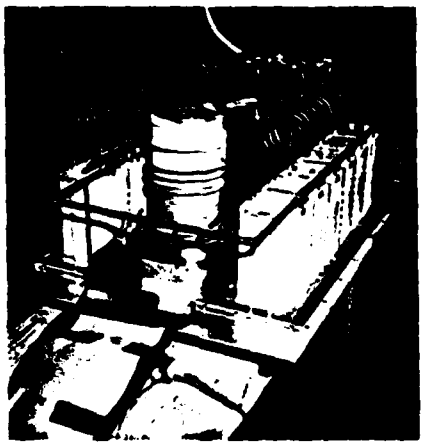


Fig. 2 View showing switch and PFN layout.

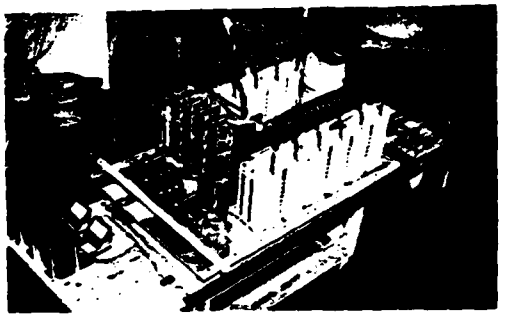


Fig. 3 View showing end of line clipper layout.

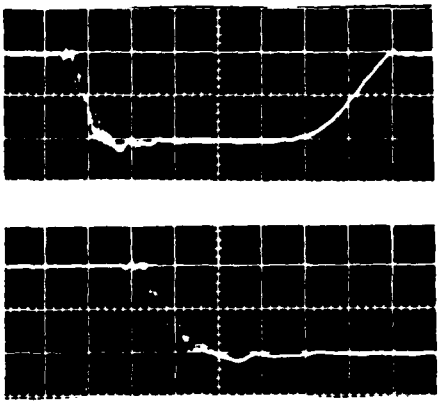


Fig. 4 (a) Peak current waveform at 5 and 1 μs/cm sweep speed.

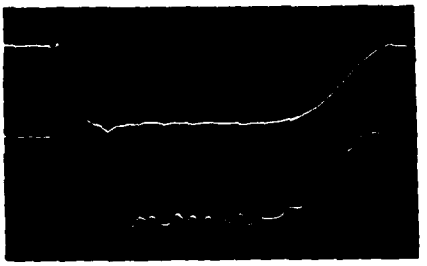


Fig. 4 (b) Peak current and load voltage at sweep speed of 5 μs/cm.

POWER SYSTEM FOR A HIGH POWER BURST MODE PULSED LOAD

T.H. Robinson

Marconi Research Laboratories, Chelmsford, U.K.

Summary

A novel power system, recently completed and commissioned, is described. Operating directly from an 11 kV, 50 Hz public supply, it provides the electrical energy for a burst mode, pulsed load. In each burst the minimum energy delivered by the power system is 100 kJ at a rate of 330 kW.

The pulse modulator operates at a peak charge of 105 kV and is capable of switching 200 MW over a range of pulse lengths and repetition rates. The high voltage, high current thyratrons used as the charge, discharge and PFN energy dump switches were specially developed, four-gap, double-ended CX 1190B thyratrons.

Supply voltage step-up transformers were designed to operate over bursts of variable pulse number, length and rate, with the rectified unfiltered transformer output directly feeding the modulator charging circuit at up to 65 kV. Polarising effects in the transformer core caused by the use of repetition rates equal to, or harmonically related to, the supply frequency were analysed and effectively eliminated. Special winding techniques were developed to provide the strength and insulation for withstanding fault transients.

While the power supply is capable of limiting fault currents occurring in the modulator and load, normal full system protection is provided by PFN energy dumping and, in the a.c. supply, by fast-acting vacuum contactors. Comprehensive control, monitoring and mode-selection are based on micrologic elements.

By using direct, high voltage modulation considerable flexibility is possible. The various alternative arrangements which derive from this design concept are explained. In addition, factors which determined the major features of the equipment are reviewed. The construction, layout and performance are illustrated.

Introduction

This versatile equipment is primarily designed to supply bursts of high power pulses to the load, without being restricted in its performance by any burst energy storage components.

By operating directly from a high capacity 11 kV, 3 phase public supply and pulse modulating at high voltage in series with the load, the power system can be used to provide the wide variety of modes, each requiring different pulse energies, pulse lengths, number of pulses and repetition rates.

The main output parameters are variable within the limits set by the following list of maxima:

Burst energy rating for 1 second, 400 kJ
(under favourable load conditions).
Burst energy rating for 0.3 second, 100 kJ
(under all load conditions, except malfunction).
Pulse energy, 6 kJ.
Pulse length (T), 90 μS.
Pulse power, 200 MW.
Pulse repetition frequency (PRF), 200 Hz.
Mean burst power into the load, 330 kW.
Load pulse voltage, 36 kV to 72 kV.
Load impedance, resistive part 7.5 Ω to 90 Ω.

Choice of System

The load required power from positive polarity pulses set to an accurately predetermined amplitude. The pulsing pattern could be chosen to have a content selected from:

- single pulse, followed by a rest interval;
- single pulses of approximately 1 Hz repetition frequency, and
- a burst of pulses, followed by a rest interval, containing a preset number and PRF, within the boundary conditions set by the modulator impedance and pulse length, or the likely performance of the experimental load.

The variation of the pulse top amplitude over the effective pulse length was required to be less than 10% and the amplitude variation between the largest and smallest pulses within the burst group, less than 10%.

Alternative methods of achieving this general specification were studied in considerable detail. A brief summary of the factors involved in the choice of system are discussed in two parts: the power supply, i.e. the circuit from the power source or the incoming 11 kV supply to the rectifier output, and the pulse modulator.

Power Supply

The essential feature in choosing the method of supplying power is the source of the burst energy. Motor-alternators and battery power supplies were considered, in addition to extracting the burst power directly from the a.c. public supply. While the former two options remove the risk of supply-transmitted interference, alternators capable of maintaining an amplitude change of less than 10% over the period of the burst require to be of low reactance for such good transient regulation, or use field boost, and in the absence of a PRF smoothing filter the alternator will be subject to the polarising effects described below. A battery installation needs regular maintenance and bus-bar switching to cover the wide load voltage range; in addition, a means of high ratio step-up from battery voltage is required, and stabilisation against as much as ± 20% input voltage variation.

The choice of a.c. supply was made because of the flexibility it offered over other approaches for the widely varying conditions of load operation. It is also more economic to charge the pulse forming networks (PFNs) directly from an unfiltered supply if the ripple output can be held to an acceptable level. Although this increases the harmonic distortion introduced onto the supply, and can cause transformer core polarisation when the PRF is near, or harmonically related to the supply frequency, these effects can be contained, and are preferable to solve than the problems that occur from burst power being drawn either via

CH1371-4/78/0000-0267$00.75 © 1978 IEEE

a PRF smoothing filter, or from an energy storage filter.

Problems of Direct Extraction: In a PFN modulator, the load current drawn by the power supply between each pulse will be the charging current into the PFNs. The effect of drawing a train of charging current pulses directly from the rectifier is compared for a resistive and modulator load in FIGURE 1 (a). The harmonic content clearly differs, being not only dependent on the number of rectifiers, but also on the charging current shape and PRF; the frequency components will be harmonically related to the PRF, and sub-harmonics of the supply frequency may be present under some operating conditions. While these produce harmonic distortion and necessitate, in addition to the need for obtaining low peak-to-peak ripple, the use of 12-pulse rectification, the more serious effect is polarisation of the transformer core produced by the modulator operating near to the supply frequency or its sub-harmonics. Under these conditions, the transformer can draw an excessive and asymmetric magnetising current.

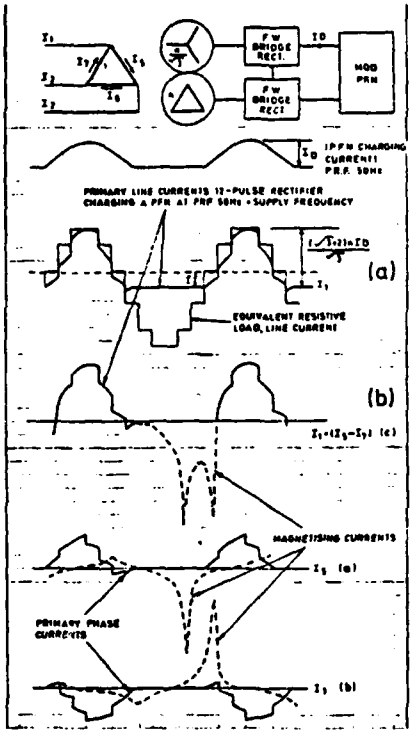


Figure 1. Primary currents - 12 pulse rectifier.

It can be seen from the waveform in FIGURE 1 (a) that the mean value of current is not zero: the synchronisation of the PRF with the supply frequency results in a d.c. component. A flux imbalance is caused by the voltage dropped across the source impedance by the load current. Flux equilibrium is reached only as the core flux climbs into the saturation region, so that the magnetising current drawn between load pulses is sufficient to produce an equal voltage drop. FIGURE 1 (b) shows the addition of the into-saturation magnetising current 'spike' resulting from polarisation on two phase currents and the resultant line current. (The phase displacement of the currents results in a double-peak magnetising component on the input line current). As the PRF departs from the supply frequency, the polarising current will occur as the difference frequency of the supply frequency (50 Hz) and the PRF. At sub-harmonics, the polarising current will be of constant amplitude but reduced in value by the ratio of the harmonic number. The peak amplitude of the magnetising current will depend on the B-H loop shape of the core material.

To solve the problem, a compromise is necessary between: using a heavily gapped core which will cause high magnetising current; having poor utilisation of a larger core; obtaining a tolerable value of leakage reactance. It is this last factor which is of particular concern as it will act as a limiting impedance under fault conditions. This use of the leakage reactance, and the compromises it causes, is discussed in more detail below.

Problems of Input Filter: Reduction of core polarisation is also possible by using an input filter. However, in order to be able to operate at low PRFs and achieve low variation of pulse amplitude over the burst, large value filter components are needed. In addition, the use of a large reservoir capacitor increases the likelihood of thyratron and load damage in the event of 'arc-through', and necessitates a 'crowbar' device with all its associated problems and limitations.

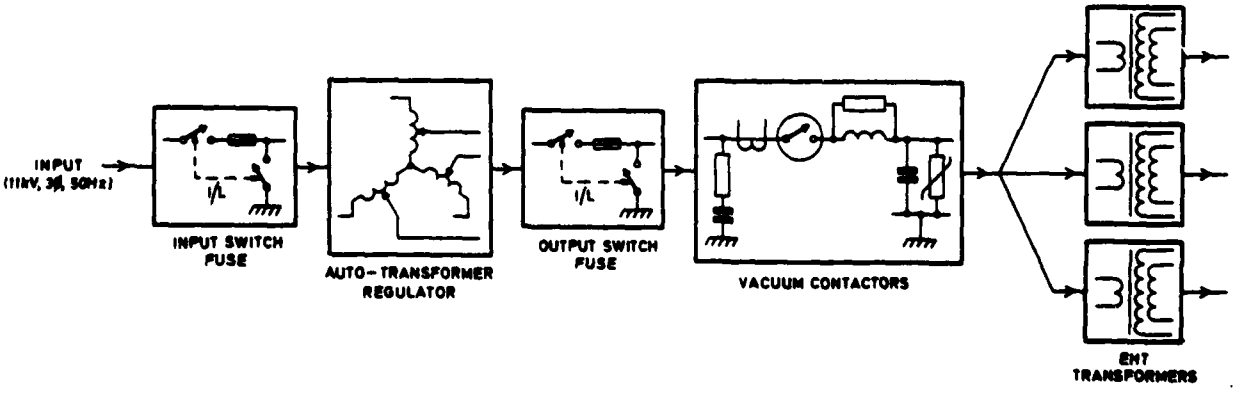


Figure 2. Power Supply

Pulse Modulator

Conventional modulators use step-up pulse transformers to achieve the desired high voltage output because of the difficulties of pulse switching at high voltage and of engineering high voltage circuits. The requirements for this power system are in principle within the range of conventional techniques, if the problems of using a number of circuits in parallel are solved. It was considered valuable, however, to obtain the versatility of direct modulator coupling to the load, particularly the advantage of being able to easily vary the pulse lengths over a wide range. With self-switching loads (for example, a gridded TWT), direct coupling gives independence from the use of a discharge switch which can limit the rating and performance of the pulse circuit. It also offers the prospect of ultimately achieving a more compact equipment.

Energy Storage: Two types of direct coupled modulator were considered: bulk capacitor energy storage and PFN energy storage.

Bulk capacitor storage in the direct coupled modulator requires either a self-commutating switch or a self-triggering load. The total energy stored in the capacitor must be many times the energy of a single pulse if the droop is to be low enough: the capacitance is therefore much larger than that of the equivalent PFN. Fault currents and energy levels are also much greater, even if the power supply is prevented from feeding the fault. Effective 'crowbar' protection is particularly difficult at high voltage and low impedance. The engineering advantages of lower peak charge, lower load hold-off voltage and the absence of PFN coils, do not offset the cost of storing and safely controlling the greatly increased energy.

The PFN energy store has the disadvantage that the load must withstand at least twice working voltage and, providing the power supply can be prevented from feeding faults in the modulator or load, the maximum load current under short circuit is a pulse of twice normal current. At the end of the PFN discharge pulse the load must be able to hold-off the mismatch voltage on the PFN or protection must be provided, which at very high power levels is difficult.

Reasons for Choice: PFN energy storage was preferred, firstly, because of the lack of a suitable self-commutating switch capable of high voltage operation; secondly, because the load was likely to be unreliable and could have a high arc rate, and thirdly, because thyratron switches were available offering reliable operation at 105 kV, 7.5 kA pulse and 5A average (burst).

Description of System

Power Supply

The power supply, shown in block diagram form in FIGURE 2, is capable of providing nominally 65 kV d.c. at 5A, to the pulse modulator.

The input power is controlled by a continuously variable tap-changing auto-transformer which enables the 11 kV supply to be smoothly varied over the full range.

Protection: Fuse switches are placed either side of the regulating auto-transformer as protection. The input fuse rating is selected to withstand the anticipated inrush of current when initially connected to the 11 kV supply. The output fuse switch is used as back-up protection and to isolate the equipment from the supply.

The primary fast acting protection is provided by vacuum contactors using a novel method of operation. In the event of a fault, they are normally operated after the modulator charging thyratron has been blocked. Provision is made to minimise the possibility of the contactors re-striking by fitting damping circuits which limit the rate of rise of voltage across the contacts. In addition, the operation is delayed until the current in either direction has just exceeded a threshold which is in excess of the minimum arc sustaining current. In this way, the contactors are always actuated at the start of a current half-cycle, and the maximum electrode separation will then have been achieved before the end of the half-cycle, when extinction at the minimum arc sustaining current would be likely to generate a voltage transient; so the possibility of re-striking is reduced. Under this arrangement, the three contactors are not operated simultaneously; the delay interval being selected sequentially for each phase.

EHT Transformers

Three single phase EHT transformers are connected in a three phase configuration. The primary windings are delta connected and fed from the vacuum contactors. The secondary windings are connected to provide 30° phase displacement, which is achieved by using two secondaries, one delta connected and one star. Each secondary output feeds a full wave bridge rectifier. The two bridges are connected in series to form a 12-pulse rectifier.

As the operating PRF could equal, or be harmonically related to the supply frequency, a gapped transformer core is used to overcome the polarising effect and the resultant excessive magnetising current 'spikes' drawn from the supply. By using C cores, the gaps can be adjusted to suit the circuit conditions and three transformers made to a manageable size and weight.

The leakage reactance is used to limit the fault current for 30 mS to 50A, ten times the mean d.c. current, in the event of an 'arc-through' of the charging thyratron. The leakage reactance also limits the transformer short circuit current, with a consequent reduction in the mechanical forces acting on the windings. However, the reactance must not adversely affect the transformer regulation.

Depending on where the rectifier commutation occurs during the charging cycle, the commutation overlap angle will vary. As the PRF is not locked to the supply frequency, commutation regulation can cause pulse-to-pulse jitter if the transformer reactance is excessive. The use of a gapped core also increases this problem since the available flux is halved. The number of turns cannot simply be doubled without increasing the leakage reactance too far, so the core volume must be increased. To provide sufficient limiting of the short circuit current, without having excessive leakage reactance, involves using the technique of magnetically coupled star and delta secondaries.

The final configuration therefore, consists of a triple winding on each core limb. The primary and two secondaries are split into two equal parts and distributed in series on both core limbs. By transposing the positions of the delta and star secondaries relative to the primaries on each core limb, equal leakage reactance is preserved for both secondaries. In addition, coupling the secondaries increases the short-circuit

reactance without increasing the regulation.

Short Circuit Effects: Under short-circuit, mechanical forces will act radially between primary and secondary, which will tend to drive the windings apart - the primary subjected to compression, causing the winding to collapse between the oil ducts unless the wire is supported, and the secondary subjected to hoop stress. The estimated total radial force between primary and secondaries under short circuit is estimated as 10 tonnes. Axial forces will also occur between windings unless they are situated on the same magnetic centre - wire size tolerances make symmetry almost impossible. The construction must therefore resist end thrust and prevent conductors from riding over each other. A displacement of 1 cm over a length of 65 cm produces an axial force on the winding of 0.5 tonne.

Transient Voltages: The transformer leakage inductance also represents a substantial proportion of the modulator charging inductance; a proportion of the charging voltage is therefore distributed across the windings.

When the modulator discharges, a high rate of change of voltage appears in the transformer. It is also anticipated that transient voltages might be induced in the transformer windings if the vacuum contactors re-struck during fault operation. For these reasons it is necessary to design the transformer to withstand high transient voltages; layer windings are used rather than disc windings and each winding is fitted with an electrostatic shield - FIGURE 3 shows a complete transformer primary with electrostatic shield slotted to reduce circulating eddy current losses. Layer spacing in relation to the shields is arranged so as to avoid circulating currents and to provide uniform transient voltage distribution throughout the winding. To be successful, each layer needs separate termination and the end returned through the inter-layer insulation to the start of the next layer. The layers are connected in series by external stress relieved links.

A view down onto the primary and two secondary windings, in FIGURE 4, shows the electrostatic shield and corona rings and the solid barrier insulation between each winding.

Pulse Modulator

Load Conditions: The modulator circuit is designed to operate over a very wide range of load impedances, maintain operation through some load fault conditions and provide rapid and safe protection for the load and the power system.

The amplitude, pulse length and number of pulses in each burst can be adjusted to fit the expected load impedance. However, the load impedance is only predictable to within a factor of 2:1, either of higher or lower value than the projected impedance, and the impedance tends to vary over the duration of each pulse and also over the duration of the burst. The load is also liable to 'arc-through' or 'current-extinction', presenting the modulator with an instantaneous short or open-circuit condition. This erratic behaviour can occur either during a pulse or for the complete pulse length. Indeed, both short and open circuit conditions can occur within the duration of a single pulse. The modulator is required to operate throughout the selected burst duration while these load faults occur or, from monitoring and comparing the levels with pre-determined boundary conditions, stop at any time in order to reduce the possibility of damage to the load. The modulator is capable of dissipating the full burst energy, if necessary, and can absorb the effects of faults without over-volting the load. Throughout these conditions, succeeding pulses are maintained at the amplitude selected for normal load operation, so that faults occurring on one pulse do not necessarily cause the loss of the remaining pulses in the burst.

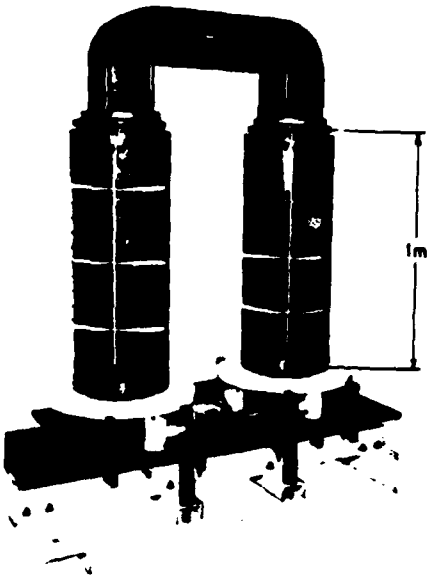


Figure 3. Transformer primary with Electrostatic Shield

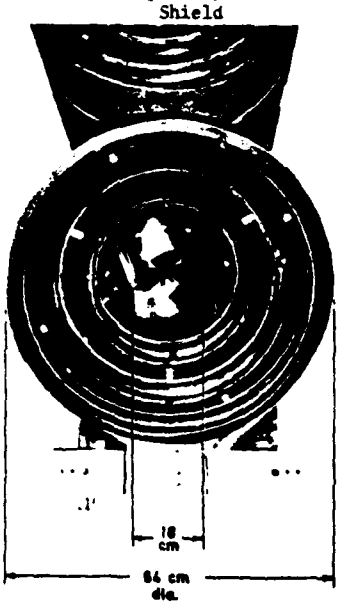


Figure 4. End view of transformer windings.

PFN Arrangement: The pulse energy-storage is divided into PFN modules which can be selected or grouped for each pulse energy and pulse length required. By careful choice, it is possible to match the load approximately for each major regime by using three 7 section networks of $Z_o = 42\Omega$ and $T = 30\ \mu S$. These can be easily coupled in series-parallel arrangements and

provide the coarse setting of pulse length. Further adjustment, to finer limits, can be made by operating the 'dump' thyratron, which produces controlled pulse shortening.

Cross-connection of the PFNs has been designed to minimise disturbance of the pulse shape by using a low amount of mutual coupling between sections of the PFN (7%), rather than the more normal 15%, and arranging for the end sections to be half-value coils. The join is not made at a PFN capacitor but at the inductance or half-section, using a compensating increase in the self-inductance of the coils, but still with some mutual coupling to the preceding sections. FIGURE 5 shows the pulse waveform of two series connected PFNs, without 'tail-biter' pulse shortening.

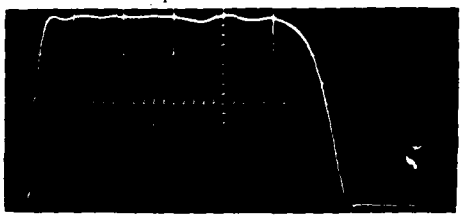


Figure 5. 60 μS pulse by joining two 30 μS PFNs.

Choice of Pulse Switches: In order to achieve reliable operation into the highly under or over matched load, particular emphasis was placed upon the selection and testing of the thyratron switches. Thyratron testing and the derivation of the operational limits are discussed in more detail in a companion paper.

While large single-ended multi-gap thyratrons are available for this type of operation, de-rating would have been essential since the tubes are likely to quench on the longer pulse lengths. Another disadvantage is the longer de-ionisation time of the tube centre-gaps, leading to slower recovery; only the lowest gap recovers quickly, with grid bias assistance, so the reverse, or re-applied forward voltage amplitude is limited to a single gap hold-off for about 250 μS after conduction.

Long pulse performance can be greatly improved by using the double-ended tube construction, where the anode is replaced by a second cathode/grid structure, plus a second reservoir - this adds to the free gas available at the anode end which improves the long pulse rating, reducing the prospect of quenching. The double-ended thyratron offers equally good operation for conduction in both directions. Forward and reverse recovery times are not improved, but the tube will safely conduct in the reverse direction without the risk of a damaging arc. The circuit operation of double-ended thyratrons is described in an earlier paper.[3]

Switch Positions: The main thyratron discharge switch is coupled directly in series with the load but, because the load cathode is grounded, the thyratron has to be incorporated into a high voltage 'floating deck' arrangement. The same thyratron type is used as the PFN charge control switch and the 'dump' switch (this includes the functions of inverse switch, 'crowbar' and 'tail-biter').

Three identical and interchangeable tanks contain each complete thyratron assembly and its auxilaries. FIGURE 6 shows one tank in the main discharge position, together with the power system load.

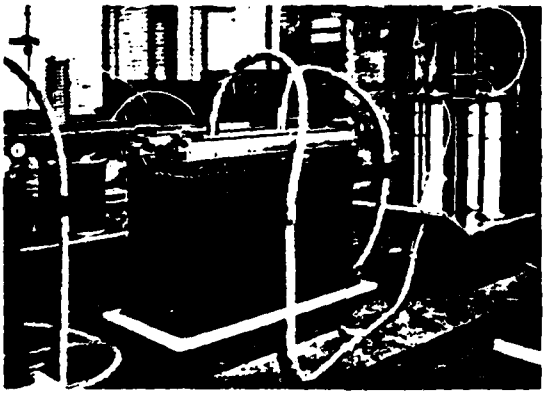


Figure 6. Thyratron tank in main discharge position.

Modulator Layout: The modulator layout is shown in the circuit, FIGURE 7. At the input, the power supply rectifiers are protected from voltage transients by non-linear resistor clipping and damping circuits. High frequency damping is a CR filter which matches the characteristic impedance of the EHT cable; this attenuates switching transients, produced by the charge control thyratron, passing into the power supply. Lower frequency damping is achieved in a filter, effectively the transformer leakage inductance and the total stray capacitance (mainly the EHT cable).

Charging Circuit: The charge control thyratron is part of a circuit with a large stray capacitance and there is therefore an extended turn-off time, by positioning the thyratron with its own stray capacitance at a point with significant additional strays, these effects do not influence the pulse shape, which could occur if the thyratron was positioned after the diode stack. If positioned after the charging choke, it would increase the energy in the choke strays, which form an oscillatory circuit. The position chosen also has the further advantage of minimising the voltage of the thyratron assembly relative to ground.

Three series-parallel, tapped, charging inductors are included after the charge thyratron tank. They are air-cored; because of this they remain effective under short circuited modulator or load conditions. The value of charging inductor is selected to match the PFN, depending on the particular operating regime, to fill the available charging time, reduce the peak current and the harmonic distortion introduced back into the supply. A typical burst of charging current cycles is shown in FIGURE 8.

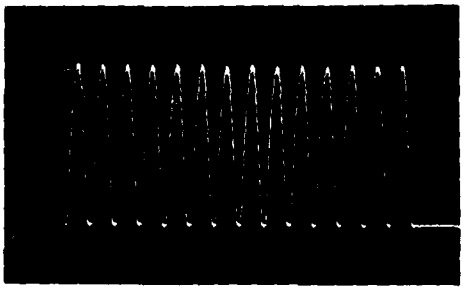


Figure 8. Burst of charging current cycles at 65 kV dc, PRF 100 Hz.

Inverse Protection: The inverse load is connected at the rear end of the PFNs to prevent the PFN voltage overturning. To give a more accurate match for all the PFN arrangements, the load can be adjusted in small steps. This arrangement for close matching ensures rapid discharge of the PFN energy under fault conditions. A semiconductor diode stack is included to provide permanent inverse protection. The modulator is then able to operate without the 'dump' thyratron tank connected under more normal load conditions (the interchangeability of the thyratron tanks enables the 'dump' thyratron tank, for example, to be used as a spare in either of the other two positions).

'Dump' Switch: The 'dump' thyratron is connected directly across the inverse diode. It may be triggered at any time to discharge the PFN energy:

- if the load pulse is overmatched, to remove the mismatch energy and establish normal conditions prior to the next charge cycle so that the amplitudes of the subsequent pulses are correct;
- 'crowbar' the PFN during the pulse in order to remove the energy under fault conditions;
- adjust the duration of the pulse to any desired length less than the nominal PFN pulse length, and
- improve the shape of the output pulse rear edge, by triggering the thyratron at a time for it to be effective as a 'tail-biter' (typical improvement is a 7 μS tail reduced to 3 μS).

Modulator Dummy Load: This is provided for test purposes, but it incorporates a CR filter so that the front edge of the output pulse can be modified to suit the particular load transient response. The circuit can also be connected to damp the rate-of-rise of voltage under fault conditions when the load open-circuits; this gives time for the fault sensing circuits to respond and 'crowbar' the PFN, so reducing the peak fault voltage appearing across the load.

Control and Interlocks: A safe working environment for the equipment and for the operators is provided by the careful layout; planning of the grounding routes and connections; screening, and filtering cable inlets and outlets.

The low-level control circuits were commissioned and used with a minimum of trouble; particularly so considering their close proximity to the high power circuits and the difficulties of monitoring burst operation when faults are present in the system.

A compressed air-controlled network, of grounding arms to discharge high voltage components and interlocks for the doors and enclosures, functioned as a 'fail-safe' method of isolating dangerous areas.

The complex electronic control and protection circuits are based on the wide use of micrologic devices. In addition to a slow acting control loop, a fast acting series of interlocks checkout the

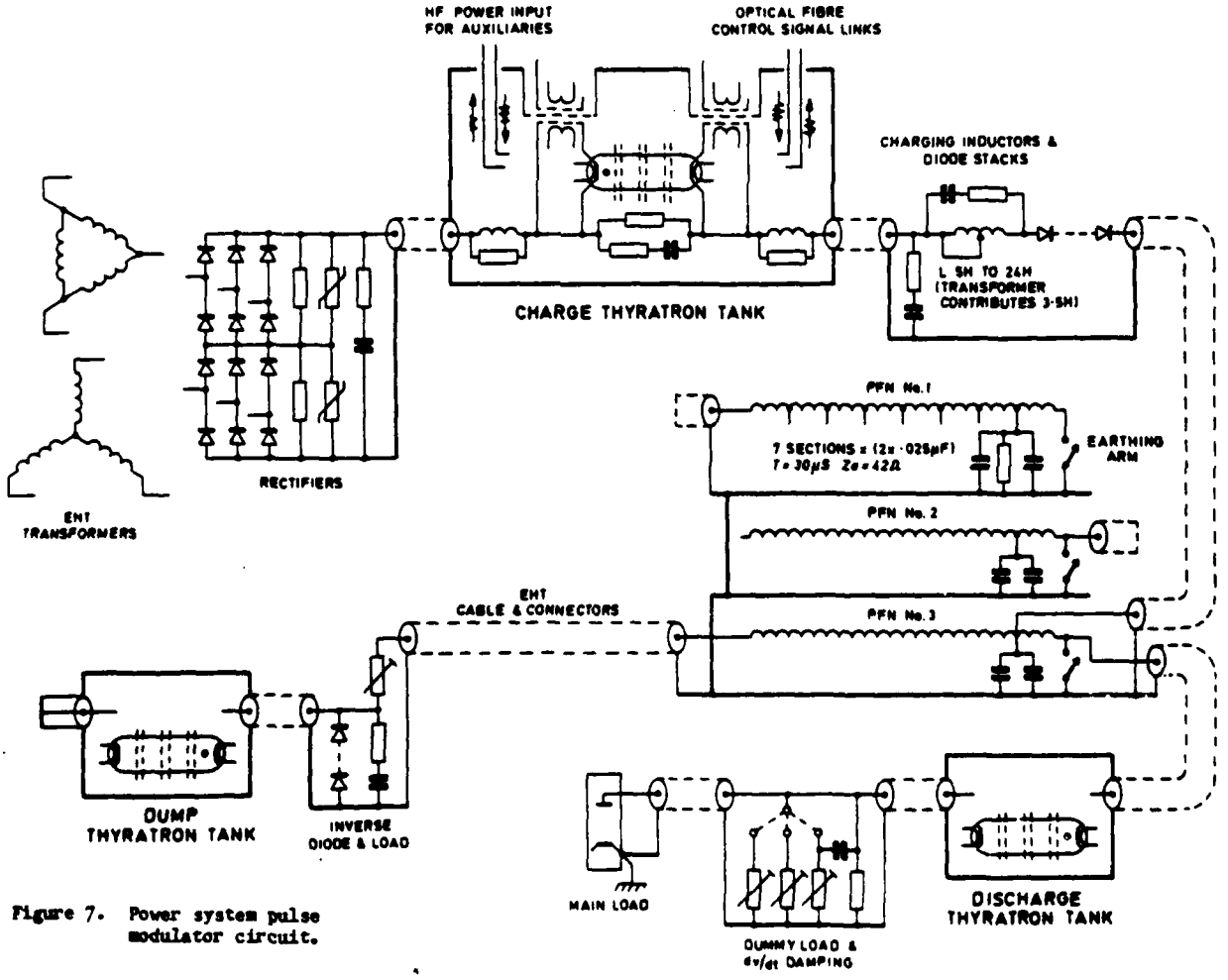


Figure 7. Power system pulse modulator circuit.

system and operate, or inhibit, trigger pulses to the thyratron switches in the modulator and the vacuum contactors in the power supply, depending on the selected mode or fault conditions.

Conclusions

The power system has operated successfully for nearly a year without any major problems occurring.

It demonstrates some significant steps forward in particular high power pulse techniques:

- direct modulation at high voltage and power, without the constraints of pulse voltage transformation. (therefore the possibility of later use with a self-switching load) or bulk capacitor storage, with the associated problem of reliably diverting large currents from a frequently faulting load;
- operation into a greatly under or over matched load impedance;
- effective protection of the load under both short and open circuit conditions;
- obtaining the burst energy directly from the public supply without energy storage;
- charging the modulator directly, at the final high voltage, from the power transformer and limiting the fault current level by incorporating large leakage inductance, and
- the utilisation of the particular advantages of power rating and fault control made possible by the double-ended, multi-gap thyratrons which are installed in all the switch positions in the pulse modulator.

A general view of most of the equipment used for the power system is shown in FIGURE 9.

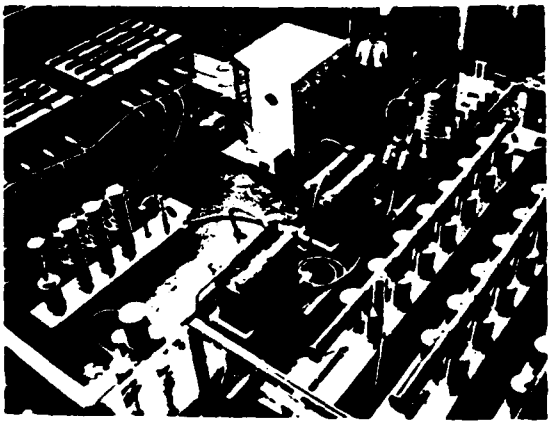


Figure 9. Part of the power system for a high power burst mode, pulsed load.

AVERAGE BURST POWER ≥ 330kW

NUMBER OF PFNs	1	2	3	2	3
ARRANGEMENT	–	PARALLEL	PARALLEL	SERIES	SERIES
Z_0	42	21	14	42	42Ω
τ	30	30	30	60	90μS
PULSE ENERGY STORED	2	4	6	4	6kJ
LOAD IMPEDANCE (MIN) (REAL PART)	22·5	11·25	7·5	22·5	22·5Ω
LOAD IMPEDANCE (MAX)	90	45	30	90	90Ω
PULSE ENERGY DELIVERED	1·7	3·4	5·1	3·4	5·1kJ
PULSE POWER (MIN)	57	114	170	57	57MW
PULSE POWER (MAX)	67	133	200	67	67MW
PRF	200	100	67	100	67Hz
CHARGE VOLTAGE PFN (MAX)			105kV		
DISCHARGE PULSE CURRENT (MAX)	1600	2400	4000	1000	1000A
PEAK FAULT CURRENT	2500	5000	7500	2500	2500A
LOAD PULSE VOLTAGE			36kV – 72kV		
AVERAGE DISCHARGE CURRENT (MAX)			9·6A		
AVERAGE POWER SUPPLY CURRENT			7·35A		
BURST LENGTH (MIN) – ALL LOAD CONDITIONS			0·3 SECS. (100kJ)		
BURST LENGTH (MAX) – MATCHED LOAD			1·0 SECS. (600kJ)		

TABLE OF THE PULSE MODULATOR BASIC ARRANGEMENTS

Acknowledgements

This work has been carried out with the support of the Procurement Executive, Ministry of Defence, U.K. The author wishes to thank the Technical Director, GEC-Marconi Electronics Ltd., for permission to publish this paper.

Acknowledgement is made of the helpful and continuous co-operation of the sponsors, but particularly during the final equipment commissioning period.

The author wishes to acknowledge the work of Mr. P.G. Kenyon, Mr. A.W. Cameron, Mr. R.B. Molyneux-Berry, and the whole team involved with the project, from the High Power Systems Group, Marconi Research Laboratories.

References

1. N.S. Nicholls, Patent No. 1473837, "Improvements relative to Electrical Switchgear".

2. R.B. Molyneux-Berry, "Double-ended Thyratron in High Power Burst Mode Pulse Modulator Applications", Proceedings of the IEEE 13th Pulse Power Modulator Symposium, 1978.

3. R.B. Molyneux-Berry, "Symmetrical Double-ended Thyratrons in Pulse Modulators", Proceedings of the IEEE 12th Modulator Symposium, 1976.

PULSE POWER REQUIREMENTS FOR LASER ISOTOPE SEPARATION

by

Phillip N. Mace, Walter L. Willis
Los Alamos Scientific Laboratory, University of California
Los Alamos, New Mexico 87545

Abstract

Laser systems being developed for laser isotope separation applications have pulse power requirements which will demand the ultimate capability of pulse power technology. Although the energy per pulse is small by many pulse power standards, the requirement for currents in excess of 100 kA, voltage of about 100 kV, and pulse repetition rates of 1 kHz constitute a set of requirements not previously imposed on pulse power systems. In this paper measurements made at low repetition rates on excimer laser discharges are presented, and the implications for pulse power components are discussed. Currently available switches and energy storage systems are discussed, and requirements for future development are given.

Introduction

The Los Alamos Scientific Laboratory is developing a molecular laser isotope separation which promises to have a significant impact on uranium enrichment technology in the years ahead. Key components include pulsed infrared and ultraviolet lasers, which must operate reliably for long periods of time. These laser systems have pulsed power requirements which involve significant advances in the state-of-the-art for successful operation of the lasers. This paper discusses these requirements and steps which are being taken to develop systems capable of meeting all specifications. Although the infrared laser requirements are by no means trivial, only the excimer laser system requirements are discussed here, since they are far more severe and will require much more effort to generate satisfactory solutions.

Table I summarizes the characteristics of the pulse power system for a typical excimer laser required by late FY 1980.

TABLE I

PULSE POWER SYSTEM REQUIREMENTS, 1980 EXCIMER LASER

Energy Storage System	Switch System
Operating voltage: 50-100 kV	Operating voltage: 50-100 kV
Pulse repetition rate: 1 kHz	Pulse repetition rate: 1 kHz
Total energy stored per pulse: 100-200 J	Peak current: 50-150 kA
Per cent reversal: < 20%	dI/dt: 5×10^{13} A/s
	Pulse width: 10-30 ns
	Jitter: < 10 ns
Effective impedance: 0.25 - 2 ohms	MTBF: 10^7 shots
MTBF: 10^7 shots	

Energy Storage

Neglecting repetition rate and reliability, the most important characteristics of energy storage systems for excimer lasers are operating voltage and impedance. The gas discharge created in an excimer laser cavity presents an unstable, collapsing impedance to the power supply, with effective resistance falling to ∿ 50 mohm within 20-30 ns. In order to effectively deposit energy in this gas a very low impedance power supply is required. The operating voltage must be high enough to effectively couple energy into the excimer gas mix, which requires voltages of 50-100 kV for typical systems. The discharge current typically peaks at the time the voltage passes through zero (the balance of the energy is stored in the laser cavity inductance); therefore the power supply must be able to drive as much current as possible through the cavity before the zero voltage point is reached, which just states again that a low impedance source is essential. In 1 Hz lasers built at Los Alamos, we have used low impedance coaxial cable as the energy storage system. By connecting cables in parallel, the source impedance can be reduced until the density of cables is so great that low inductance connections to the laser cavity are no longer possible. Table II gives characteristics of two cables used at LASL.

TABLE II

SPECIFICATIONS OF CABLES USED AT LASL

Essex Type 40/100

Z_o = 30.4 Ω

C/m = 204 pF

L/m = 188 nH

τ_{CH} = 6.2 ns/m

Average insulation thickness = 3.6 mm

Diameter of center conductor = 7.7 mm

Overall diameter = 19.3 mm

17/14 HV Graded

Z_o = 23 Ω

C/m = 247.6 pF

L/m = 131 nH

τ_{CH} = 5.7 m/m

Average insulation thickness = 3.6 mm

Diameter of center conductor = 11 mm

Overall diameter = 27 mm

We have not had any failures of the cables used to feed the laser cavity, but have observed failures in cables used for power supply output, apparently from reflected high voltage pulses. GTE Sylvania has used 40/100 cables in a 1 kHz laser with no serious problems, but in their case the voltage was limited to less than 30 kV. Operation at high pulse rates does produce one phenomena which must be dealt with: the carbon particles which are imbedded in the PVC jacket used to grade the cable are not securely bound, and when operated at high repetition rates they are shaken loose by the electrostatic forces and sift down the main polyethylene insulation. This leads to corona and cable failure, so it is necessary to contain the carbon by installing shrink tubing over the PVC layer near the cable end. Coaxial cables have some serious problems when considering their use for large kHz laser systems; the energy storage density is low, the impedance per cable is fairly high, and as a result a large number of cables is needed per system. Any time the component count in a system goes up, the reliability goes down. An alternate system is therefore needed which does not have this drawback. The most obvious is some form of liquid capacitor, and we are investigating use of water or other liquid dielectric units. Advantages possessed by water include the self-healing nature of the dielectric, high specific energy storage, and ease of designing low impedance systems. There are, however,

CH1371-4/78/0000-0274$00.75 © 1978 IEEE

questions which must be addressed on purity, chemistry, and cooling in designing a successful system. If water is used, fairly stringent requirements are placed on the charging power supply, to provide charging times on the order of 1 μs. If operation at high pressure can be obtained, this charge time can be increased somewhat.

Low impedance, solid dielectric pulse forming lines are still a possibility, but the well-known problems of reliability of solid dielectric capacitors makes this approach less attractive for long life systems.

Switches

One major problem which any switch design must address is the loss during closure time. Due to the very short pulse durations in excimer lasers, the loss mechanisms of a closing switch not only produce significant heating effects, but may also impact the total power transfer efficiency and thus the overall process economics. To obtain optimum performance from electrical discharge pumped excimer lasers, it is necessary to apply the exciting electric field to the cavity in as short a time as possible. The switch may be used either as a series switch or as a closing switch to initiate an L-C ring up. The specifications for a suitable switch, which have been given in Table I, have all been met, but unfortunately not in the same device. Table III lists the types of switches we have investigated for this application, with their main advantages and disadvantages.

TABLE III

SWITCHES

TYPE	ADVANTAGES	DISADVANTAGES	POTENTIAL FOR FAST SYSTEMS
Spark Gaps	High Voltage, High Current High dI/dt	Potential Reliability, Life Problems, Triggering, Cooling	Good
Thyratrons	Reliability, Life	(Heater Power), Limited Voltage, Current, dI/dt	Good
LASS	Reliability, dI/dt	Triggering System, Packaging for High Voltage, Current	Fair
RSR's, SCR's	Reliability, Peak Current	Low dI/dt, Packaging, Voltage	Poor
Power Transistors	Life	Low Current, Voltage dI/dt	Poor
Vacuum Gaps	High Peak Current, dI/dt	Life, Jitter	Poor
Hard Tubes	Reliability	Low Peak Current, dI/dt, Packaging	Poor
Ignitron	High Peak Current, Voltage	Slow Turn On, Unknown Reliability	Poor
Ignitrons	High Peak Current Reliability	Slow Turn On, Limited Voltage	Poor
Microwave Coupled Spark Gap	High dI/dt, Peak Current Voltage, Inherent Transformer Action	Much Development Required	Unknown
Saturable Inductor	High Repetition Rate, Basically Nondestructive, Long Life	Much Development Required	Unknown

We will discuss first the types of switches deemed unsuitable (at least at present) for further development for our application. LASS (Light Activated Silicon Switches) have been discussed in another paper at this conference; the reliability of a solid state device is always an attractive feature, and the demonstrated capability of working at high dI/dt is important. However, the present devices require kHz lasers of dubious reliability to provide the triggering light pulse, so the total system reliability is poor. Also a considerable effort would be required to engineer these devices into packages which could work at the total voltages and currents required. We are not able to actively support developments in this area, but will continue to follow progress.

RSR's and SCR's have also been discussed in other papers; in addition to the packaging problems just mentioned for LASS devices, they are inherently too slow for our application and cannot handle the dI/dt required. Power transistors fall into this same category.

Vacuum gaps have received careful attention as potential switches for excimer lasers; however, they have inherently high jitter, and life is limited because of the high electrode erosion rates. This erosion results from the fact that the current carrying medium is a metal plasma generated from the electrodes.

Hard tubes have been suggested many times as potential switches for excimer lasers; hard tubes are used as switches in the Stanford Linear Accelerator with excellent reliability. However, the peak current and dI/dt capability of the best hard tubes are orders of magnitude less than the requirements given in Table I, and power transfer efficiency is low.

The Gamitron, or crossed field closing switch, has also been discussed in an earlier paper. It came to our attention because of its rugged construction and high current handling ability. In common with several devices already discussed, it has the problem of slow closure time.

Ignitrons have been used for over forty years to switch high currents; unfortunately, their operating voltage is limited, and too much time is required to fully establish tube conduction.

The last two devices listed in Table II, Microwave Coupled Spark Gaps and Saturable Inductor Switches, may have unique characteristics which will make them extremely interesting for future use in fast pulsed power supplies. However, at this time, there is not enough data available to make an intelligent engineering decision as to their ultimate utility, and funding limitations preclude development programs at this time.

The two switch types which are receiving both in-house effort and contractual support are spark gaps and thyratrons. These two have been chosen since the spark gap offers a near-term solution in a device which can meet all of the system requirements (after appropriate development) with the probable exception of life, and thyratrons have promise of longer life, but must be improved to meet the specifications of voltage, peak current, and dI/dt. (The possibility of using several devices in parallel has not been overlooked, and specifications can be modified accordingly).

Two spark gap switches have been investigated in this program, and work will continue to develop a prototype system switch. One approach, proposed and developed by the Garrett Corporation, is to use many pairs of electrodes in parallel, with a saturable inductance in series with each gap to provide an initial impedance during the resistive phase of the plasma formation which is absent at later times of the current pulse. The waveforms predicted for this gap are shown in Fig. 1.

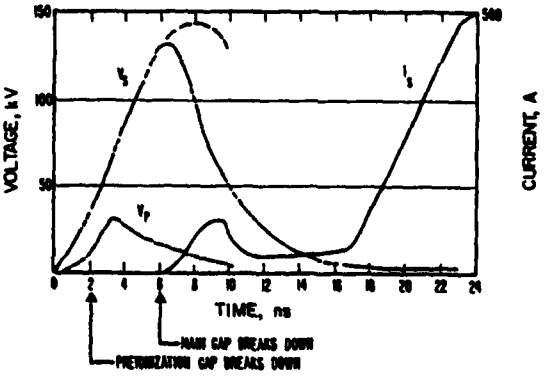


Figure 1.

The voltage which initially appears across the gap supports formation of the gap current, but collapses as the gap moves out of the resistive phase. The impedance of the saturable inductor then collapses, and the load current begins to flow. Spark gap losses are thus minimized, and the small amount of charge transfer during the resistive phase can serve to provide initial charge for stray or peaking capacitors associated with the laser cavity. Calculations show that this should be small enough to have negligible impact on the laser dV/dt. By using many gaps in parallel the total switch inductance can be reduced, and life extended to about 10^8 shots.

Some geometries preferred for excimer laser systems are not amenable to use of a single large switch system such as the one just described, and require use of a more compact switch. The Veradyne Corporation has developed a toroidal spark gap described in another paper at this conference for use in an accelerator program at the Lawrence Livermore Laboratory. We are now working with Veradyne to produce a scaled-down version of this switch which will operate at 100 kV (vs 250 kV in the original version), have inductance of < 15 nH, and life of about 10^8 shots. New electrode materials, a simplified air flow system and better triggering circuits will be incorporated. By using these switches in an appropriate circuit design, it should be possible to obtain reliable operation while still keeping the switch loss to less than 10% of the total energy transferred.

The spark gap switches just discussed are intended to provide an interim solution to the switch problem; however, systems operating at 1 kHz with an MTBF of 10^8 shots can be expected to fail after only 277 hours of operation, which, in a plant operating 16 hours/day is only 17 days. A device with much improved reliability is therefore required, and we are supporting thyratron development with this in mind. The thyratron program which is being carried out by EG&G Inc., has the following major goals:

1. Increase the peak current capability
2. Increase the dI/dt capability
3. Demonstrate subnanosecond jitter
4. Investigate tube heating during the leading edge of the current
5. Investigate tube recovery, both the time required, and the need for reverse voltage protection.

The approach being used involves both obtaining a better fundamental understanding of how thyratrons work, and making modifications to tube design to meet the design specifications. This work has been described in more detail in the paper by Friedman, et al., given earlier at this conference.

The pulse power requirements for laser isotope separation are placing new demands on devices and systems. The devices discussed in this paper may turn out to be interim solutions; new systems as yet undefined, are likely to be the ones having the ultimate performance required. Developments in pulse power systems may turn out to be pacing items in achieving the goals of the laser isotope separation program, and will have significant impact on other high power system development.

ANALYSIS OF AN INDUCTIVE ENERGY HIGH PERVEANCE ELECTRON BEAM GENERATOR

Maurice Weiner
Electronics Technology and Devices Laboratory
USA Electronics R&D Command
Fort Monmouth, New Jersey 07703

Summary

Recently Slivkov and Dolgachev[1] proposed an interesting type of electron beam generator, consisting of a high voltage triode in series with a storage inductor. During the storage time the triode operates with a depressed collector voltage. A high energy current pulse is obtained when the triode is switched from a high perveance state to a low perveance one.

In this paper, the circuit model for the beam generator was expanded to take into account grid capacitance and beam loss. Computer results based on the new circuit model predict a train of sinusoidal like pulses in the triode output when the grid is suddenly connected to a portion of the storage inductor. An electron beam generator, capable of producing a train of megavolt pulses at high currents, appears to be feasible.

Introduction

In recent years much attention has been given to beam generators which utilize inductive energy storage. Compared to capacitive energy storage, inductive storage has an inherently large ratio of stored energy to weight. For applications which have a low weight requirement, therefore, inductive energy storage is an approach worth exploring.

In most beam generator designs considered previously, the operation was limited to either single shot or involved coercive pulsing, i.e., an external switching voltage was supplied for each output pulse. Less consideration has been given to the burst mode of operation, i.e., to the generation of a train of pulses. Unlike coercive pulsing, a switching voltage is required only to start and terminate the pulse train. The burst mode therefore places less stringent requirements on the switch, particularly when rapid pulsing at high power levels is sought.

Recently Slivkov and Dolgachev[1] proposed an interesting type of electron beam generator, consisting of a high voltage triode in series with a storage inductor. The triode operates with a depressed collector voltage. A foil window is provided at the anode end to extract the electron beam.

An attractive feature of this design has to do with the fact that the switch and beam accelerator functions are performed in the same structure. In previous designs utilizing inductive energy storage, the switch and accelerator functions were performed in separate components. Thus the new design is simpler and the system is made more compact.

The analytic treatment previously considered was geared toward single shot and coercive pulsing. In this paper the circuit model for the generator has been modified so as to allow for the existence of oscillations, i.e., the burst mode of operation. Computer results based on the new model clearly indicate that strong oscillations are present under a variety of conditions. Modifications in the generator design which are more suitable to the burst mode of operation, and to higher voltage operation, are discussed.

Basic Circuit Description

The basic circuit with no allowances for oscillations is shown in Figure 1. Initially a large voltage is placed on the grid. When the contact at B is closed, current will start to build up, resulting in energy storage in the inductors L_1 and L_2. During the storage interval the grid voltage will exceed the anode voltage. When the current has built up to a point close to its maximum value, signifying the end of the storage interval, the spark gap at P is fired. The grid potential is then suddenly reduced to the potential at the point of the tapped inductance. As a result of the reduced grid voltage, a large rate of change in the current will occur, accompanied by a build-up of voltage across the inductors, L_1 and L_2. This voltage will appear across the triode, producing the high voltage electron beam.

In the circuit of Slivkov and Dolgachev the voltage reduction is instantaneous since no allowances are made for grid capacitance. The circuit model also does not include the effect of beam losses. In this paper both grid capacitance and beam loss are incorporated into the circuit model.

Modified Circuit Model

The more detailed circuit model is shown in Figure 2, where the grid cathode capacitance C_g, and a resistance, R_c, shunt the inductor. R_g represents grid losses associated with beam interception and beam loading. Initially the grid cathode capacitance is charged to the voltage V_g. When the spark gap is fired current from V_c begins to flow in L_1. After a time roughly equal to L_1/R_c, where R_c is the charging resistance, the voltage across L_1, R_g, and C_g will significantly decrease and the grid cathode capacitance will start to discharge. This will be followed by oscillations in the grid voltage, associated with the L_1 C_g circuit. The oscillations in V_g will introduce corresponding variations in the triode impedance, which in turn will give rise to large variations in the inductive voltage. The inductive voltage oscillations then will appear across the triode. The oscillations will be affected by the losses given by R_g, Rc, as well as by the variation in voltage across L_1 induced by the changes in the primary current flowing in L_1.

Simple conditions under which oscillations will occur may be obtained as follows. In order for oscillations to occur, the fall time of the voltage across L_1 should be less than the period of oscillation. Thus $L_1/R_c \ll 2\pi (L_1C_g)^{1/2}$, or $R_c \gg (1/2\pi)(L_1/C_g)^{1/2}$. Similarly the grid resistance should satisy the condition $R_g \gg (1/2\pi)(L_1/C_g)^{1/2}$. In addition the oscillation period should be less than the fall time of the primary current. The fall time will be discussed later.

U.S. GOVERNMENT WORK NOT PROTECTED BY U.S. COPYRIGHT.

An alternative grid circuit for exciting oscillations is shown in Figure 3. Instead of using a bias voltage, the grid-cathode is pulsed during the storage interval. The pulse voltage is then removed at the same time that the spark gap is fired. If the fall time of the pulse is small compared to the period of oscillation, $2\pi(L_1C_g)^{1/2}$, the grid-cathode capacitance will be "shock" excited and grid oscillations will occur, which in turn will give rise to high voltage oscillations across the accelerator. The requirements that $R_g \gg (1/2\pi)(L_1/C_g)^{1/2}$, and that the oscillation period be less than the fall time of the primary current, also prevail.

In general, grid pulsing with a steep fall time will result in somewhat larger amplitude oscillations, compared to the bias mode where one has a finite R_c in the circuit. The two modes are equivalent when $R_c \to \infty$. Choosing a very large value R_c is prohibitive since this implies extremely large values of V_c at the same grid current levels. Another potential advantage of grid pulsing is that, after a pulse train has died out, little or no current flows through the spark gap and it is relatively easy to open up the grid circuit in preparation for generating another pulse train. The potential advantages of grid pulsing, however, must be balanced against the added circuit complexity needed to supply the grid pulse with a steep fall time.

Voltage Current Relationship in Triode

In order to obtain numerical results, the relationship among the grid voltage V_g, the anode-cathode potential, V_a, and the current, I, must be assumed. For this purpose the following is adopted:[2]

$$I = K\left(V_g + \frac{V_a}{\mu}\right)^{3/2} \qquad (1)$$

where K is the triode perveance and μ is the amplification factor. During the storage interval V_g is normally larger than V_a. If $V_g \gg V_a$, then Equation (1) reduces to the diode equation

$$I = KV_g^{3/2} \qquad (2)$$

When the switch is closed, however, it will no longer be true that $V_g \gg V_a$ since V_g may decline rapidly.

In order to demonstrate how the large voltage oscillations develop, it is instructive to solve Equation (1) for V_a,

$$V_a = \mu\left[\left(\frac{I}{K}\right)^{2/3} - V_g\right] \qquad (3)$$

Shortly before the spark gap is fired $\mu(I/K)^{2/3}$ and μV_g represents two large quantities whose difference is equal to the power supply voltage. When the spark gap is fired μV_g will undergo rapid oscillations while $\mu(I/K)^{2/3}$ will change slowly because of the energy storage in the inductive elements. Assuming V_g drops to about $V_g \approx 0$, the magnitude of the voltage swing in V_a will be approximately μV_{go}, where V_{go} is the initial voltage on the grid. If we allow V_g to become negative, voltage peaks of $\approx 2\mu V_{go}$ may be attained.

Circuit Response After Firing of Spark Gap at P

Computer results have been obtained for both the biased and pulsed grid cases. In particular, the variation in V_a and I as a function of time, subsequent to the firing of the spark gap, have been obtained. In obtaining the results for the acceleration interval the triode nature of the device is fully taken into account. Equations which govern the circuit, as well as the computer programs used for their solution, are discussed briefly in the Appendix.

Typical megavolt (MV) oscillations in V_a, for the biased grid case, are shown in the upper curve of Figure 4. The corresponding decline in the induction current, from which the energy for the oscillations is derived, is shown in the lower curve of Figure 4. Damping of the oscillations occurs when R_c, the charging resistance, is decreased. A similar damping occurs when the shunt resistance, R_g, is decreased. Eventually the current decays to a value determined by Equation (1) with $V_g = 0$ and $V_a = V_b$.

Computer results were obtained for various values of the tapped inductance, L_1. As expected, the pulse-width is narrowed by decreasing L_1. The narrower pulses usually are accompanied by an increase in amplitude, indicative of the wider swing in grid voltage permitted when L_1 is decreased.

Figure 5 shows that similar oscillations are present when the grid is pulsed. The parameters of Figure 5 are identical to those of Figure 4, except for the omission of V_c and R_c. An infinitely steep fall time is assumed. As mentioned previously, somewhat higher amplitude oscillations are expected for the pulsed grid case, because of the presence of R_c and the assumption of an infinitely steep fall time in the grid pulse.

Since the output voltage amplitude is $\approx \mu V_g$, the required grid voltage may be decreased by increasing the amplification factor, μ. Figure 6 shows the MV oscillations which are present when $V_g = 100$ kV and $\mu = 10$, compared to the values $V_g = 390$ kV and $\mu = 2.5$ in Figures 4 and 5.

Fall Time

The fall time of the primary current may be approximated if we assume the current flowing through L_1 is equal to I, i.e., we ignore the currents in the secondary loops (Figure 2). Under these circumstances the differential equation governing the current is

$$V_b = (L_1 + L_2)\frac{dI}{dt} + \mu\left[\left(\frac{I}{K}\right)^{2/3} - V_g\right] \qquad (4)$$

The form of Equation (4) is identical to that of the diode if we regard the power supply voltage as

$$V_b' = V_b + \mu V_g \qquad (5)$$

and the diode perveance as

$$K' = \frac{K}{\mu^{3/2}} \tag{6}$$

The fall time constant, t_f, for the diode case is[1]

$$t_f = (L_1 + L_2)K' V_b'^{1/2} \tag{7}$$

Making use of Equations (5) and (6), the fall time for the triode is

$$t_f = \frac{(L_1 + L_2)K (V_b + V_g)^{3/2}}{\mu^{3/2}} \tag{8}$$

For the parameters listed in Figure 4, for example, $t_f \approx 6.4\mu s$. Note that the fall time calculated from Equation (8) is in approximate accord with the exact computer results shown in the curves of Figure 4. As mentioned previously the oscillation period must be less than t_f in order to achieve large amplitude oscillations.

Inductive Storage Interval

During the storage interval it is important to know how quantities such as the current I, and anode-cathode potential, V_a, and the efficiency, η_s, vary with time, t. These quantities have been calculated previously[1] for the case of the vacuum diode, and are shown in Figure 7.

A similar calculation for the triode is complicated by the fact that, during the storage interval, Equation (3) does not apply. During the bulk of the storage interval, Equation (3) states that $V_g < 0$, which is contrary to fact if we assume the grid does not supply any appreciable energy to the beam. The reason for the discrepancy lies in the fact that Equation (3) does not account for the beam deacceleration in the grid-anode region. In order to accurately relate V_a to I and V_g, during the storage interval, a beam analysis should be undertaken.

A rough approximation of the storage behavior may be obtained, however, from the diode results. We adopt the view that V_g has the effect of increasing the effective perveance of the generator. For the same current, I, and anode-cathode voltage drop, V_a, one has

$$I = K_e V_a^{3/2} = K\left[V_g + \frac{V_a}{\mu}\right]^{3/2} \tag{9}$$

and

$$K_e = K\left[\frac{V_g}{V_a} + \frac{1}{\mu}\right]^{3/2} \tag{10}$$

where K_e is the equivalent perveance of the diode and V_a is evaluated at the end of the storage interval. As an example, K_e may be evaluated for the parameters listed in Figure 4. Making use of Equation (10), $K_e = 160 \times 10^{-6}$ perveance. From Figure 7, at I = 1000A, the storage time is $\approx 23\mu s$, at which point 38 percent of the maximum storage current and 52 percent of the maximum anode-cathode voltage is achieved. The storage efficiency is approximately 56 percent at this point in time.

A general expression for the storage time constant t_r, analogous to L/R, is given by $(L_1 + L_2)K_e V_b^{1/2}$. The time constant for the aforementioned example is 408 μs, indicating we have chosen to fire the spark gap before t_r. Choosing to fire the spark gap at a time much larger than the time constant is wasteful of energy, since the efficiency is low and little gain in energy storage is achieved. On the other hand, choosing a firing time much less than the time constant, although highly efficient, may not provide sufficient storage energy.

Periodic Focusing

The use of a single control electrode is probably not the optimum type of structure to achieve MV pulses at high beam currents. In order to avoid breakdown a fairly large anode-cathode space is needed. Given such a large space the transmission of the beam current with only a single grid is difficult to achieve without heavy beam losses, caused by space charge effects. One possible means for overcoming this problem is to use a quasi-periodic electrostatic focusing[3], as shown in Figure 8. The grids alternate in potential during the storage interval. One set is connected to a high grid potential. The other set is connected to various points on the inductor. When the spark gaps are activated, the grid potentials are suddenly reduced, giving rise to a large rate of current change, which in turn produces a high voltage burst of beam current. If all the acceleration grid voltages are switched simultaneously then the total change in grid voltage will be nV_g where V_g is the voltage applied to each grid, with respect to its adjacent electrode. n is the total number of grids. The amplitude of the output voltage will then be nuv_g. The circuit equivalent may be considered that shown in Figure 9.

Trajectory calculations for a planar beam in the presence of such a periodic potential indicates fair transmission, approximately 80 percent.[3] No trajectory results have been obtained for the case of a cylindrical beam, however. In addition, no trajectory results were obtained which apply to the acceleration interval. This is a particularly important area of investigation since there exists the possibility that the beam will blow up during the acceleration time, thereby reducing the beam transmission.

Heating of the Anode Foil

Heating of the foil will present severe problems. Suppose a design corresponds to the parameters of Figure 4, and that a 1 mil thick gold foil with a 20 cm^2 area is chosen for the anode. At one mil thickness the 1 MV electrons will pass through the foil largely unattenuated while the storage state electrons will be absorbed. A beam area of 20 cm^2 is chosen since, for a current of 1000 amps, the cathodes now available yield current density of $10A/cm^2$.

By the end of one storage interval the beam will have delivered energy to the foil in the amount

$$\tfrac{1}{2}(L_1+L_2)\, I^2(1-\eta_s)/\eta_s .$$

For the previous example $\eta_s = 0.58$, $L_1 + L_2 = 10^{-2}H$,

and $I = 10^3$ amps, so that the energy dissipation in the foil is 3600 joules, assuming all the beam energy is absorbed. Assuming that no heat is conducted or radiated away during the storage interval, 233μs, the foil will attain a flash temperature of about 28,000 °C. Although the actual temperature will be much lower because of heat losses, the example is indicative of the severe heating problem one may expect. One possible approach is a trade-off which reduces the storage energy. For example, using 10^{-3}H instead of 10^{-2}H, will reduce the calculated temperature by an order of magnitude, although the droop in the oscillation will be increased.

A more desirable technique for reducing foil dissipation involves defocusing of the beam during the storage state, so that the beam does not strike the foil but is instead collected by adjacent electrodes able to withstand the dissipation (Figure 10). During the acceleration state the beam is focused into the foil. The focusing may be accomplished, possibly, by proper design of the electrostatic control grids, so that during acceleration the high voltage automatically refocuses the beam onto the foil. The focusing may be aided perhaps by a pulsed longitudinal magnetic field which is introduced shortly before the start of the acceleration cycle.

Conclusions And Recommendations

A circuit analysis was performed on a beam generator design utilizing inductive energy storage. The design resembles that of a triode with a depressed collector anode. The results of the analysis indicated that MV pulse trains at high current levels will occur. The analysis also strongly suggests that such oscillations will occur in a multi-gridded structure having a periodic potential. The multi-gridded structure will allow the extension to higher acceleration voltages.

Suggested areas for further design study include the following:

1) A beam trajectory study for the periodic potential should be undertaken to determine the quality of transmission. High levels of beam transmission are required in order for the oscillations not to damp out. Such a study also will dictate the choice of circuit parameters and the dimensions of the structure.

2) The concept of defocusing the beam at the anode during the storage interval should be incorporated into the beam trajectory analysis. As mentioned previously, defocusing the beam will ease the thermal dissipation problems associated with the window.

3) Design consideration should be given to minimizing the voltage drop across the accelerator during the storage interval, while maintaining high current levels. This means resorting to a structure with a large effective perveance. A lower voltage drop will make the concept compatible with voltage generating machines, which are capable of supplying high currents at a few kV.

4) The use of supercooled inductors should be considered in the design. At low impedance levels the resistive losses in the storage inductors should be as low as possible in order to take advantage of the concept of inductive-energy storage.

5) Consideration must be given to the technique which will be used to open up the grid circuit after each burst of oscillations. As mentioned previously the problem is lessened in the grid pulsing case. One possible approach is the placement of a repetitive series interrupter (RSI) in the grid circuit.

6) In order to obtain reasonably small diameter beams, fairly large current densities are required. A cathode study must be undertaken to determine whether such cathodes are feasible. Large convergence ratio cathodes may be one approach for obtaining the high current density levels.

Appendix

The loop equations for the circuit of Figure 2 are:

$$V_b = V_a + L_1 \frac{d\,(I-I_2-I_3-I_4)}{dt} + L_2 \frac{dI}{dt} \qquad (A1)$$

$$L_1 \frac{d\,(I-I_2-I_3-I_4)}{dt} = I_2 R_g \qquad (A2)$$

$$I_2 R_g = V_g \qquad (A3)$$

$$I_2 R_g = V_c + I_4 R_c \qquad (A4)$$

$$L_1 \frac{d^2\,(I-I_2-I_3-I_4)}{dt^2} = \frac{dI_2}{dt} R_g \qquad (A5)$$

$$\frac{dI_2}{dt} R_g = \frac{dI_4}{dt} R_c \qquad (A6)$$

$$\frac{dI_2}{dt} R_g = \frac{I_3}{C_g} \qquad (A7)$$

V_a is given by

$$V_a = \mu \left[\left(\frac{I}{K} \right)^{4/3} + V_g \right] \qquad (A8)$$

where V_g is replaced by $-V_g$ because of the sign convention of the circuit. The initial conditions are:

$$I = I_o \qquad (A9)$$

$$I_3 = 0 \qquad (A10)$$

$$I_4 = -I_2 = V_c/(R_c + R_g) \qquad (A11)$$

Equations (A1) - (A8) were solved by an iterative procedure using a Burroughs 5500 computer. The computer program employed a Runge-Kutta-Nystrom starting procedure followed by the Hamming method. Details of the programs are found elsewhere.[4]

References

1. I. Slivkov, G. Dolgachev, "Accelerating and Switching Optoelectronic Systems of a High Powered Acceleration with an Inductive Element, Prib. i Tekh. Eksper, No. 3, pp. 27-30, 1975.

2. K. Spangenberg, Vacuum Tubes, McGraw Hill, New York, New York, 1948.

3. A. Koslov, A. Maslov, G. Prokhova, I. Slivkov, " A Multielectrode Electron-Optic System with an Inductive Storage Device for a High-Current Accelerator", Prib. i. Tekn Eksper., No. 3, pp. 25-27, 1975.

4. A. Pixley, A. Macek, "A B5000 ALGOL 60 Program for the Solution of a System of First Order Differential Equations (Hamming Method)", Burroughs Technical Bulletin MRS-126, Feb 1964.

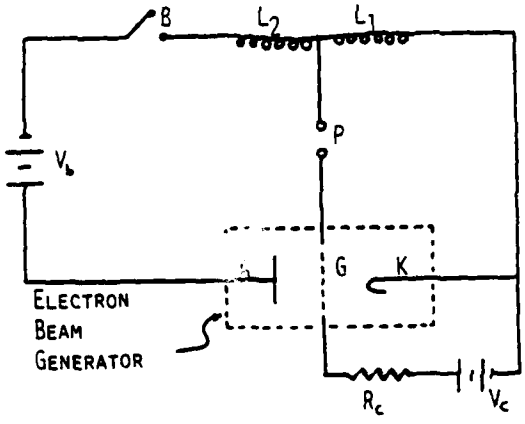


Fig. 1 Beam Circuit for Electron Beam Generator Utilizing Inductive Energy Storage.

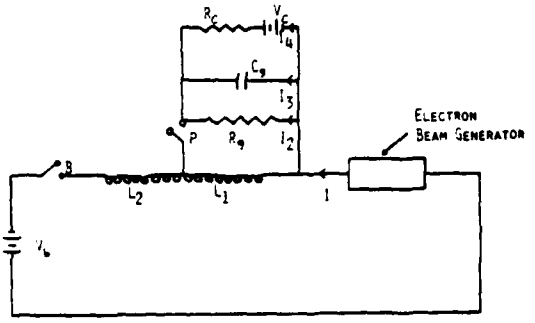


Fig. 2 Circuit Model of Electron Beam Generator Utilizing Inductive Energy Storage. Model Includes Grid Capacitive Effects and Beam Loss.

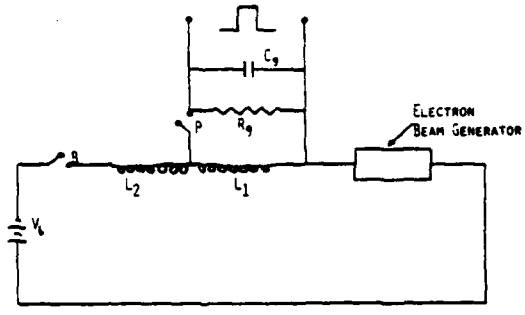


Fig. 3 Circuit Model of Electron Beam Generator Utilizing Inductive Energy Storage. Model Includes Capacitive Effects and Beam Loss. Grid Pulsed During Storage Interval.

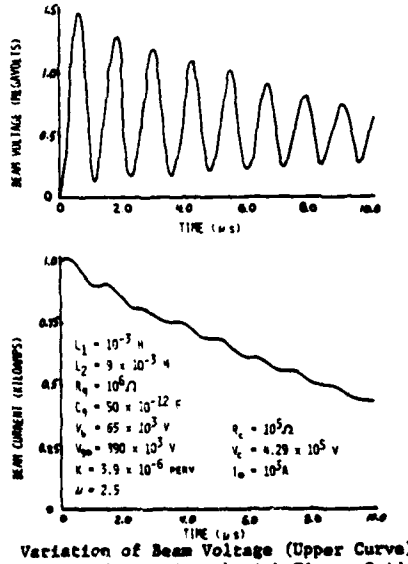


Fig. 4 Variation of Beam Voltage (Upper Curve) and Current (Lower Curve) with Time. Grid Bias Mode.

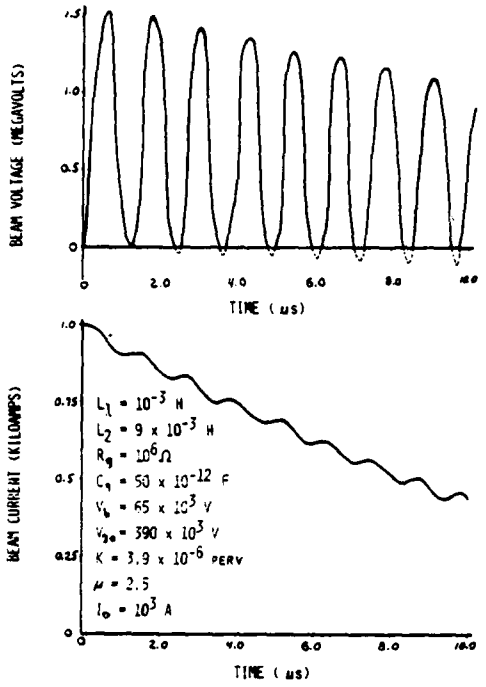


Fig. 5 Variation of Beam Voltage (Upper Curve) and Current (Lower Curve) with Time. Grid Pulse Mode.

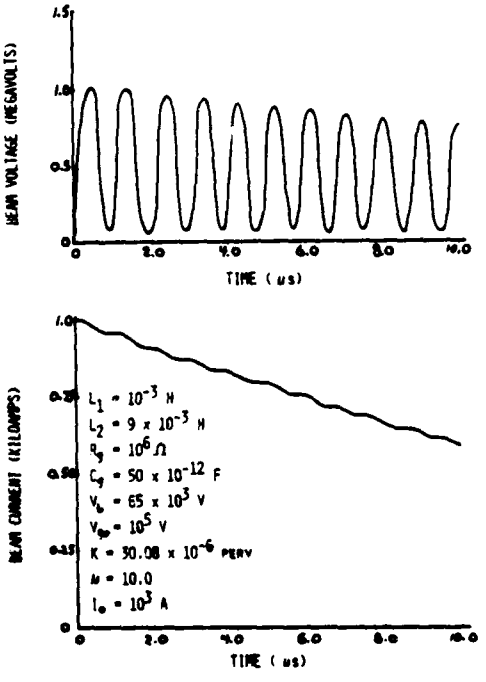


Fig. 6 Variation of Beam Voltage (Upper Curve) and Current (Lower Curve) with Time. Grid Pulse Mode.

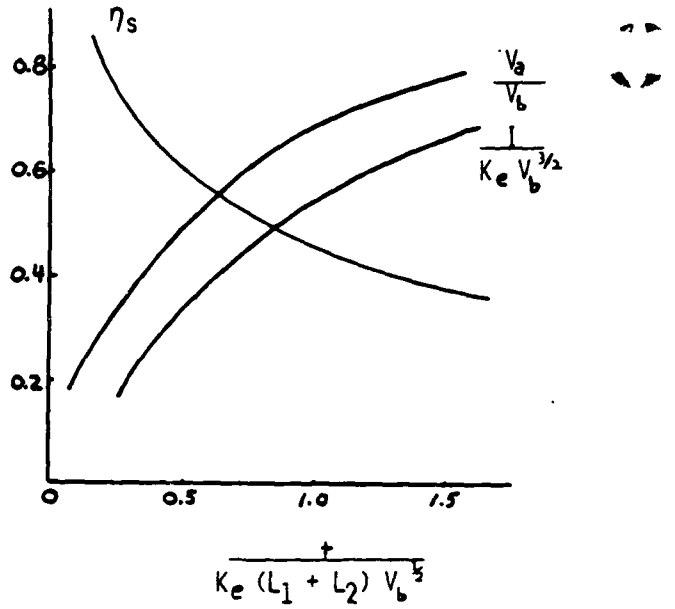


Fig. 7 Diode Dependence of Current, Voltage and Efficiency with Time (Ref. 1)

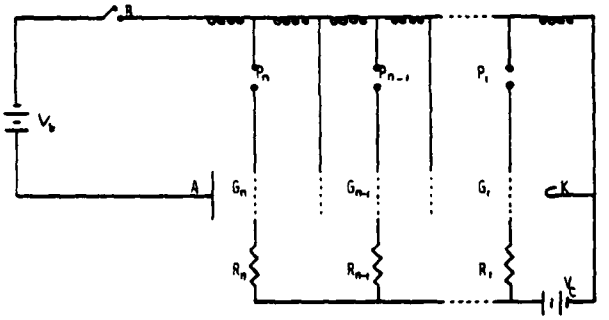


Fig. 8 Electron Beam Generator with Quasi-Periodic Focusing.

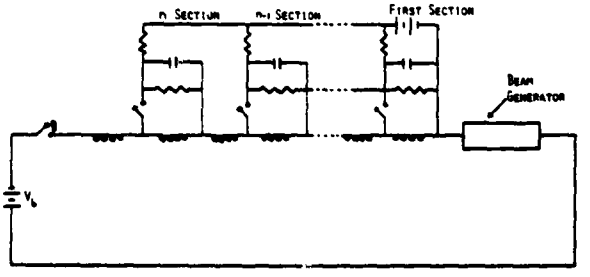
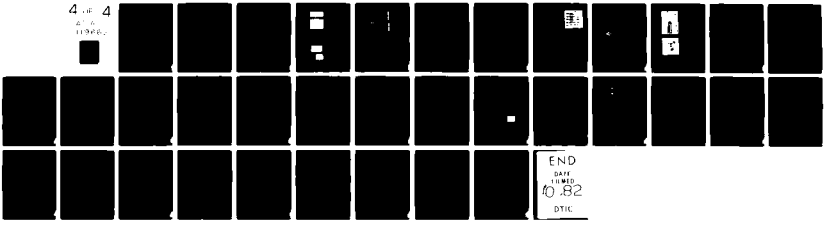


Fig. 9 Circuit Model of Beam Generator with Quasi-Periodic Focusing.

AD-A119 662 PALISADES INST FOR RESEARCH SERVICES INC NEW YORK F/G 9/5
IEEE CONFERENCE RECORD OF 1978 THIRTEENTH PULSE POWER MODULATOR--ETC(U)
1978
UNCLASSIFIED 78-CH-1371-4-ED NL



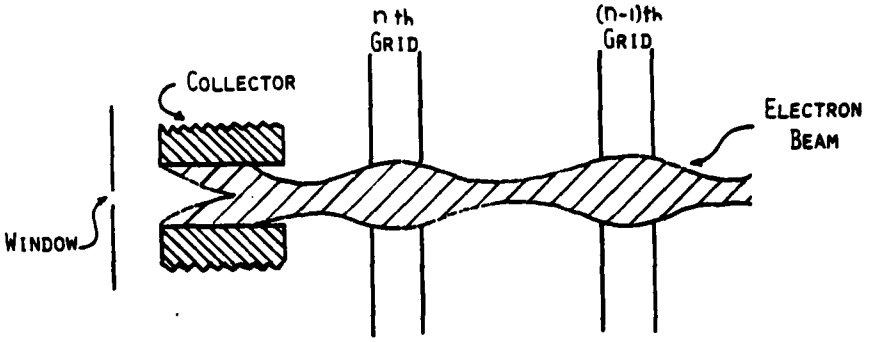


Fig. 10 Defocusing of Electron Beam During Storage Cycle.

INDUCTIVE STORAGE PULSE-TRAIN GENERATOR

R. D. Ford and I. M. Vitkovitsky

Naval Research Laboratory
Washington, D. C. 20375

Introduction

Utilization of inductive storage in production of intense charged particle beams, laser beams and hot dense plasmas of interest in thermonuclear fusion studies and in other research areas is very attractive because of its inherent compactness associated with energy storage in the form of magnetic fields. A major problem in utilizing inductive energy sources with sufficient output power for such beams and plasmas is the development of an opening switch. In some instances repetitive pulse output is required, so that switches must open repeatedly at a frequency determined by the needs of the experiment. If only a small number of pulses is needed, then use of one switch per pulse in the train becomes a practical method for generating pulse trains with peak power determined by the performance of individual switches. Formation of pulse trains with peak pulse power in the range of 10^9 to 10^{10} Watts was studied. This study included the investigation of single switch elements to determine methods for extending the operating power to higher levels.

Earlier experimental study[1,2] of high current, high voltage, fast opening switches has shown that 10^{10} Watt pulses can be generated by interrupting a current in the inductor. These switches employ an explosively actuated interruption of current, typically occurring in 20 μsec, with subsequent commutation to an auxiliary fuse. This allows rapid voltage recovery in the first stage (exploding switch) to take place. The exploding switch provides high current capability, while the rapidly increasing nonlinear resistance of the fuse in a period of about 2 μsec produces high inductive voltage. At present, such a configuration has been tested to 300 kV. The high current and high voltage properties of the exploding switch and fuse combination, as well as the low energy consumption of the exploding switch, make it suitable for use in pulse train forming networks with high pulse repetition rates.

Inductive circuit configurations have been studied and tested to demonstrate the feasibility of using explosively actuated opening switches with commutating fuses to generate pulse trains with pulse-to-pulse separation time of less than 10 μsec, i.e., with repetition rates up to 100 kHz. The power supply used for generation of such pulse trains consists of a 90 kJ inductive store (using 80 μH inductance). The current rises in the inductor to 35 kA in approximately 1 millisecond. The energy and pulse time are sufficient to test generation of as many as 6 pulses with peak power of 2×10^9 Watts and with output voltage level of 75 kV, while operating near peak current with essentially constant power in each of the pulses. Tests were conducted with both open circuit output and with power delivered to a 2.5 Ohm resistive load.

Pulse Train Generator

Figure 1 shows two methods for connecting a series of opening switches to an inductive store, L, to provide a pulse train output. The first method uses parallel opening switch modules (denoted by letter E, with a switch number in the subscript) separated from each other by closing switches (denoted by letter S, with switch number in the subscript). At the start of the pulse train formation all the closing switches, S, are in an open state, and the load resistance, R_L, is significantly greater than that of the opening switch, so that current flow in the inductor and in the first opening switch, E_1, are almost identical. Analogously, the current in the second circuit, shown in Fig. 1, is initially flowing in all opening switch modules, E_1 through E_n. Opening the first switch in either circuit transfers some of the current to the load until the first switch, S_1, is closed. The amount of current sharing between the opening switch E_1 and the load, depends on the relative values of R_L and opening switch resistance during the process of current transfer. With S_1 resistance low, relative to the load resistance, the inductor current is transferred back to opening switch, E_2, via S_1. Subsequent opening and closing of the remaining switches produces the same results, provided that the source continues to deliver current. Thus a train of pulses whose repetition rate is limited only by the time required for operation of the opening switch-fuse module can be generated. Figure 2 depicts schematically such a train of pulses.

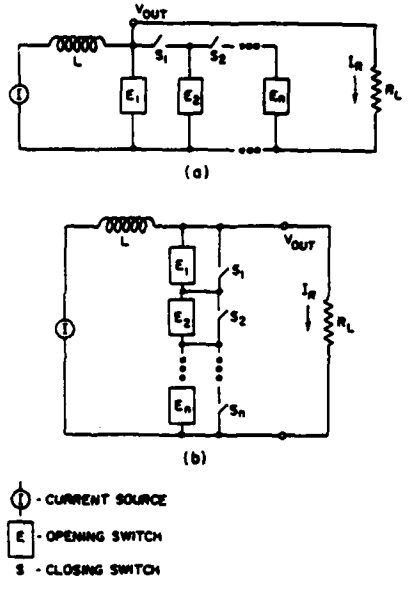


Fig. 1 - Circuit diagrams of inductive storage power supply for generation of pulse train output.

A dashed line superimposed on the top waveform in Fig. 2 shows the maximum inductor current, I_m, that would flow through the exploding switches without opening the switches. Before the switch opening, current in the inductor and in the exploding switch is the same. As the exploding switch initiates the current interruption (without significant energy dissipation[4]), the current is transferred to the first fuse. In addition to generating inductive voltage much higher than that produced by the opening of the exploding switch, because of the much more rapid change in the non-linear resistance of the fuse, it also dissipates the stored energy until the time when the second exploding switch and fuse module is actuated. To determine the change in the inductor current as a result of this dissipation, as well as that due to absorption in the load,

U.S. GOVERNMENT WORK NOT PROTECTED BY U.S. COPYRIGHT

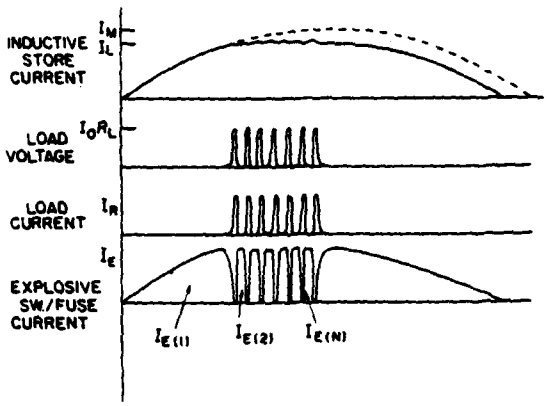


Fig. 2 - Current and voltage waveforms associated with the circuits of Fig. 1.

consider the energy balance in the circuit. The energy in the inductor, L, at time t_i when 1/2 of exploding switch-fuse pairs were actuated, is:

$$W(t_i) = \tfrac{1}{2}L\,[I(t_i)]^2 \qquad (1)$$

with

t_0 - time of opening of the first exploding switch

t_1 - time of transfer of current to the first fuse

t_2 - time of opening of the second exploding switch

.
.
.

The energy removed from the inductor in time $t_i - t_{i-2}$, is:

$$\Delta W^{(i)} = W_F^{(i)} + W_L^{(i)} - W_S^{(i)} \qquad (2)$$

where the superscript refers to the i-th pair. The subscripts denote components of circuit energy:

W_F - energy dissipated in the fuse

W_L - energy delivered to the load

W_S - energy delivered to the inductor from the incompletely discharged current source (such as capacitor or flywheel)

The energy and current in the inductor after the i-th pulse are

$$W(t_i) = W(t_0) - \Delta W, \qquad [\Delta W = \textstyle\sum \Delta W^{(i)}] \qquad (3)$$

$$I(t_i) = [2(W_0 - \Delta W)/L]^{1/2} \qquad (4)$$

By initiating the pulse train before the current peak, the current in each pulse of the train can be kept constant over a large fraction of the period of the source current. By limiting the pulses to those with constant current, the amplitude of the output voltage and peak pulse power will remain constant.

The measured inductor current as well as output voltage, V, and current, I, associated with the circuit derived from that of Fig. 1 is shown in Fig. 3. The output voltage waveform depends on details of current transfer from the explosively actuated switch to the fuse. Reference 1 describes the behavior of the voltage waveform during the transfer. Typically, in those experiments as well as in those reported here, the ratio of peak voltage generated by the fuse to that generated by the exploding switch during the transfer is about 50 to 100.

The circuit of Fig. 3 has been operated successfully with pulsing rates up to 15 kHz. As the pulsing rate is increased to 20 kHz, occasional pulse dropout occurs. However, at 20 kHz and higher (pulse-to-pulse spacing of less than 50 μsec), energy dissipated in exploding foil fuses decreases to a level more acceptable for an efficient pulser. A voltage stress of 3-4 kV/cm can be generated by the fuse, so that a compact switching arrangement illustrated by the circuit in Fig. 4 becomes practical for very high frequency pulsing. Because high energy inductive storage systems require inductor charging to be relatively long, efficient system operation requires that an explosively actuated switch be used as the first switch. Subsequent switches can then be simple exploding foil fuses interconnected by closing switches as shown in Fig. 4. The first fuse must be such that the exploding switch transfer of the inductor current does not open the fuse for a time sufficient to allow high voltage recovery across the opening switch. Subsequent exploding foils are designed to generate pulses after time delay, Δt_p, which determines output pulse-to-pulse separation. By limiting this type of pulser to applications where short time between pulses is required, each fuse carries current only for short times, so that efficient pulse train formation is achieved. Figure 4 shows a typical pulse train obtained using the circuit shown. Current is 35 kA and pulse forming fuse F_1 indicated in Fig. 4 consists of an aluminum foil with the following dimensions: 0.0025 cm x 2.5 cm x 40 cm long. Succeeding switches F_2 through F_6 use foils of 1.2 cm width. Voltage generated is approximately 75 kV per fuse. The pulses are separated at approximately 20 μsec intervals (50 kHz rep. rate). No attempt was made to time precisely each pulse in this demonstration of feasibility. [Data dealing with the interaction of sequential opening switch stages obtained in studies of two stage switching configurations[3] indicate that repetition rates as high as 1 MHz should be possible using the method shown in Fig. 4.]

Capacitive, inductive and resistive loads can be driven with repetitive pulses formed by circuits shown in Figs. 3 and 4. Load impedance dictates the choice of either of the circuits shown in Fig. 1. For example, in resistive loads, efficient transfer of energy may be impaired as the increasing number of switch modules is engaged in a parallel opening switch circuit. Such impairment would occur at the time when the generator has switched n modules of the array and the load resistance, R_L, must compete with the switch resistance, R_0/n, where R_0 is the resistance of one switch module at late time relative to its firing.* To avoid the degradation

*The internal resistance of the circuits in Fig. 1 has a complex form associated with the time dependence of the resistance of switch in the opened state. For example, T. H. Lee[4] shows that uncommutated arc resistance increases over two orders of magnitude over millisecond periods.

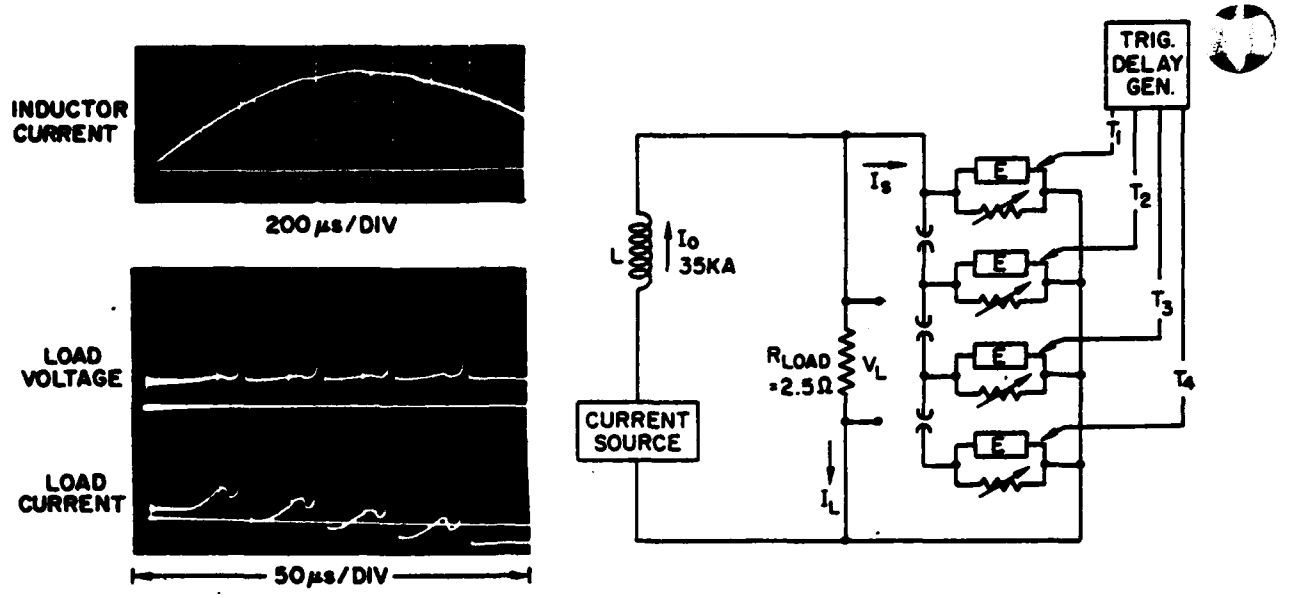


Fig. 3 - Typical inductor charging and output (voltage and current) pulse train characteristics associated with power supply shown schematically.

of performance, a generator with series switch modules can be used. The resistance competing for the output current at the time of engagement of n modules would then be nR_o.

Switch Modules for Pulse Train Generation

Part of the development of the pulse train generator included studies of single switch elements when full pulse train application could not be tested because of the current source limitation. The mechanical and electrical performance of two types of explosively actuated switches in inductive storage systems and their limitations and potential improvements have been described in ref. [1]. Both are shown in Fig. 5. The first type, a switch design with cylindrical conductor (with diameter of 6.35 cm) using steel rings to control the cutting of the conductor by explosively driven

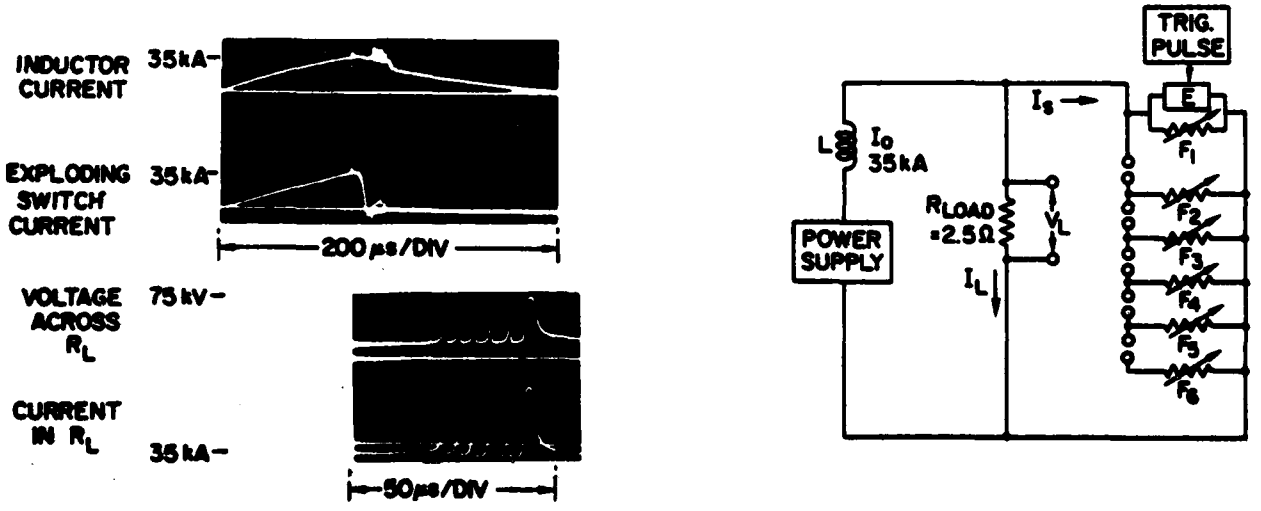


Fig. 4 - Typical 20 to 100 kHz repetitive output (voltage and current) associated with the power supply shown schematically.

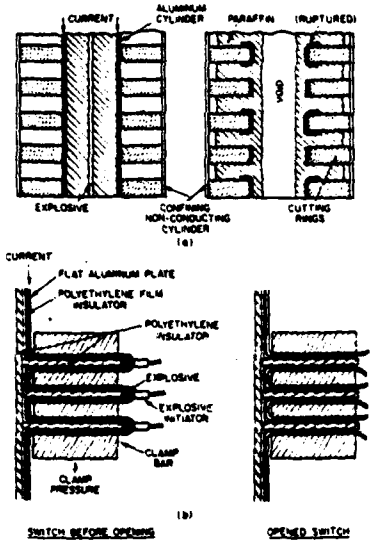


Fig. 5 - Cylindrical and flat opening switch assemblies before and after current interruption.

pusher, has been investigated thoroughly. Its performance, when used with a parallel exploding foil fuse, is described in ref. 3. The second switch design, using flat conductors, was also tried, and shows potential for high voltage applications. Both of these designs along with various fuse assemblies were studied further to extend their performance and to provide modifications needed in pulse train forming applications.

Cylindrical Switch

One of the obvious techniques for improving switch high voltage capability is to increase effective length of the switch by either adding more sections or by operating switches in series.[1] However, as switch length increases beyond one meter, the explosive detonation propagation time given by the shock velocity of approximately 7 x 10^5 cm/s becomes significant relative to the desired switching time. Additionally, when switch modules are connected in series, detonator triggering of ungrounded modules becomes a problem. A simple solution to both of these problems is shown in Fig. 6. Detonators are installed at the center of the explosive in each switch module (S_1 and S_2) allowing explosive detonation to propagate in two directions. The detonator for each module is connected in series by passing the firing circuit wire between the steel rings and the cylindrical conductor via one of the many axial grooves in the conductor. Upon initiation, there is a delay of at least 40 microseconds before high voltage appears across switch module as described in Ref. 1. During this delay, the conducting cylinder of the switch and the detonator firing wires are sheared at each cutting ring and folded back to form an insulating gap between each steel ring pair. At the time high voltage is developed by the exploding foil fuse, the electrical connection that the detonator wires provided between the high voltage and ground terminals of the switch is completely removed.

The value of the field that can be maintained without restrike in the switch depends upon the time of current transfer to the fuse, t_f, and more importantly on the time, t_{HV}, at which high voltage is developed as the fuse explodes (both being referenced to the instant

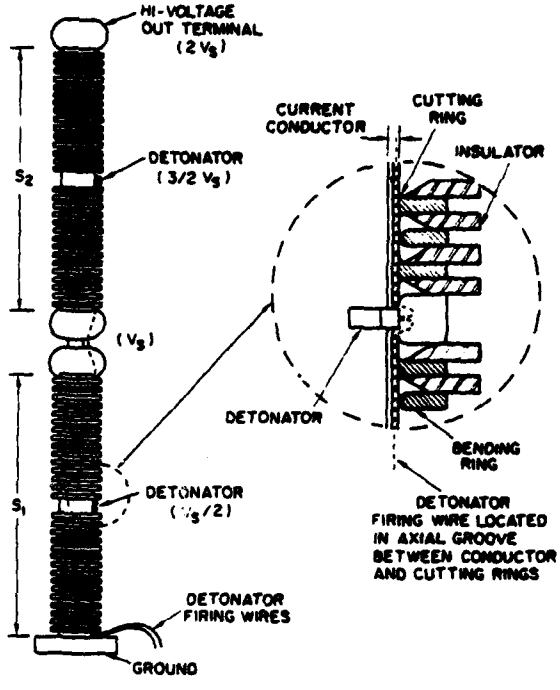


Fig. 6 - Opening switch modules assembled for high voltage operation. Method for simultaneous initiation of explosive actuation of large number of modules is shown.

when conductor rupture is initiated). Table I lists the results of tests performed to determine voltage recovery ability of the switch.

TABLE I: HIGH VOLTAGE PERFORMANCE OF 70 cm CYLINDRICAL EXPLOSIVELY-ACTUATED SWITCH

t_{HV} (μsec)	Voltage Across Switch, V (kV)	Type of Breakdown
40	200	along inner wax surfaces
45	230	along inner wax surfaces
70	300	none

Flat Switch

A second switch design which shows promise for higher voltage stress uses a flat rather than cylindrical conductor as shown in Fig. 5. Preliminary studies of this switch have been performed in configurations using up to six gaps, in both air and in water dielectric. The switch develops approximately 2 kV arc voltage per gap as compared to 0.8 kV per gap for the cylindrical switch, and has held off approximately 45 kV/cm at 40 microseconds after explosive initiation, when used with current commutation into an exploding foil fuse. Although these values are very promising, further development and more extensive testing is required to deal effectively with the effects of high pressure on the surroundings, before this switch is available for practical applications.

Fuse Assembly

Foil fuse assemblies used during switch development were functional but unwieldy. In order to demonstrate that such fuses could be produced simply, and made easily replaceable, the assembly shown in Fig. 7 was constructed and tested. In this assembly, cemented lucite components contain multiple foil fuses in water medium, with each fuse separated by lucite partitions. A spark gap closing switch electrode becomes an integral part of the foil clamp assembly. A six section assembly, of 3.85 cm (1.5 inch) in width, was tested and shown to be both reliable and convenient to use.

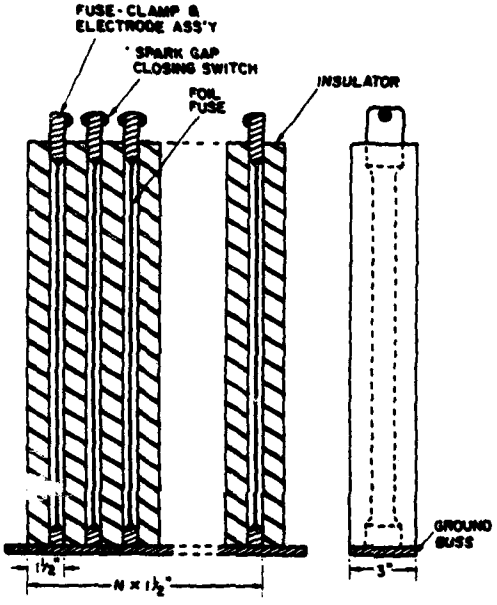


Fig. 7 - Compact assembly for an array of fuses used in generation of high frequency pulse trains.

Conclusion

A method for generating high frequency pulse trains at power levels previously not available has been developed. Pulse trains, with pulse-to-pulse separation equivalent to 100 kHz frequency can be generated. Single switch module performance suggests that peak power level of the pulses within the train of more than 10^{11} W can be obtained in practical laboratory devices.

References

1. R.D. Ford, I.M. Vitkovitsky, Explosively Actuated 100 kA Opening Switch for High Voltage Applications, NRL Memorandum Report 3561, (1977).

2. Glukhikh, V.A., Gusev, O.A., Kostenko, A.I., Larinov, B.A., Monoszon, N.A., Stolov, M.A., Trokhachev, G.V., Pulsed Sources of Energy Based on Inductive Storage, D.V. Efremov, Research Institute, Report 8-0299, Leningrad, USSR, 1976.

3. D. Conte, R.D. Ford, W.H. Lupton, I.M. Vitkovitsky, Two Stage Opening Switching Techniques for Generation of High Inductive Voltages, Seventh Symposium on Engineering Problems of Fusion Research, IEEE Pub. No. 77CH1267-4-NPS, Knoxville, Tenn., 1066-1070, October, 1977.

4. Lee, T.H., Physics and Engineering of High Power Devices, MIT Press, Cambridge, Mass. (1975).

5. D. Conte, M. Friedman, M. Ury, A Method for Enhancing Exploding Aluminum Foil Fuses For Inductive Storage Switching, Proceedings of First IEEE International Pulsed Power Conference, IEEE Cat. No. 76H1147-8 REG-5, Lubbock, Texas, Nov., 1976.

HIGH DENSITY Z-PINCH PULSE POWER SUPPLY

W. C. Nunnally, C. A. Ekdahl, J. E. Hammel, K. W. Hanks, and L. A. Jones
Los Alamos Scientific Laboratory*
Los Alamos, New Mexico 87545

Summary

The pulse-power supply for the High Density Z-Pinch (HDZP) experiment at LASL, described in this paper, is required to produce a peak voltage on the order of 1 MV and a peak current of 1 MA in a small, high-pressure gas load. The experimental load is a small diameter (100 μm) current filament between two electrodes spaced 10 cm apart with a 20-cm diameter coaxial return conductor. The current filament is to be initiated with an 18-J, 18-ns, Q-switched Nd:glass laser. The HDZP system consists of a 75-nH, 600-kV, 72-kJ marx bank that resonantly charges a water-insulated intermediate storage line. A prototype of 1/12 of the system is also described. The prototype has been tested at its design values. The large system is to become operational in November 1978.

Introduction

The High Density Z-Pinch experiment at Los Alamos Scientific Laboratory is being constructed to investigate the plasma parameters of a laser-initiated current channel in a high-pressure neutral gas. A 1 GW neodymium glass laser will be used to initiate a conducting channel with a radius on the order 100 μm and a length on the order of 10 cm between two electrodes as shown schematically in Fig. 1. Ideally, the pulse-power supply for the HDZP must produce a pressure-dependent current waveform with a specific rate of rise and amplitude to maintain a constant plasma channel radius and ohmically heat the $\approx 10^{20}$ cm^{-3} plasma to several kilovolts.

The theoretical current waveforms required for three filling pressures that maintain a constant channel radius are shown in Fig. 2. The initial experiment will investigate the first several hundred nanoseconds of the channel initiation and conduction. The effect of initial laser energy, the current risetime, and maximum current amplitude on the plasma channel will be studied to evaluate the theoretical predictions and to confirm numerical calculations.

Pulse Power Supply Design

*Work performed under the auspices of U.S. Department of Energy.

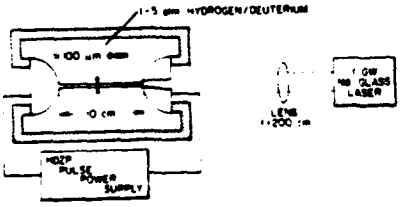


Fig. 1.
HDZP schematic.

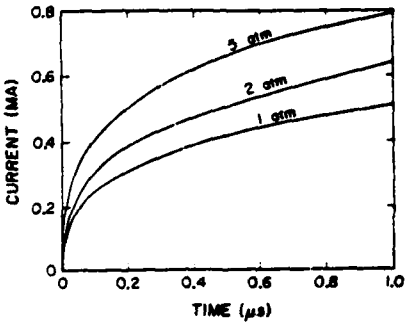


Fig. 2.
HDZP current waveform.

The gas load with conducting channel has an inductance of approximately 100 nH. In order to obtain the desired $\dot{I}$ at channel initiation of approximately $0.5\text{-}1.0\times10^{13}$ A/s, the initial voltage across the load must be approximately $0.5\text{-}1.0\times10^{6}$ V. The maximum current required from the power supply is also shown in Fig. 2. Another important consideration is the voltage risetime across the gas load electrodes before laser initiation. In order to increase the current risetime, the load inductance must be reduced, however, reducing the inductance of the load reduces the open circuit or preinitiation voltage hold-off of the load electrode structure. Thus, a fast-rising, open-circuit voltage is desired to permit reducing the load inductance by increasing the maximum open circuit breakdown voltage for a given structure.

Several circuit configurations were evaluated and simulated using a circuit analysis code. A system consisting of a water-insulated, intermediate storage line resonantly charged by a low-inductance marx circuit was chosen as the most versatile system. The basic circuit for the HDZP pulse-power supply is shown in Fig. 3. The system can be operated with a wide range of current risetimes and current amplitude by laser initiating the current channel at various times during the resonant charge of the water line. The

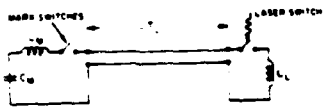


Fig. 3.
Basic HDZP pulse power supply circuit.

CH1371-4/78/0000-0289$00.75 © 1978 IEEE

line impedance is designed to be varied between 0.25 Ω and 1 Ω with a transit time of 90 ns. The marx bank is designed to operate at a nominal 500 kV. The maximum transient voltage across the load is determined by the ratio of the line capacitance to the marx capacitance.

Marx Bank Design

The inductance of the marx bank, L_M, is of prime importance in that it determines the voltage risetime across the load electrodes for a given line impedance Z_L or L_M/Z_L. In addition, the inductance determines the energy transfer efficiency to the load and the isolation of the marx from the transmission line. The marx inductance was designed to be less than the load inductance of 100 nH. The minimum energy storage of the marx is determined by the maximum desired inductive load energy of 50 kJ. The maximum marx fault current was designed to be 1 MA at 500 kV.

In order to accomodate the maximum marx current and reduce the marx inductance, 12, 6-stage marx modules, each of which stores 4.3 kJ at 500 kV and provides a maximum fault current of 83.3 kA, were paralleled. The individual marx module circuit diagram is shown in Fig. 4 and pictured in Fig 5. Each marx module stage consists of two parallel 0.1 μF, 100 kV Maxwell Series S capacitors and one Physics International T670 triggered spark gap. Each capacitor has a maximum rated current of 50 kA, and the spark gap has a maximum rated current of 100 kA. The capacitors were specified with 50% voltage reversal to accommodate a marx output fault and resulting 75% voltage reversal at 500 kV output voltage.

The marx trigger system was designed to erect all the marx modules in a small fraction of the minimum voltage rise on the water transmission line or within approximately 20 ns. The trigger circuit chosen is shown in Fig. 6. This trigger marx arrangement is a variation of trigger circuits suggested by Fitch[1] and was selected because the trigger pulse of the marx module gaps can be controlled in amplitude, risetime, and arrival time very precisely. In addition, each marx module spark gap can be trigered with a similar trigger pulse without loading the marx system. The simultaneous trigger pulses are generated by shorting 12 coaxial cables charged to a maximum of 100 kV with a spark gap that also serves as the trigger marx stage

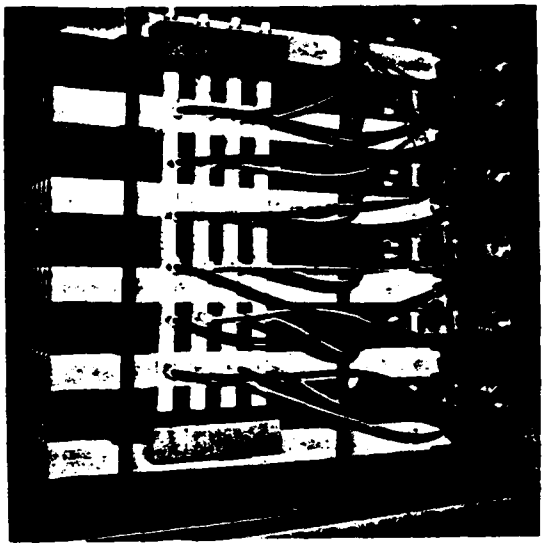


Fig. 5.
Picture of HDZP marx module.

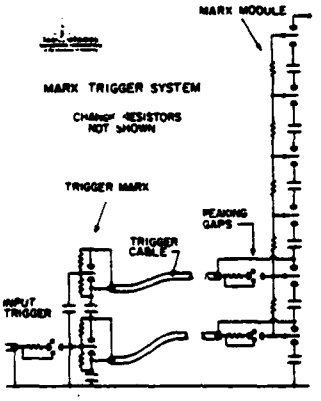


Fig. 6.
HDZP parallel marx trigger circuit.

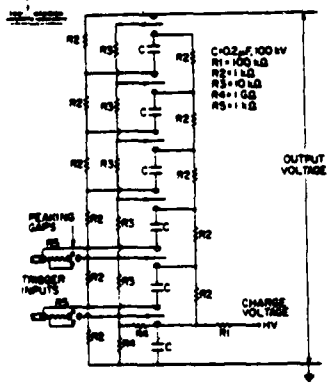


Fig. 4.
HDZP marx module circuit.

gap. The trigger marx stage capacitors serve to bias the shorted cable trigger generators at a potential similar to that of the main marx and isolate the main marx stage voltage from ground. A two-stage trigger marx that triggers only the first two stages of the 12 marx modules will be used because initial test show additional stages are unnecessary. The coaxial trigger cable charge voltage is isolated from the main gap trigger electrodes by an "inside-out" trigatron peaking gap. The peaking gap shown in Fig. 7 also reduces the trigger pulse risetime seen by the main gap trigger electrode to less than 7 ns with a jitter spread of less than 2 ns. The two-stage trigger marx is initiated by an 8-stage ceramic capacitor micromarx generating a 200-kV pulse with risetime of less than 20 ns. The micromarx is shown in Fig. 8.

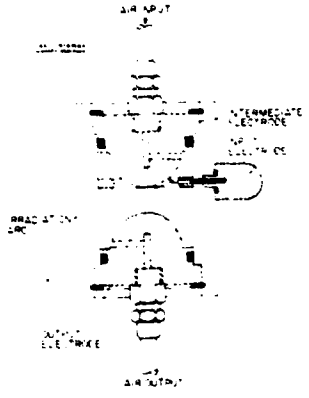


Fig. 7.
HDZP trigger pulse sharpening gap.

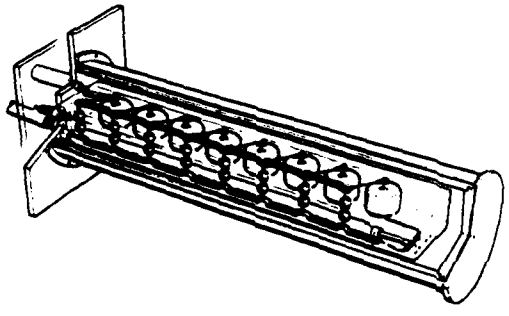


Fig. 8.
Trigger micromarx.

Transmission Line Design

The water insulated transmission line system is shown in Fig. 9. A parallel plate transmission line was chosen over a coaxial transmission line for two reasons. First, the impedance can be easily varied by changing the number and size of the parallel plates. A large water tank was designed to hold the transmission line leaving a large amount of room for line variations. Secondly, the point sink nature of the laser initiated plasma channel requires storing the pulse energy very close physically to the center line of the pinch channel to reduce the transition inductance. A disk transmission line with radial marx current feed would be the optimum configuration but building space limitations prevented using this design.

Gas Load

The desired characteristics of load geometry at the end of the water transmission line are a minimum inductance configuration, a uniform electric field distribution in the pinch region, and visibility and maximum access for diagnostics. An initial load chamber design is shown in Fig. 10 that provides uniform electric field and minimum inductance but diagnostic visibility is restricted. The gas load design is being modified with diagnostic visibility in mind.

Prototype Results

A prototype of the final system has been constructed of one marx module, a 60-ns, 6-Ω coaxial, water-insulated, transmission line and a high-pressure gas pinch chamber. The prototype system is shown in Fig. 11.

The 6-stage marx module has been tested to its maximum charge voltage (100 kV per stage) or 600 kV and a maximum current of 100 kA. The marx module inductance is 900 nH, which extrapolates to an inductance of 75 nH for 12 parallel modules. A single module is triggered with a two-stage trigger marx, shown in Fig. 12, that erects with a jitter of less than ±3 ns. The measured jitter is the cumulative system jitter determined by triggering a scope with one time-delay channel and triggering the marx with another time delay-channel. The marx module erection follows the trigger marx with a total jitter of ±5 ns. The parallel erection of 12 marx modules should have an extrapolated jitter spread of less than 20 ns.

The 6-Ω prototype water insulated transmission line has been tested to 900 kV. The integral current and voltage probes have been tested and calibrated. The prototype system uses fiber-optic technology for control and timing as well as monitoring spark gap

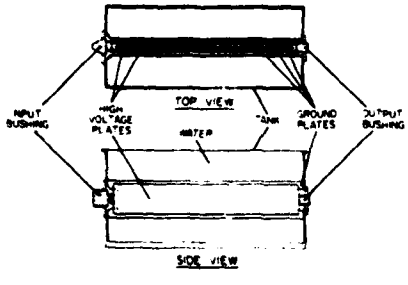


Fig. 9.
HDZP water insulated transmission line.

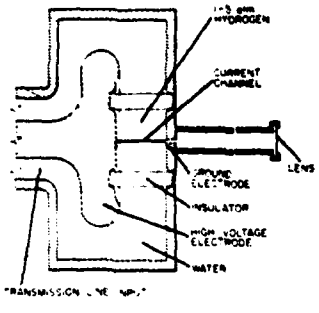


Fig. 10.
Initial HDZP gas load design.



Fig. 11.
Picture of HDZP prototype system.

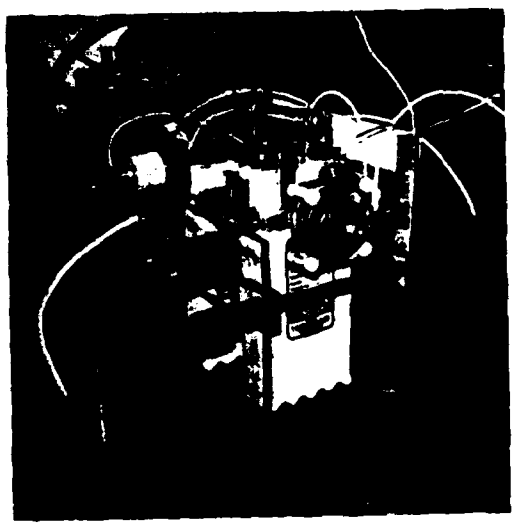


Fig. 12.
Prototype two-stage trigger marx.

control and timing as well as monitoring spark gap switching and laser pulse monitoring. The final HDZP system control will use air lines or fiber-optic links for all systems.

The HDZP system is now being constructed. The initial checkout of the parallel marx system is scheduled for the latter part of 1978. Plasma channel experiments should begin before 1979. The final HDZP system is illustrated in Fig. 13.

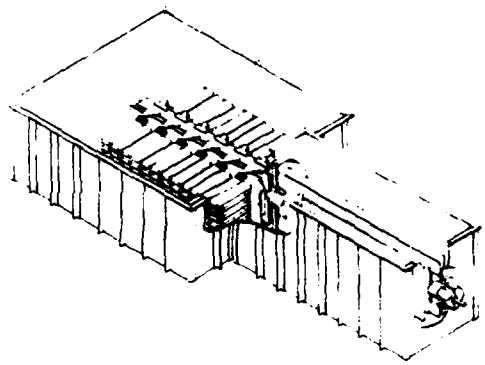


Fig. 13.
Illustration of HDZP system.

Reference

1. R. A. Fitch, "Marx and Marx-Like High-Voltage Generators," Maxwell Labs, Inc., IEEE Trans. on Nuclear Science NS18 4, (1971).

MG ENERGY STORAGE AND SWITCHED PULSE POWER SUPPLY

Karl I Selin

The JET Project, Abingdon, Oxon., U.K.

Abstract

For the JET (Joint European Torus) device there are four main pulse power supplies for the following loads:

(a) the poloidal field circuit
(b) the toroidal field magnets
(c) the plasma positioning
(d) the plasma additional heating.

The (a) supply will be described in this paper. It is presently in the design stage at GEC Machines Limited, U.K. and is scheduled for operation in 1982. A motor-generator with integrated rotor and flywheel will be used in a pulsed mode. The time between load pulses (9 minutes) is used for acceleration of the flywheel-generator. The generator output AC is rectified in a diode convertor. The nominal energy extracted from the flywheel-generator-convertor (FGC) is 2600 MJ at a maximum rate of 400 MW. A magnetic energy storage is included in order to reach a still larger load power.

Introduction

The purpose of the ohmic heating coil of the poloidal field circuit in a Tokamak plasma fusion device is to ignite the gas and to initiate and maintain a current in the hydrogen plasma in the Torus vessel. The coil is the primary winding of a transformer in which the plasma is the short-circuited secondary.

The rectified output current and voltage from the generator is shown in Fig. 1 for a typical experiment run with 3.9 MA in a D-shaped plasma. Also shown is the flux change required for the build-up of the plasma current.

Extensive system studies and generator design evaluations have been made to ascertain that the speed of response of the generator through excitation control is satisfactory and SCR control of the generator output is not necessary.

An experimental run will last a few, up to 20 s. During the pulse the generator and its magnetic circuit shall facilitate a change of 400 MW and 6 kV in 0.4 s and shall be able to supply a power integral of 2600 MJ (722 MWh).

MG Kinetic Energy Storage

Considering the pulsing of the JET device every 10 minutes it is feasible to store the energy in the generator prior to the pulse and to extract the energy through a speed drop during the pulse. A speed drop of 50% from 225 rpm to 112.5 rpm releases the rated energy of the system, 2600 MJ. The moment of inertia is 13100 tonnes m^2 and the weight of the rotor is 795 tonnes. For starting the set and for the acceleration between pulses the following drive schemes could be used: induction motor with wound rotor connected to a liquid rheostat - induction motor with slipring energy recovery - static variable frequency supply feeding into generator armature winding.

In the present design there is a slipring induction motor mounted above the top bearing. It has 26 poles and is rated 8.8 MW continuous, which may be compared with the peak power of 300 MW in Fig. 1a.

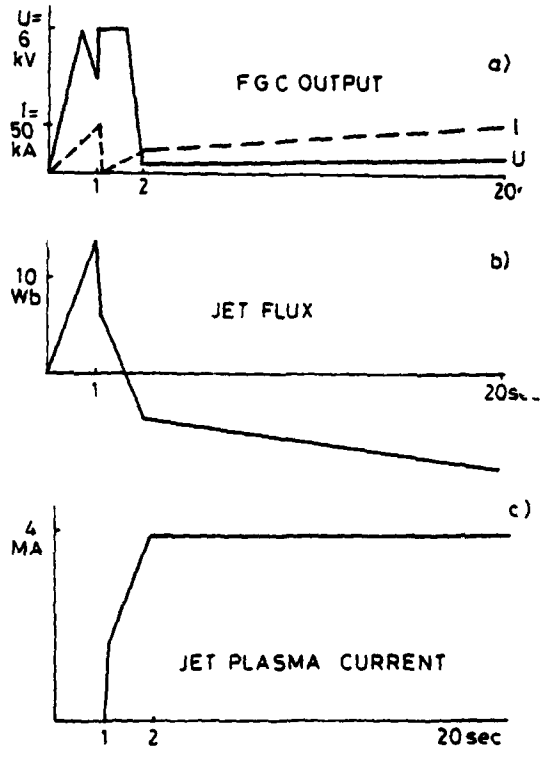


Fig. 1a) The rectified output voltage and current from the generator
Fig. 1b) The flux of the central column
Fig. 1c) The toroidal current in the plasma

The energy is stored kinetically in the slow rotation of a vertical shaft body. The power output is regulated by the generator exciter. The hydroelectric type of generator with a vertical shaft transmits torque easier to the surroundings as compared with a horizontal shaft machine. Normally there are no critical speeds to pass through and the speed excursion is therefore not mechanically limited as can be the case with a horizontal shaft arrangement having a number of resonance frequencies. With 48 poles the speed range corresponds to an induced electric frequency of 90-45 Hz. The generator and convertor will be erected in a deep pit of 20 m diameter.

The large air gap diameter (about 10 m) and the heavy rotor rim facilitates a large inertia. The laminated rotor rim is made of steel sheet metal, it extends below and above the poles and it is assembled in situ. The pole-rim fixing and pole end plates and the Tee heads whereby the poles are attached to the rim are problems of a safe mechanical fatigue stress design.

CH1371-4/78/0000-0293$00.75 ©1978 IEEE

The centrifugal force on each pole weighing 886 kg (160 kg of field winding copper) is 2472000 N at the maximum speed of 121 m/s in air gap.

The vertical shaft is supported on a thrust bearing below the rim and by guide bearings above and below the rim.

In view of the pulse duty (6 pulses per hour) the stator core will be built on site in a complete circle without joints. Then the stator winding also will be completed on site. The stator will be lowered on the rotor built in the generator pit. There are two 3-phase stator windings each one supplying a 6-pulse Graetz bridge rectifier. The induced voltages are in phase and the rectified voltage has a 6-pulse character.

The electrical voltage/current/power output is limited by the generator exciter and ultimately by the magnetic saturation curve shown in Fig. 3. A static exciter system will be used rated 1.2 kV and 2.8 kA/22 s and 5.6 kA/5 s.

The overall maximum output power is about 400 MW which is not enough for the JET experiment for which the poloidal field peak power is 40 kV x 80 kA = 3.2 GW. A power amplification is made through an inductive energy storage. The pulse sequence is shown in Fig.4 where positive power is defined directed to the JET Device.

Power modulation

The power modulation is done by a rather complicated circuit in which are combined both the ohmic heating and the equilibrium coils; a simplified equivalent circuit is shown in Fig. 5. The switching network and the static exciter of the generator co-operate in shaping the power pulse at the terminals of the JET device whose equivalent resistance and inductance change drastically during the pulse; following gas breakdown the coils and plasma is equivalent to about 60 mH and 10 mΩ for this experimental scenario.

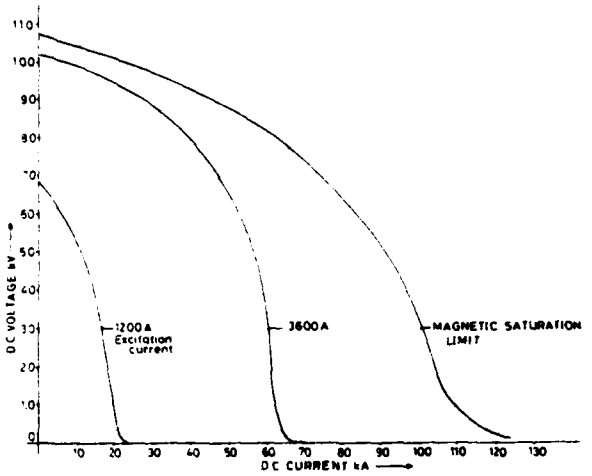


Fig. 3: Generator-Convertor output at two values of field current and at magnetic saturation

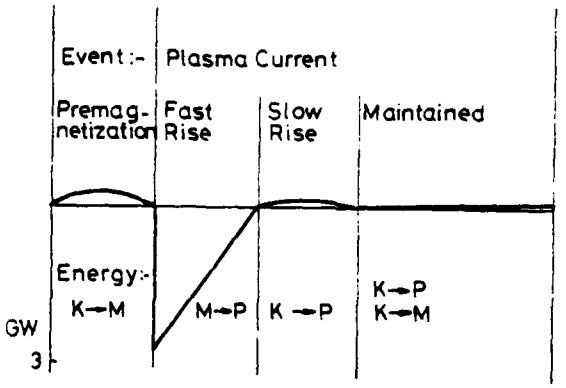


Fig. 4: Energy Conversion at Load Terminals
K = Kinetic, M = Magnetic, P = Plasma

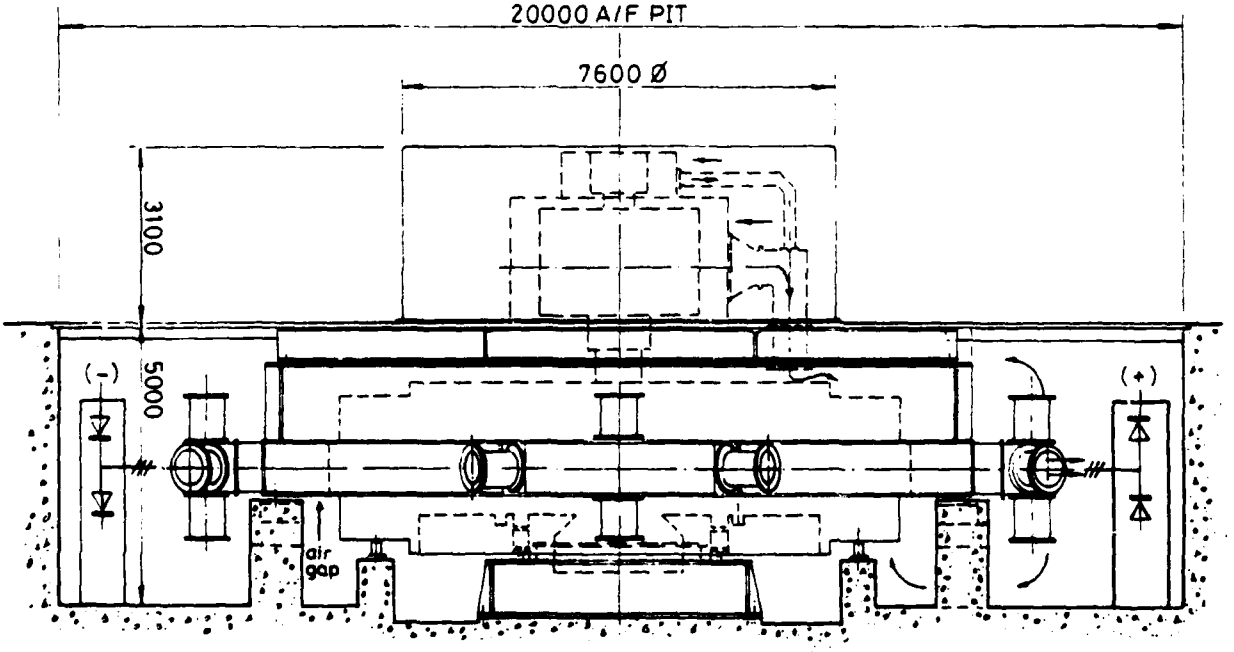
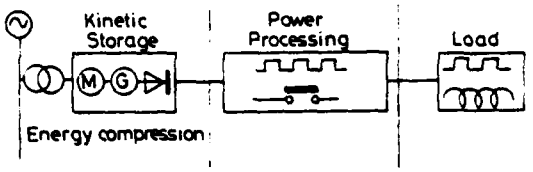


Fig. 2: Flywheel-Generator with vertical shaft mounted in pit together with output convertors



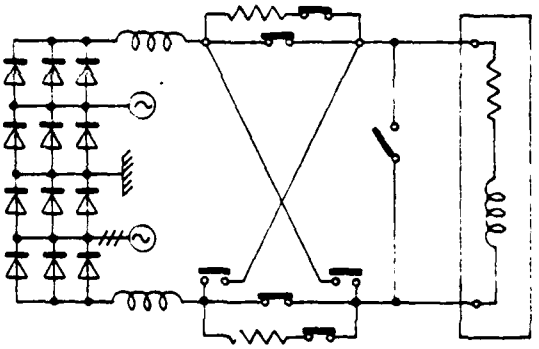


Fig.5: The FGC supplying the switching network and the poloidal field coils

The switched resistive network between the generator-convertor and the JET device performs in three ways: (1) It makes a direct connection from the power supply to the device for magnetization. (2) It switches resistors into the high current circuit, thereby creating a high voltage demagnetizing effect and a turn voltage in the vessel high enough for gas breakdown and plasma heating. (3) In the third phase it changes the polarity of the convertor connections relative to the JET terminals in order to magnetize the core in the opposite direction.

The main switch of the 2nd phase is shown in Fig. 6 and in Fig.7 are performance oscillograms of voltage and current during a switch opening test.

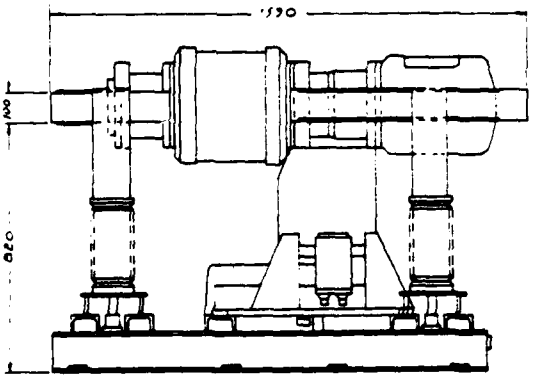


Fig. 6: Circuit Breaker AP 4970 revised for OH service

The AEG circuit breaker AP 4970 was developed in Germany by AEG as a back-up breaker for high current test laboratories. It has a peak current carrying capability asymmetric AC of 400 kA. It can switch (break) 120 kA DC when aided by capacitor current commutation. The air pressure in the chamber is 80 bar. The contacts begin to open within 7 ms from

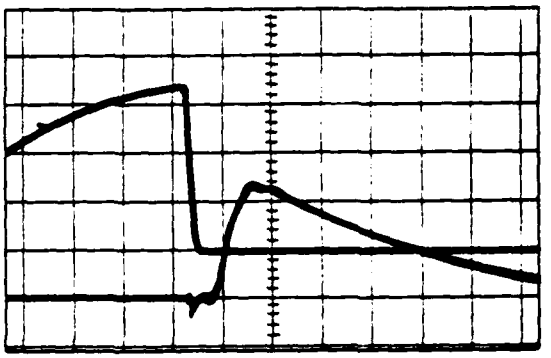


Fig. 7: Current and voltage in the circuit breaker during test. The current drops from 70 kA to zero in 200μs through capacitor discharge. Lower curve shows recovery voltage of 23 kV. Scale per square: 20 kA, 9.5 kV, 1 ms.

the time of tripping with a jitter less than ± 40 μs. The contact opening speed is 12 m/s.

Economics of a Rotating vs a Static Pulse Power Supply

A generator power supply of this size with auxiliaries, generator house, etc., costs about 15 £/kW or 2.1 £/kJ. If a power line (400 kV or above) is available near the test site it may be possible to supply the load directly by a number of mixed rectifier and SCR bridges. As compared with a power supply from the mains the power available from a MG set is speed dependent; if the generator is magnetically fully utilized at top speed the peak power (or voltage) available is proportional to the shaft speed; with a 50% speed drop the available generator voltage and power drops correspondingly.

Assuming a "minimum" installation in which a 400 kV circuit breaker, a step-down transformer and the diode-thyristor transformers and convertors are included, the installation cost would be about £11/kW.

The differential or marginal capital cost for stored energy for a vertical shaft energy machine is about 20% of the average. For a supply from the mains it is even less since it only influences the thermal rating of the transformers. For very large energy demands the installation cost of a mains supply will ultimately prove to be cheaper (assuming a reactive power compensation can be avoided).

The electricity bill for the FGC reported could be (10,000 pulses of full energy) 0.28 M£/year. The static system would have a higher efficiency. Therefore the cost of energy may be only 0.15 M£. On the other hand, the cost of peak power (400 MW) when the load is directly supplied from the mains would be 0.33 M£/year.

Technical Limitations of a Static Pulse Power Supply

Decisive for the choice between a rotating and a static power supply, apart from closeness to a power line, is the ability of the network to supply large power, large power derivatives and reactive power swings. The network available at the JET site does not allow the type of pulse power needed for the poloidal field load to be supplied from the mains. The reactive load power demand may be diminished through over-sizing the system components. Otherwise a local installation of variable reactive power generation is needed. Switched capacitors are suitable for this purpose but their

capital cost (about 10£/kVAR) is such that it can decisively influence the choice of the pulse power source. Another method used for reactive power compensation, is capacitors connected in series with the pulse load. As the load most often is transformer connected the ferro-resonance state of the third subharmonic is easily excited. Consequently the voltage monitoring becomes important and attenuating resistors must eventually be switched in parallel to the series capacitor.

Summary

A generator and circuit is described for ignition of about 200 m^2. of magnetically confined hydrogen plasma and for induction of about 4 MA of plasma current in a Tokamak plasma vessel. The magnetic field coil inducing the plasma current will be supplied from a generator of 400 MW peak power presently in the design stage at GEC Machines Limited, U.K. The generator output voltage can be varied up to 20-40 kV/s at currents from 0-80 kA through generator excitation control. The kinetically stored energy will be 3500 MJ of which 2600 MJ can be exhausted through a speed drop from 225 rpm to half speed. The integrated rotor-flywheel will be mechanically designed for 100,000 pulses; its rim will be constructed from sheath metal and will be erected at the site of the experiment. The stator and winding will also be assembled in situ.

A peak load power of 3200 MW is attained through a switching network in which an inductive energy storage is incorporated and a power magnification of eight times is reached. The main switching is made by an air blast circuit breaker. Alternative circuits are being considered and evaluated from the standpoint of the number of switches, current drain, energy losses and severity of fault conditions for the protection of the power supply.

The JET Project is sited near one of the CEGB 400 kV lines and its high pulse loading capacity will be used for other pulse loads of the JET device.

REFERENCES

1 The JET Design Team "The JET Project - Design Proposal for the Joint European Torus" EUR-5516e 1976

2 K Kriechbaum "A half cycle air blast generator breaker for high power testing fields" IEEE Transactions Vol. PAS-91, No.3 pp.747-753.

HIGH-VOLTAGE PULSER DEVELOPMENT

by

Harold Watson
AiResearch Manufacturing Company of California
Torrance, California

Abstract

This paper highlights the development of a pulse generator that utilizes a single, midplane, triggered spark gap (TSG) to discharge a pulse-forming network (PFN) into a CS_2 laser cavity load.

The PFN is a four-section line pulser. When charged to 116 kv, it can discharge 300 joules in 700 nsec, full width half maximum (FWHM). The system operates at 0 to 50 pps.

In designing the PFN inductors, the pulse rise time was kept long enough to avoid excessive ringing in the output cables. Such ringing can cause arcing in the cavity or damage to the cables themselves. The PFN capacitors were potted into a coaxial configuration to minimize inductance.

As the pulse repetition rate increases or the charge duration decreases, special consideration must be given to design of the midplane TSG voltage grading network to ensure the trigger electrode always stays at some set fraction of the PFN voltage during charge. This paper describes a circuit that makes operation of the grading network independent of frequency and charge duration, within certain limits.

Tests were run in synthetic air and in nitrogen to evaluate operating voltage and the amount of jitter and misfire as a function of pressure.

The work was partially supported by the U.S. Energy Research and Development Administration under contract number EY-77-C-04-3745.

Introduction

The objective was to design and build a device to furnish pulse power to the cavity of a pulsed electron-beam electric discharge CS_2 laser. The specifications are shown in Table 1.

The circuit was kept simple by using a single TSG and PFN that can operate up to a relatively high voltage, 116 kv. To keep the structure and lead inductance from being too large, the assembly was designed to operate in pressurized nitrogen. A pressure vessel was designed for up to 80 psig to accommodate the assembly.

The system was required to produce pulses with energy from 100 to 300 joules at 0 to 50 pps. The PFN voltage was varied to change the energy in the pulse. The PFN employed was a four-section line pulser, discharged with a nonsealed, midplane-triggered, spark gap.

Normally, TSG's do not perform well over a large voltage range, e.g., 80 percent of the static breakdown may be considered the best operating voltage (V_o). If V_o is higher, the TSG may self-fire and if it is lower, the jitter may be too high. If it is too low, the TSG may not turn on at all.

To get the nonsealed TSG to operate over the voltage range needed to produce the 3-to-1 energy range, the pressure was changed in the tank. In this way, the optimum operating voltage on the TSG could be externally adjusted to match the voltage needed to produce the desired energy.

The requirements for the PFN are not unusual. However, there are some interesting tradeoffs when the PFN voltage is very high and when the load impedance becomes low enough that the load inductance and the internal inductance of the capacitors and the output cables become a significant part of the PFN.

Table 1

Specification

General	
Pulse repetition rate	0 to 50 pps
Number of pulses per burst	10,000
Switch life	10^6 pulses
Pulse length (FWHM)	700 nsec
Rise time	100 nsec (10 to 90 percent)
Fall time	unspecified
Jitter	±100 nsec
Ambient temperature	10 to 30 C
Performance repeatability	90 percent
Condition 1	
Pulse repetition rate	0 to 17 pps
Energy per pulse	300 joules
PFN voltage	116 kv
Load voltage	58 kv
Condition 2	
Pulse repetition rate	17 to 50 pps
Energy per pulse	100 joules
PFN voltage	67 kv
Load voltage	33.5 kv

Notes:

1. The PFN cannot be matched over the full power level because of the power characteristics of the cavity. The high power level mismatch was chosen to realize more cavity voltage for a given PFN voltage.
2. The above numbers are design goals.

In addition, when operating the midplane TSG with a PFN that is being charged up in a relatively short time, (in this case ac resonant charging is used to charge it in 7.5 msec) it may be difficult to keep the midplane voltage at a set percentage of the PFN voltage during the charge. To make it work under this condition, the usual low-rate circuitry had to be modified.

Pulse-Forming Network

The PFN is a four-section line pulser. Although it is fairly standard, several interesting design tradeoffs were required to produce a reasonably good 700-nsec, 300-joule pulse from a 116-kv PFN at a load 5 ft from the pulser.

Because the inductance per section is so low, less than 700 nanonenries (nh), any inductance in the output cables, plugs and jacks, and load becomes a significant part of the PFN circuit. The total inductance and capacitance needed to produce the 300-joule pulse is as follows:

$$L_{total} = (tp/2)^2 V^2/2\varepsilon = 2.74 \text{ uh}$$

$$C_{total} = 2\varepsilon/V^2 = 0.0446 \text{ uf}$$

CH1371-4/78/0000-0297$00.75 © 1978 IEEE

where

ϵ = 300 joules of energy in pulse

V = 116-kv PFN voltage

tp = 700 nsec pulse duration

In addition, with a large mismatch between the cables and the load, high-frequency ringing in the cables could be high enough to either damage the cables or cause arcing in the load if the relative inductance between the output capacitor and the output cables is too low or if the mutual inductance between PFN coils is too high.

For this application, two parallel 5-ft cables with a total impedance of 26 ohms were used to connect the pulser with a 7.8-ohm load. This was mainly to lower the cable inductance, but it also lowered the inductance in the cavity by allowing the power to be fed into two places in the cavity.

Inductance from the two cables plus load and plugs and jacks was calculated to be approximately 350 nh—250 nh for the cable and 100 nh for plugs, jacks, and cavity load. (The plugs were designed for low inductance.) The total cable capacitance is 350 pf.

Partly because of the potential problem of ringing in the cables, the PFN was designed with just enough mutual inductance between coils to cancel out the internal inductance of the capacitors. This has the effect of creating a PFN without any mutual inductance between coils. As the mutual inductance is lowered, the rise and fall times will increase. This in turn reduces ringing in the cable. Past experience indicates a PFN without mutual inductance would produce a pulse shape acceptable for this application.

Figure 1 shows the ideal equivalent circuit of a four-section line pulser defined by Perkins (ref 1). If all capacitors in this figure are equal, the best (most rectangular) pulse occurs when there is significant magnetic coupling between neighboring coils, but insignificant coupling between any other coils. This mutual inductance shows up in the equivalent circuit as a negative inductance in series with capacitors 2, 3, and 4 and their respective internal inductance, L_c. When the capacitor inductance is significant, it must be considered as part of the circuit. Therefore, the sum of the mutual and capacitive inductances should be negative; it also should equal 5 to 15 percent of the self-inductance of the two coils that cause the mutual inductance.

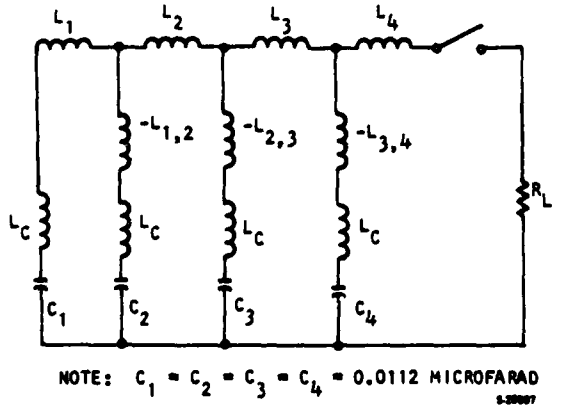


Fig. 1. Equivalent circuit of line pulser

Capacitors

The capacitors in a partial coaxial configuration (Figure 2) had a calculated inductance of approximately 61.3 nh.

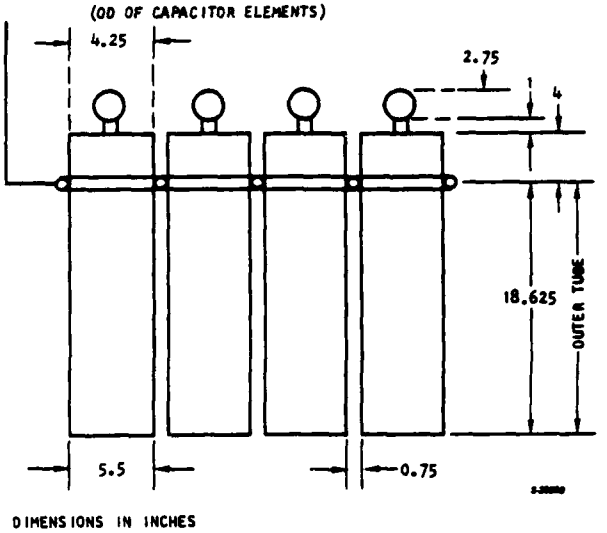


Fig. 2. Side view of PFN capacitors

These capacitors are rated at 150 kv and 0.0112 μf; they are made in multiple series sections by Condenser Products Inc. of Florida. Each section looks like a large hockey puck with a small hole in the center. They are connected by pressure in such a way that all sections stacked together make up an almost solid cylindrical element. When current flows uniformly through all the elements, its internal inductance becomes a significant value. Capacitor inductance can be calculated from the following equation, partly derived from the work of M. Zaret (ref. 2).

$$L = L_{ext} + L_{int} = \frac{\mu_V}{2\pi}\left\{\ln \frac{r_2}{r_1} + \frac{A_2}{4A_1}\right\} L/L_m = \quad (1)$$

30.84 nh + 30.46 nh = 61.3 nh

where

L_{ext} = inductance due to flux from the outside of the cylinder to the boundary

L_{int} = inductance due to flux in the cylinder minus the small hole

μ_V = permeability of a vacuum, $4\pi \times 10^{-7}$ henry/meter

A_1 = cross sectional area of small hole, $\pi/4$

A_2 = cross sectional area of cylinder without hole $4.25^2\pi/4$

L = length of element, 18 and 4 in.

L_m = inches in one meter 39.4 in.

r_2 = radius or distance to boundaries, $\frac{5.5}{2}$ and $\frac{7}{2}$ in. (The inductance had to be calculated for two sections of the capacitor, see Figure 2.)

r_1 = radius of the sections

A full coaxial configuration would have given 56 nh; however, the outer tube would have had to extend to the top, and this may have compromised the high-voltage integrity of the assembly. Capacitors with 40 nh were available, but the 4-month delivery time was prohibitive. In addition, they cost 43 percent more and some potting may still have been necessary.

Inductors

A long helix-type inductor was designed with the correct inductance of 2.7 μh for the 700-nsec pulse. Each section, (L_1, L_2, etc.) had an even number of turns. In addition, it had a mutual inductance at each capacitor, which was approximately equal to the capacitor inductance.

To make the mutual inductance approximately equal to the capacitor inductance, it had to be made lower than usual. This was done by keeping the number of turns low so the distance between loops was large enough to achieve low mutual inductance. To make up for the loss in inductance, the diameter of the conductor was kept small; therefore, the self-inductance of each loop was relatively high. In designing the helix and mutual inductance, the equations and tables of Grover were used (ref. 3).

Although the design selected had slightly less than 61 nh of mutual inductance, it had enough to cancel out most of the capacitor inductance. Therefore, the sum of the mutual and capacitor inductances was low enough to make the PFN act as if there were no inductance. The design used type RG-16/u cable without the shield for the conductor; properties of this helix coil are defined as follows:

Mechanical Parameters	Electrical Parameters
Conductor diameter = 1/8 in.	L_c = 62 nh
Number of turns = 8	
Coil diameter = 4.5 in.	L_m = 39 nh (note: $L_c - L_m$ = +23 nh)
Coil length = 20 in.	L_s = 631.5 nh (L_S = $L_1 = L_2 = L_3$)
Pitch = 2.5 in.	L = 2.694 μh (for full helix)
Conductor-to-conductor distance = 2.38 in.	

Note: $L_c \neq L_m$, but the percent of difference is low. For example,

$$\frac{L_c - L_m}{L_2 + L_3} \times 100 = 1.8 \text{ percent} \qquad (2)$$

In the actual PFN, the helix was simulated by four separate coils. Since the insulation on the cable was stiff, no structure was needed to hold the coils in place; however, this feature also made it difficult to form the coils. Consequently, the final assembly deviated somewhat from the helix design.

The output inductor was designed to equal 350 nh; therefore, the external inductance was included as part of the PFN. The actual output is shown in Figure 3. Except for cable-ringing, it compares favorably to the waveshape taken on a test PFN. The test PFN comprised four 10-μf capacitors and four 624-nh toroidal inductors. (Because the flux is contained there is no mutual inductance.) Note that such a PFN has approximately 44 percent more peak power than one that puts out the more rectangular pulse, or

$$\frac{(I_2^2 - I_1^2)R}{I_1^2 R} \times 100 = 44 \text{ percent} \qquad (3)$$

where

I_2 = the peak current of the nonoptimum PFN

I_1 = the peak current of the optimum PFN

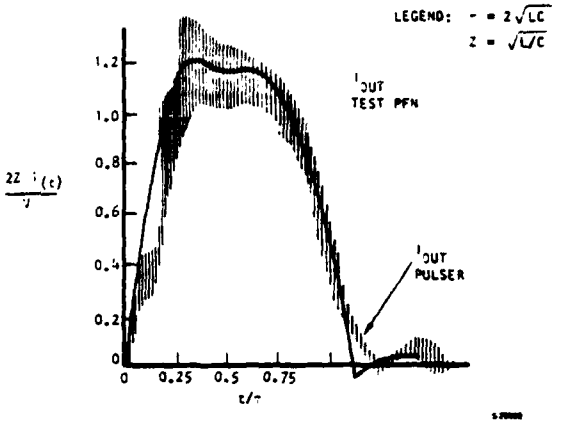


Fig. 3. Current from pulser vs current in four-section test PFN

As a matter of interest, several helix coils were designed to see if it were possible to realize the needed 5 percent minimum equivalent negative inductance. The conclusion was that even with the best available capacitors of 40 nh inductance, it would have been difficult.

Main Discharge Switch

A single gap, or distortion gap, type of triggered spark gap is used to discharge the PFN. The TSG, made by the Ion Physics Corporation, is shown in Figure 4. Elkonite electrodes were used to increase the life; to date, there have been approximately 10,000 shots on the TSG with very little noticeable electrode ablation. (The switch is designed for 10^6 shots, for a total of 5173 coulombs of charge transfer at the 300-joule pulse level. This sintered Elkonite mix comprised 75 percent tungsten and 25 percent copper by weight, and 58 percent tungsten and 42 percent copper by volume.

A spark gap made of a similar mix has been able to accommodate up to 28,000 coulombs in a recent research spark gap program (ref 3). Although operating conditions are different, there is a strong possibility such a design will accommodate the required 5173 coulombs.

Ion Physics Corporation had to slightly modify the TSG for operation at this voltage. This amounted to changing the radius slightly on the electrodes. The final product is outlined in Figure 4.

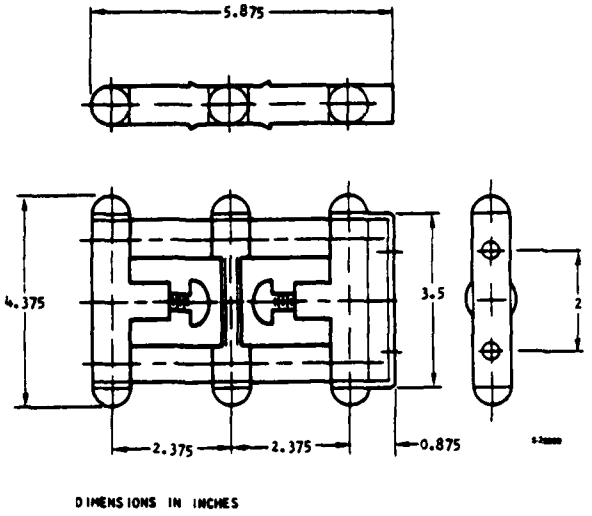


Fig. 4. Main discharge switch

TSG Grading Network

Special consideration had to be given to the midplane biasing and triggering network because the PFN was being resonantly charged in approximately 7.5 msec.

Figure 5 shows the midplane TSG with trigger circuit. Resistors R_1 and R_2 are used to hold the trigger electrode at 1/2 V . This fraction of V should remain constant during and after charge; however, if the circuit time constant (τ) is greater than 0.1 times the charge time constant (t_{chg}), a misfire can occur.

CIRCUIT TIME CONSTANT:

$$\left\{(R_1 \| R_2) + R_4 + R_5\right\} C_2 = \tau$$

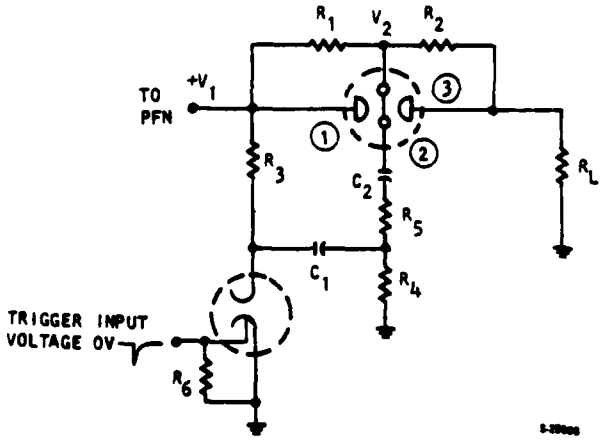


Fig. 5. Midplane TSG with trigger circuit

If the voltage drops below 1/2 V_1 by a large enough amount, it will overstress gaps 1 and 2 and cause prefire during t_{chg}. Figure 6 illustrates what happens if the time constants are not right. The top wave represents a typical resonant charge of the PFN. The next wave is half of the PFN voltage all during t_{chg}. This is the desired condition. The bottom wave shows what can happen if τ is too long.

ACCEPTABLE CONDITION FOR MIDPLANE CHARGING VOLTAGE:

$$V_2 = (0.955)\left(\tfrac{1}{2} V_1\right), \text{ if } \tau = 0.1\ t_{chg}$$

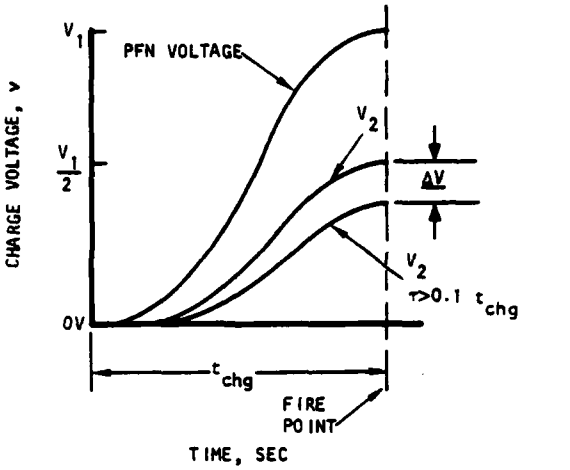


Fig. 6. Charge voltage on PFN and V_2 in figs. 5 and 7

For the circuit in Figure 5, the voltage can be expressed as follows if the PFN is resonantly charged:

$$V_{PFN_{(t)}} = V_{(t)} = V_o\,(1 - \cos \omega t)/2 \qquad (4)$$

In this case, the voltage on the midplane V_2 can be found any time during the charge in the following manner:

$$V_{2(t)} = \frac{V_o\,\omega RC}{4\left[(\omega RC)^2 + 1\right]} \left\{\omega RC(1 - e^{-t/RC}) + \frac{1}{\omega RC}(1 - \cos\omega t) - \sin\omega t\right\} \qquad (5)$$

$$V_2 = V_o \left\{(\omega RC)^2(1 - e^{-t/RC}) + 2\right\} / \; 4\left\{(\omega RC)^2 + 1\right\} \qquad (6)$$

where

$V_{2(t)}$ = voltage on midplane during charge

V_2 = peak voltage on midplane

V_o = peak voltage on the PFN

$R = R_1 \| R_2 + R_4 + R_5$

$C = C_2$

$\omega = 2\pi/2t_p = \pi/t_p$

t = time, sec

It may be impractical to decrease C_2 or R to lower τ in circuits where t_{chg} is too short. If C_2 is too low, there may be insufficient charge to turn on the TSG; if R is too low, the power losses, especially at high voltage, may be too high. An improved circuit is shown in Figure 7.

The voltage grading system was modified to make it less sensitive to frequency. This is basically a capacitive divider; when $C_2 = C_3$, the charge voltage tends to divide up in such a way as to keep V_2 at 1/2 V_1 all during t_{chg}.

$$V_{2(t)} \approx V_{PFN(t)} \, C_1/(C_1 + C_2) \qquad (7)$$

where V_2 = the voltage on the trigger electrode of the TSG.

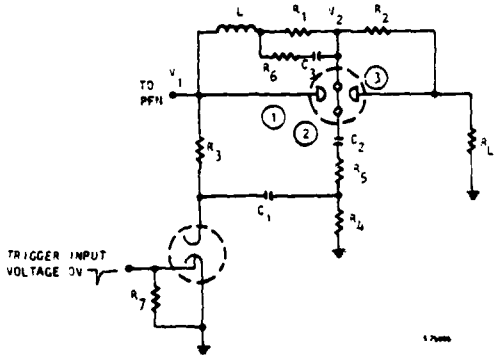


Fig. 7. Midplane TSG with modified grading network

Because R_4, R_5, and R_6 are relatively small, they drop little voltage while C_2 is being charged. Thus, they can be neglected as far as the t_{chg} period is concerned. The function of the inductor, L, is to keep C_3 from putting a capacitive load on the trigger circuit. However, it's reactance must be low during the charge period to keep from introducing a significant reactive voltage drop.

Inductor L is effectively in series with C_3. It therefore must be designed with a low interwinding capacitance to prevent overloading the trigger circuit.

Pulser System Circuit

As shown in the pulser system circuit, Figure 8, the trigger circuit consists of an SCR pulse generator driving a hydrogen thyratron. The thyratron in turn drives a trigatron-type TSG that turns on the midplane TSG. In addition, an overvoltage gap (OVG) is used in case the TSG's prefire or if the load is missing due to a malfunction in the laser system. If this happens, the PFN will discharge through the OVG into R_9 and be ready for the next pulse.

The charging circuit always allows at least 3 msec of off time for the TSG's to recover before the PFN starts to recharge. In addition, to augment recovery, a small fan was placed next to each TSG to blow a small amount of gas across the gaps.

Results

All tests were done on a dummy resistive load of 7.8 ohm. Monitoring waveforms proved to be a difficult task because high-level radiation from the pulser and the load generated interference on the scope. For this reason, no definite percentage of the high frequency hash in Figure 3 can be attributed to cable ringing. The laser cavity should produce less EMI. In addition, improved EMI shielding of the scope should result in more representative results.



Fig. 8. Pulser generator circuit

Figures 9 and 10 show how the pulser operates in industrial-grade synthetic air and in nitrogen. The jitter is slightly worse in air than in nitrogen. Also, increased jitter was probably experienced because the trigatron was operated in an inferior mode, i.e., the trigger was driven negative while the anode was positive. This was an easy way to trigger the midplane; however, it undoubtedly added to the jitter and prefire problem. The 10 percent prefire does not preclude use of the pulser to power the CS_2 cavity. If prefire occurs before the E-beam turns on, the output voltage will be high enough to turn on the overvoltage gap. The energy will be absorbed in R_9 and the PFN will be ready to be charged up for the next pulse.

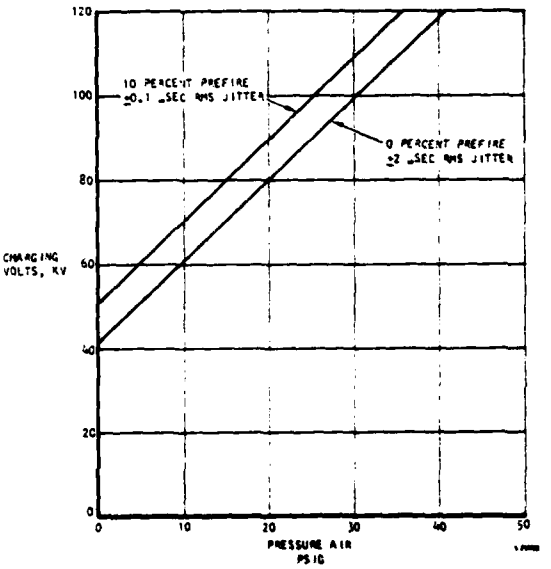


Fig. 9. CS_2 pulser performance in air

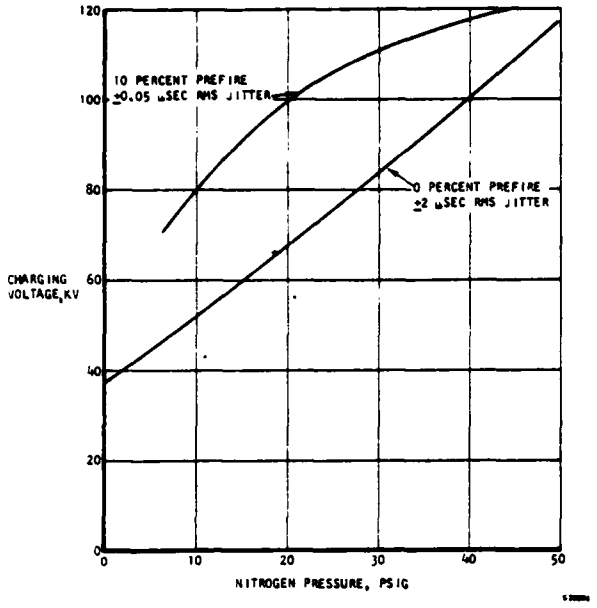


Fig. 10. CS_2 pulser performance in nitrogen

The original intent was to house the assembly in 80 psig of nitrogen when operating at full voltage; however, tests showed that the TSG gaps could be increased and the assembly could be operated with a pressure as low as 45 psig.

The assembly was well-shielded for corona. The first voltage tests showed it could be subjected to 50 kvdc in 1 atmosphere of air with no noticeable corona.

Conclusions

The pulser should work well for the purpose it was intended.

The waveform is not too rectangular; however, the peak power is significantly higher in this type of wave than in the better PFN, e.g., it is at least 44 percent higher. It may be that for the pulsed electron-beam electric discharge laser, this would produce the most laser power.

The PFN capacitors, made by Condenser Products, worked well in this circuit; however, this type is probably not the best-configured capacitor for low inductance because there is no way to lower the internal flux, and therefore the internal inductance.

In this laser, the operating voltage on the cavity is significantly below the static breakover point. Therefore, the cable-ringing on the pulse will probably be acceptable. If this ringing does present a problem, more inductance between the output of the PFN and the input of the cables would lower the ringing and probably would not appreciably increase the output pulse rise and fall time.

Recent work done to extend the useful life of TSG's makes them an inexpensive alternative to the thyratron, especially for applications that require very high voltages and short pulses (ref 4).

In this application, as the PFN voltage increases, the jitter decreases; however, the percentage of cycles with prefire increases. This high incidence of prefire is probably because the trigatron is not being operated in the best mode.

Acknowledgements

MAURICE FIALKOFF designed the packaging--a difficult task in view of the conflicting requirements of providing high voltage insulation, and at the same time keeping critical inductance low enough to realize a usable output pulse.

WALTER HENDRICKSON designed all the logic controls for the pulser as well as for the complete laser system.

ALAN MACKNIGHT, the project engineer on the CS_2 program, was involved in all phases of checkout and test evaluation. His assistance solving the high-voltage TSG problems helped considerably in checking out the pulser.

H. MILDE and G. TRIPOLI of Ion Physics Corporation contributed significantly by way of developing TSG's and basic trigger circuitry for the system.

References

1. Pulse Generators, G. Glasoe and J. Lebocay, editors, Dover Publications, New York, 1965, p. 205

2. Zaret, M., Electro-Magnetic Theory, Regents Publishing Inc., New York, 1965, p. 125

3. Grover, F. W., Inductance Calculations--Working Formulas and Tables, Dover Publications, New York, 1962

4. Clark, W., High Power Spark Gap Development, AFAPL, TR-75-41, May 1975

OPERATION OF A 300 kV, 100 Hz, 30 KW AVERAGE POWER PULSER*

M. T. Buttram and G. J. Rohwein
Sandia Laboratories, Albuquerque, New Mexico 87185

Introduction

Applications for efficient and reliable pulse power systems with long lifetimes (>10^8 shots) are foreseen for electron beam generators, ion beam accelerators and lasers leading eventually to inertially confined fusion reactors. These systems will have to be capable of continuous operation for sustained periods without requiring major maintenance or repair. High operating efficiency will be required not only to minimize power consumption but also to avoid heat build up and consequent damage to components. The system described in this paper represents an initial effort to develop an efficient energy handling high voltage pulser to study the problems of long life components.

General Description

The 350 kV, 35 kA, 30 ns, 100 pps accelerator, shown in Fig. 1, consists of a low voltage modulator section, a voltage step-up transformer, a pulse forming line (PFL), a high-voltage switch and a load resistor or diode. To date only the resistive load has been used. Figure 2 is an electrical schematic of the system. The modulator converts dc power at 11.5 kV to primary pulsed power at 21 kV by resonant charging a 1.5 uF capacitor from a 14.5 uF capacitor. The 1.5 uF capacitor is subsequently discharged through the primary of the voltage step-up transformer to charge the PFL to 700 kV. Near the peak of the charge cycle, the output switch self fires and energizes the load. At full voltage and 100 pps, the average power output of the system is 30 kW.

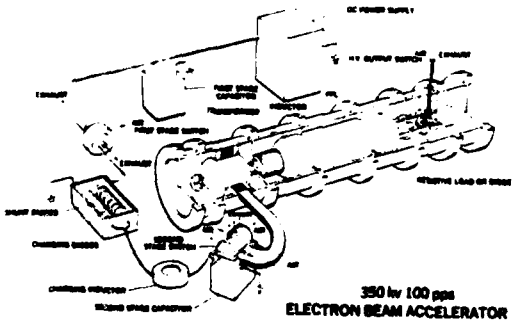


FIGURE 1.

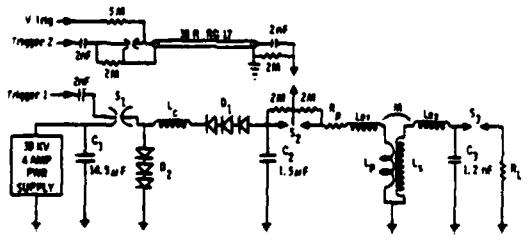


FIGURE 2.

Dual resonance transformer charging was chosen for this repetitive pulser application because of the high-energy transfer efficiency attainable with this method. In the present system, 94 percent of the energy stored in the 1.5 uF capacitor is transferred to the PFL. The 6 percent energy loss is dissipated in the 1.5 uF capacitor, the switch, and the transformer.

The complete pulser system has undergone tests lasting a few minutes at rates up to 100 pps and 30 kW average power. The longest continous run was one million shots at 40 pps and 7 kilowatts average power. A total of approximately 2 x 10^7 shots have been fired since the machine became operational. Throughout all the tests runs there have been no major component failures or damaging heat build up problems.

Low Voltage Section (Modulator)

A modulator was built into the low voltage section of the pulser to facilitate control of the pulse rate and operating voltage as well as to control the grace (no voltage) period on switch S_2 between the 1.5 uF capacitor and transformer.

The modulator consists of a 14.5 uF first stage capacitor (C_1) which resonantly charges the 1.5 uF second stage capacitor (C_2) through a diode stack, a 170 mH inductor and the first stage spark gap switch (S_1). With C_1 maintained at 11.5 kV, C_2 is charged to 21 kV for a 1.83 voltage ringing gain. The series diode stack, D_1, prevents reverse current flow between C_2 and C_1 before S_2 is fired. This allows S_1 to self extinguish when the charging current goes to zero and to be cleaned by continous flowing air for approximately 2 ms before S_2 is fired. The charging voltage waveform at C_2 is shown in Fig. 3.

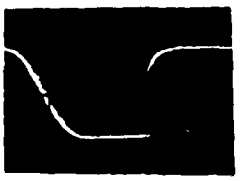


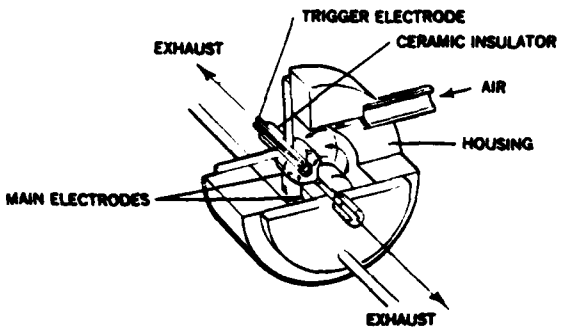
FIGURE 3.

During the dual resonance discharge cycle, a 54 percent voltage reversal occurs across C_2. The output electrode of S_1 is clamped to ground with a diode stack, D_2, during this reversal. Without the shunt diodes, S_1 would be required to stand off nearly twice the normal voltage or approximately 18 kV.

The switches S_1 and S_2 are shown in Figs. 4 and 5. Switch S_1 is a trigatron spark gap which operates at a maximum of 30 A. It has a tubular recessed trigger electrode insulated from the main electrode with a high strength alumina ceramic tube. By recessing the trigger electrode approximately 2 mm, it was found that erosion of the trigger electrode was virtually

*This work was supported by the U.S. Department of Energy, under Contract AT(29-1)-789.

CH1371-4/78/0000-0303$00.75 ©1978 IEEE



FIRST STAGE SWITCH

FIGURE 4.

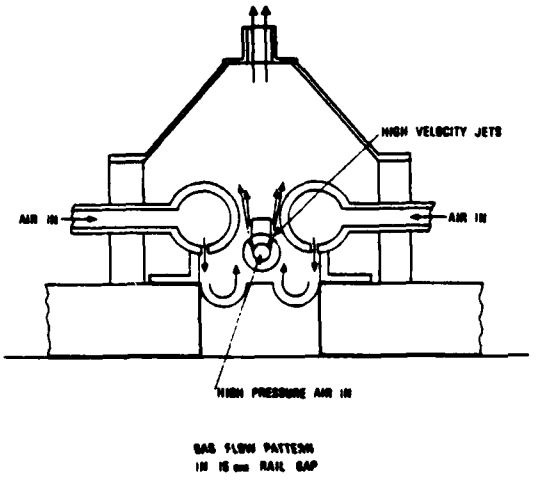


FIGURE 5.

eliminated. With copper main electrodes the tip of the ceramic tube will remain intact for greater than 10^6 shots before it is necessary to renew the end by light sanding to remove resolidified metallic electrode debris.

The switch housing is purged at a rate of approximately 10 SCFM with a continuous air stream which is introduced at the periphery of the acrylic housing cavity and forms a vortex flow pattern through the switch. Residual ionized gas and electrode debris are expelled from the switch through the center of both electrodes.

Switch S_2 is a 15 cm long rail gap with a 6 mm wide trigger bar backed by a perforated air distribution tube. At maximum power it operates at 21 kV and 32 kA. It has a polycarbonate housing and a brass cover through which the hot gas and debris are expelled. Cooling air is delivered to both the main electrodes and to the trigger electrode. The gap is continuously swept by air flow as indicated in Fig. 5. The jetting action from the perforations in the tube below the trigger bar draws air from below the main electrode uniformly up through both sides of the gap. This flow pattern not only effectively cools the electrodes but also prevents debris from being deposited anywhere on the insulating surfaces of the housing.

The gap is normally operated with a spacing of 4.8 mm on the high voltage side and 3 mm on the output side. It has a wide triggering range as illustrated in Fig. 6 which results in highly reliable performance when operated in the range of 50 to 60 percent of self break. The gap is triggered with a 50 Ω coaxial discharge cable coupled to the trigger electrode through a 2 nF capacitor and a peaking gap. With this arrangement the measured risetime of the trigger pulse is 3 ns and the switch typically fires with an average of two to three current channels.

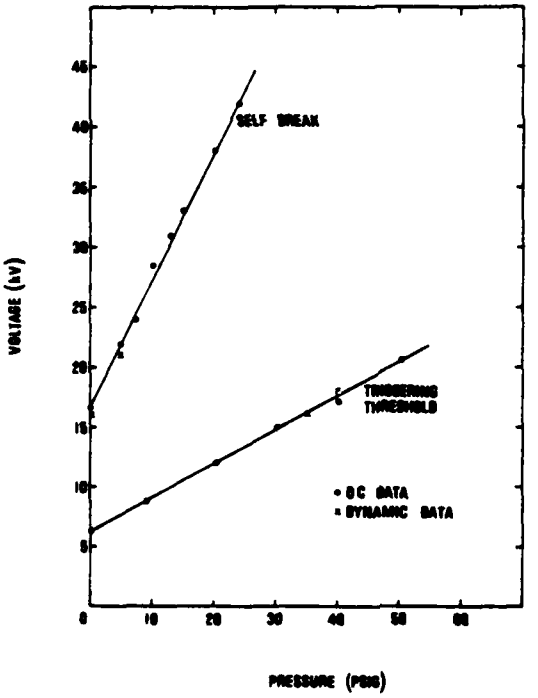


FIGURE 6.

Transformer and Pulse Forming Line

The PFL charging transformer (Fig. 7) is an air core spiral strip design with a 60 cm diameter single turn primary surrounding a 44 turn copper-mylar secondary winding. The width of both windings is 10 cm. The electric field on either side of the windings is constrained to a coaxial distribution by concentric field shaping rings on the core and case. This scheme minimizes the field enhancement at the edges of the spiral strip and prevents breakdowns which would otherwise occur from the edges of the secondary winding. At full voltage the winding stress is 125 kV/cm which should provide a life of greater than 10^9 shots. The external case, flanges and core are fiberglass reinforced epoxy composition with an epoxy filling between the field shaping rings. The windings and the open volume inside the transformer are impregnated with an oxidation inhibited mineral oil (Exxon 2930 x-ray oil). In separate tests this oil in combination with mylar-copper windings had a breakdown strength of 580 kV/cm. The ends of the transformer case are covered with 2.5 cm thick acrylic plates to confine the oil and support the ends of the core.

The transformer has a 1 μH primary inductance, a 1280 μH secondary inductance, and a 30 μH mutual

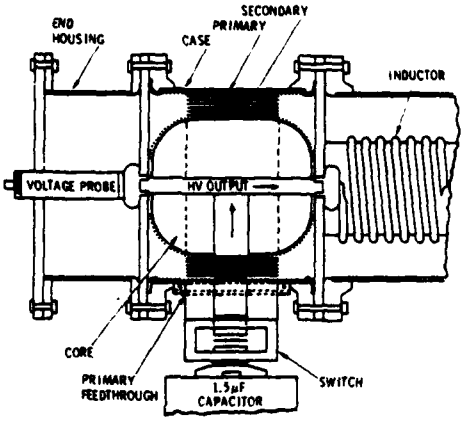


FIGURE 7.

inductance which results in a coupling coefficient of 0.84. To adapt the transformer to dual resonance charging, external inductances of 0.420 μH and 488 μH were added to the primary and secondary sections of the circuit, respectively, to match the frequencies and reduce the effective coupling coefficient to 0.6. (Dual resonance charging results when the primary and secondary frequencies are equal, i.e., $L_1C_1 = L_2C_2$, and the effective coupling coefficient of the transformer is 0.6. Under these conditions the maximum charge transfer occurs at the peak of the second or reverse voltage excursion of the secondary capacitor C_2. In a lossless system, 100 percent of the energy is transferred from C_1 to C_2.)[1-5] Figure 8 is a plot of the charging voltage on the PFL for this system. The measured transfer efficiency is 94 percent. A 21 kV charge on C_2 is required to reach 700 kV on the PFL.

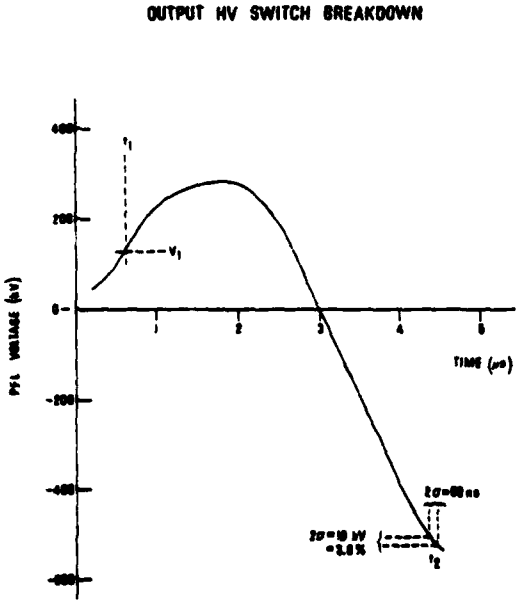


FIGURE 8.

The PFL is a 10 Ω oil-insulated, coaxial transmission line with inner and outer diameters of 46 and 61 cm, respectively. Its electrical length is 15 ns. It is connected to the transformer through the 488 μH tuning inductor, a helix of 12 gauge insulated wire wrapped on a 30 cm acrylic tube.

High Voltage Switch

The output high voltage switch is the untriggered gas spark gap shown in cross section in Fig. 9. Air was the dielectric for most of the work done to date although some data with SF_6 are now available. The maximum operating parameters for this switch are breakdown at 700 kV followed by a 35 kA current pulse lasting 30 ns (into a matched load). Minimum recovery time is 10 ms. With the exception of the current which is typically held in the range of 12 to 20 kA with an overmatched load these parameters have been achieved in short runs. Typical operating parameters have been 500 kV, 13 kA, 40 pps for the longer runs (in excess of 10^5 shots).

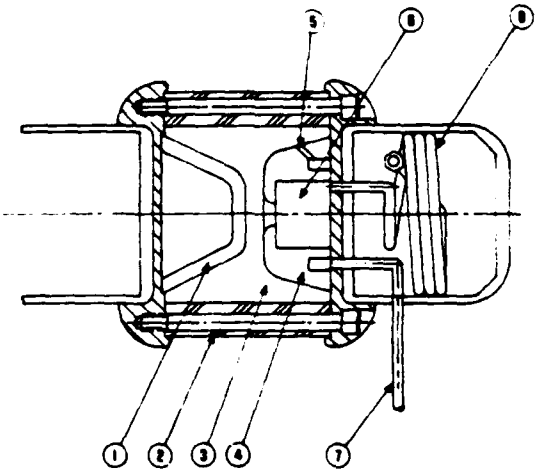


FIGURE 9.

The switch operates at pressures up to 10 atm with a gap length of 1.3 to 3.8 cm. Its cylindrical acrylic housing (2) has a 20 cm diameter and is 19 cm long. Compressed air or SF_6 is injected tangentially through two 1 cm ports in the acrylic wall (not shown in figure) and/or (4) through 8 ports in the large electrode (5) to form a rotary flow pattern which sweeps and cleans the housing. By this procedure housing damage in 2×10^7 shots has been reduced to a yellowing of the acrylic. There is no reason to believe that housing damage will limit the lifetime of this switch. Exhaust gas exits through the center of the large electrode passing through a copper cooling coil (8) located within the high voltage structure before entering nylon lines through the high field region. Because of a slight field enhancement, breakdown occurs over a 60 cm^2 band at the flat portion of the large electrode (1) during normal operation. In a stable operating regime the spark strikes randomly over this area from shot to shot. Grossly unstable operation (corresponding to a large spread in breakdown voltage including breakdown on the positive half cycle of the dual resonance waveform) is generally accompanied by a "settling in" of the spark at one spot on the electrodes. Presumably this spot becomes overheated weakening the

dielectric strength of the gas in its vicinity and switch performance degrades rapidly.

To achieve optimal power flow efficiency the spread in switch closure times must be minimized and the switch should close as close as possible to the peak of the charging voltage waveform. Because of the spread in breakdown times, closure too near to peak leads to ringovers, i.e., pulses in which the switch does not close. Ringovers must be minimized to avoid energy dissipation in sensitive elements of the pulser, particularly the transformer and second stage capacitor. The magnitude of the statistical spread in breakdown voltage determines the maximum fraction of peak PFL voltage at which the output switch may be operated.

Stability of the breakdown of the output switch is monitored as shown in Figs. 10 and 11. Voltage on the PFL (denoted by Vc_2 in the figures) is sampled by a capacitive probe. (Resistive probes are also used but have a tendency to overheat.) A start signal is generated by discriminator D_1 when the probe voltage crosses a preset threshold V_1 at time t_1. This threshold is set to be above the switching noise at t = 0. This signal starts a time-to-digital converter (TDC) which digitizes the elapsed time to a stop signal generated by differentiating the voltage waveform and triggering a descriminator on the rapid rise of the dv/dt waveform at time t_2. The digitized time interval (with a 5 ns least count) is fed through a CAMAC compatible interface to a PDP-11 computer.

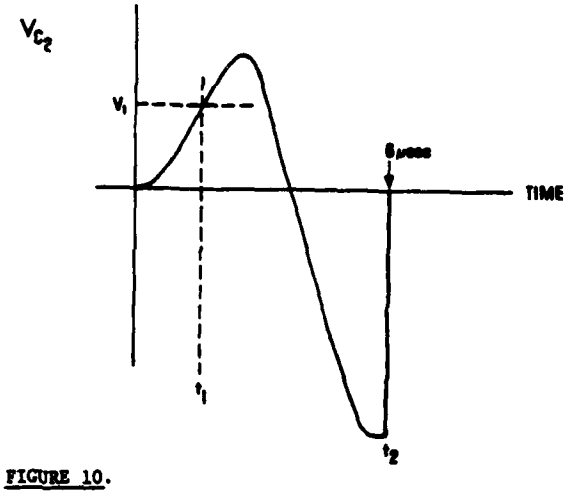


FIGURE 10.

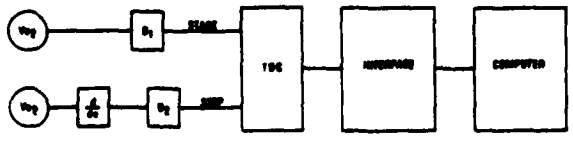


FIGURE 11.

Histograms of the type shown in Fig. 12 are produced online. This sequence is taken at a constant maximum PFL voltage of 530 kV and constant repetition frequency of 40 pps with a varying flow rate. For the lowest flow rate the distribution of breakdown times has a pronounced tail toward early time. This is accompanied by breakdown on the positive portion of the charging waveform (prefires). As the gas flow

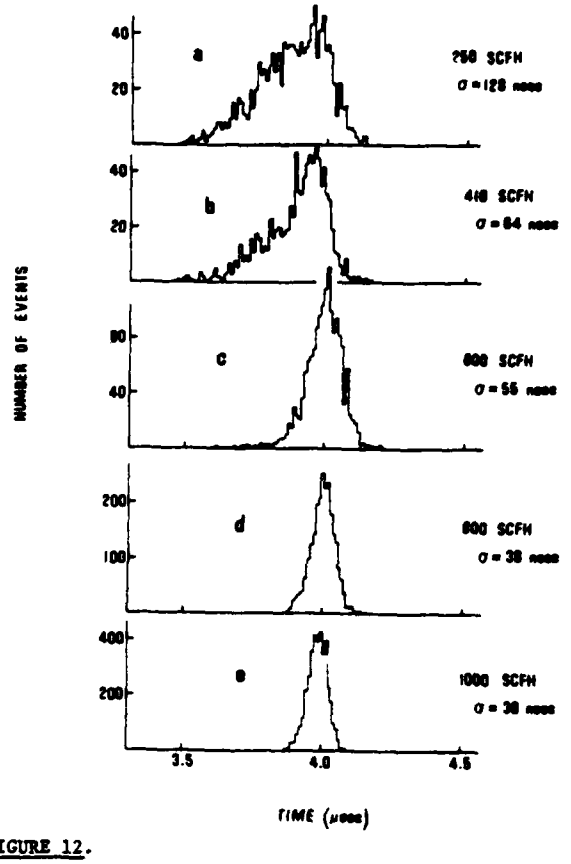


FIGURE 12.

rate is increased, the early time tail and prefires vanish leaving an approximately Gaussian distribution. Figure 13 illustrates this approach to stability by plotting the standard deviation of the breakdown time distribution versus flow rate. Stable switch operation requires a gas flow rate corresponding to the flat portion of the curve. In this regime there are no breakdowns outside the normal tails of the Gaussian distribution.

Figure 14 displays the time distribution for a run of 10^6 consecutive shots overlaid with a Gaussian matched to the data. The standard deviation for these

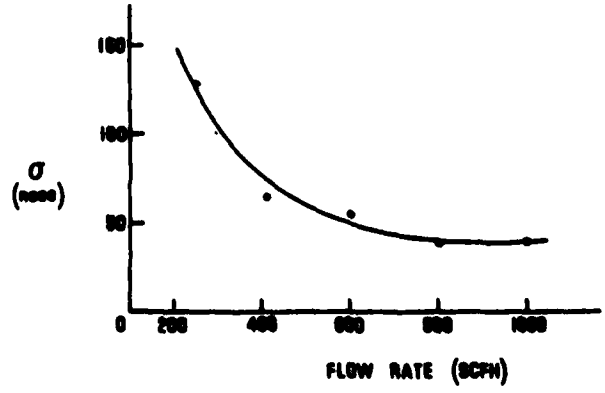


FIGURE 13.

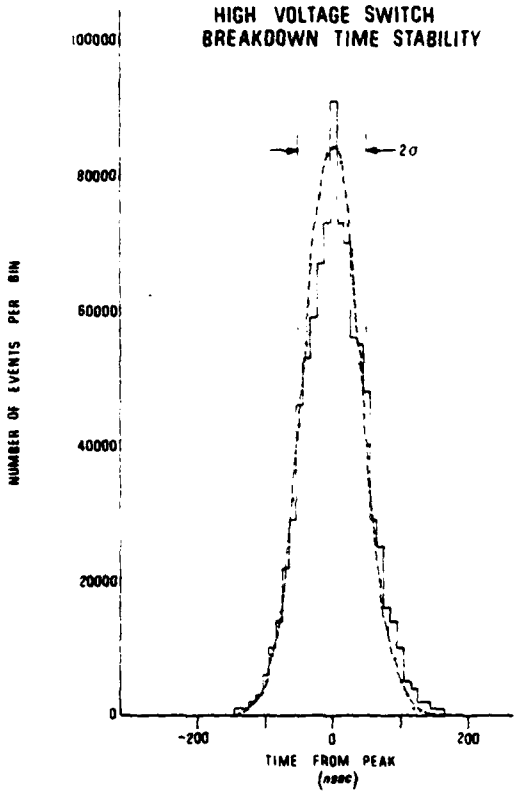


FIGURE 14.

data is 44 ns. In this case the standard deviation is artificially broadened by drifts in the switch pressure during the run which lasted over seven hours. For shorter runs, during which the pressure was more nearly constant, the typical standard deviation was 30 ns. Figure 8 displays the PFL voltage waveform together with two standard deviation wide bands in time and voltage. Note that 44 ns jitter in time corresponds to 1.8 percent spread in the breakdown voltage at the operating point for the 10^6 shot run.

Assuming the breakdown time distribution is truly Gaussian, it is possible to estimate the ringover rate. Defining a ringover very conservatively as any breakdown occurring after voltage peak, the criterion for a fraction f of ringovers is that the tail of the Gaussian beyond peak voltage have an area f (where the total area under the Gaussian is normalized to 1). For one ringover in 10^6 shots, the mean breakdown time should be 4.8 σ before peak or 144 ns for the typical observed 30 ns width. At that time the voltage is 97 percent of peak. Allowing for other instabilities such as are observed in the gas system the typical operating point has been reduced to 90-95 percent of peak. Assuming that the same stability could be achieved in a triggered switch, there should be no prefires for operation at any reasonable point, e.g., less than 90 percent of the selfbreak voltage.

A 30 ns standard deviation is 0.5 percent of the total duration of the dual resonance waveform. Previous data taken with this same switch (and UV preionization) at 1 pps using a 1.7 μs quasi-dual resonance waveform gave a 12.5 ns standard deviation which is 0.7 percent of the total waveform duration. UV preionization was essential to stabilize the switch for 1 pps operation. The standard deviation of the breakdown voltage distribution was below 1 percent with good preionization (the jitter was essentially unmeasurable from oscilloscope traces). Without UV it was in the range of 3 to 5 percent of the mean breakdown voltage. While detailed measurements of switch stability with preionization have not been made at higher repetition rates, the time jitter data given above indicate that with sufficient gas flow the stability at higher repetition rates without preionization is similar to the stability at lower rates with preionization. This would imply a conditioning of the gas by previous shots decaying with characteristic time which might be in the range of 0.1 sec.

Similar results have been obtained using SF_6. (For economic reasons air was preferred to SF_6 before a recirculating system became available.) Preliminary data with SF_6 show a Gaussian breakdown distirbution for 700 kV, 50 pps operation at 450 SCFH with a gap spacing of 1.3 cm. The standard deviation was 30 ns as should have been expected for air. The required flow rate for air would have been about 25 SCFM under these conditions in a 3.8 cm gap. Thus the SF_6 flow rate is roughly down from the air flow rate in proportion to the gap ratio.

Switch Lifetime

A primary goal of this work is to establish and enhance the lifetime of spark gaps which is assumed to be limited by electrode erosion. All spark gap electrodes were weighed before and after the previously mentioned 10^6 shot run. Waveforms were monitored to establish the charge transfer and action integral per shot. The following tables summarize the results:

Table I. Rail Gap Switch

Mass loss, main electrode #1 (brass), g	2
Mass loss, main electrode #2 (brass), g	1.9
Mass loss, trigger electrode (60/40 Elkonite), gm	5.4
Charge transfer per shot, $(\int I dt)$, coulombs	36×10^{-3}
Charge transfer total, coulombs	36×10^{3}
Action per shot, $(\int I^2 dt)$, amp^2-sec	592
Action, total, amp^2-sec	592×10^{6}
Erosion, g/coulomb	
Main electrode #1	55.6×10^{-6}
Main electrode #2	52.8×10^{-6}
Trigger (half of 2-arc total)	75.0×10^{-6}
Erosion, g/amp^2-sec	
Main electrode #1	3.38×10^{-9}
Main electrode #2	3.21×10^{-9}
Trigger (half of 2-arc total)	4.56×10^{-9}

The average power dissipation in the rail gap was monitored during the million shot run by measuring the temperature rise (75°) in the air flowing (2.23 lb/min) through the switch. Based on these measurements the average power dissipation was 704 watts or 17.6 J/pulse, a full 10 percent of the total system power. This energy is dissipated during the PFL charge cycle and

during a lower amplitude ringdown period after the high voltage switch fires if residual energy is left in the system.

Data show that 6 percent of the energy stored in the 1.5 μF capacitor is lost during the dual resonance charge cycle. From measured values of equivalent series resistance in the capacitor and transformer it is estimated that each accounts for approximately 17 percent of the energy loss leaving 66 percent assumed dissipated in the rail gap switch, the only other significant loss element in the primary circuit. With the output switch operating at 95 percent of peak, 10 percent of the originally stored energy remains in the primary side of the circuit when the PFL is discharged. Calculations have shown that very little of this energy couples through the transformer and is dissipated in the PFL load during the ensuing ringdown. For the conditions of the million shot run, therefore, an estimated 1.7 J/pulse was dissipated in both the transformer and capacitor and 6.5 J/shot in the rail gap switch during the PFL charge cycle and 17 J/pulse remained in the primary side after the output switch fired. Assuming that the proportionate energy loss remained constant during the late time ringdown, an additional 2.9 joules were deposited in the transformer and capacitor and 11.2 joules in the switch making a total of 4.6 J/pulse in the transformer and capacitor and 17.7 J/pulse in the switch.

Although the absolute accuracy of the close correlation to the measured 17.6 J/pulse may be viewed with considerable reservation, it does illustrate the significant heat deposition that can occur in system components when comparatively small fractions of energy are left in the system.

Table II. Interstage Gap

Mass loss, main electrodes (copper), g	negligible
Charge transfer per shot, coulombs	24×10^{-3}
Charge transfer total, coulombs	24×10^{3}
Action per shot ($\int I^2 dt$), amp^2-sec	.58
Action total amp^2-sec	580×10^{3}

Table II presents erosion data for the interstage gap. The weight loss from the main electrodes was unmeasurable with the instrument used. Assuming, however, that the erosion rate of the copper electrodes could be scaled with the action integral and the data for the brass electrodes in the rail gap switch the expected erosion of the interstage gap electrodes would have been approximately 2×10^{-3} g which could not have been measured. This would have made the erosion rate in terms of charge transfer $.083 \times 10^{-6}$ g/coulomb which is much lower than that for the rail gap. Since the total charge transfer through the interstage gap was comparable to the rail gap and the erosion was not, this result strongly suggests that electrode erosion can not be accurately estimated with charge transfer considerations where widely different current densities are involved.

Table III presents erosion data for the high voltage switch. Based on these data for the large electrode of the high voltage switch, the erosion rate is 2×10^{-8} cm^3/shot ($\rho = 18$ g/cm^3). The damage pattern on this electrode has an area of 60 cm^2. Assuming that an erosion induced increase in the gap of 10 percent can be tolerated, the switch could survive removal of 0.2 cm from the face of this electrode corresponding to a total volume loss of 12 cm^3. At the observed erosion rate of 2×10^{-8} cm^3/pulse, the estimated switch lifetime is 6×10^{8} pulses.

Table III. High Voltage Switch

Mass loss, large electrode (Elkonite), g	0.352
Mass loss, small electrode (Elkonite), g	0.187
Charge transfer per shot, coulombs	6.5×10^{-4}
Charge transfer total, coulombs	650
Action per shot, amp^2-sec	5
Action total, amp^2-sec	5×10^{6}
Erosion, g/coulomb	
Large electrode	5.4×10^{-4}
Small electrode	2.9×10^{-4}
Erosion, g/amp^2-sec	
Large electrode	7×10^{-8}
Small electrode	4×10^{-8}

Conclusion

The 100 Hz, 350 kV, 30 KW time averaged power pulser has operated successfully for over 10^7 shots with runs ranging from full power for a few minutes to a continuous run of 10^6 shots (7 hours) at reduced power. Throughout the testing, the transformer and capacitors have shown no signs of deterioration indicating expected lifetimes in excess of 10^7 shots.

The three spark gap switches used in the circuit have also performed satisfactorily. The low current trigatron interstage switch which controls the charging of the second stage capacitor and the rail gap in the primary circuit of the transformer require service intervals in excess of 10^6 shots without using heavy metal electrodes. With tungsten alloy electrodes these service intervals should at least approach 10^7 shots.

The untriggered 700 kV output switch has been shown to have a stable operating regime for each voltage and repetition rate at which the system may be operated. Estimates based on the data indicate that the switch ought to operate stably at a mean breakdown voltage of 95 percent of peak and no more than one ringover per 10^6 shots with lifetime near 10^9 shots.

Acknowledgements

The authors wish to thank K. R. Prestwich for his valuable comments and suggestions in support of this work. The assistance of J. P. Corley and M.W. O'Malley is also acknowledged.

References

1. G. J. Rohwein, IEEE Trans. Nucl. Sci. NS-22 (1975).
2. T. H. Martin, SC-RR-71 0341 (1971).
3. E. A. Abramyan, IEEE Trans. Nucl. Sci. NS-18 (1971).
4. D. Finkelstein, P. Goldberg, and J. Shuchatowitz, Rev. Sci. Instr., 37, No. 2 (1966).
5. C. R. J. Hoffman, Rev. Sci. Instr., 46, No. 1 (1975).

AUTHOR INDEX

NAME/SESSSION NO.	PAGE
Alcock, A.J.–V-4	94
Bajda, J.–I-1	1
Bayless, J.–V-2	83
Bird, S.R.–IX-2	242
Blinchikoff, H.J.–III-1	38
Bowman, C.D.–VIII-8	213
Brewster, J.B.–VII-1	149
Buffa, A.J.–X-2	264
Burkes, T.R.–III-3, VII-6	46,173
Buttram, M.T.–Post-Deadline-2	303
Carder, B.M.–I-2	5
Caristi, R.F.–VIII-11	227
Cary, W.K., Jr.–VII-5	167
Cervone, P.–IV-5	75
Chesterman, A.–V-5	98
Cole, R.C.–II-1	14
Cook, E.–II-5, V-5	27,98
Corbiere, P.A.–X-1	260
Corson, C.A.–II-6	34
Creedon, J.E.–IV-1, V-1, VI-7, X-2	60, 79,135,264
Dethlefsen, R.–VIII-10	222
Dexter, W.–II-3, V-5	19,98
Dolbear, D.–VI-4	117
Dollinger, R.–VII-4, VIII-5, VIII-6, VIII-8, VIII-9	163, 200,204,213,217
Ekdahl, C.A.–X-7	289
Faltens, A.–V-5	98
Fleischer, D.–VI-4	117
Ford, R.D.–X-6	284
Friedman, S.–VI-6	129
Gardenghi, R.A.–III-1, III-2	38,43
Gauch, H.–V-1	79
Gilmour, A.S., Jr.–VIII-5, VIII-6, VIII-7, VIII-8, VIII-9	200, 204,208,213,217
Goldberg, S.–VI-6	129
Gray, B.R.–IV-3	70
Hagler, M.–VII-6	173
Hamilton, J.–VI-6, VI-7	129,135
Hammel, J.E.–X-7	289
Hanks, K.W.–X-7	289
Harrison, J.–III-5	55
Harvey, R.J.–V-1	79
Haumesser, R.–IV-4	71
Hester, R.–V-5	98
Holly, R.W.–V-1	79
Honig, E.M.–VIII-3, VIII-4	189,194
Hooper, E.H.–IX-2	242
Hopkins, D.C.–VIII-6	204
Ishikawa, K.Y.–IX-1	235
Jones, L.A.–X-7	289
Kettle, L.J.–VI-1	102
King, C.J.–VIII-6	204
Kolibas, R.E.–X-1	260
Kristiansen, M.–VII-6	173
Leopold, K.E.–V-4	94
Levy, S.–IV-1	60
Lockwood, D.–IV-4	71
Lowry, L.R.–VII-3	159
McCown, C.J.–IX-1	235
McGowan, J.–VI-7, X-2	135,264
McMullin, P.G.–VII-3	159
McNees, S.G.–VIII-1	180
Mace, P.N.–X-4	274
Malone, D.P.–VIII-8	213
Manikopoulos, C.N.–VIII-9	217
Masten, L.B.–III-3	46
Mazzie, J.–VII-5	167
Menown, H.–VI-2, VI-5	105,125
Merz, S.–VI-4, VI-6, VI-7	117,129,135
Miller, R.N.–VIII-5, VIII-6	200,204
Moeny, W.M.–III-4	52
Molyneux-Berry, R.B.–VI-8	144
Moran, S.L.–IX-4	254
Moriarty, J.J.–X-1	260
Morreall A.F.–VIII-2	183
Myers, A.–II-3	19
Mylius, J.–VIII-10	222
Neale, C.V.–VI-1, VI-5	102,125
Newton, B.P.–VI-1	102
Nicholls, N.S.–VI-2	105
North, W.–IX-3	247
Nunnally, W.C.–X-7	289
O'Loughlin, J.P.–III-4	52
Parten, M.E.–III-3	46
Pedano, A. –VIII-6	204
Plante, R.–VI-4, VI-6, VI-7	117,129,135
Portnoy, W.–VII-6	173
Porzio, P.–II-4	22
Pruitt, D.L.–II-2, VII-2	15,157
Rambo, S.I.–III-2	43
Ramrus, A.–V-3	88
Reginato, L.–II-3, II-5, V-5	19,27,98
Reinhardt, N.–VI-4, VI-7	117,135
Roark, R.M.–III-3	46
Robinson, T.H.–X-3	267
Rogers, D.–II-3	19
Rohwein, G.J.–Post-Deadline-2	303
Rosenfeld, M.–VIII-9	217
Sarjeant, W.J.–V-4	94
Scerch, G.–IV-5	75
Scheffler, C.–VII-4	163
Schneider, S.–X-2	264
Schwartz, P.–VIII-9	217
Scoles, G.J.–I-3	9
Selin, K. I.–X-8	293
Sherboody, G.M.–VII-1	149
Simon, R.P.–VIII-11	227

AUTHOR INDEX

NAME/SESSION NO.	PAGE
Snelling, R.L.–I-3	9
Stronks, G.E.–IX-1	235
Swen, Y.–VIII-7	208
Tarantino, F.–II-4	22
Taylor, R.S.–V-4	94
Turnquist, D.–VI-4, VI-6, VI-7, VIII-11	117, 129,135,227
Vitkovitsky, I.M.–X-6	284
Warren, R.W.–VIII-3, VIII-4	189,194
Watson, H.–Post-Deadline-1	297
Weiner, M.–X-5	277
Welsh, J.–IV-4	71
Wheldon, R.J.–VI-2, VI-3	105,113
Willis, W.L.–X-4	274
Wright, W., Jr.–IV-2, V-2	66,83
Yokata, T.–V-5	98
Zimmerman, A.–II-3	19

LIST OF ATTENDEES

1978 THIRTEENTH PULSE POWER MODULATOR SYMPOSIUM

Kris Aaland	Lawrence Livermore Laboratory
Garry R. Allen	Los Alamos Scientific Laboratory
E.R. Altschul	Aydin Energy Division
Robert A. Anderson	Lawrence Livermore Laboratory
G.P. Bagley	Brookhaven National Laboratory
Kenneth C. Baile	Naval Surface Weapons Center
Joseph Bajda	Cober Electronics Company
Don G. Ball	Lawrence Livermore Laboratory
Glenn C. Barber	Oak Ridge National Laboratory
John Barnes	Varian Associates
Bart Barton	Maxwell Laboratory
David M. Benenson	SUNY at Buffalo
Stephen Bird	Westinghouse Electric Corporation
Rudolph M. Bonitch	AIL
L.P. Bradley	Lawrence Livermore Laboratory
Jerome B. Brewster	Westinghouse Electric Corporation
T.R. Burkes	Texas Tech University
Malcolm T. Buttram	Sandia Laboratories
W. J. Caldwell	Lawrence Livermore Laboratory
Richard J. Calliger	Lawrence Livermore Laboratory
James Calpin	Westinghouse Electric Corporation
Nguyen Ngoc Can	Thomson-CSF
Bruce M. Carder	Lawrence Livermore Laboratory
Robert Caristi	EG&G, Inc.
James J. Carlins	Union Carbide Corporation
John L. Carter	U.S. Army ERADCOM
William K. Cary, Jr.	Naval Surface Weapons Center
Robert N. Caselaro	RCA
Matija Cevanovic	Ontario Hydro
Piero Cervone	Selenia S.p.e.
Phil Champney	Physics International
S.R. Childerhose	Veradyne Corporation

LIST OF ATTENDEES

Gerald Clark	EG&G, Inc.
Stanley R. Clark	Hughes Aircraft Company
L. Colin	Thomson-CSF
Dominick Coute	U.S. Naval Research Laboratory
Edward G. Cook	Lawrence Livermore Laboratory
Don Cooke	Carborundum Company
Charles A. Corson	Westinghouse Electric Corporation
Carl R. Crager	Litton Industries
John P. Craig	Texas Tech University
John E. Creedon	U.S. Army ERADCOM
Jack Cutting	Lawrence Livermore Laboratory
Frederick J. Dahl	General Electric Company
Stephen J. Davis	Lawrence Livermore Laboratory
Terry DeHart	Northwest, Inc.
Stephen Delligatti	Sperry Gyroscope
Frank DeLargio	Emerson Electric Company
F. DeRoos	ITT Corporation
Rolf Dethlefsen	Gould Inc.
Dennis R. Dettman	SUNY at Buffalo
Warren L. Dexter	Lawrence Livermore Laboratory
Richard Dolbear	EG&G, Inc.
Richard Dollinger	SUNY at Buffalo
Michael P. Dougherty	Air Force Aero-Propulsion Laboratory
John W. Dzimianski	Westinghouse Electric Corporation
Donald Eccleshall	USA Ballistic Research Laboratory
Carl J. Eichenauer	General Electric Company
Jim Eshleman	RCA Corporation
Edward Fennell	REL, Inc.
Richard D. Ford	Naval Research Laboratory
James Forsythe	Garrett Corporation
Bill Fox	Maxwell Laboratories, Inc.
Steven Friedman	EG&G, Inc.
B. Fudim	Calvert Electronics Company
John D. Galbraith	EG&G, Inc.

LIST OF ATTENDEES

Robert A. Gardenghi	Westinghouse Electric Corporation
Leonard Genova	Stanford University
K. J. Germeshausen	EG&G, Inc.
Antonio Giacometti	Contraves Italiana Spa
Richard A. Gibson	AiResearch
A. S. Gilmour, Jr.	SUNY at Buffalo
M. Therese Glancy	Naval Surface Weapons Center
Saul Gold	Varian Associates
Jerry A. Goldlust	Dielectric Sciences, Inc.
Robert Goldstein	Lasermetrics Inc.
A. E. Gordon	ITT Corporation
Bobby R. Gray	Rome Air Development Center
Ronald Gripshover	Naval Surface Weapons Center
H. C. Grunwald	ITT Corporation
Arthur H. Guenther	Air Force Weapons Laboratory
Marion Hagler	Texas Tech University
Robin Harvey	Hughes Research Labs
J. R. Hall	Rocketdyne
Jerome Hamilton	EG&G, Inc.
Hildegarde Hammond	Palisades Institute for Research Services
Neville W. Harris	Ion Physics Company
John Harrison	Maxwell Laboratories, Inc.
Lynn L. Hatfield	Texas Tech University
R. A. Hill	Naval Electronic Systems Command
W. Wayne Hofer	Lawrence Livermore Laboratory
Emanuel M. Honig	Los Alamos Scientific Laboratory
Edward H. Hooper	Westinghouse Electric Corporation
Craig Howton	Maxwell Laboratories, Inc.
Joseph A. Howarth	Raytheon Company
Don Ho Huang	SUNY at Buffalo
Daniel Hudgings	Los Alamos Scientific Laboratory
T. G. Ianes	Lawrence Livermore Laboratory
Ken Y. Ishikawa	Hughes Aircraft Company
Sandford Jacobson	Cober Electronics Company

LIST OF ATTENDEES

Jon Jasper	Exxon Nuclear Company, Inc.
Rodney M. Johnson	Wantagh, N.Y.
William A. Johnson	SLAC, Stanford University
Warren L. Jones	Westinghouse Electric Corporation
Morris Katzman	Naval Elec. Lab. Center
John Keane	Brookhaven National Laboratory
Dean O. Kippenhan	Lawrence Livermore Laboratory
Leonard Klein	Palisades Institute for Research Services
Marc A. Kolpin	Physics International
Robert Kuenning	Lawrence Livermore Laboratory
Bernhard Kulke	Lawrence Livermore Laboratory
Dick Larkin	Larkin & Company
Alan G. Larmen	Raytheon Company
Joe L. Lee	SUNY at Buffalo
Jeff Levatter	Encinitos, CA
Stephen Levy	U.S. Army ERADCOM
Edward Logan	International Laser Systems, Inc.
C. M. Loring, Jr.	Oak Ridge National Laboratory
L. R. Lowry	Westinghouse Electric Corporation
Lawrence H. Luessen	Naval Surface Weapons Center
James Lunsford	Los Alamos Scientific Laboratory
Helmut Lustig	AEG-Telefunken
Phillip N. Mace	Los Alamos, NM
Wilbert Manley	Bendix Corporation
Irwin Marson	Sperry Gyroscope
V. Nicholas Martin	GTE Laboratories
Glen McDuff	Beverly, MA
Paul G. McMullin	Westinghouse Electric Corporation
Sterling G. McNees	EIMAC, Division of Varian
Bernard A. McNulty	Lawrence Livermore Laboratory
H. Menown	English Electric Valve Co., Ltd.
Spencer Merz	EG&G, Inc.
Bob Michelak	Dei Electronics
Richard N. Miller	SUNY at Buffalo

LIST OF ATTENDEES

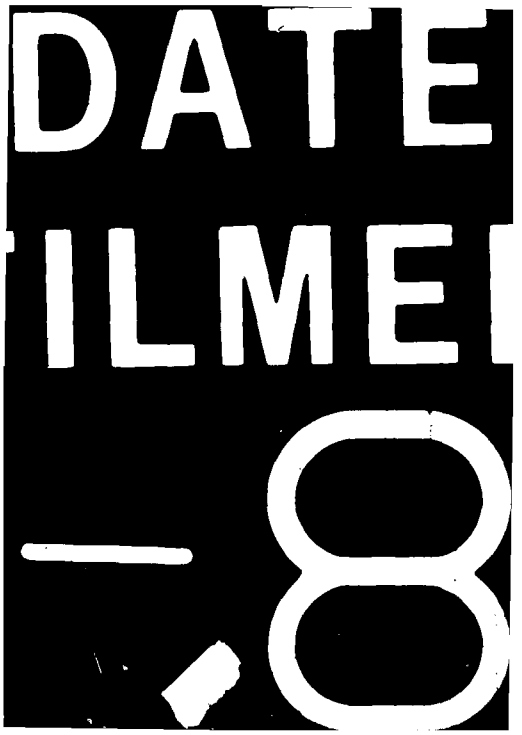
Mark L. Mitscher	R. W. Mitscher Company
Douglas Moll	SUNY at Buffalo
Stuart L. Moran	Naval Surface Weapons Center
J. J. Moriarty	Raytheon Company
Dave Morman	Varian Associates
Merle Morozowich	Westinghouse Electric Corporation
Albert F. Morreall	Utica, NY
Louis Motta	Raytheon Company
John Mulrey	EG&G, Inc.
John Brian Murray	Sierra Research Corporation
Justus Mylius	Gould, Inc.
Harvey C. Nathanson	Westinghouse Electric Corporation
William R. Neal	Spire Corporation
C. V. Neale	English Electric Valve Co., Ltd.
L. K. Neher	Los Alamos Scientific Laboratory
Nigel S. Nicholls	Royal Signal & Radar Establishment
William R. North	GTE Sylvania
W. C. Nunnally	Los Alamos Scientific Laboratory
Martin J. Nutter	Los Alamos Scientific Laboratory
Fred Nylander	Varian Associates
Henry B. Odom, III	Naval Surface Weapons Center
Joseph P. O'Donnell	Axel Electronics, Inc.
Dennis O'Kula	Varian Associates
James P. O'Loughlin	Albuquerque, NM
Thomas J. Pacala	Jet Propulsion Laboratory
John L. Pack	Westinghouse Electric Corporation
R. H. Parkes	EEV Canada, Ltd.
Edward M. Piechowiak	Westinghouse Electric Corporation
Roger Plante	EG&G, Inc.
John Power	Beverly, MA
Kenneth R. Prestwicit	Sandia Laboratories
Joseph Proud	GTE Laboratories
D. L. Pruitt	RCA Corporation
S. Ivan Rambo	Westinghouse Electric Corporation

LIST OF ATTENDEES

Al Kamrus	Maxwell Laboratories, Inc.
William R. Rapoport	Lawrence Livermore Laboratory
Louis L. Reginato	Lawrence Livermore Laboratory
Richard Reid	Hipotronics, Inc.
Nicholas Reinhardt	Consultant
D. B. Remsen, Jr.	General Atomic Company
G. Ribakous	Lumonics Research
B. G. Rice	ITT Corporation
Robert L. Ritter	Varian Associates
A. D. Roach	SLAC, Stanford University
T. H. Robinson	Marconi Research Laboratories
Ricki M. Roark	Texas Tech University
David A. Rogers	General Electric Company
Doyle Rogers, Jr.	Lawrence Livermore Laboratory
Gerald J. Rohwein	Sandia Laboratories
M. F. Rose	Naval Surface Weapons Center
Herbert Rosebrock	Sierra Research Corporation
Robert M. Rowe	SLAC, Stanford University
D. G. Samaras	AFOSR, Air Force Office of Scientific Research
Ralph Sanders	Brookhaven National Laboratory
W. J. Sarjeant	National Research Council, of Canada
Merrald B. Shrader	EIMAC, Division of Varian
Paul R. Schwartz	SUNY at Buffalo
Karl L. Selin	The Jet Project
George Sinclair	Sinclair Radio Labs, Ltd.
Franklin R. Smith	U.S. Army Engineers
Ian D. Smith	Ian Smith, Inc.
R. L. Snelling	English Electric Valve Co., Ltd.
Dennis O. Sparks	Oak Ridge National Laboratory
R. J. Spreadbury	Westinghouse Electric Corporation
Jere D. Stahley	RCA Corporation
Brian Steer	Varian Associates
Robert H. Stone	Raytheon Company

LIST OF ATTENDEES

Dale E. Suddeth	Argonne National Laboratories
James S. Sullivan	SUNY at Buffalo
P. J. Swan	EMI Varian, Ltd.
Thomas F. Sweam, Jr.	STD Research Corporation
Patrick P. Tam	SUNY at Buffalo
Francesco Tarantino	Selenia S.p.A.
Will S. Tate	Hughes Aircraft Company
Gordon F. Thomas	Naval Surface Weapons Center
Jim Thompson	University of South Carolina
David Trzcinski	SUNY at Buffalo
David Turnquist	EG&G, Inc.,
Vance Valencia	Exxon Nuclear Co., Inc.
S. James Veraldi	Veradyne Corporation
Ihor M. Vitkovitsky	Naval Research Laboratory
George Vogtlin	Lawrence Livermore Laboratory
Gerald J. Volk	Argonne National Laboratories
George M. Walter	Bendix Corporation
Richard J. Wasneski	Naval Air Systems Command
Harold Watson	AiResearch Mfg. Company
R. W. Weeks	Lumonics Research
Maurice Weiner	U.S. Army ERADCOM
William C. Weiss	Lawrence Livermore Laboratory
James P. Welsh	Thermal Technology Laboratory
Kenneth E. Williams	Avco Everett Research Laboratory
Robert H. Wills	Naval Ocean Systems Center
Raoul E. Wright	Oak Ridge National Laboratory
William H. Wright, Jr.	U.S. Army ETDL
Donald C. Wunsch	BDM Corporation
B. Zarkower	Cober Electronics, Inc.
S. W. Zimmerman	Cornell University
Stanley Zweig	Axel Electronics, Inc.


DATE
ILME
8